



MATRUSRI ENGINEERING COLLEGE

(Sponsored by Matrusri Education Society, Estd.1980)
(Approved by AICTE & Affiliated to Osmania University)
#16-1-486, Saidabad, Hyderabad – 500 059, Ph: 040-24072764
Email: matrusri.principal@gmail.com, www.matrusri.edu.in

INDEX

3.2.2 Number of books and chapters in edited volumes/books published and papers published in national/ international confere proceedings per teacher during last five years

A.Y: 2017-18

Sl. No	Name of the teacher	Title of the book/chapters published	Title of the paper	Title of the proceedings of the conference	Year of publication	ISBN/ISSN number of the proceeding	Whether at the time of publication Affiliating Institution Was same Yes/NO	Name of the publisher	Page NO
1	D.Nagaraju	-	Pothole Detection System: 'Monitoring Road Surface Aberrations Using a Wireless Sensor Network'	Proceedings of 1st National Conference on Trends in Science, Engineering & Technology (NTSET-2018)	2017-18	97881-936274-0-2.	Yes	Matrusri Engineering College	1-5
2	Dr.Y.Aparna	-	Synthesis and antimicrobial activity of substituted 4-arylidene,2-(hydroxy phenyl) oxazol-5(4h)- ones	National Conference On Trends In Science, Engineering & Technology by Matrusri Engineering College	2017-18	978-1-5386-1959-9	Yes	Matrusri Engineering College	6-17
3	Dr.Y.Aparna	-	synthesis of novel imidazolones, their Antimicrobial Studies and molecular docking studies	Indian Council of Chemists	2017-18	-	Yes	NITK Mangalore	17-24

4	Dr.M.Yuvaraj	-	Optimization of web service quality control through Goal programming	National Conference On Trends In Science, Engineering & Technology by Matrusri Engineering College	2017-18	978-1-5386-1959-9	Yes	Matrusri Engineering College	25-29
5	Dr.G.Ravindranath	-	Graphical user interface load flow solution of radial distribution network	National Conference On Trends In Science, Engineering & Technology by Matrusri Engineering College	2017-18	97881-936274-0-2	Yes	Matrusri Engineering College	30-36
6	Dr.G.Ravindranath	-	A Noval electric vechile control- Electronic differential-strategy using Five phase Induction Motor	National Conference On Trends In Science, Engineering & Technology by Matrusri Engineering College	2017-18	97881-936274-0-2	Yes	Matrusri Engineering College	37-45
7	P.Kishor	-	SPWM Techniques in five level inverters	National Conference On Trends In Science, Engineering & Technology by Matrusri Engineering College	2017-18	97881-936274-0-2	Yes	Matrusri Engineering College	46-52
8	M.Saritha	-	Modelling of SSSC to Enhance power system stability using MATLAB	National Conference On Trends In Science, Engineering & Technology by Matrusri Engineering College	2017-18	97881-936274-0-2	Yes	Matrusri Engineering College	53-59
9	P.Anil Kumar	-	Single phase quasi-Z-source modified cascaded multilevel inverter with half bridge cell	National Conference On Trends In Science, Engineering & Technology by Matrusri Engineering College	2017-18	97881-936274-0-2	Yes	Matrusri Engineering College	60-67
10	M V Subramanyam	-	SPWM techniques in five level inverters	National Conference On Trends In Science, Engineering & Technology by Matrusri Engineering College	2017-18	97881-936274-0-2	Yes	Matrusri Engineering College	68-74
11	M Srinivas Reddy	-	Simulation of solar PV Array Using MATLAB/SIMULINK	National Conference On Trends In Science, Engineering & Technology by Matrusri Engineering College	2017-18	97881-936274-0-2	Yes	Matrusri Engineering College	75-80

12	Mrs. N.Kalpana	-	Modelling of SSSC to Enhance power system stability using MATLAB	National Conference On Trends In Science, Engineering & Technology by Matrusri Engineering College	2017-18	97881-936274-0-2	Yes	Matrusri Engineering College	81-87
13	M.Praveen Reddy	-	Simulation of solar PV Array Using MATLAB/SIMULINK	National Conference On Trends In Science, Engineering & Technology by Matrusri Engineering College	2017-18	97881-936274-0-2	Yes	Matrusri Engineering College	88-93
14	Prof.G.Manohar	-	Optimum Design of Multi-Storeyed Building against Blast Loads	National Conference on Trends in Science, Engineering & Technology (NTSET-2018)	2017-18	97881-936274-0-2	Yes	Matrusri Engineering College	94-102
15	P.V.S.Koteswar Rao	-	A Study on Recycled Bituminous Pavement Materials using Bitumen VG-30	National Conference on Trends in Science, Engineering & Technology (NTSET-2018)	2017-18	97881-936274-0-2	Yes	Matrusri Engineering College	103-108
16	G.Satyavathi	-	Impact Of Moisture Deficit Stress On Growth, Biomass And Yield Parameters Of Cluster Bean (CyamopsisTetragonolobaL. Taub.) Genotypes	National Conference on Trends in Science, Engineering & Technology (NTSET-2018)	2017-18	97881-936274-0-2	Yes	Matrusri Engineering College	109-117
17	S.Lokeswari	-	Study Of Concrete Using Ld Slag As Partial Replacement Of Coarse Aggregate	National Conference on Trends in Science, Engineering & Technology (NTSET-2018)	2017-18	97881-936274-0-2	Yes	Matrusri Engineering College	118-129
18	K.S.SugunaLeela	-	Outer Ring Road Traffic Analysis And Prediction	National Conference on Trends in Science, Engineering & Technology (NTSET-2018)	2017-18	97881-936274-0-2	Yes	Matrusri Engineering College	130-139
19	T.RajaRamanna	-	Manufacturing Of Elliptical Shape Concrete Hollow Bricks Using Granulated Blast Furnace Slag As A Fine Aggregate	National Conference on Trends in Science, Engineering & Technology (NTSET-2018)	2017-18	97881-936274-0-2	Yes	Matrusri Engineering College	140-148

20	P.Prashanth	-	Experimental Study On Geopolymer Concrete	National Conference on Trends in Science, Engineering & Technology (NTSET-2018)	2017-18	97881-936274-0-2	Yes	Matrusri Engineering College	149-155
21	M.Srividya	-	Numerical Modelling Of Contaminant Transport In Soil	National Conference on Trends in Science, Engineering & Technology (NTSET-2018)	2017-18	97881-936274-0-2	Yes	Matrusri Engineering College	156-165
22	Dr.M.V.Kishore	-	An Experimental Study On The Mechanical Properties Of Thixoformed Components in Aluminum Alloys	National Conference On Trends In Science, Engineering & Technology by Matrusri Engineering College	2017-18	97881-936274-0-2	Yes	Matrusri Engineering College	166-172
23	Mr. C. Venkateshwar Reddy	-	Experimental characterization of inconel-718 by GTAW process using different sheild gases	National Conference On Trends In Science, Engineering & Technology by Matrusri Engineering College	2017-18	97881-936274-0-2	Yes	Matrusri Engineering College	173-180
24	Mr.M.Krishna	-	Failure Criticality Analysis using FishiKawa Diagram (A Case study of Dumpers at OCP, Ramagundam)	National Conference On Trends In Science, Engineering & Technology by Matrusri Engineering College	2017-18	97881-936274-0-2	Yes	Matrusri Engineering College	181-189
25	Mr.V.Harinath	-	Factors and mechanisms responsible for heat transfer enhancement using nano fluid	National Conference On Trends In Science, Engineering & Technology by Matrusri Engineering College	2017-18	ISBN 97881-936274-0-2	Yes	Matrusri Engineering College	190-197
26	Mr. A. Kalyan Charan	-	Extraction of liquid hydrocarbon fuel from waste plastic	National Conference On Trends In Science, Engineering & Technology by Matrusri Engineering College	2017-18	ISBN 97881-936274-0-2	Yes	Matrusri Engineering College	198-206
27	Mr. A. Kalyan Charan	-	Thermal Analysis on Rectangular Plate Fin with perforations using ANSYS	National Conference On Trends In Science, Engineering & Technology by Matrusri Engineering College	2017-18	97881-936274-0-2	Yes	Matrusri Engineering College	207-214

28	Mr.P.NaveenKishore	-	Review paper on friction stir welding of various materials and aluminium matrix composites	National Conference On Trends In Science, Engineering & Technology by Matrusri Engineering College	2017-18	97881-936274-0-2	Yes	Matrusri Engineering College	215-223
29	Mr.T.SomaSekhar	-	Review paper on processing of metal matrix composites & its properties.	National Conference On Trends In Science, Engineering & Technology by Matrusri Engineering College	2017-18	97881-936274-0-2	Yes	Matrusri Engineering College	224-231
30	Mr.S.Sampath	-	Design and Analysis of thermo mechanical loading for a turbine housing using FEA	National Conference On Trends In Science, Engineering & Technology by Matrusri Engineering College	2017-18	97881-936274-0-2	Yes	Matrusri Engineering College	232-243
31	Dr. P.Vijaya Pal Reddy	-	Nativity Language age and prediction using a document weighted Approach	National Conference On Trends In Science, Engineering & Technology	2017-18	ISBN 97881-936274-0-2	Yes	Matrusri Engineering College	244-250
32	Dr. P. Hara Gopal Mani	-	Dynamic Evaluation of Embedded Systems	NTSET-2018	2017-18	ISBN 97881-936274-0-2	Yes	Matrusri Engineering College	251-260
33	A.Narmada	-	Raspberry pi based global industrial process monitoring through wireless communication	NTSET-2018	2017-18	ISBN 97881-936274-0-2	Yes	Matrusri Engineering College	261-270
34	Aruna kokkula	-	Effective food grain loss reduction technique using IOT	NTSET-2018	2017-18	ISBN: 97881-936274-0-2.	Yes	Matrusri Engineering College	271-278
35	Aruna kokkula	-	Design and implementation of All digital phase locked loop on FPGA	NTSET-2018	2017-18	97881-936274-0-2.	Yes	Matrusri Engineering College	279-286
36	B.Indira Priyadarshini	-	RTL generation using a high performance DIF algorithm using 'C'	NTSET-2018	2017-18	97881-936274-0-218.	Yes	Matrusri Engineering College	287-293
37	B.Indira Priyadarshini	-	A 64 bit MAC Unit Design using Reversible Logic gate and Vedic Multiplier	NTSET-2018,	2017-18	97881-936274-0-2.	Yes	Matrusri Engineering College	294-300

38	B.Indira Priyadarshini	-	Improved Design of Low Power TPG using LP LFSR	NTSET-2018	2017-18	97881-936274-0-2.	Yes	Matrusri Engineering College	301-306
39	B.Indira Priyadarshini	-	Defects Detection in Printed Circuit Board using Integrated frame work	4th International conference on Science, Technology & Management (ICSTM-2017)	2017-18	978-93-87433-00-7	Yes	Institution of Electronics and Telecommunication Engineers, MAHARASHTRA	307-313
40	Dr.Pallavi Khare	-	Defects Detection in Printed Circuit Board using Integrated	4th International conference on Science, Technology & Management (ICSTM-2017)	2017-18	978-93-87433-00-7	Yes	Institution of Electronics and Telecommunication Engineers, MAHARASHTRA	314-320
41	DR.M.Ramesh	-	Optimal solution of linear programming with Fuzzy variables	NTSET-2018	2017-18	97881-936274-0-2.	Yes	Matrusri Engineering College	321-325
42	Aruna kokkula	-	High Speed Architecture for Orthogonal Code Convolution	International Conference on Intelligent Sustainable Systems (ICISS 2017)	2017-18	978-1-5386-7808-4	Yes	IEEE	326-334
43	Aruna kokkula	-	Performance comparison of weighted modulo (2n+1) adder using different prefix structures	ICRTESSM-2017	2017-18	978-81-934288-0-1	Yes	Institution of Electronics and Telecommunication Engineers	335-342
44	A S Keerthi Nayani	-	Effective food grain loss reduction technique using IOT	NTSET-2018	2017-18	97881-936274-0-2.	Yes	Matrusri Engineering College	343-350
45	A S Keerthi Nayani	-	Performance comparison of weighted modulo (2n+1) adder using different prefix structures	ICRTESSM-2017	2017-18	978-81-934288-0-1	Yes	Institution of Electronics and Telecommunication Engineers.	351-358
46	Dr. Pallavi Khare	-	A Review on Mixed IRIS Spoofing Attacks Detection	Proceedings of 1st National Conference on Trends in Science, Engineering & Technology (NTSET-2018)	2017-18	97881-936274-0-2.	Yes	Matrusri Engineering College	359-364

47	Dr. Pallavi Khare	-	A Smart Integrated System for Bike riders : A Review	Proceedings of 1st National Conference on Trends in Science, Engineering & Technology (NTSET-2018)	2017-18	97881-936274-0-2.	Yes	St.Martins Engineering College & IOSR Journals	365-371
48	Mr.P.NaveenKishore	-	Thermo acoustic refrigeration	National Conference On "Innovative Approaches In Mechanical Engineering" by St.Martins Engineering College	2017-18	2278-1684,p-ISSN: 2320-334X	Yes	St.Martins Engineering College & IOSR Journals	372-377
49	K.Koteswara Rao	-	Investigation of linearly polarized RMPA embedded with 2D-EBG ground plane	International Conference on Wireless Communications, Signal Processing and Networking (WiSPNET)	2017-18	978-1-5090-4442-9	Yes	IEEE	378-384
50	Mr. P Ravindra	-	Survival prediction for titanic data using machine learning algorithms	Ist national conference on Trends in Science,Engineering and Technology NTSET 2018	2017- 18	97881-936294-0-2	Yes	Matrusri Engineering College	385-389
51	Mrs.B J Praveena	-	Cloud computing and IoT in health care system	Ist national conference on Trends in Science,Engineering and Technology NTSET 2018	2017- 18	97881-936294-0-2	Yes	Matrusri Engineering College	390-395
52	Mrs.G.Pratibha	-	Parsing sentiment in telugu language sentences	Ist national conference on Trends in Science,Engineering and Technology NTSET 2018	2017- 18	97881-936294-0-2	Yes	Matrusri Engineering College	396-401
53	Dr. K Sunil Manohar Reddy	-	Analysing various face Recognition Techniques using Neural Networks	Ist national conference on Trends in Science,Engineering and Technology NTSET 2018	2017- 18	97881-936294-0-2	Yes	Matrusri Engineering College	402-406

54	Dr. G. Shyama Chandra Prasad	-	Particle Swarm Optimization Methodology for Classification of Images	Ist national conference on Trends in Science, Engineering and Technology NTSET 2018	2017-18	97881-936294-0-2	Yes	Matrusri Engineering College	407-414
55	Dr. Pallavi Khare	Exploring the convergence of Big Data and the Internet of Things	Chapter: 08: Internet of Things for Smart Cities	-	2017-18	DOI: 10.4018/978-1-5225-2947-7.	Yes	IGI-Global	415-420
56	Dr. G. Shyama Chandra Prasad	Get Ready for placements	-	Get Ready for placements	2017-18	978-81-920425-3-4	Yes	UMA Publications	421-424
57	Dr. Pallavi Khare	Exploring the convergence of Big Data and the Internet of Things	Chapter 13: Data Mining for the Internet of Things	-	2017-18	10.4018/978-1-5225-2947-7.	Yes	IGI-Global	425-430



Principal

Principal

Matrusri Engineering College
Saidabad, Hyderabad.

POTHOLE DETECTION SYSTEM: 'MONITORING ROAD SURFACE ABERRATIONS USING A WIRELESS SENSOR NETWORK'

¹D.Nagaraju, ²D.Prithvi Krishna Parasar, ³V.Mounika, ⁴V.Sai Deepthi

¹ Asst.Prof, ^{2,3,4} Student

^{1,2,3,4}Dept of ECE, ^{1,2,3,4}Matrusri Engineering College, Hyderabad.

¹nagaraju.devajji@gmail.com, ²prithvi.duggirala@gmail.com, ³vmounikareddy814@gmail.com,

⁴deepthililly6@gmail.com

ABSTRACT: Potholes are a major obstacle for road transport which greatly affect the commute time and comfort. Detecting and locating the potholes ensures a better commute and helps in preventing any possible fatalities. The system would be installed on a vehicle and would perform the function of road surface monitoring, using the inherent mobility of the vehicle. The system would consist of a sensing unit, micro-controller unit and a GPS subsystem. The sensing unit consists of accelerometers, deployed at specific positions which would help them make use of the accelerations generated during the motion of the vehicle. The data generated from the accelerometers would indicate the presence of potholes or severe road surface anomalies. The micro-controller unit then collects the data, which is then processed utilizing the Machine Learning algorithms. This onerous task of data processing, leads to the distinguished possibilities of pothole detection or vibrations generated due to a severe lateral unevenness on the surface of the road. At the time of the detection, the GPS unit logs the co-ordinates of that location, which then can be represented on a map and shared through a mobile application, enabling the users to choose alternative ways depending on the conditions of the road in their respective routes of travel.

I. INTRODUCTION

Municipalities around the world spend millions of dollars to maintain and repair their roadways. Keeping our roadways in good condition is a challenging problem, due to the harsh weather conditions and normal wear and tear. Because municipal budgets are constrained, determining which roads need to be fixed becomes important. Alarming the drivers regarding the road surface conditions at night or when the lighting is poor is extremely needful as well. In recent years, fast economic growth and rapid technology advance have led to significant impact on the quality of traditional transport system. Road surface monitoring is a problem which fundamentally requires mobility to solve; it cannot be solved by using static sensors on the road surfaces. The data is to be dynamically sensed through sensors installed on the vehicle. The use of sensors in the smart phones as in [1], [2] can lead to the dampening of vibrations, and also disorientation of the sensors, as the position of the phone is not fixed. This can lead to false detection, and it has been seen that the potholes cannot be detected when the vehicle is moving at slower speeds. The method in [1] will not always work because magnetometer is not present in all phones and is also susceptible to magnetic interference and increases battery consumption. In addition, the performance of this algorithm was not evaluated for various different types of speed-breakers, vehicles and drivers. The pothole patrol [3] required manual intervention for most of the process, which is not desired. The accelerometer approaches however have a universal disadvantage, as typical drivers strive to avoid potholes, so the probability of hitting a road anomaly is considerably lower than what would be expected.

II. PROPOSED PROTOTYPE

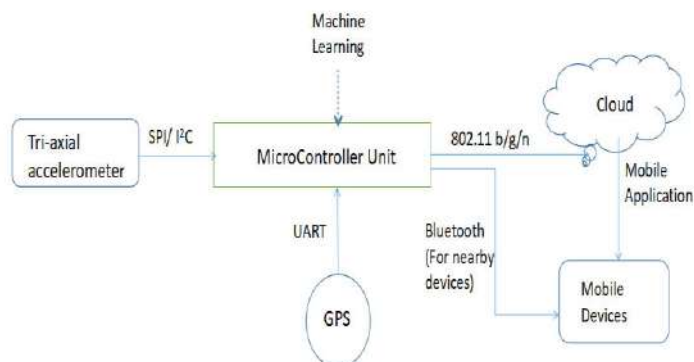


Fig.1 Block Diagram

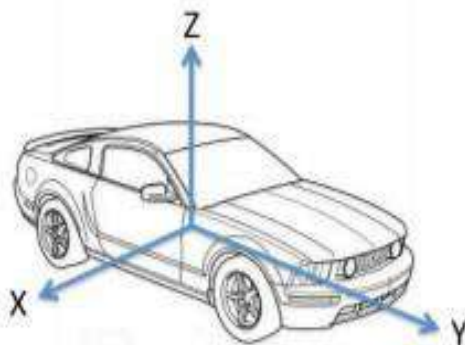


Fig2 . Axes with respect to the vehicle

The sensing unit would consist of tri-axial accelerometers, which would record the vibrations/accelerations produced in the three different directions x, y and z. The data obtained from the accelerometers can be visually represented as g-force vs. time. The vibrations along z and x axis would indicate the vibrations due to the depth of the anomalies and lateral unevenness respectively. The vibrations along the z axis would represent the rapid accelerations and the braking of the vehicle. It is to be noted that the directions along y direction can also be obtained without any interaction with a pothole, but rather due to intense braking. The data obtained from the accelerometers can be visually represented as g-force vs. time. The accelerometers would have to be placed at a specific position on the vehicle, where the vibrations produced would not get dampened by the suspensions. As the processing of the data highly depends on the sensitivity of the vibrations obtained, this is a predominant aspect of the system. The capacitance based accelerometers are preferred for this application due to its lower impedance, which is useful for the A-D conversion to be efficient. Accelerometer breakout boards with a desired sensitivity of $\pm 8g$ are interfaced with the Micro-controller unit using either of the SPI or I2C protocols.

The GPS subsystem logs the co-ordinates of the location, as soon as anomaly detection is triggered. A GPS unit with a hot start is desired, as the time to be taken for recording the co-ordinates, is very minimal (0.5-2 sec). This unit would also provide information about the velocity of the vehicle, through the nmea sentences, which are recorded as the output. The form factor of the GPS unit is also important as the size of the system is to be maintained as small as possible, in order to be feasible for the installation on the vehicle. The GPS unit would be interfaced with the MCU using the UART protocol.

The micro-controller unit acts as the central node for collecting the data from the subsystems, and then processing the data. This unit would also be responsible for storing the data onto the cloud, and also transmit the data to the nearby devices. The MCU is chosen according to the memory requirements of the algorithm, integrated modules for wireless connectivity (802.11 b/g/n), and the desired software compatibility for running the algorithms as well as for using the technologies like Android nearby, Bluetooth Low Energy to transmit the data to the mobile devices in proximity.

These three units together form the integral hardware unit of the pothole detection system, and are predominantly responsible for collecting and storing the raw data.

III. MACHINE LEARNING

Machine learning is used to process the data, into the possible set of outputs i.e. speed bumps, potholes etc., and is chosen as the system has to adapt itself over time, based on the speed of the vehicle and the conditions of the road surfaces. Machine learning makes this possible as it acts as a self-adapting medium, based on the written algorithm.

3.1 Algorithm approach

The algorithm has to differentiate the data from the accelerometers, and classify them into the possible outputs. The output variables would be assigned a predefined threshold values. The initial approach to the algorithm is done using the classification algorithm based on supervised learning. Supervised learning is a branch of machine learning, which requires a training set of data to be provided in order to determine the relation between the input data and the output variables. In order to eliminate the possibilities of inaccuracies of human observations, the training set would be defined with the help of a semi/unsupervised anomaly detection algorithm. Amidst the continuous data being obtained, this algorithm would differentiate the abnormal recordings, and these observations can be used to define the thresholds.

The above algorithm is the main approach for the classification purpose. However, the system may come across some unspecified conditions, where the traditional algorithm finds it difficult to produce the correct output. Two other approaches for their own specific purposes are:

- 1) Instance based learning: This can be used when a certain recorded data, cannot be classified into the defined set of outputs. This uses a nearest neighbour approach, estimated using a similarity parameter. Thus, the data under dilemma is considered into the category of the estimated nearest neighbouring data.
- 2) Ensemble Learning (Boosting): This is used when the errors are observed in the processed data. The data which are wrongly classified, are given more weight sequentially, and thus more significance. This helps in decreasing the possibilities of a false detection or assigning data to the wrong set of output.

3.2 SVM Learner / Classifier

A kernel is a similarity function. It is a function that is provided to a machine learning algorithm. It takes two inputs and spits out how similar they are.

Support Vector Machines are based on the concept of decision planes that define decision boundaries. In the case of binary classification, it builds two dimensional boundaries, to classify the data. Support Vector Machine (SVM) is primarily a method that performs classification tasks by constructing hyper planes in a multidimensional space that separates cases of different class labels. A decision plane is one that separates between a set of objects having different class memberships. In this case, the different class memberships would be the different possible outputs like potholes speed bumps, minor bumps etc.. Classification tasks based on drawing separating lines to distinguish between objects of different class memberships are known as hyper plane classifiers. This is done by mapping (transformation) and rearranging the objects using a set of mathematical functions known as kernels. Support Vector Machines are particularly suited to handle such tasks. SVM by definition is well suited for binary classification. In order to perform multi-class classification, the problem needs to be transformed into a set of binary classification problems. There are two such approaches:

One vs. Rest Approach (OvR): This strategy involves training a single classifier per class, with the samples of that class as positive samples and all other samples as negatives. This strategy requires the base classifiers to produce a real-valued confidence score for its decision, rather than just a class label; discrete class labels alone can lead to ambiguities, where multiple classes are predicted for a single sample.

One vs. One Approach (OvO): In the one-vs.-one (OvO) strategy, one trains $K(K-1)/2$ binary classifiers for a K -way multi-class problem; each receives the samples of a pair of classes from the original training set, and must learn to distinguish these two classes. At prediction time, a voting scheme is applied: all $K(K-1)/2$ classifiers are applied to an unseen sample and the class that got the highest number of “+1” predictions get predicted by the combined classifier. Like OvR, OvO suffers from ambiguities in that some regions of its input space may receive the same number of votes.

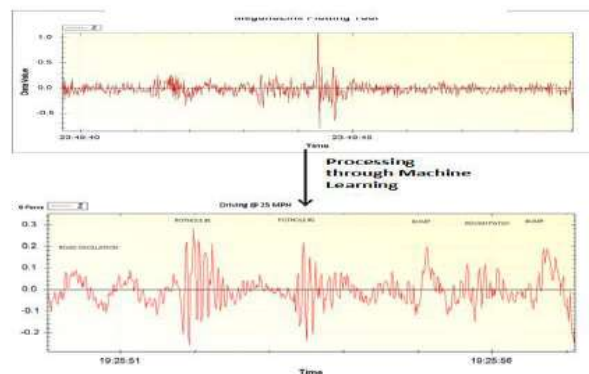


Fig3. Classified accelerometer data

IV. CLOUD COMPUTING

Cloud computing is the delivery of on-demand computing services from applications to storage and processing power typically over the internet. Cloud computing services cover a vast range of options, from the basics of storage, networking, and processing power through to natural language processing and artificial intelligence and standard office applications. Pretty much any service that doesn't require you to be physically close to the computer hardware that you are using can now be delivered via the cloud. This application would use either of the PaaS or SaaS aspects of the cloud computing, which would help in effectively storing the data and managing it through the back end. As mentioned, the cloud would further be related to two other aspects of the system, which are data representation and management. These are done through a mobile application and a crowd-sourcing platform respectively.

4.1 Crowd-sourcing/Continuous data curation

The concept of crowd-sourcing comes into picture when the system is installed on a multitude of vehicles. The data is continuously obtained from all these sources/nodes, and the data in the mobile application is to be updated accordingly, by curating this data recorded in the database. The veracity of the data is to be verified for maintaining the efficacy of the system. Data Tamer, ZenCrowd, CrowdDB, Qurk are some examples of the data curation platforms. The assumptions made by a general RDBMS are restrictive; and some queries cannot be completely

answered by machines only. Processing such queries requires human input for providing information that is missing from the database, performing computationally difficult functions, and for matching, ranking, or aggregating results based on fuzzy criteria. CrowdDB is one such platform which uses human input via crowd-sourcing. These methods of continuous data curation would be responsible for monitoring the data from the multitude of systems, and establish the veracity of the visualized data.

4.2 Mobile Application

The mobile/web application would represent the obtained location data on a digital map. The application can be built by using the PaaS aspect of cloud computing. Besides the crowd-sourcing applications mentioned above, open source applications like OpenStreetMap can be used for representing the locations, and further monitor them as well.



Fig4. Visual representation of the data in the mobile application.

The locations in the map are updated in the mobile application in analogous to the data obtained after the back end management. This is significant as a number of vehicles may travel through the same routes, and it has to be updated with respect to the continuously obtained data from the vehicles.

If multiple options for data transfer are desired, it can be transferred to the devices in the required proximity via Bluetooth Low Energy etc. Technologies like Android Nearby as well can be treated as alternatives for data transfer, for compatible devices. It is to be noted that all of these additional options may lead to the increase in power consumption.

V.CONCLUSION

The severe disorientations in the road surfaces have lead to a multitude of accidents, some of them even being fatal. The proposed Pothole Detection System is an efficient system for monitoring the road surface anomalies, using an array of sensors and effective communication media. Since satellite navigation has almost become prevalent, integrating this application with it would be beneficial in alerting the driver about the conditions of road surfaces in their respective routes of travel. This system is superficial in terms of portability as the accelerometers don't have to be re-oriented, once installed. The algorithm being implemented has no compromises whatsoever for every aspect of detection of aberrations. The future work would include installing the system on different types of vehicles, and determine the best position on the vehicle for the sensors, and envisage even simpler media of communication.

REFERENCES

- [1].Bhoraskar,R.,Vankadhara,N.,Raman,B., Kulkarni, P. 'Wolverine: Traffic and road condition estimation using smartphone sensors. In Communication Systems and Networks (COMSNETS),' 2012 Fourth International Conference on (jan. 2012), pp. 1-6.
- [2] Mednis, A., Strazdins, G., Zviedris, R., Kanonirs, G., and Selavo, L. 'Real time pothole detection using android smartphones with accelerometers' Distributed Computing in Sensor Systems and Workshops, International Conference on 0 (2011), 1-6.
- [3] Eriksson, J., Girod, L., Hull, B., Newton, R., Madden, S., and Balakrishnan, H. 'The Pothole Patrol: Using a Mobile Sensor Network for Road Surface Monitoring'. In The Sixth Annual International conference on Mobile Systems, Applications and Services (MobiSys 2008) (Breckenridge, U.S.A., June 2008)
- [4] P. Mohan, V. N. Padmanabhan, and R. Ramjee. 'Nericell: Rich monitoring of road and traffic conditions using mobile smartphones.' In Proceedings of the 6th ACM conference on Embedded network sensor systems, SenSys '08, pages 323-336, New York, NY, USA, 2008. ACM.
- [5] S. Gaonkar, J. Li, R. R. Choudhury, L. Cox, and A. Schmidt. Micro-Blog: Sharing and Querying Content through Mobile Phones and Social Participation. In MobiSys, 2008.
- [6] B. Hull, V. Bychkovsky, K. Chen, M. Goraczko, A. Miu, E. Shih, Y. Zhang, H. Balakrishnan, and S. Madden. The CarTel Mobile Sensor Computing System. In SenSys, 2006



- [7] R. Chandra, J. Padhye, A. Wolman, and B. Zill. 'A Location-based Management System for Enterprise Wireless LANs' NSDI, 2007.
- [8] R. Chang, T. Gandhi, and M. M. Trivedi. 'Vision Modules for a Multi-Sensory Bridge Monitoring Approach.' In IEEE Intelligent Transportation Systems Conference, 2004



**NTSET
2018**

1ST NATIONAL CONFERENCE ON TRENDS IN SCIENCE, ENGINEERING AND TECHNOLOGY

(NTSET - 2018)

February 2nd & 3rd - 2018

TECHNICAL PAPER ABSTRACTS



ORGANIZED BY

MATRUSRI ENGINEERING COLLEGE

(Approved by AICTE, Affiliated to Osmania University)

#16-1-486, Saidabad, Hyderabad - 500059



Sponsored by

MATRUSRI EDUCATION SOCIETY

ISBN: 97881-936274-0-2





1st NATIONAL CONFERENCE
ON TRENDS IN SCIENCE, ENGINEERING AND TECHNOLOGY
(NTSET - 2018)



2nd & 3rd February, 2018

Patron

Dr. K. P. SRINIVAS RAO

Chairman, Matrusri Education Society

Chair Person

Dr. D. HANUMANTHA RAO

Principal, Matrusri Engineering College

Convener

Dr. P. HARA GOPAL MANI

Prof. of ECE, Matrusri Engineering College

Organized By



MATRUSRI ENGINEERING COLLEGE

(Approved by AICTE, Affiliated to Osmania University)

#16-1-486, Saidabad, Hyderabad, - 500059

Sponsored by



MATRUSRI EDUCATION SOCIETY
HYDERABAD



Synthesis and Antimicrobial Activity of Substituted 4-Arylidene 2 -(Hydroxy Phenyl) Oxazol-5(4h)-Ones

Y.Aparna¹, Prof L.N.Sharada²

¹Matrusri Engineering College, Saidabad, aparnayeddala@gmail.com

²University college of Science, Osmania University

A series of (4Z)-4-(Arylidene)-2-(2-Hydroxyphenyl)oxazol-5(4H)-ones were synthesized by condensation of substituted hippuric acid with different aromatic aldehydes in the presence of fused sodium acetate, acetic anhydride in catalytic amount, ethanol as solvent under reflux conditions. All the synthesized compounds were confirmed and characterized by using various spectral techniques like IR, ¹H NMR, ¹³C NMR, and mass spectral studies. All the synthesized oxazolone derivatives displayed moderate to potent activity.

Keywords: Oxazolones, Azlactones, Antibacterial Activity, Antifungal activity Studies.

Study of Low Temperature DC Conductivity on Co_xZn_{1-x}S Mixed Semiconductor Compounds

V. Laxminarasimha Rao¹, T. Shekharam², Y. Vasudevareddy³, M. Nagabhushanam⁴

^{1,2,3,4}Department of Physics,
University College of Science,
Osmania University, Hyderabad-500007,
Telangana, India.

Polycrystalline semiconductor compounds of Co_xZn_{1-x}S (0 ≤ x ≤ 0.1) samples have been synthesized by a controlled co-precipitation technique. The samples are characterized by X-ray diffraction (XRD). DC conductivity studies were performed in the temperature region 77–300K by using a two probe method. The dc conductivity plots show the Arrhenius behavior with three different activation energies (E_a) in three different temperature regions I (300–165K), II (165–100K), III (100–77K), and they exhibited the variable range hopping conduction (VRH) mechanism at low temperature region (100–77K).

Keywords: Co-precipitation technique, DC conductivity, Variable range hopping (VRH).



MATRUSRI ENGINEERING COLLEGE

(Approved by AICTE, Affiliated to Osmania University)

#16-1-486, Saidabad, Hyderabad - 500059



Sponsored by

MATRUSRI EDUCATION SOCIETY



ISBN: 97881-936274-0-2



SYNTHESIS AND ANTIMICROBIAL ACTIVITY OF SUBSTITUTED 4-ARYLIDENE 2-(HYDROXY PHENYL) OXAZOL-5(4H)-ONES

¹Y. Aparna, ²L. N. Sharada

¹Assistant Professor, ²Retd. Professor

¹Department of Sciences and Humanities, ²Department of Chemistry

¹Matrusri Engineering College, Hyderabad, Telangana, India. ²University College of Science, Osmania University, Hyderabad, Telangana, India

Abstract: A series of (4Z)-4-(Arylidene)-2-(2-Hydroxyphenyl)oxazol-5(4H)-ones were synthesized by condensation of substituted hippuric acid with different aromatic aldehydes in the presence of fused sodium acetate, acetic anhydride in catalytic amount, ethanol as solvent under reflux conditions. All the synthesized compounds were confirmed and characterized by using various spectral techniques like IR, ¹H NMR, ¹³C NMR, and mass spectral studies. All the synthesized oxazolone derivatives displayed moderate to potent antibacterial activity.

Keywords: Oxazolones, Azlactones, Antibacterial Activity, Antifungal Activity Studies.

I. INTRODUCTION

Oxazolones are heterocyclic compounds which are known to be multifunctional as they showed prolific development in synthetic chemistry through C=C, C=N, C=O bonds.

Oxazolone were first reported by Ploch¹ and named it as 'azlactone'. These compounds exhibit important biological activities such as antimicrobial², antibacterial³, analgesic⁴, antifungal⁵, anticancer^{6,7}, anti-inflammatory⁸, neuroleptic⁹, sedative¹⁰, antidiabetic¹¹ and antiobesity¹². Azlactones are important intermediates in the preparation of several chemicals including amino acids¹³, peptides¹⁴, some heterocyclic precursors¹⁵ as well as coupling and photosensitive devices for proteins¹⁶. They exhibit promising photophysical and photochemical activities^{17,18,19} and as pH sensors²⁰. Few benzimidazole derivatives were synthesized which showed good antimicrobial activity²¹.

Over past few years there is an increase in public concern on environmental pollution and there is a need for new antibiotics either plant based or synthetic or both products. The development of new antibiotics is prime concern which paved way to further develop bacterial resistant drugs.

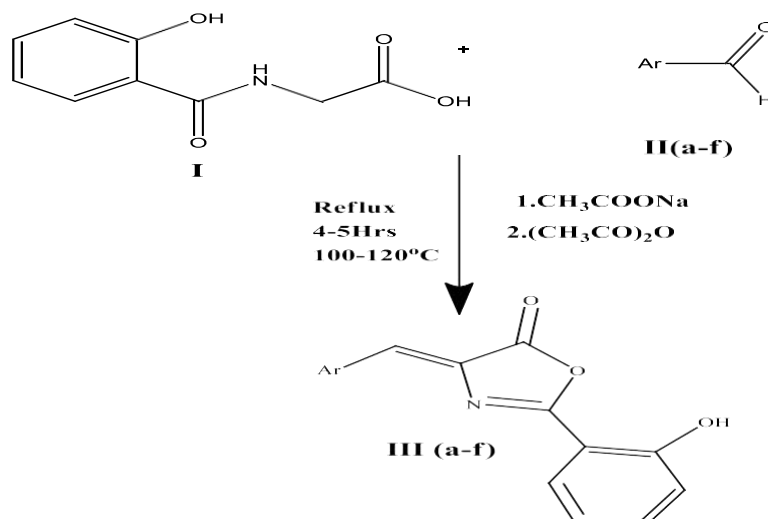
Azlactones possess imidazole nucleus and known to exhibit antifungal, antibacterial and anti-inflammatory activities. In this line we synthesized new derivatives of oxazolones²² and were screened for their anti-bacterial and antifungal activity. These compounds showed moderate to potent activity.

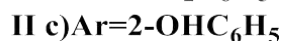
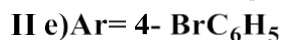
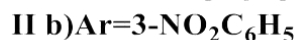
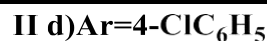
The scheme of synthesis for some compounds in this paper along with their antimicrobial and antifungal activity has been discussed.

II. EXPERIMENTAL

General method for the preparation of (4Z)-4-(arylidene)-2-(2-hydroxyphenyl)oxazol-5(4H)-ones

A mixture of 1mmol (0.195 gms) of 2-hydroxy hippuric acid, 1mmol (0.185 gms) of suitable aldehyde, 3mmol of acetic anhydride and 1 mmol (0.082 gms) of fused anhydrous sodium acetate was heated on an oil bath at 140-150°C for 3-4 Hrs and then cooled. Then 5ml of ethanol is added slowly to the contents of the flask and the mixture is allowed to stand overnight. The compound is filtered under suction, washed with 10ml of ice cold ethanol and then with 10ml of boiling water and air dried and recrystallised from Hexane.





,

,

Antimicrobial testing

The compounds synthesized were screened for their antimicrobial activity by Disc Diffusion Method²³. In this method the sensitivity of the compounds is measured by determining the zone of inhibition after placing the paper disc dipped in solution of compounds, on LBS agar medium, which was previously inoculated with test organism. These results were compared with the zone of inhibition produced after placing disc dipped in the solution of standard antibiotic. The diameter of zone of inhibition is directly proportional to antimicrobial activity of the compound. The size of zone of inhibition depends on rate of antibiotic diffusion, rate of bacterial growth and incubation condition, concentration of organism.

Materials used 1. Sterilized Petri dishes, 2. Sterilized test tubes and watch glasses, 3. Micropipette and micro-tips, 4. Cotton swabs

Test organism used in the study**Bacterial cultures used:**

1. Pseudomonas aeruginosa – Gram positive bacteria
2. Bacillus subtilis – Gram positive bacteria.
3. Staphylococcus aureus – Gram positive
4. Escherichia Coli – Gram negative

Subculture: One day prior to the testing, the organisms obtained from the laboratory stock were subculture into sterile nutrient broth and incubated at 37 ° C for 18-24hrs. The culture growth thus obtained was used as inoculums for the antibacterial testing.

Fungal Cultures used:

1. Candida albicans ,
2. Rizopusmicrosporus var. oligosporus

Subculture: Two days before the testing the culture is prepared by inoculating the fungus from master culture into potato dextrose medium and incubated for 48 hrs at room temperature.

Drugs Control: 1. Penicillin (antibacterial), 2. Griseofulvin (antifungal)

Concentration: all the test compounds were tested at 25 to 100 µg/ml concentrations.

Solvent: Methanol.

Preparation of paper discs

Paper disc of 6mm diameter and 2mm thickness was used for the test. These disks were sterilized by autoclaving at 121° C (15 lbs psi) for 15 minutes.

Preparation of culture medium

Culture media provides all essential nutrients for the growth of microorganism. Luria Broth (LB) Agar was used to inoculate bacterial strains and PDA (Potassium-dextrose agar) medium for fungal strains.

Nutrient media thus prepared was sterilized by autoclave at 121° C for 20 mins at 15 lbs pressure.

Procedure

Petri dishes were filled to depth of 3-4mm with a nutrient agar medium. This poured medium was allowed to set and then inoculated with susceptible test organism culture using cotton swab under aseptic conditions under laminar air flow unit. Each plate was divided into six equal positions along the diameter. Each portion was used to place one disc. Five discs of each sample was placed on five portions using sterilized forceps. Two discs were placed one each with ciprofloxacin disc and a disc impregnated with the solvent. The petri dishes were incubated at 37°C for 24 h for bacterial culture and incubated for 28 °C for 4 days for fungal culture. Diameter of the zone of inhibition was measured and the results are shown in Table. The diameter obtained for the test samples were compared with that produced by standards. Diameter of the zone of inhibition was measured in mm.

Table-1: Activity against Bacillus subtilis

Compd No	Code	Activity against Bacillus subtilis (MTCC No.6544)		
		25µg/ml	50µg/ml	100µg/ml
1	IIa	8	14	18
2	IIb	9	13	19
3	IIc	8	10	19
4	IId	10	15	19
5	IIe	12	16	20
6	IIf	8	14	18
Pencillin	Standard	17	39	48

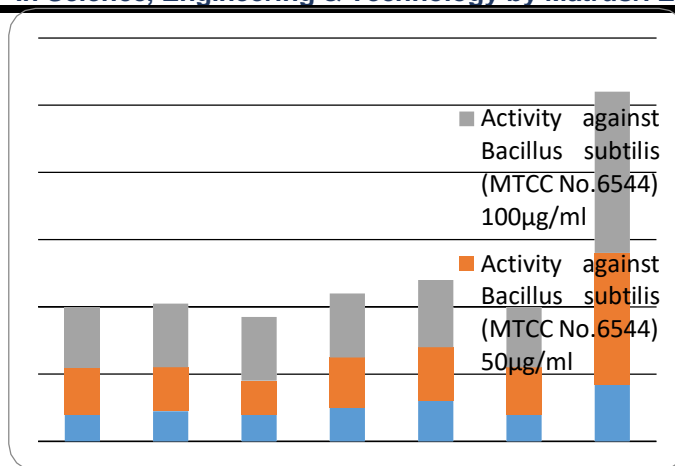


Fig-1: pictorial representation

Table-2: Activity against Staphylococcus aureus

Compd No	Code	Activity against Staphylococcus aureus (MTCC No.3160)		
		25µg/ml	50µg/ml	100µg/ml
1	Ia	5	8	10
2	Ib	6	8	10
3	Ic	2	8	11
4	Id	7	10	13
5	Ie	5	5	7
6	If	6	9	12
	Pencillin	14	36	40

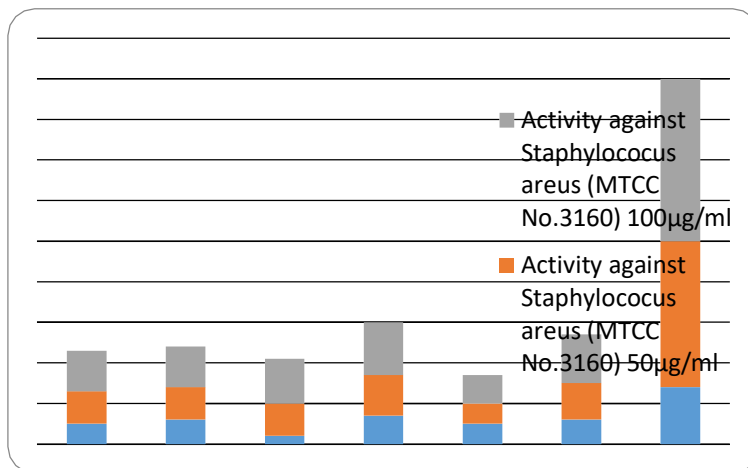


Fig-2: pictorial representation

Table-3: Activity against Pseudomonas aeruginosa

Compd No	Code	Activity against Pseudomonas Aeruginosa (MTCC No.1034)		
		25µg/ml	50µg/ml	100µg/ml
1	Ia	4	9	13
2	Ib	5	12	15
3	Ic	4	12	15
4	Id	6	11	13
5	Ie	5	8	12
6	If	6	10	15
	Pencillin	14	36	40

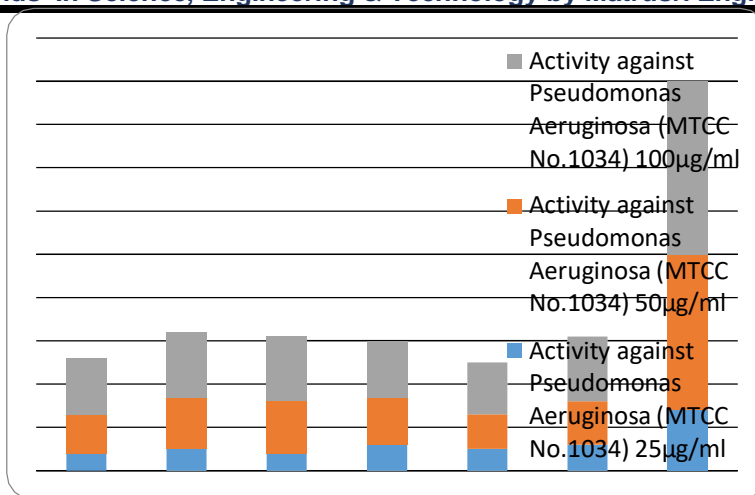


Fig-3: pictorial representation

Table-4: Activity against Escherichia Coli

Compd No	Code	Activity against E.Coli (MTCC No.42)		
		25µg/ml	50µg/ml	100µg/ml
1	IIa	5	7	7
2	IIb	2	5	9
3	IIc	9	11	17
4	IId	9	12	17
5	IIe	4	10	12
6	IIf	8	12	20
Pencillin	Standard	17	39	48

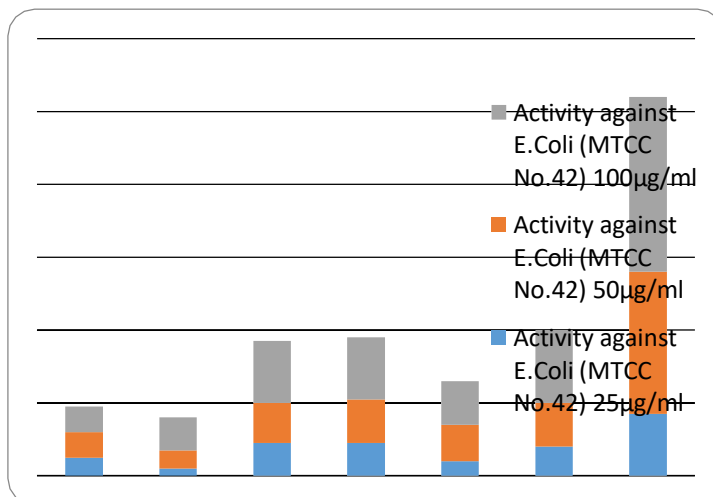


Fig-4: pictorial representation

Table-5: Activity against Candida Parapsolosis

Compd No	Code	Activity against Candida Parapsolosis (MTCC No..3017)		
		25µg/ml	50µg/ml	100µg/ml
1	IIa	9	10	12
2	IIb	7	8	10
3	IIc	-	-	11
4	IId	-	-	-
5	IIe	-	-	-
6	IIf	-	10	12
Griseofulvin	Standard	14	18	23

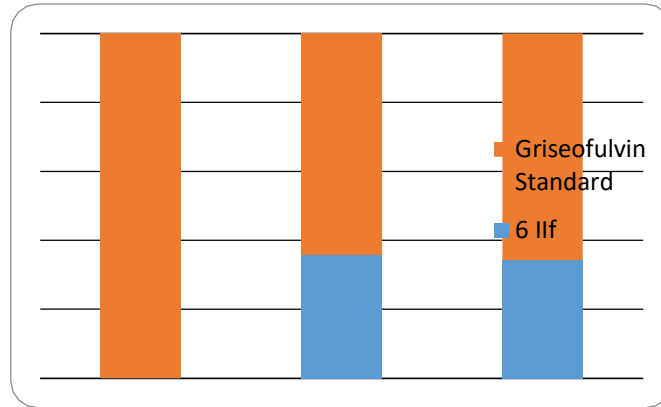


Fig-5: pictorial representation

Table-6: Activity against Rizopus microsporus var. oligosporus

Compd No	Code	Activity against Rizopus microsporus var. oligosporus (MTCC No.2785)		
		25µg/ml	50µg/ml	100µg/ml
1	IIa	-	10	14
2	IIb	5	10	12
3	IIc	2	8	12
4	IId	-	4	6
5	IIe	4	12	15
6	IIf	3	9	12
Griseofulvin	Standard	19	22	33

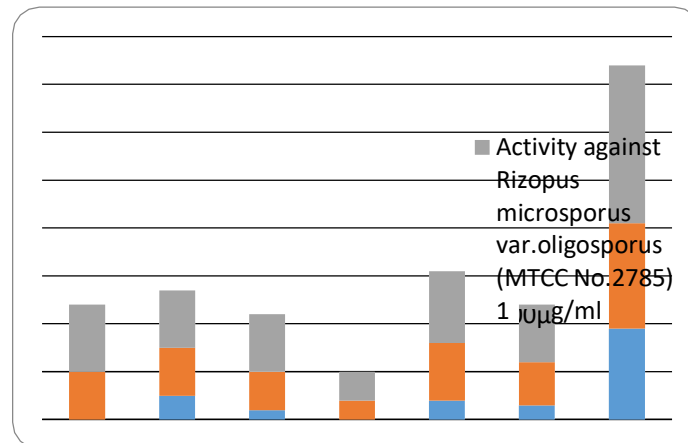
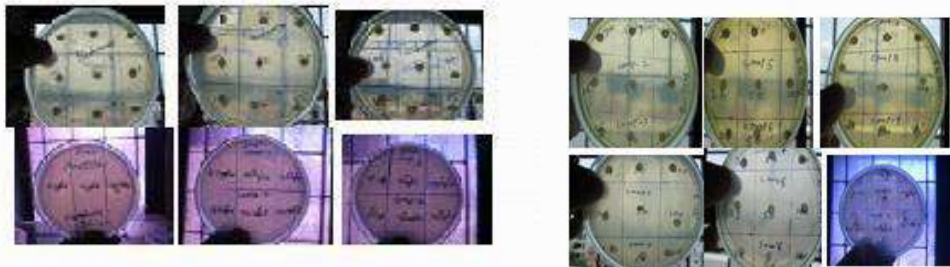


Fig-6: pictorial representation



Images of activity against Bacterial Strains



Images of activity against Fungal Strains

III. CONCLUSION

The activity studies of all the synthesized compounds against gram positive and gram negative bacterial strains revealed that the compounds 1,2,3,4,5 and 6 showed moderate to good activity against bacterial strains compared with standard penicillin. Activity against Fungi *Rizopus oligosporus* revealed that the compounds 1 and 4 showed activity only above 50 μ g/ml concentrations and compounds 2,3,5 and 6 showed good to moderate activity compared with standard Griseofulvin. Activity against *Candida Parapsolosis* revealed that compound 3 showed activity at 100 μ g/ml only while 4 and 5 showed no activity but 6 showed good activity. Hence these substituted oxazolones displayed moderate to potent activity against microbial and fungal strains.

The antimicrobial screening was carried by disc fusion method. The most eye catching features of these compounds are their utility in pharmaceutical industry²⁴ and there is further scope for their exploration. The present focus is on DNA binding studies of these synthesized compounds.

IV. ACKNOWLEDGEMENT

I thank our Research Supervisor Prof L. N. Sharada for her able guidance. I am grateful to the Head, Department of Chemistry, Osmania University. I also thank the Management, Principal, Head Department of S&H and Chemistry Staff for encouraging me to carry research work at Matrusri Engineering College.

REFERENCES

- [1] Ploch I, Ber., 16, 2815 (1883).
- [2] Desai N.C., Bhavasar A.M., and Baldaniya B.B., Synthesis and antimicrobial activity of 6-imidazolone derivatives, *Indian Journal of Pharmaceutical Sciences*, 2009, 71, 90-94.
- [3] Shinde DB, Aaglawe MJ, Dhole SS, Bahekar SS, Wakte PS, Synthesis and antimicrobial activity of some Oxazolone derivatives. *J Korean Chem Soc* 2003; Vol. 47, No. 2, 133-136.
- [4] Jakeman DL, Farrell S, Yong N, Doucet RJ, Timmons SC, Revel jadomycins incorporation of non-natural and natural amino acids, *Bioorg Med Chem Lett* 2005; vol. 15, No 5, PP1447-1449.
- [5] Sah P, Nair S, Garg SP, Synthesis and antimicrobial activity of some new oxazolone derivatives of 4,5-disubstituted-2-aminothiazole. *J Indian Chem Soc* 2006; vol. 83, No. 2, 205-207.
- [6] Benedl, D.; Daniel, V. *J. Med. Chem.* 1994, 37, 710.
- [7] L.R. Jat, R. Mishra and D. Pathak, Synthesis and anticancer activity of 4-Benzylidene-2-phenyloxazol-5(4H)-one derivatives. *International Journal of Pharmacy and Pharmaceutical sciences* vol 4, Issue 1, 2012.
- [8] Crespo MI, et al, Synthesis and biological evaluation of 3,4-diaryloxazolones. A new class of orally active cyclooxygenase-2 inhibitors. *J Med Chem* 2000; vol 43, No. 2, 214-223.
- [9] Cascio G, Manghisi E., Fregnan G, 5-piperazinylalkyl-2-3(H)-oxazolones with neuroleptic activity. *J Med Chem* 1989; Vol 32, No. 10, 2241-2247.
- [10] Mesaik .A., Rahat S., Khan .M., Ullah Z., Choudary, M.I., Murad S., Ismail, Z., Rahman A., and Ahmad A., Synthesis and immunodilatory properties of selected oxazolone derivatives, *Bioorganic and Medicinal Chemistry*, 2004, 12, 2049-2057.
- [11] Pereira, E.R.; Sancelme, M.; Voltaire, A.; Prudhomme, M. *Bio-org, Med-Chem. Lit.* 1997, 7(190), 2503.
- [12] Viti, G.; Namicine, R.; Ricci, R.; Pestelline, V.; Abeli, L.; Funo, M. *Euro. J. Med. Chem.* 1994, 29, 401.
- [13] a) F.M. Bautista, J.M. Campelo, A. Garcia, D. Lona, J.M. Marinas, *Amino acids* 2(1992)87-95;
b) K. Gottwald, D. Seebach, *Tetrahedron* 55(1999)723-738;
c) E. Bunuel, C. Cativela, M.D. D Villegas, *Tetrahedron* 51(1995)8923-8934.
- [14] F. Cavalier, J. Verducci, *Tetrahedron Lett.* 36(1995)4425-4428.
- [15] a) P.D. Croce, R. Ferraccioli, C. La-Rosa, *J. Chem. Soc. Perkin Trans. 1* (1994) 2499-2502;
b) R. Cannella, F. Clerici, M.L. Gelmi, M. Penso, D. Pocar, *J. Org. Chem.* 61(1996)1854-1856;
c) R. Bossio, S. Marcaccini, R. Pepino P. Paoli, *J. Heterocycl. Chem.* 31(1994)729-732.

- [16] a) M.A. Gonzalez-Martinez, R. Puchades, A. Maquieira, I. Ferrer, M.P. Marco, D. Barcelo, *Anal. Chim. Acta* 386 (1999) 201-210;
b) G.T. Hermanson, G.R. Mattson, R.I. Krohn, *J. Chromatogr. A* 691 (1995) 113-122.
- [17] Palcut M., Spectral properties of novel 1,3-oxazol-5[4H]ones with substituted benzylidene and phenyl rings., *Acta chimica slovenica*, 2009, 56, 362-368
- [18] Barotte M., Schmitt M., Wend A., F. Pigaut C., Haiech I., and Bourguignon J.J., Fluorophores related to the green protein, *Tetrahedron Letters*, 2004, 45, 6343-6348.
- [19] Jung B., Kim H., and Park B.S., Photo decarbonylation of 2-phenyl-4-alkylidene-5(4H)-Oxazolones, *Tetrahedron Letters*, 1996, 37, 4019-4022.
- [20] Canan Karapire, Siddik cli, Serap Alp, Kadriye Ertokin, Errin Yenigul and Emur Henden, Fluorescence emission studies of an azlactone derivative in polymer films; An optical sensor in pH Measurements.
- [21] Y. Aparna, N. J. Prameela Subhashini, Azlactones in heterocyclic synthesis: Part-V- Condensation of Azlactones with 4-nitrobenzene-1,2-diamine; *J. Chem. Pharm. Res.*, 2010, 2(3):473-477.
- [22] Prof L. N. Sharada, Y. Aparna, Saba, Sunita, Lakshmi Viveka, Synthesis, Characterization and Molecular Docking Studies Of New Erlenmeyer Azlactones, *IOSR Journal of Applied Chemistry (IOSR-JAC)* e-ISSN: 2278-5736. Volume 8, Issue 8 Ver. II (Aug. 2015), PP 30-36.
- [23] A. Espinel-Ingroff, "Standardized Disk Diffusion Method for Yeasts," *Clinical Microbiology Newsletter*, Vol. 29, No. 13, 2007, pp. 97-100. doi:10.1016/j.clinmicnews.2007.06.001.
- [24] Tella. Lakshmi Viveka, Mariyam Saba, S.N.T. Sunitha, Y. Aparna, L. Nalanda Sharada, Synthesis and anti-microbial agents of novel (E)-N'-4,4'-difluoro-cyclohexanecarboxylic acid (substituted-benzylidene)-hydrazide derivatives, *World Journal of Pharmacy and Pharmaceutical Sciences*, Volume-4, Issue-5, 1087-1105.

INDIAN COUNCIL OF CHEMISTS



www.chemicc.com

XXXVII ANNUAL CONFERENCE 2018

ABSTRACTS BOOK



National Institute of
Technology Karnataka (NITK), Surathkal
Mangalore - 575025 (Karnataka)

12th - 14th DECEMBER, 2018

Editor : Prof. R.K.S. Dhakarey

Welcome

Dear Fellow Researchers & Scientists

On behalf of the Indian Council of Chemists, it is my pleasure and honour to welcome you all to the XXXVII Annual Conference of ICC from 12th - 14th December, 2018 at National Institute of Technology Karnataka (NITK) Surathkal, Mangalore - 575025 (Karnataka).

The leading researchers and key opinion leaders in Chemistry have been invited to facilitate sessions and deliver lectures at XXXVII National Conference of ICC.

A series of scientific and educational activities have also been planned for delegates participating during the conference. There will be vast range of learning opportunities at invited talks, oral, poster presentations and symposium session. Participants can also look forward to expanding their network at various networking events such as conference lunch, dinner and cultural programme. Apart from the scientific programme, there are many tourist attractions in and around Mangalore. You can enjoy there too.

Again Welcome you for your participation.

Prof. R.K.S. Dhakarey
Secretary, ICC

Elemental analysis for their characterization Antimicrobial activity of these compounds has been evaluated by standard methods and attempts have been made to correlate structural characteristics with antimicrobial properties of these complexes.

OO-18 : Synthesis of Novel Imidazolones, their Antimicrobial Studies and Molecular Docking Studies

L. N. Sharada^{1*}, Y. Aparna² and N. J. P. Subhashini¹

¹*Department of Chemistry, Osmania University, Hyderabad, Telangana*

²*Matrusri Engineering College, Saidabad.*

A three step procedure was performed for the synthesis of eleven 2-(2-hydroxyphenyl)-4-(arylidene)-1-phenyl-1H-imidazol-5(4H)-ones by cyclodehydration and condensation of oxazol derivatives with substituted aromatic amines with the aid of vilsmeier Haack reagent. These imidazolone derivatives have been synthesised by condensation of 2-hydroxy hippuric acid with aromatic amines, fused sodium acetate and acetic anhydride in catalytic amounts in presence of Vilsmeier Haack reagent. The structures of the compounds were evaluated based on ¹H-NMR, ¹³C-NMR, EI-MS and FT-IR spectroscopy and elemental analysis. All the compounds were screened for their antibacterial, antifungal activity and molecular docking studies were performed. The antibacterial activity was tested against two gram positive and two gram negative species *Bacillus subtilis*, *Staphylococcus aureus*, *Escherichia Coli*, *Klebsiella Pneumonia* and antifungal activity was carried on *Phytophthora nicotiana*, *Fusarium ricini*. All the compounds showed moderate to good antibacterial and antifungal activity. Molecular docking was performed on these imidazolones and they showed better docking score. Docking studies were performed on Linux operating system using Schrodinger suite 2009. The focus on docking is to study the relative orientation and nature of bonding between imidazolones and bacterial protein.

OP-CYSA-01 : Synthesis, Characterization of a New Class of Symmetrically Substituted Thiophene-1,3,4-Oxadiazole Derivatives and their Optoelectronic Properties

Manjunatha Garbhagudi and Imtiyaz Ahmed M. Khazi*

Department of Chemistry, Karnatak University, Pavate Nagar, Dharwad, Karnataka 580003

^{*}*E-mail : drimkorgchem@gmail.com*

A series of a new class of symmetrically substituted thiophene-

Synthesis of novel Imidazolones, their antimicrobial studies and Molecular docking studies

Y.Aparna,^a L.N.Sharada^{b*}

^aMatrusri Engineering College,Saidabad500059,Hydererabad,India

^aDepartment of ChemistryDepartment of Chemistry,Hyderabad500007,India.

Abstract

Imidazolones were prepared by condensation of 4-benzylidene-2-phenyloxazol-5(4H)-ones with aromatic amines in presence of glacial acetic acid and sodium acetate. They were also prepared by condensation of 2-(4-(arylidene)-5-oxo-4, 5-dihydrooxazol-2-yl) phenyl acetate with aromatic amines in presence of Vilsmeier haack reagent. Synthesis of 2-(4-(arylidene)-5-oxo-4, 5-dihydrooxazol-2-yl)phenyl acetate derivatives were carried by condensation of 2-hydroxy Benzoyl Glycine with different aromatic aldehydes. The constitution of all the compounds has been established by their physical properties, elemental analysis and spectral analysis (¹H NMR, ¹³C NMR, IR and Mass).All the compounds were screened for their antibacterial activity

Keywords: imidazolones,antibacterial study,docking study

1.Introduction

These compounds exhibit important biological activities such as antimicrobial, antibacterial, analgesic, antifungal,anticancer, anti-inflammatory,neuroleptic, sedative, antidiabetic and antiobesity.Imidazolones are carbonyl dihydro-imidazoles, also known as oxoimidazolines.They are five-membered heterocyclic ring systems with three carbon atoms and two nitrogen atoms at positions 1 and 3. In general, imidazolones are of many types, e.g. 2-, 4-, or 5-imidazolones. The number indicates the position of the carbonyl group. Literature assessment reveals that a variety of imidazolone-5-ones hold an extensive band of pharmacological and biological actions which are exhibited by their use as CNS depressant,antifungal, antihelmentic and anticancer, anticonvulsant, anti-Parkinsonian and monoamineoxidase inhibitory agents. Few new disubstituted imidazolones were proved as anticonvulsant and succinate dehydrogenase suppressive agents.Thus, the quest to explore many more modifications on imidazole moiety needs to be sustained. Based on the position of carbonyl group,Imidazolines are classified as 2-oxo-imidazoline,4-oxoimidazoline and 5-oxo-imidazoline. Imidazolines are structurally related to guanidines and amidines. Besides the vast distribution of heterocycles in natural products, they are also the major components of biological molecules such as DNA and RNA.

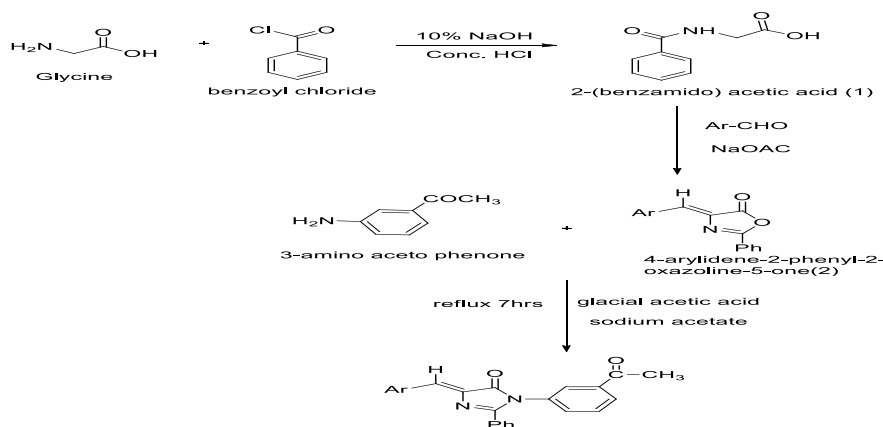
2. Materials and methods

Materials All chemicals and reagents were of analytical grade and purchased from Merck and SD Fine-Chem limited .

3.Preparation of imidazolones

Benzoylchloride on reaction with glycine gives benzoyl glycine which on condensation with an assortment of aromatic aldehydes followed by condensation gave Substituted 4-arylidene-2-phenyloxazol-5(4H)-ones.These substituted oxazolones when refluxed with p-amino acetophenone in glacial acetic acid and sodium acetate,1-(3-acetylphenyl)-4-arylidene-2-phenyl-1H-imidazol-5(4H)-ones were obtained in good yield.A novel series of 10 substituted imidazolones were prepared by cyclocondensation of oxazolones with aromatic aldehydes.

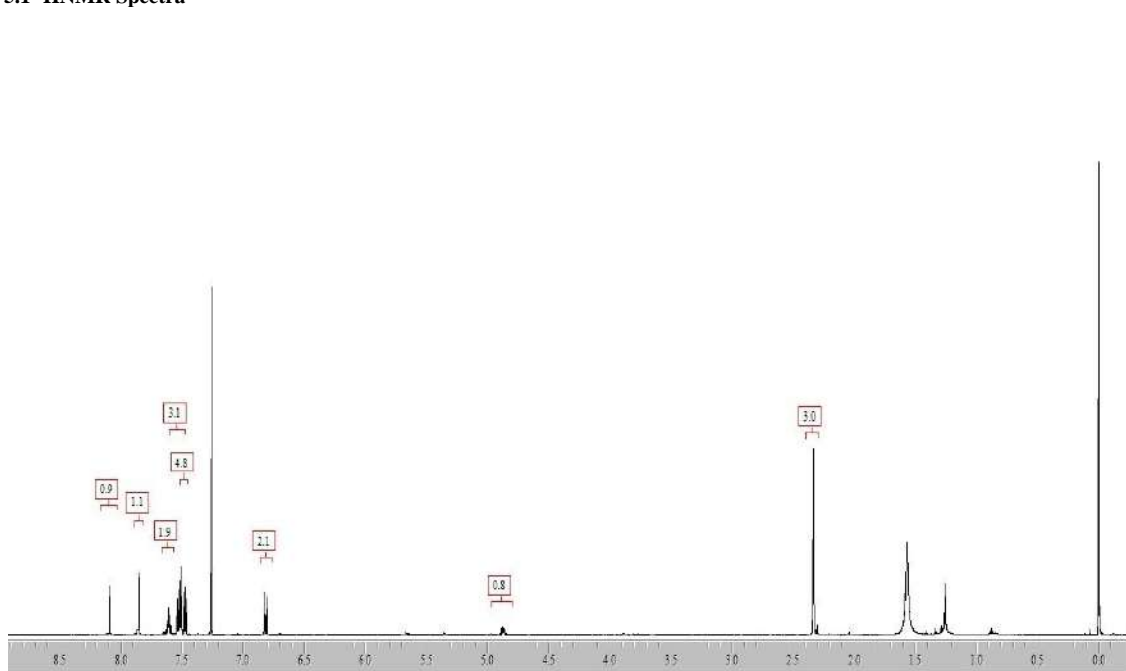
4.synthesis of imidazolones



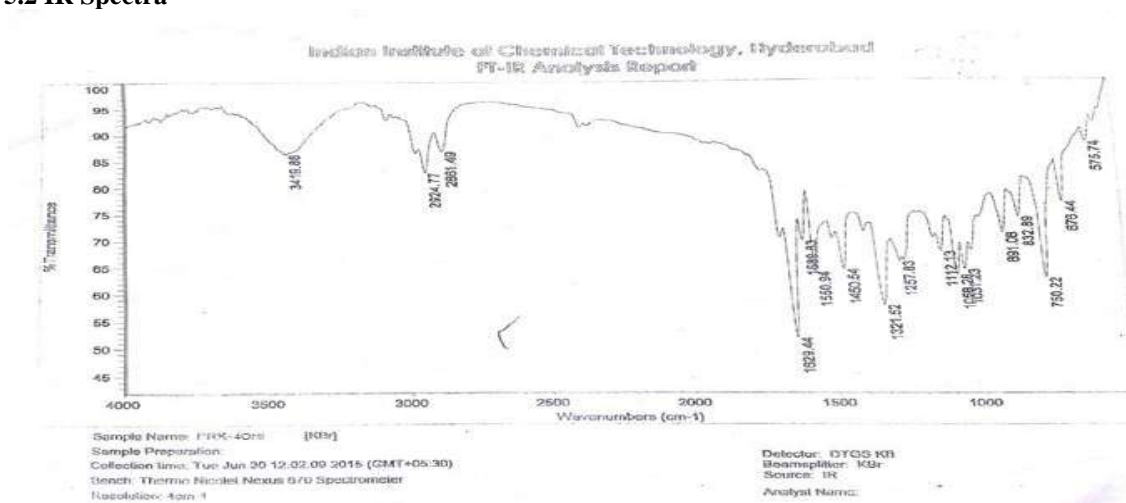
5. Results and discussion

The structures of imidazolones were confirmed based on ^1H NMR, ^{13}C NMR and Mass spectral data. As a representative case the spectral analysis of 1-(3-acetylphenyl)-4-(4-hydroxybenzylidene)-2-phenyl-1H-imidazol-5(4H)-one is discussed below. In the IR spectrum the stretching frequency at 3421cm^{-1} and 2922cm^{-1} indicates absorption due to aliphatic (C-H) group. The characteristic (C=N) absorption was observed at 1550cm^{-1} and (C-N) group absorption 1321cm^{-1} . The ^1H NMR spectrum (400 MHz, CDCl_3) of compound showed multiplet between δ 7.48-7.51 due to aromatic protons and δ 7.86 due to arylidene proton. ESI-MS mass spectrum of compound showed m/z 383 ($\text{M}+\text{H}$) $^+$ appeared as base peak.

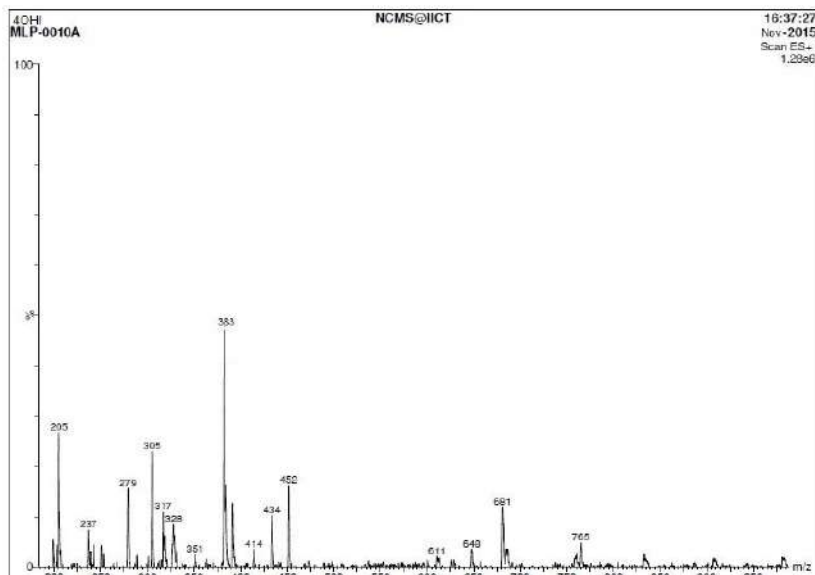
5.1 ^1H NMR Spectra



5.2 IR Spectra

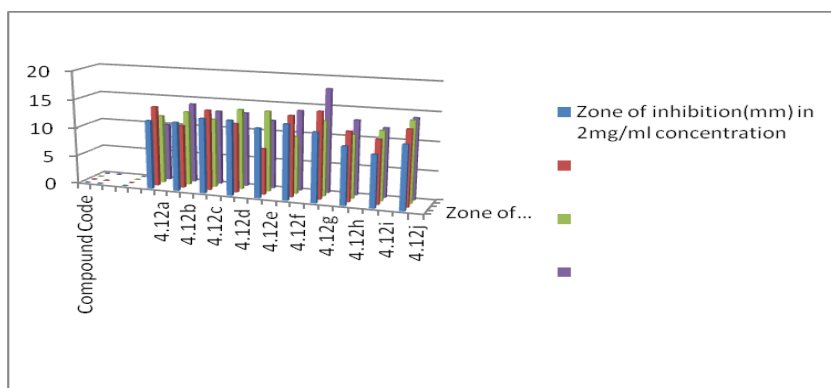


5.3 Mass Spectrum



6. Antibacterial studies

Petri plates containing 20ml Muller Hinton medium were seeded with 24hr culture of bacterial strains. Wells were cut and 10 μ l of the compounds were added. The plates were then incubated at 37°C for 24 hours. The antibacterial activity was assayed by measuring the diameter of the inhibition zone formed around the well. The solvent, methanol was used as a control. Different concentrations of drug were prepared. Stock solution of 5mg/ml was prepared at first. Different dilutions were made from that i.e. 2mg/ml, 1mg/ml, 0.5mg/ml, 0.2mg/ml and 0.1mg/ml. Wells were made in the agar plate using a borer. The sample solutions of different concentrations were pipetted into the wells. The plates were incubated for 24hrs. Then the zone of inhibition was measured and recorded.

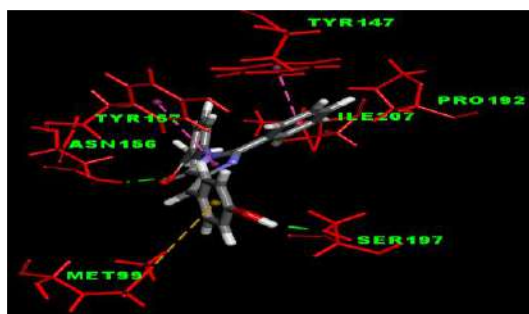
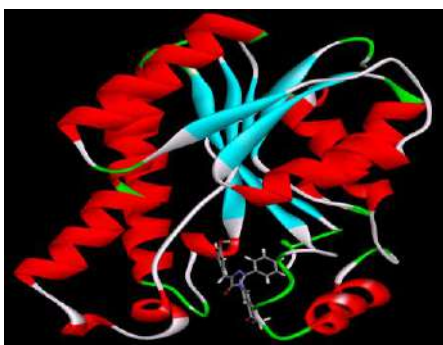


Compound Code	Zone of inhibition(mm) in 2mg/ml concentration			
	Gram -ve	Gram -ve	Gram +ve	Gram +ve
	E.coli	P. aeruginosa	B.subtilis	S. aureus
3a	12	14	12	10

3b	12	11	13	14
3c	13	14	12	13
3d	13	12	14	13
3e	12	8	14	12
3f	13	14	10	14
3g	12	15	13	18
3h	10	12	11	13
3i	9	11	12	12
3j	11	13	14	14

7.Molecular docking studies

Substituted imidazole and benimidazole molecules are reported as inhibitors of *Staphylococcus aureus* and *Escherichia coli* enoyl acyl carrier protein reductase (FabI). In order to elucidate the mode of interaction and binding of synthesized imidazole derivatives molecular docking studies were carried out on X-ray crystal structure of FabI of *Staphylococcus aureus* (pdb id: 4NZ9) obtained from protein data bank (www.rcsb.org).



Conclusion

Compounds 3a, 3c, 3d, 3g and 3i shows maximum potent activity against all the micro organisms. Of these five compounds which are further diluted with concentration 2g/ml, 1g/ml, 0.5g/ml, 0.2g/ml, 0.1g/ml. In these dilutions 3a & 3g compounds showed maximum activity for *Bacillus subtilis*, 3c, 3d & 3i compounds showed maximum activity for *Staphylococcus aureus*. Molecular docking studies with bacterial host DNA inferred conformational results for binding affinity of the compounds in accordance with experimental data. All the compounds showed moderate to good docking score indicating that they are inhibitors of enoyl acyl carrier protein reductase. Among all the entries 3g showed highest dock score of -10.318 kcal/mol.

References

- [1] Plochl, Ber., 16, 2815 (1883).
- [2] Desai N.C., Bhavasar A.M., and Baldaniya B.B., Synthesis and antimicrobial activity of 6-imidazolone derivatives, Indian Journal of Pharmaceutical Sciences, 2009, 71, 90-94.
- [3] Shinde DB, Aaglawe MJ, Dhole SS, Bahekar SS, Wakte PS, Synthesis and antimicrobial activity of some Oxazolone derivatives. J Korean Chem Soc 2003; Vol. 47, No. 2, 133-136.
- [4] Jakeman DL, Farrell S, Yong N, Doucet RJ, Timmons SC, Revel jadomycins incorporation of non-natural and natural amino acids, BioorgMed Chem Lett 2005; vol. 15, No. 5, PP1447-1449.
- [5] Sah P, Nair S, Garg SP, Synthesis and antimicrobial activity of some new oxazolone derivatives of 4,5-disubstituted-2-aminothiazole. J Indian Chem Soc 2006; vol. 83, No. 2, 205-207.
- [6] Benedl, D; Daniel, V. J. Med. Chem. 1994, 37, 710.
- [7] L.R. Jat, R. Mishra and D. Pathak, Synthesis and anticancer activity of 4-Benzylidene-2-phenyloxazol-5(4H)-one derivatives. International Journal of Pharmacy and Pharmaceutical sciences vol 4, Issue 1, 2012.
- [8] Crespo MI, et al, Synthesis and biological evaluation of 3,4-diaryloxazolones. A new class of orally active cyclooxygenase-2 inhibitors. J Med Chem 2000; vol 43, No. 2, 214-223.
- Cascio G, Manghisi E., Fregnan G, 5-piperazinylalkyl-2-3(H)-oxazolones with neuroleptic activity. J Med Chem 1989; Vol 32, No. 10, 2241-2247.
- [10] Mesaik A., Rahat S., Khan M., Ullah Z., Choudary, M.I., Murad S., Ismail, Z., Rahman A., and Ahmad A., Synthesis and immunodilatory properties of selected oxazolone derivatives, Bioorganic and Medicinal Chemistry, 2004, 12, 2049-2057.

OPTIMIZATION OF WEB SERVICE QUALITY CONTROL THROUGH GOAL PROGRAMMING

Yuvaraju Macha

Asst.Professor of Mathematics

Department of Sciences and Humanities

Matrusri Engineering College, Hyderabad, Telangana, India.

Abstract: As business environment is changed and become complex, a more efficient and effective process management is needed. More and more enterprises and organizations are recently trying to build flexible and integrated information systems with web services in order to satisfy the changing needs of the customers. The web service can currently recognized as a new alternative for integrating the scattered information assets within an enterprise or an organization. Due to the increasing number of web service applications and the service suppliers, however customers were confronted with the problem of selecting the most suitable web service. In this chapter the new methodology for marshaling the composite web service satisfying web service Quality of service (QoS) goals are suggested. This provides theoretical basis from which a goal programming model is identified by which web service QoS can be quantified.

Keywords – Goal Programming Model, Web Quality of Service, Optimization techniques

I. INTRODUCTION

The experimental scenario is devised as shown in Figure 1. The purchasing process is executed Web Services, and each process has 1.1 tasks.

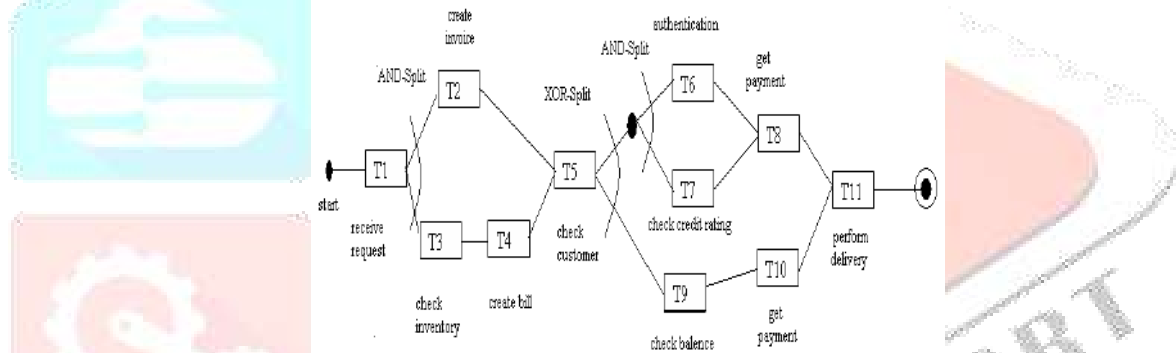


Fig 1 Purchasing Process for Simulated Scenario

After receiving the orders form customers (T1), invoice is issued (T2), inventory is checked and the bill is prepared(T3). After all previous tasks are confirmed (T5). If the payment is to be processed by credit card, the customer's identification is verified (T6), and credit status is checked (T7), then the payment is approved (T8). If the payment is to be processed by bank account , the balance is checked(T9) and the payment is approved (T10). If the product is delivered to customer after the payment is confirmed(T11). The customer, Who are involved in this purchasing process, is assumed make SLA (Service Level Agreement) Shown in Table 1 with the service supplier of purchasing process.

Table 1: SLA for QoS

	SLO (Service Level Objective)	Penalty
Execution Duration	60s	5/s
Execution Costs	800	Over costs
Reliability	95%	100
Availability	95%	50
Reputation	8	50

The goal of this experimentation is to evaluate the plausibility of Goal programming. If the service suppliers are chosen the execution cost will be exceeded by 0.6 and the reputation is lowered by 0.1after composition.

Table 2: QoS For Web Service Suppliers QoS

		Duration	Cost	Reliability	Availability	Reputation
Task 1	X ₀₁₀₁	6.3	91.5	0.993	0.9985	10
	X ₀₁₀₂	9	75.4	0.9942	0.9948	6.1
Task 2	X ₀₂₀₁	19.8	156	0.9945	0.9967	7.4
	X ₀₂₀₂	17.5	195.2	0.9909	0.9973	6.1
Task 3	X ₀₃₀₁	8.4	91.2	0.9973	0.9985	7.1
	X ₀₃₀₂	8	94.4	0.9969	0.9924	9.1
Task 4	X ₀₄₀₁	9	80.5	0.995	0.9948	7.9
	X ₀₄₀₂	10.3	89.5	0.992	0.9987	6.5
Task 5	X ₀₅₀₁	7.6	91.6	0.995	0.9928	8.2
	X ₀₅₀₂	8.2	74.5	0.9976	0.9974	8.2
Task 6	X ₀₆₀₁	8.7	82.5	0.9961	0.9939	9.7
	X ₀₆₀₂	7.5	91.4	0.9947	0.9923	7.3
Task 7	X ₀₇₀₁	7.4	83.4	0.9932	0.9919	8.8
	X ₀₇₀₂	9.4	73.4	0.9999	0.9929	8.6
Task 8	X ₀₈₀₁	7	81.2	0.9948	0.9917	8.9
	X ₀₈₀₂	6.5	70.4	0.9917	0.9918	7.3
Task 9	X ₀₉₀₁	14.7	149.1	0.9984	0.9984	7.1
	X ₀₉₀₂	10.2	133.8	0.9971	0.9915	9.6
Task 10	X ₀₁₀₀₁	12.8	121.5	0.9904	0.9985	9.5
	X ₀₁₀₀₂	12.8	104.4	0.9912	0.9909	7.2
Task 11	X ₀₁₁₀₁	6.8	93.5	0.9994	0.9994	6.8
	X ₀₁₁₀₂	9.3	90.4	0.9919	0.9927	6.7

II. QoS FOR WEB SERVICES

Process structure is said to be the ordered relation defined between the units task consisted of process. In this chapter, SWR (Stochastic work flow reduction) Algorithm, which is the approach to reduce the predefined process structure into single task to estimate the process quality, is opted. Workflow process structure is classified as serial and parallel block. Serial block has one path along which no branching and combining is not happened. Parallel block has multiple paths between the branching unit task (a_s) and combining unit tasks (a_m).

2.1 QoS Requirements for Web Services

The requirements of Web Service QoS proposed by IBM include the non-functional Attributes like the process time of Web Service, cost, reliability, etc. In this chapter, the criteria for selecting the Web Service partners is set based on the QoS of Services Requested by consumers, which can be evaluated quantitatively as follows.

Execution Duration – is the time elapsed from the customer request of service to the receipt of response from the Web Service supplier. Hence, it may be composed of the request time, service time and the needed for sending the results.

Execution Cost – is defined as the cost to be paid for the execution of Web service

Reliability – is the probability of the processing result within the expected duration Time set randomly, when the Web Service is requested. It may be considers the Measure to guarantee the message transmission between customer and service supplier.

Availability – is the criteria for evaluating the immediate availability of web service. It can be computed as the ratio of the service time to the total time of the observation.

Time of observation.

Availability = $\frac{\text{Total time} - (\text{Up time} + \text{Down time})}{\text{UP time}}$

Reputation – is the factor for evaluating the service reliability based on the Customer's experience. In this chapter, it is defined as the average of the final Customer's evaluation on the Web Services.

$$\text{Reputation} = \frac{1}{n} \sum_{i=1}^n \langle \text{userratings} \rangle . 2$$

2.2 Hypothesis

The plausible selection of Web Service suppliers is set up as the determining variable from this perspective, AND Structure and XOR structure are taken into consideration in the case of parallel structure of web service process. The evaluation criteria for QoS can be formulated according to the each process structure, then the results are combined. Each QoS criteria can be an objective function, so there come out multiple Objective functions, which the constraints of goal programming to minimize the deviation from the QoS demanded by customer. The formulation of criteria is done under the following assumptions .

Independency: all tasks resided in process are mutually independent.

Trustfulness: the quality level of services is reliable

Active Selection: Web Service customer can arbitrarily select a path among the

Paths characterized by XOR branching.

2.3 WS QoS MODELLING

2.3.1 Notation

The problem defined in this chapter is to find optimal Web Service supplies to perform the task in process, when composing the complex web services. Hence the determining variable can be characterized by plausibility of selection of particular web service suppliers.

X_{ij} : The selection value j^{th} supplier among i^{th} task (0: unselected,1: selected),

S_{ij} : The set of all service suppliers in i^{th} task

S^{XORn} : n^{th} XOR set

S^{XORn} : the set of all service suppliers in the i^{th} task within n^{th} XOR set

The qualities characterized by service suppliers performing particular task is represented as follows;

r_i : reliability of i^{th} task

c_{ij} : The cost of i^{th} task performed by j^{th} service supplier

t_{ij} : The execution duration of i^{th} task performed by j^{th} service supplier

r_{ij} : The reliability of j^{th} service supplier in i^{th} task

av_{ij} : the availability of j^{th} service supplier in i^{th} task

re_{ij} : the reputation of j^{th} service supplier in i^{th} task

Reliability, Availability and Reputation are nonlinearly expressed and formulated by regarding the quality of service suppliers to the quality of selected task. So the quality of the task is represented as follows:

r_i : the reliability of i^{th} task

av_i : the availability of i^{th} task

re_i : the reputation of i^{th} task

T_i : the execution duration process of i^{th} task

T_{start} : the initial time of process

T_{end} : the ending time of process

The level of QoS demanded by customer is represented as follows:

C: The execution cost of complex web service requested by customer

T: The execution time of complex web service requested by customer

R: The reliability of complex web service requested by customer

Av: The availability of complex web service requested by customer

Re : The reputation of complex web service requested by customer

Based on the structural information mentioned above, the web service is defined as below

Definition 1 All web services existent from the n^{th} XOR set S^{XORn} to k^{th} path is $\Phi^n(k)$

In case of XOR set S^{XORn} , there exists k paths. The possibility of selection of each path is defined as w_k^n . That is if w_k^n is set to 1, the k^{th} path in n^{th} XOR set is selected. Otherwise it is set to zero

(not selected).Based on the definitions above, the additional constraints within XOR structure are as follows:

$$\sum_{j \in S_i^{XORn}}^n x_{ij} = w_k, \text{ where for all } x_{ij} = 0 \text{ or } 1 \text{ and } x_{ij} \text{ belongs to } \Phi(k) \dots \dots \dots (9.3)$$

$$\sum_{i=1}^k w_i = 1, \text{ where for all } w_k = 0 \text{ or } 1 \dots \dots \dots (9.4)$$

2.3.2 Nested XOR Structure

In case of the nested AND structure or XOR structure, the nested structure is preferred depending on the resultant selection of the nested paths. This can be theorized as follows:

Theorem 1: If the and structures are nested within the k^{th} path $\Phi^n(k)$ of XOR structure, the execution of task in the AND structure is

performed depending on the resultant selection of nested paths ($\sum_{j \in S_{i_i}}^n x_{ij} = w_k^n$)

Theorem 2:The $n+1^{th}$ XOR structure is nested within the k^{th} path of n^{th} XOR structure is performed depending up on the resultant selection

of k^{th} path of n^{th} XOR structure ($\sum_{i_{ii}} w_i^{n+1} = w_k^n$)

If another XOR structure is nested within XOR structure, the execution of $n+1^{th}$ XOR structure is performed depending on the value $w^n(k)$ of by theorem 2.Hence the additional constraint imposed on the $n+1^{th}$ XOR structure is as follows:

$$\sum_i^3 w_i^{n+1} = w_k^n \dots \dots \dots (5)$$

2.3.3 Quality Driven Web Service Selection

As mentioned above, Goal Programming is used for minimizing the QoS deviation. The deviation variable and its penalty are described as follows:

S_i^+ : Amount by which we numerically exceed the i^{th} goal

S_i^- : Amount by which we numerically exceed the i^{th} goal

P_i = The penalty for un- fulfillment of i^{th} goal

Optimal web service suppliers which are process-independent are picked using the following equations under consideration of QoS.

Minimize $S_1^+ + P_2 S_2^+ + P_3 S_3^- + P_4 S_4^- + P_5 S_5^-$

Subject to : $\sum_i \sum_{j \in S_j} a_{ij} x_j + S_1^- - S_1^+ = C \dots \dots \dots (6)$

$T_{end} - T_{start} + S_2^- - S_2^+ = T \dots \dots \dots (7)$

$$\prod_i r_i + S_4^- - S_4^+ = R \dots\dots\dots (8)$$

$$\prod_i av_i + S_3^- - S_3^+ = R \dots\dots\dots (9)$$

$$1/n (\sum_i \sum_{j \in S_i} re_{ij} x_{ij}) + S_5^- - S_5^+ = R_e \dots\dots\dots (10)$$

$$\sum_{j \in S_i} x_{ij} = 1, \forall x_{ij} = 0 \text{ or } 1 \dots\dots\dots (11)$$

$$n = \sum_i \sum_{j_i} x_{ij} \dots\dots\dots // \dots\dots\dots (2)..$$

$$\sum_{j \in S_i} x_{ij} = 1 \dots\dots\dots w_k^{n-1}, \text{ where } x_{ij} \in \phi^{n-1}(k) \dots\dots\dots (13)$$

$$\sum_i w_i^n = 1 \dots\dots\dots w_i^{n-1}, \text{ where } S^{XOR^{n-1}} \in S^{XOR^{n-1}} \dots\dots\dots (14)$$

$$\forall x_{ij} \text{ and } w_i^n = 0 \text{ or } 1 \dots\dots\dots (15)$$

Equation (6) computes the execution cost by summing the total cost after selecting a service supplier from each task. The execution time in sequential structure corresponds to the execution time of task taken by the selected service supplier. The equation is modified as equation (7) by considering AND structure, computing the execution time elapsed along the critical path using PERT/CPM algorithm. Equation (8) and (9) computes the reliability and availability, multiplying reliability of particular service supplier performing task with availability. Equation (10) represents the reputation of the web service ,averaging the reputations of tasks. Equation (13) claims that only one service supplier should be selected for performing task and the result comes out depending on the resultant selection of the path that is the only path in XOR branching. Equation (14) claims that only one XOR structure should be selected and the result comes out depending on the resultant selection of the path which is nested in XOR structure.

IV. RESULT AND ANALYSIS

The solution is obtained by using QSB+ computer software as follows.

Table 3(a): Service Provider

Task 1	2 nd SP
Task 2	1 st SP
Task 3	2 nd SP
Task 4	1 st SP
Task 5	2 nd SP
Task 6	1 st SP
Task 7	2 nd SP
Task 8	2 nd SP
Task 9	
Task 10	
Task 11	2 nd SP
Task 12	

Table 3(b): Result Analysis

	Customers requirement	result
Duration	60s	59.7s
Cost	800\$	800.6\$
reliability	95%	96.88%
availability	95%	95.35%
reputation	8	7.9%

V. CONCLUSION

The requirements of web service QoS proposed by IBM include the non functional attributes like the process time of web service cost, reliability etc. The criteria for selecting the web service partners is based on the QoS services requested by consumers. The web service can be currently recognized as a new alternate for integrating the scattered information assets within an enterprise or an organization. This model provides the critical basis from which Goal Programming Model is identified by which web service QoS can be quantified. The model is extended for the composite web service satisfying the problem of selecting the most suitable web services.

REFERENCES

- [1] Ana Barcus and Gilberto Montibeller [2008]: Supporting the allocation of software development work in distributed teams with multi-criteria decision analysis. *Omega*, 36(3):464 – 475.
- [2] Aouni B, Ben Abdelaziz F and Martel M [2005]: Decision-makers preferences modeling in the stochastic goal programming, *European Journal of Operational Research*, 162(3), 610-618.
- [3] Blahe, John t., Carter, Micheal W [2007]: A goal programming Approach to strategic resource allocation in acute care hospitals. *European Journal of operational Research*. 541-561.
- [4] DOMINIQUE BOLLINGER AND JACQUES PICTET [2008]: Multiple criteria decision analysis of treatment and land-filling technologies for waste incineration residues. *Omega*, 36(3), 418 – 428.
- [5] FIGUEIRA J, GRECO S., V. MOUSSEAU V. AND SLOWINSKI R.[2008]: Interactive Multiobjective Optimization using a Set of Additive Value Functions., *Multiobjective Optimization Approaches*, pages 99--122.
- [6] FERNANDO GARCÍA , FRANCISCO GUIJARRO ,AND ISMAEL MOYA [2010] A goal programming approach to estimating performance weights for ranking firms.
- [7] HODGKIN J, BELTON V AND KOULOURI A [2005]: European Supporting the Intelligent MCDA user: A Case Study in Multi-person Multicriteria Decision Support, *Journal of Operational Research*, 160, 1, 172-189, 1st January 2005.
- [8] JAEWOOK LEE, SUK-HOKANG, JAY ROSENBERGER & SEOUNG BUM KIM [2010]: A hybrid approach of goal programming for weapon systems selection portal. 521-527.
- [9] JAVAD DODANGEH, ROSNAH BT MOHD YUSUFF AND JAVAD JASSBI [2010]: Using Topsis Method with Goal Programming for Best selection of Strategic Plans in BSC Model, *Journal of American Science* 2010, 6(30).
- [10] JULIANA REGUEIRA ABATH AND ADIEL TEIXEIRA DE ALMEIDA [2009]: Outsourcing multicriteria decision model based on promethee method, *Journal of the Academy of Business and Economics*.
- [11] LIS, BEULLENS P, JONES DF & TAMIZ M [2008]: An Integrated queuing & multi-Objective Bed allocation model with Application to hospital in china *Journal of the Operational research society* 59, 1-9.
- [12] LIU D AND STEWART T J [2004]: Object-oriented decision support system modeling for multicriteria decision making in natural resource management, *Computers and Operations Research*, 31, 985- 999.
- [13] MAHESH O; SRINIVASAN G [2006]; Multi-objectives for incremental cell formation problem, *Annals of Operations Research*, 143(1), 157-170.
- [14] M E NJA AND VDOFIA G.A.[2009] Formulation of the mixed-integer Goal programming model for flour producing companies, *Asian Journal on mathematics & statistics volume 2, Issue-3, 55-64*.
- [15] MISHRA S, PRAKASH, TIWARI M K AND LASHKARI R S [2006]: A fuzzy goal-programming model of machine-tool selection and operation allocation problem in FMS: a quick converging simulated annealing-based approach, *International, Journal of Production Research*, 44 (1), 43-76.
- [16] ODDOYE JP, JONES D F, TAMIZ M, FOUROUGHI A A SCHMITH P.[2007]: A multi-Objective model to determine efficient resource levmedical assessment unit *Journal of the operations research society* 58, 1563-1573.
- [17] PAQUETE L. AND STÜTZLE T. [2009]: Design and analysis of stochastic local search for the multiobjective traveling salesman problem, *Computers & Operations Research*, 36(9):2619-2631.
- [18] ROMERO C. AND REHMAN .T. [2008]: Goal Programming and multiple criteria decision-making in farm planning: some extensions *Journal of Agricultural Economics Volume 36 Issue 2, Pages 171 – 185*.
- [19] S DHOUB, A KHARRAT' & H CHABCHOUB [2010]: Goal programming using multi objective hybrid meta heuristic algorithm. *Journal of the Operation Research society advance online pu*

1ST NATIONAL CONFERENCE ON TRENDS IN SCIENCE, ENGINEERING AND TECHNOLOGY (NTSET - 2018)

February 2nd & 3rd - 2018

TECHNICAL PAPER ABSTRACTS



ORGANIZED BY

MATRUSRI ENGINEERING COLLEGE

(Approved by AICTE, Affiliated to Osmania University)

#16-1-486, Saidabad, Hyderabad - 500059



Sponsored by

MATRUSRI EDUCATION SOCIETY

ISBN: 97881-936274-0-2

**NTSET
2018**





GRAPHICAL USER INTERFACE LOAD FLOW SOLUTION OF RADIAL DISTRIBUTION NETWORK

G.Pranava¹, Gurram Ravindranth², K.Ramesh Reddy³

¹Assistant Professor, Department of EEE, Vasavi College of Engineering, Hyderabad

² Professor, Department of EEE, Matrusri Engineering College, Hyderabad

³ Professor, Department of EEE, GNITS, Hyderabad

Email: ¹pranavag@yahoo.com, ²g_ravindranath@hotmail.com, ³kollirameshreddy@yahoo.com

Abstract: Power flow computation of a distribution system is very important for the system operation, reconfiguration and for placing the FACTS devices. This paper presents a development of distribution Power System of Radial Distribution Network with laterals Load Flow Analysis tool based on the Tellegen theorem based method by using a User Friendly Graphical User Interface (GUI) Matlab Program. This tool introduces a simple interface for the user to perform load flow analysis. It is also designed for a user to view power flow results for each iteration and thus will facilitate especially undergraduate electrical students to verify their manual calculation of load flow solution. By just point and click, the students will easily get the required solution. The load flow tool is evaluated by solving the load flow of several test systems and the GUI tool gives the complete Voltage Profile and Power Losses in the system. The well proved Tellegen theorem is used to obtain the load flow solution of Radial Distribution Network. 12.6KV Distribution system for 12, 28, 33 and 69 bus system. The result shows that all the answers displayed in GUI for every required calculation steps for Tellegen theorem based load flow are successfully verified with the manual calculation. Thus, this tool helps student and lecturer to learn and verify their manual calculation and at the same time reduce their calculation time.

Keywords: GUI(Graphical User Interface) tool ; Radial Distribution Network; Tellegen theorem.

I. INTRODUCTION

The distribution network structure is radial with laterals and sublaterals. The network branches have high r/x ratio. Due to these features the conventional load flow studies fail to converge.

Luis A F.M.Ferreira^[1] et al proposed the idea of Tellegen theorem application for Power systems. Hsia-Dong Chiang^[2] et al developed decoupled load flow method for distribution networks. D.Das^[3] et al proposed a novel method for solving radial distribution networks. S. Sivanagaraju^[4] et al proposed a loop based load flow method for weakly meshed distribution network. ^{[2][4]}papers had higher order terms and trigonometric equations. Memory storage requirement were high and it involved high computational time. The authors of this paper ^[5] and ^[6] have proposed and applied Tellegen theorem algorithm for load flow solution of radial distribution network. It is proved to have less memory storage requirements and computational time.

The simple and well proved Tellegen theorem algorithm is used for load flow analysis of the distribution network. It has good convergence rate. The algorithm is applied to the distribution network without and with laterals. At start flat voltage profile is assumed. The objective and other necessary equations used in this process does not have any higher order terms and trigonometric functions and the memory is observed to be less and computation time is also less. The voltage magnitudes at every node along with active and reactive power losses in the network.

Load flow solution is required for continuous monitoring of the system. The solution is necessary for future expansion of the system and is used in various ways, i.e, for reconfiguration of the system, load changes, voltage profile improvement and design of the protection equipment. In this process the algorithm has to be execute large number of times. Algorithms which give accurate solutions have to be adopted. At the same time reading the data with a user friendly tool is always appreciable. The Substation Engineer requires the complete solution of the system along with the interconnections with a click of a button. Input data along with the results with a pictorial representation of the system in one single window gives the idea of the system at a glance. An attempt to achieve the above is made in the paper.

II. RESEARCH METHOD

A. Load Problem Formulation

Load flow solution of radial distribution network

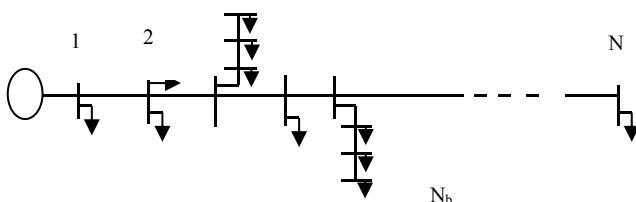


Fig1. Radial Distribution network with laterals



The Tellegen theorem is that “Sum of instantaneous complex powers in a network is equal to zero”,

$$\sum_{k=1}^{N_b} V_k I_k^* = 0 \quad (1)$$

V_i and I_i represents the voltages and currents at the i th buses respectively.

For the given distribution network

$$(0 - V_1)I_1 + (V_1 - V_2)I_1 + P_{L1} + jQ_{L1} + (V_2 - V_3)I_2 + \dots + (V_{NB-1} - V_{NB})I_{NB-1} + P_{LNB} + jQ_{LNB} = 0 \quad (2)$$

The loads at each node are represented by $P_{Li} + jQ_{Li}$.

The voltage at $(i+1)$ th node is obtained with i th voltage known.

$$V(i+1) = \frac{(V(i) * V(i) - k3)}{V(i)} \quad (3)$$

The power injected at the i th bus is given by $P(i) + jQ(i)$. The resistance and reactance at the i th bus is represented by $r(i) + jx(i)$.

$$\text{where } k3 = \sqrt{(P(i)^2 + Q(i)^2)(r(i)^2 + x(i)^2)} \quad (4)$$

The distribution system with laterals is solved in in two stages [1] and [2]

1) First stage

Initially the loads at the laterals are lumped at their respective start nodes thus reducing it to a main feeder case. The load flow study for main feeder case is executed.

2) Second stage

Now the voltage at the node where the lateral is connected is taken as the source node. The algorithm for the load flow is run at each lateral. This gives the entire load flow solution.

B. Graphical User Interface Tool

A Graphical User Interface tool developed in Matlab environment which gives the complete load flow solution of radial distribution network with laterals. The load flow solution includes voltage profile and power losses. A network diagram is displayed along with the Load Flow Solution. The diagram indicates the interconnection of the buses and the voltage at the corresponding bus.

C. Sequence of steps involved in developing the tool

Matlab Graphical User Interface is used to develop this user friendly tool.

1. Input data required for load flow solution are to be read. Static text, edit text, tables are used in order to read the data. Input data includes
 - (i) Number of buses, number of laterals, sublaterals.
 - (ii) Lateral connection data: number of laterals connected at each node.
 - (iii) Source Node, Start node and end node of laterals. The node at which lateral is connected is called source node. The node number of the lateral after the source node in the lateral is called start node. The last node number of that lateral is called end node.
 - (iv) Resistance and Reactance data of the lines in pu
 - (v) Active and Reactive power loads at each bus in pu
2. A push button is used to execute the algorithm for load flow solution of the fed radial distribution network.
3. The well proved Tellegen theorem algorithm is programmed and linked with the pushbutton for execution.
4. On execution the results are displayed on the panel and the tables
 - (i) Voltages in pu at each bus and power losses in KW and KVAR of the system are displayed in two separate tables.
 - (ii) The connections of the nodes are displayed in the panel. The connections indicate the main feeder along with its laterals
 - (iii) The bus number with their corresponding voltages are displayed on the plot axes.

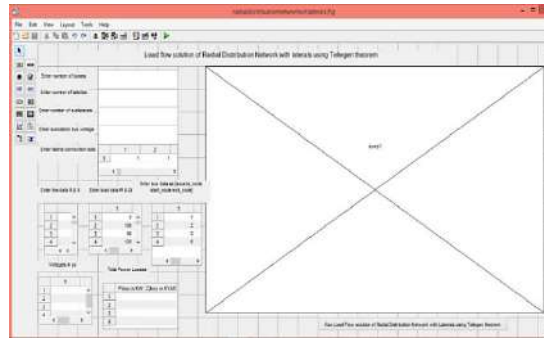


Fig2. Graphical User Interface tool for Load flow solution of Radial Distribution network with laterals

The GUI tool shown in Fig2 is modeled with text boxes to enter the feeder data with number of buses, laterals, sublaterals. Tables are provided to enter the data of lateral connection data, line data and load data. After execution the connection diagram of the buses is generated at a click of the push button along with the voltage profile and power losses of the system. The output values are shown in the tables provided. The connection diagram is displayed in the plot axes.

III.RESULTS AND DISCUSSIONS

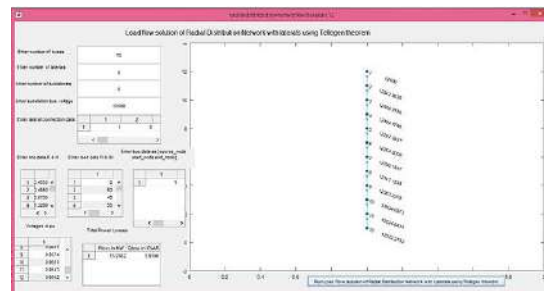


Fig 3. Load flow solution of 12.6KV, 12 bus Radial Distribution network – main feeder case.

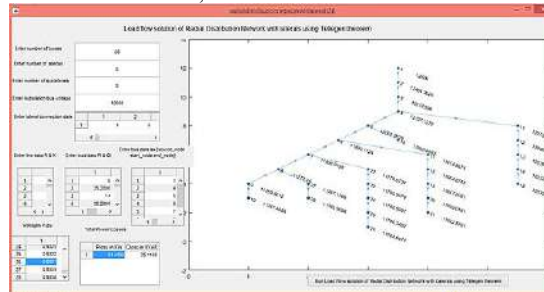


Fig 4. Load flow solution of 12.6KV, 28 bus Radial Distribution network with laterals

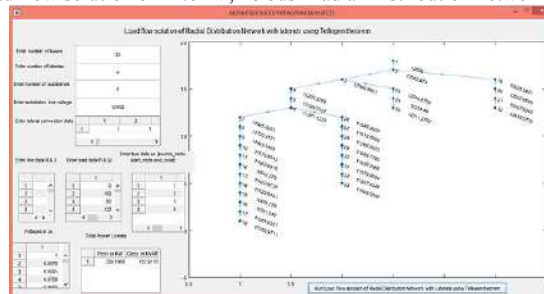


Fig 5. Load flow solution of 12.6KV,33 bus Radial Distribution network with laterals

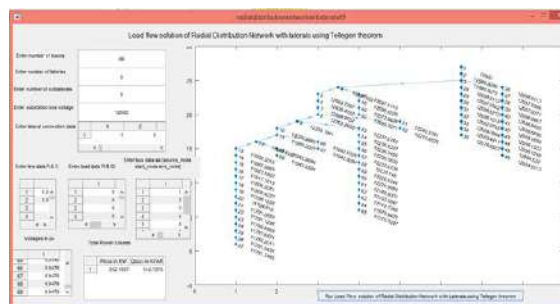


Fig 6. Load flow solution of 12.6KV,69 bus Radial Distribution network with laterals



TABLE I

	12 bus	28 bus	33 bus	69 bus
Power Losses in KW	15.28	51.41	204.19	252.15
Power Losses in KVAR	5.91	35.11	133.91	118.73

Power Losses in 12.6KV Radial Distribution network- 12 bus, 28 bus, 33 bus and 69 bus

Figures 3 to 6 give the picture of the load flow data along with the voltage profile, power losses and interconnection of buses for 12.6KV-12, 28,33 and 69 buses. 12 bus system is a simple radial feeder without laterals. 28,33 and 69 buses are radial feeders with laterals. The power losses and voltage profile for all the systems are tabulated separately in Tables 1 and 2.

TABLE II

S.No	12 bus	28 bus	33 bus	69 bus
1	1.0000	1.0000	1.0000	1.0000
2	0.9955	0.9892	0.9970	0.9999
3	0.9913	0.9740	0.9831	0.9999
4	0.9845	0.9633	0.9756	0.9998
5	0.976	0.9524	0.9682	0.9987
6	0.9734	0.9439	0.9501	0.9872
7	0.9711	0.9370	0.9449	0.9753
8	0.9641	0.9343	0.9310	0.9725
9	0.9574	0.9341	0.9246	0.9714
10	0.9551	0.9339	0.9186	0.9545
11	0.9543	0.9582	0.9177	0.9508
12	0.9542	0.9561	0.9161	0.9482
13		0.9552	0.9098	0.9449
14		0.9550	0.9071	0.9417
15		0.9548	0.9055	0.9384
16		0.9515	0.9041	0.9379
17		0.9424	0.9017	0.9370
18		0.9417	0.9010	0.9370
19		0.9403	0.9965	0.9364
20		0.9396	0.9927	0.9361
21		0.9391	0.9919	0.9358
22		0.9347	0.9912	0.9358
23		0.9334	0.9794	0.9357
24		0.9325	0.9726	0.9355
25		0.9322	0.9691	0.9352
26		0.9321	0.9480	0.9351
27		0.9339	0.9453	0.9350
28		0.9338	0.9339	0.9999
29			0.9274	0.9998
30			0.9234	0.9996
31			0.9190	0.9996
32			0.9181	0.9994
33			0.9177	0.9991
34				0.9987
35				0.9984
36				0.9999
37				0.9998
38				0.9998
39				0.9997
40				0.9997
41				0.9997
42				0.9996
43				0.9996
44				0.9996
45				0.9996
46				0.9996
47				0.9998
48				0.9997
49				0.9978
50				0.9967
51				0.9717
52				0.9693
53				0.9713
54				0.9712
55				0.9711
56				0.9711
57				0.9708
58				0.9707
59				0.9705
60				0.9702
61				0.9642
62				0.9630
63				0.9612
64				0.9508
68				0.9346
66				0.9478
67				0.9478
69				0.9479
69				0.9479

Voltage Profile of 12.6KV Radial Distribution network- 12 bus, 28 bus, 33 bus and 69 bus

IV. CONCLUSIONS

Graphical user interface tool developed using Matlab 2015a has been tested with various number of feeders. Data and output results are shown in the same window. The tool has been developed to visualize data and output in the same window. At a click of the push button, solution appears on the screen. It is a user friendly tool which clearly indicates input information and the



outputs. As previously, programs need not be executed every time. Data can be easily modified in this window, instead of re-entering every time in the command window whenever there is change in data.

REFERENCES

- [1] Luis A F.M.Ferreira, "Tellegen's Theorem and Power Systems-New Load Flow Equations", New Solution Methods, IEEE Transactions on Circuits and Systems, vol 37, No 4, April 1990
- [2] Hsia-Dong Chiang, "A decoupled load flow method for distribution networks: algorithms, analysis and convergence study, Electric Power and Energy Systems", Vol 13, No 3, June 1991, pp130-138.
- [3] D.Das, H.S. Nagi, D.P.Kothari, "Novel method for solving radial distribution networks", IEE Proc.-Gener.Transm.Distrib., Vol.141, No.4, July 1994, pp291-298.
- [4] S. Sivanagaraju, J. Viswanatha Rao and M. Giridhar, "A loop based load flow method for weakly meshed distribution network", ARPN Journal of Engineering and Applied Sciences, VOL. 3, NO. 4, AUGUST 2008 ISSN 1819-6608, pp 56-59.
- [5] G.Pranava, Gurraravindranth, K.Ramesh Reddy, "Tellegen Theorem Based Load Flow Solution Of Radial Distribution Network", First International Conference On Recent Innovations In Engineering And Technology (ICRIEATt-2016), pp1402-1405.
- [6] G.Pranava, Gurraravindranth, K.Ramesh Reddy, "Tellegen theorem based Load Flow Solution of Radial Distribution Network with Laterals", 2015 International Conference on Power and Advanced Control Engineering (ICPACE), pp 99-103.



MATRUSRI ENGINEERING COLLEGE

(Approved by AICTE, Affiliated to Osmania University)

#16-1-486, Saidabad, Hyderabad - 500059



Sponsored by

MATRUSRI EDUCATION SOCIETY



ISBN: 97881-936274-0-2



1ST NATIONAL CONFERENCE ON TRENDS IN SCIENCE, ENGINEERING AND TECHNOLOGY (NTSET - 2018)

February 2nd & 3rd - 2018

TECHNICAL PAPER ABSTRACTS



ORGANIZED BY

MATRUSRI ENGINEERING COLLEGE

(Approved by AICTE, Affiliated to Osmania University)

#16-1-486, Saidabad, Hyderabad - 500059



Sponsored by

MATRUSRI EDUCATION SOCIETY

ISBN: 97881-936274-0-2

NTSET 2018



A NOVEL ELECTRIC VEHICLE CONTROL- ELECTRONIC DIFFERENTIAL-STRATEGY USING FIVE PHASE INDUCTION MOTOR

Y.Laxmi Narasimha Rao¹, G.Ravindranath²

¹Assistant Professor, Department of EEE, MVSR Engineering College, Hyderabad

²Professor, Department of EEE, Matrusri Engineering College, Hyderabad

Email: lyalavarthi1234@gmail.com, g_ravindranath@hotmail.com

Abstract: Three phase Induction motors especially multiphase motor drives has proved to be much efficient for high power drives application such as Electric vehicles/Hybrid Electric vehicles. In this paper a simulated Electric Vehicle (EV) with four-wheel-drive with Electronic Differential System (EDS) is presented. The Electric Vehicle (EV) is controlled with five phase induction motor and the EDS distributes torque and power to each in-wheel motor according to the requirements, adapts the speed of motor to the driving conditions and simulates the behavior of a differential. The working conditions including the condition of the vehicle with the constant speed, accelerating and decelerating are studied, and the control strategy of the EDS for the vehicle with four in-wheel motors is designed and simulated. The simulation with Matlab/Simulink is made and the results are verified with the rationality of the EDS controller, and proved that the system has more favorable dynamic performance.

Index Terms: Electric Vehicle, Electronic Differential System

I. INTRODUCTION

The principal constraints in vehicle design for transportation are the development of a non-polluting high safety and comfortable vehicle. Taking into account these constraints, our interest has been focused on the Electrical Vehicle, with independent driving wheel-motor drive shaft. This configuration is a conceivable solution, the pollution of this vehicle is strongly decreased and electric traction gives the possibility to achieve accurate and quick control of the distribution torque. Torque control can be ensured by the inverter, so this vehicle does not require a mechanical differential gear or gearbox. One of the main issues in the design of this vehicle (without mechanical differential) is to assume the car stability. During normal driving condition, all drive wheel system requires a symmetrical distribution of torque in the both sides. In recent years, due to problems like the energy crisis and environmental pollution, the Electric Vehicle (EV) has been researched and developed more and more extensively.

Three phase squirrel cage induction motor are well known for their simple and robust construction, reliability, ruggedness, low maintenance and low cost. The speed control of induction motor is complicated when used for variable speed application. However, due to the development in the power electronic devices, the control of induction motor have become easier and flexible. In addition to this, the numbers of phases have become a design parameter. The development of the solid-state inverter and control schemes has opened a new range of applications for induction machines in areas where dc machines were dominant. In almost any kind of application, three phase induction machines have been employed. However, when the machine is not directly fed from standard power sources, there is no need for specified number of phases. Higher numbers of phases are more advantageous. Multiphase machine has several advantages over the conventional three phase motor such as reduced torque pulsation, reduced per phase rotor harmonic current, high reliability and high fault tolerance. E.E. Ward and Harrer have presented the preliminary investigation on inverter fed five phase induction motor and suggested that the amplitude of the torque pulsation can be reduced by increasing the number of phases. H.A. Toliyat, J.C. White, and T.A. *et al* Lipo evaluated the performance of induction machine with different number of phases for operation with static converter in. Nelson and Krause *et al* derived the voltage equations in phase variables and the transformed in to d-q-o reference frame of a multi-phase machine with symmetrical phase displacement. G.K. Singh *et al* developed a two-axis (d-q) model of the multi-phase machine in an arbitrary reference frame analyzed the machine under balanced, and unbalanced (open circuit and short circuit both) operating condition.

II. PROBLEM FORMULATION AND ANALYSIS

A. ELECTRIC VEHICLE DESCRIPTION

According to Figure 1(a) the opposition forces acting to the vehicle motion are: the rolling resistance force F_{tire} due to the friction of the vehicle tires on the road; the aerodynamic drag force F_{aero} caused by the friction on the body moving through the air; and the climbing force F_{slope} that depends on the road slope

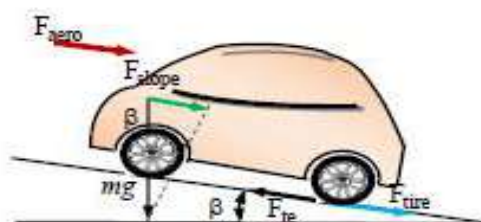


Figure 1

The forces acting on a vehicle moving along a slope.

$$F_r = F_{\text{tire}} + F_{\text{aero}} + F_{\text{slope}} \quad (1)$$

The total resistive force is equal to F_r and is the sum of the resistance forces, as in (1).

The rolling resistance force is defined by:

$$F_{\text{tire}} = mgF_r \quad (2)$$

The aerodynamic resistance torque is defined as follows

$$F_{\text{aero}} = \frac{1}{2}(\rho_{\text{air}} A_f C_d V^2) \quad (3)$$

The rolling resistance force is usually modeled as:

$$F_{\text{slope}} = m g \sin(\beta) \quad (4)$$

The main purpose of the electronic differential is to substitute the mechanical differential in multi-drive systems providing the required torque for for each driving wheel

$$V_1 = W_v(R-d/2) \quad (5)$$

$$V_2 = W_v(R+d/2) \quad (6)$$

Where $R = L/(\tan\delta)$

δ is the steering angle d is the width of the car where this angle is zero we are in the straight road. The angular speeds in the curved roads are

$$W_1 = ((L-(d/2)\tan\delta)/L) W_v \quad (7)$$

$$W_2 = ((L+(d/2)\tan\delta)/L) W_v \quad (8)$$

Where L is the length of the car and W_v is the centre of the turn angular speed's is given by

$$W_v = (W_1+W_2)/2 \quad (9)$$

B.CONSTRUCTION AND WORKING PRINCIPLE OF MULTIPHASE INDUCTION MOTOR

Similar to the working of three phase induction motor, five phase induction motor works on the application of Faraday's law and Lorentz force on conductor. When five phase ac supply is given to the stator winding which are spatially and time displaced by 72° the rotating magnetic field is produce which rotates at synchronous speed. When short circuited rotor (squirrel cage) is placed in rotating magnetic field an EMF is induced in the rotor conductor due to electromagnetic induction. Due to this EMF, current starts flowing in the rotor conductor and sets up its own magnetic field. Due to interaction of these two magnetic fields, a torque is produced and conductor tends to move. The scheme of five phase motor drive is shown in Fig. (2). The field winding of the induction motor is housed in the stator which is excited by five leg inverter. Stator winding of an n-phase machine can be designed in such a way that the spatial displacement between any two consecutive stator phases equals, $\alpha = 2\pi/n$ in this case a symmetrical multiphase machine results. This will always be a case if the number of phases is an odd prime number. In three phase induction machine the three phases are spatially displaced by 120 degree whereas in five phase machine by 72 degrees as shown in Fig. (3) .

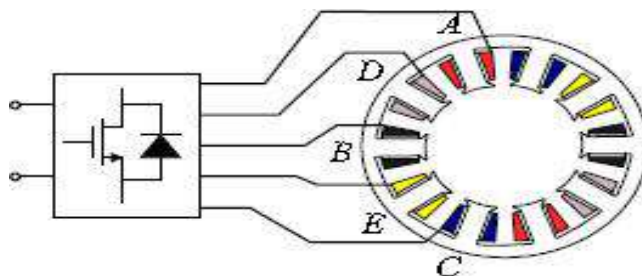


Fig.2 Scheme of the five-phase motor drive.

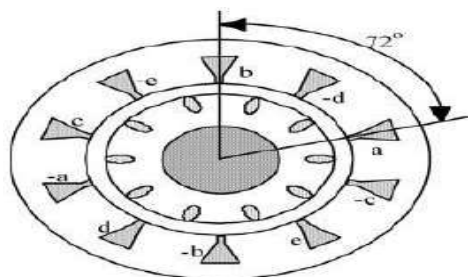


Fig. 3 five-phase concentrated winding induction machine

It is not practically possible to directly implement the five phase stator winding into standard three phase machine stator slots. Five phase machine requires custom laminations for the machine stator and custom inverter to supply the five phase motor. The standard squirrel cage rotor of three f machine can be used. The advantage of using squirrel cage rotor is that, it can adjust to any number of phases which is not possible in case if wound rotor. A five phase induction machine may have five phase distributed winding or fractional slot concentrated winding.

Characteristics of Multiphase Induction Machines

To achieve a motor drive with high fault tolerance, it is important to choose the motor exhibiting an intrinsic fault-tolerant capability. Fractional slot winding motors with non-overlapped coils are suitable for fault-tolerant applications. They allow a physical separation among the phases, limiting the propagation of the fault. They are also characterized by a high self-inductance, necessary to limit the short circuit current. In addition, a suitable combination of slots and poles yields a very low mutual coupling between phases. For better performance of the machine, the mutual coupling between the phases should be less, so that when fault occurs on one phase of a machine it is not carried to the other phase mutually.

The stator excitation in multiphase machine produces a field with lower harmonic content, so the efficiency of the machine is increased than that with three phase machine. Multiphase machine have greater fault tolerance than their three phase counterparts. If one phase of the three phase machine becomes open-circuited the machine becomes single phase. It may continue to run but requires some external means for starting, and must be massively de-rated. But in case of multi-phase machine if one phase is open circuited, it will self-start and will run with minimal de-rating. Multiphase machines are less susceptible than their three phase counterparts to time harmonic components in the excitation waveform. Such excitation components produce pulsating torques at even multiple of fundamental excitation frequency. All the above aspects are elaborated in detail in.

Over the years, many advantages of multiphase machines have been recognized, including higher machine torque density, reduced torque ripples, reduced harmonic currents, better transient and steady-state performance, and more robust control offered by current harmonic injection.

Concerning the five phase motor drive advantages and drawbacks are as follow:

The main advantages of using a five phase motor drive are found in its reliability to operate properly also in faulty conditions. It can operate with one or two open circuited

C. MATHEMATICAL MODEL OFFIVE-PHASE INDUCTIONMOTOR

The parameter equations such as voltage and torque that describe the dynamic behavior of an induction motor are time-varying in nature. Such equations involve complexity while solving as differential equations. A change of variables from time varying to time invariant can be used to minimize the complexity from the voltage equations of motor due to relative motion of electric circuit. By this technique, a multi-phase winding can be reduced to a set of two phase winding (d-q) which are in quadrature to each other. In other words, the stator and rotor variables (voltage, current and flux linkages) of an induction motor are transferred to arbitrary reference frame.

The steady state model and equivalent circuit of induction motor are useful for studying the performance of the machine in steady state. Fig.4 shows a q-d-0 equivalent circuit of an Induction motor. The circuit comprises of various time varying inductances which are to be simulated to analyze the dynamic behavior of five-phase Induction motor.

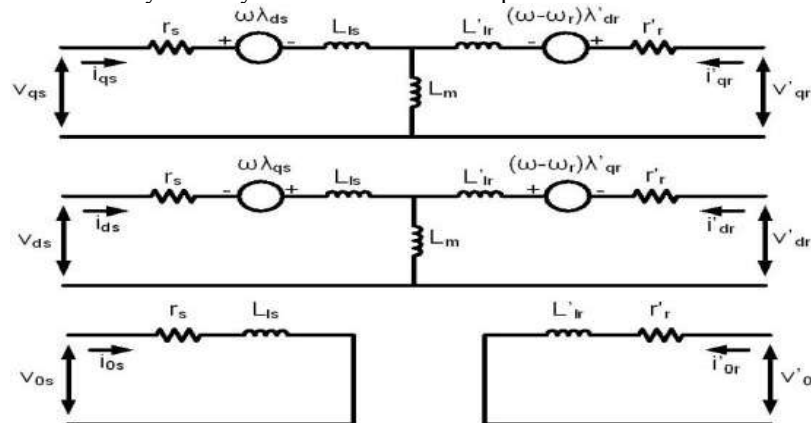


Fig.4 A d-q-0 axis equivalent circuit of five phase Induction machine in arbitrary reference frame

Five phase stator voltage of induction motor under balanced condition is expressed as follows.

$$V_a = 2V_{rms} \sin \omega t$$

$$V_b = 2V_{rms} \sin (\omega t - 2\pi/5)$$

$$V_c = 2V_{rms} \sin (\omega t - 4\pi/5)$$

$$V_d = 2V_{rms} \sin (\omega t + 4\pi/5)$$

$$V_e = 2V_{rms} \sin (\omega t + 2\pi/5)$$

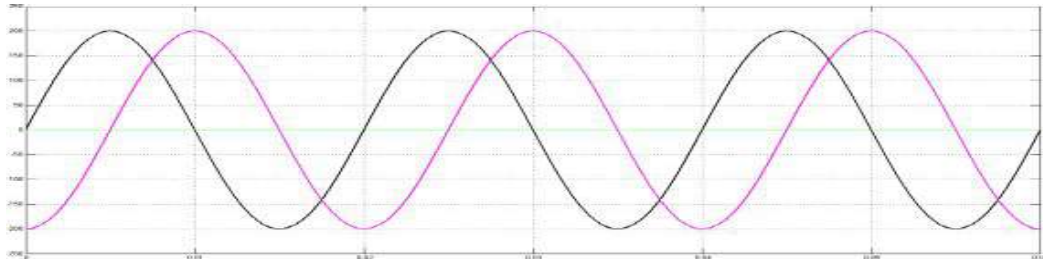


Fig 5 q- and d- axis stator voltages

As stator to rotor coupling takes place in only d-q equations, rotational transformation is applied to these two pairs of equation. The nature of this equation is identical to the three phase machine equations. Assuming that the machine equations are transformed into arbitrary frame of references rotating at angular speed, ω_a .

As stator to rotor coupling takes place in only d-q equations, rotational transformation is applied to these two pairs of equation. The nature of this equation is identical to the three phase machine equations. Assuming that the machine equations are transformed into arbitrary frame of references rotating at angular speed, ω_a , the model of five phase induction machine with Stator side voltage equations in d- and q- reference frame are given as follows

$$\begin{aligned} V_{ds} &= R_s i_{ds} - \omega_a \phi_{qs} + \rho \phi_{ds} \\ V_{qs} &= R_s i_{qs} + \omega_a \phi_{ds} + \rho \phi_{qs} \\ V_{xs} &= R_s i_{xs} + \rho \phi_{xs} \\ V_{ys} &= R_s i_{ys} + \rho \phi_{ys} \\ V_{0s} &= R_s i_{0s} + \rho \phi_{0s} \end{aligned}$$

Rotor side voltage equations in d- and q- reference frame are given as,

$$\begin{aligned} V_{dr} &= R_r i_{dr} - \omega_a - \omega \phi_{qr} + \rho \phi_{dr} \\ V_{qr} &= R_r i_{qr} + \omega_a - \omega \phi_{dr} + \rho \phi_{qr} \\ V_{xr} &= R_r i_{xr} + \rho \phi_{xr} \\ V_{yr} &= R_r i_{yr} + \rho \phi_{yr} \\ V_{0r} &= R_r i_{0r} + \rho \phi_{0r} \end{aligned}$$

Flux equation of stator side of five phase induction motor is given as,

$$\begin{aligned} \phi_{qs} &= L_{ls} + L_m i_{ds} + L_m i_{dr} \\ \phi_{ds} &= L_{ls} + L_m i_{qs} + L_m i_{qr} \\ \phi_{xs} &= L_{ls} i_{xs} \\ \phi_{ys} &= L_{ls} i_{ys} \\ \phi_{0s} &= L_{ls} i_{0s} \end{aligned}$$

Flux equation of rotor side of five phase induction motor is given as,

$$\begin{aligned} \phi_{qr} &= L_{lr} + L_m i_{dr} + L_m i_{ds} \\ \phi_{dr} &= L_{lr} + L_m i_{qr} + L_m i_{qs} \\ \phi_{xr} &= L_{lr} i_{xr} \\ \phi_{yr} &= L_{lr} i_{yr} \\ \phi_{0r} &= L_{lr} i_{0r} \end{aligned}$$

Where, $L_m = (n/2) * M$ and M is the maximum value of the stator to rotor mutual inductances in the phase-variable model.

Symbols R and L stand for resistance and inductance, v, i and ϕ denote voltage, current and flux linkage, while indices s, r identify stator/rotor variables/parameters. Index l identifies leakage inductances.

From the above equations the Torque and rotor speed can be determined as,

$$\begin{aligned} T &= \frac{5}{2} \left(\frac{P}{2} \right) * \frac{1}{\omega_b} (\phi_{ds} i_{qs} - \phi_{qs} i_{ds}) \quad (35) \\ \omega_r &= \int \frac{P}{J} (T_e - T_l) \quad (36) \end{aligned}$$

Where, P is the number of poles; J moment of inertia; TL Load Torque; Te electromechanical torque; ω_r Rotor Speed.

Mathematical model equations for d-q components and the torque equation are identical as for a three-phase induction machine. The only difference between five phase machine model and corresponding three phase machine model is the presence of x-y components in voltage and flux equations. Rotor x-y components are fully decoupled from d-q components and one from other. Since rotor winding is short circuited, x-y components does not appear in the rotor winding. Zero sequence component equations for both stator and rotor can be omitted from further consideration due to short-circuited rotor winding and star connection of stator winding. Finally, since stator x-y components are fully decoupled from d-q components and one from the other, the equations for x-y components can be omitted from further consideration as well. This means that the model of five phase induction motor in arbitrary reference frame is identical to the model of three phase induction machine and the same control schemes can be apply to multiphase induction machines as for three-phase machines. However, existence of xy equations means that utilization of a voltage source that creates stator voltage x-y components will lead to a flow of potentially large stator x-y current components, since these

are restricted only by stator leakage impedance. These x-y components correspond to certain voltage and current harmonics, the order of which depends on the machine's number of stator phases. Hence the inverter, used to supply a multiphase induction machine, must not create low-order voltage harmonics that will excite stator current low-order harmonic flow in x-y circuits.

D. MATALB/SIMULINK IMPLIMENTATION

The voltage, flux, torque equations and transformation matrices are used to implement the model of five phase induction motor in MATLAB/Simulink as shown in Fig. 6. The input to the motor is the five phase sinusoidal voltage supply. The five phase to two phase conversion block transfers the five phase stator voltages to d- and q- axis voltages. This block gives stator current, rotor currents and fluxes in direct and quadrature axis. Current-flux to torque- speed block gives the rotor speed and torque using above equations. The simulation of the internal structure of five phases induction motor is run assuming different load condition. The stator and rotor currents in d and q references frame are transferred to machine variable as i_{as} , i_{bs} , i_{cs} , i_{ds} and i_{es} using inverse transformation matrices to analyze the nature of the stator and rotor currents.

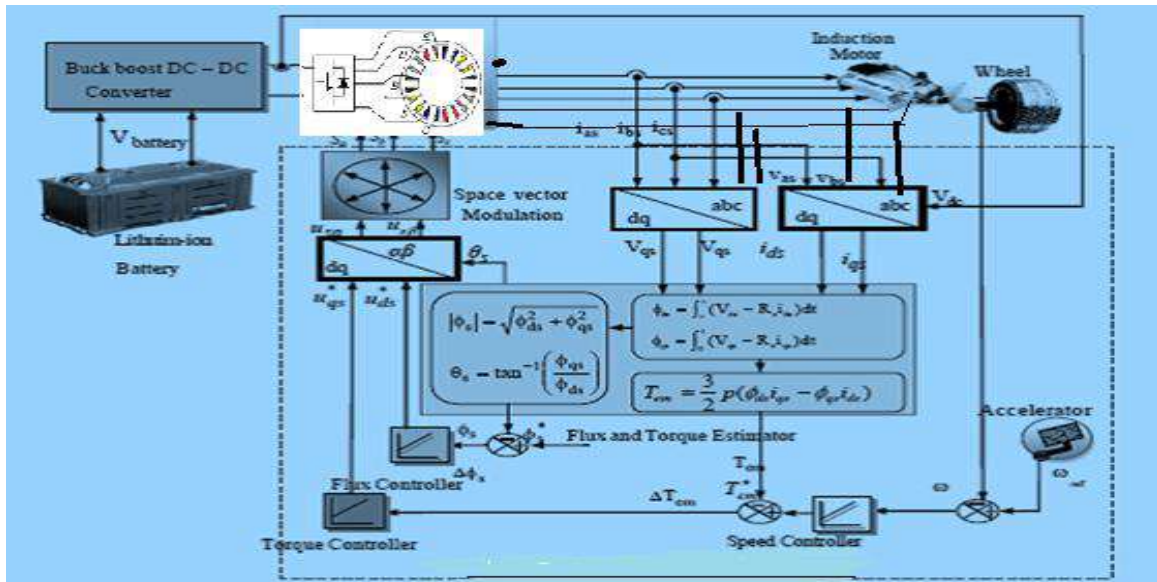


Fig 6. Implementation of Electric Vehicle with Five phase Induction Motor

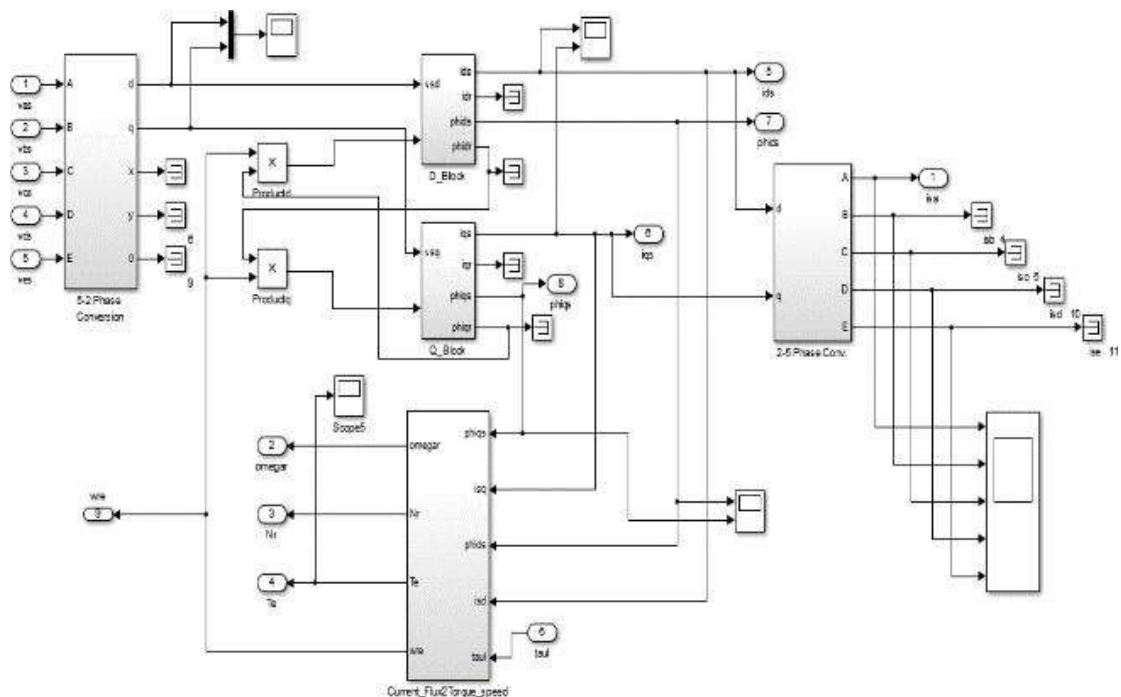


Fig7. Mathematical Model of Five phase Induction Motor

SIMULATION RESULTS:

For electric drive the following paths are chosen path 1 corresponds to straight road, Path 2 corresponds Right curve , Path 3 corresponds to straight road and path 4 corresponds to left curve. Simulation of novel electric vehicle using five phase induction motor is modeled and simulated in Matlab. It is observed that the torque and current ripples for five phase induction motor is reduced and at the same time, time response is improved. Following are the results compared with the conventional three phase induction motor to the proposed five phase induction motor

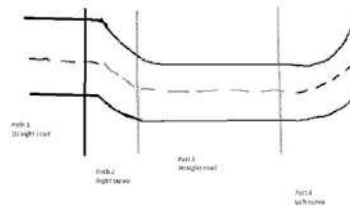


Fig 8. Road path for the Electric Drive

Path	Time (sec)	Road Topology
1	0<t<0.5	Straight road
2	0.5<t<1.5	Right curve
3	1.5<t<2.5	Straight road
4	2.5<t<3	Left curve

Table.1 For Road path

A) Five phase Induction Motor(2- level Inverter)

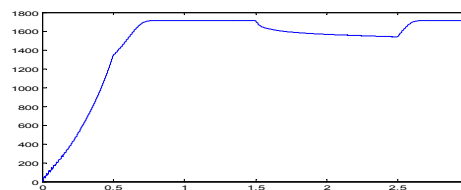


Fig 9.Speed curve for right tire

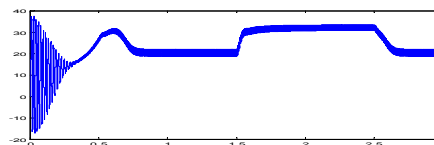


Fig 10.Torque for right tire

Table 2. Comparison of 3phase and 5 phase of two Level Inverter

S.no		Conventional 3 Phase (2level Inverter)	Proposed 5 Phase (2-level Inverter)
1	Torque (Fund)	26 N-m	29 N-m
2	Current (Fund)	7 A	8.5 A
3	Torque ripple	10.8(%)	7.23(%)
4	Current ripple	18.9(%)	15.23(%)

Table 3. Transient Response

Transient response	Rising time (sec)
Proposed 5phase(2-level Inverter)	.54
Conventional 3 phase(2- Level Inverter)	.752

Rated phase voltage (V)	250
Rated Power (Hp)	5
Rated Phase current (A)	10
Rated frequency (Hz)	50
Number of Poles	2
Rated Speed (rpm)	1440



REFERENCES:

- [1] E.E. Ward and H.Harer, "Preliminary investigation of an inverter fed five-phase induction motor", Proc. IEE 116 (6), 1969, pp. 980-984.
- [2] N. Bianchi, S. Bolognani, and M. D. Pre, "Strategies for the fault-tolerant current control of a five-phase permanent-magnet motor," IEEE Trans. on Ind. Appl., vol. 43, no. 4, pp. 960–970, July/Aug. 2007
- [3] G. K. Singh and V. Pant, "Analysis of multi-phase induction machine under fault condition in a phase redundant AC drive system", Elect. Mach. Power System, vol. 28, no. 6, pp. 577-590, 2000.
- [4] H.A. Toliyat, T.A. Lipo and J.C. White, "Analysis of concentrated winding machine for adjustable speed drive applications-Pat II: Motor design performance", IEEE Tras. Energ Conv., vol. 6, no. 4, pp. 684-692, Dec. 1991.
- [5] D.C. White, H.H. Woodson, "Electromechanical energy conversion", Wiley, New York, 1959.
- [6] R.H. Nelson, P.C. Krause, "Induction machine analysis for arbitrary displacement between multiple winding sets", IEEE Trans. 93 (1974) 841–848.
- [7] Y Zhao, T.A. Lipo, "Space vector PWM control of dual three phase induction machine using vector space decomposition", IEEE Trans. IA-31 (5) (1995) 1100–1109.
- [8] Y. Zhao, T.A. Lipo, "Modeling and control of multi-phase induction machine with structural unbalance, part I- Machine modeling and multi-dimensional current regulation", IEEE Trans. Energy Conversion EC-11 (3) (1996) 570–577.
- [9] V. Pant, G.K. Singh, S.N. Singh, "Modeling of a multiphase induction machine under fault condition", in: Proceedings IEEE The Third International Conference on Power Electronics and Drive Systems, PEDS'99, Hong Kong, July 26–29, 1999, Vol. 1, pp. 92–97.
- [10] G.K.Singh, "Multi-phase induction machine drive research – a survey," Electric Power System Research, vol. 61, pp. 139-147, 2002.
- [11] M. Barcaro, N. Bianchi, E. Fornasiero, and F. Magnussen, "Experimental comparison between two fault-tolerant fractional-slot multiphase PM motor drives," in Proc. ISIE, 2010, pp. 2160– 2165.
- [12] J. Faiz, M. B. B. Sharifian, A. Keyhani, A. B. Proca, , "Sensorless direct torque control of induction motors used in electric vehicle," IEEE Trans. Energy Conversion, vol. 18, no. 1, Mars. 2003.
- [13] J. Faiz, S.H. Hossieni, M. Ghaneei, A. Keyhani, A. B. Proca, "Direct torque control of induction motor for electric propulsion system," Electric Power System Research, vol. 51, pp. 95-101, Aug. 1999.
- [14] K. Jezemik, "Speed sensorless torque control of induction motor for EVs," Proc. IEE Intl. Workshop on Advanced Motion Control, 2002, pp. 236-241.
- [15] Cao, Xianqing, Zang, Chunhua, Fan, Liping, "Direct Torque Controlled Drive for Permanent Magnet Synchronous Motor Based on Neural Networks and Multi Fuzzy Controllers, " IEEE International Conference on Robotics and Biomimetics, 2006. ROBIO '06. pp. 197 – 201, 2006.



MATRUSRI ENGINEERING COLLEGE

(Approved by AICTE, Affiliated to Osmania University)

#16-1-486, Saidabad, Hyderabad - 500059



Sponsored by

MATRUSRI EDUCATION SOCIETY



ISBN: 97881-936274-0-2



1ST NATIONAL CONFERENCE ON TRENDS IN SCIENCE, ENGINEERING AND TECHNOLOGY

(NTSET - 2018)

February 2nd & 3rd - 2018

TECHNICAL PAPER ABSTRACTS



ORGANIZED BY

MATRUSRI ENGINEERING COLLEGE

(Approved by AICTE, Affiliated to Osmania University)

#16-1-486, Saidabad, Hyderabad - 500059



Sponsored by

MATRUSRI EDUCATION SOCIETY

ISBN: 97881-936274-0-2

NTSET 2018



SPWM TECHNIQUES IN FIVE LEVEL INVERTER

M.V.Subramanyam¹, P.Kishor², M.Srinivas³

¹Assistant Professor, Department of EEE, Matrusri Engineering College, Hyderabad

²Assistant Professor, Department of EEE, Matrusri Engineering College, Hyderabad

³Assistant Professor, Department of EEE, Matrusri Engineering College, Hyderabad

Email: subramanyam.mvs@gmail.com, parellykishore@gmail.com, srinureddy2005@gmail.com

Abstract: The five level inverter is most widely used inverter in medium and high voltage applications, since it has many advantages and easy to develop when compared to higher level(7 or 9) inverters. There are several modulation techniques and most popular among them is Sinusoidal Pulse Width Modulation.(SPWM). There are different Sinusoidal Pulse width Modulation techniques such as In Phase Disposition(IPD), Anti Phase Disposition(APD), Phase Opposition Disposition(POD), Phase shift(PS), Anti-Phase Shift(APS), Variable Frequency(VF), Anti-Variable Frequency(AVF) and Carrier Overlap(CO)The THD of different Sinusoidal Pulse width Modulation techniques are found as carrier frequency is varied and compared .

Keywords: five level inverter, modulation technique, pulse width modulation, phase disposition, phase shift, variable frequency.

I. INTRODUCTION

Multilevel Inverters have many advantages compared with and well known two level converters [1]. These advantages are fundamentally focused on improvements on the output quality and a nominal power increase in the inverter. The five level inverter is most widely used inverter in medium and high voltage applications, since it has many advantages and less complex architecture compared to higher level (7 or 9) inverters. There are several modulation techniques that can be used with 5 level inverters such as i) Sinusoidal Pulse Width Modulation (SPWM) technique ii) Selective Harmonic Elimination(SHE) and iii) Space Vector Modulation (SVM) technique. [2]. There are again different methodologies in SPWM technique such as 1)In Phase Disposition PWM (IPDPWM) 2)Phase Opposition Disposition PWM (PODPWM) 3)Alternative Phase Opposition & Disposition PWM(APODPWM) 4) Phase Shift PWM(PSPWM) 5) Alternate Phase Shift PWM(APSPWM) 6)Carrier Overlap PWM(COPWM) 7)Variable Frequency PWM (VFPWM) 8)Alternate Variable Frequency PWM(AVFPWM) 9)Alternate Phase Disposition & Alternate Phase Shift PWM(APDAPSPWM)[2].

II. MULTI LEVEL INVERTERS

Traditional two level and three level high frequency Pulse width modulated (PWM) inverters for motor drives has several problems associated with high frequency switching which produce common mode voltages and high rate of voltage change (dv/dt) to motor windings. The concept of using multiple small voltages to perform power conversion was introduced. These converters recently have found many applications in medium and high power applications. Recent advances in Power electronics made the multilevel concept practical. Based on the output voltage levels, inverters can be classified as two level inverters and Multi-level inverters. The inverters with voltage level 3 or more are referred as Multi-level inverters.[3]

The fundamental multilevel inverter topologies are diode clamped, flying capacitor and multilevel H-bridge. Diode clamped Multilevel Inverter is a very general and widely used topology for real power flow control. Normally n-level diode clamped Multilevel Inverter has 2(n-1) main switches and 2(n-1) main diodes. In addition, this topology needs 2(n-2) clamping diodes [4]. So in the five level diode clamped inverter 8 main switches, () 8 main diodes (D1 to D8) and 6 clamped diodes (DB1 to DB6) are used.[5] Fig.1 illustrates five level diode clamped multilevel inverter.

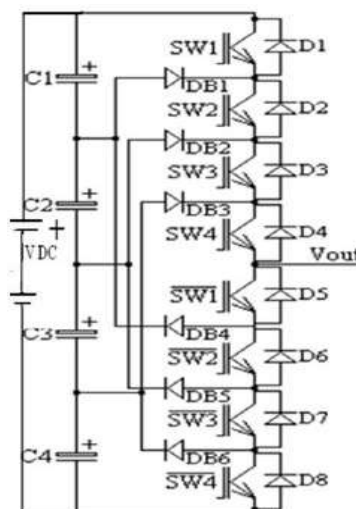


Fig. 1 One leg of Five Level diode clamped Multi-level inverter

III. SPWM MODULATION TECHNIQUES

In Phase Disposition PWM (IPDPWM): In this method all four carrier waves are in phase. The converter is switched to $+V_{dc}/2$ when the sine wave is greater than both upper carrier waves. The converter is switched to $+V_{dc}/4$ when the sine wave is greater than first upper carrier waves. The converter is switched to zero when sine waveform is lower than upper carrier waveforms and higher than lower carrier waveforms. The converter is switched to $-V_{dc}/4$ when sine wave is less than first lower carrier waveform. The converter is switched to $-V_{dc}/2$ when sine wave less than both lower carrier waveforms. This method is shown Fig. 2

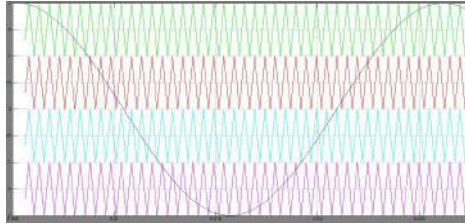


Fig. 2 In Phase Disposition Pulse Width Modulation (IPDPWM)

Phase Opposition Disposition PWM (PODPWM): In this method, four carrier waveforms are arranged so that all carrier waveforms above zero are in phase and they are 180° out of phase with those below zero. This is shown in Fig. 3

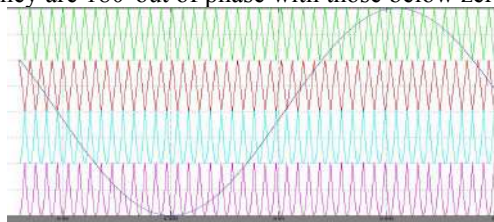


Fig.3 Carrier arrangement for Phase opposition disposition PWM (PODPWM)

Alternate Phase Opposition & Disposition PWM (APODPWM) : In this method, four carrier waveforms are arranged so that alternate carriers waveforms are 180° out of phase with those other two alternate waveforms. This is shown in Fig. 4

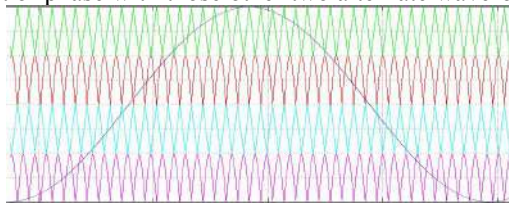


Fig.4 Carrier arrangement for Alternate Phase opposition disposition PWM (APODPWM)

Phase Shift PWM (PSPWM): In this method four carrier waveforms are arranged so that there is phase shift of 90° between each carrier waveforms. This is shown in Fig. 5

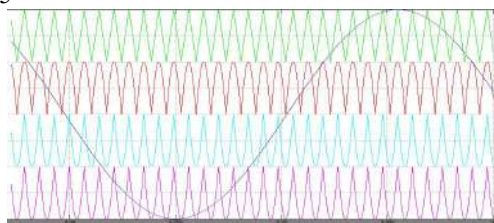


Fig. 5 Carrier arrangement for Phase Shift PWM (PSPWM)

Alternate Phase Shift PWM (APSPWM): In this method alternate carrier wave forms are shifted by 90° . This is shown in fig. 6

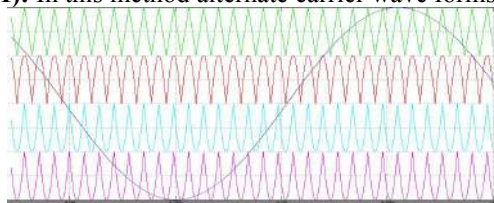


Fig. 6 Carrier arrangement for Alternate Phase Shift PWM (APSPWM)

Carrier Overlap PWM(COPWM): In this method four carrier waveforms overlap each other .This is shown in Fig. 7

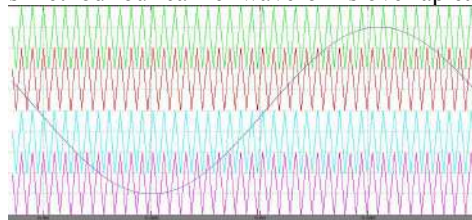


Fig. 7 Carrier arrangement for Carrier Overlap PWM(COPWM)

Variable Frequency PWM (VFPWM):In this method four carrier waveforms have different frequencies .This is shown in Fig. 8.

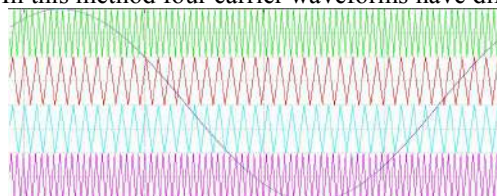


Fig. 8 Carrier arrangement for Variable Frequency PWM (VFPWM)

Alternate Variable Frequency PWM(AVFPWM): In this method alternate carrier waveforms frequencies are varied. This is shown in Fig. 9.

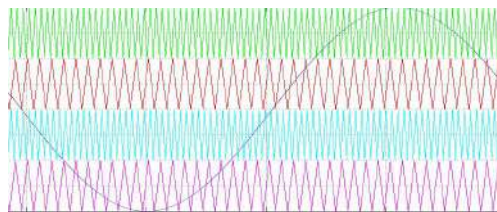


Fig. 9 Carrier arrangement for Alternate Variable Frequency PWM (AVFPWM)

Alternate Phase Disposition & Alternate Phase Shift PWM(APDAPSPWM): In this method , two alternate waveforms are 180⁰ out of phase and remaining two alternate waveforms are 90⁰ phase shift. This is shown in Fig. 10 .

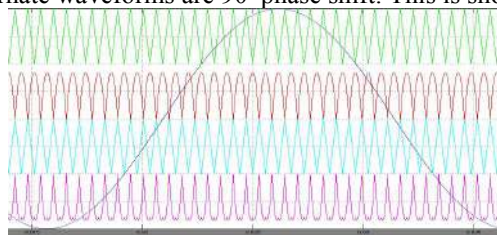


Fig. 10 Carrier arrangement for Alternate Phase Disposition & Alternate Phase Shift PWM(APDAPSPWM)

The above modulation techniques are having their own advantages and disadvantages several authors[6 - 8] compared their performances using simulation techniques.

V. RESULTS

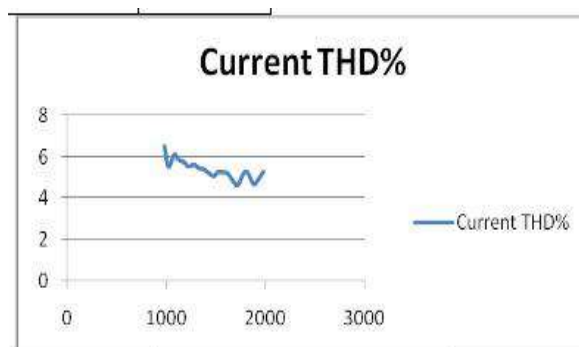


Fig. 11.In Phase Disposition PWM Stator Current THD

Fig. 11.Illustrates the variation of Stator Current THD with carrier frequency in- In Phase Disposition PWM .As the carrier frequency is varied from 980 Hz. to 1980 Hz. , the THD is varying between 4% and 7%.The minimum THD is 4.61 at 1720 Hz.

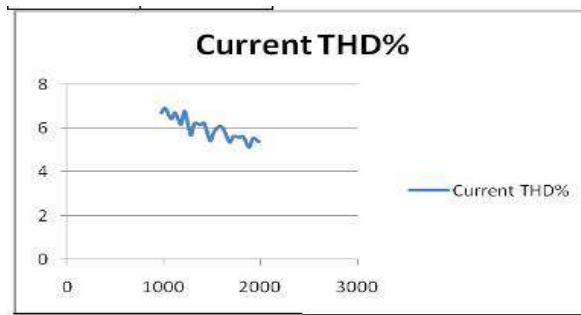


Fig. 12 Phase Opposition Disposition PWM Stator Current THD

Fig. 12. Illustrates the variation of Stator Current THD with carrier frequency in Phase Opposition Disposition PWM. As the carrier frequency is varied from 980 Hz. to 1980 Hz., the THD is varying between 5% and 7%. The minimum THD is 5.13 at 1880 Hz.

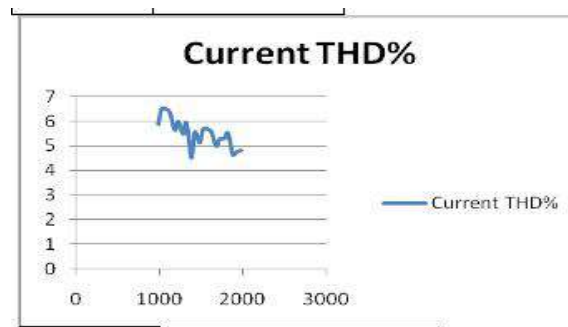


Fig. 13 Alternative Phase Opposition & Disposition PWM Stator Current THD

Fig. 13. Illustrates the variation of Stator Current THD with carrier frequency in Alternative Phase Opposition & Disposition PWM. As the carrier frequency is varied from 980 Hz. to 1980 Hz., the THD is varying between 4% and 7%. The minimum THD is 4.5 at 1380 Hz.

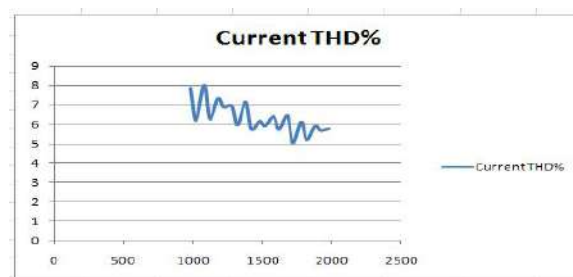


Fig. 14 Phase Shift PWM Stator Current THD

Fig. 14. Illustrates the variation of Stator Current THD with carrier frequency in Phase Shift PWM. As the carrier frequency is varied from 980 Hz. to 1980 Hz., the THD is varying between 5% and 8%. The minimum THD is 5.02 at 1720 Hz.

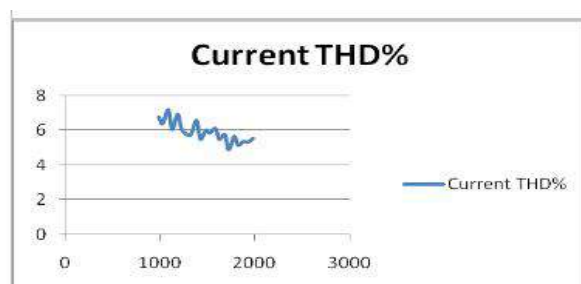


Fig. 15 Alternate Phase Shift PWM Stator Current THD

Fig. 15. Illustrates the variation of Stator Current THD with carrier frequency in Alternate Phase Shift PWM. As the carrier frequency is varied from 980 Hz. to 1980 Hz., the THD is varying between 4.5% and 7.5%. The minimum THD is 4.89 at 1720 Hz.

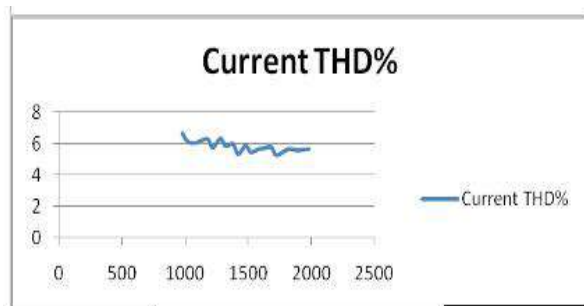


Fig. 16 Carrier Overlap PWM Stator Current THD

Fig. 16 .Illustrates the variation of Stator Current THD with carrier frequency in Carrier Overlap PWM .As the carrier frequency is varied from 980 Hz. to 1980 Hz. , the THD is varying between 5% and 7%.The minimum THD is 5.25 at 1720 Hz.

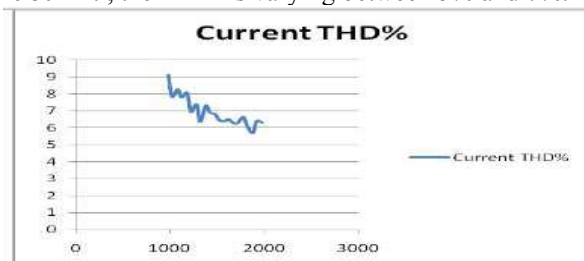


Fig. 17 Variable Frequency PWM Stator Current THD

Fig. 17 .Illustrates the variation of Stator Current THD with carrier frequency in Variable Frequency PWM .As the carrier frequency is varied from 980 Hz. to 1980 Hz. , the THD is varying between 5.5% and 9.5%.The minimum THD is 5.71 at 1880 Hz

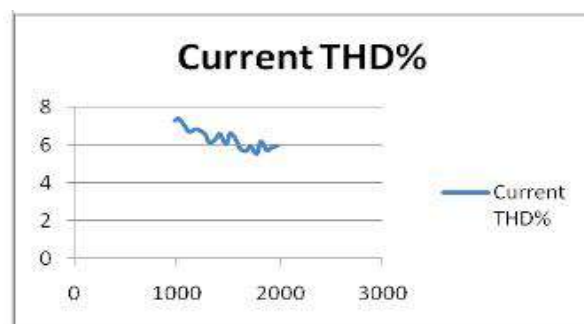


Fig. 18 Alternate Variable Frequency PWM Stator Current THD

Fig. 18 .Illustrates the variation of Stator Current THD with carrier frequency in Alternate Variable Frequency PWM .As the carrier frequency is varied from 980 Hz. to 1980 Hz. , the THD is varying between 5.5% and 7.5%.The minimum THD is 5.51 at 1780 Hz

VI. CONCLUSION

It is clear from above results that the In Phase Disposition PWM , Alternative Phase Opposition & Disposition PWM and Alternate Phase Shift PWM techniques are best as the THD is below 5% . As per IEEE standards the THD should be below 5%.

REFERENCES

- [1] Jose Ignacio Leon Galvan "Multilevel converters: topologies, modeling, SVM techniques and optimization"; Doctoral thesis, University of Seville
- [2] M.V.Subramanyam, P.V.N.Prasad "SPWM Techniques in closed loop control of five level inverter fed 3 Φ Induction motor" , The IUP Journal of Electrical and Electronics Engineering, Vol VII, no. 4,2014,pp 43-53
- [3] R.Teodorescu, F.Beaabjerg, J.K.Pedersen, E.Cengeki, S.Sulistijo,Woo and P.Enjeti "Multi-Level Converters ; A Survey" in Proc. European power electronics conference, Switzerland 1999
- [4] Ying Cheng, Mariesa L Crow "A Diode Clamped Multi-level Inverter for the Statcom/BESS"; University of Missouri, USA
- [5] M.V.Subramanyam,S.Mani Kuchibhotla. P.V.N. Prasad-"Effect of carrier frequency on THD in closed loop control of 5-level Multi-Level Inverter fed 3 phase induction motor"- International Journal of Scientific & Engineering Research. Volume 4. Issue 5, May -2013. pp 804—809.
- [6] Reddy V Naga Bhaskar, Babu Ch. Sai and Suresh K, "Advanced Modulation Techniques for Diode Clamped Multi Level Inverter Fed Induction Motor" ARPJ Journal of Engineering and Applied Sciences. Vol. 6, No. 1,ISSN 1819 – 6608, 2011.
- [7] F arid Berrezzek and F arid Berrezzek "A Study of New Techniques of Controlled PWM Inverters ", European Journal of Scientific Research, Vol. 32, No. 1,pp 77-87,ISSN 1450-218X, 2009.
- [8] Balamurgan C R, Natrajan S P, and Bensraj R "Investigations on Three Phase Five Level Diode Clamped Multi Level Inverter" , International Journal of Modern Engineering Research(IJMER), Vol. 2, No. 3, pp 1273 – 1279,ISSN 2249 6645, 2012.



MATRUSRI ENGINEERING COLLEGE

(Approved by AICTE, Affiliated to Osmania University)

#16-1-486, Saidabad, Hyderabad - 500059



Sponsored by

MATRUSRI EDUCATION SOCIETY



ISBN: 97881-936274-0-2



1ST NATIONAL CONFERENCE ON TRENDS IN SCIENCE, ENGINEERING AND TECHNOLOGY (NTSET - 2018)

February 2nd & 3rd - 2018

TECHNICAL PAPER ABSTRACTS



ORGANIZED BY

MATRUSRI ENGINEERING COLLEGE

(Approved by AICTE, Affiliated to Osmania University)

#16-1-486, Saidabad, Hyderabad - 500059



Sponsored by

MATRUSRI EDUCATION SOCIETY

ISBN: 97881-936274-0-2

**NTSET
2018**





MODELLING OF SSSC TO ENHANCE THE POWER SYSTEM STABILITY USING MATLAB

N.Kalpana¹, M.Saritha²

¹Assistant Professor, Department of EEE, Matrusri Engineering College, Hyderabad

²Assistant Professor, Department of EEE, Matrusri Engineering College, Hyderabad

Email: 'kalpana924@yahoo.com, ² saritha.nagasai@gmail.com

Abstract: In this paper, a very efficient approach to control the power flow through the transmission line is given. A static synchronous series compensator (SSSC) is used as controller. It controls the active and reactive power as well as damping power system oscillation in transient mode. The SSSC is equipped with a source of energy in DC link can apply or absorb the reactive power to or from the transmission line. Simulation results are obtained for the selected bus-2 in two machine power system which shows the efficiency of this compensator as one of the FACTS devices member in controlling the power flow, achieving the desired value of active and reactive powers, and damping the power oscillation.

Key words: Static synchronous series compensator(SSSC), FACTS, Active and reactive powers and transmission line.

I. INTRODUCTION

Now a days reliability of power system is big concern to ensure uninterrupted power supply. becoming more complex from operation, control and stability maintenances a big issue when they meet ever increasing load demand[1] The power flow in ac power system give the significant electrical storage, the electrical generation and load must balance at all times [2]. One of the most important problems in the control of power transmission systems is the reactive power compensation. Reactive power causes the increase in the transmission systems losses, decrease in power capacity carried decrease in power transfer capacity in the transmission lines and leads to voltage instability. Hence it is necessary to improve Active and reactive powers in order to increase transmittable power, and provide voltage stability.

This paper investigates the static synchronous series compensator (SSSC) that belongs to the Flexible AC Transmission Systems (FACTS) family to control power flow and improve active and reactive powers by injecting the voltage in series with the transmission line where it is connected. It consists of a solid state voltage source converter (VSC) which generates a controllable alternating current voltage at fundamental frequency. When the injected voltage is kept in quadrature with the line current, it can emulate as inductive or capacitive reactance so as to influence the power flow through the transmission line [2,3]. While the primary purpose of a SSSC is to control power flow in steady state, it can also improve transient stability of a power system.

II. FLEXIBLE AC TRANSMISSION SYSTEM (FACTS)

Flexible AC Transmission System (FACTS) is the well-known concept which is more needed [4]. The FACTS devices have main purposes of power flow regulation, power loss reduction, power oscillation damping, cost reduction and transmission routes power flow control [8].

The of FACTS devices has many advantages that are listed below,

- Control of Power flow
- Rise of transmission capability
- Increase the loading capability
- Reactive power compensation with controllers
- System security
- Provides greater flexibility
- The problem of voltage fluctuation and flickers can be reduced
- Reduce the reactive power flows and loop flow
- Prevention of cascading outages by contributing to emergency control

III. BASIC SSSC CONFIGURATION

Fig. 1 shows The basic circuit diagram of the SSSC. The compensator is equipped with a source of energy, which helps in supplying or absorbing active power to or from the transmission line along with the control of reactive power flow. The dc capacitor has been replaced by an energy storage device such as a high energy battery installation to allow active as well as reactive power exchanges with the ac system. The SSSC's output voltage magnitude and phase angle can be varied in a controlled manner to influence power flows in a transmission line. The phase displacement of the inserted voltage, with respect to the transmission line current, determines the exchange of real and reactive power with the ac system [3]

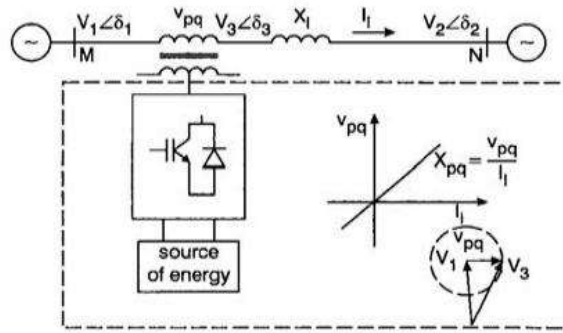


Fig1: Static Synchronous Series compensator (SSSC)

IV.TWO MACHINE MODEL OF SSSC

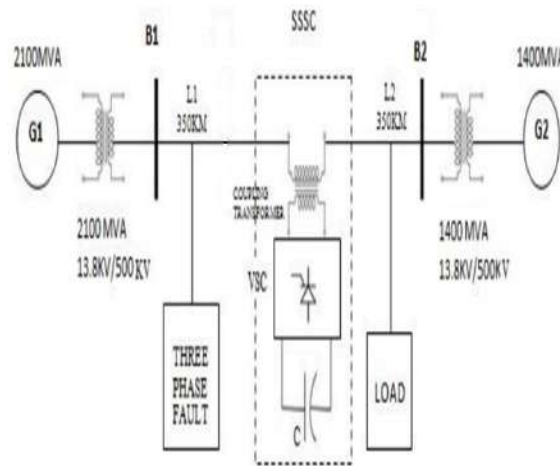


Fig2. Single line diagram of two machine power system

V. FLOW CHART OF WORKING OF SSSC

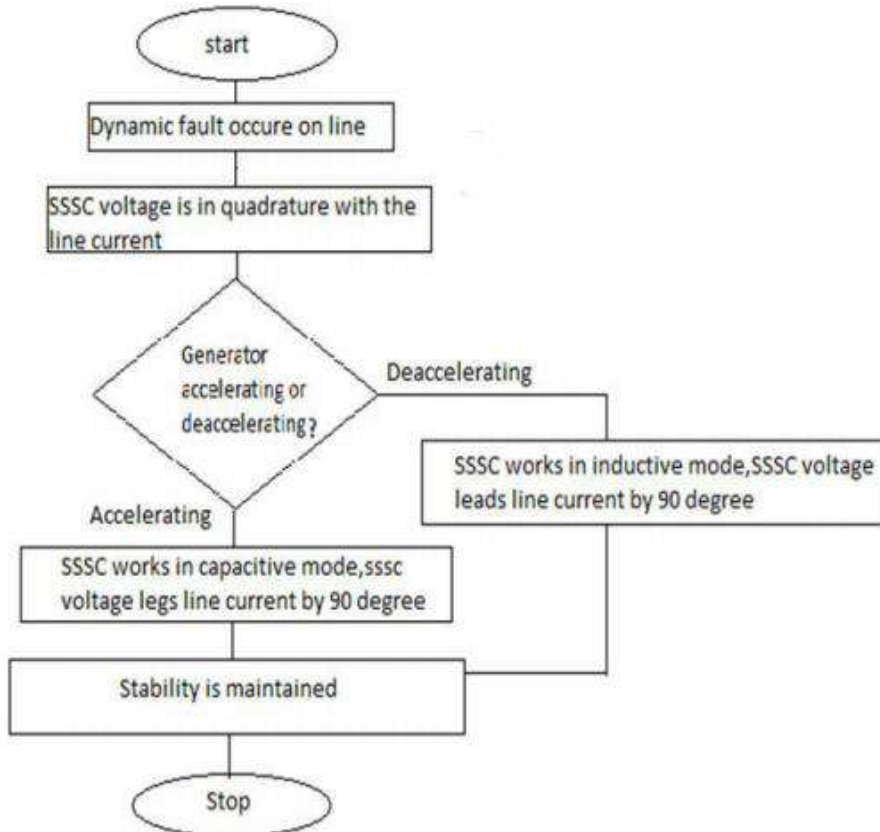


Fig3.Flow chart of working of SSSC using in to the power system

VI. SIMULATION RESULTS WITH MATLAB/SIMULINK

The functional performance of SSSC is given by the real time voltage wave forms. By using the MATLAB environment tool shown in fig. , it is obtained on real time, in proposed simulation SSSC is coupled to the power transmission line of having 500KV by coupling transformer. The proposed system is having made into ring mode which consist of two buses(B1 and B2) connected to the transmission line having 500kv transmission lines. The system is having two sources of three phase of 500KV and the base voltage is also 500KV.

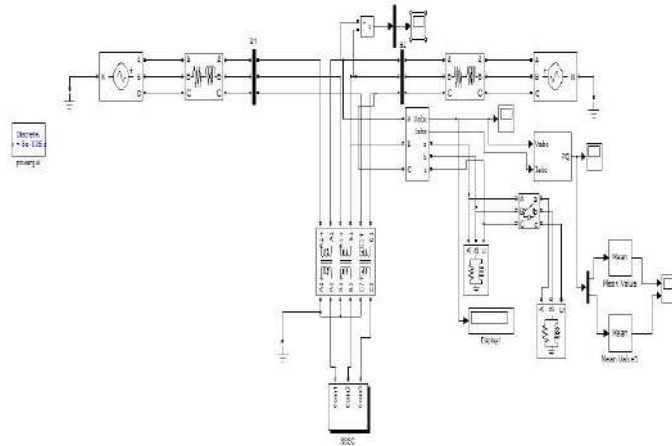


Fig4: Simulation of two machine bus system

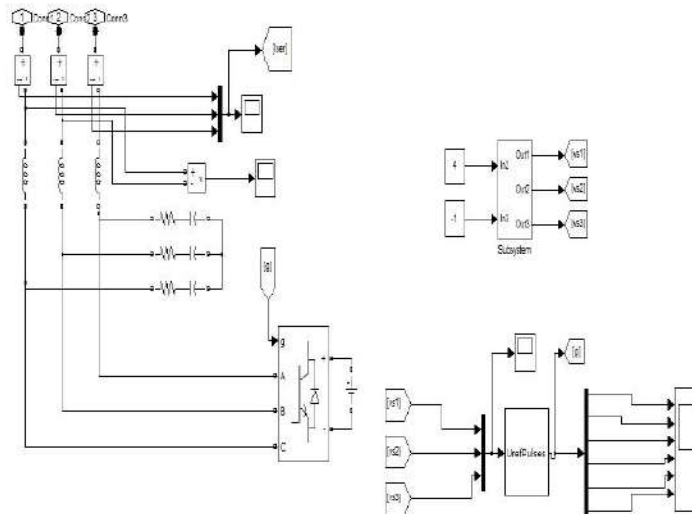


Fig5: Simulation of SSSC

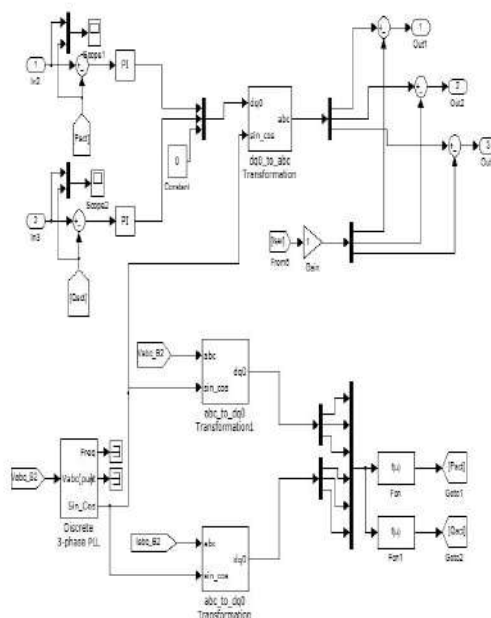


Fig6: Simulation of sub system



VII. EXPERIMENTAL RESULTS

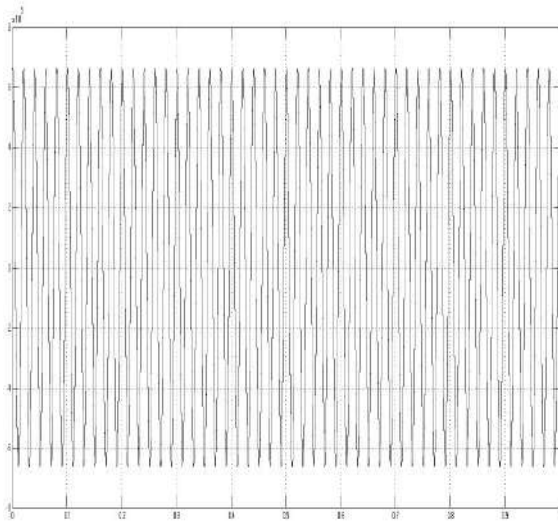


Fig7:Waveform of voltage of bus 2 with out SSSC

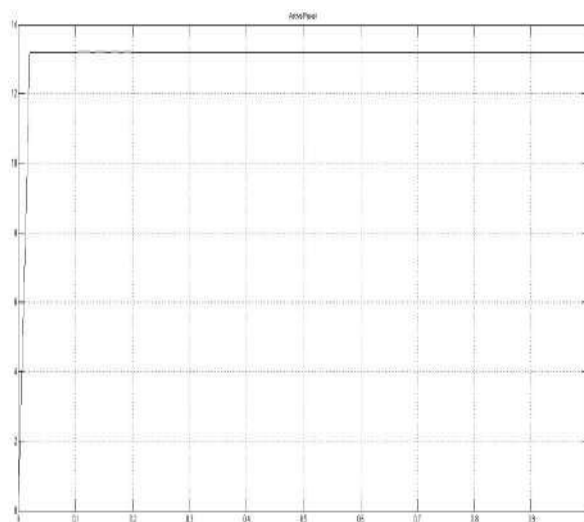


Fig8. Waveform of active power with out SSSC

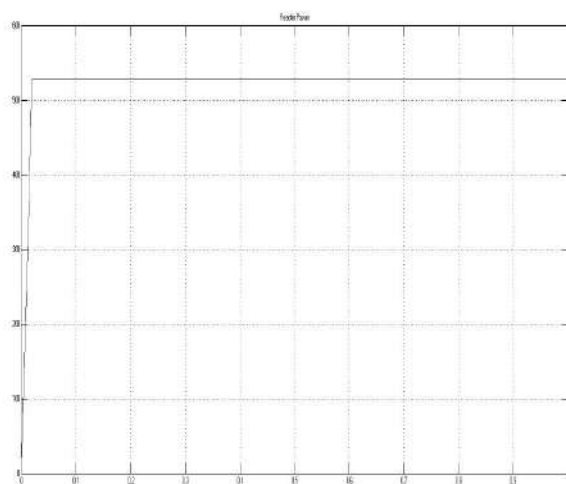


Fig9.:waveform of reactive power with out SSSC

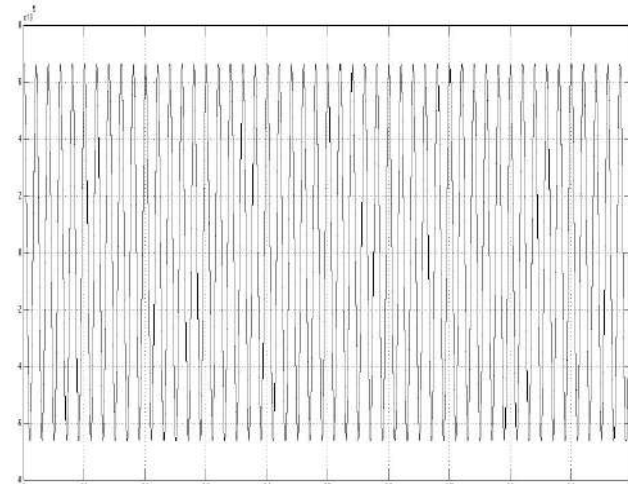


Fig10:waveform of voltage of bus 2 with SSSC

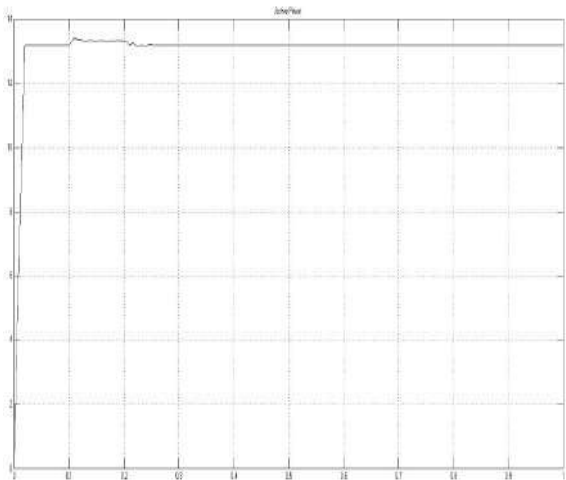


Fig11:waveform of active power with SSSC

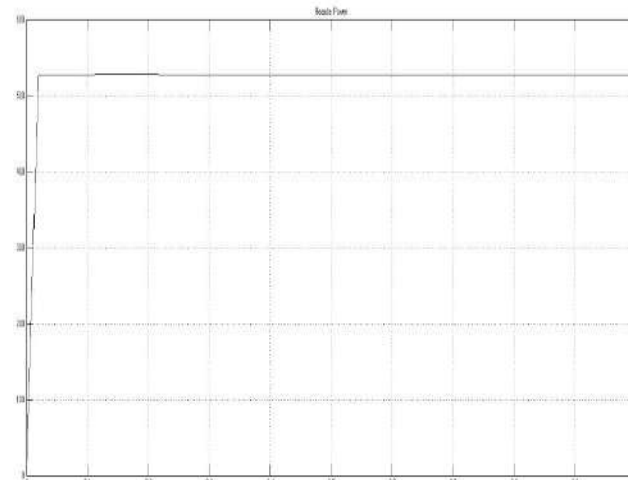


Fig12: waveform of reactive power with SSSC

The changes into the parameter like voltage. Active and reactive power is obtained in to the real time. Regarding to that, system having large loads causes the system active power of bus-2 got oscillated and it keep continuing, the oscillations of the active power are more than that of the reactive power because the ohmic parts of the loads are greatly more.



REFERENCES

- [1] SSSC-static synchronous series compensator: theory, modeling, and application [IEEE Transactions on Power Delivery](#) Volume: 13, [Issue: 1](#), Jan 1998.
- [2] N.G Hingorani, 201 1, "Understanding facts: concepts Technology of flexible AC transmission system",IEEE Power Engg. IEEE press, Wiley India.
- [3] B.Suresh Kumar, Enhancement of Voltage Stability using Static Synchronous Series Compensator (SSSC) with PI Controller LLLG Fault, International Journal of Advanced Research in Engineering & Technology (IJARET), Volume 4, Issue 5, 2013, pp. 164 175, ISSN Print: 0976 6480, ISSN Online: 0976 6499
- [4] "Power System Stability Enhancement Using Static synchronous Series Compensator (SSSC)" by M. Faridi & H. Maeiiat Electrical Engg, EEE department. Islamic Azad University-Ahar-Branch, Ahar, Iran, IEEE, 2011.
- [5] "Dynamic Compensation of AC transmission line by solid- state synchronous voltage sources" by Laszlo gyugi, fellow, IEEE Westinghouse Electric Corporation Pittsburg, Pennsylvania 15235, IEEE Transaction on power delivery, Vol.9, No. 2, April 1994.
- [6] Stability Improvement and Power Oscillation Damping Using Static Synchronous Series Compensator (SSSC) International Journal of Advanced Research in Science, Engineering and Technology Vol. 2, Issue 1 , January 2015 . Mythili



MATRUSRI ENGINEERING COLLEGE

(Approved by AICTE, Affiliated to Osmania University)

#16-1-486, Saidabad, Hyderabad - 500059



Sponsored by

MATRUSRI EDUCATION SOCIETY



ISBN: 97881-936274-0-2





SINGLE PHASE QUASI-Z-SOURCE BASED MODIFIED CASCADED MULTILEVEL INVERTER WITH HALF-BRIDGE CELL

K.Kartheek¹, B.Madhukar², P.Anil Kumar³

¹Assistant Professor, Department of EEE, Matrusri Engineering College, Hyderabad

²Assistant Professor, Department of EEE, Matrusri Engineering College, Hyderabad

³Assistant Professor, Department of EEE, Matrusri Engineering College, Hyderabad

Email: kkartheek19@gmail.com, madhukar148@gmail.com, anilkumar.palarapu@gmail.com

Abstract: In this paper a new Quasi-Z-Source Modified Cascaded Multilevel Inverter with Half-Bridge Cell is presented and proved to be advantageous over conventional Cascaded Multilevel Inverter with voltage boost ability and reduced switches. The proposed topology is comprised of cascaded auxiliary units and a full H-bridge inverter, where the auxiliary unit includes half bridge cell with quasi Z Source network. With quasi Z Source network shoot-through state control, the output voltage amplitude can be boosted, which is not limited to DC source voltage summation similar to conventional cascaded Multilevel Inverter. The performance parameters of quasi Z Source Modified Cascaded Multilevel Inverter with various multicarrier PWM control methods are analyzed with simulation results and portrayed here.

Keywords—CHB, MLI, SPWM

1. INTRODUCTION

A circuit that converts dc power into ac power at desired output voltage and frequency is called an inverter. Some industrial applications of inverters are for adjustable speed ac drives, induction heating, stand by air-craft power supplies, UPS (uninterruptible power supplies) for computers, HVDC transmission lines etc. The dc power input to the inverter is obtained from an existing power supply network or from a rotating alternator through a rectifier or a battery, fuel cell, photovoltaic array or magneto hydrodynamic (MHD) generator. The configuration of ac to dc converter and dc to ac inverter is called a dc-link converter. The rectification is carried out by standard diodes or thyristor converter circuits. Inverters can be broadly classified into two types: voltage source inverters and current source inverters[1].

Now a day's many industrial applications have begun to require high power. Some appliances in the industries however require medium or low power for their operation. Using a high-power source for all industrial loads may prove beneficial to some motors requiring high power, while it may damage the other loads. Some medium voltage motor drives and utility applications require medium voltage. The multi-level inverter has been introduced since 1975 as alternative in high power and medium voltage situations. The Multi-level inverter is like an inverter and it is used for industrial applications as alternative in high power and medium voltage situations.

The need of multilevel converter is to give a high output power from medium voltage source. Sources like batteries, super capacitors, solar panel are medium voltage sources.

The multi-level inverter is to synthesize a near sinusoidal voltage from several levels of dc voltages. As number of levels increases, the synthesized output waveform has more steps, which provides a staircase wave that approaches a desired waveform. Also, as steps are added to waveform, the harmonic distortion of the output wave decreases, approaching zero as the number of voltage levels increases. The Multi-level inverters can be classified into three types. 1. Diode – clamped Multi-level inverter 2. Flying – capacitor Multi-level inverter 3. Cascade Multi-level inverter.

2. CASCADED H-BRIDGE MULTI-LEVEL INVERTER

Cascaded H-Bridge (CHB) configuration has recently become very popular in high power AC supplies and adjustable-speed drive applications. A cascade multilevel inverter consists of a series of H-bridge (single-phase full bridge) inverter units in each of its three phases. Each H-bridge unit has its own dc source, which for an induction motor would be a battery unit, fuel cell or solar cell. Each SDC (separate D.C. source) is associated with a single phase full-bridge inverter. The ac terminal voltages of different level inverters are connected in series. Through different combinations of the four switches, S1-S4, each converter level can generate three different voltage outputs, +Vdc, -Vdc and zero. The AC outputs of different full bridge converters in the same phase are connected in series such that the synthesized voltage waveform is the sum of the individual converter outputs.

3. NEW DESIGN OF MULTI-LEVEL INVERTER

3.1 Introduction

In recent trends, the quasi-Z-source inverter has engrossed ever-increasing applications in renewable energy sources such as Photovoltaic (PV) and wind energy systems [2]. The modern research revealed that the quasi-Z-source concept has been applied to cascaded H-bridge multilevel inverter that provides the combined advantages of traditional Cascaded Half-Bridge Multilevel Inverter [3], [4] and quasi-Z-Source Inverter. Quasi-Z-source cascaded multilevel inverter offered numerous merits over traditional Cascaded Half-Bridge Multilevel Inverter in distributed generation applications [5]. The balanced dc-link voltage and voltage boost capability are the most fruitful advantages of the quasi-Z-Source Cascaded Half-Bridge Multilevel Inverter. The switching device count increases as the number of levels increases in the conventional Cascaded Half-Bridge Multilevel Inverter that leads to higher switching losses and increased cost for designing the module. Modified Cascaded H-Bridge Multilevel Inverter has fascinated extensive interests in recent researches as it leads to reduced number of switches and minimized manufacturing cost.

Until now, there is no literature to provide the complete analysis of Quasi-Z-Source Based Modified Cascaded Multilevel Inverter. The novelty of this paper is to propose the Quasi-Z-Source Modified Cascaded Multilevel Inverter with Half-Bridge Cell presenting gorgeous advantages over conventional cascaded Multilevel Inverter with voltage boost ability and reduced number of switches. The quasi-Z-Source Modified Cascaded Multilevel Inverter has the ability of single stage power conversion with improved reliability and wide voltage control through boost factor and modulation index. The Quasi-Z-Source Modified Cascaded Multilevel Inverter also provides reduced THD and reliability against short-circuits. A multilevel output voltage waveform of the Quasi-Z-Source Modified Cascaded Multilevel Inverter is synthesized by the combination of multicarrier pulse width modulation technique and simple boost control that launches shoot-through states into the traditional zero states to control the Quasi-Z-Source Modified Cascaded Multilevel Inverter module. The boost control methods uses maximum modulation index to provide output voltage with high voltage gain. In this paper, Phase Disposition Pulse Width Modulation control scheme in combination with simple boost control on the proposed topology are analysed.

The conventional quasi-Z-Source Cascaded Half-Bridge Multilevel Inverter is shown in Fig 1. It has quasi Z source network consisting of two inductors (L1, L2), capacitors (C1, C2) and one diode (D1). The quasi Z source network shares the common ground with inverter, and the current drawn by the dc source is continuous.

This topology is a simplified Cascaded Half-Bridge inverter symmetric topology. The main advantage of proposed topology is less number of switches compared with conventional multilevel inverter.

- Number of Level (m)= 2n+1
- Number of Main Switches (s switch) = 2n
- Number of low frequency switches(s switches)=4

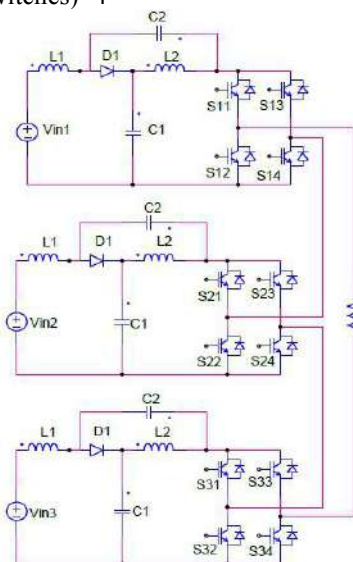


Fig.1 Conventional quasi-z-source cascaded h-bridge

Where 'm' is the number of output voltage level, 'n' number DC source switches. Figure.1 shows the general circuit diagram of proposed multilevel inverter. If number levels increases add one switch for each level, simple control circuitry. The Unique modulation strategies are applicable for this topology. The numbers of switches are required for each level and switches can be calculated from the above equations. To get a Positive half, properly turn ON the switches and the current flow from the point A to B will generate a positive polarity, the flow from B to A will generate the negative polarity as shown in below figure. In general, in order to achieve an equal voltage steps, the equal and same dc source voltage to be use. The unequal V_{dc} generate the different voltage steps. There are several multilevel inverters are commercialized for high power applications such as Flexible AC Transmission Systems Controllers, Train Traction, Automotive applications, renewable energy power conversion and transmission etc. This project proposes a new PV system based on quasi Z Source Cascaded Half-Bridge multilevel inverter. Now-a-days, the Z-source inverter and the quasi-Z-source inverter have been widely applied for renewable energy power generation system due to some unique features. They can implement voltage boost and power conversion simultaneously in a single stage, and improve the reliability due to the shoot-through cases no longer destroying the inverter. PV systems purely depends on solar energy and it is consistently shows its great potential to serve as a clean and inexhaustible renewable energy source.

At shoot-through states each PV array and quasi Z Source capacitors charge the inductors and diode is cut-off due to negative voltage.

3.2 Proposed Quasi-Z-Source Modified Cascaded Multilevel Inverter

The proposed topology of the Quasi-Z-Source Modified Cascaded Multilevel Inverter with Half-Bridge Cell is depicted as in the Fig.2. The circuit of the Quasi-Z-Source Modified Cascaded Multilevel Inverter is developed such that it can produce multi-level outputs with reduced number of semiconductor switches.

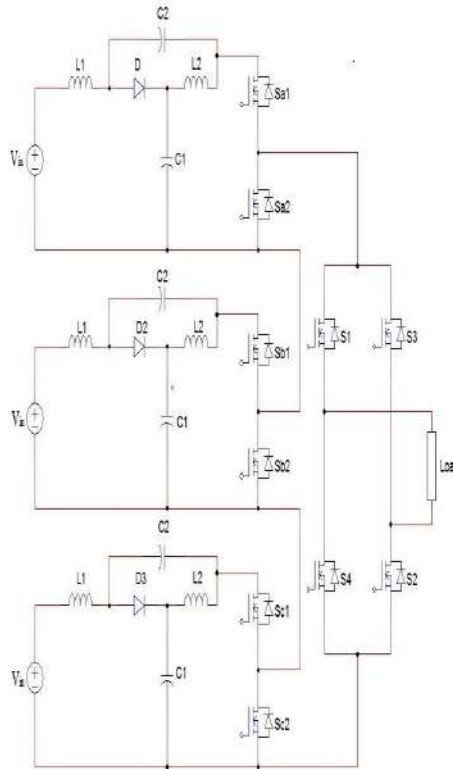


Fig.2 Reduced topology

This topology has cascaded auxiliary units and a full H-bridge inverter, where the auxiliary unit includes half bridge cell with quasi Z Source network. The quasi Z Source Modified Cascaded Multilevel Inverter module has a single stage voltage boost and inversion capability.

4. DESIGN PROCEDURE AND CIRCUIT OPERATION

4.1 New Design

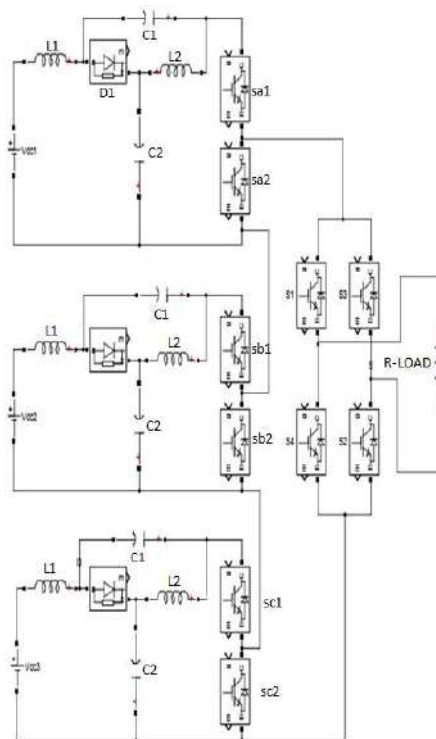


Fig.3 New design

Fig 3 shows a new 7-level inverter which consists of three main switches which are high frequency switches and also there four low frequency switches which are for polarity generation For V_{dc} the S2, S7, S3 switches are ON. The S1 is connected in positive terminal of the load and S3 is connected with negative terminal of the load through S7 for $+2V_{dc}$ and $+3V_{dc}$, switches S2 and S7. This new design has three DC sources.



4.2 Operation

The number of levels to be generated is based on the mathematical formula which is given as $m=2n+1$ where n =no of dc sources based on this the number of levels to be generated is calculated. The number of switches is also calculated using the mathematical formula i.e., $S=2n$

Hence for 7-level inverter three Dc sources are required and number of switches required is three. The number of low frequency switches is calculated by using mathematical formula

$$S=4$$

The frequency of low frequency switch is 50 HZ whereas the frequency of high frequency switch is 10 KHZ

4.3 Switching Sequence

The output voltage +1Vdc (first level) is produced across the load when switching on controlled switches Sa2, Sb2, Sc1, S1 and S2, and maintaining the remaining switches in off state. The output voltage +2Vdc (second level) is produced across the load by turning on the switches Sa2, Sb1, Sc1, and S2. Similarly, the output voltage +3Vdc is obtained by switching on Sa1, Sb1, Sc1, S1 and S2.

The following table shows the switching sequence of all the levels of proposed topology.

Sa1	Sb1	Sc1	Sa2	Sb2	Sc2	S1	S2	S3	S4	Voltage level
0	0	1	1	1	0	1	1	0	0	+ Vdc
0	1	1	1	0	0	1	1	0	0	+2 Vdc
1	1	1	0	0	0	1	1	0	0	+3 Vdc
1	1	1	1	1	1	1	1	1	1	0
1	1	0	0	0	1	0	0	1	1	-Vdc
1	0	0	0	1	1	0	0	1	1	-2 Vdc
0	0	0	1	1	1	0	0	1	1	-3 Vdc

This topology is operated in 2 modes

1. Shoot through state
2. Non-shoot through state

4.4 Shoot Through State

The shoot-through zero state is provided by the LC and diode network. This network defends the circuit from damage during the shoot-through zero state by storing energy in L and C. The quasi Z Source network boosts the dc-link voltage with the help of stored energy in the network elements.

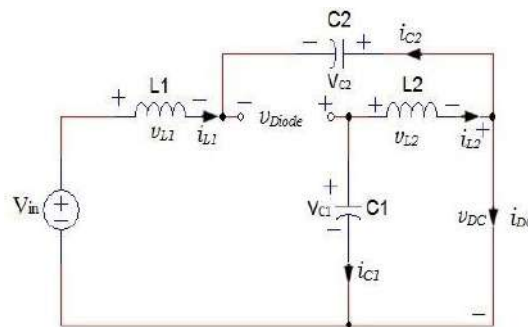


Fig.4 Equivalent circuit of quasi Z Source Modified Cascaded Multilevel Inverter in shoot-through state

4.5 Non-Shoot Through State

But, in non-shoot through state the power is transmitted from dc side to ac side. There is no power transmission during shoot-through state since the dc-link voltage is zero.

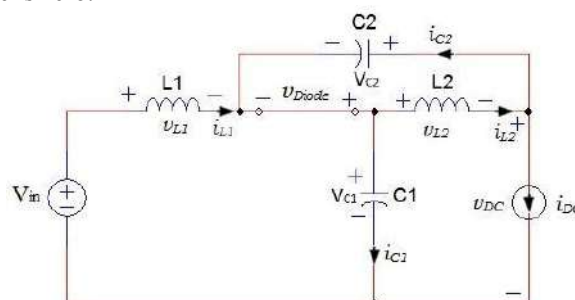


Fig.5 Equivalent circuit of quasi Z Source Modified Cascaded Multilevel Inverter in non-shoot-through state

4.6 Equations

The fundamental equations governing the operation of the quasi Z Source Modified Cascaded Multilevel Inverter are given below. The average value of the voltage across capacitor C1 is given

$$v_{c1} = \frac{1-D}{1-2D} v_{in}$$

The average value of the voltage across capacitor C2 is given

$$v_{c2} = \frac{D}{1-2D} v_{in}$$

The average value of the currents through the inductors L1 and L2 are given

$$I_{L1} = I_{L2} = \frac{1-D}{1-2D} V_{in}$$

The average value of DC link voltage is given

$$V_{DC} = \frac{1}{1-2D} V_{in} = BV_{in}$$

The average value of AC output voltage is given

$$V_{ac} = M * B * \frac{V_{in}}{2}$$

The boost factor B is given

$$B = \frac{1}{1-2D}$$

The voltage gain G is given

$$G = M * B$$

Where, M is the modulation index and V_{in} is the input dc voltage to the quasi-Z-Source network.

Each boosted voltage from the quasi-Z-Source network is connected in cascade with other boosted voltages through the half bridge cell comprising of one active switch and one diode that can generate multilevel positive output voltage. The full H-bridge unit is connected with the cascaded auxiliary units to acquire both positive and negative multilevel positive output voltage.

I. MODULATION TECHNIQUES

The following are the multilevel Modulation techniques.

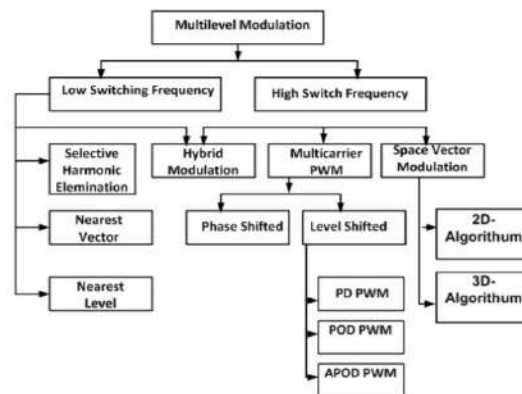


Fig 6 Multilevel modulation techniques

Multiple Pulse Width Modulation Technique is used in three level or more than three levels. These are classified into two types: - Level Shift, Phase Shift. In this paper we used the level shifted modulation technique[6,7].

There are three different types of level shifted SPWM strategies with differing phase relationships:

Phase disposition(PD)- All carrier waveforms are in phase.

Phase opposition disposition

(POD) – All carrier waveforms above zero reference are in phase and are 180° out of phase with those below zero.

Alternate phase disposition

(APOD) – Every carrier waveform is in out of phase with its neighbor carrier by 180°.

In this paper simulation results using POD method are shown

5.1 Phase Opposition Disposition (POD)

In phase opposition disposition (POD) modulation all carrier waveforms above zero reference are in phase and are 180 degrees out of phase with those below zero.

Carrier arrangements for PODPWM strategy The rules for the phase opposition disposition method, when the number of level $N = 7$ are The $N - 1 = 6$ carrier waveforms are arranged so that all carrier waveforms above zero are in phase and are 180 degrees out of phase with those below zero. There are 3 carrier waveforms above the reference zero line and other 3 carrier waveforms with 180 degree shift are below the zero reference line. The converter switches to + Vdc when the reference is greater than 1st positive carrier waveform. The converter switches to +2Vdc when the reference is greater than the 2nd positive carrier

waveform. The converter switches to +3Vdc when the reference is greater than the uppermost 3rd positive carrier waveform. The converter switches to 0 when the reference is lesser than all positive carrier waveforms as well as lesser than negative carrier waveforms.

The converter switches to - Vdc when the reference is lesser than 1st negative carrier waveform. The converter switches to - 2Vdc when the reference is lesser than 2nd negative carrier waveform. The converter switches to - 3Vdc when the reference is lesser than 3rd lowermost negative carrier waveform.

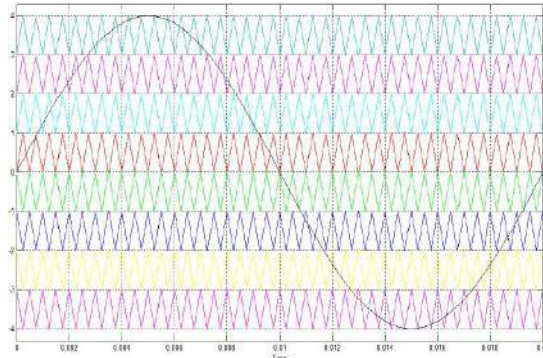


Fig.7 POD technique

For phase opposition disposition (POD) modulation all carrier waveforms above zero reference are in phase and are 180 degrees out of phase with those below zero[6,7].

II. SIMULATION DESIGN AND RESULTS

6.1 Matlab/Simulation Design of Proposed MLI

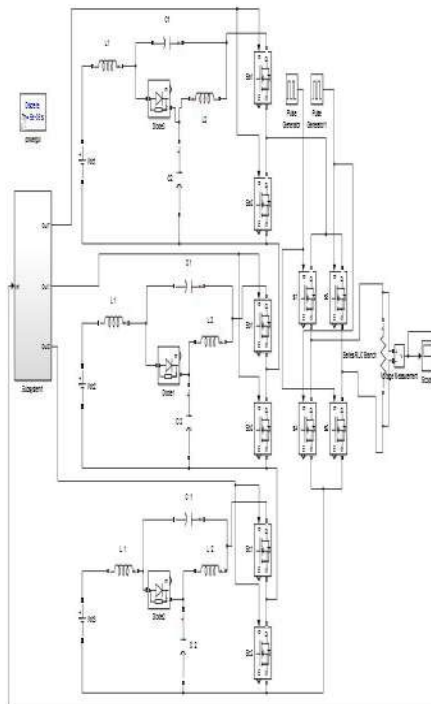


Fig.8 Proposed 7 level quasi Z Source Modified Cascaded Multilevel Inverter topology

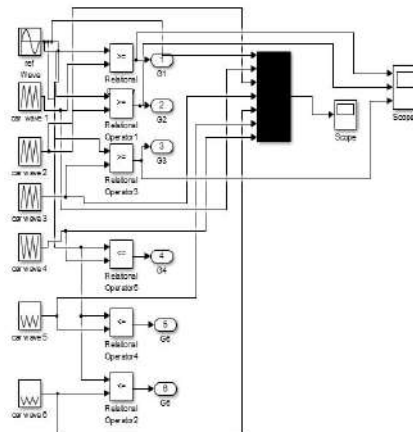


Fig.9 Sub-system of Simulink model of Sinusoidal Pulse with modulation.

Components used:

- 1) Number of dc sources = 3
- 2) Number of IGBT high frequency switches = 6
- 3) Number of IGBT high frequency switches = 4
- 4) Resistive load = 50 ohms

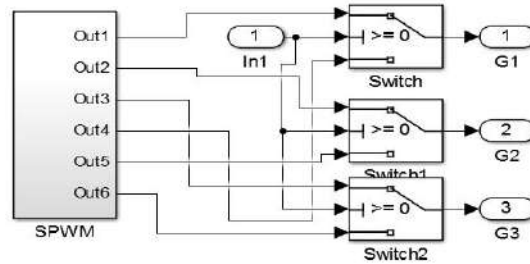


Fig.10 Sub-system of Proposed MLI using SPWM inverter topology.

It is the 7-level cascaded multilevel Inverter output.

6.3 Output of Phase Disposition

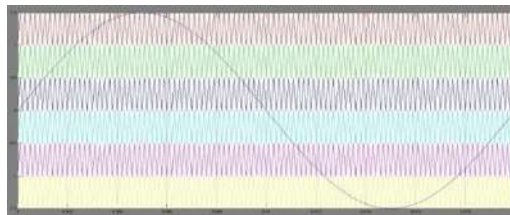


Fig.12 Phase Disposition

- **Phase disposition (PD)** – Here all carrier waveforms are in phase with each other.

6.4 Output of Impedances and Dc Link Voltages

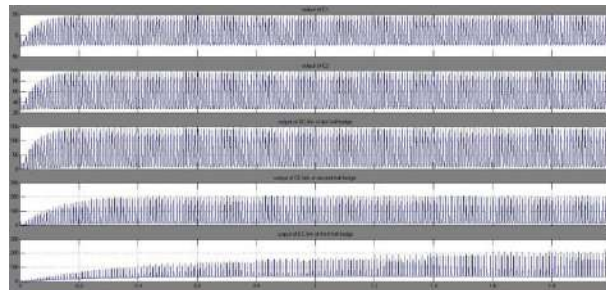


Fig.13 Impedances and DC link voltages

6.5 Output of Proposed Quasi Z Source Multilevel Inverter

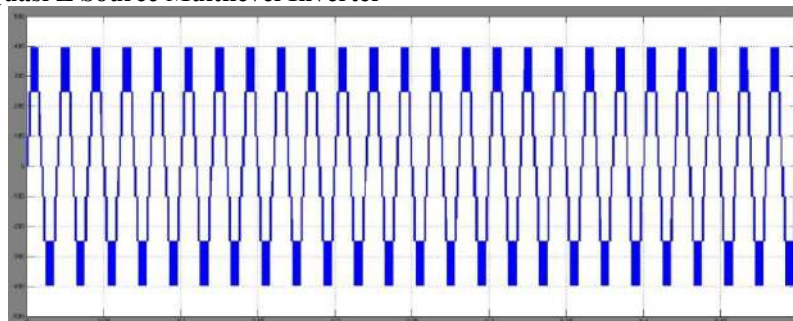


Fig.14 Cascaded half-bridge output with Z-source

In the fig 11 we observe that the output voltage is 150V which is equal to input magnitude but the output of quasi-Z-source multilevel inverter which is shown in fig 14 has boosted to 400V.

III. CONCLUSION

The proposed quasi Z Source Modified Cascaded Multilevel Inverter topology provides attractive advantages like reduced number of switches, voltage boost ability not limited to input voltage (DC source) summation, single stage conversion and reliability against short-circuits. Using Phase Disposition PWM control method, the quasi Z Source Modified Cascaded Multilevel Inverter performance parameters are analysed and presented. The Phase Disposition-PWM control method combined with simple boost control technique provides better results. This proposed quasi Z Source Modified Cascaded Multilevel Inverter topology is more suitable and can be effectively used for Photo Voltaic based applications.



REFERENCES

- [1] L.G. Franquelo, J.Rodríguez, J.I.Leon, S. Kouro, R. ortillo, and M.A.M. Prats, “ The age of multilevel converters arrives,” IEEE Industrial Electronics Magazine, June 2008.
- [2] Yuan Li, Shuai Jiang, J.G. Cintron-Rivera, Fang Zheng Peng, "Modelling and control of quasi-Z-source inverter for distributed generation applications," IEEE Transactions on Industrial Electronics, vol. 60, no. 4, pp. 1532-1541, Apr. 2013.
- [3] J. Rodriguez, J.-S. Lai, and F. Z. Peng, “Multilevel inverters: A survey of topologies, controls, and applications,” IEEE Trans. Ind. Electron., vol. 49, no. 4, pp. 724–738, Aug. 2002.
- [4] J. Rodriguez, S. Bernet, B. Wu, J. O. Pontt, and S. Kouro, “Multilevel voltage-source-converter topologies for industrial medium- voltage drives,” IEEE Trans. Ind. Electron., vol. 54, no. 6, pp. 2930–2945, Dec. 2007.
- [5] Yushan Liu, Baoming Ge, Abu-Rub H., Peng F.Z., "An effective control method for quasi-Z-source cascade multilevel inverter-based grid-tie single-phase photovoltaic power system," IEEE Transactions on Industrial Informatics, vol.10, no.1, pp.399-407, Feb. 2014.
- [6] Y. Liu, B. Ge, H. Abu-Rub, Iqbal A., F. Z. Peng, "Modelling and controller design of quasi-Z-Source inverter with battery based photovoltaic power system," in 2012 IEEE Energy Conversion Congress and Exposition (ECCE), 15-20 Sept. 2012, pp.3119-3124.
- [7] J. Anderson and F. Z. Peng, “A class of quasi-Z-source inverters,” in Conf. Rec. IEEE IAS Annu. Meeting, Edmonton, Alta, Canada, Oct.2008, pp.1-7.
- [8] Y. Liu, B. Ge, H. Abu-Rub, F. Peng, “Phase-shifted pulse-width amplitude modulation for quasi-Z-source cascade multilevel inverter applied to PV power systems,” 2013 IEEE Energy Conversion Congress & Exposition (ECCE), Denver, USA, pp. 94-100, 15-20 Sept. 2013.

1ST NATIONAL CONFERENCE ON TRENDS IN SCIENCE, ENGINEERING AND TECHNOLOGY (NTSET - 2018)

February 2nd & 3rd - 2018

TECHNICAL PAPER ABSTRACTS



ORGANIZED BY

MATRUSRI ENGINEERING COLLEGE

(Approved by AICTE, Affiliated to Osmania University)

#16-1-486, Saidabad, Hyderabad - 500059



Sponsored by

MATRUSRI EDUCATION SOCIETY

ISBN: 97881-936274-0-2

**NTSET
2018**



SPWM TECHNIQUES IN FIVE LEVEL INVERTER

M.V.Subramanyam¹, P.Kishor², M.Srinivas³

¹Assistant Professor, Department of EEE, Matrusri Engineering College, Hyderabad

²Assistant Professor, Department of EEE, Matrusri Engineering College, Hyderabad

³Assistant Professor, Department of EEE, Matrusri Engineering College, Hyderabad

Email: subramanyam.mvs@gmail.com, parellykishore@gmail.com, srinureddy2005@gmail.com

Abstract: The five level inverter is most widely used inverter in medium and high voltage applications, since it has many advantages and easy to develop when compared to higher level(7 or 9) inverters. There are several modulation techniques and most popular among them is Sinusoidal Pulse Width Modulation.(SPWM). There are different Sinusoidal Pulse width Modulation techniques such as In Phase Disposition(IPD), Anti Phase Disposition(APD), Phase Opposition Disposition(POD), Phase shift(PS), Anti-Phase Shift(APS), Variable Frequency(VF), Anti-Variable Frequency(AVF) and Carrier Overlap(CO)The THD of different Sinusoidal Pulse width Modulation techniques are found as carrier frequency is varied and compared .

Keywords: five level inverter, modulation technique, pulse width modulation, phase disposition, phase shift, variable frequency.

I. INTRODUCTION

Multilevel Inverters have many advantages compared with and well known two level converters [1]. These advantages are fundamentally focused on improvements on the output quality and a nominal power increase in the inverter. The five level inverter is most widely used inverter in medium and high voltage applications, since it has many advantages and less complex architecture compared to higher level (7 or 9) inverters. There are several modulation techniques that can be used with 5 level inverters such as i) Sinusoidal Pulse Width Modulation (SPWM) technique ii) Selective Harmonic Elimination(SHE) and iii) Space Vector Modulation (SVM) technique. [2]. There are again different methodologies in SPWM technique such as 1)In Phase Disposition PWM (IPDPWM) 2)Phase Opposition Disposition PWM (PODPWM) 3)Alternative Phase Opposition & Disposition PWM(APODPWM) 4) Phase Shift PWM(PSPWM) 5) Alternate Phase Shift PWM(APSPWM) 6)Carrier Overlap PWM(COPWM) 7)Variable Frequency PWM (VFPWM) 8)Alternate Variable Frequency PWM(AVFPWM) 9)Alternate Phase Disposition & Alternate Phase Shift PWM(APDAPSPWM)[2].

II. MULTI LEVEL INVERTERS

Traditional two level and three level high frequency Pulse width modulated (PWM) inverters for motor drives has several problems associated with high frequency switching which produce common mode voltages and high rate of voltage change (dv/dt) to motor windings. The concept of using multiple small voltages to perform power conversion was introduced. These converters recently have found many applications in medium and high power applications. Recent advances in Power electronics made the multilevel concept practical. Based on the output voltage levels, inverters can be classified as two level inverters and Multi-level inverters. The inverters with voltage level 3 or more are referred as Multi-level inverters.[3]

The fundamental multilevel inverter topologies are diode clamped, flying capacitor and multilevel H-bridge. Diode clamped Multilevel Inverter is a very general and widely used topology for real power flow control. Normally n-level diode clamped Multilevel Inverter has $2(n-1)$ main switches and $2(n-1)$ main diodes. In addition, this topology needs $2(n-2)$ clamping diodes [4]. So in the five level diode clamped inverter 8 main switches, () 8 main diodes (D1 to D8) and 6 clamped diodes (DB1 to DB6) are used.[5] Fig.1 illustrates five level diode clamped multilevel inverter.

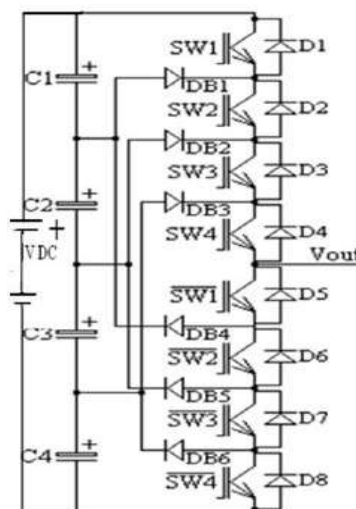


Fig. 1 One leg of Five Level diode clamped Multi-level inverter

III. SPWM MODULATION TECHNIQUES

In Phase Disposition PWM (IPDPWM): In this method all four carrier waves are in phase. The converter is switched to $+V_{dc}/2$ when the sine wave is greater than both upper carrier waves. The converter is switched to $+V_{dc}/4$ when the sine wave is greater than first upper carrier waves. The converter is switched to zero when sine waveform is lower than upper carrier waveforms and higher than lower carrier waveforms. The converter is switched to $-V_{dc}/4$ when sine wave is less than first lower carrier waveform. The converter is switched to $-V_{dc}/2$ when sine wave less than both lower carrier waveforms. This method is shown Fig. 2

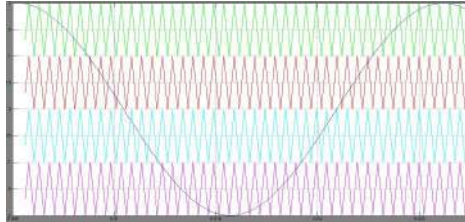


Fig. 2 In Phase Disposition Pulse Width Modulation (IPDPWM)

Phase Opposition Disposition PWM (PODPWM): In this method, four carrier waveforms are arranged so that all carrier waveforms above zero are in phase and they are 180° out of phase with those below zero. This is shown in Fig. 3



Fig.3 Carrier arrangement for Phase opposition disposition PWM (PODPWM)

Alternate Phase Opposition & Disposition PWM (APODPWM) : In this method, four carrier waveforms are arranged so that alternate carriers waveforms are 180° out of phase with those other two alternate waveforms. This is shown in Fig. 4

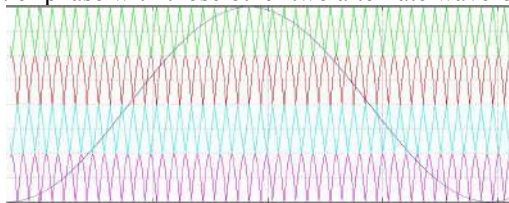


Fig.4 Carrier arrangement for Alternate Phase opposition disposition PWM (APODPWM)

Phase Shift PWM (PSPWM): In this method four carrier waveforms are arranged so that there is phase shift of 90° between each carrier waveforms. This is shown in Fig. 5

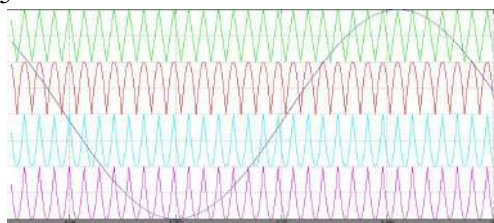


Fig. 5 Carrier arrangement for Phase Shift PWM (PSPWM)

Alternate Phase Shift PWM (APSPWM): In this method alternate carrier wave forms are shifted by 90° . This is shown in fig. 6

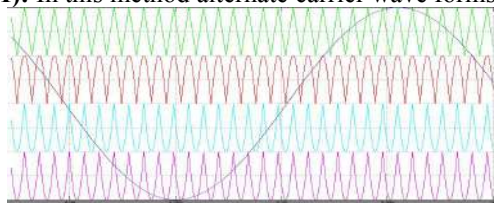


Fig. 6 Carrier arrangement for Alternate Phase Shift PWM (APSPWM)

Carrier Overlap PWM(COPWM): In this method four carrier waveforms overlap each other .This is shown in Fig. 7

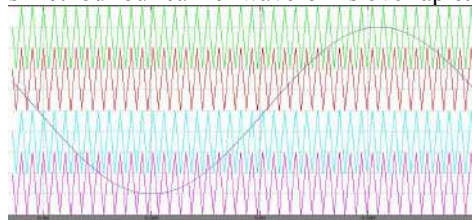


Fig. 7 Carrier arrangement for Carrier Overlap PWM(COPWM)

Variable Frequency PWM (VFPWM):In this method four carrier waveforms have different frequencies .This is shown in Fig. 8.

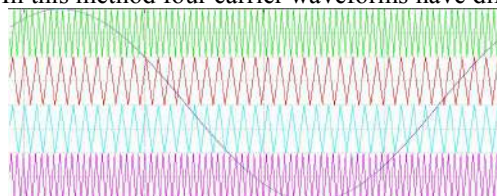


Fig. 8 Carrier arrangement for Variable Frequency PWM (VFPWM)

Alternate Variable Frequency PWM(AVFPWM): In this method alternate carrier waveforms frequencies are varied. This is shown in Fig. 9.

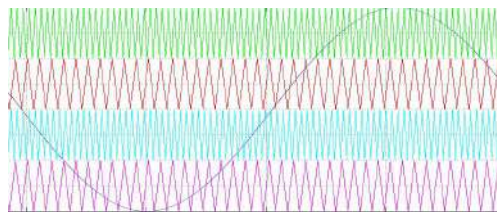


Fig. 9 Carrier arrangement for Alternate Variable Frequency PWM (AVFPWM)

Alternate Phase Disposition & Alternate Phase Shift PWM(APDAPSPWM): In this method , two alternate waveforms are 180^0 out of phase and remaining two alternate waveforms are 90^0 phase shift. This is shown in Fig. 10 .

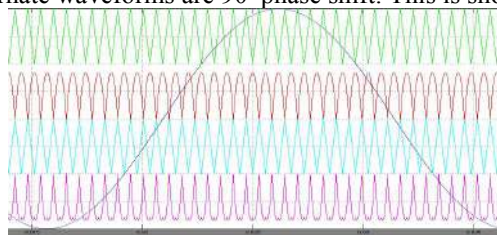


Fig. 10 Carrier arrangement for Alternate Phase Disposition & Alternate Phase Shift PWM(APDAPSPWM)

The above modulation techniques are having their own advantages and disadvantages several authors[6 - 8] compared their performances using simulation techniques.

V. RESULTS

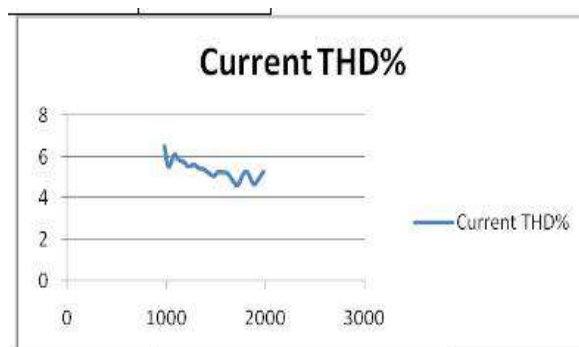


Fig. 11.In Phase Disposition PWM Stator Current THD

Fig. 11.Illustrates the variation of Stator Current THD with carrier frequency in- In Phase Disposition PWM .As the carrier frequency is varied from 980 Hz. to 1980 Hz. , the THD is varying between 4% and 7%.The minimum THD is 4.61 at 1720 Hz.

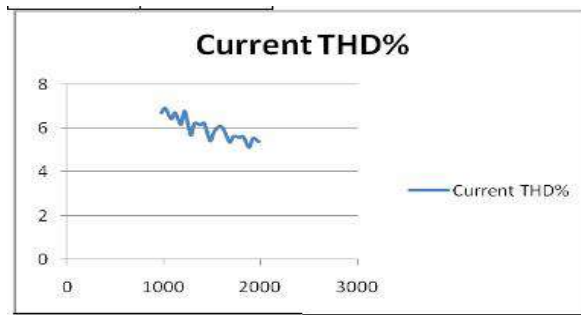


Fig. 12 Phase Opposition Disposition PWM Stator Current THD

Fig. 12. Illustrates the variation of Stator Current THD with carrier frequency in Phase Opposition Disposition PWM. As the carrier frequency is varied from 980 Hz. to 1980 Hz., the THD is varying between 5% and 7%. The minimum THD is 5.13 at 1880 Hz.

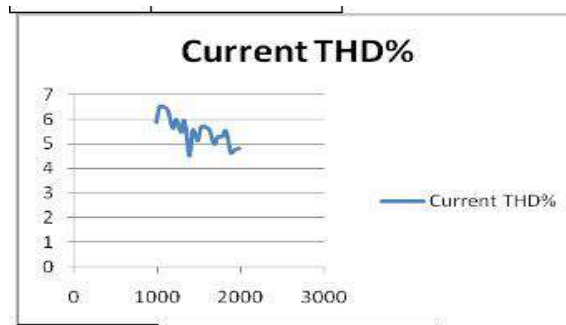


Fig. 13 Alternative Phase Opposition & Disposition PWM Stator Current THD

Fig. 13. Illustrates the variation of Stator Current THD with carrier frequency in Alternative Phase Opposition & Disposition PWM. As the carrier frequency is varied from 980 Hz. to 1980 Hz., the THD is varying between 4% and 7%. The minimum THD is 4.5 at 1380 Hz.

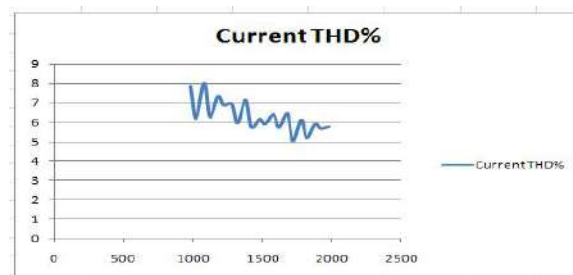


Fig. 14 Phase Shift PWM Stator Current THD

Fig. 14. Illustrates the variation of Stator Current THD with carrier frequency in Phase Shift PWM. As the carrier frequency is varied from 980 Hz. to 1980 Hz., the THD is varying between 5% and 8%. The minimum THD is 5.02 at 1720 Hz.

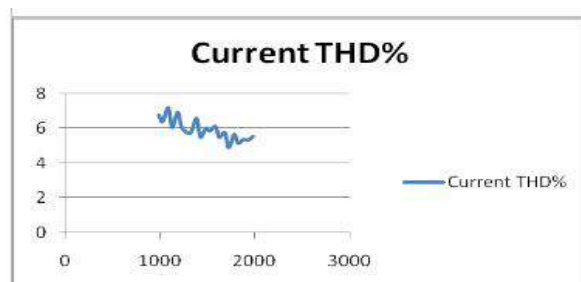


Fig. 15 Alternate Phase Shift PWM Stator Current THD

Fig. 15. Illustrates the variation of Stator Current THD with carrier frequency in Alternate Phase Shift PWM. As the carrier frequency is varied from 980 Hz. to 1980 Hz., the THD is varying between 4.5% and 7.5%. The minimum THD is 4.89 at 1720 Hz.

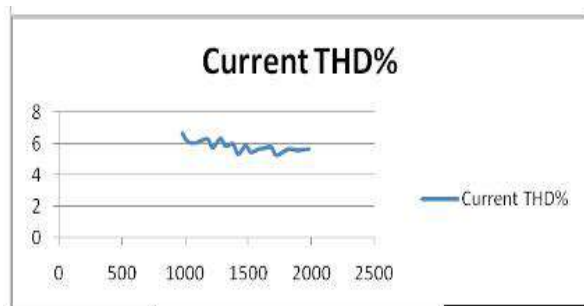


Fig. 16 Carrier Overlap PWM Stator Current THD

Fig. 16 .Illustrates the variation of Stator Current THD with carrier frequency in Carrier Overlap PWM .As the carrier frequency is varied from 980 Hz. to 1980 Hz. , the THD is varying between 5% and 7%.The minimum THD is 5.25 at 1720 Hz.

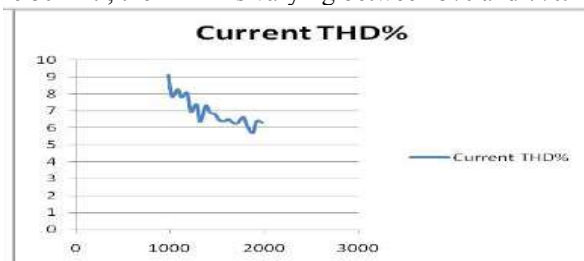


Fig. 17 Variable Frequency PWM Stator Current THD

Fig. 17 .Illustrates the variation of Stator Current THD with carrier frequency in Variable Frequency PWM .As the carrier frequency is varied from 980 Hz. to 1980 Hz. , the THD is varying between 5.5% and 9.5%.The minimum THD is 5.71 at 1880 Hz

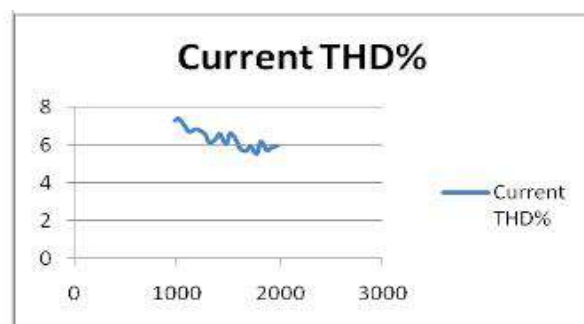


Fig. 18 Alternate Variable Frequency PWM Stator Current THD

Fig. 18 .Illustrates the variation of Stator Current THD with carrier frequency in Alternate Variable Frequency PWM .As the carrier frequency is varied from 980 Hz. to 1980 Hz. , the THD is varying between 5.5% and 7.5%.The minimum THD is 5.51 at 1780 Hz

VI. CONCLUSION

It is clear from above results that the In Phase Disposition PWM , Alternative Phase Opposition & Disposition PWM and Alternate Phase Shift PWM techniques are best as the THD is below 5% . As per IEEE standards the THD should be below 5%.

REFERENCES

- [1] Jose Ignacio Leon Galvan "Multilevel converters: topologies, modeling, SVM techniques and optimization"; Doctoral thesis, University of Seville
- [2] M.V.Subramanyam, P.V.N.Prasad "SPWM Techniques in closed loop control of five level inverter fed 3 Φ Induction motor" , The IUP Journal of Electrical and Electronics Engineering, Vol VII, no. 4,2014,pp 43-53
- [3] R.Teodorescu, F.Beaabjerg, J.K.Pedersen, E.Cengeki, S.Sulistijo,Woo and P.Enjeti "Multi-Level Converters ; A Survey" in Proc. European power electronics conference, Switzerland 1999
- [4] Ying Cheng, Mariesa L Crow "A Diode Clamped Multi-level Inverter for the Statcom/BESS"; University of Missouri, USA
- [5] M.V.Subramanyam,S.Mani Kuchibhotla. P.V.N. Prasad-"Effect of carrier frequency on THD in closed loop control of 5-level Multi-Level Inverter fed 3 phase induction motor"- International Journal of Scientific & Engineering Research. Volume 4. Issue 5, May -2013. pp 804—809.
- [6] Reddy V Naga Bhaskar, Babu Ch. Sai and Suresh K, "Advanced Modulation Techniques for Diode Clamped Multi Level Inverter Fed Induction Motor" ARPJ Journal of Engineering and Applied Sciences. Vol. 6, No. 1,ISSN 1819 – 6608, 2011.
- [7] F arid Berrezzek and F arid Berrezzek "A Study of New Techniques of Controlled PWM Inverters ", European Journal of Scientific Research, Vol. 32, No. 1,pp 77-87,ISSN 1450-218X, 2009.
- [8] Balamurgan C R, Natrajan S P, and Bensraj R "Investigations on Three Phase Five Level Diode Clamped Multi Level Inverter" , International Journal of Modern Engineering Research(IJMER), Vol. 2, No. 3, pp 1273 – 1279,ISSN 2249 6645, 2012.



MATRUSRI ENGINEERING COLLEGE

(Approved by AICTE, Affiliated to Osmania University)

#16-1-486, Saidabad, Hyderabad - 500059



Sponsored by

MATRUSRI EDUCATION SOCIETY



ISBN: 97881-936274-0-2



1ST NATIONAL CONFERENCE ON TRENDS IN SCIENCE, ENGINEERING AND TECHNOLOGY

(NTSET - 2018)

February 2nd & 3rd - 2018

TECHNICAL PAPER ABSTRACTS



ORGANIZED BY

MATRUSRI ENGINEERING COLLEGE

(Approved by AICTE, Affiliated to Osmania University)

#16-1-486, Saidabad, Hyderabad - 500059



Sponsored by

MATRUSRI EDUCATION SOCIETY

ISBN: 97881-936274-0-2



NTSET 2018



SIMULATION OF SOLAR PV ARRAY USING MATLAB/SIMULINK

M.Srinivas¹, M.Praveen Reddy²

¹Assistant Professor, Department of EEE, Matrusri Engineering College, Hyderabad

²Assistant Professor, Department of EEE, Matrusri Engineering College, Hyderabad

Email: ¹srinureddy2005@gmail.com, ²maalipravin@gmail.com

Abstract-Solar radiant energy accounts for most of the usable renewable energy on this earth. Photovoltaic (PV) is a method of generating electrical power by converting solar radiation into direct current electricity using semiconductor that exhibits the photovoltaic effect. This paper presents a method of modeling and simulation of photovoltaic array in MATLAB/SIMULINK using solar cell block from SimElectronics® library. The method is used to implement and determine the characteristics of a particular photovoltaic cell panel and it can be used to build a solar PV system with any photovoltaic array. All modules which form the photovoltaic system model are individually modeled and validated in MATLAB/SIMULINK.

Keywords: Simulation, Photovoltaic, MATLAB/SIMULINK

I. INTRODUCTION

Photovoltaic(PV) and Renewable Energy Sources(RES) have experimented a great development in recent years[1], mainly because of the growing concern about climate change and the oil price increase, which has lead many countries to adopt new regulations to promote this kind of energy. Photovoltaic systems are very low exploitation costs (free fuel), limited maintenance requirements, reliable, silent and easy to install. In addition, in some stand alone applications photovoltaic systems are certainly convenient in comparison with other energy sources, especially in those places that are not accessible, which is unprofitable to install traditional power lines[2].

II. MODEL OF SOLAR CELL

Any photovoltaic cell model is based on diode behavior, which gives to photovoltaic cell its exponential characteristic. The solar cell can be modeled with three modeling systems[3].The first possibility of modeling can be done with instruments which can implement any differential equation or algebraic relationship of a highly complex mathematical model. Another possibility is given by Simscape®, which allows direct modeling using physical components of the electric field(resistors, capacitors and diodes) to implement exactly the same mathematical equation. A modeling system more complex than those described above is performed using SimElectronics® advanced component library, which contains a block called Solar Cell. The solar cell from MATLAB/SIMULINK is a solar current source, which includes solar induced current and temperature dependence[4].

III. SOLAR INDUCED CURRENT

Solar cell block is formed from a single solar cell as a resistance R_s connected in series with a parallel combination of a current source, two exponential diodes and a parallel resistance R_p as shown in Figure.1[4][5].

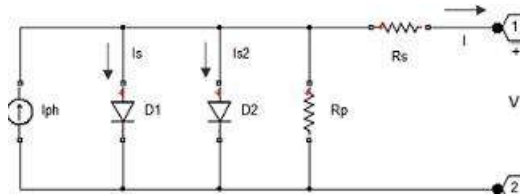


Figure 1: Two diode model of Solar cell

The output current is given by the equation $I = I_{ph} - I_s \left(e^{(V+IR_s)/(N_1V_t)} - 1 \right) - I_{s2} \left(e^{(V+IR_s)/(N_2V_t)} - 1 \right) - (V + IR_s) / R_p$ where I_{ph} is solar induced current. $I_{ph} = I_{pho} \cdot I_r / I_{ro}$, where I_r is irradiance in W/m^2 which fall on cell surface; I_{pho} is measured solar generated current for the irradiance I_{ro} ; I_s is the saturation current of the first diode; I_{s2} is the saturation current of the second diode; $V = kT/q$ is the thermal voltage, depend on temperature of the device T , k is the Boltzmann constant and q is elementary charge of the electron; N_1 is the quality factor (the emission coefficient for the diode) of the first diode; N_2 is the quality factor (the emission coefficient for the diode) of the second diode; V is the voltage at the terminals of solar cell[8].

This block allows choosing one of two models: a model with 8 parameters in which the previous equation describes the output current, and a model with 5 parameters implied for this equation with the following simplified assumptions: the impedance of the parallel resistor is infinite and the saturation current of the second diode is zero. The model with 5 parameters allows optimization of this block according to the equivalent circuit model parameters or by short circuit current and open circuit voltage[3].

IV. TEMPERATURE DEPENDENCE

Several solar cell parameters (the solar-induced current I_{ph} , the saturation current of the first diode I_s , the saturation current of the second diode I_{s2} , the series resistance R_s and the parallel resistance R_p) depend on temperature. Photovoltaic cell temperature is specified by value of the fixed circuit temperature parameter, TFIXED[4]. Between the solar induced current I_{ph} and temperature of solar cell T [4-8] appears in the equation

$I_{ph}(t) = I_{ph}(1 + TIPH1(T - T_{meas}))$ where $TIPH1$ is the first temperature coefficient for I_{ph} ; T_{meas} is the parameter extraction temperature.

V. MODEL OF PHOTOVOLTAIC ARRAY

In the model Figure 2 represents a PV cell array connected to a variable resistor. This resistor has an input ramp which just varies resistance linearly in closed circuit until it reaches the 30th steps. Inside the array subsystem are 8 rows of photovoltaic solar cells connected in series, formed by 8 solar cells of SimElectronics® library as shown in Figure 3. This structure can be built in any configurations by connecting multiple strings of solar cells in series or in parallel.

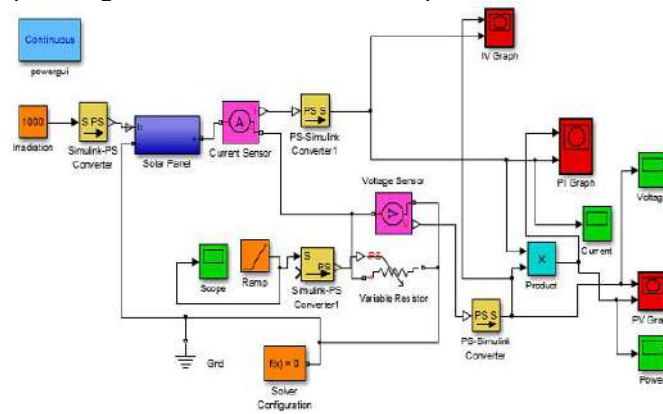


Figure 2: The Simulink model of photovoltaic array

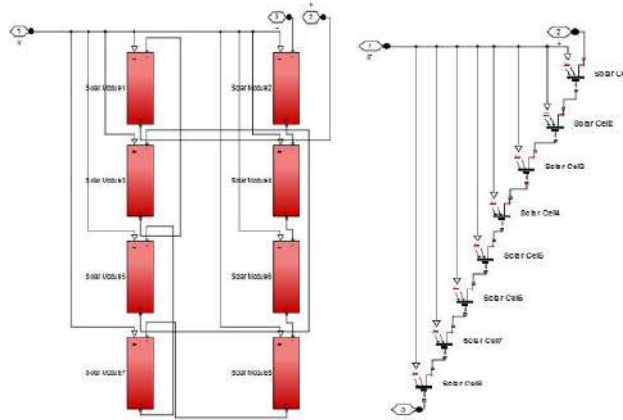


Figure 3: Connection of Solar cells in PV panel subsystem

The advantage of using of this high level of implementation is to create a simple equivalent circuit, which have much more complex parameters, including the effect of temperature in the device which is very important for behavior of this type of system. The photovoltaic panel model is validated by simulating at a value of irradiance of 1000 W/m^2 and a temperature of 25°C .

Parameter	Value
Short-circuit current [A]	$I_{sc} = 7.34$
Open-circuit current [V]	$V_{oc} = 0.6$
Quality factor	$N = 1.5$
Series resistance [Ω]	$R_s = 0$
First order temperature coefficient for I_{ph} [1/K]	$TIPH1 = 0$
Temperature exponent for I_s	$TXIS1 = 3$
Temperature exponent for R_s	$TRS1 = 0$
Parameter extraction temperature [$^\circ\text{C}$]	$T_{meas} = 25$
Fixed circuit temperature [$^\circ\text{C}$]	$TFIXED=25$

Table 1: The parameters of single solar cell

VI. SIMULATION RESULTS

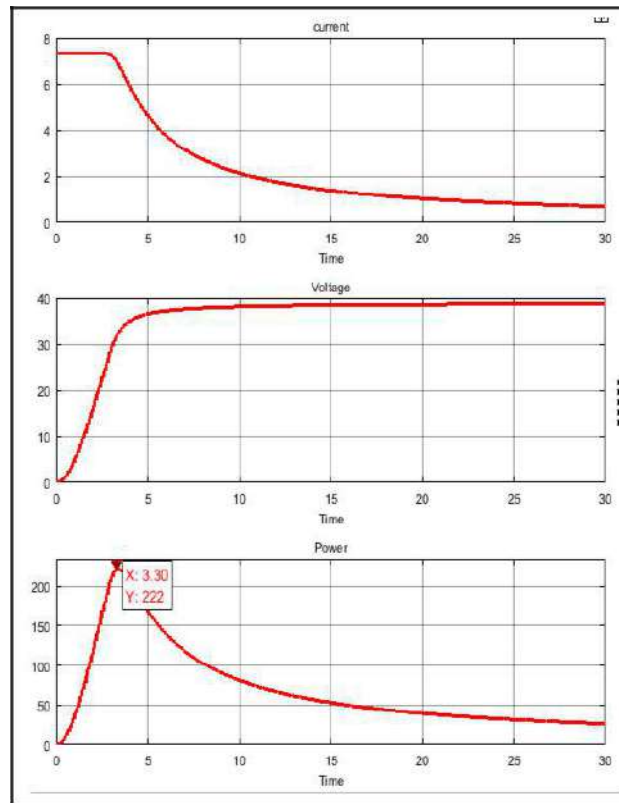


Figure 4: Current, Voltage and Power curves for PV array

In Figure 4, are shown the current, voltage and power which are obtained at output of PV array. These are the curves of current, voltage and power versus time. When the resistance varies, the current and voltage vary depending on the voltage-time relationship, which gives the power curve.

The characteristics of V-I and P-V of the photovoltaic array is given in Figure 5 and Figure 6. The V-I curve represent the standard behavior of the photovoltaic cell and photovoltaic array respectively. In the middle of this characteristic is the maximum power point. This point is very critical for this kind of system for maximum power extraction from the photovoltaic array. Result that the main objective is to try operating around of this maximum point in order to make the photovoltaic cells to work at maximum efficiency.

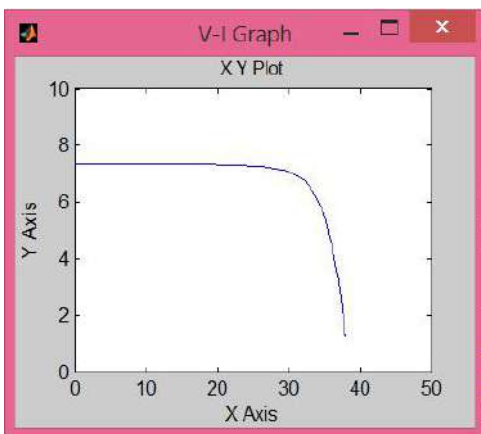


Figure 5: V-I Characteristic of PV array

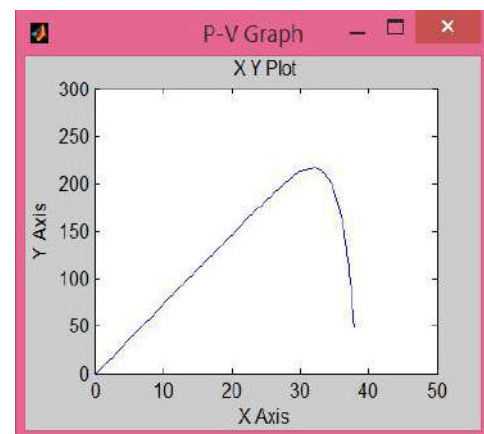


Figure 6: P-V Characteristic of PV array

The V-I characteristic for radiation incident on the photovoltaic cells is amended in Figure 7. If the irradiance decreases, the photovoltaic current generated decreases proportionally to that and variation of no-load voltage is very small.

PV Array V-I Characteristics-Data

Irradiance effect on PV array performance at T=25°C

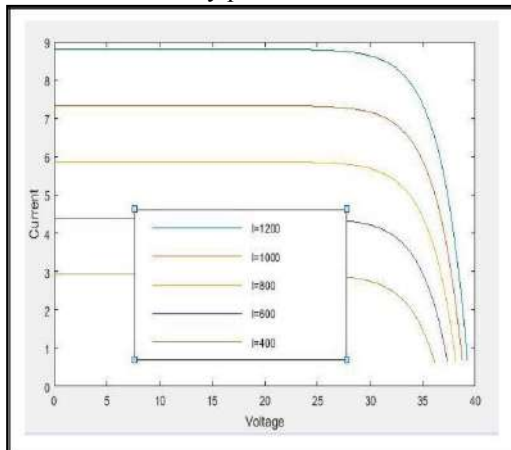


Figure 7: V-I characteristics for different values of solar radiation at temperature of 25°C

Temperature effect on PV array performance at irradiance of 1000 W/m²

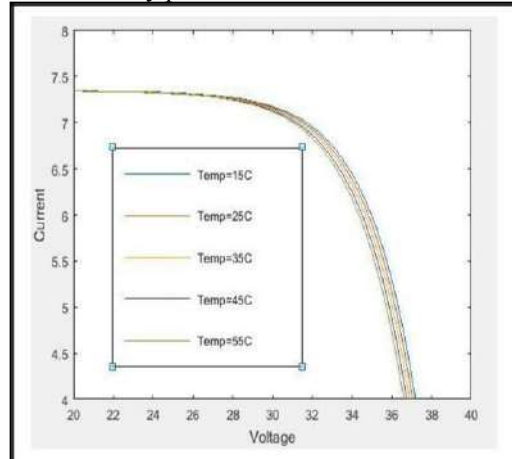


Figure 8: V-I characteristics for different temperatures

As shown in Fig.7, when the temperature of module increases the voltage decreases and the produced current remains practically constant. In terms of produced electric power is a reduction in the performance of the PV array[2].

In Figure 9 are represented the P-V characteristics of the photovoltaic array for a level of irradiation of 1000 W/m² and for different temperatures and respectively in Figure 10 are given the P-V characteristics for different levels of solar radiation at the temperature of 25°.

Temperature effect on PV array performance at irradiance of 1000 W/m²

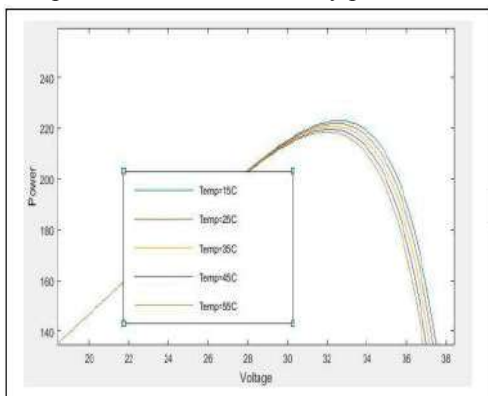


Figure 9: P-V characteristics for different temperatures
Irradiance effect on PV array performance at T=25°C

From Figure 9, it is observed that for an irradiance of 800 W/m², which corresponds to yellow curve is obtained a maximum power of 170 W and for an irradiance of 1000 W/m² which corresponds to dark blue curve, the PV array provide a maximum power of 222 W. That gives an idea of measure in the power produced by a photovoltaic array is affected by changing irradiance.

VII. CONCLUSION

This work describes a new implementation of solar cell by using MATLAB®/Simulink® of photovoltaic array and modeling using experimental data. Photovoltaic array is build by using the solar cell block and the power produced by a photovoltaic array is affected by changing of irradiance. The implemented model is validated through simulation. The simulation results show that the proposed method is efficient in terms of modeling of the functioning of the photovoltaic system.

REFERENCES

- [1] Bevrani H., Ghosh A., Ledwich G.: 'Renewable energy sources and frequency regulation: survey and new perspectives', IET Renewable Power Generation, 2010, 4, (5), pp.438-457.
- [2] ABB, Technical application papers No.10 Photovoltaic plants.
- [3] www.mathworks.com, Osorio C., Recorded Webinar-Model-Based Design for Solar Power Systems.
- [4] www.mathworks.com, Help-Solar Cell Blocks.
- [5] Messenger R.A., Ventre J., Photovoltaic Systems Engineering, CRC Press LLC, 2000.
- [6] Gow J.A., Manning C.D., Development of a photovoltaic Array Model for use in Power Electronics Simulation Studies, IEE Proceedings of Electric Power Applications, Vol.146, No.2, March 1999, pp.193-200.
- [7] Villalva M.G., Gazoli, Filho E., Comprehensive Approach to Modeling and Simulation of Photovoltaic Arrays, IEEE Transactions on Power Electronics, Vol.24, No.5 May, 2009, pp.1198-1208.
- [8] Pavan Kumar A.V., Parimi A.M., Uma Rao K., "Performance Analysis of a Two Diode model of PV cell for PV based generation in MATLAB", in Advanced Communication Control and Computing Technologies (ICACCCT).



MATRUSRI ENGINEERING COLLEGE

(Approved by AICTE, Affiliated to Osmania University)

#16-1-486, Saidabad, Hyderabad - 500059



Sponsored by

MATRUSRI EDUCATION SOCIETY



ISBN: 97881-936274-0-2



1ST NATIONAL CONFERENCE ON TRENDS IN SCIENCE, ENGINEERING AND TECHNOLOGY

(NTSET - 2018)

February 2nd & 3rd - 2018

TECHNICAL PAPER ABSTRACTS



ORGANIZED BY

MATRUSRI ENGINEERING COLLEGE

(Approved by AICTE, Affiliated to Osmania University)

#16-1-486, Saidabad, Hyderabad - 500059



Sponsored by

MATRUSRI EDUCATION SOCIETY

ISBN: 97881-936274-0-2

NTSET 2018





MODELLING OF SSSC TO ENHANCE THE POWER SYSTEM STABILITY USING MATLAB

N.Kalpana¹, M.Saritha²

¹Assistant Professor, Department of EEE, Matrusri Engineering College, Hyderabad

²Assistant Professor, Department of EEE, Matrusri Engineering College, Hyderabad

Email: 'kalpana924@yahoo.com, ² saritha.nagasai@gmail.com

Abstract: In this paper, a very efficient approach to control the power flow through the transmission line is given. A static synchronous series compensator (SSSC) is used as controller. It controls the active and reactive power as well as damping power system oscillation in transient mode. The SSSC is equipped with a source of energy in DC link can apply or absorb the reactive power to or from the transmission line. Simulation results are obtained for the selected bus-2 in two machine power system which shows the efficiency of this compensator as one of the FACTS devices member in controlling the power flow, achieving the desired value of active and reactive powers, and damping the power oscillation.

Key words: Static synchronous series compensator(SSSC), FACTS, Active and reactive powers and transmission line.

I. INTRODUCTION

Now a days reliability of power system is big concern to ensure uninterrupted power supply. becoming more complex from operation, control and stability maintenances a big issue when they meet ever increasing load demand[1] The power flow in ac power system give the significant electrical storage, the electrical generation and load must balance at all times [2]. One of the most important problems in the control of power transmission systems is the reactive power compensation. Reactive power causes the increase in the transmission systems losses, decrease in power capacity carried decrease in power transfer capacity in the transmission lines and leads to voltage instability. Hence it is necessary to improve Active and reactive powers in order to increase transmittable power, and provide voltage stability.

This paper investigates the static synchronous series compensator (SSSC) that belongs to the Flexible AC Transmission Systems (FACTS) family to control power flow and improve active and reactive powers by injecting the voltage in series with the transmission line where it is connected. It consists of a solid state voltage source converter (VSC) which generates a controllable alternating current voltage at fundamental frequency. When the injected voltage is kept in quadrature with the line current, it can emulate as inductive or capacitive reactance so as to influence the power flow through the transmission line [2,3]. While the primary purpose of a SSSC is to control power flow in steady state, it can also improve transient stability of a power system.

II. FLEXIBLE AC TRANSMISSION SYSTEM (FACTS)

Flexible AC Transmission System (FACTS) is the well-known concept which is more needed [4]. The FACTS devices have main purposes of power flow regulation, power loss reduction, power oscillation damping, cost reduction and transmission routes power flow control [8].

The of FACTS devices has many advantages that are listed below,

- Control of Power flow
- Rise of transmission capability
- Increase the loading capability
- Reactive power compensation with controllers
- System security
- Provides greater flexibility
- The problem of voltage fluctuation and flickers can be reduced
- Reduce the reactive power flows and loop flow
- Prevention of cascading outages by contributing to emergency control

III. BASIC SSSC CONFIGURATION

Fig. 1 shows The basic circuit diagram of the SSSC. The compensator is equipped with a source of energy, which helps in supplying or absorbing active power to or from the transmission line along with the control of reactive power flow. The dc capacitor has been replaced by an energy storage device such as a high energy battery installation to allow active as well as reactive power exchanges with the ac system. The SSSC's output voltage magnitude and phase angle can be varied in a controlled manner to influence power flows in a transmission line. The phase displacement of the inserted voltage, with respect to the transmission line current, determines the exchange of real and reactive power with the ac system [3]

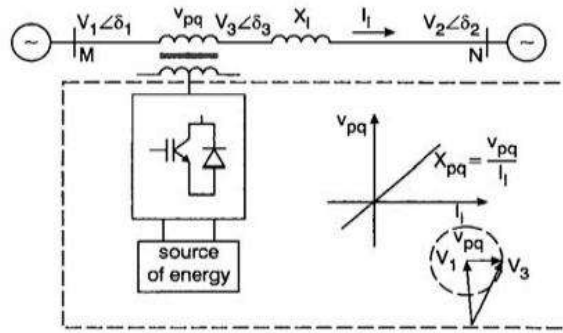


Fig1: Static Synchronous Series compensator (SSSC)

IV.TWO MACHINE MODEL OF SSSC

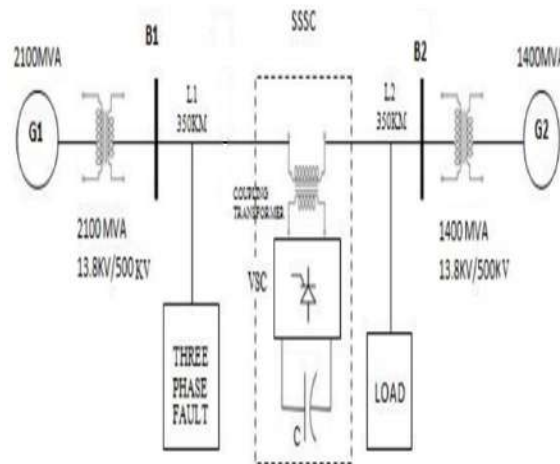


Fig2. Single line diagram of two machine power system

V. FLOW CHART OF WORKING OF SSSC

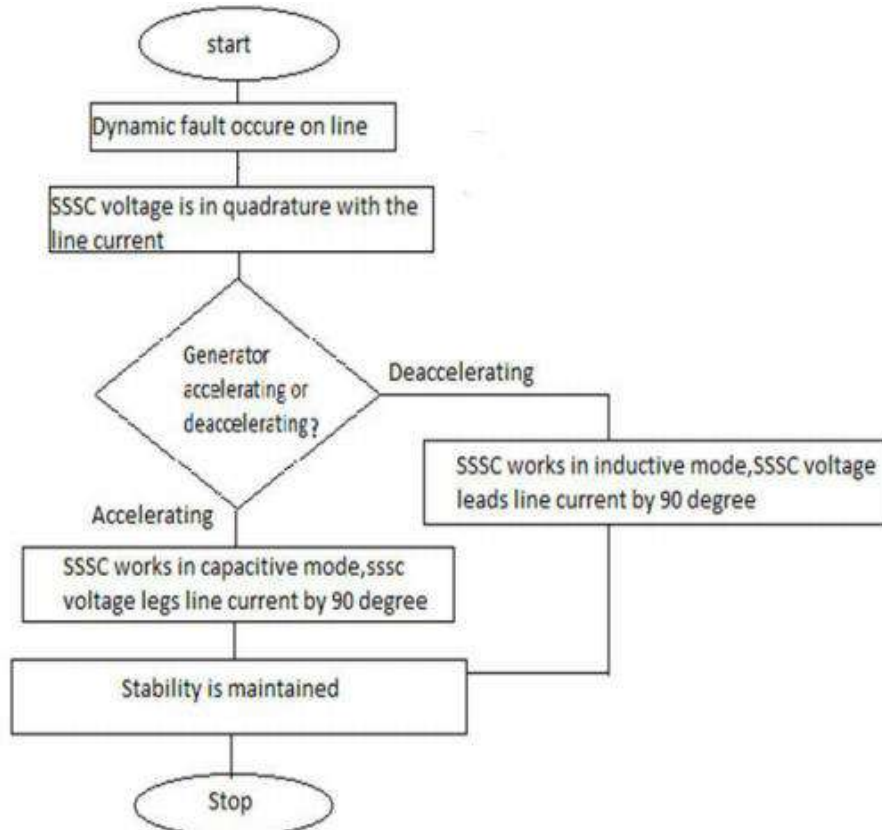


Fig3.Flow chart of working of SSSC using in to the power system

VI. SIMULATION RESULTS WITH MATLAB/SIMULINK

The functional performance of SSSC is given by the real time voltage wave forms. By using the MATLAB environment tool shown in fig. , it is obtained on real time, in proposed simulation SSSC is coupled to the power transmission line of having 500KV by coupling transformer. The proposed system is having made into ring mode which consist of two buses(B1 and B2) connected to the transmission line having 500kv transmission lines. The system is having two sources of three phase of 500KV and the base voltage is also 500KV.

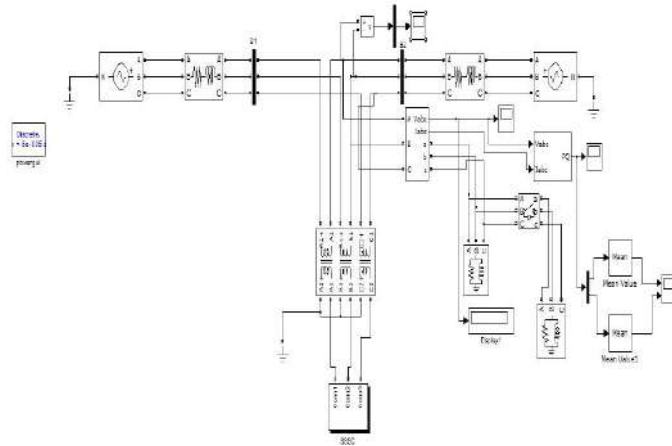


Fig4: Simulation of two machine bus system

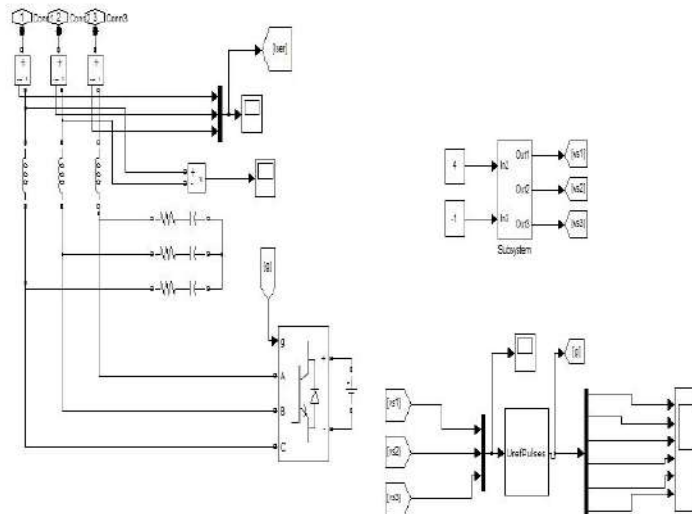


Fig5: Simulation of SSSC

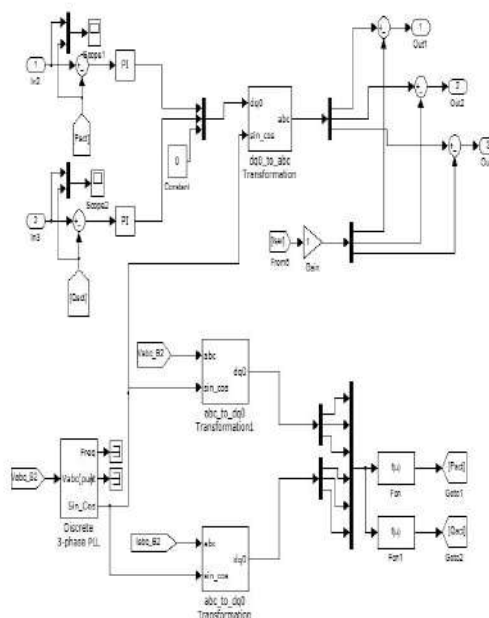


Fig6: Simulation of sub system



VII. EXPERIMENTAL RESULTS

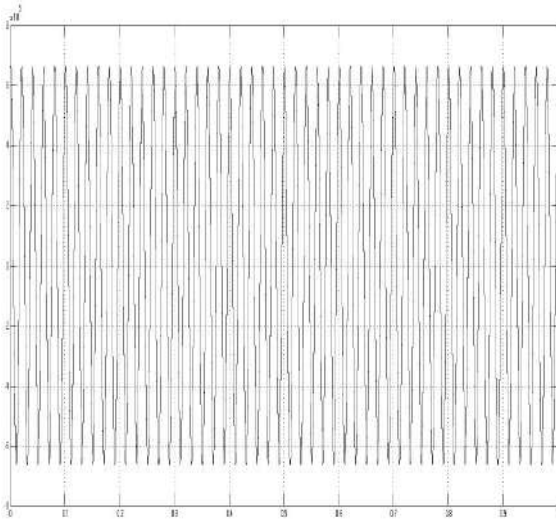


Fig7: Waveform of voltage of bus 2 with out SSSC

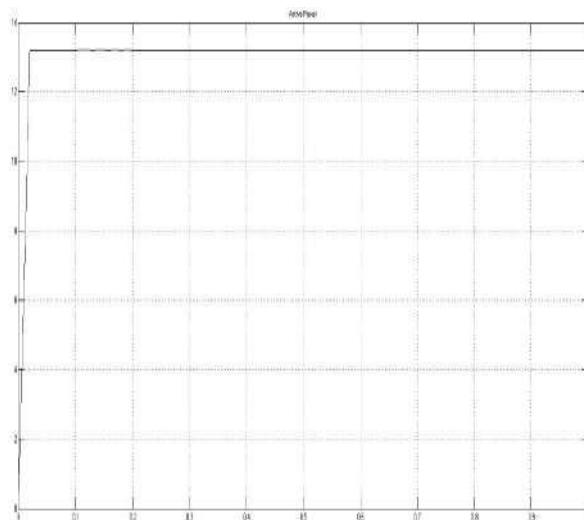


Fig8. Waveform of active power with out SSSC

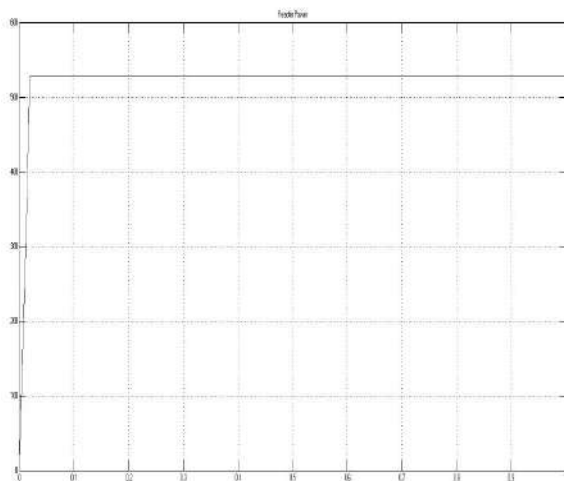


Fig9.: waveform of reactive power with SSSC

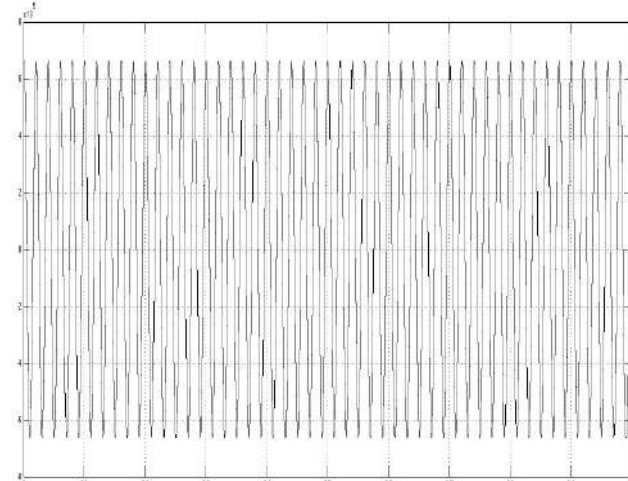


Fig10: waveform of voltage of bus 2 with SSSC

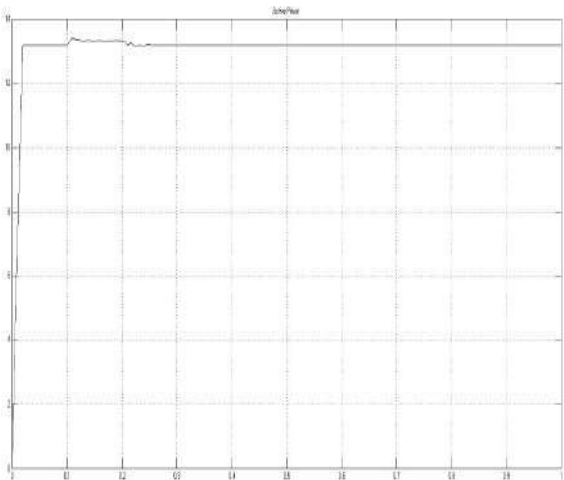


Fig11: waveform of active power with SSSC

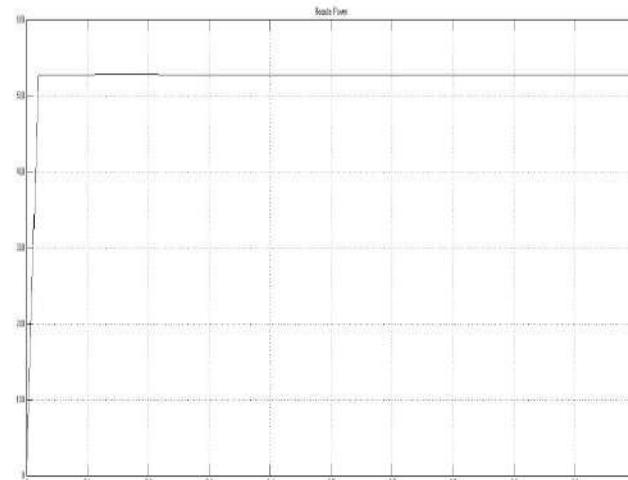


Fig12: waveform of reactive power with SSSC

The changes into the parameter like voltage. Active and reactive power is obtained in to the real time. Regarding to that, system having large loads causes the system active power of bus-2 got oscillated and it keep continuing, the oscillations of the active power are more than that of the reactive power because the ohmic parts of the loads are greatly more.



REFERENCES

- [1] SSSC-static synchronous series compensator: theory, modeling, and application [IEEE Transactions on Power Delivery](#) Volume: 13, [Issue: 1](#), Jan 1998.
- [2] N.G Hingorani, 201 1, "Understanding facts: concepts Technology of flexible AC transmission system",IEEE Power Engg. IEEE press, Wiley India.
- [3] B.Suresh Kumar, Enhancement of Voltage Stability using Static Synchronous Series Compensator (SSSC) with PI Controller LLLG Fault, International Journal of Advanced Research in Engineering & Technology (IJARET), Volume 4, Issue 5, 2013, pp. 164 175, ISSN Print: 0976 6480, ISSN Online: 0976 6499
- [4] "Power System Stability Enhancement Using Static synchronous Series Compensator (SSSC)" by M. Faridi & H. Maeiiat Electrical Engg, EEE department. Islamic Azad University-Ahar-Branch, Ahar, Iran, IEEE, 2011.
- [5] "Dynamic Compensation of AC transmission line by solid- state synchronous voltage sources" by Laszlo gyugi, fellow, IEEE Westinghouse Electric Corporation Pittsburg, Pennsylvania 15235, IEEE Transaction on power delivery, Vol.9, No. 2, April 1994.
- [6] Stability Improvement and Power Oscillation Damping Using Static Synchronous Series Compensator (SSSC) International Journal of Advanced Research in Science, Engineering and Technology Vol. 2, Issue 1 , January 2015 . Mythili



MATRUSRI ENGINEERING COLLEGE

(Approved by AICTE, Affiliated to Osmania University)

#16-1-486, Saidabad, Hyderabad - 500059



Sponsored by

MATRUSRI EDUCATION SOCIETY



ISBN: 97881-936274-0-2



1ST NATIONAL CONFERENCE ON TRENDS IN SCIENCE, ENGINEERING AND TECHNOLOGY (NTSET - 2018)

February 2nd & 3rd - 2018

TECHNICAL PAPER ABSTRACTS



ORGANIZED BY

MATRUSRI ENGINEERING COLLEGE

(Approved by AICTE, Affiliated to Osmania University)

#16-1-486, Saidabad, Hyderabad - 500059



Sponsored by

MATRUSRI EDUCATION SOCIETY

ISBN: 97881-936274-0-2

**NTSET
2018**



SIMULATION OF SOLAR PV ARRAY USING MATLAB/SIMULINK

M.Srinivas¹, M.Praveen Reddy²

¹Assistant Professor, Department of EEE, Matrusri Engineering College, Hyderabad

²Assistant Professor, Department of EEE, Matrusri Engineering College, Hyderabad

Email: ¹srinureddy2005@gmail.com, ²maalipravin@gmail.com

Abstract-Solar radiant energy accounts for most of the usable renewable energy on this earth. Photovoltaic (PV) is a method of generating electrical power by converting solar radiation into direct current electricity using semiconductor that exhibits the photovoltaic effect. This paper presents a method of modeling and simulation of photovoltaic array in MATLAB/SIMULINK using solar cell block from SimElectronics® library. The method is used to implement and determine the characteristics of a particular photovoltaic cell panel and it can be used to build a solar PV system with any photovoltaic array. All modules which form the photovoltaic system model are individually modeled and validated in MATLAB/SIMULINK.

Keywords: Simulation, Photovoltaic, MATLAB/SIMULINK

I. INTRODUCTION

Photovoltaic(PV) and Renewable Energy Sources(RES) have experimented a great development in recent years[1], mainly because of the growing concern about climate change and the oil price increase, which has lead many countries to adopt new regulations to promote this kind of energy. Photovoltaic systems are very low exploitation costs (free fuel), limited maintenance requirements, reliable, silent and easy to install. In addition, in some stand alone applications photovoltaic systems are certainly convenient in comparison with other energy sources, especially in those places that are not accessible, which is unprofitable to install traditional power lines[2].

II. MODEL OF SOLAR CELL

Any photovoltaic cell model is based on diode behavior, which gives to photovoltaic cell its exponential characteristic. The solar cell can be modeled with three modeling systems[3].The first possibility of modeling can be done with instruments which can implement any differential equation or algebraic relationship of a highly complex mathematical model. Another possibility is given by Simscape®, which allows direct modeling using physical components of the electric field(resistors, capacitors and diodes) to implement exactly the same mathematical equation. A modeling system more complex than those described above is performed using SimElectronics® advanced component library, which contains a block called Solar Cell. The solar cell from MATLAB/SIMULINK is a solar current source, which includes solar induced current and temperature dependence[4].

III. SOLAR INDUCED CURRENT

Solar cell block is formed from a single solar cell as a resistance R_s connected in series with a parallel combination of a current source, two exponential diodes and a parallel resistance R_p as shown in Figure.1[4][5].

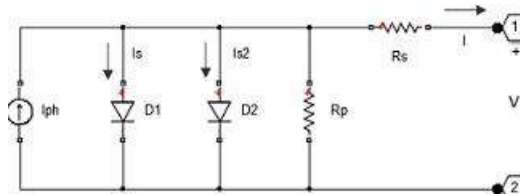


Figure 1: Two diode model of Solar cell

The output current is given by the equation $I = I_{ph} - I_{s1} \left(e^{(V+IR_s)/(N_1V_t)} - 1 \right) - I_{s2} \left(e^{(V+IR_s)/(N_2V_t)} - 1 \right) - (V + IR_s) / R_p$ where I_{ph} is solar induced current. $I_{ph} = I_{pho} \cdot I_r / I_{ro}$, where I_r is irradiance in W/m^2 which fall on cell surface; I_{pho} is measured solar generated current for the irradiance I_{ro} ; I_{s1} is the saturation current of the first diode; I_{s2} is the saturation current of the second diode; $V = kT/q$ is the thermal voltage, depend on temperature of the device T , k is the Boltzmann constant and q is elementary charge of the electron; N_1 is the quality factor (the emission coefficient for the diode) of the first diode; N_2 is the quality factor (the emission coefficient for the diode) of the second diode; V is the voltage at the terminals of solar cell[8].

This block allows choosing one of two models: a model with 8 parameters in which the previous equation describes the output current, and a model with 5 parameters implied for this equation with the following simplified assumptions: the impedance of the parallel resistor is infinite and the saturation current of the second diode is zero. The model with 5 parameters allows optimization of this block according to the equivalent circuit model parameters or by short circuit current and open circuit voltage[3].

IV. TEMPERATURE DEPENDENCE

Several solar cell parameters (the solar-induced current I_{ph} , the saturation current of the first diode I_s , the saturation current of the second diode I_{s2} , the series resistance R_s and the parallel resistance R_p) depend on temperature. Photovoltaic cell temperature is specified by value of the fixed circuit temperature parameter, TFIXED[4]. Between the solar induced current I_{ph} and temperature of solar cell T [4-8] appears in the equation

$I_{ph}(t) = I_{ph}(1 + TIPH1(T - T_{meas}))$ where $TIPH1$ is the first temperature coefficient for I_{ph} ; T_{meas} is the parameter extraction temperature.

V. MODEL OF PHOTOVOLTAIC ARRAY

In the model Figure 2 represents a PV cell array connected to a variable resistor. This resistor has an input ramp which just varies resistance linearly in closed circuit until it reaches the 30th steps. Inside the array subsystem are 8 rows of photovoltaic solar cells connected in series, formed by 8 solar cells of SimElectronics® library as shown in Figure 3. This structure can be built in any configurations by connecting multiple strings of solar cells in series or in parallel.

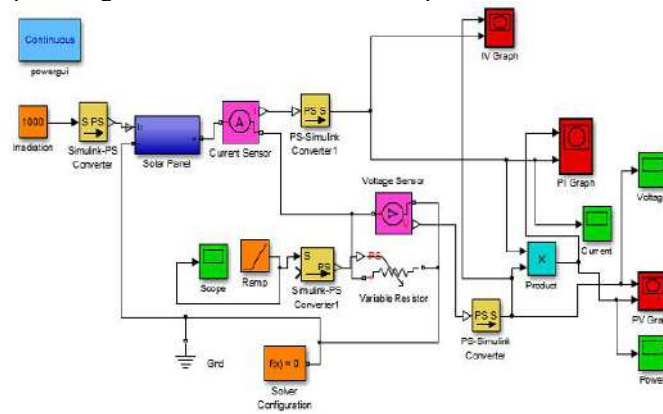


Figure 2: The Simulink model of photovoltaic array

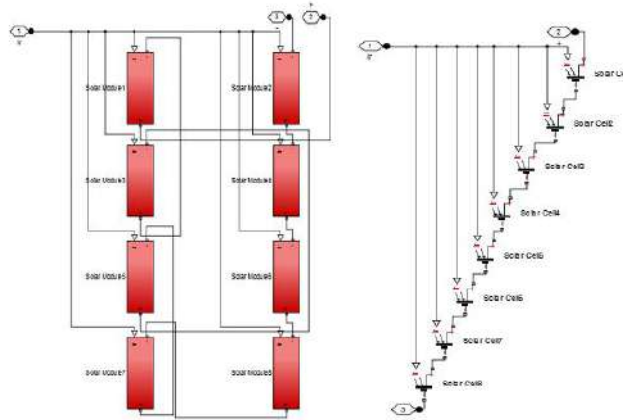


Figure 3: Connection of Solar cells in PV panel subsystem

The advantage of using of this high level of implementation is to create a simple equivalent circuit, which have much more complex parameters, including the effect of temperature in the device which is very important for behavior of this type of system. The photovoltaic panel model is validated by simulating at a value of irradiance of 1000 W/m^2 and a temperature of 25°C .

Parameter	Value
Short-circuit current [A]	$I_{sc} = 7.34$
Open-circuit current [V]	$V_{oc} = 0.6$
Quality factor	$N = 1.5$
Series resistance [Ω]	$R_s = 0$
First order temperature coefficient for I_{ph} [1/K]	$TIPH1 = 0$
Temperature exponent for I_s	$TXIS1 = 3$
Temperature exponent for R_s	$TRS1 = 0$
Parameter extraction temperature [$^\circ\text{C}$]	$T_{meas} = 25$
Fixed circuit temperature [$^\circ\text{C}$]	$TFIXED=25$

Table 1: The parameters of single solar cell

VI. SIMULATION RESULTS

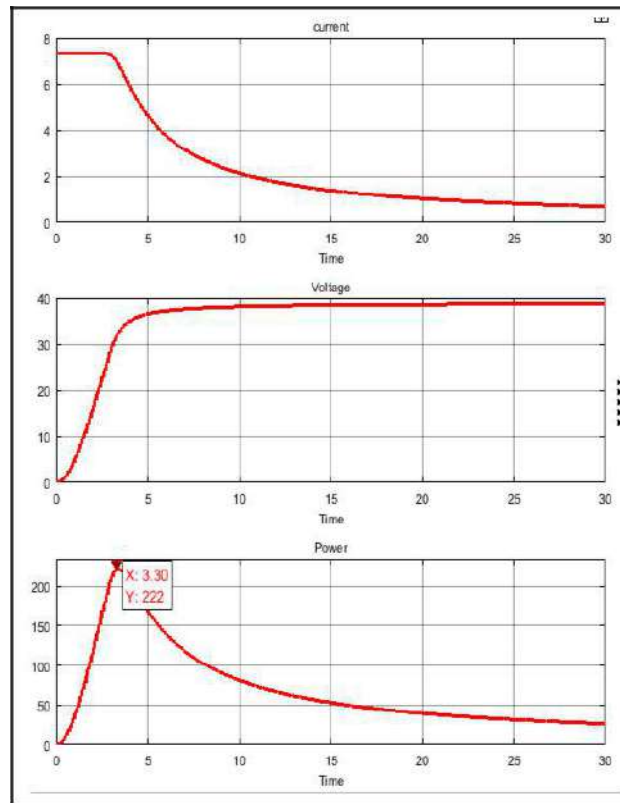


Figure 4: Current, Voltage and Power curves for PV array

In Figure 4, are shown the current, voltage and power which are obtained at output of PV array. These are the curves of current, voltage and power versus time. When the resistance varies, the current and voltage vary depending on the voltage-time relationship, which gives the power curve.

The characteristics of V-I and P-V of the photovoltaic array is given in Figure 5 and Figure 6. The V-I curve represent the standard behavior of the photovoltaic cell and photovoltaic array respectively. In the middle of this characteristic is the maximum power point. This point is very critical for this kind of system for maximum power extraction from the photovoltaic array. Result that the main objective is to try operating around of this maximum point in order to make the photovoltaic cells to work at maximum efficiency.

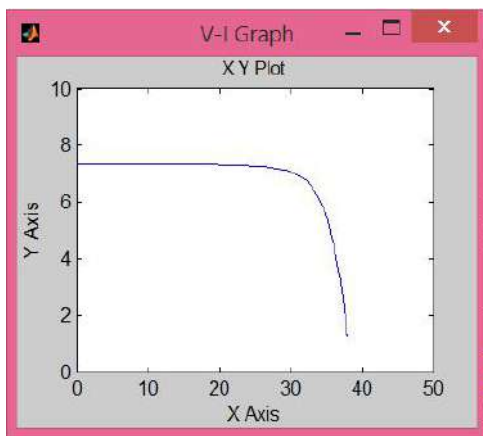


Figure 5: V-I Characteristic of PV array

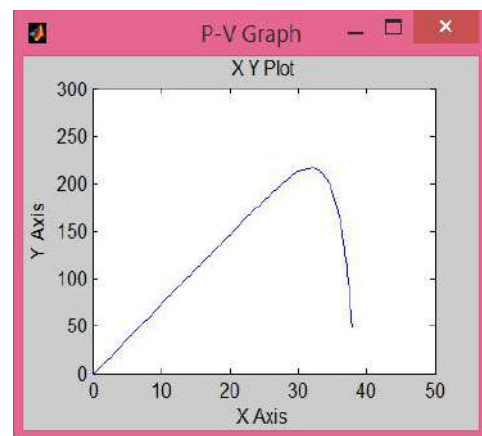


Figure 6: P-V Characteristic of PV array

The V-I characteristic for radiation incident on the photovoltaic cells is amended in Figure 7. If the irradiance decreases, the photovoltaic current generated decreases proportionally to that and variation of no-load voltage is very small.

PV Array V-I Characteristics-Data

Irradiance effect on PV array performance at T=25°C

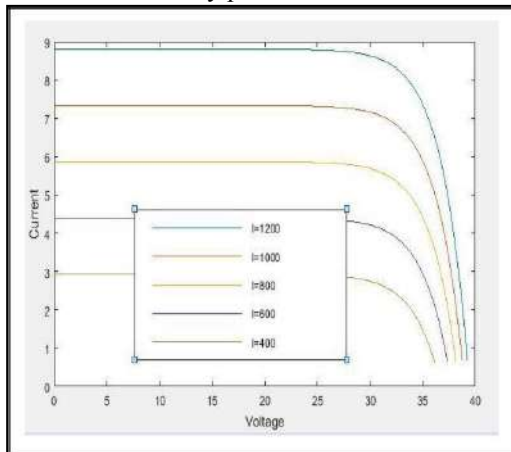


Figure 7: V-I characteristics for different values of solar radiation at temperature of 25°C

Temperature effect on PV array performance at irradiance of 1000 W/m²

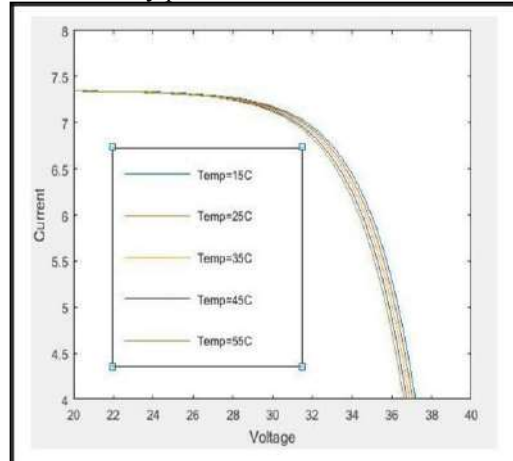


Figure 8: V-I characteristics for different temperatures

As shown in Fig.7, when the temperature of module increases the voltage decreases and the produced current remains practically constant. In terms of produced electric power is a reduction in the performance of the PV array[2].

In Figure 9 are represented the P-V characteristics of the photovoltaic array for a level of irradiation of 1000 W/m² and for different temperatures and respectively in Figure 10 are given the P-V characteristics for different levels of solar radiation at the temperature of 25°.

Temperature effect on PV array performance at irradiance of 1000 W/m²

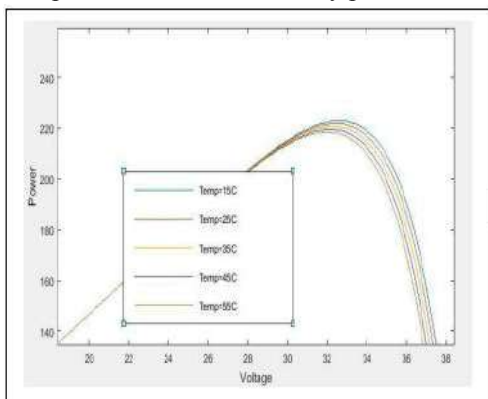


Figure 9: P-V characteristics for different temperatures
Irradiance effect on PV array performance at T=25°C

From Figure 9, it is observed that for an irradiance of 800 W/m², which corresponds to yellow curve is obtained a maximum power of 170 W and for an irradiation of 1000 W/m² which corresponds to dark blue curve, the PV array provide a maximum power of 222 W. That gives an idea of measure in the power produced by a photovoltaic array is affected by changing irradiance.

VII. CONCLUSION

This work describes a new implementation of solar cell by using MATLAB®/Simulink® of photovoltaic array and modeling using experimental data. Photovoltaic array is build by using the solar cell block and the power produced by a photovoltaic array is affected by changing of irradiance. The implemented model is validated through simulation. The simulation results show that the proposed method is efficient in terms of modeling of the functioning of the photovoltaic system.

REFERENCES

- [1] Bevrani H., Ghosh A., Ledwich G.: 'Renewable energy sources and frequency regulation: survey and new perspectives', IET Renewable Power Generation, 2010, 4, (5), pp.438-457.
- [2] ABB, Technical application papers No.10 Photovoltaic plants.
- [3] www.mathworks.com, Osorio C., Recorded Webinar-Model-Based Design for Solar Power Systems.
- [4] www.mathworks.com, Help-Solar Cell Blocks.
- [5] Messenger R.A., Ventre J., Photovoltaic Systems Engineering, CRC Press LLC, 2000.
- [6] Gow J.A., Manning C.D., Development of a photovoltaic Array Model for use in Power Electronics Simulation Studies, IEE Proceedings of Electric Power Applications, Vol.146, No.2, March 1999, pp.193-200.
- [7] Villalva M.G., Gazoli, Filho E., Comprehensive Approach to Modeling and Simulation of Photovoltaic Arrays, IEEE Transactions on Power Electronics, Vol.24, No.5 May, 2009, pp.1198-1208.
- [8] Pavan Kumar A.V., Parimi A.M., Uma Rao K., "Performance Analysis of a Two Diode model of PV cell for PV based generation in MATLAB", in Advanced Communication Control and Computing Technologies (ICACCCT).



MATRUSRI ENGINEERING COLLEGE

(Approved by AICTE, Affiliated to Osmania University)

#16-1-486, Saidabad, Hyderabad - 500059



Sponsored by

MATRUSRI EDUCATION SOCIETY



ISBN: 97881-936274-0-2



1ST NATIONAL CONFERENCE ON TRENDS IN SCIENCE, ENGINEERING AND TECHNOLOGY

(NTSET - 2018)

February 2nd & 3rd - 2018

TECHNICAL PAPER ABSTRACTS



ORGANIZED BY

MATRUSRI ENGINEERING COLLEGE

(Approved by AICTE, Affiliated to Osmania University)

#16-1-486, Saidabad, Hyderabad - 500059



Sponsored by

MATRUSRI EDUCATION SOCIETY

ISBN: 97881-936274-0-2

NTSET 2018





OPTIMUM DESIGN OF MULTI-STORIED BUILDING AGAINST BLAST LOADS

¹MohammedAsra Jabeen,²Dr Manohar. G, ³Prashanth.P.

¹ Research Scholar, Noida International University, Noida, India

² Professor, Department of Civil Engineering, Matrusri Engineering College, Hyderabad.

³Asst. Prof. Department of Civil Engineering, Matrusri Engineering College, Hyderabad.

ABSTRACT

Apart from natural calamity, there are numerous manmade disasters that is compelling structural engineers to come up with more advancement in designing the structures. One of the biggest manmade disasters is growing terrorists' attacks. In order to design blast resistant building, dynamic loads must be considered as an essential parameter. The objective of this study is to understand the design theories that safeguards structure designs against the harmful effects of explosions. Firstly different types of explosions are being explained, then the detail process of explosion are illustrated for a clarity on the behavior of explosives on buildings studying the characteristics of explosion will help to design blast resistant structure in the best possible manner using requisite knowledge.

Keywords: blast resistant, dynamic load, explosives, structural response and designs

INTRODUCTION

Damage to the assets, loss of life and social panic are factors that have to be minimized if the threat of terrorist action cannot be stopped. Designing the structures to be fully blast resistant is not possible in reality and does not prove to be an economical one. Here with the help of engineering and architectural knowledge new as well as existing buildings can be safeguarded from the explosive effects. The aim of the study is to provide knowledge to structural engineers and spreading awareness of protection against explosions for human lives, valuables and various buildings. The blast explosion nearby or within structure is due to pressure or vehicle bomb or quarry blasting. These causes catastrophic damage to the building both externally and internally (structural frames) resulting in collapsing of walls, blowing out of windows, and shutting down of critical life-safety systems. Buildings, bridges, pipelines, industrial plants dams etc are the lifeline structures and they play an important role in the economy of the country and hence they have to be protected from dynamic and wind loading.

The study of blast effects on structures has been an area of formal technical investigation for over 60 years. A bomb explosion within or immediately nearby a building can cause catastrophic damage on the building's external and internal structural frames, collapsing of walls, blowing out of large expanses of windows, and shutting down of critical life-safety systems. Loss of life and injuries to occupants can result from many causes, including direct blast-effects, structural collapse, debris impact, fire, and smoke. The indirect effects can combine to inhibit or prevent timely evacuation, thereby contributing to additional casualties. In addition, major catastrophes resulting from gas-chemical explosions result in large dynamic loads, greater than the original design loads, of many structures.

SIGNIFICANCE

To design a blast resistant building against explosions caused by terrorist, providing protection to losses incurred due to explosives.

Blast Loading and Its Behavior

Explosion Science

An explosion is a rapid release of stored energy characterized by a bright flash and an audible blast. Part of the energy is released as thermal radiation (flash); and part is coupled into the air as air blast and into the soil (ground) as ground shock, both as radially expanding shock waves. To be an explosive, the material will have the following characteristics.

1. Must contain a substance or mixture of substances that remains unchanged under ordinary conditions, but undergoes a fast chemical change upon stimulation.

2. This reaction must yield gases whose volume—under normal pressure, but at the high temperature resulting from an explosion—is much greater than that of the original substance.
3. The change must be exothermic in order to heat the products of the reaction and thus to increase their pressure. Common types of explosions include construction blasting to break up rock or to demolish buildings and their foundations, and accidental explosions resulting from natural gas leaks or other chemical/explosive materials.

Effects on Structures

Blast effects on building structures can be classified as primary effects and secondary effects. Primary effects include

1. **Air blast:** the blast wave causes a pressure increase of the air surrounding a building structure and also a blast wind.
2. **Direct ground shock:** an explosive which is buried completely or partly below the ground surface will cause a ground shock. This is a horizontal (and vertical, depending on the location of the explosion with regard to the structural foundation) vibration of the ground, similar to an earthquake but with a different frequency.
3. **Heat:** a part of the explosive energy is converted to heat. Building materials are weakened at increased temperature. Heat can cause fire if the temperature is high enough.
4. **Primary fragments:** fragments from the explosive source which are thrown into the air at high velocity (for example wall fragments of an exploded gas tank). Secondary effects can be fragments hitting people or buildings near the explosion. They are not a direct threat to the bearing structure of the building, which is usually covered by a facade. However, they may destroy windows and glass facades and cause victims among inhabitants and passers-by.

Blast loading on structures can be explained by three main loading conditions (figure1)

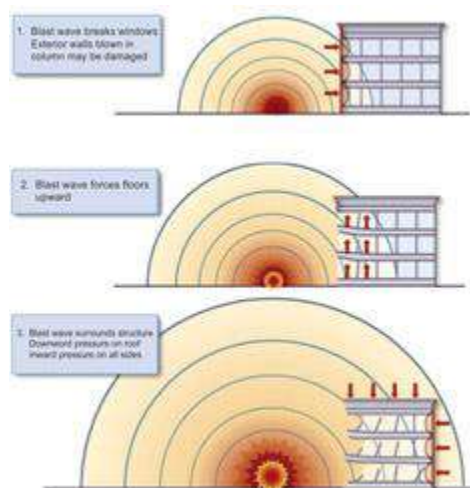


Figure 1: Blast Pressure Effects on a Structure

- In the first type a relatively large shock wave reaches a structure relatively small enough that the blast wave encloses the entire structure. The shock wave effectively acts on the entire structure simultaneously. Additionally, there is a drag force from the rapidly moving wind behind the blast wave. The structure is, however, massive enough to resist translation.



- The second condition also involves a relatively large shock wave and a target much smaller than the previous case. The same phenomena happen during this case, but the target is sufficiently small enough to be moved by the dynamic, drag pressure.
- In the final case, the shock burst is too small to surround the structure simultaneously and the structure is too large to be shifted. Instead of simultaneous loading, each component is affected in succession. For a typical building, the front face is loaded with a reflected overpressure.

LITERATURE REVIEW

In the past, few decades' considerable emphasis has been given to problems of blast and earthquake. The earthquake problem is rather old, but most of the knowledge on this subject has been accumulated during the past fifty years. The blast problem is rather new; information about the development in this field is made available mostly through publication of the Army Corps of Engineers, Department of Defense, U.S. Air Force and other governmental office and public institutes.

Much of the work is done by the Massachusetts Institute of Technology, The University of Illinois, and other leading educational institutions and engineering firms. Due to different accidental or intentional events, the behavior of structural components subjected to blast loading has been the subject of considerable research effort in recent years. Conventional structures are not designed to resist blast loads; and because the magnitudes of design loads are significantly lower than those produced by most explosions. Further, often conventional structures are susceptible to damage from explosions. With this in mind, developers, architects and engineers increasingly are seeking solutions for potential blast situations, to protect building occupants and the structures.

This study is very much useful for design the buildings constructed for industries where chemical process is the main activity. An increasing number of research programs on the sources of these impact loads a dynamic analysis and preventive measures are being undertaken. Just in design some areas takes into account the effects of earthquakes, hurricanes, tornadoes and extremes snow loads, likewise even explosive or blast loads has to be taken into design consideration. This does not mean design and consideration of special shelter facilities but simply the application of appropriate design techniques to ordinary buildings, so that one can achieve some degree of safety from sudden attacks.

Philip Esper in 2003, after the Four major bombing incidents took place in Mainland UK within the last ten years; the 1992 St Mary's Axe, the 1993 Bishopsgate, the 1996 Docklands and Manchester bombs the author was involved in the investigation of damage and reinstatement of numerous commercial buildings, and in providing advice to building owners and occupiers on blast protection measures for both existing and proposed buildings. These detonation devices were estimated as 450 kg, 850 kg, 500 kg and 750 kg of TNT equivalent, respectively. As a result, the author was involved in the investigation of damage and reinstatement of numerous commercial buildings, and in providing advice to building owners and occupiers on blast protection measures for both existing and proposed buildings. Numerical modeling as well as laboratory and on-site testing were used in the investigation of damage and assessing the dynamic response of these buildings and their floor slabs to blast loading. The finite element (FE) analysis technique used in this investigation is described, and the correlation between the results of the FE analysis and laboratory and on-site testing is highlighted. It was concluded that the ductility and natural period of vibration of a structure governs its response to an explosion. Ductile elements, such as steel and reinforced concrete, can absorb significant amount of strain energy, whereas brittle elements, such as timber, masonry, and monolithic glass, fail abruptly.

LUCCIONI et al in 2005, studied the effects of mesh size on pressure and impulse distribution of blast loads with the aid of hydro codes. A computational dynamic analysis using AUTODYN-3D was carried out over the congested urban environment that corresponds to the opposite rows of buildings of a block, in the same street. The results obtained for different positions of the explosive charge are presented and compared. The effect of mesh size for different boundary conditions is also addressed. It is concluded that the accuracy of numerical results is strongly dependent on the mesh size used for the analysis. On the other side the mesh size is also limited by the dimensions of the model and the computer capacity. One of the major features in the numerical



simulation of blast wave propagation in large urban environments is the use of an adequate mesh size.

Ghani Razaqpur et al in 2006, investigated the behavior of reinforced concrete panels, or slabs, retrofitted with glass fiber reinforced polymer (GFRP) composite, and subjected to blast load. Eight 1000 x 1000 x 70 mm panels were made of 40 MPa concrete and reinforced with top and bottom steel meshes. Five of the panels were used as control while the remaining four were retrofitted with adhesively bonded 500 mm wide GFRP laminate strips on both faces, one in each direction parallel to the panel edges. The panels were subjected to blast loads generated by the detonation of either 22.4 kg or 33.4 kg ANFO explosive charge located at a 3-m standoff. Blast wave characteristics, including incident and reflected pressures and impulses, as well as panel central deflection and strain in steel and on concrete/FRP surfaces were measured. The post-blast damage and mode of failure of each panel was observed, and those panels that were not completely damaged by the blast were subsequently statically tested to find their residual strength. It was determined that the reflected blast pressure and impulse measured at the same location during different shots using the same charge size and standoff distance were generally reasonably close, but in some cases significant deviation occurred. The results of this study indicate that the GFRP retrofit may not be suitable in every situation and that quantifying its strengthening effects will need more actual blast testing rather than merely theoretical modeling or pseudo-dynamic testing.

Ray Singh Meena in 2009, focused on the design techniques for the loading on roof structures and the resistance of open web steel joists, a common roof component. Blast loads are dynamic, impulsive and non-simultaneous over the length of a roof.

To design against explosions, a procedure has been developed to devise a uniform dynamic load on a roof that matches the response from blast loads. The objective of this research was to test and compare its results to the deflections from blast loads using FEM of analysis and to compare them to equivalent loading response. It is recommended that additional research is to be done on the prediction of blast pressures on roofs and on the development of an equivalent uniform dynamic load. It is also recommended that an analytical resistance function for open web steel joists be clearly defined, which includes all failure limit states.

Ngo ET AL in 2007, carried an analytical study on RC column subjected to blast loading and progressive collapse analysis of a multi-storied building were carried out. The 3D model of the column was analyzed using the nonlinear explicit code LS-Dyna 3D (2002) which takes into account both material nonlinearity and geometric nonlinearity. It was observed that the increase in flexural strength was greater than that of shear strength. Thus, the increase in the material strengths under dynamic conditions may lead to a shift from a ductile flexural failure to a brittle shear failure mode. In the progressive collapse analysis study which is based on the local damage assessment due to bomb blast at ground level, progressive collapse analyses was performed on the example building. The structural stability and integrity of the building were assessed by considering the effects of the failure of some perimeter columns, spandrel beams and floor slabs due to blast overpressure or aircraft impact. In addition to material and geometric nonlinearities, the analyses considered membrane action, inertia effects, and other influencing factors. The results show that the ultimate capacity of the floor slab is approximately 16.5kPa which is 2.75 times the total floor load (dead load plus 0.4 live load).

Alok Goyal in 2008, discussed through an overview to quantify blast loads as high pressure, short duration shock loading for the building as a whole and on each individual structural component. The study concluded that the most difficult part of the blast-resistance design is to define the blast wave parameters with acceptable probability of exceedance, and to quantify desired performance parameters in terms of crack widths, rotations, ductility factor capacities of elements or story drifts. Considerable efforts and skill is required to numerically predict the blast induced pressure field and highly non-linear response. Even then, the results may be meaningless due to modeling limitations and uncertainties associated with blast loads. The developed systems therefore should be tested in field and the data collected should be used to improve the design and the mathematical model.

Khadiid et al., studied the fully fixed stiffened plates under the effect of blast loads to determine the dynamic response of the plates with different stiffener configurations and considered the effect of mesh density, time



duration and strain rate sensitivity. He used the finite element method and the central difference method for the time integration of the nonlinear equations of motion to obtain numerical solutions.

A.K. Pandey et al., studied the effects of an external explosion on the outer reinforced concrete shell of a typical nuclear containment structure. The analysis has been made using appropriate non-linear material models till the ultimate stages. An analytical procedure for nonlinear analysis by adopting the above model has been implemented into a finite element code DYNAIB.

Alexander M. Remennikov, studied the methods for predicting bomb blast effects on buildings. When a single building is subjected to blast loading produced by the detonation of high explosive device. Simplified analytical techniques used for obtaining conservative estimates of the blast effects on buildings. Numerical techniques including Lagrangian, Eulerian, EulerFCT, ALE, and finite element modeling used for accurate prediction of blast loads on commercial and public buildings.

J. M. Dewey, studied the properties of the blast waves obtained from the particle trajectories. First time he introduced the effect of spherical and hemispherical TNT (trinitrotoluene) in blast waves and determined the density throughout the flow by application of the Lagrangian conservation of mass equation which used for calculating the pressure by assuming the adiabatic flow for each air element between the shock fronts. The temperature and the sound speed found from the pressure and density, assuming the perfect gas equation of states.

Kirk A. Marchand et al, reviews the contents of American Institute of Steel Construction, Inc. for facts for steel buildings give a general science of blast effects with the help of numbers of case studies of the building which are damaged due to the blast loading i.e. Murrah Building, Oklahoma City, Khobar Towers, Dhahran, Saudi Arabia and others. Also studied the dynamic response of a steel structure to the blast loading and shows the behavior of ductile steel column and steel connections for the blast loads.

M. V. Dharaneepathy et al., studied the effects of the stand-off distance on tall shells of different heights, carried out with a view to study the effect of distance (ground-zero distance) of charge on the blast response. An important task in blast-resistant design is to make a realistic prediction of the blast pressures. The distance of explosion from the structure is an important datum, governing the magnitude and duration of the blast loads. The distance, known as 'critical 6 ground-zero distance', at which the blast response is a maximum. This critical distance should be used as design distance, instead of any other arbitrary distance.

METHODOLOGY

A careful study of blast waves, air shock waves and ground shock waves generated during explosion and plotting a graph with the behavior of pressure with respect to time. Blast resistant dynamic design also uses the limit state design techniques which are collapse limit design and functionality limit design. It provides sufficient ductility to the building which gives rise to the distribution of explosion energy within the structure to avoid risk of collapse.

Structural Response or Analysis to Blast Loading

Blast loading is a short duration load also called impulsive loading. Mathematically blast loading is treated as triangular loading. The ductility and natural period of vibration of a structure governs its response to an explosion. There are three kinds of explosions which are unconfined explosions, confined explosions and explosions caused by explosives attached to the structure.

Unconfined explosions can occur as an air-burst or a surface burst. In an air burst explosion, the detonation of the high explosive occurs above the ground level and intermediate amplification of the wave caused by ground reflections occurs prior to the arrival of the initial blast wave at a building (Figure 2) As the shock wave continues to propagate outwards along the ground surface, a front commonly called a Mach stem is formed by the interaction of the initial wave and the reflected wave.

However a surface burst explosion occurs when the detonation occurs close to or on the ground surface. The initial shock wave is reflected and amplified by the ground surface to produce a reflected wave. (Figure 3) Unlike the air burst, the reflected wave merges with the incident wave at the point of detonation and forms a single wave. In the majority of cases, terrorist activity occurs in built-up areas of cities, where devices are placed on or very near the ground surface.

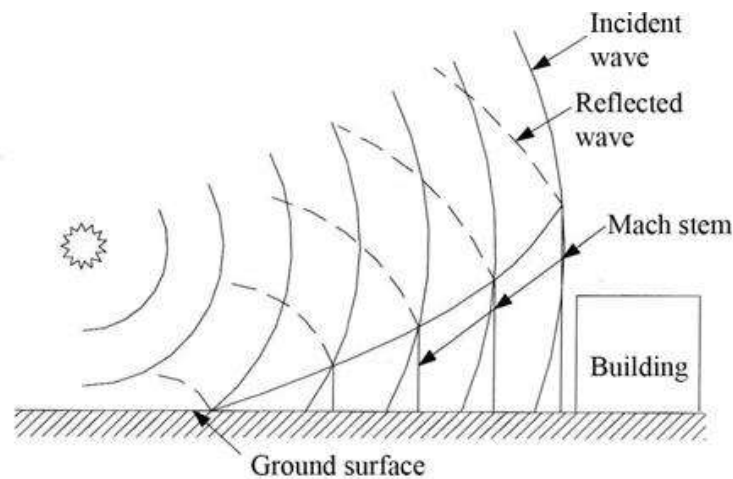


FIGURE-2 AIR BURST WITH GROUND REFLECTIONS

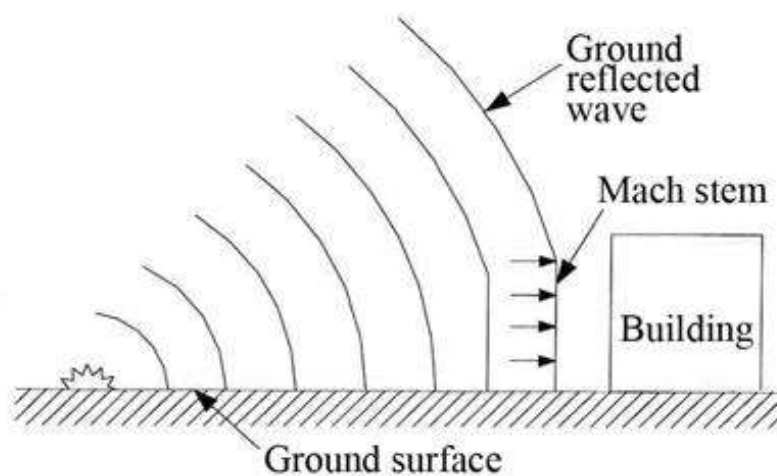


FIGURE 3 SURFACE BLAST

When an explosion occurs within a building, the pressures associated with the initial shock front will be high and therefore will be amplified by their reflections within the building. This type of explosion is called a confined explosion. In addition and depending on the degree of confinement, the effects of the high temperatures and accumulation of gaseous products produced by the chemical reaction involved in the explosion will cause additional pressures and increase the load duration within the structure. Depending on the extent of venting, various types of confined explosions are possible. (Figure 4)

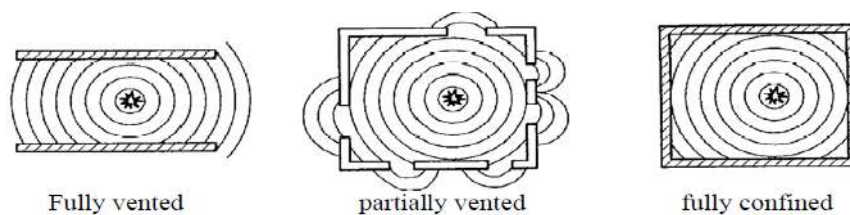


FIGURE-4 FULLY VENTED, PARTIALLY VENTED AND FULLY CONFINED EXPLOSIONS

If detonating explosive is in contact with a structural component, e.g. a column, the arrival of the detonation wave at the surface of the explosive will generate intense stress waves in the material and resulting crushing of the material. Except that an explosive in contact with a structure produces similar effects to those of unconfined or confined explosions. There are many forms of high explosive available and as each explosive has its own detonation characteristics, the properties of each blast wave will be different. TNT is being used as the standard benchmark, where all explosions can be expressed in terms of an equivalent charge mass of TNT. The most common method of equalization is based on the ratio of an explosive's specific energy to that of TNT.

REFERENCES



1. 'Prediction of blast loading and its impact on buildings', Nitesh. N. Moon national institute of technology Rourkela- 2009
2. 'ARCHITECTURAL AND STRUCTURAL DESIGN FOR BLAST RESISTANT BUILDINGS', Zeynep Koccaz, *Institute of Science, Technical University, Taskisla, and Istanbul, Turkey 2008*
3. A.GhaniRazaqpur, Ahmed Tolba and EttoreConstestabile, Blast loaing response of reinforced concrete panels reinforced with externally bonded GFRP laminates. Science direct, Composites: Part B 38 (2007) 535-546.
- 4 AlokGoyal, Blast resistant design: Critical issues, proceedings of the sixth structural engineering convection, pp IPXI-1-10, Dec 2008
5. AnatolLonginow A, and Mniszewski KR., "Protecting buildings against vehicle bomb attacks," Practice Periodical on Structural Design and Construction, ASCE, New York, pp. 51-54, 1996.
6. B. Lu, P. Silva, A. Nanni, and J. Baird, Retrofit for Blast-Resistant RC Slabs with Composite Materials, University of Missouri–Rolla, SP-230—76
7. B.M. Luccioni¹, R. D. Ambrosini & R.F. Danesi¹, Assessment of blast loads on structures, WIT Transactions on Engineering Sciences, Vol 49, 2005
8. Mario Paz, Structural dynamics, second edition, CBS publishers and distributors, 2004.
9. Philip Esper, investigation of damage to buildings under blast loading and recommended protection measures, 9th International Structural Engineering Conference, Abu Dhabi, November 2003
10. Ray Singh Meena, BE thesis report, National Institute of Technology, Rourkela (2009)
11. Smith and Hetherington (1994) Blast and ballistic loading of structures, Oxford Butterworth-Heinemann.
12. T. Ngo, P. Mendis, A. Gupta & J. Ramsay, "Blast Loading and Blast Effects on Structures – An Overview", The University of Melbourne, Australia, EJSE Special Issue: Loading on Structures (2007)
13. T.D. Ngo, P.A. Mendis, & G. Kusuma, "Behavior of high-strength concrete columns subjected to blast loading, The University of Melbourne, Australia (2002).



MATRUSRI ENGINEERING COLLEGE

(Approved by AICTE, Affiliated to Osmania University)

#16-1-486, Saidabad, Hyderabad - 500059



Sponsored by

MATRUSRI EDUCATION SOCIETY



ISBN: 97881-936274-0-2



1ST NATIONAL CONFERENCE ON TRENDS IN SCIENCE, ENGINEERING AND TECHNOLOGY

(NTSET - 2018)

February 2nd & 3rd - 2018

TECHNICAL PAPER ABSTRACTS



NTSET 2018



ORGANIZED BY

MATRUSRI ENGINEERING COLLEGE

(Approved by AICTE, Affiliated to Osmania University)

#16-1-486, Saidabad, Hyderabad - 500059



Sponsored by

MATRUSRI EDUCATION SOCIETY

ISBN: 97881-936274-0-2





A STUDY ON RECYCLED BITUMINOUS PAVEMENT MATERIALS USING BITUMEN VG-30

P V S Koteswara rao¹, P.Suresh Babu² and R. Srinivasa Kumar³

¹Assoc Prof, civil Engg dept, Matrusri Engg College; ²Research Scholar Osmania University, Hyderabad; ³Asst. Professor, Dept. of Civil Eng. University College of Eng. Osmania University, Hyderabad.

ABSTRACT

In general, any good road construction requires large quantities of construction materials from natural resources. Continuously utilization of natural resources particularly the stone aggregates creates future shortfall and environmental imbalances. In view of utilization of reclaimed asphalt pavement (RAP) for recycling of bituminous pavements has got significance now.

With the above serious concern, the present study has been carried to use of recycled bituminous pavement (RAP) with new aggregates collected from quarry materials and mixed with bitumen (VG-30) grade. The prepared several combinations of trial mixes of Dense Bituminous Macadam (DBM) mixture sample were then tested conducted as per MORTH (2013) specification.

It has been observed that mix combination of 40% of RAP with 60% of new aggregates is within the specified limits of MORTH (2013) Specifications¹. Hence it is found that RAP can be used in place of new formation of roads in Urban & Rural roads.

1. INTRODUCTION

In order to reduce the usage of natural aggregate, recycled asphalt pavement can be used as partially or fully replacement of new materials. The Reclaimed asphalt pavement (RAP) is the term used to collect from existing old pavements by milling equipment. RAP material is tested with the bitumen extraction test, identify bitumen percentage and aggregate gradation and the obtained material is reused by suitably blending with processed new aggregate and bitumen

There has been considerable research carried out on the reusability of RAP over the past 1980s and this has grown considerably over the past years as the various agencies²⁻⁷, Central and State Governments have recognized the need for greater sustainability in construction. As an example of Indian practice, Clause No.519.2.1, MORTH also recommends to reuse of RAP for production of bituminous macadam (BM) and dense bituminous macadam (DBM) by suitably blending with new bitumen and the aggregates subjected to the maximum proportion of RAP materials used is limited to not greater than 60%.

With the above importance, the present research work is under taken and the details of objectives and scope of the study are as follows.

2.0 OBJECTIVE AND SCOPE OF THE STUDY

2.1 Objectives

The objectives of the present study are listed below:

- To study the suitability of RAP materials for production of DBM by partial replacement with natural aggregate by conducting required laboratory tests
- To determine the strength characteristics of the blended RAP material by conducting Marshall Stability Tests and determine its compliance with MORTH Specification (2013).

2.2 Scope of the study

The following are the details of scope of the work.

- Investigation the prospects of recycling of the RAP material obtained from exiting old bituminous pavement NH-202.
- To evaluate engineering properties of the RAP samples collected from NH-202.
- To blend the aggregates to meet the standard graduation requirement of DBM as per MORTH 2013.
- Determination of optimum percent replacement of virgin aggregate by the RAP.
- Determination of strength characteristics of RAP as DBM mix by conducting Marshall Stability Test with the following trail mixes.

3. EXPERIMENTAL PROCEDURE

The details of methodology and the steps followed in the laboratory evaluation of RAP are brief below: Source of RAP materials are from deteriorated surface NH-202 at Ghatkesar junction in Hyderabad and evaluate its engineering properties by conducting bitumen extraction test, sieve analysis and other tests on the aggregate obtained from the RAP as per standard specifications.



Fig. 1 Collection RAP material and bitumen extraction test on RAP

After conducting the above tests RAP, analysis is carried out to examine the inherent characteristics of RAP so as to determine optimum proportion of different sizes of natural aggregates required to be added to the extracted RAP materials and optimum bitumen. To validate the experiments results with MORTH & MS-2 Specifications were adopted.

The engineering properties of the natural aggregate used and the aggregates obtained from the RAP are tested and the details are presented in Table 1. The new natural aggregate was procured from a stone crusher near Hyderabad.

Table 1 Summary of the Test results of Natural aggregate and Aggregate Obtained from RAP material.

Physical	Test	Specification	Test Results	
			Natural Aggregate	RAP Material
Impact Value	IS:2386 (Part IV)	27% Max.	21.73%	22.26%
Water Absorption	IS:2386 (Part III)	2%	27-12 mm	0.547
			5-0 mm	0.879
Specific Gravity	IS:2386 (Part III)	2.5-3.2	27-12 mm	2.680
			5-0 mm	2.556

The engineering properties of the bitumen used for preparing the Marshall mix samples are presented in Table 2

Table 2 Physical properties of bitumen (VG-30) used

Property	Bitumen test results	Requirement as per IS 73:2006 ⁸
Penetration value (mm)	62 mm	40 (min)



Ductility (cm)	86.50 cm	40(min)
Specific gravity	1.020	0.98-1.02
Softening point	49.40 C	47 C(min)

Trial Marshall-mix samples of the proposed DBM were prepared by varying proportion of RAP material as 35%, 40%, 50% s 65%, 60% and 50% with new aggregates, and the each sample was mixed with bitumen (VG-30) content of 3%, 3.5%, 4%, 4.5% and 5%.

The Marshall test data of the above samples were drawn for Unit weight Vs Bitumen Content, Air Voids Vs Bitumen Content, VMA Vs Bitumen Content, VFB Vs Bitumen Content, Marshall Stability Vs Bitumen Content and Flow Vs Bitumen Content.

4. TEST RESULTS

The suitability of reusability RAP in DBM was evaluated and the details are as follows:

Marshall test results obtained on the DBM Grading II design mix proportioned with 35%, 40% and 50% of RAP are presented Table 4, Table 5 and Table 6, respectively. Summary of Marshall test results obtained with optimum bitumen content for the RAP proportions used are presented in Table 7.

Table 4 Marshall stability test results of DBM with 35 % RAP

Bitumen %	Density	Stability	Air Voids	VMA	VFB	Flow
3.00	2.340	27.25	7.80	14.13	44.80	3.87
3.50	2.348	28.57	6.75	14.26	52.67	4.13
4.00	2.345	33.83	6.16	14.81	58.43	4.20
4.50	2.343	29.88	5.55	15.34	63.84	5.07
5.00	2.354	28.57	4.39	15.39	71.46	5.33

Table 5 Marshall stability test results of DBM with 40 % RAP

Bitumen %	Density	Stability	Air Voids	VMA	VFB	Flow
3.00	2.309	27.74	8.93	15.15	41.04	3.73
3.50	2.313	30.43	8.08	15.44	47.70	5.93
4.00	2.316	32.39	7.28	15.79	53.90	4.50
4.50	2.337	29.11	5.71	15.45	63.03	4.97
5.00	2.330	30.98	5.31	16.16	67.14	6.33

Table 5 Marshall stability test results of DBM with 50 % RAP

Bitumen %	Density	Stability	Air Voids	VMA	VFB	Flow
3.00	2.311	25.07	9.17	15.49	40.82	4.20
3.50	2.313	27.98	8.39	15.86	47.08	4.60



4.00	2.318	25.14	7.51	16.13	53.42	5.60
4.50	2.329	26.78	6.34	16.15	60.73	6.60
5.00	2.248	25.19	8.93	19.50	54.19	7.00

Table 7 Summary of Marshall test results obtained with optimum bitumen content for the RAP proportions used

Mix Proportion with RAP %	Bitumen (%)			Density (g/cc)	Stability (kN)	Air Voids (%)	VMA (%)	VFB (%)	Flow (mm)
	Existing	Additional	Overall						
Mix-I (35%)	4.40	0.75	5.15	2.337	26.45	4.96	16.62	70.19	5.57
Mix-II (40%)	4.40	0.25	4.65	2.347	28.57	5.18	15.34	66.23	4.95
Mix-III (50%)	4.40	0.85	5.25	2.314	24.99	5.87	17.51	66.5	5.88

5. CONCLUSIONS

Based on the laboratory experiments carried out in this study, the following conclusions have been drawn: For the materials used in this study, it was found that, the proportion of 40% RAP material and 60% of virgin material by weight, proved to be optimum. The engineering properties of this RAP substituted mix are found to be satisfactory and comparable to that of the 100% virgin material.

Hence it is concluded that the experimental results showed that, the RAP materials can be used effectively together with the virgin material such that, the RAP materials utilization is environmentally favourable and energy saving. Further, milling of RAP from the old existing urban roads can result to maintain the top levels of roads in an urban area will be within the limit as before overlay, so that, urban drainage problems can be eliminated.

REFERENCES

1. MORTH (2013), "Specifications for Road and Bridge Works: (Clause 519 Recycling of Bituminous Pavement", Ministry of Road Transport and Highways (MORTH), Indian Roads Congress, New Delhi, pp.242-250.
2. Riddish A. Shah and Jayesh hai R. Pitroda, (2011), Recycling of Construction of mate-rials for sustainability, Journal of National Conference on Recent trends in Engineering & Technology.
3. Ravi Patel, Chetna M Vyas and Darshana R. Bhatt (2013), Experimental investigation for Re-cycled Coarse aggregate replaced for natural Course aggregate in Concrete, International Journal of Civil, Structural, Environmental and Infrastructure Engineering and Development, Volume 3 issue 2.
4. Betenson W. D. (1979), Recycled asphalt concrete in Utah, Proceedings of the Association of Asphalt Paving Technologists, Vol.48, , pp.272-295.
5. Mallick B. R., lecture notes, A 3-day workshop on recycling and other pavement rehabilitation methods, IIT Kanpur, 8-10th February, 2005, pp.58-350.
6. Ikeda, T., and Kimura, M., Recent developments in recycling asphalt pavements in Japan, Proceedings of 8th international conference on asphalt pavements, Seattle, Washington, 1997, pp. 99-106.
7. Epps J.A., Terrel R. L., Little, D. N. and Holmgreen R. J., Guidelines for recycling asphalt pavements, Proceedings of the Association of Asphalt Paving Technologists, Vol.49, 1980, pp.144-176.
8. IS.73-1992-Paving Bitumen Specification, BIS, New Delhi, 2nd Revision.



MATRUSRI ENGINEERING COLLEGE

(Approved by AICTE, Affiliated to Osmania University)

#16-1-486, Saidabad, Hyderabad - 500059



Sponsored by

MATRUSRI EDUCATION SOCIETY



ISBN: 97881-936274-0-2



1ST NATIONAL CONFERENCE ON TRENDS IN SCIENCE, ENGINEERING AND TECHNOLOGY

(NTSET - 2018)

February 2nd & 3rd - 2018

TECHNICAL PAPER ABSTRACTS



ORGANIZED BY

MATRUSRI ENGINEERING COLLEGE

(Approved by AICTE, Affiliated to Osmania University)

#16-1-486, Saidabad, Hyderabad - 500059



Sponsored by

MATRUSRI EDUCATION SOCIETY

ISBN: 97881-936274-0-2

NTSET 2018





Impact of moisture deficit stress on growth, biomass and yield parameters of cluster bean (*Cyamopsis tetragonoloba* L.Taub.) genotypes

Satyavathi. P¹., Vanaja M², Vagheera P³. and Ira Khan⁴
¹Matrusri Engineering College, Saidabad, Hyderabad- 500059
E-mail: [1ganiseti.satyavathi@gmail.com](mailto:ganiseti.satyavathi@gmail.com)

Abstract

Drought stress is considered as one of the most adverse abiotic stresses which is a threat to majority of the plant growth and productivity. Therefore, the aim of the present study was to identify the drought tolerant genotype/s of Cluster bean (*Cyamopsis tetragonoloba* L.Taub.) for the semi-arid regions. Abiotic stresses have considerable influence on biomass and seed yield parameters of crop plants. A field experiment was conducted to evaluate the moisture deficit stress on biomass and seed yield parameters of three cluster bean genotypes RGC-1025, RGC-936 and HGS-563 during winter season 2014. The stress was imposed during the initiation of flowering stage and the observations were recorded at the time of harvest for growth, biomass and seed yield parameters. All the selected genotypes recorded reduction under stress condition as compared with well watered condition for morphological, biomass and seed yield traits, however the magnitude of reduction varied with genotype. Among the three genotypes, the total biomass at harvest was highest with HGS-563 while with RGC-936 under stress. The seed yield was highest with RGC-936 under both moisture levels while HGS-563 recorded lowest seed yield as well as highest reduction with stress. Among all the three genotypes assessed, the genotype RGC-936 performed best in both moisture levels for biomass and seed yield parameters.

Key words: Guar, genotypes, biomass, water deficit stress, seed yield, HI

Introduction

Cluster bean (*Cyamopsis tetragonoloba* L. Taub.), is also known as *guar*, is an important commercial crop which is grown both in arid and semi-arid region. Cluster bean is a drought resistant annual legume crop. Being a leguminous crop, it fixes the atmospheric nitrogen and enriches the soil fertility. The crop is mainly grown during rainy season as well as under irrigated condition in summer season.

Drought stress impairs the plants growth and yield. Drought can be defined as the lack of required amount of moisture which is necessary for a plant to grow healthy (Zhu 2002). Even though cluster bean is a minor crop but due to its gum qualities it is considered as an important cash crop for industrial gum production. The discovery of the galactomannan gum in the endosperm during 1948, led to this hitherto insignificant plant gaining importance as an industrial crop. The gum is utilized for many food items like ice creams, baked and dairy products etc. Moreover, its gum also used in many other industries like pharmaceuticals, cosmetics, mining, textile, paper, oil drilling, explosive industry etc. The productivity of this crop can be significantly



increased with the use of improved production technologies. Owing to the significant applications in industries there is an obvious need to undertake studies in cluster bean to identify suitable genotypes for semi-arid regions in order to expand its area under cultivation.

Materials and Methods:

Field experiments were conducted with 3 genotypes of cluster bean- RGC-1025, RGC-936 and HGS-563 during winter season of 2014, and their yield potentials were quantified both under irrigated and moisture deficit stress conditions. The germplasm was obtained from Rajasthan Seed Corporation and raised at CRIDA (HRF), Hyderabad. The selected genotypes were sown in 2.25m × 2.0m plots maintaining 15cm space between plants and 45cm between rows with three replications for both irrigated and moisture deficit stress treatments. The crop was maintained moisture and nutrient stress free by irrigating at regular intervals and applying recommended dose of fertilizers. Moisture deficit stress was imposed during the initiation of flowering stage by withholding irrigation till wilting symptoms appeared then stress was released and maintained stress free till harvest. The observations were recorded at the time of harvest for growth, biomass and seed yield parameters such as stem length (SL, cm); stem dry weight (SDW, g/plant); number of clusters (NOC); number of pods (PN); pod weight (PW, g/plant); fodder dry weight (FDW, g/plant); vegetative biomass (VBM, g/plant); total biomass (TBM, g/plant); seed yield (SY, g/plant); test weight (TW, g/plant) and harvest index (HI, %) under each treatment.

The data was statistically analyzed using a two-way analysis of variance (ANOVA) to test the significance of genotypes, moisture levels and their interactions

Results and Discussion

Based on ANOVA, it was observed that there was highly significant ($p < 0.01$) difference for genotypes for all the traits- plant height, number of clusters, pod number, stem dry weight, pod weight, seed yield, vegetative biomass, total biomass, harvest index and significant ($p < 0.05$) for test weight, while non-significant for fodder biomass (Table 1). The moisture levels were highly significant ($p < 0.01$) for all the parameters except for stem weight, seed weight and vegetative biomass. The interaction of genotypes x seasons were highly significant ($p < 0.01$) for all the parameters while stem length, number of pods, pod weight and vegetative biomass were significant.

The *per se* values of the parameters studied were presented in Table 2 and the % of reduction of these parameters due to stress was presented as Fig.1.

The cluster bean genotypes response for growth and biomass parameters were significant for moisture levels. Moisture deficit stress reduced growth and biomass parameters such as stem length, number of clusters, number of pods, stem weight, pod weight, seed weight, test weight and total biomass at the time of harvest. The results are in line with earlier reports of Baroowa *et al.* (2016) who observed reduced growth and biomass parameters under stress condition in black gram and green gram genotypes. Siddiqui *et al.* (2015) also reported that the growth parameters of Faba Bean were reduced



due to drought stress.

The stem length of the cluster bean genotypes under well watered condition ranged from 49.2 cm (RGC-936) to 45 cm (RGC-1025) with genotypic mean of 47.7cm whereas it ranged from 38.1cm (HGS-563) to 32.2cm (RGC-1025) with a mean of 34.4cm under moisture stress. Dahanayake *et al.* (2014) also observed significant reduction in stem length under water stress condition in black gram.

The highest number of clusters per plant under both well watered and stress condition were recorded by HGS-563 (23.2 & 15.6) while the genotypes RGC-1025 and RGC-936 maintained similar number of clusters (19.8) under irrigated conditions and recorded similar reduction with moisture deficit stress. The highest number of pods per plant under well watered condition were recorded by RGC-1025 (65.6) and lowest by HGS-563 (58.6), while under moisture deficit stress it was RGC-936 (53.8) and HGS-563 (50.6) respectively, revealing that though the pod number of genotype HGS-563 was lowest its reduction due to stress was also minimum (13.65 %). Moisture deficit stress reduced pod weight of all the genotypes and significant variation was observed for genotypes, treatments and their interaction. RGC-936 (14.42g/pl) recorded maximum pod weight at well watered condition and minimum by HGS-563 (11.48 g/pl). Whereas RGC-936 (11.72g/pl) recorded maximum and RGC-1025 (8.51g/pl) minimum pod weight under water deficit condition.

The seed weight of RGC-936 was highest under irrigated (8.1g/pl) and stress condition (6.6g/pl) followed by RGC-1025 (6.16 g/pl 5.23 g/pl) and HGS-563 (5.6g/pl & 4.3g/pl). Among the three genotypes, RGC-1025 recorded highest seed yield under both moisture levels with lowest reduction due to moisture stress (15.1%). In White bean, Habibi (2011) also recorded reduced number of pods and seed yield with drought stress. There was a significant variation in genotypes, moisture levels and their interaction for test weight. The test weight of genotypes was 3.12g under stress and 3.47g under well watered periods showing the stress impacted the seed filling. Among the genotypes, RGC-1025 (3.6g) maintained highest test weight under well watered condition while HGS-563 (3.32g) under drought stress. Under moisture deficit stress, the reduction in the seed yield of cluster bean genotypes was due to the reduction in number of pods, seed number and test weight.

There was a significant variation in genotypes, moisture levels and their interaction for HI. Among all the genotypes, RGC-1025 recorded an improvement of 18.58% in HI with stress as compared with its performance under irrigated condition, revealing that though biomass and seed yield was reduced with stress the impact was higher on biomass than seed yield of this genotype. The genotypes HGS-563 (69.87 g/pl & 69.88 g/pl) recorded maximum and RGC-936 (54.45g/pl & 56.31g/pl) recorded minimum fodder biomass under both well watered and drought stress periods. While the genotype HGS-563 maintained the fodder biomass in both the conditions. Maximum vegetative biomass was observed in HGS-563 (41.17g/pl) and



minimum in RGC-1025 (24.75 g/pl) under well watered period whereas in stress RGC-1025 (32.58 g/pl) recorded maximum and RGC-936 (22.07g/pl) recorded minimum.

From the results it can be concluded that the genotype RGC-936 is ideal to grow under semi arid regions as it recorded better seed yield under both irrigated and moisture deficit stress conditions. The genotype HGS-563 is suitable for biomass production even under stress conditions.



Table 1. ANOVA of morphological, biomass and yield parameters of guar genotypes under irrigated and stress conditions- Winter Season 2014

Parameter	Genotypes	Moisture levels	G×ML
Stem Length	**	**	*
Number of Clusters	**	**	**
Number of pods	**	**	*
Stem weight	**	NS	**
Pod Weight	**	**	*
Seed Weight	**	NS	**
Test Weight	*	**	**
Total Biomass	**	**	**
Harvest Index	**	**	**
Vegetative Biomass	**	NS	**
Fodder Biomass	NS	**	**



Table 2. The *per se* values of morphological, biomass and yield parameters of guar genotypes under irrigated and stress conditions- Winter Season 2014

Parameters	Stem length (cm)		No. of Clusters		No. of Pods	
	Irrigated	Stress	Irrigated	Stress	Irrigated	Stress
RGC 1025	45.00	32.2	19.8	13.8	65.6	52.4
RGC 936	49.2	32.8	19.8	14.2	62.6	53.8
HGS 563	49	38.1	23.2	15.6	58.6	50.6
	Stem Wt. (g/pl)		Pod Wt. (g/pl)		Total Biomass (g/pl)	
RGC 1025	4.06	3.39	14.26	8.51	17.79	12.63
RGC 936	5.34	2.59	14.42	11.72	17.74	15.04
HGS 563	7.01	3.26	11.48	9.71	18.57	14.30
	Seed Wt. (g/pl)		Test Wt. (g)		HI (%)	
RGC 1025	6.16	5.23	3.62	3.01	35.49	42.08
RGC 936	8.08	6.57	3.16	3.04	46.22	44.29
HGS 563	5.59	4.31	3.54	3.32	32.03	30.23
	Vegetative biomass (g/pl)		Fodder Biomass (g/pl)			
RGC 1025					58.58	
RGC 936					56.31	
HGS 563					59.88	

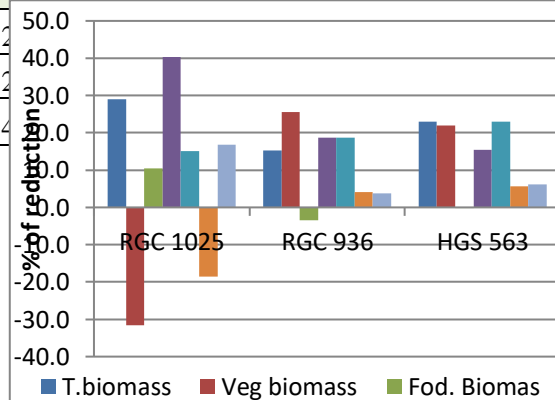


Fig. 1 The reduction in different biomass and yield parameters of cluster bean genotypes due to moisture deficit stress



References

- Zhu Q. (2002). Salt and drought stress signal transduction in plants. *Annu. Rev. Plant Biol.*, 53, 247-273.
- Baroowa B. and Gogoi N. (2016). Morpho-physiological and yield responses of black gram (*Vigna mungo* L.) and Green gram (*Vigna radiata* L.) genotypes under drought at different growth stages. *Research Journal of Recent Sciences* 5(2): 43-50.
- Dahanayake N., Ranawake AL and Senadhipathy DD. (2014). Effects of water stress on the growth and reproduction of black gram (*Vigna mungo* L.). *Tropical Agricultural Research & Extension* 17(1):
- Habibi G. (2011). Influence of drought on yield and yield components in white bean. *International Journal of Biological, Biomolecular, Agricultural, Food and Biotechnological Engineering* 5 (7).
- Siddiqui MH., Mutahhar Y., Al-Khaishany, Mohammed A., Al-Qutami, Mohamed H. Al-Whaibi, Anil Grover, Hayssam M. Ali, Mona S. Al-Wahibi and Najat A. Bukhari (2015). Response of different genotypes of faba bean plant to drought stress. *International Journal of Molecular Sciences* 16(5): 10214-10227.



MATRUSRI ENGINEERING COLLEGE

(Approved by AICTE, Affiliated to Osmania University)

#16-1-486, Saidabad, Hyderabad - 500059



Sponsored by

MATRUSRI EDUCATION SOCIETY



ISBN: 97881-936274-0-2



1ST NATIONAL CONFERENCE ON TRENDS IN SCIENCE, ENGINEERING AND TECHNOLOGY

(NTSET - 2018)

February 2nd & 3rd - 2018

TECHNICAL PAPER ABSTRACTS



ORGANIZED BY

MATRUSRI ENGINEERING COLLEGE

(Approved by AICTE, Affiliated to Osmania University)

#16-1-486, Saidabad, Hyderabad - 500059



Sponsored by

MATRUSRI EDUCATION SOCIETY

ISBN: 97881-936274-0-2

NTSET 2018





STUDY OF CONCRETE USING LD SLAG AS PARTIAL REPLACEMENT OF COARSE AGGREGATE

B.Udayasree¹, S.Lokeswari², T. Raja Ramanna³,

^{1,2,3} Assistant Professor, Matrusri Engineering College (MECS), Santosh Nagar, Hyderabad,
Email: ¹udayaregella@gmail.com, ²sankaralokeswari@gmail.com, ³trajaramanna@gmail.com,

ABSTRACT

India has an enormous growth in steel industry and Slag is a byproduct of the same which has to be disposed properly. Steel industry generate large quantities of Slags from their iron-making and steel-making processes. Iron making Slags are recycled in cement making and steel-making Slags are dumped because they are unsuitable for the cement industry owing to the high iron content and other impurities. Reuse of waste in integrated steel plants is important with regard to environmental and economic consideration.

LD Slag is a byproduct of the iron ore and steel making industry. It is produced in large quantities and poses a substantial disposal problem. The letters **LD** means **L**inz and **D**onawitz, towns in Austria where the process was invented. The generation of LD Slag in Indian steel plants is about 200 kg per ton of hot metal produced. Out of this only 25% is being reutilized in India compared to 70-100% in other countries.

The objective of the present study is to study the possibility of using LD Slag as partial replacement of coarse aggregate and to compare the properties of the proposed concrete with that of existing conventional concrete. An experimental investigation was carried out to evaluate the effect of replacing coarse aggregate by LD Slag on flexural strength and compressive strength of concrete. Coarse aggregate was replaced with three percentages (1%, 2% and 3%) of LD Slag by volume in M25 grade of concrete with 0.5 water cement ratio (w/c).

Key words: LD Slag, Partial Replacement

INTRODUCTION

Concrete is widely used structural material consisting essentially of a binder and mineral filler. It has the unique distinction of being the only construction material actually manufactured on the site, whereas other materials are merely shaped to use at the worksite. Steel making slag is a product resulting from the industrial processes carried out to produce first, pig iron and second, steel. LD slag is generated in the steel-making process resulting from the transformation of pig iron in liquid steel. The letters LD come from the fact that the steel is produced in an LD type oxygen converter, **LD** meaning **L**inz and **D**onawitz, towns in Austria where the process was invented. This process is also called as Basic Oxygen Process. The generation of LD slag in Indian steel plants is about 200 kg per ton of hot metal produced. Out of this only 25% is being reutilized in India compared to 70-100% in other countries.

Present Uses of LD Slag:

a) LD Slag as Railway Ballast

LD Slag bolder is used in road making and floor preparation for its high hardness and cementing property. All the steel plants in India are selling more than 50% LD Slag for road making and ground filling. LD Slag has been proved to be an excellent railway ballast material and, as such, is being used by Indian Railways.



b) LD Slag in Cement:

LD Slag is used as Cement making for replacement of clinker. LD Slag has higher CaO content in comparison to BF Slag, which acts as an activator and gives better strength.

c) The others areas where LD Slag is used are:

Road base and sub-base, Yard paving, Asphaltic cover, Soil corrective element for agricultural use, Cleaning of metallic structures, Anti-dust treatment, Rock Plugs, Recycling in steel products, Landfills, River beds, Acidic water treatment.

Properties of LD Slag:

Resistance to heavy load/compression, Resistance durability, free drainage, interconnected angled particles, Resistance to skidding, Inertia, Basicity/ CaO content, Soluble P₂O₅ content.

Chemical composition of LD Slag:

The chemical composition of typical LD slag samples generated at steel plant is shown in the following table.

Table 1:Chemical Composition of LD Slag

Type of Waste (Non-hazardous)	FeO	CaO	MgO	SiO ₂	Al ₂ O ₃	MnO
LD Slag	5.89	50.75	10.31	17.99	1.02	1.30

Table 2: Physical Properties of LD Slag

S.No.	Properties	Test results
1	Fineness modulus	7.93
2	Specific gravity	2.15

CONCEPT OF MIX DESIGN

It will be a worthwhile to recall at this stage the relationship between aggregates and pastes which are the two essential ingredients of concrete. Workability of the mass is provided by the lubricating effect of the paste and it is influenced by the amount and dilution of paste. The strength of the concrete is limited by the strength of the paste, since mineral aggregates with rare exception are for stronger than the quality and continuity of the paste, since little water flows through aggregates either under pressure or capillarity. Further, the predominant contribution to drying shrinkage of concrete is that of paste.

MIX DESIGN OF M25 GRADE CONCRETE

- Grade Designation - M25
- Type of Cement - OPC 53 grade
- Maximum Nominal - 20mm
- Aggregate
- Minimum Water Content - 300 Kg/m³
- Maximum Water Cement ratio - 0.50
- Workability-Slump - 60 mm



Compacting Factor	-	0.94
Exposure Conditions	-	Moderate
Type of Aggregate	-	Crushed Angular
Type of Admixture	-	Super Plasticizer

Test Data for Materials:

Cement used	-	Jaypee OPC 53 grade
Specific Gravity of Cement	-	3.08
Specific Gravity of Water	-	1.00
Chemical Admixture	-	Armstrong Chemical
Specific Gravity of Aggregate	-	2.67
Specific Gravity of Sand	-	2.75

MATERIALS REQUIREMENT FOR M25 GRADE

Mix proportions for one cum of Concrete:

Mass of Cement	-	383.16	Kg
Mass of Water	-	191.58	lit
Mass of Fine Aggregate	-	679.905	Kg
Mass of Coarse Aggregate	-	1228.584	Kg
Water Cement Ratio	-	0.50	

Mix Proportion by Weight/by Volume

Mix M25	Cement	Fine Aggregate	Coarse Aggregate	Water
Weight (Kg)	383.16	679.90	1228.58	191.58
Ratio	1	1.77	3.20	0.50

Batching Proportions for M25 grade Concrete

Table 3: Batching Proportions for M25 Grade Concrete per m³ in Flexure

S.No.	% of LD Slag	Cement	Fine Aggregate	Coarse Aggregate	Water	LD Slag	Super Plasticizer
1.	0 %	18.10	32.06	58.03	9.05	-	108.6
2.	1 %	18.10	32.06	57.44	9.05	0.580	108.6
3.	2 %	18.10	32.06	56.86	9.05	1.160	108.6
4.	3 %	18.10	32.06	56.28	9.05	1.740	108.6

Table 4: Batching Proportions for M25 Grade Concrete per m³ in Compression

S.No.	% of LD Slag	Cement	Fine Aggregate	Coarse Aggregate	Water	LD Slag	Super Plasticizer
1.	0 %	11.63	20.61	34.54	5.80	-	69.78
2.	1 %	11.63	20.61	34.19	5.80	0.345	69.78



3.	2 %	11.63	20.61	33.84	5.80	0.690	69.78
4.	3 %	11.63	20.61	33.50	5.80	1.036	69.78

Observations of Flexural Strength(N/mm²):

Table 5: Flexural Strength of M25 Grade Concrete for 7 days

S.No.	Specimen size (150x150x700)	% of LD Slag	Span (Cm)	Distance of fracture	Load (KN)	Avg. Load (KN)	Avg.* Strength (N/mm ²)
1.	1	0 %	70	25.00	25.50	25.50	5.28
2.	2	1 %	70	31.00	25.50	25.50	5.28
3.	3	2 %	70	29.30	26.00	26.00	5.39
4.	4	3 %	70	28.90	26.00	26.00	5.39

Table 6: Flexural Strength of M25 grade Concrete for 14 days

S.No.	Specimen size (150x150x700)	% of LD Slag	Span (Cm)	Distance of fracture	Load (KN)	Avg. Load (KN)	Avg.* Strength (N/mm ²)
1.	1	0 %	70	30.50	26	26	5.39
2.	2	1 %	70	25.50	29	29	6.01
3.	3	2 %	70	33.00	29	29	6.01
4.	4	3 %	70	30.00	32	32	6.63

Table 7: Flexural Strength of M25 Grade Concrete for 28 days

S.No.	Specimen size (150x150x700)	% of LD Slag	Span (Cm)	Distance of fracture	Load (KN)	Avg. Load (KN)	Avg.* Strength (N/mm ²)
1.	1	0 %	70	27.10	28	28	5.80
2.	2	1 %	70	34.50	31	31	6.42
3.	3	2 %	70	33.00	31.5	31.5	6.53
4.	4	3 %	70	29.00	33	33	6.84

Table 8: % Increase of Flexural Strength in N/mm² of Concrete with LD Slag with respect to conventional Concrete

S.No.	% of LD Slag	Flexural Strength (N/mm ²)			% increase		
		7 days	14 days	28 days	7 days	14 days	28 days
1.	0	5.28	5.39	5.80	-	-	-
2.	1	5.28	6.01	6.42	-	11.5	10.68
3.	2	5.39	6.01	6.53	2.08	11.5	12.58
4.	3	5.39	6.63	6.84	2.08	23	17.93

Observation of Compressive Strength (N/mm²):

Table 9: Compressive Strength of Concrete for 7 days

S.No.	Specimen size (150x150x700)	% of LD Slag	Load (KN)	Avg. Load (KN)	Compressive Strength (N/mm ²)
1.	1		750		



	2	0 %	820	706.6	31.40
	3		550		
2.	1	1 %	650	680.0	30.22
	2		640		
	3		750		
3.	1	2 %	690	700.0	31.11
	2		700		
	3		710		
4.	1	3 %	750	696.6	30.96
	2		650		
	3		690		

Table 10: Compressive Strength of Concrete for 14 days

S.No.	Specimen size (150x150x700)	% of LD Slag	Load (KN)	Avg. Load (KN)	Compressive Strength (N/mm ²)
1.	1	0 %	830	936.66	41.62
	2		980		
	3		1000		
2.	1	1 %	730	793.33	35.25
	2		800		
	3		850		
3.	1	2 %	820	853.33	37.92
	2		850		
	3		890		
4.	1	3 %	800	823.33	36.59
	2		830		
	3		840		

Table 11: Compressive Strength of Concrete for 28 days

S.No.	Specimen size (150x150x700)	% of LD Slag	Load (KN)	Avg. Load (KN)	Compressive Strength (N/mm ²)
1.	1	0 %	940	960.00	42.66
	2		1000		
	3		940		
2.	1	1 %	970	920.00	40.88
	2		950		
	3		840		
3.	1	2 %	940	960.00	42.66
	2		1010		
	3		940		
4.	1	3 %	980	966.66	42.96
	2		1000		
	3		920		

Table 12: % Increase/ Decrease of Compressive Strength in N/mm² of Concrete with



LD Slag with Respect to Conventional Concrete.

S.No.	% of LD Slag	Compressive Strength (N/mm ²)			% increase			% decrease		
		7 days	14 days	28 days	7 days	14 days	28 days	7 days	14 days	28 days
1.	0	31.40	41.62	42.66	-	-	-	-	-	-
2.	1	30.22	35.25	40.88	-	-	-	3.76	15.31	4.17
3.	2	31.11	37.92	42.66	-	-	-	0.92	8.89	0.00
4.	3	30.96	36.59	42.96	-	-	0.70	1.4	12.09	-

Flexural Strength

In the present investigation 150 x 150 x 700 mm size beams are used. Flexural Strength of Concrete was determined on these specimens, which were cured in clean water until the date of test. One beam was tested in every case at different % of LD Slag for 7 days, 14 days and 28 days respectively.

- Table 5 gives the results of flexural strength of beams at different % of LD slag i.e., 0%, 1%, 2%, 3% for 7days.
- Table 6 gives the results of flexural strength of beams at different % of LD slag i.e., 0%, 1%, 2%, 3% for 14days.
- Table 7 gives the results of flexural strength of beams at different % of LD slag i.e., 0%, 1%, 2%, 3% for 28days.
- Table 8 gives the percentage increase/decrease of Flexural Strength of Concrete with LD Slag with respect to Conventional Concrete.

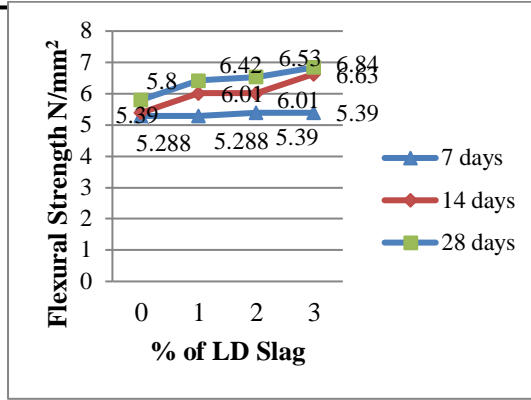
Compressive Strength

- In the present investigation 150 x 150 x 150 mm size cubes are used. Compressive strength of concrete was determined on these specimens, which were cured in clean water until the date of test. Three cubes were tested in every case and the average value is taken in assessing Compressive Strength at different % of LD Slag for 7 days, 14 days and 28 days respectively.
- Table 9 gives the results of Compressive Strength of beams at different % of LD Slag i.e., 0%, 1%, 2%, 3% for 7days.
- Table 10 gives the results of Compressive Strength of beams at different % of LD Slag i.e., 0%, 1%, 2%, 3% for 14days.
- Table 11 gives the results of Compressive Strength of beams at different % of LD Slag i.e., 0%, 1%, 2%, 3% for 28days.
- Table 12 gives the percentage increase/decrease of Compressive Strength of Concrete with LD Slag with respect to Conventional Concrete.

GRAPHS

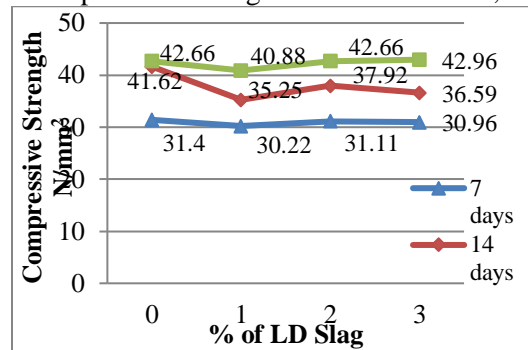
- FLEXURAL STRENGTH:

Graph-1: Flexural Strength of M25 grade Concrete for 7, 14, 28 days



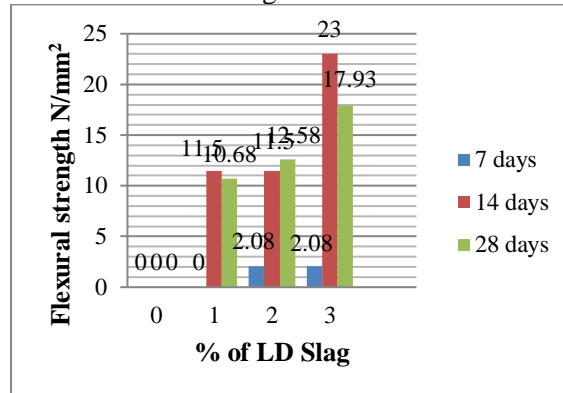
b) COMPRESSIVE STRENGTH

Graph-2: Compressive Strength of Concrete for 7, 14, 28 days



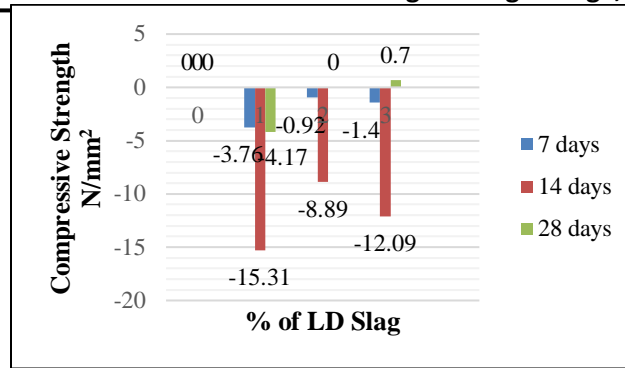
c) RELATION SHOWING % INCREASE OF FLEXURAL STRENGTH

Graph-3: Comparison of Flexural Strength of M25 Grade Concrete at 7, 14, 28 days



d) RELATION SHOWING % INCREASE/DECREASE IN COMPRESSIVE STRENGTH

Graph-4: Comparison of Compressive Strength of M25 Grade Concrete at 7, 14, 28 days



CONCLUSIONS:

Based on the experimental results following conclusions were made:

1. The Specific Gravity of LD Slag is low as compared to the Coarse Aggregate.
2. 1%, 2%, 3% of Coarse Aggregate was replaced by LD Slag resulted that the Compressive Strength is reduced when compared with the Conventional Concrete.
3. The Compressive Strength at 28 days for 2% LD Slag replacement was same as Conventional Concrete Strength.
4. The Compressive Strength at 28 days for 3% LD Slag replacement indicated increase in strength compared to Conventional Concrete.

The percentage increase of Strength with respect to Conventional Concrete was 0.7%.

5. The Flexural Strength of Concrete was found to be increasing with replacement of LD Slag at all percentage, the maximum Flexural Strength was achieved at 3% replacement of LD Slag at 7, 14 and 28 days.
6. The maximum Compressive Strength was achieved at 3% replacement of Slag at 28 days.

Environmental Aspect

1. No substantial leaching of the Slag metal content to underground or surface water representing little or no concern regarding potable water quality.
2. Slag has no impact on animals or other forms of life in the areas of use or areas nearby. There is no bioaccumulation of metals present in the slag in the soil.
3. LD slag can be safely used in aquatic environments such as rivers, lakes and water streams with no impact on the quality of the water or aquatic life. Such environments allow enough dilution protect against high pH alteration. It is necessary to be careful when using the slag in smaller water bodies with low water flow such as wet terrains or shallow channels.
4. Slag used in cement manufacturing has partially replaced the use of clinker reducing energy consumption and, therefore CO₂ emissions.
5. Environmental impacts caused by mineral extraction can be eliminated with the use of Slag.

Advantages of using LD Slag:

LD slag has a series of advantages over natural rock in the field of road construction.



a. Greater Hardness

Slag has a greater resistance to wear. This is the result of its mineral composition. The consequences: less wear and longer road lifetimes. Roads constructed using LD slag demonstrates reduced rutting.

b. Better Adhesion

LD Slag has micro pores and therefore, it retains its adhesiveness with wear. In contrast, natural rock becomes smooth with wear - its surface becomes polished and slippery. As a result, tires can grip better on surfaces constructed using LD Slag and this is particularly important on highways and in curves.

c. Greater Stability and Reduced Wear

LD Slag is harder and internally bound. Natural gravel does not have the same stability and load bearing capacity. As LD slag is harder and more compact than natural rock, roads last longer as there is less wear, particulate pollution is reduced



References:

- [1]. IS 456-2000, Indian standard plain and reinforced concrete-code of practice.
- [2]. Utilization of LD Slag - An overview, Journal of Metallurgy and Materials Science, 45 (2). pp. 61-72., Pal J and Chaudhary, P N and Goswami, M C (2003)
- [3]. L. Zeghichi (2006), "The Effect of Replacement of Natural Aggregates by Slag Products on the Strength of Concrete", Asian Journal of Civil Engineering (Building and Housing) Vol. 7, No. 1, pp 27-35.
- [4]. IS 10262-2009, recommended guide lines for Concrete mix design.
- [5]. Concrete technology by M.S.Shetty.
- [6]. Design of Concrete Mixes by Krishna Raju N.
- [7]. Characterization of LD Slag of Bokaro Steel Plant and its feasibility study of manufacturing commercial 'fly ash-LD Slag' bricks. International Journal of Environmental Technology and Management, 2013 Vol.16, No.1/2, pp.129 – 145. Rajeev Singh, A.K. Gorai, R.G. Segaran.
- [8]. A study on Flexural behavior of reinforced Concrete beam by replacement of Linz-Donawitz (LD) Slag as fine aggregate. International Journal of Civil and Structural Engineering Research Vol. 2, Issue 1, pp.: (89-96), Month: April 2014 - September 2014, Naveen, K.V. Mahesh Chandra, Asst. Professor.



MATRUSRI ENGINEERING COLLEGE

(Approved by AICTE, Affiliated to Osmania University)

#16-1-486, Saidabad, Hyderabad - 500059



Sponsored by

MATRUSRI EDUCATION SOCIETY



ISBN: 97881-936274-0-2



1ST NATIONAL CONFERENCE ON TRENDS IN SCIENCE, ENGINEERING AND TECHNOLOGY

(NTSET - 2018)

February 2nd & 3rd - 2018

TECHNICAL PAPER ABSTRACTS



ORGANIZED BY

MATRUSRI ENGINEERING COLLEGE

(Approved by AICTE, Affiliated to Osmania University)

#16-1-486, Saidabad, Hyderabad - 500059



Sponsored by

MATRUSRI EDUCATION SOCIETY

ISBN: 97881-936274-0-2



NTSET 2018





OUTER RING ROAD TRAFFIC ANALYSIS AND PREDICTION

1.K.Smitha Suguna Leela, 2.Mr.P.Vamsi Krishna, 3.Ms.Mounika Chandram Assistant
Professor, M.Tech student, B.E Graduate

Dept. of Civil Engineering

Matrusri Engineering college Saidabad, Hyderabad, RR district, India.^{1,3}

CVR Engineering college Ibrahimpatnam, Hyderabad, RR district, India.²

ABSTRACT: Traffic congestion is becoming a serious problem in Hyderabad like any other city in India. Therefore, there is pressing and growing need to measure congestion levels in a consistent manner and it is needed to improve the road facilities in order to connect different areas with no loss of time. A multi-disciplinary approach is needed in understanding the problem and providing solutions. Hyderabad is the fifth largest city of India with a total extent of 1868 sq.km. A huge amount of traffic moves daily and in order to divert the highway traffic bypassing through the city and to reduce the travel time and to connect all the places around the city without connecting to inner ring road, an outer ring road is essential. The backbone of any successful traffic management system for a metropolis is reliable, accurate and real time data. Traffic flowing, travel time and traffic increments are the three most important factors considered in TMS for analysing and predicting the traffic and controlling congestions. It is observed that major congestion problems are caused due to poor network of roads. This study presents manual counting of traffic flowing on ORR as well as at underpasses and the traffic is predicted for future years. The main aim of our project is to de-congest metropolitan area and inner ring road and to meet future demand. A comparative statistical analysis was performed on traffic predictions. Information about ITS is specified which helps in decongestion of traffic on ORR due to increased vehicular traffic. Moreover, our study conveys the importance of transportation engineering in our day to day life.

Keywords: Traffic Analysis, Travel Time, Traffic Prediction and Intelligent Transport System.

INTRODUCTION

Transport plays a significant role in the overall economic development. Transportation results into growth of infrastructure, industrialization and massive production. Advancement in the transport sector has resulted into comfort and convenience. Well-functioning transportation systems form the basis for economic prosperity and social wellbeing of societies.

Road network in India is one of the largest networks in the world. The country's road network consists of Expressways, National Highways, State Highways, Major District Roads, Other District Roads and Village Roads. Roads are the dominant mode of transportation in India.

They are an indispensable means of communication and has come a long way. It is today regarded as one of the most ideal and cost effective modes of transportation in India. The Indian Roadways play a crucial role in connecting the different parts of India. One of the most important advancement in transportation system is outer ring road, which helps in the development of the state or city.

The outer ring road is the rim of the cartwheel. While it is now also used by the traffic to bypass a town, its original purpose was to link the outer communities and promote development infill by acting as a distributor between radials, thus these ring roads are generally located within the lower density outer fringes of urban development, and they tend to be more circumferential than inner ring roads. Their quality of demand and completeness depend upon needs at specific locations. Outer ring roads are not heavily used by public transport, it is mainly to divert the heavy motor vehicles from the inner city traffic.

METHODOLOGY

TRAFFIC STUDIES

Traffic studies are carried out to analyse the traffic characteristics. It helps in geometric design and traffic control, which tends to a safe



and efficient traffic movement. The traffic studies in collection of data is also known as traffic census. There are multiple methods for the collection of traffic data and traffic characteristics either manually or mechanically. The different types of traffic studies are:

1. Traffic volume study
2. Speed study
3. Origin and destination study

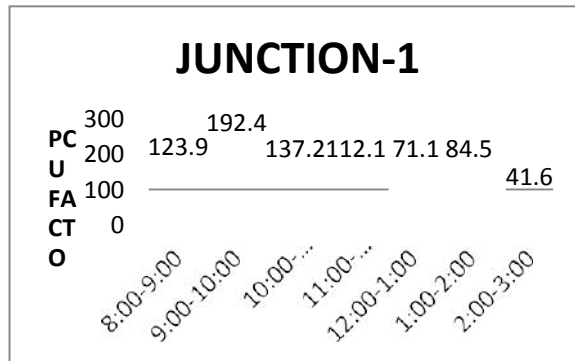


4. Traffic flow characteristics study
5. Traffic capacity study
6. Parking study
7. Accident study

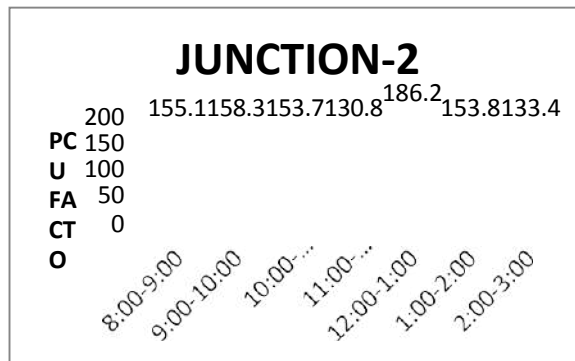
The traffic study in this case is done using “Traffic volume study”.

The case study includes the stretch Bongulur- Ghatkesar. The distance between the two junctions is 32.1km. The stretch consists of 16 vehicle under passes (VUP). But the survey was conducted in 6 vehicle under passes only. The data is collected and represented graphically as follows:

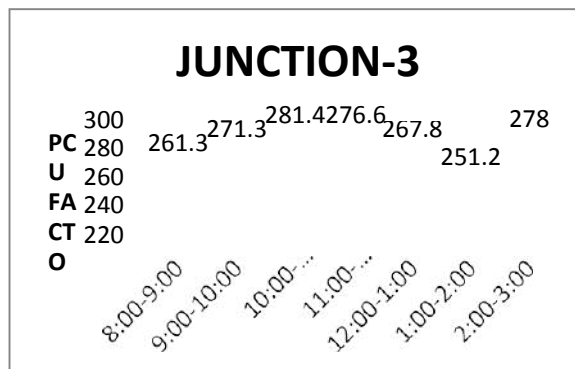
Graph 1: PCU vs. TIME



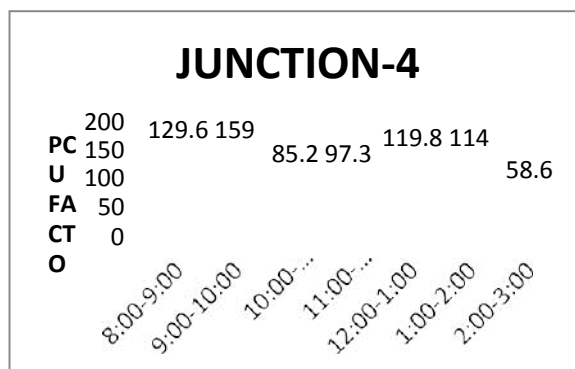
Graph 2: PCU vs. TIME



Graph 3: PCU vs. TIME

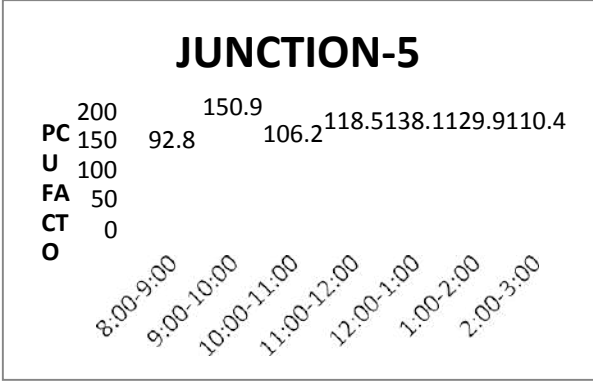


Graph 4: PCU vs. TIME

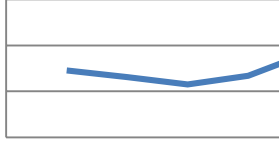
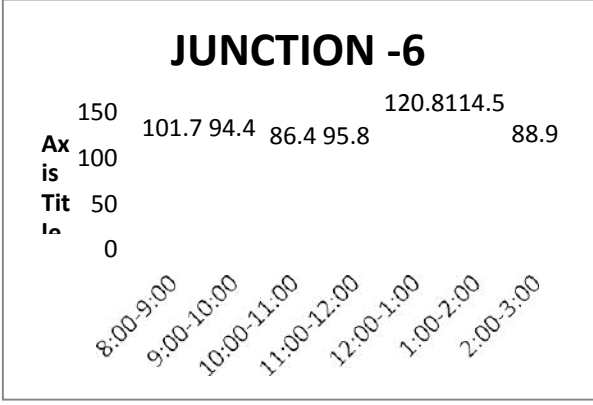




Graph 5:PCU vs. TIME



Graph 6: PCU vs. TIME



REGRESSION MODEL

In this model an additive functional form is assumed to exist between the factors which affect trip-generation and the number of trips generated. This model is very helpful in determining the number of trips generated in a zone when the parameters of the regression function are known. These parameters can be determined using estimation techniques like Ordinary Least Squares or Maximum Likelihood Technique on empirically obtained data on variables.

The formula generated is as follows:
 $y = a + b(x)$

Where, y= dependent variable (vehicular registered data),
 a= intercept,
 b= slope of the line,
 x= independent variable (GDP).

OUR CONCEPT

Taking vehicular registered data as dependent variable and GDP as independent variable, using regression technique in excel a relation between them is created, based on that equation vehicular registration for future year is calculated and an average growth rate per year is obtained. Based on that growth rate the traffic on ORR is predicted for future years.

The method, Elasticity based model using regression, is used in predicting the traffic which is based on the assumption that traffic volume is dependent on growth rate which in turn depends on the number of vehicular registrations. Based on this assumptions predictions are performed.

Regression analysis is a causal / econometric forecasting method. Some forecasting methods use the assumption that it is possible to identify the underlying factors that might influence the variable that is being forecast.

Regression analysis includes several classical assumptions. Regression analysis includes many techniques for modelling and analysing several variables when the focus is on the relationship between a dependent variable and one or more independent variables.

A large body of techniques for carrying out regression analysis has been developed. Familiar methods, such as linear regression and ordinary least squares regression, are parametric.

REGRESSION TECHNIQUE:

year	vehicles registered in hyddist	vehicles registered in rrdist	Total Registered Vehicles	GDP (USD BILLIONS)



1st National Conference on Trends in Science, Engineering & Technology, 2nd-3rd, Feb., 2018

Matrusri Engineering College, Saidabad, Hyderabad-500 059

2011	1849087	1302186	3151273	74	
2012	2012816	1489806	3502622	79.476	
2013	2176560	1679030	3855590	85.357224	
2014	2340869	1881518	4222387	91.67365858	



2015	2520309	2025083	4615692	9845750931	
Matrusri Engineering College, Saidabad, Hyderabad-500059					
	TOTAL VEHICULAR TRAFFIC ON ORR	TOTAL TRAFFIC IN OUR STRETCH			GROWTH RATE
2016	16212984	853248	5044875.13	105.743365	9.20%
2017	17542448.69	923214.336	5503176.52	113.568374	9.00%
2018	18980929.48	998917.9116	5995392.212	121.9724337	8.90%
2019	20537365.7	1080829.18	6524031.865	130.9983938	8.82%
2020	22221429.69	1169457.173	7091790.853	140.6922749	8.70%
2021	24043586.92	1265352.661	7701564.005	151.1035033	8.60%
2022	26015161.05	1369111.58	8356460.371	162.2851625	8.50%
2023	28148404.25	1481378.729	9059819.068	174.2942645	8.42%
2024	30456573.4	1602851.785	9815226.309	187.1920401	8.34%
2025	32954012.42	1734285.631	10626533.69	201.0442511	8.27%
2026	35656241.44	1876497.053	11497877.81	215.9215257	8.20%
2027	38580053.24	2030369.811	12433701.39	231.8997185	8.14%
2028	41743617.6	2196860.136	13438775.93	249.0602977	8.08%
2029	45166594.25	2377002.667	14518225.98	267.4907598	8.03%
2030	48870254.97	2571916.886	15677555.33	287.285076	7.99%
2031	52877615.88	2782814.07	16922675.05	308.5441716	7.94%
2032	57213580.38	3011004.824	18259933.63	331.3764403	7.90%
2033	61905093.97	3257907.22	19696149.35	355.8982969	7.87%
2034	66981311.68	3525055.612	21238645.04	382.2347708	7.83%
2035	72473779.24	3814110.172	22895285.4	410.5201439	7.80%
2036	78416629.14	4126867.206	24674517.15	440.8986345	7.77%
2037	84846792.73	4465270.317	26585412.04	473.5251335	7.74%
2038	91804229.73	4831422.483	28637713.17	508.5659934	7.72%
2039	99332176.57	5227599.126	30841884.57	546.1998769	7.70%
2040	107477415	5656262.255	33209164.66	586.6186678	7.68%
				AVG GROWTH	8.21%

SUMMARY OUTPUT						
<i>Regression Statistics</i>						
Multiple R	0.999967178					
R Square	0.999934357					
Adjusted R Square	0.999901535					
Standard Error	4749.006444					
Observations	4					
<i>ANOVA</i>						
	<i>df</i>	<i>SS</i>	<i>MS</i>	<i>F</i>	<i>Significance F</i>	
Regression	1	6.87094E+11	6.87094E+11	30465.6675	3.28222E-05	
Residual	2	45106124.42	22553062.21			

Total	3	6.87139E+11				
	<i>Coefficients</i>	<i>Standard Error</i>	<i>t Stat</i>	<i>P-value</i>	<i>Lower 95%</i>	<i>Lower 95.0%</i>
Intercept	- 1148386.886	29871.8553	- 38.44377508	0.00067593 9	- 1276915.106	- 1276915.106
74	58568.8002	335.5528861	174.5441706	3.28222E-05	57125.0326 5	57125.0326 5

RESULTS AND CONCLUSIONS

According to the survey done and data obtained, the predictions are performed by regression process. The vehicular traffic is predicted till the year 2040. The traffic may be **6.2** times greater than the present traffic. Since there is a huge increase in the number of vehicles, the present design may not be sufficient. To meet the future need some changes have to be implemented.

One of the best ways to decongest the road is to properly managing the traffic. This can be done by implementing new technologies in the toll management and variable message systems.

The study has given a lead to the scientific planning in the Cantonment from planning, management and engineering perspectives. In the planning front, the future urban longitudinal and transitional corridors are identified by defining the hierarchy of the road systems. The link prioritization, identification of potential junctions to be developed, recommendations on land use controls are some of the key outputs from the planning distance that have been achieved in the study. The management issues have been dealt in the road safety auditing of links and junctions in the study area. An engineering face lift is given by the junction designs and link designs. It is further recommended for regular road safety audits to propose any improvements catering to the demands. A better practice of transportation planning and related policy making as suggested in the study must be followed. Improvement of the mobility based on access and hierarchy is the objective that has been accomplished in the study. Managing transportation accessibility from different parts of the area is the key concept framed in the study. The planning and design proposed in the study will be supportive in the smooth transition of the sprawl to an urban fabric. The study advocates the idea that, when the capability of new construction of roads is limited, a thoroughly designed road systems that fills the sprawl space better and improves the accessibility within the area can provide a larger transportation capability to serve more people and a better economy.

HMDA has taken initiation to implement ITS on the outer ring road. Smart cards, variable message systems etc. They will be installed and implemented by the year 2017. Hyderabad is the first city to implement ITS. The use of ITS improves the traffic flow and reduces the problems.

REFERENCES

- [1]. <http://www.nptel.ac.in/courses/105104098/32>
- [2]. https://en.wikipedia.org/wiki/Transportation_forecasting
- [3]. <http://www.hmda.gov.in/>
- [4]. IRC108: Guidelines for traffic prediction
- [5]. Hyderabad urban development authority, Hyderabad
- [6]. HMDA, ITS Zone.



MATRUSRI ENGINEERING COLLEGE

(Approved by AICTE, Affiliated to Osmania University)

#16-1-486, Saidabad, Hyderabad - 500059



Sponsored by

MATRUSRI EDUCATION SOCIETY



ISBN: 97881-936274-0-2



1ST NATIONAL CONFERENCE ON TRENDS IN SCIENCE, ENGINEERING AND TECHNOLOGY

(NTSET - 2018)

February 2nd & 3rd - 2018

TECHNICAL PAPER ABSTRACTS



ORGANIZED BY

MATRUSRI ENGINEERING COLLEGE

(Approved by AICTE, Affiliated to Osmania University)

#16-1-486, Saidabad, Hyderabad - 500059



Sponsored by

MATRUSRI EDUCATION SOCIETY

ISBN: 97881-936274-0-2

NTSET 2018





MANUFACTURING OF ELLIPTICAL SHAPE CONCRETE HOLLOW BRICKS USING GRANULATED BLAST FURNACE SLAG AS A FINE AGGREGATE

T Raja Ramanna ¹ , M Govardhan ² , P.Dhanamma ³

^{1,3} Assistant Professor, Civil Engineering Department, Matrusri Engineering College (MECS),
Santosh Nagar, Hyderabad, Telangana

² Student, Civil Engineering Department, PJMS Engineering College, Bairamalguda, Karmanghat,
Hyderabad, Telangana.

¹ trajaramanna@gmail.com, ² govardhanchari@yahoo.com

ABSTRACT

By using GBFS which is a by-product of steel industry as a fine aggregate, we can save the natural resources and environment. The GBFS provides durability and better engineering properties and the elliptical shape which helps in enhanced thermal properties.

The experiment helps in find out the economical and technical features of the product by conducting different tests like economical mix proportions, compressive strength, to meet the standards and to develop eco-friendly building block.

Since, it is designated as Green Building Material it would help to get GRIHA (Green Rating for Integrated Habitat Assessment) as well as the LEED (Leadership in Energy and Environmental Design) certification.

Systematic laboratory tests were carried out with different proportions of cement, river sand and slag sand to compare the quality, durability and technical feasibility.

Key words: Concrete Bricks, Ordinary Portland Cement (OPC), Ground Granulated Blast furnace Slag (GGBS), Granulated Blast furnace Slag (GBS).



INTRODUCTION

Shelter is one of the three basic requirements of human being. Initially ancient man started living in caves excavated below ground level on near the hill ends. Thereafter, they started constructing walls from mud, and in due course of time, they developed the techniques of burnt clay brick masonry to form the structural part of the shelter. The desire for search of new structural materials paved the way for hollow concrete blocks due to the following advantages

1. Adequate strength and structural stability.
2. Superior thermal insulation and acoustic characteristics.
3. Resistance to fire.
4. Light weight.
5. Speedy work.
6. Economy

Building construction is a multi disciplined technology. It involves an exchange of thoughts, experience and ideas among those engaged in the various disciplines of the construction activity in order to achieve overall economy and proper serviceability of the construction project at hand. It should also make use of innovative methods in the field of material technology by use of new/improved materials resulting in the production of economical, aesthetically acceptable and durable structure. The resistance to any change comes not only from the artisans and makers but even from engineers, contractors, owners and public in general. It is a human attitude of unwillingness to come out of a well established route. The modern recommended practice is to dispense with several 'on the spot' operations and replace them with the manufactured materials. That site operation is often left to workers who do not have the skills to the desirable extent and cannot adequately supervised, resulting in such work often being shoddy and expensive. Economical and efficient construction techniques demand excellent micro-planning, determining as to which of the building materials should be manufactured on a mass scale, setting out and promoting such manufacturing facilities and popularizing their use. The development of construction technology is closely related to the development of adequate mechanization and handling technology, the latter involves both the provisions of equipment as well as the handling dexterity.

Hollow concrete block is an important addition to the types of masonry units available to the builders and its use for masonry is consistently increasing, some of the advantages of hollow concrete block construction resulted in reduced mortar consumption, light weight and greater speed of masonry work compared to traditional brick masonry. Since many builders are yet to become familiar with the use of hollow concrete blocks, this will help them to appreciate the essential constructional details and adopt hollow concrete block masonry in a large scale wherever it is economical.

We did an experiment on concrete hollow bricks of size **24×12×6 - inch** by introducing an elliptical shaped hollow portion to reduce the material and to get more load bearing capacity and also to improve all engineering properties by using Granulated Blast Furnace Slag (GBS/Slag sand) & Ground Granulated Blast Furnace Slag (GGBS/Slag Cement). This project work carried out by following the instructions given in **“IS: 2185 (Part 1) – 1979 (Reaffirmed 2003), Edition 3.1 (1984-05): SPECIFICATION FOR CONCRETE MASONRY UNITS; HOLLOW AND SOLID CONCRETE BLOCKS (Second Revision)”**

MATERIALS USED

Type 1: Ordinary Portland Cement 53 Grade, Stone dust, Granulated Blast furnace Slag (GBS), 6mm Aggregate

Type 2: OPC of 53 grade, Ground Granulated Blast furnace Slag (GGBS), Stone dust, Natural sand, 6mm Aggregate

Slag: “Slag” is a non-metallic product consisting essentially of glass containing silicates and Alumino Silicates of lime. It is the by-product obtained in the manufacture of pig Iron in blast furnaces at around 1400° to 1500°C in the molten form. The granulated slag is obtained by rapidly chilling (Quenching) the molten ash from the furnace by means of water or steam and air.



Granulated Blast furnace Slag

Granulated Blast furnace Slag is an alternative for river sand. The natural sand being successfully obtained from river bed thought to be everlasting supply, now the sand resources are getting depleted and exhausted. The physical properties of the slag was evaluated in a reputed testing Lab of **National council for Cement and Building materials (NCCBM), Hyderabad** and the test results shown that the Slag is meeting the requirements of IS 383-1973(reaffirmed) for sand.

MATERIALS AND METHODS

Slag Sand (GBS) and Slag Cement (GGBS) used for this study were provided by JSW CEMENT LIMITED, Secunderabad. Other locally available materials 53grade Ordinary Portland Cement, Fine aggregate (Natural Sand), Quarry dust and Coarse Aggregate (6mm chips) were obtained for this study. Potable water available in the campus conforming to the requirements of water for concreting and curing was used throughout the project.

PROPERTIES OF GBS

Chemical composition

The primary components of iron and steel slag are:

- a) Lime (CaO) and
- b) Silica (SiO₂)

The other components include alumina (Al₂O₃) and magnesium oxide (MgO), as well as a small amount of sulfur (S).

Physical properties

Reliable Quality:

Blast furnace slag fine aggregate is a product for industrial use manufactured under suitable, quality-controlled conditions.

No deleterious materials:

Blast furnace slag fine aggregate does not contain materials that may affect the strength and durability of concrete, such as chlorides, organic impurities, clay and shells.

Increased long term Strength:

The compressive strength of the mortar and concretes achieved with BF slag as sand is similar to that of natural sand at a material age of 7days and 28 days.It also helps in the continuous strength gain beyond 28 days.

Alkali-aggregate Reactions:

Since no siliceous and clayey materials are present in BF Slag it doesn't generate Alkali-Silica Reaction, and the concrete made with slag sand is more durable

PROPERTIES OF GGBS

Concrete Properties:

Slag cement is a more uniform product as a result concrete made with slag cement will generally have more uniform properties.

Plastic Properties:

Water reduction:

The use of either material should result in a reduction of the required water content to reach a given consistency. This effect with slag cement is due to its influence on paste characteristics and absorption.

Air Entrainment:

Slag cement does not contain carbon and does not cause instability in the entrained air content.

Time of Set:

Time of initial set is influenced by the use of slag cement. Concrete made with slag cement can have faster set times than concrete made with other cementitious materials.

Pumpability and Finishability:



Pumpability with slag cement is generally improved largely due to the addition of fines to the matrix. Finishability is also improved.

Hardened Properties:

Strength:

At 28 days, slag cement will achieve higher strength than straight Portland cement in concrete mixtures.

Permeability:

At normally specified replacement levels, concrete made with slag cement will have lower permeability than concrete when tested according to ASTM 1206 (rapid chloride permeability test).

Sulfate Attack and Alkali-Silica Reaction (ASR): Slag cement provides protection against sulfate attack and ASR.

Time of Set: Time of initial set is influenced by the use of slag cement. Concrete made with slag cement can have faster set times than concrete made with other cementitious materials.

Chemical composition: The ternary diagram, shown in Table1 shows that slag cement is more closely related to Portland cement than other cementitious materials.

Parameter	GGBS	As per IS: 12089-1987 (Reaffirmed 2008)
CaO	37.34%	---
Al ₂ O ₃	14.42%	---
Fe ₂ O ₃	1.11%	---
SiO ₂	37.73%	---
MgO	8.71%	Max. 17.0%
MnO	0.02%	Max. 5.5%
Sulphide sulphur	0.39%	Max. 2.0%
Loss On Ignition	1.41%	---
Insoluble Residue	1.59%	Max. 5%
Glass Content	92%	Min. 85%
Chemical Moduli: 1. $\frac{CaO+MgO+1/3Al_2O_3}{SiO_2+2/3Al_2O_3}$ 2. $\frac{CaO+MgO+Al_2O_3}{SiO_2}$	1.07 \geq 1.0 1.60 \geq 1.0	The presence of major oxides with granulated slag shall satisfy at least one of the equation



Chemical composition of slag cement

Physical properties:

The following are the physical properties of GGBS,

Blaine fineness, m²/ kg - 400

Specific gravity - 2.94

Good quality GGBS

1. Fineness : Typically about 300 M²/Kg
2. Manganese Oxide : Max. 5.5%
3. Magnesium Oxide : Max. 17.0%
4. Sulphide sulphur : Max. 2.0%
5. Glass content : Min. 85%
6. Insoluble Residue : Max. 5%

MIX DESIGN AND PRODUCTION OF THE BLOCK SAMPLES

There is no proper mix design for concrete bricks, the nominal mix proportion used is, cement, fine aggregate, coarse aggregate; 1: 4: 8.

Mix

Mixing was done by following IS: 2185 (Part 1). Mix proportion taken for both the types is, cement, fine aggregate, stone dust, coarse aggregate 1: 3: 3: 6. Constant water cement ratio is applied which is 0.8 in every mix.

Type 1: In this investigates 53grade OPC, GBS as fine aggregate, stone dust and 6mm chips as coarse aggregate were used.

Type 2: In investigates 53grade OPC was replaced with 50% GGBS, natural sand as fine aggregate, stone dust and 6mm aggregate

Materials	Type 1	Type 2
OPC	35	17.5
GGBS	---	17.5
Stone dust	105	105
Natural Sand	---	105
GBS	105	---
6mm Chips	210	210

Mix proportions of concrete brick

Preparation of test specimen

The experimental investigation has been carried out on the test specimens to study the strength properties as a result using GBS as fine aggregate. The test specimens were cast in steel molds and wooden elliptical shaped hollow making part. The inside of the mold was applied with oil to facilitate the easy removal of specimens. The raw materials were weighed accurately. The concrete was mixed thoroughly in dry condition. Initially, 75% of water was added to the dry mix, and they were mixed thoroughly. Then the remaining 25% of water was added to the mix. The mixing was continued until a uniform color was obtained. Fresh concrete was placed in the mold in three layers, and each layer was compacted using tamping rod. The concrete specimen cast is a 24 × 12 × 6-inch hollow brick. After (before initial setting (5-10 minutes) the elliptical portion should be removed to make easy work) 24 hrs from casting, the test specimens were taken out and placed in a curing tank, until the age of the specimens. The prepared specimens were analyzed for workability and compressive strength as per IS standards.

COMPRESSIVE STRENGTH

The compressive strength of the brick samples was determined in accordance with the standard procedure



for concrete masonry units (IS 2185 Part 1). Samples were taken from curing tank before testing. Nine sample bricks were crushed each at 7, 14 and 28 days after casting of type 1 and type 2 using the compressive testing machine in the concrete laboratory of Civil Engineering Department, JNTU Hyderabad.

WATER ABSORPTION

The test specimens were completely immersed in water at room temperature for 24 hours. The specimens were then be weighed, while suspended by a metal wire and completely submerged in water. Then removed from the water and allowed to drain for one minute by placing them on a coarser wire mesh, visible surface water being removed with a damp cloth, and immediately weighed. Then all specimens dried in a ventilated oven at 100 to 115°C for not less than 24 hours and weighed. The difference between two weights then determined and percentage of water absorption calculated.

BLOCK DENSITY

Three blocks taken and dried to constant mass in suitable oven heated to 100°C. After cooling the blocks to room temperature, the dimensions of each block were measured volume was computed. Block then weighed in Kilograms and the density of each block calculated.

RESULTS AND DISCUSSIONS

COMPRESSIVE STRENGTH TEST

The specified minimum required compressive strength of hollow blocks for both Type 1 and Type 2 is 3.5 N/mm² as per IS 2185 (Part 1). The test results have shown increase of strength by replacing OPC with GGBS compared to blocks made with only OPC. The average data for strength against curing age is shown in **Table 4**. The results clearly indicated that strength increased with time. Further it is observed that GGBS and GBS reach the optimum values of strength at 60 days. Partial replacement of cement with GGBS has better commercial viability due to reduced cost. Strength development of blocks containing GBS and GGBS can perform well in gaining ultimate strength and durability.

Days	Type 1 brick	Type 2 brick
7	3.63	3.57
14	4.13	5.35
28	4.69	5.98

Compressive strength N/mm²

WATER ABSORPTION TEST

The water absorption tests were conducted as per IS 2185 (Part 1). After 28 days of curing, the average value of the water absorption of Type 1 and Type 2 are 5.32% and 2.55% respectively. The maximum allowable water absorption is 10% by mass and result obtained was well within the limits.

DENSITY TEST

Test conducted by following procedure given in IS 2185 (Part 1). As per standards, density should not be less than 1500 Kg/m³ for Grade A hollow load bearing unit. Our test results for type 1 and type 2 are 1848.15 Kg/m³ and 1870.37 Kg/m³ respectively. So, these blocks meeting the requirement of Grade A.

CONCLUSION

This project work concluded that,



- 1) The use of Blast Furnace Slag in concrete works makes environmental friendly constructions. The lower specific gravity of slag helps in reduction of weight of concrete and improves the strength and durability.
- 2) The study shows that the concrete bricks prepared using slag sand (GBS) as fine aggregate comes under **Grade A(4.5)** and 50% of cement replaced with GGBS comes under **Grade A(5.5)** as per IS 2185-1979 (Part1) hollow load bearing units.
- 3) The manufacturing of Red bricks consumes lot of fertile alluvial soil and energy causing environment pollution. The hollow blocks made with Slag (GBS & GGBS) are environment friendly and helps in conserving the natural resources.
- 4) This elliptical hollow portion reduces the material quantity and improves load bearing capacity which is economically feasible with better engineering properties.
- 5) These building blocks can be used in place of beams and columns in non- engineering buildings.
- 6) These bricks have high heat resistance and eco-friendly properties. Finally these units can be recommended for low cost building.

REFERENCES

1. IS: 2185 (Part 1) – 1979 (Reaffirmed 2003), Edition 3.1 (1984-05): “*SPECIFICATION FOR CONCRETE MASONRY UNITS; HOLLOW AND SOLID CONCRETE BLOCKS* (Second Revision)”
2. IS 10262 : 2009 – Concrete Mix Proportioning-Guidelines
3. Concrete Technology By, M. S. Shetty.
4. Building Materials and construction Planning By, MahabubBasha.
5. *CEMENT CONCRETE BLOCK* By, Glass & Ceramic Division, MSME-DI, 3rd CGO Complex, Sanjay place Agra.
6. *LOAD CARRYING CAPACITY OF HOLLOW CONCRETE BLOCK MASONRY COLUMN* By, IOSR Journal of Engineering (IOSRJEN) e-ISSN: 2250-3021, p-ISSN: 2278-8719, www.iosrjen.org Volume 2, Issue 10 (October 2012, PP 05-08.
7. nkk technical review no.87 (2002)By, Dr. Tatsuhito Takahashi, Chief Engineer, Steel Technology Center, Dr. Kazuya Yabuta Manager, Ceramic Engineering Lab. Applied Technology Research Center.
8. International Journal of Scientific & Engineering Research Volume 3, Issue 8, August-2012 1 ISSN 2229-5518.
9. Ramesh et al. International Journal of Energy and Environmental Engineering 2013, 4:3.
10. Journal of Wuhan University of Technology-Mater. Sci. Ed. Oct 2008, DOI 10. 1007/s11595-007-5737-3.
11. *INTERNATIONAL JOURNAL OF CIVIL AND STRUCTURAL ENGINEERING*, Volume 3, No 1, 2012. ISSN 0976 – 4399.
12. IOSR Journal of Mechanical and Civil Engineering (IOSRJMCCE) ISSN: 2278-1684 Volume 2, Issue 6 (Sep-Oct 2012), PP 26-30, www.iosrjournals.org.
13. Mohammed Nadeem, Dr. A. D. Pofale / International Journal of Engineering Research and Applications (IJERA) ISSN: 2248-9622 www.ijera.com Vol. 2, Issue 5, September- October 2012, pp.1258-1264.
14. International Journal of Earth Sciences and Engineering, ISSN 0974 5904, Volume 04, No 06 SPL, October 2011, pp. 949-952
15. International Journal of Scientific & Engineering Research Volume 3, Issue 8, August-2012 1 ISSN 2229-5518.



MATRUSRI ENGINEERING COLLEGE

(Approved by AICTE, Affiliated to Osmania University)

#16-1-486, Saidabad, Hyderabad - 500059



Sponsored by

MATRUSRI EDUCATION SOCIETY



ISBN: 97881-936274-0-2



1ST NATIONAL CONFERENCE ON TRENDS IN SCIENCE, ENGINEERING AND TECHNOLOGY

(NTSET - 2018)

February 2nd & 3rd - 2018

TECHNICAL PAPER ABSTRACTS



ORGANIZED BY

MATRUSRI ENGINEERING COLLEGE

(Approved by AICTE, Affiliated to Osmania University)

#16-1-486, Saidabad, Hyderabad - 500059



Sponsored by

MATRUSRI EDUCATION SOCIETY

ISBN: 97881-936274-0-2

NTSET 2018





EXPERIMENTAL STUDY ON GEOPOLYMER CONCRETE

P.Prashanth ¹, M.Prasanna Lakshmi ², , Dr. G.Manohar ³,

¹Assistant Professor, ²Graduate student, ³Professor,

Civil Engineering Department, Matrusri Engineering College, Hyderabad

ABSTRACT

The objective of this research work was to produce a carbon dioxide emission free cementitious material. The geopolymer concrete is such a vital and promising one. In this present study the cement is replaced by GGBS(Ground Granulated Blast Furnace Slag) and Fly Ash .The Alkaline liquids used in this study for the polymerization process are the solutions of sodium hydroxide (NaOH) and sodium silicate (Na_2SiO_3). A 10 Molarity solution was taken to prepare the mix. The cube compressive strength was calculated for 10 M solution for different mix Id i.e. $G_{10}F_{90}$, $G_{20}F_{80}$, $G_{30}F_{70}$, and $G_{40}F_{60}$ (Where F and G are, respectively, Fly Ash and GGBS and the numerical value indicates the percentage of replacement of cement by fly ash and GGBS). The cube specimens are taken of size 150 mm x 150 mm x 150 mm. Ambient curing of concrete at a temperature of 35-40^oc was adopted. In total 6 cubes and 3 beams were cast for different mix Id and the cube and beam specimens are tested for their compressive strength at age of 7 days, 14 day and 28 days respectively. The result shows that geopolymer concrete gains strength with increase in the GGBS content without water curing at ambient temperature. Also the strength of Geopolymer concrete was increased with increase in period of curing.

INTRODUCTION

Geopolymer concrete is an innovative and ecofriendly construction material and an alternative to Portland cement concrete. Use of geopolymer reduces the demand of Portland cement which is responsible for high CO₂ emission.

Geopolymer was the name given by Daidovits in 1978 to materials which are characterized by chains or networks or inorganic molecules. In 1978, Davidovits proposed that binders could be produced by a polymeric reaction of alkaline liquids with the silicon and the aluminium in source materials of geological origin or by-product materials such as fly ash. He termed these binders as geopolymers. Two main constituents of geopolymers are source materials and alkaline liquids. The source materials of alumino-silicate should be rich in silicon (Si) and aluminium (Al). Geopolymer cement concrete is made from utilization of waste materials such as fly ash and ground granulated blast furnace slag(GGBS). Fly ash is the waste product generated from thermal power plant and ground granulate blast furnace slag is generated as waste material in steel plant.

The threat of climate change is considered to be one of the major environmental challenges for the society. The production of cement contributes to the emission of CO₂ through the decarbonization of limestone. Cement is one of the most important building materials used worldwide for the production of concrete. The cement industry is a major source of carbon emissions and deserves attention in the assessment of carbon emission reduction options. It is responsible for about 6% of all CO₂ emissions, because the production of one ton of Portland cement emits approximately one ton of CO₂ into the atmosphere. The contribution of Ordinary



Portland Cement (OPC) production worldwide to greenhouse gas emissions is estimated to be approximately 1.35 billion tons annually or approximately 7% of the total green house gas emission to the earth's atmosphere. This research aims at 100% replacement of cement with fly ash as an alternative binding material.

METHODOLOGY

MATERIALS USED

GGBS(GROUND GRANULATED BLAST FURNACE SLAG)

Ground granulated blast furnace slag (GGBS) is a by-product from the blast-furnaces used to make iron.

FLY ASH

Fly ash (FA) is a by-product of the combustion of pulverized coal in thermal power plants. It is a fine grained, powdery and glassy particulate material that is collected from the exhaust gases by electrostatic precipitators or bag filters.

ALKALINE SOLUTIONS

The solutions of sodium silicate and sodium hydroxide are used as alkaline solutions in the present work. Sodium hydroxide in pellets form and sodium silicate solution are used.

Fly ash was taken from thermal power plant, Ramagundam, karimnagar, Telangana .GGBS slag was obtained from JSW suppliers, Hyderabad. Locally available river sand having a specific gravity 2.65 was used. Crushed granite coarsed aggregate of 20 mm maximum size having a specific gravity of 2.56 was used. Distilled water was used in a concrete mix.

PREPARATION OF SOLUTIONS

In this work the strength of Geopolymer concrete is examined for the mixes of 10 molarity of sodium hydroxide. Molecular weight of sodium hydroxide is 40. To prepare 10 Molarity 400 g of sodium hydroxide flakes are weighed and they can be dissolved in distilled water to form litre solution. Volumetric flask of 1 litre capacity is taken, sodium hydroxide flakes are added slowly to distilled water to prepare 1 litre solution.

MIX PROPORTIONS

As there are no provisions for the mix design of geopolymer concrete, the design is done according to IS 10262 provisions. The alkaline liquid to fly ash and GGBS ratio is kept as 0.4. The ratio of sodium hydroxide to sodium silicate is kept as 2.5. The conventional method used in the making of normal concrete is adopted to prepare geopolymer concrete.

CASTING AND CURING

Firstly, the fine aggregates and coarse aggregates, fly ash and GGBS are mixed in dry condition for 3-4 minutes and then the alkaline solution which is a combination of sodium hydroxide solution and sodium silicate solution. Water is taken as 10% of the cementious material(fly ash GGBS). The mixing is done for about 6-8 mins. For proper bonding of all the materials. After mixing is done, cubes are casted by giving proper compaction in three layers.

The demoulded specimen are kept at a temperature of 35-40^oc for air curing until testing. Water is not involved in the chemical reaction of Geopolymer concrete and instead water is expelled during curing and subsequent drying. This is in contrast to the hydration reactions that occur when Portland cement is mixed with water, which produce the primary hydration products calcium silicate hydrate and calcium hydroxide

MATERIALS REQUIRED FOR 1 M³



Fly ash+GGBS	Sodium hydroxide	Sodium silicate	Fine aggregate	Coarse aggregate
478.95 kg/m ³	136.825 kg/m ³	54.73 kg/m ³	475.05 kg/m ³	1113.88 kg/m ³
Distilled water: 10% of the total cementitious material				

TEST RESULTS

The cubes are tested in compression and flexure testing machines to determine their compressive strength and flexural strength at the age of 1 day, 7 days and 28 days of curing. The results are shown in the following table.

COMPRESSIVE STRENGTH(N/mm²)

Mix	curing period					
	7 days		14 days		28 days	
A G ₁₀ F ₉₀	11.56	11.11	12	13.33	11.11	12
B G ₂₀ F ₈₀	24.44	24.889	25.33	27.11	32	32
C G ₃₀ F ₇₀	29.78	30.22	24.44	26.67	33.33	37.78
D G ₄₀ F ₆₀	28.89	26.22	27.556	32	33.33	33.78

FLEXURAL STRENGTH(N/mm²)

Mix	curing period		
	7 days	14 days	28 days
A G ₁₀ F ₉₀	3.214	2.69	3.32
B G ₂₀ F ₈₀	3.629	4.25	4.35
C G ₃₀ F ₇₀	3.629	3.111	3.73
D G ₄₀ F ₆₀	3.733	3.007	4.25

A G₁₀F₉₀- GGBS 10% FLYASH 90%

B G₂₀F₈₀- GGBS 20% FLYASH 80%

C G₃₀F₇₀- GGBS 30% FLYASH 70%

D G₄₀F₆₀- GGBS 40% FLYASH 60%



Casting



failure of cube



casting of cubes



failure of beam



Compression testing machine



Solution of NaOH and Sodium Silicate



CONCLUSION

User-friendly geopolymer concrete can be used under conditions similar to those suitable for ordinary portland cement concrete. Replacement of 100% of cement with GGBS is made possible without compromise in compressive strength.

GGBS was effectively used as a mineral admixture in modifying the microstructure of geopolymer concrete and also in the polymerisation process. It also developed very good binding property with alkaline liquids to yield a better strength and alkali activation process. These constituents of Geopolymer Concrete shall be capable of being mixed with a relatively low-alkali activating solution and must be curable in a reasonable time under ambient conditions

From the limited experiments conducted, it was found that,

- With the increase in the GGBS content from 10% - 40% of cement there is slight increase in the compression and flexural strengths of the member.
- With the increase in the period of curing there is slight increase in the strengths.
- This type of geopolymer concrete not only serves to replace the cement to a greater extent and also for making use of industrial waste products to minimize its disposal problem.

REFERENCES

1. IS : 10262 – 2009, “Concrete Mix Proportioning-Guidelines”.
2. IS SP : 23-1982, “Hand Book On Concrete Mixes”.
3. “GEOPOLYMER CONCRETE- A REVIEW”, *International Journal of Engineering Sciences and Emerging Technologies*.
4. Journal on “Geopolymer Concrete an Eco-friendly Construction Material”, *International Journal of Research in Engineering and Technology*.
5. Journal on “30 Years of Success and Failures in Geopolymer Applications”, Prof. Dr. Joseph Davidovits, Geopolymer Institute, France
6. “Geopolymer concrete-Green Concrete for the Future-A Review”, *International Journal of Civil Engineering Research*.
7. “Mechanical Properties of Fly Ash Based Geopolymer Concrete with Addition of GGBS as Smart Material”, Dr. V.Bhikshma.
8. “A Brief Review on Geopolymer Concrete”, *International Journal of Advanced Research*.
9. “Compressive Strength Of Thermal Cured Ggbfs Based Geopolymer Concrete”, *Asian Journal Of Civil Engineering*, Vol. 17.
10. “Strength Characteristics Of Low Calcium Fly Ash Based Geopolymer Concrete”, *IOSR Journal of Engineering*.
11. A Technical Paper on “Geopolymer Concrete For Environmental Protection” *The Indian Concrete Journal*.
12. “Geopolymer Concrete Using Different Source Materials”, *International Journal of Emerging Technology and Advanced Engineering*.
13. “A Brief Review on Geopolymer Concrete”, *International Journal of Advanced Research in Education Technology*.
14. [https://www.researchgate.net/publication/Geopolymer Concrete For Ambient Curing Condition](https://www.researchgate.net/publication/Geopolymer+Concrete+For+Ambient+Curing+Condition)
15. N. Krishna Raju, “Design of Concrete Mixes”, CBS Publishers and Distributors.
16. M.S. Shetty, “Concrete Technology”.



MATRUSRI ENGINEERING COLLEGE

(Approved by AICTE, Affiliated to Osmania University)

#16-1-486, Saidabad, Hyderabad - 500059



Sponsored by

MATRUSRI EDUCATION SOCIETY



ISBN: 97881-936274-0-2



1ST NATIONAL CONFERENCE ON TRENDS IN SCIENCE, ENGINEERING AND TECHNOLOGY

(NTSET - 2018)

February 2nd & 3rd - 2018

TECHNICAL PAPER ABSTRACTS



**NTSET
2018**



ORGANIZED BY

MATRUSRI ENGINEERING COLLEGE

(Approved by AICTE, Affiliated to Osmania University)

#16-1-486, Saidabad, Hyderabad - 500059



Sponsored by

MATRUSRI EDUCATION SOCIETY

ISBN: 97881-936274-0-2





NUMERICAL MODELLING OF CONTAMINANT TRANSPORT IN SOIL

M. Srividya ¹, Jayatheja Muktinutalapati², Dr. G.Manohar ³

¹ Assistant Professor, Department of Civil Engineering, Matrusri Engineering College, Hyd.

² Ph.D scholar, department of Civil engineering, BITS, Hyderabad.

³ Professor, Department of Civil Engineering, Matrusri Engineering College, Hyderabad

ABSTRACT:

The study of migration or the fate of the contaminant miscible in ground water from waste site, dumping yards or landfills is essential for preparation of ground water contamination models. Numerical methods are generally adopted to measure the key parameters at a small scale as it is time consuming and costly to determine them in the field and used for quantifying flow and transport in large scales in in-situ conditions applied to simulate real contaminant transport models. These methods need a number of key parameters such as porosity, hydrodynamic dispersion, velocity of contaminant flow and Temperatures. The main aim of this research is to evaluate the nonlinear variation of the Distribution coefficient with parameters like porosity, power factor and bulk density based on detailed experimentation carried out on physical models in the laboratory and development of a suitable and appropriate numerical model. The batch and column tests were conducted to evaluate the distribution coefficient and sorption capacity.

Keywords: Contamination, Distribution Coefficient, Dispersion Coefficient

INTRODUCTION

Soil is a vibrant system in which numerous chemical, physical, and biological reactions occur singly or simultaneously. Evaluation of fluid flows is essential part to understand subsurface phenomena including contaminant transport and waste contaminant. Subsurface contamination is the acute problem faced by mankind. Understanding the long- term behavior of contaminants in the subsurface is essential to avoid ground water contamination. Once groundwater is contaminated, it is important to understand how the contaminant moves in the subsurface environment. Proper understanding of the contaminant fate and transport is necessary in order to characterize the risks associated with the contamination. The parameters known as the Distribution coefficient (K_d) and Retardation factor (R) are the most important parameters used in estimating the migration potential of contaminants present in aqueous solutions in contact with surface, subsurface and suspended solids. Hence evaluating these parameters is very important to predict the extent of contamination at a particular site. Numerical methods are in general superior to analytical methods in terms of being able to solve much more practical problems. Numerical methods usually subdivide the time and spatial coordinates into smaller pieces, such as finite differences, finite elements, and finite volumes, and reformulate the continuous form of governing partial differential equations in terms of a system of algebraic equations. To obtain solutions at certain times, numerical methods generally require intermediate simulations (time-stepping) between the initial condition and the points in time for which the solution is needed. The object of the present work is to develop a method of analysis to determine the Linear and Nonlinear variation of the Distribution Coefficient with different physical parameters. Laboratory studies were conducted on soil columns of 15 to 95cm length. Analytical solution (Fried, 1975) was used for obtaining the Distribution coefficient from the Break-through curves. A numerical method introducing constant dispersion coefficient was developed.

LITERATURE REVIEW

Wu et al. (1997) proposed a stochastic model for modelling solute transport for heterogeneous soils. In this approach, a hydrologic environment is divided into sub-environments based on the knowledge of the omains deterministic spatial variability. The sub environments are assumed to form statistically independent soil columns within which vertical flow occurs. Each sub-environment is discredited based on morphological



horizon information as many layers with varying thickness to form modelling units that are statistically independent. Selected soil properties in each sub environment are described with a multivariate normal random vector. Several realisations of the soil properties are then generated for each of the modelling units. Monte-Carlo runs of the model are then carried out to provide statistical information of the output variables of the column.

Srinivas and Krishna Reddy (1996) presented the adsorption tests results for hexavalent chromium, Cr (VI) The break-through time due to combined advection, diffusion and nonlinear adsorption will be greater than that of advection and diffusion but lower than that of advection, diffusion and linear sorption. Further different contaminants get absorbed in different amounts to the same adsorbate. For example, the adsorption of inorganic contaminants is primarily dependent on the cation or anion exchange capacity of the clay, and different clays have different adsorption mechanisms Therefore even in linear adsorption different distribution coefficient values are possible leading to different break-through times for different contaminants.

DEVELOPMENT OF NUMERICAL MODEL

The theoretical basis for the equation describing solute transport has been well documented in literature (Bear, 1997). Changes in chemical; concentration occur in a dynamic soil system due to the different processes of transport involved, such as advective transport, dispersion, sorption, biodegradation etc. In the present study, advective and dispersive transport along with sorption for reactive contaminant has been considered for deriving the governing equations. These governing partial differential equations can be solved numerically. The continuous differential equation, which defines solute concentration every-where in the system, is replaced by a finite number of algebraic equations that defines concentrations at different time periods.

The various steps involved in development of numerical model are as follows:

- Conceptualization of the model.
- Mathematical model expressing the set of assumptions into a set of differential equations associated with a set of auxiliary boundary conditions.
- Convective dispersive equation with sorption
- Finite difference method of solution of the partial differential equation.

Conceptualization of the model

The contaminant disperses through the low permeable layer into the next layer. the flow through the low permeable layer is considered as one – dimensional. For conceptualization of the model the assumptions made are

- The flow is considered to be one –Dimensional.
- The source of contamination is continuous with the same concentration of C_0 .
- The depth of the porous medium under consideration is finite.
- The porous medium is saturated.
- The concentration of the contaminant initially is zero in the porous medium.

Mathematical modeling

The second step of modeling process involves the translation of conceptual model in to the mathematical terms by a set of partial differential equations with an associated set of auxiliary boundary conditions. Based on the assumptions made, the governing equations is as follows

- Convective- Advective Equation for a reactive contaminant is given by

$$D_x \frac{\partial^2 C}{\partial x^2} - V_x C = R \quad (1)$$

Where

D_x : Hydrodynamic dispersion coefficient V_x : Contaminant flow velocity R : Retardation coefficient.

- The Initial boundary conditions are

$$C(x, 0) = 0 \quad \text{at } t=0$$

In many practical situations the most hazardous pollutant has a maximum concentration, c_0 initially (zero time). This concentration will then decrease with time as leachate is transmitted through the soil. Though this assumption of constant concentration is extremely conservative still, it is used because it covers many important aspects of the problem of



pollutant migration through a finite layer. Therefore, it is assumed that

$$C(0, t) = C_0 \quad \text{for } t > 0$$

It is assumed that the concentration in the underlying permeable stratum does not vary with vertical or horizontal position. Therefore

$$C(L_1, t) = C(L, t) \quad L_1 > L$$

L: the total depth or thickness of the stratum.

Convective - dispersive equation with sorption: Convective-dispersive equation with retardation factor to include the sorption effect of the soil was considered in framing the governing equation as given above

NON - LINEAR SORPTION

The solute Retardation factor for nonlinear adsorption is not constant, as is the case for linear adsorption, but changes as a function of concentration. Many models have been used in the past to describe nonlinear sorption. The most commonly used nonlinear sorption models are those by Freundlich (1909) is

$$S = K_d C^N \quad (2)$$

Non - linear variation of distribution coefficient

Taking into consideration nonlinear variation of the distribution coefficient, and differentiating

$$\frac{\partial C}{\partial t} = D_x \frac{\partial^2 C}{\partial x^2} - V_s \frac{\partial C}{\partial x} - \frac{\rho_d}{n} \frac{\partial S}{\partial t} \quad (3)$$

$$\frac{\partial C}{\partial t} = D_x \frac{\partial^2 C}{\partial x^2} - V_s \frac{\partial C}{\partial x} - \frac{\rho_d}{n} \frac{\partial S}{\partial C} \quad (4)$$

$$S = K C^N \quad (5)$$

By differentiating above equation we get

$$\frac{\partial S}{\partial C} = K N C^{N-1} \quad (6)$$

Substituting Eq 6 in Eq 4 one gets

$$\begin{aligned} \frac{\partial C}{\partial t} &= D_x \frac{\partial^2 C}{\partial x^2} - V_s \frac{\partial C}{\partial x} - \frac{\rho_d}{n} K N C^{N-1} \frac{\partial C}{\partial t} \\ \text{On simplification the equation reduces to} \\ D_x \frac{\partial^2 C}{\partial x^2} - V_s \frac{\partial C}{\partial x} &= \frac{\rho_d}{n} K N C^{N-1} \frac{\partial C}{\partial t} + \frac{\partial C}{\partial t} \\ \frac{\partial^2 C}{\partial x^2} - V_s \frac{\partial C}{\partial x} &= (1 + \frac{\rho_d}{n} K N C^{N-1}) \frac{\partial C}{\partial t} \end{aligned} \quad (7)$$

Normalizing Equation with $X = \frac{x}{L}$ and $T = t/t_0$

$$\partial X = \frac{1}{L} \partial x \quad \partial T = \frac{1}{t_0} \partial t$$

$$\partial^2 X = \frac{1}{L^2} \partial x^2 \quad \partial t = t_0 \partial T$$

$$D_x \frac{\partial^2 C}{L^2 \partial X^2} - V_s \frac{\partial C}{L \partial X} = (1 + \frac{\rho_d}{n} K N C^{N-1}) \frac{\partial C}{t_0 \partial T}$$

$$D_x \frac{\partial^2 C}{L^2 \partial X^2} - V_s \frac{\partial C}{L \partial X} = (1 + \frac{\rho_d}{n} K N C^{N-1}) \frac{\partial C}{\partial T} \quad (8)$$

Substituting $t_0 = L/V_x$ in Eq. (8) the following expression was obtained

$$\left(\frac{D_x}{V_x L}\right) \frac{\partial^2 C}{\partial X^2} - \left(\frac{V_s}{V_x}\right) \frac{\partial C}{\partial X} = (1 + \frac{\rho_d}{n} K N C^{N-1}) \frac{\partial C}{\partial T}$$

If $R = (1 + \frac{\rho_d}{n} K N C^{N-1})$ the above Eq. Reduces to

$$\left(\frac{D_x}{V_x L}\right) \frac{\partial^2 C}{\partial X^2} - \left(\frac{V_s}{V_x}\right) \frac{\partial C}{\partial X} = (R) \frac{\partial C}{\partial T} \quad (9)$$

From finite difference method the Eq. (14) one obtained as

$$\begin{aligned} \left(\frac{D_x}{RV_x L \Delta X^2}\right) (C_{i+1,t} - 2C_{i,t} + C_{i-1,t}) - \left(\frac{1}{\Delta X}\right) C_{i+1,t} - C_{i-1,t} &= \frac{C_{i,t+\Delta t} - C_{i,t}}{\Delta t} \\ \left(\frac{D_x \Delta t}{RV_x L \Delta X^2}\right) (C_{i+1,t} - 2C_{i,t} + C_{i-1,t}) - \left(\frac{1 \Delta t}{R 2 \Delta X}\right) C_{i+1,t} - C_{i-1,t} &= C_{i,t+\Delta t} - C_{i,t} \end{aligned}$$

$$\text{Let } \alpha = \left(\frac{D_x \Delta t}{R V_x L \Delta x^2} \right) \quad \beta = \frac{\Delta t}{R 2 \Delta X}$$

Then above Equation in terms of α and β is given by

$$\alpha (C_{i+1,t} - 2C_{i,t} + C_{i-1,t}) - \beta (C_{i+1,t} - C_{i-1,t}) = C_{i,t+\Delta t} - C_{i,t}$$

On further simplification

$$(\alpha - \beta) C_{i+1,t} + (1 - 2\alpha)C_{i,t} + (\alpha + \beta)C_{i-1,t} = C_{i,t+\Delta t} \quad (10)$$

Checking the convergence and stability of the cdm with sorption for nonlinear variation

For a reactive contaminant with nonlinear variation of the distributive coefficient, with distance

$$\alpha = \left(\frac{D_x \Delta t}{R V_x L \Delta x^2} \right) \quad \beta = \frac{\Delta t}{R 2 \Delta X}$$

Table 1 Input Parameters to Check Stability of the Model for Nonlinear Variation of Distributive Coefficient for Reactive Contaminant

L	15	15
ρ_d	0.0016	0.0016
N	0.6	0.6
K	100	100
N	5	5
C	1	1
N-1	4	4
$\rho_d/nx(KxNx C^{N-1})$	1.333333	1.333333
R	2.333333	2.333333
A	0.111561	0.200809
B	0.054665	0.098397
$\alpha-\beta$	0.056896	0.102413
$1-2\alpha$	0.776879	0.598382
$\alpha+\beta$	0.166225	0.299206

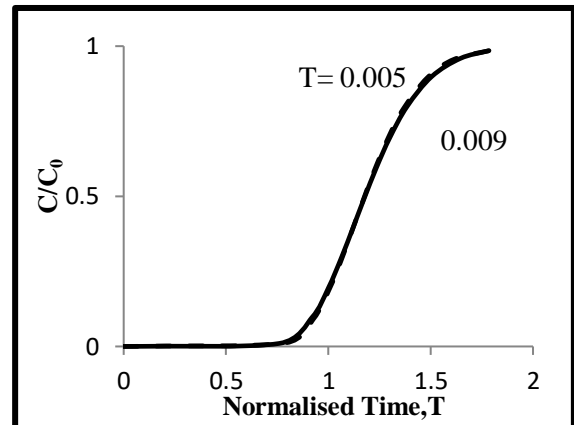


Fig 1 Breakthrough Curves for Different ΔT Values to Check the Convergence and Stability of the Model

The equation for unknown concentration is $(\alpha - \beta) C_{i+1,t} + (1 - 2\alpha)C_{i,t} + (\alpha + \beta)C_{i-1,t} = C_{i,t+\Delta t}$

Using this expression, the concentrations were calculated at each node of the column using the input parameters shown in the table 3 The Break-through curves are furnished in Fig 3.

Fig 1 shows the Break-Through curves for $D_x = 3 \times 10^{-6} \text{cm}^2/\text{sec}$, $V_x = 1 \times 10^{-5} \text{cm}/\text{sec}$, and for ΔT values of 5×10^{-2} and 9×10^{-2} minutes. It is observed that the curves corresponding to $\Delta T = 5 \times 10^{-2}$ and $\Delta T = 9 \times 10^{-2}$ converge to the same breakthrough curve. for these values of ΔT , for $\Delta X = 0.0196$ the values $\alpha + \beta$, $\alpha - \beta$ and $1 - 2\alpha$ are positive. For $\Delta T = 2 \times 10^{-2}$ the value of $1 - 2\alpha$ is negative. While the other two are positive, therefore these values do not yield proper solution. Hence to obtain convergence of the curves, the size of time step, ΔT should not exceed 2×10^{-2} for values of $\Delta X = 0.0196$. It is also observed that the initial normalized time is at about 1.4 and attained the maximum point at a normalized time of about 3.4. the range of the curve remains constant for different normalized time (ΔT) values.

PARAMATRIC STUDY FOR NON - LINEAR VARIATION

The governing equation for nonlinear variation of distributive coefficient and retardation is given by a equation This CDM with sorption considers the nonlinear variation of distributive coefficient with length of the column. The sensitivity of the model was carried out by studying the effect of these key parameters Distribution coefficient (K), Power factor(N), Bulk density (ρ_d), Porosity (n), and contaminant flow velocity (V_x) on the Break-Through curves. The range of Distribution Coefficient K for this study ranges from 10 to 1000, Power factor(N) from 1 to 10 Bulk density (ρ_d) from 0.0013 to 0.0018 and Porosity (n) from 0.4 to 0.9 contaminant flow velocity (V_x) for $1 \times 10^{-5} \text{cm}/\text{sec}$ and $1 \times 10^{-6} \text{cm}/\text{sec}$. The resulted breaks through curves are presented in Figures below.

Effect of power factor 'n' on break through curves

The sensitivity of parameter power factor(N) on break-through curves was studied by varying N values from 1 to 10 for values of bulk density (ρ_d) = 0.0016 and porosity(n) = 0.6, Distribution coefficient K = 10.

Table2 Input Parameters for Different Power Factor Values for K=10



L	15	15	15	15
ρ_d	0.0016	0.0016	0.0016	0.0016
n	0.6	0.6	0.6	0.6
K	10	10	10	10
N	2	5	7	10
C	1	1	1	1
N-1	1	4	6	9
$\rho_d/nx(KxNx C^{N-1})$	0.053333	0.133333	0.186667	0.266667
R	1.053333	1.133333	1.186667	1.266667
α	0.247128	0.229684	0.219361	0.205506
β	0.121093	0.112545	0.107487	0.100698
$\alpha-\beta$	0.126035	0.117139	0.111874	0.104808
$1-2\alpha$	0.505744	0.540633	0.561278	0.588987
$\alpha+\beta$	0.368221	0.342229	0.326848	0.306205

From the Fig 2 it is observed that initial time for N=2 is 0.6 and final normalized time is around 1.5. for N=5 the initial normalized time is 0.6 and final time is around 1.8. for N=7 and N=10 it is observed that the initial normalized time is slightly increasing with increasing Power factor (N), whereas the final normalized break-through curves are almost coinciding at 1.8

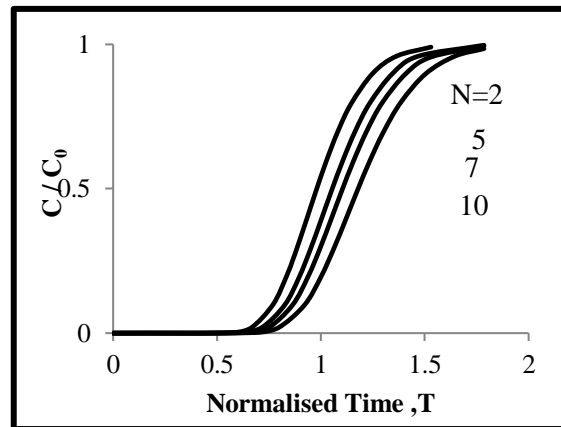


Fig :2 Breakthrough Curves for Different N Values for K=10

From these plots it is observed that as Power factor (N) value increases the Normalized time (T) increases for any given value of C/C_0

Effect of distribution coefficient 'k' on break through curves

The sensitivity of parameter K on break-through curves was studied by varying K values for Power Factor N=1, bulk density(ρ_d) =0.0016 and porosity(n)=0.6

Table 3 Input Parameters for Varying Distribution Coefficient Values for N=1

L	15	15
D_x	0.000003	0.000003
V_x	0.00001	0.00001
ΔT	0.005	0.005
ΔX	0.0196	0.0196
ΔX^2	0.000384	0.000384
ρ_d	0.0016	0.0016
n	0.6	0.6
K	1	10
N	1	1
C	1	1
N-1	0	0
$\rho_d/nx(KxNx C^{N-1})$	0.002667	0.026667



1)		
R	1.002667	1.026667
α	0.259616	0.253547
β	0.127212	0.124238
$\alpha-\beta$	0.132404	0.129309
$1-2\alpha$	0.480768	0.492906
$\alpha+\beta$	0.386828	0.377785

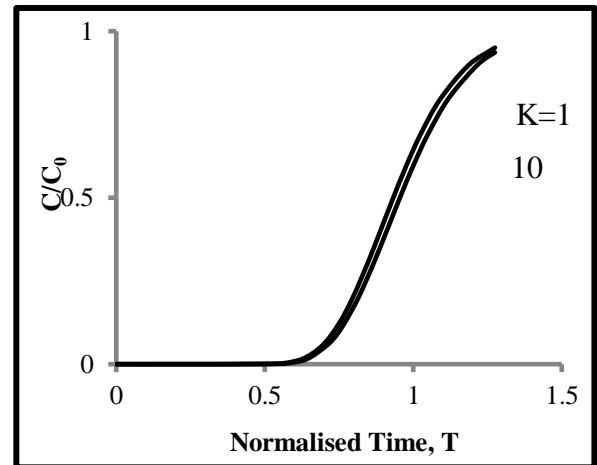


Fig 3 Breakthrough Curves for Different K Values for N=1

From Fig 3 it is observed that the break through curves for K=1 and K=10 are almost coinciding. The initial normalized time for both the break-through curves is 0.6 and final normalized time interval is 1.5. The sensitivity of parameter K on break-through curves was studied by varying K values for Power Factor N=5, $\rho_d=0.0016$ and $n=0.9$

Table 4 Input Parameters for Different Distribution Coefficient Values for N=5

L	15	15	15	15
D_x	0.000003	0.000003	0.000003	0.000003
ΔT	0.005	0.005	0.005	0.005
ΔX	0.0196	0.0196	0.0196	0.019
ΔX^2	0.000384	0.000384	0.000384	0.000384
ρ_d	0.0016	0.0016	0.0016	0.0016
n	0.6	0.6	0.6	0.6
K	10	100	500	1000
N	5	5	5	5
C	1	1	1	1
N-1	4	4	4	4
$\rho_d/nx(KxNx C^{N-1})$	0.133333	1.333333	6.666667	13.33333
R	1.133333	2.333333	7.666667	14.33333
α	0.229684	0.111561	0.033953	0.018161
β	0.112545	0.054665	0.016637	0.008899
$\alpha-\beta$	0.117139	0.056896	0.017316	0.009262
$1-2\alpha$	0.540633	0.776879	0.932094	0.963678
$\alpha+\beta$	0.342229	0.166225	0.05059	0.02706

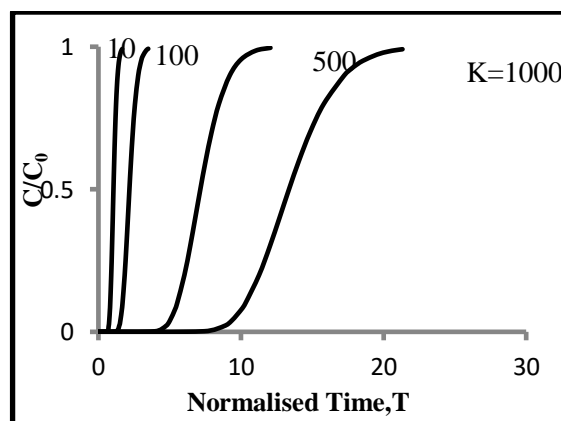


Fig 4 Break through Curves for Different K Values and N=10

From Fig 4 it could be observed that as Distribution coefficient increases normalized time also increases for any given value of C/C_0 . By comparing Fig 4 and Fig 5 it could be observed that the initial normalized time attained by the break-through curves for $K < 500$ has almost remained same, whereas for $K=1000$ it is observed that the initial and final normalized time has increased with increased porosity and power factor.

The initial normalized time for $K=1000$ is around 9.5, whereas in Fig 5 the initial normalized time has increased to 11 and the final normalized time has also increased from 18 to 29. From these plots it is observed that as Distribution coefficient (K) value increases the Normalized time (T) increases for any given value of C/C_0 .

Effect of different bulk density ρ_d on break through curves

The sensitivity of the parameter ρ_d on break-through curves was studied by varying ρ_d values from 0.0013 to 0.0018 for $n = 0.6$ and $K=10$ and Power Factor $N=2$.

Table 5 Input Parameters for Different Bulk Density (ρ_d) Values for $K=10, N=2$

L	15	15	15
ρ_d	0.0013	0.0016	0.0018
n	0.6	0.6	0.6
K	10	10	10
N	2	2	2
C	1	1	1
N-1	1	1	1
$\rho_d/nx(KxNx C^{N-1})$	0.043333	0.053333	0.06
R	1.043333	1.053333	1.06
α	0.249497	0.247128	0.245574
β	0.122253	0.121093	0.120331
$\alpha-\beta$	0.127243	0.126035	0.125243
$1-2\alpha$	0.501007	0.505744	0.508852
$\alpha+\beta$	0.37175	0.368221	0.365905

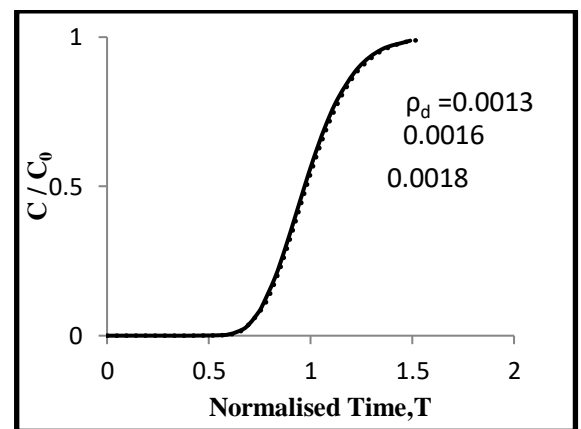


Fig 5 Breakthrough Curves for Different ρ_d Values for Input Parameters $K=10, N=2$

From Fig 5 it is observed that the normalized time attained for different values of bulk density ρ_d is constant. The initial normalized time is 0.5 and attains final normalized time at 1.6 Distribution coefficient (K) and Power factor (N) values are increased from $K=10$ and $N=2$ to $K=1000$ and $N=10$. variation of the break-through curves is observed in Fig 7

Table 6 Input Parameters for Different Bulk Density Values for $K=1000, N=10$

L	15	15	15
ρ_d	0.0013	0.0016	0.0018
n	0.4	0.4	0.4
K	1000	1000	1000
N	10	10	10
C	1	1	1
N-1	9	9	9
$\rho_d/nx(KxNx C^{N-1})$	32.5	40	45
R	33.5	41	46
α	0.00777	0.006349	0.005659
β	0.003807	0.003111	0.002773
$\alpha-\beta$	0.003963	0.003238	0.002886
$1-2\alpha$	0.984459	0.987302	0.988682
$\alpha+\beta$	0.011578	0.00946	0.008432

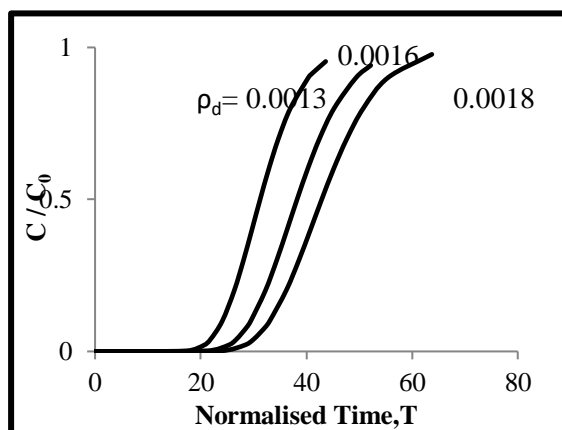


Fig 6 Breakthrough Curves for Different ρ_d Values for Input Parameters $K=10$, $N=2$

From Fig 6 it could be observed that for bulk density $\rho_d < 0.0018$ the normalized time for any given value of C/C_0 decreases with decrease in bulk density. It is also observed that when Distribution coefficient (K) and power factor (N) values are increased from $K=10$ and $N=2$ to $K=1000$ and $N=10$ for varying bulk density values, the normalized time increases almost 40 times the initial values.

CONCLUSION

Based on the Numerical Modeling and the analytical results obtained, the following conclusions are obtained

- Variation of Distribution coefficient depends on the parameters Porosity, Bulk density and Power factor.
- For reactive contaminant in nonlinear variation, bulk density, Power factor are directly proportional to Distribution coefficient. Whereas Porosity is inversely proportional to Distribution coefficient.
- When Retardation factor is high nonlinear variation of Distribution coefficient is observed.
- Break-through curves coincide for low Retardation factor. But as Retardation factor increases range of the Break-through curve increases.

REFERENCES

1. A Lj Bojic, M Purenovic and D Bojic. 2014 Removal of chromium (VI) from water by micro-alloyed aluminium composite (MAIC) under flow conditions. Water SA Vol. 30. pp 2-5.
2. Abriola, L.M, Pennell K.D, Weber Jr, W.J. Lang, J.R. and Wilkins M.D. 1999. Persistence and interphase mass transfer of organic contaminants in the unsaturated zone: Experimental observations and mathematical modelling. Vadose Zone Hydrology: Cutting Across Disciplines. Oxford University Press, New York, pp. 210–234.
3. Anderson, M.P. 1984 Movement of contaminants in groundwater: Groundwater transport–advection and dispersion. In Groundwater Contamination, National Academy Press, Washington, D.C. pp. 37–45.
4. Aniszewski. 2005. An Experimental verification of the contaminant transport in the aquifer incorporating advection, dispersion and sorption processes, J. Environ Fluid Mech. Springer.
5. A.R. Rahmani, M.T. Samadi, R. Noroozi. 2011. Hexavalent Chromium Removal from Aqueous Solutions by Adsorption onto Synthetic Nano Size Zero Valent Iron (nZVI). J. WASET. Vol 3, 195-212
6. Alaerts GI, Jitjarurunt V, Kelderman P. 1989. Use of coconut shell based activated carbon for chromium (VI) removal J. Water. Sci. Technology. 21:171-179.
7. Ajamal, A. Mohammad and S. Anwar, 2001. Sorption studies of heavy metals on teak leave using thin layer and column chromatographic technique. Pollution Research, 20(3): 425-428.



MATRUSRI ENGINEERING COLLEGE

(Approved by AICTE, Affiliated to Osmania University)

#16-1-486, Saidabad, Hyderabad - 500059



Sponsored by

MATRUSRI EDUCATION SOCIETY



ISBN: 97881-936274-0-2



1ST NATIONAL CONFERENCE ON TRENDS IN SCIENCE, ENGINEERING AND TECHNOLOGY

(NTSET - 2018)

February 2nd & 3rd - 2018

TECHNICAL PAPER ABSTRACTS



ORGANIZED BY

MATRUSRI ENGINEERING COLLEGE

(Approved by AICTE, Affiliated to Osmania University)

#16-1-486, Saidabad, Hyderabad - 500059



Sponsored by

MATRUSRI EDUCATION SOCIETY

ISBN: 97881-936274-0-2

NTSET 2018





AN EXPERIMENTAL STUDY ON THE MECHANICAL PROPERTIES OF THIXOFORMED COMPONENTS IN ALUMINUM ALLOYS

M.V. Kishore ^{1,a*}, D. Hanumantha Rao ^{2,b}, M. Manzoor Hussain ^{3,c}

¹ Associate Professor, Department of Mechanical Engineering, Matrusri Engineering College, Saidabad, Hyderabad, India.

² Principal, Matrusri Engineering College, Saidabad, Hyderabad, India.

³ Professor, Department of Mechanical Engineering, Jawaharlal Nehru Technological University Hyderabad, India.

^{a*}mylavarakishore@yahoo.com, ^bdharwada.rao@gmail.com, ^cmanzoorjntu@gmail.com

Abstract: Semisolid metal processing or Thixoforming is a developing technology where the material is processed in the freezing range. Thixoforming process results in components with better mechanical properties as compared to conventional processes. The material at this temperature is very soft and as a result lower loads may be applied to obtain the final shape of the component. Process parameters like ram speed, temperature of the billet and die temperature influence the mechanical properties like tensile strength, hardness and wear behavior of thixoformed component. In the present study an attempt is made to understand the effect of process parameters on the mechanical properties of aluminum alloy by carrying out experimental studies. The results indicate the significant influence of billet temperature and die temperature on the tensile strength and hardness of the material.

Keywords: Thixoforming, A356, Mechanical Properties, experimental study.

I. INTRODUCTION:

Semisolid metal processing (SSMP) or Thixoforming is a technology employed for production of near net shaped components. This process is carried out at a temperature range between its liquidus and solidus temperature [1]. The origin of SSMP can be traced to the experiments conducted by David Spencer at MIT in 1971 as part of his doctoral thesis under the supervision of Martin Flemings [2]. The process combines a number of advantages of casting and forging. Compared to casting, SSMP provides a more stable filling front places lower thermal loads on the metal dies and less shrinkage. Semisolid metal processing (SSMP) is also known as thixoforming or thixocasting depending on the initial condition of the billet and process adopted [3]. Some of the alloys which are suitable for carrying out the semisolid metal processing are alloys of aluminum and copper A356.0 and 356.0 are a 7% Si, 0.3% Mg alloy with 0.2 Fe (max) and 0.10 Zn. The alloys have very good casting and machining characteristics. They are used in the heat-treated condition. The schematic view of thixocasting and thixoforging processes is shown in Fig.1. The three important steps in this process are billet production, reheating to semi-solid condition and forming operation [4]. The process combines a number of advantages of casting and forging. Compared to casting, SSMP provides a more stable filling front places lower thermal loads on the metal dies and less shrinkage.

The alloys have very good casting and machining characteristics. They are used in the heat-treated condition. The resistance to corrosion is excellent and the weldability characteristics are good. The components when given a solution and aging treatment have very good mechanical properties. However to derive the benefits of this process to the full potential, the billets must have a non-dendritic microstructure. To achieve this several methods are available. For the present study mechanical stirring is employed to modify the dendritic microstructure to a globular form.

II. STUDIES ON MECHANICAL PROPERTIES

The mechanical properties of a material determine the range of usefulness and also service life of the component. The elastic and plastic behavior of the material under various loading conditions helps us to understand the characteristics like bending, deformation and hardness of the material. The mechanical properties are not constant and are functions of temperature, type of loading and relative movement between two components. Some of the properties that give a measure of these characteristics include the tensile strength, ductility and wear resistance. Therefore tensile test, hardness test and wear test are conducted to determine the mechanical properties. Bouzakis K.D. [5] conducted experimental and numerical study to determine the influence of temperature and shear rate and concluded that the increasing both the variables led to deterioration of mechanical and rheological properties. Michel Bellet [6] carried out experimental and simulation studies to characterize the flow behavior of aluminum alloy in semi-solid condition. The experimental results are validated with the finite element simulation results. The process parameters such as initial temperature of the specimen, mould temperature and piston velocity are considered. Freitas De E. [7] performed extensive experimentation to assess the flow behavior, mechanical properties, microstructure evolution and porosity levels. Samples of Al 356 obtained by different methods are prepared and the above properties are evaluated. It is observed that the tensile properties are better as compared to conventionally cast alloys. Shueiwan H. Juang [8] studied the mechanical properties of A356 alloy with preformed billets having thixotropic structure. The results of tensile, impact and fatigue tests are reported for two different heat treated specimens. It is observed that the superior mechanical properties can be achieved with globular microstructure. Manjunath Patel [9] carried out experimental study to optimize the process parameters in squeeze cast process. The process parameters chosen are squeeze pressure, pouring temperature and die temperature. The output parameters of surface roughness and surface density are calculated. The results are analyzed using Taguchi and grey rational analysis methods. Thus it is essential to study the combined effect of process parameters on mechanical properties.

III. EXPERIMENTAL STUDIES

The billets required for this study are initially prepared by stirring the molten alloy of Al 356 in an electric arc furnace and cast into billets. Mechanical stirring is employed as it involves usage of less sophisticated equipment and the process is also economically viable. The billets are now heated to semisolid temperature and load is applied using hydraulic press after placing the hot billet in the die. The process parameters considered for the present study are billet temperature and die temperature. Three levels are chosen for each of two factors. L9 experiments (3 Levels and 2 factors) are designed using Taguchi design of experiment approach. The temperatures considered for billet are 580^oC, 590^oC and 600^oC and die temperatures chosen are 30^oC, 125^oC and 250^oC.

Table 1 lists the arrangement of runs for experimental studies. Fig. 1 represents the schematic representation of die used for making the thixoformed component. Tensile specimens are prepared as per ASTM E8 standards. The tensile test specimen used is shown in Figure 2. The diameter of the specimen is 12 mm. The length of the specimen is about 95mm and the gauge length is about 50 mm. A 40 ton Universal Testing machine is used for conducting the tensile tests. The data is recorded and results are tabulated at Table 2. Fig. 3 represents the tensile specimen after the test. The experimental data is analyzed to determine the effect of process parameters on the mechanical properties of the component formed by thixoforming process. The process parameters used for conducting the L9 experiments are billet temperature and die temperatures. The tensile strength for various experimental data is plotted and is shown in Fig 4. The plot indicates that tensile strength is varying for different runs. The influence of process parameters is observed. A maximum value of 171.602 N/mm² is obtained for run order no.1. The BHN values are recorded for all the nine specimens at three different locations and the mean value is tabulated at Table 2. A graph is plotted for the hardness values recorded for different run orders as shown in Fig.5.

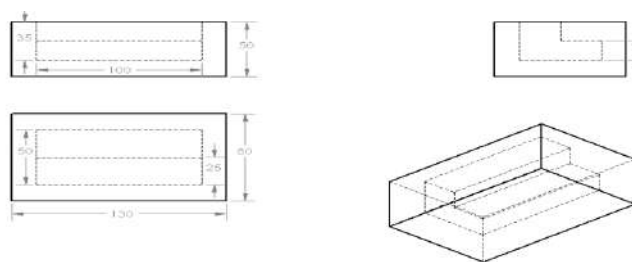


Fig 1 Schematic representation of die used in making Thixoformed Component



Table 1.DOE using L9 Orthogonal array

Run No	Billet Temp °C	Die Temp °C
1	580	30
2	600	250
3	590	250
4	590	30
5	580	250
6	580	125
7	590	125
8	600	30
9	600	125



Fig. 2 Tensile test specimen



Fig. 3 Tensile test specimen after the test.

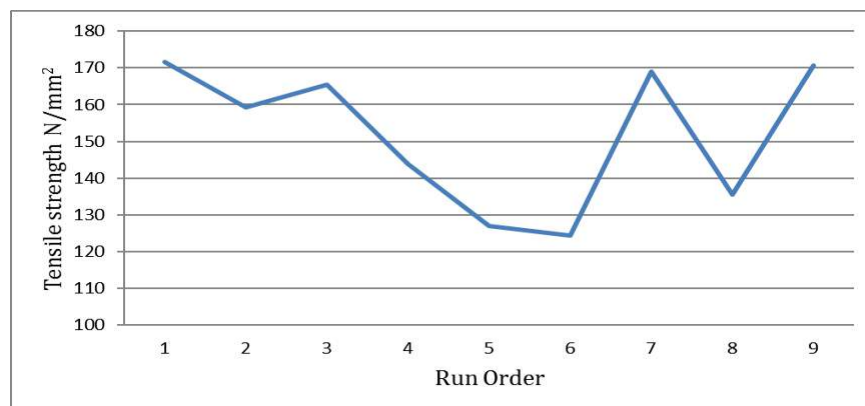


Fig. 4 Plot showing the tensile strength for different run orders.



Fig. 5 Plot showing the BHN values for different run orders

Table 2 Results of Tensile Strength and Hardness Tests

Run No	Billet Temp °C	Die Temp °C	Tensile Strength N/mm ²	BHN
1	580	30	171.602	95.3
2	600	250	159.347	55
3	590	250	165.485	48
4	590	30	143.952	91.7
5	580	250	126.987	69
6	580	125	124.28	66.7
7	590	125	168.994	66.7
8	600	30	135.429	88.3
9	600	125	170.691	64.3



IV. RESULTS AND CONCLUSIONS:

It is observed that the process parameters significantly influence the mechanical properties of thixoformed component of A 356 material. The average values of tensile strength obtained is better than as cast values for Al 356 alloy because of improved ductility of the material at higher loads. It is observed that with an increase in billet temperature the hardness value decreased and stayed constant beyond a value of 590 °C. The Die temperatures are found to have a major influence on hardness as compared to billet temperature. The hardness value decreased with increase in die temperature.

REFERENCES

1. Spencer, B, Mehrabian, R. and Flemings, M.C. "Rheological behavior of Sn-15 pct Pb in the crystallization range" Metallurgical Transactions, vol. 3, no. 7, pages 1925–1932, 1972
2. Thixoforming, A textbook on Semi-solid Metal Processing Edited by Gerhard Hirt and Reiner Kopp (Wiley VCH Verlag GmbH & Co KGaA 2009).
3. Thoguluva Raghavan Vijayaram and S.Thiru Chitrabalam, "Rheocasting and Thixocasting : Semi-solid casting technologies", Indian Foundry Journal, Vol 56, pages 23 – 27, 2010.
4. Flemings, M.C. ' Behavior of metal alloys in the semisolid state', Metallurgical Transactions A, 22 (5), pages 957 – 981, 1991.
5. K.D. Bouzakis, G Maliaris, A. Tsouknidas, ' Development of an experimental-analytical procedure to determine the mechanical properties of semi-solid aluminum alloys at thixo-temperatures', 3rd International Conference on Manufacturing Engineering, Oct 2008, pp325-340
6. Michel Bellet and Serge Moto Mpong, 'Determination of the constitutive equation of a thixotropic Al alloy and FEM modeling of the thixoforming process' , The international conference on Numerical Methods in Industrial forming processes' , 2001, pages 1-5.
7. E. de Freitas, M. Ferrante, C.T. Ruckert, W.W. Bose Filho, ' Thixocasting of an A356 alloy: Fluidity, porosity distribution and thermo-mechanical fatigue behavior', Materials Science and Engineering A 479, 2008, pages 171 – 180.
8. Shueiwan H. Juang and Shyn-Ming Wu, 'Study on mechanical properties of A356 alloys enhanced with preformed thixotropic structure', Journal of Marine Science and Technology', Vol. 16, No.4, 2008, pages 271-274.
9. Manjunath Patel G.C., Prasad Krishna and Mahesh B. Parappagoudar, ' Optimization of squeeze cast process parameters using Taguchi grey relational analysis', Procedia Technology, Vol.14, 2014, pages 157-164.



MATRUSRI ENGINEERING COLLEGE

(Approved by AICTE, Affiliated to Osmania University)

#16-1-486, Saidabad, Hyderabad - 500059



Sponsored by

MATRUSRI EDUCATION SOCIETY



ISBN: 97881-936274-0-2



1ST NATIONAL CONFERENCE ON TRENDS IN SCIENCE, ENGINEERING AND TECHNOLOGY

(NTSET - 2018)

February 2nd & 3rd - 2018

TECHNICAL PAPER ABSTRACTS



ORGANIZED BY

MATRUSRI ENGINEERING COLLEGE

(Approved by AICTE, Affiliated to Osmania University)

#16-1-486, Saidabad, Hyderabad - 500059



Sponsored by

MATRUSRI EDUCATION SOCIETY

ISBN: 97881-936274-0-2

NTSET 2018





EXPERIMENTAL CHARACTERIZATION OF INCONEL-718 BY GTAW PROCESS USING DIFFERENT SHIELDING GASES

¹C. VenkateshwarReddy, ²P. Thrilochan Sharma, ³G. Sainithin.

¹Asst.prof., Department of Mechanical Engineering, Matrusri Engineering College, Saidabad, Hyderabad.Telangana, India.

^{2&3}Students, Department of Mechanical Engineering, Matrusri Engineering College, Saidabad, Hyderabad,Telangana,India.

Abstract: In the present study effect of shielding gases in welding process which results in weld bead characteristics of metal was studied. The welding was carried out by using the GTAW(Gas Tungsten Arc Welding)/TIG (Tungsten Inert Gas) process. GTAW is very commonly used in the areas such as rail, car manufacturing, automotive and chemical industries. The material Inconel718 is a nickel-based super alloy generally used at elevated temperature applications including turbine engines and power generation because of its superior mechanical properties. In the present experimentation, An attempt was made to study the weld characteristics of Inconel718alloy weld samples with different shielding gases of Argon and Argon-hydrogen gas.

Key words: GTAW, shielding gases, Hardness, NDT, Ultrasonic Test.

I. INTRODUCTION

Inconel718 alloy is a high-strength, corrosion-resistant nickel chromium material suitable for service at temperature ranges from -423° to 1300°F. The easy and economy with which Inconel718 alloy can be fabricated with similar and dissimilar metals. Its good tensile, fatigue, creep, and rupture strength have resulted in its use in a wide range of applications. These components are used for rings, casings and various sheet metal formed parts for aircraft and land-based gas turbine engines and cryogenic tanks. It is also used for fasteners and instrumentation parts. The age-harden able alloy can be readily fabricated, even into complex parts. Its welding characteristics are resistance to post weld cracking results in many applications.

GTAW is a process in which the source of heat is an arc formed in between non-consumable tungsten electrode and the base metal. The arc and the molten weld pool are protected with shielding gas from the atmospheric contamination. The inert gases such as argon, helium, or argon helium mixture are used in this welding process. It is accepted that GTAW is the one of the advanced high- quality metal joining process. The weld quality is effectively recognized by the weld bead geometry, the mechanical properties of welded joints are determined by the dimensions of weld bead. It is very essential to select the welding process parameters for obtaining most favorable weld bead characteristics. Ultrasonic Testing (UT) is the most preferred Non-Destructive Testing(NDT) technique for characterization of material properties. The material is volumetric in nature the ultrasonic examination can give an idea about the bulk material properties. The ultrasonic testing parameters are significantly indicate the changes in micro structural or mechanical properties of materials.

II. SAMPLE PREPARATION

2.1 Selection of input parameters and their range:

Based on previous studies, the effect of welding process parameter on weld bead profile characters, the following TIG welding process parameters are considered as input parameters. They are Welding Current (I), Welding Voltage (V), Welding Speed(S), and Shielding Gas (G). The welding process parameters and their ranges are shown in Table 1.

Table 1: Welding Parameters.

Welding Parameter	Notation	Value
Welding Current (Amp)	I	90
Welding Voltage(Volts)	V	50
Welding Speed (mm/s)	S	2
Shielding gas	G	1.Argon 2.Argon (95%)+H2(5%)

Table 2. Welding Process parameters.

Process Parameter	Constant Value
Gas Flow Rate (l/min)	15
Electrode Diameter (mm)	2.4
Electrode Material type	2% Thorated

The nickel based alloy Inconel718 alloy was received from M/S Ashtavinayaka metals was used as a base metal. The thickness of the base metal is 3mm.size is 5mmx5mm.The below table shows the chemical composition of the alloy at laboratory level.

Table 3- Chemical Composition of Inconel718

Alloy Elements	Percentage	Alloy Elements	Percentage
Nickel (plus Cobalt)	50.00-55.00	Aluminum	0.20-0.80
Chromium	17.00-21.00	Cobalt	1.00 max.
Iron	Balance*	Carbon	0.08 max.
Niobium (plus Tantalum)	4.75-5.50	Manganese	0.35 max.
Molybdenum	2.80-3.30	Silicon	0.35 max.
Titanium	0.65-1.15	Phosphorus	0.015 max.
Copper	0.30 max.	Sulfur	0.015 max.
Boron	0.006 max.		

The welding joints have been fabricated by using an automatic TIG welding machine both in continuous mode and pulsated modes. Before welding, the Inconel 718 alloy plates was cleaned to remove the rust, dirt and any surface impurities with the help of acid and wire brush. The edge preparation is made as per the standard procedure. The samples were welded in accordance with the combination of TIG process parameters with Argon as shielding gas and Argon-Hydrogen shielding gas. The thickness of base metal is 3mm a single weld pass procedure is performed to fabricate the test specimens. The photographs of fabricated test specimens are shown in fig 1.



Fig1(a) specimen welded with Argon



Fig1 (b) specimen welded with Argon-hydrogen

Then the welded samples were cut in small pieces by using abrasive cutting wheel and then some of samples were mounted using cold mounting process. These mounted samples were used to observe micro and macro structural analysis and to perform micro hardness test.

III.RESULTS & DISCUSSION:

3.1. Microstructure :

The Inconel718 samples welded with Gas Tungsten Arc Welding (GTAW) in two different shielding conditions was studied with standard metallographic techniques and then evaluated using optical microscope with 200X. Microstructure of weld specimens in the weld zone was studied at different regions. Heat input increases when argon-hydrogen is used as shielding gas. Significant grain refinement was observed in HAZ with increases in heat input. It was also found that average dendrite length and inter dendritic spacing in weld zone increases with increase in heat input which is the main reason for observable changes in the microstructure of weld joints welded with different shielding gases.

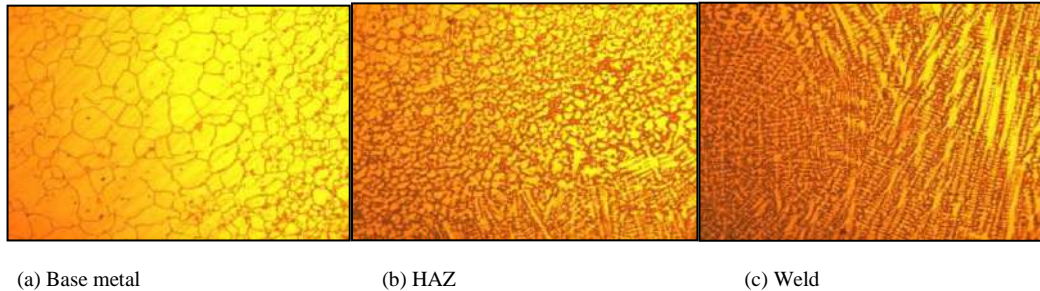


Fig.2(a): Microstructure of sample welded with Argon as shielding gas

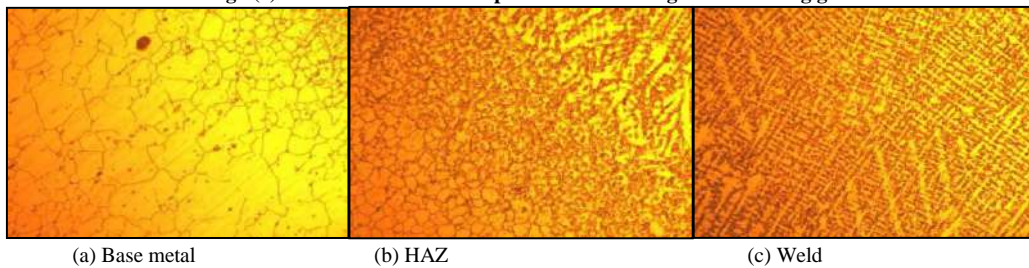


Fig.2(b): Microstructure of sample welded with Argon-hydrogen as shielding gas

3.2. Macrostructure:

To compare the bead size of the both the specimens, their macrostructure was captured at 7X. These bead profile specimens were polished using disc polisher with different grades (320 – 1200 grit sizes) emery papers of different grit sizes and final polishing was done with diamond paste. To expose the bead profile characters the specimens are deeply etched with oxalic acid. Bead Depth (BD) and bead width (BW) were measured using 3D profile projector (make: Sipcon) based on illustration of bead profile shown in Fig. 4. The measured values of WD, WW and DW are presented in Table 4. Then weld bead width and weld penetration are calculated using IMAGE J software from the obtained macrographs of the weld samples.



Fig 3. Macrostructure of weld (a) with Argon shielding gas (b) with Argon-Hydrogen shielding gas

Comparing the bead size of the both the specimens, we observed a broader bead along with a deeper penetration in the case of the sample welded with Argon-Hydrogen as shielding gas. Addition of Hydrogen to Argon changes the static characteristic of the welding arc, increases arc power and consequently the quantity of material melted. In GTAW welding with 10% increase in the quantity of hydrogen, melting of parent metal increased by four times. Thus, we get a wider weld bead when we use Argon-Hydrogen as the shielding gas. Ionization potential of Argon-Hydrogen shielding is more than only Argon shielding, resulting a deeper penetration.

Table 4: Bead width of test specimens welded with Argon and Argon-Hydrogen as shielding gas

Shielding Gas	Weld penetration (cm)	Weld Bead width (cm)
Argon	1.8	3.2
Argon-Hydrogen	2.8	2.7

3.3. Micro Hardness:

After the samples were prepared using standard metallographic techniques, they are evaluated using Vickers Micro hardness testing. The Micro Vickers hardness test method consists of indenting the test material with a diamond indenter in the form of a right pyramid with a square base and an angle of 136° between opposite faces. The test piece was subjected to a load of 500 gm-f, applied for a dwell time of 10 seconds. The two diagonals of the indentation left in the surface of the material after removal of the load were measured using microscope at 50X magnification. Using the MINUTEMAN software the length of the diagonals of indent was measured. And hence using these values the Vicker's Hardness of the specimen is determined at varied positions (at micron distances) along the weld surface ranging from the weld region to the base metal and Hardness Vs distance graph is plotted.

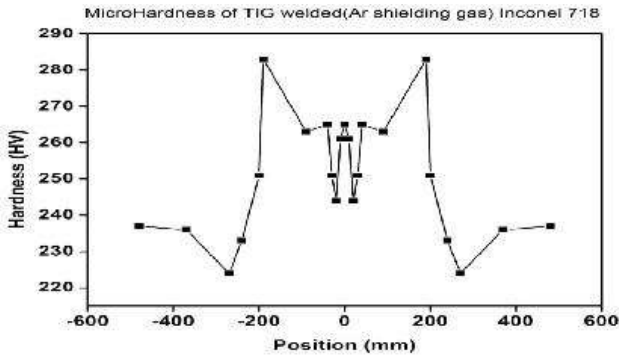


Fig.4 (a) Micro Hardness using Argon Gas

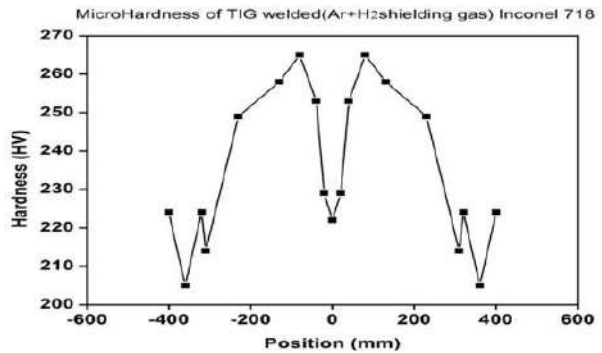


Fig.4(b) Micro Hardness using Argon Gas-Hydrogen Gas

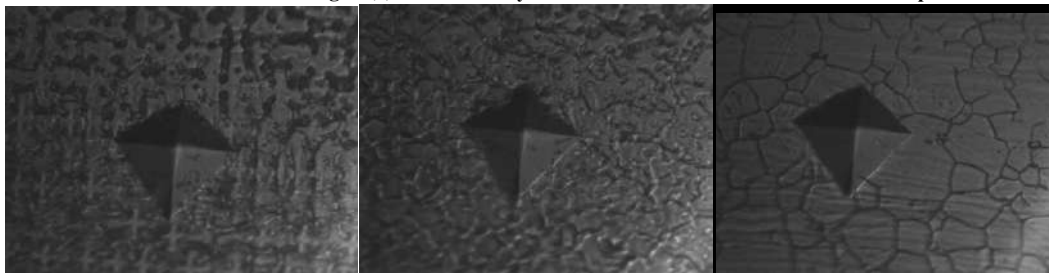


Weld

HAZ

Base metal

Fig 5: (a) Indentation by vicker's hardness tester on Ar welded samples.



Weld

HAZ

Base metal

Fig 5: (b) Indentation by vicker's hardness tester on Ar-H₂ welded samples.

The results shows that hardness variation in HAZ is much greater than weld and base metal areas. Analysis of the results showed that each of the experimental variables and interactions had statistically significant effects on one or more of the hardness value measured. It was found that the mechanical properties of the joint in welds were made under the conditions of higher heat input in the case of Argon-Hydrogen shielding, because of which it has lower hardness than the other case.

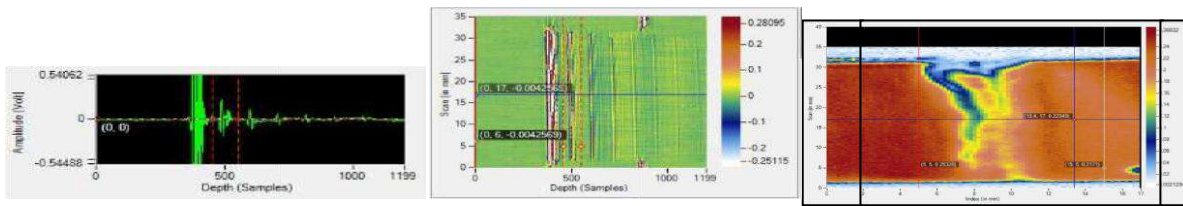
3.4 Ultrasonic Testing:

Ultrasonic data can be collected and displayed in a number of different formats. The three most common formats are known in the NDT world as A-scan, B-scan and C-scan presentations. Each presentation mode provides a different way of looking at and evaluating the region of material being inspected. Modern computerized ultrasonic scanning systems can display data in all three presentation forms simultaneously.

A-Scan Presentation: The A-scan presentation displays the amount of received ultrasonic energy as a function of time. In the A-scan presentation, relative discontinuity size can be estimated by comparing the signal amplitude obtained from an unknown reflector to that from a known reflector.

B-Scan Presentation: The B-scan presentations is a profile (cross-sectional) view of the test specimen. From the B-scan, the depth of the reflector and its approximate linear dimensions in the scan direction can be determined.

C-Scan Presentation: The C-scan presentation provides a plan-type view of the location and size of test specimen features. The plane of the image is parallel to the scan pattern of the transducer. The C-scan presentation provides an image of the features that reflect and scatter the sound within and on the surfaces of the test piece.



6(a) Ultrasonic A Scan

6(b) Ultrasonic B Scan

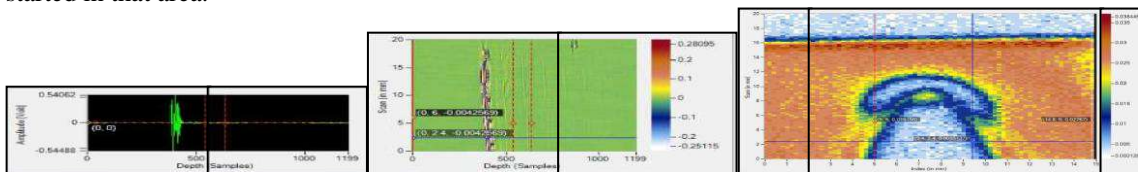
6(c) Ultrasonic C Scan

Fig.7 Observations of Ultrasonic Test for weld specimen using Argon Gas.

Fig 7 (a) shows the absence of defect echo and hence we conclude that there is no defect in the welded specimen.

Fig 7(b) does not characterize the location of the defect as it is not present in the specimen.

Fig 7(c) highlights the base metal region in orange, the HAZ region in pink and the weld in yellow. The blue color highlights the variation in thickness in the weld region because of insufficient heat accumulation in that region as the welding had been started in that area.



7(a) Ultrasonic A Scan

7(b) Ultrasonic B Scan

7(c) Ultrasonic C Scan

Fig.8 Observations of Ultrasonic Test for weld specimen using Argon Gas- Hydrogen Gas.

Fig 8(a) shows the absence of defect echo and hence the absence of any defects in the weld specimen.

Fig 8(b) characterizes the location of the defect as it is not present in the specimen.

Fig 8(c) highlights the base metal in orange, the HAZ in yellow and the weld region in blue colour.

The uniformity in color in the weld region describes the absence of any irregularities and characterizes a continuous weld being done.

$$V = \sqrt{\frac{C_{ij}}{\rho}}$$

$$V_L = \sqrt{\frac{E(1-\nu)}{\rho(1+\nu)(1-2\nu)}}$$

$$V_T = \sqrt{\frac{G}{\rho}}$$

Where V is the speed of sound, C_{ij} is the elastic constant in the given direction, E is Young's modulus (or the modulus of elasticity), ν is Poisson's ratio, ρ is the density, and G is the shear modulus, V_L is the longitudinal velocity and V_T is the shear velocity.

Table 5: Weld and base metal characteristics obtained from Ultrasonic A Scan

Shielding gas	Region	Poisson's Ratio	Shear Velocity (m/s)	Longitudinal Velocity (m/s)	Young's Modulus (MPa)	Shear Modulus (GPa)
Argon	Base	0.28	3100	5607.4	36.18	79.28
	Weld	0.225	3100	5405.4	36.81	79.28
Argon-Hydrogen	Base	0.234	3100	5263	37.212	79.28
	Weld	0.196	3100	5042	37.6214	79.28



Shear waves, particles oscillate at right angle to the direction of propagation. They require an acoustically solid material for their propagation and relatively weaker than longitudinal waves. In longitudinal waves, the oscillation occurs in the direction of wave propagation. Compression and expansion forces are active in these waves and they are also called "Density waves, as material density fluctuates as the wave moves. These are the velocities of the ultrasonic rays.

IV. CONCLUSION

From the experimental results, it is observed that the weld properties changed with change in shielding gases while carrying out GTAW welding. The grain size in HAZ region is dendrite length and spacing in weld region is more and deeper weld penetration and a wider bead was observed with Argon-Hydrogen as shielding gas as compared to Argon gas. A shallow penetration and narrow bead was observed from the macrostructure using Argon as shielding gas. Hardness of samples welded with Argon-Hydrogen shielding gas is lower. From Ultrasonic Testing it was found that there are no defects in the weld region. Observing the results of Ultrasonic A scan, the Young's modulus of the weld region is more that of the base metal whereas the Poisson's ratio for the base metal is higher than the weld region. Young's modulus of the specimen welded with Argon is less than that welded with Argon-Hydrogen.

REFERENCES

- [1] Hirose A, Sakata K, Jobayashi KF (1998) Microstructure and mechanical properties of laser beam welded Inconel 718. Int.J Mater Prof Technol 13 (1-2) : 28-44.
- [2] M or tezaie A, shamanian M (2014) An assessment of microstructure, mechanical properties and corrosion resistance of dissimisa welds between Inconel 718 and 310s. austenitic stainless steel. Int J press ves pip 116: 37-46.
- [3] James L (1978) Fatigue- crock growth in Inconel 718 weldments at elevated temperatures weld j res suppl 57(1) : 17s -23s.
- [4] Wang.H, ileuchi, K, Aritoshi, M, Takahashi, M and Ikeda, A. 2008. Microstructure forming in friction weld of Inconel 718 alloy. Quart J Jpn weld soc, 26(2): 159-166 (In Japanese).
- [5] M. Sundararaman and P. Mukhopadhyay, "Carbide precipitation in Inconel 718", High Temperature Materials and Processes, 11 (1993), 315-368.



MATRUSRI ENGINEERING COLLEGE

(Approved by AICTE, Affiliated to Osmania University)

#16-1-486, Saidabad, Hyderabad - 500059



Sponsored by

MATRUSRI EDUCATION SOCIETY



ISBN: 97881-936274-0-2



1ST NATIONAL CONFERENCE ON TRENDS IN SCIENCE, ENGINEERING AND TECHNOLOGY

(NTSET - 2018)

February 2nd & 3rd - 2018

TECHNICAL PAPER ABSTRACTS



ORGANIZED BY

MATRUSRI ENGINEERING COLLEGE

(Approved by AICTE, Affiliated to Osmania University)

#16-1-486, Saidabad, Hyderabad - 500059



Sponsored by

MATRUSRI EDUCATION SOCIETY

ISBN: 97881-936274-0-2

NTSET 2018





FAILURE CRITICALITY ANALYSIS USING FISHIKAWA DIAGRAM (A CASE STUDY OF DUMPERS AT OCP, RAMAGUNDAM)

M. Pradeep Kumar¹, M. Krishna², Dr. N.V.S. Raju³, Dr. M. V. Satish Kumar⁴

¹Research Scholar, JNTUH Kukatpally, Assistant Professor, KITS(s), Karimnagar, TS-India

²Assistant. Professor, MatrusriEngg. College, Hyderabad, TS - India

³Professor in Mechanical Engineering, JNTUHCE, Jagtial, TS-India

⁴Professor in Mechanical Engineering, KITS(s) Karimnagar, TS-India

Abstract: Open cast mines are one of the major sources for extracting coal to generate power. The machineries used in the open cast have prominence in producing coal. Any interruption may arise due to poor quality of assemblies or improper maintenance, which results in the production loss. In the interest of enhancing the productivity, the interruptions in the form of failures are to be avoided and the availability of the machinery in the field thence can be maximized. Some failures not only cause the interruption (production loss) but also cause damage assets and even may consume human lives. This necessitates the prediction of failures in advance. In this perspective, “fishbone” diagram, introduced by Ishikawa gained popularity in identifying the root causes of failures. This paper attempts to find criticality using C-I-N analysis and root causes of the various failures that occurred in dumpers used in mining industry. The causes and effects of failures can enlighten the maintenance managers to focus on the areas of causes of failures that considerably can minimize the failures.

Index Terms - Criticality, Fishbone diagram, dumpers.

I. INTRODUCTION

The cause and effect analysis is a preliminary tool for analysing the root causes and their effects for a problem. It was invented and incorporated by Mr. Kaoru Ishikawa, a Japanese quality control statistician. Ishikawa first proposed the seven tools for quality control, this special tool is exclusively propounded by him and is known as the most effective and powerful tool for defect analysis. The fishbone diagram and analysis typically evaluates the causes and sub-causes of one particular problem and therefore assists in predicting the problems by focusing on the root causes. In the present study, the failure categorization was done based on its criticality using C-I-N analysis. Further, root cause analysis was done for the failures occurred in the machineries used in the open cast mines. This study was carried out at the Singareni Collieries Company Limited (SCCL) which is undertaken by the Telangana govt. and union govt. of India.

Although there are various machineries were available like Drills, Dozers, Dumpers, Loaders, and Shovels etc. at the mine, for which dumpers has found giving more trouble. A failure can occur in many forms, each failure will have some cause to occur. Also there will be an effect either may be major or minor for each failure. If the causes which makes the failure to occur are known then the same failure may not be repeated. In this study, the failures of dumpers used in open cast mines were studied and root causes of each failure and their categorization were investigated using fishbone diagram and C-I-N analysis.

I. C-I-N ANALYSIS

All machines fail at one time or another. A machine will fail due to many reasons and in general situations all failures will not have the same importance due to their improper failure distribution pattern, time of repair, cost of the component, function, etc. Also, it is very difficult for maintenance department to focus on all kind of failure that occurs in equipment. Thus, care to be taken obviously differs based on the importance of failures. To have control and modeling of the failures which are of less occurring or importance, maintenance managers should establish a procedure to sort the failure based on their importance. C-I-N analysis is one such procedure that gives a clear picture on three classes of failures. This classification is also based on criticality. C-I-N classification is often used for machinery and equipment.

- C stands for critical machines/failures.
- I stands for important machines/failures.
- N stands for normal machines/failures.

II. ANALYSIS OF FAILURES

This study was carried out at the Singareni Collieries Company Limited (SCCL) which is undertaken by the Telangana govt. and union govt. of India. After a thorough study on the machineries used in open cast mines, it was found that load hauling dumpers are giving more trouble than any other machine. Concerning this, a critical study was done on the failures of dumpers and using fishbone diagram, root causes were found. Initially, data related to dumper failures for a period of two years



was collected based as per the record available. Then after, all the failures are arranged in a chronological order. It has been found that, many failures were occurred in a span of two years, some of them are shown in the table no.1 as an example.

Table 1: Examples of Some of the failures occurred

Bucket exhaust adaptor broken.	Tappet setting metal in strain.	Steering hard idle
Water leak in the exhaust pipe.	Horn not working.	PTO problem, replaced.
Steering hard, turbo charger fixed.	Wheel alignment	Right side pulling.
Engine oil leak.	Hydraulic oil leak seal fix.	Air leak
Exhaust leak.	Clutch, gears problem.	transmission oil leak
Seal broken in engine.	Breaks weak.	tie rod broken
Clutch and Gears problem	Steering oil leak.	pin jammed
Hoist cylinder leak, replaced.	Brakes weak.	crank damage
Suspension seal leak.	Steering link broken.	suspension broken

It was observed that more number of failures occurred in the stated period, all these failures were reduced to a small number for the convenience. Based on the element or the component which it belongs, these failures were categorised as seven major failures. Also a count has been taken for each failure mode about which it has been occurred in the stated period. These seven failures along with their occurrence of sub failure (in number of times) are listed in the table no.2. From the table, a total of seven failure components were listed along with their failure modes. Number of occurrences, time to repair (TTR) and average of TTR were recorded along with each failure mode. Component wise total failure occurrences, their average repair time also calculated and the product of these two gives the total production loss. Based on these value rank was assigned for each failure component C-I-N analysis were carried further.

Table 2: Seven Failure Components along with their failure modes and occurrences

F. No.	Failure Mode	TTR	Avg. of TTR	Occurrence	Avg repair time	Total No. of Failures	Production Loss	Rank	
1	Brake Failures	Brake oil leak	85	17	5	38	21	798	IV
	Air leak from brake	140	70	2					
	Brake Jam	280	56	5					
	Brake wear & air loss	99	33	3					
	Brake Anchor Leak	78	13	6					
2	Suspension Failures	Suspension Bolt Broken	98	20	5	24	34	816	III
	Suspension Oil Leak	378	27	14					
	Suspension seal leak	322	36	9					
	Suspension preventive repair	74	12	6					
3	Engine Failures	Exhaust leak	67	35	2	75	17	1275	I
	Engine replaced	731	183	4					
	Engine head failed	759	126	6					
	Engine maintenance	21	11	2					
	Engine vibration	65	22	3					
4	Transmission Failures	Toe in toe out	59	12	5	15	19	258	VI
	Gear shifting problem	90	15	6					
	Transmission oil leaked	135	17	8					
5	Steering Failures	Steering oil cylinder leak	94	13	7	11	11	121	VII
	steering box bolts replaced	16	8	2					
	Steering ball bearing broken	24	12	2					
6	Hydraulic & Hoist Failures	Hydraulic oil leak	1100	61	18	24	53	1272	II
	Hoist cylinder leak	263	20	13					
	Hoist seal leak	152	22	7					
	oil leak from seals	75	25	3					
	ELC oil change	25	8	3					
	hoist not working	76	8	9					
7	Radiator Failures	water boil in radiator	106	26	4	27	15	405	V
	Water pump leak	99	33	3					
	Turbo charger oil leak	121	40	3					
	Radiator hose problem	18	9	2					
	Radiator fan damaged	78	26	3					



III. FAILURE CRITICALITY THROUGH C-I-N

In failure criticality through C-I-N analysis initially the average repair time and the number of failures for each failure component was calculated individually. Then the total production loss is calculated by multiplying the number of failures with its respective average time to repair. Then ranking was done from the highest to the lowest production loss. Cumulative production loss was calculated and the graph between the number of failure and cumulative production loss has been plotted as shown in the figure 1 which gives the Critical, Important and Normal failures.

Table 3: C-I-N analysis calculations

S. No.	F. No.	Failures	Total Prod. loss	Cumulative TPL	% Cumulative	% Failure	C-I-N
1	3	Engine Failures	1275	1275	4.96	14.28	Critical
2	6	Hydraulic & Hoist Failures	1272	2547	9.91	28.57	Critical
3	2	Suspension Failures	816	3363	13.09	42.85	Important
4	1	Brake Failures	798	4161	16.2	57.14	Important
5	7	Radiator Failures	405	4566	17.77	71.42	Important
6	4	Transmission Failures	258	4824	18.78	85.71	Normal
7	5	Steering Failures	121	4945	19.25	100	Normal

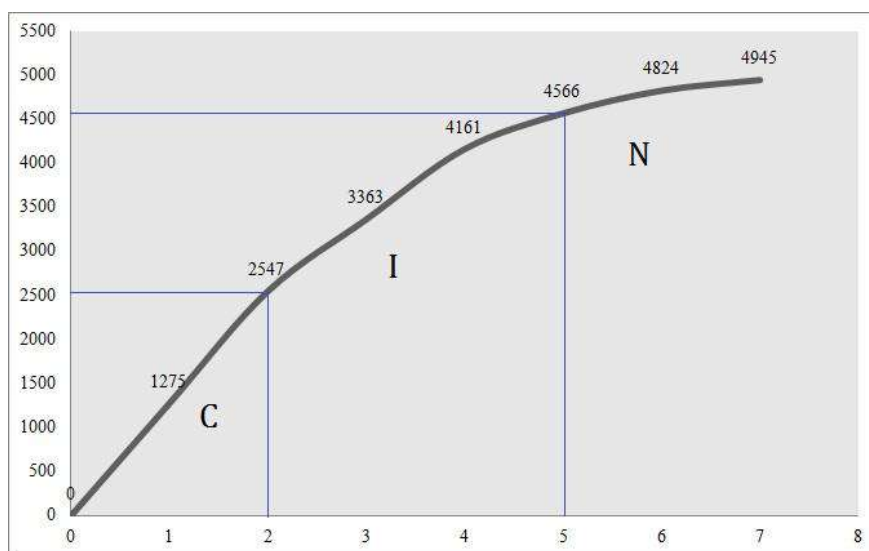


Figure 1: C-I-N analysis graph

IV. KAORU ISHIKAWA

Kaoru Ishikawa graduated from the University of Tokyo. Ishikawa ideology focused that the quality improvement is a continuous process, and it can always be taken one step further. He was the first quality guru to stress the importance of total quality control of an organization, rather than just focusing on products and services. Ishikawa also enlightened the importance of the “internal customer,” the next person in the production process. He believed that the company’s vision and the goals should be shared by each and every worker in the organization and the unity among them enhances the standard. He popularly knew for his implementation of quality circles, which are small teams of employees that volunteer to solve quality problems.

The first contribution of Ishikawa is transforming the Deming’s PDCA cycle into a six step plan. Ishikawa identified and showed the importance of seven tools of quality. His seven quality tool includes control chart, run chart, histogram, scatter diagram, Pareto chart, and flowchart. The most popularized and widely used seventh quality tool of Ishikawa is the *Fishbone Diagram*, Commonly known as the *Cause and Effect diagram* or *Fishikawa diagram*. This is the most notable of all of Ishikawa’s contributions to the field of total quality.

V. CAUSE-AND-EFFECT DIAGRAM

Cause and effect diagram is used as a way of structuring the process of determining the root cause of a problem. Although Ishikawa first proposed the seven tools for quality control, this special tool is exclusively propounded by him and is known as the most effective and powerful tool for defect analysis. It can be applied to any situation and does not need any mathematical/statistical preliminaries.

This diagram evaluates the causes and sub-causes of a particular problem and therefore assists to resolve the same. In a common fishbone diagram major problem which is to be focused has been put on central bone as problem statement, the major categories of causes are put as side bones and sub-bones as detailed causes. With the aid of fishbone diagram, one can estimate and evaluate all possible causes of a problem, and thence find the root cause of the fault, failure of a system. With the focus on the root problems, this diagram can provide considerable quality improvement from the “bottom up.”



Some Noteworthy Points about Cause-and-Effect Diagrams

- Cause-and-effect diagrams (Ishikawa diagrams) are used for understanding organizational or business problem causes.
- Organizations face problems everyday and it is required to understand the causes of these problems in order to solve them effectively. Cause-and-effect diagrams exercise is usually a team work.
- A brainstorming session is required in order to come up with an effective cause-and-effect diagram.
- All the main components of a problem area are listed and possible causes from each area are enumerated.
- Root cause analysis (also included in this category) helps in finding the true root cause of a problem.
- The most likely causes of the problems are identified to carry out further analysis.

VI. CONSTRUCTION OF ISHIKAWA (CAUSE-AND-EFFECT) DIAGRAM

The following steps will help in constructing a Fishikawa cause-and-effect diagram.

Step 1 (problem statement): A defect or an inconvenience or symptoms of such situations propel the problem. The detail of it or the definition of situation becomes the problem statement. In turn, this then becomes the label for the root effect arrow (also called spine) as shown by horizontal shaded lines in Figure

Step 2 (major causes): The second step is to identify major categories of causes. These are then drawn at an angle to the root effect arrow as shown by dotted area in Figure.

Step 3 (detailed causes): The next step is to list all the detailed causes as sub-braches on to the major categories, i.e., within each of angled bone (line).

Step 4 (principal causes): The final step is to identify the principal causes among the detailed causes. These are considered as the significant or important causes.

VII. ROOT CAUSE ANALYSIS FOR THE FAILURES

In order to construct the fishbone diagram for these seven failures, a critical study has been done by questring and inquiring the workers and mechanics working in the field. After refining the data, fishbone diagram was constructed according to the category about which that failure belongs.

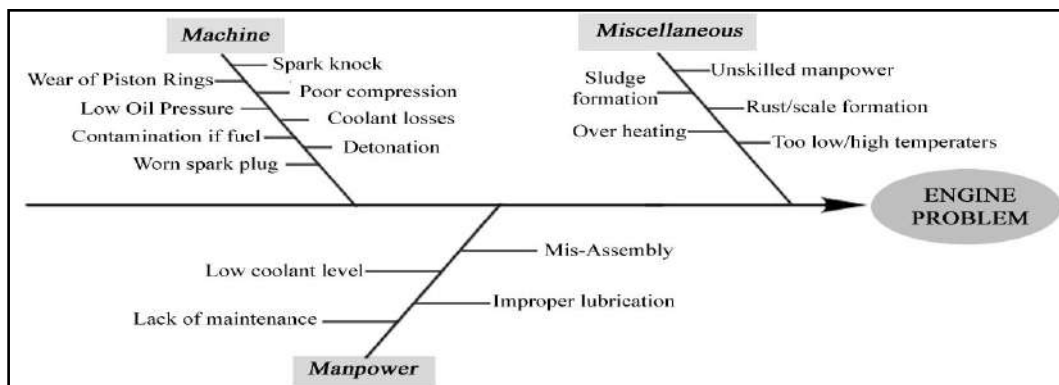


Figure2: Fish bone diagram for Engine problems

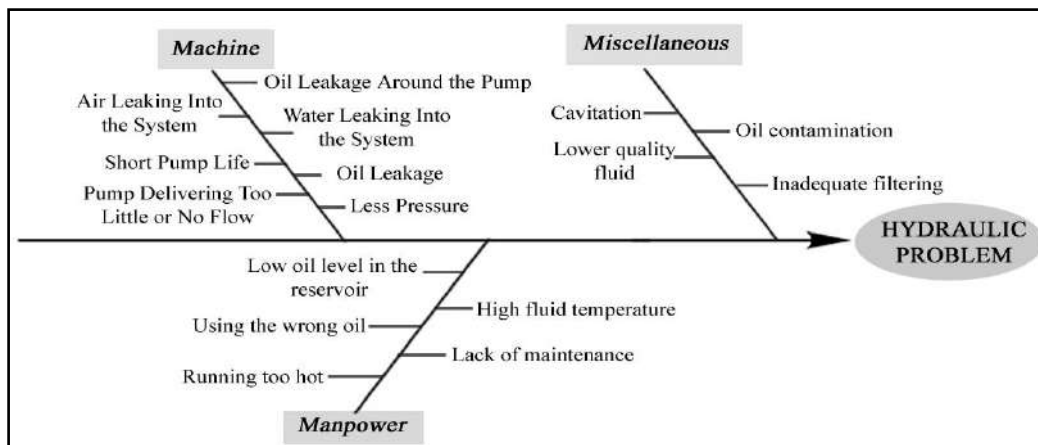


Figure 3: Fish bone diagram for Hydraulic problems

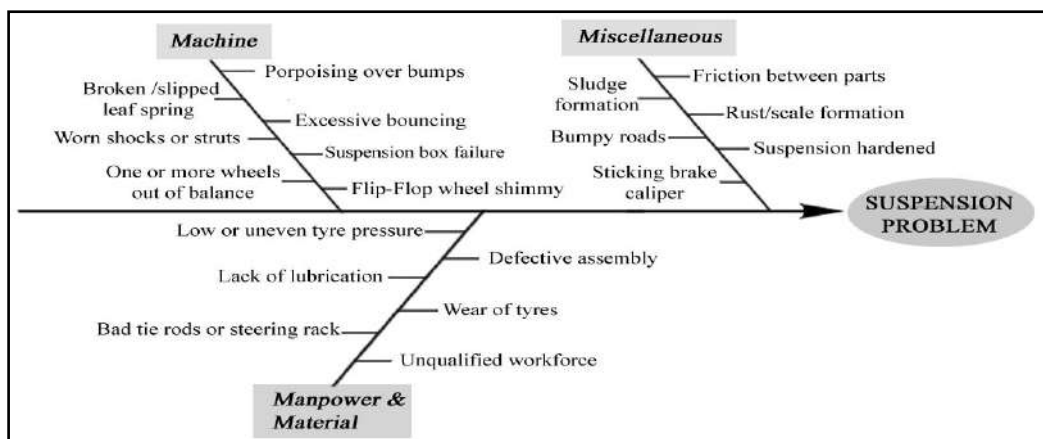


Figure 4: Fish bone diagram for Suspension problems

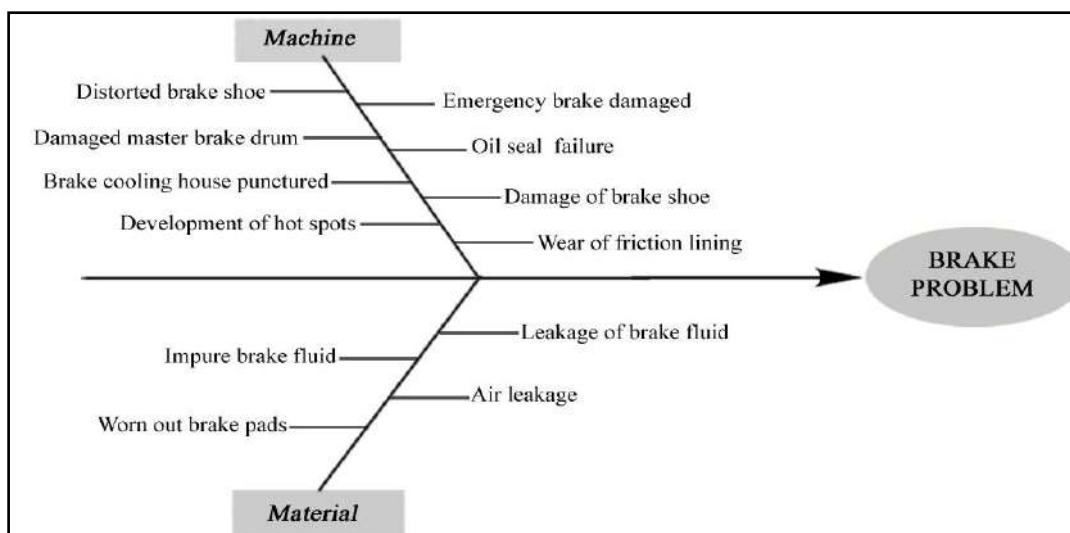


Figure 5: Fish bone diagram for Brake problems

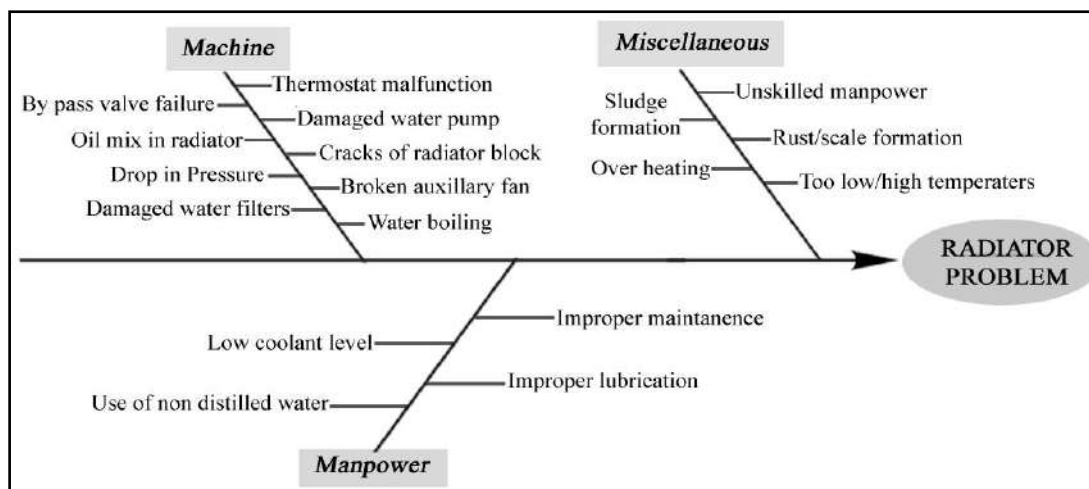


Figure 6: Fish bone diagram for Radiator problems

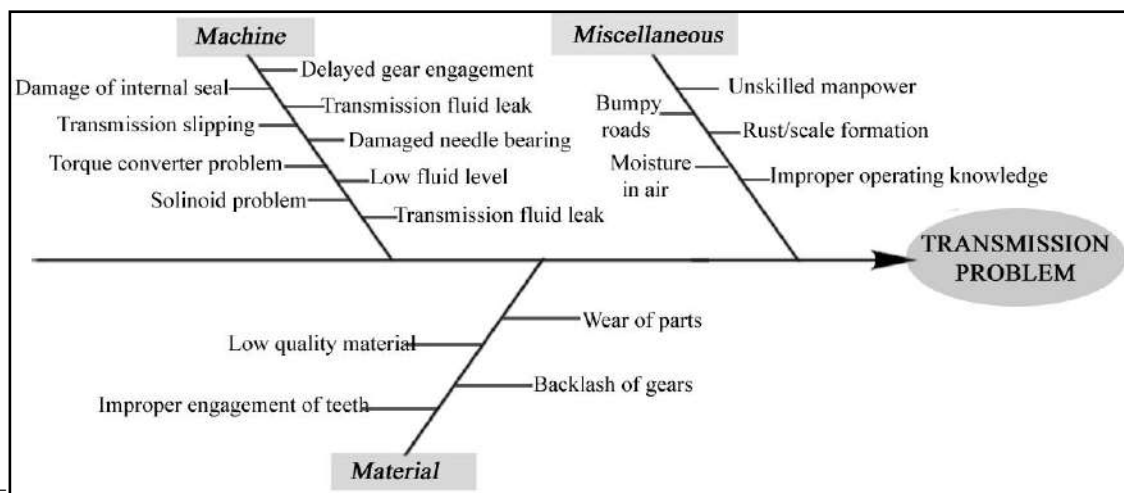


Figure 7: Fish bone diagram for Transmission problems

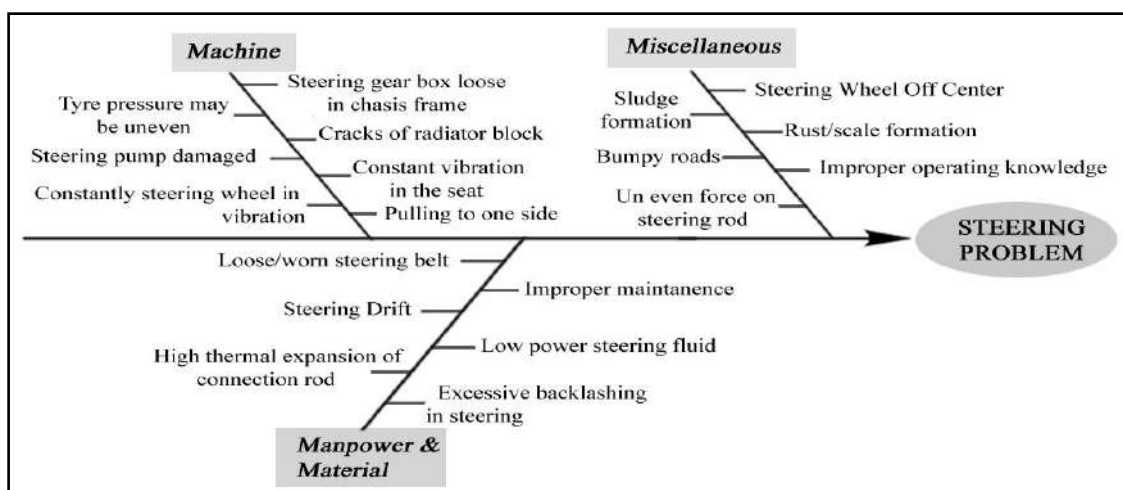


Figure 8: Fish bone diagram for steering problems

VI. FISHBONE DIAGRAM ANALYSIS

Based on the results of C-I-N analysis, it is clear that among all the seven failures, the most critical failures were engine and hydraulic failures. Although there needed attentiveness on all the failures which causes the breakdowns, though major focus should be on the failure which has highest production loss. The objective of this paper is to analyse the criticality and causes of failures using fishbone diagram. All the causes for seven failures were grouped under 4 categories i.e, man, machine, material and miscellaneous. Each failure causes were studied and noted under the category which it belongs. After drawing the network of fishbone diagram for all the failures, it was observed that, steering and suspension problem have the highest number of causes when compare the other failures. And analysing the causes according to the category, the machine category related has more number of causes.

Table 3: Fishbone diagram Causes categorization

S. No.	F. No.	Failures	Man	Machine	Material	Miscellaneous	Total
1	3	Engine Failures	4	8	-	5	17
2	6	Hydraulic & Hoist Failures	5	7	-	4	16
3	2	Suspension Failures	3	7	3	6	19
4	1	Brake Failures	-	8	4	-	12
5	7	Radiator Failures	4	9	-	5	18
6	4	Transmission Failures	-	9	4	5	18
7	5	Steering Failures	3	7	3	6	19
			19	55	14	31	

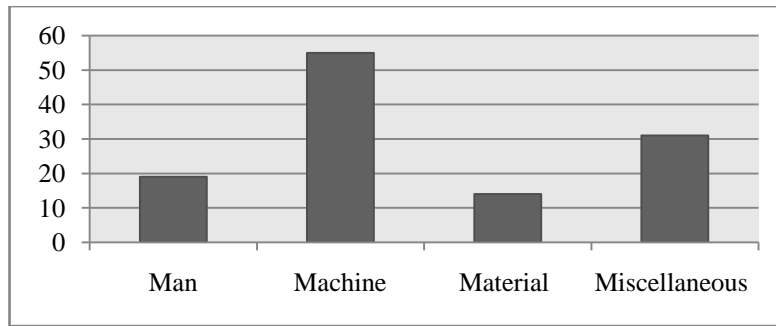


Figure 9: Contribution of man, machine, and material for causes of failures

VII. CONCLUSION

Fishbone analysis provides a template to divide and categorise possible causes of a problem by allowing quality circle to focus on the content of the problem, rather than the history. It is useful tool, which is increasingly being used in production, manufacturing and safety engineering. In this paper, cause and effect diagram is used to identify the root causes for the breakdowns that occurred in the dumpers used in the open cast mines. Initially the breakdowns (failures) were investigated and categorised as seven major failures. These seven failures were sorted and categorised as critical failures, important failures and normal failures. This is achieved by applying C-I-N analysis to the failures of the dumpers. Engine failures and Hydraulic failures have found in top 2 places in the list which indicate that are the most critical failures. After C-I-N analysis, a thorough study has been done for each failure and their various causes were noted down in the form of fishbone diagram. The diagram has been categorised as man based, machine based, material based and miscellaneous. Then each cause regarded to a particular failure has been mapped with the category about which it belongs. After the construction of fishbone diagram for each failure separately, it has been found that failures which belong to machine category has more number of causes. Also it was observed that among all the failures steering problem and suspension problem has more number of causes. The focus on the failures with highest criticality and focus on the causes with highest number can considerably improve the production rate and enhance the quality and reliability of the system.

REFERENCES

- [1] Dr. N.V.S Raju/ Industrial Engineering and Management/ Cengage Learning
- [2]. Dr. N.V.S Raju/ Total Quality Management / Cengage Learning
- [3] M. Pradeep Kumar, Dr. N.V.S. Raju, Dr. M.V. Satish Kumar, Quality of Quality Definitions –An Analysis, International Journal of Scientific Engineering and Technology/ISSN:2277-1581 / Volume No.5 Issue No.3, pp: 142-148
- [4] M.Pradeep Kumar, Dr. N.V.S Raju, K.Amarnath, When Technology Ends Art Begins -The Art and Science of TQM, International Journal of Scientific & Engineering Research, Volume 7, Issue 6, June-2016 ISSN 2229-5518
- [5] Joanna Phillips/Using fishbone analysis to investigate problems/ Nursing Times 16.04.13/ Vol 109 No 15 / www.nursingtimes.net
- [6] Kiran M, Cijo Mathew, Jacob Kuriakose/ Root Cause Analysis for Reducing Breakdowns in a Manufacturing Industry/ International Journal of Emerging Technology and Advanced Engineering/ Volume 3, Issue 1, January 2013
- [7] Joymalya Bhattacharya / Root Cause Analysis – A Practice to Understanding and Control the Failure Management in Manufacturing Industry/ International Journal of Business and Management Invention ISSN (Online): 2319 – 8028, ISSN (Print): 2319 – 801X www.ijbmi.org Volume 3 Issue 10 | October. 2014 | PP.12-20
- [8] Ishikawa, K. (1985). What is total quality control. New Jersey: Prentice Hall
- [9] Wilson, P. F., Dell, L. D., & Anderson, G. F. (1993). Root Cause Analysis: A Tool for Total Quality Management . Milwaukee: ASQC Quality Press
- [10] Analysis of Breakdowns and Improvement of Preventive Maintenance on 1000 Ton Hydraulic Press, International Journal of Emerging Technology and Advanced Engineering, Praveen Kumar R, Rudramurthy, Volume 3, Issue 8, August 2013,638
- [11] M.A. Khattak , N.Zareen , AniqueMukhtar , S.Kazi , AmenaJalil ,Zaheer Ahmed , Miraj Muhammad Jan (2016) Root cause analysis(RCA)of fractured ASTM A 53 carbon steel pipe at oil & gas company Case Studiesin Engineering Failure Analysis7(2016)
- [12] Chandna, P., & Chandra, A. (2009). Quality Tools to Reduce Crankshaft Forging Defects: An Industrial Case Study. Journal of Industrial and Systems Engineering, 3



MATRUSRI ENGINEERING COLLEGE

(Approved by AICTE, Affiliated to Osmania University)

#16-1-486, Saidabad, Hyderabad - 500059



Sponsored by

MATRUSRI EDUCATION SOCIETY



ISBN: 97881-936274-0-2



1ST NATIONAL CONFERENCE ON TRENDS IN SCIENCE, ENGINEERING AND TECHNOLOGY

(NTSET - 2018)

February 2nd & 3rd - 2018

TECHNICAL PAPER ABSTRACTS



ORGANIZED BY

MATRUSRI ENGINEERING COLLEGE

(Approved by AICTE, Affiliated to Osmania University)

#16-1-486, Saidabad, Hyderabad - 500059



Sponsored by

MATRUSRI EDUCATION SOCIETY

ISBN: 97881-936274-0-2

NTSET 2018





FACTORS AND MECHANISMS RESPONSIBLE FOR HEAT TRANSFER ENHANCEMENT USING NANO FLUID

¹V.Harinath, ²Dr.K.Srinivasa Reddy, ³Dr.K.Vijaya Kumar Reddy

¹Asst. Professor, ²Professor, ³Professor,

¹Department of Mechanical Engineering,

¹Matrusri Engineering College, Hyderabad, INDIA,

Abstract: A colloidal mixture of Nano fluid particles in a base fluid is called Nano fluid which is a new generation of Heat transfer fluid for various heat transfer applications. This paper analyses and summarizes the various factors affecting Nano-fluid thermal performance such as particle size, fluid type, temperature, volume concentration, PH, particle shape and the latest developments regarding the mechanisms that influences the enhancement of Heat transfer by using Nano fluids.

Keywords: Nano fluid, Thermal conductivity, Brownian motion

I. INTRODUCTION

Nano fluids are a new class of fluids, developed by dispersing Nano meter sized materials (Nano particles, Nano fibres, Nano tubes, Nano wires, Nano rods, Nano sheets) in the base fluids. Common base fluids include water, organic fluids, oils lubricants and bio fluids etc. Materials commonly used as Nano particles include chemically stable metals (Ex: - Ag, Au, Cu), Metal oxides (Ex:-Alumina, silica, MgO) ceramic oxides (Ex:-Al₂O₃, CuO) etc. Preparation of Nano-fluids is the first key step in experimental studies with Nano-fluids. Nano fluid is not simply liquid-solid mixtures. Some special requirements are essential, e.g., even and stable suspension, durable suspension, negligible agglomeration of particles, no chemical change of the fluid, etc. Nano fluid are produced by dispersing Nanometre-scale solid particles into base liquids such as water, ethylene glycol (EG), oils, etc. In the preparation of Nano-fluids agglomeration is a major problem. There are mainly two techniques used to produce Nano-fluids. The single-step and the two-step method. The single-step direct evaporation approach was developed by Akoh¹ et al. (1978) and is called the VEROS (Vacuum Evaporation onto a Running Oil Substrate) technique. The original idea of this method was to produce Nanoparticles, but it is difficult to subsequently separate the particles from the fluids to produce dry Nanoparticles. A modified VEROS process was proposed by Wagener² et al. (1997). They employed high pressure magnetron sputtering for the preparation of suspensions with metal Nanoparticles such as Ag and Fe. Eastman³ et al. (1997) developed a modified VEROS technique, in which Cu vapour is directly condensed into Nanoparticles by contact with a flowing low-vapour-pressure liquid (EG).

Zhu⁴ et al. (2004) presented a novel one-step chemical method for preparing copper Nano-fluids by reducing CuSO₄·5H₂O with NaH₂PO₂·H₂O in ethylene glycol under microwave irradiation. Results showed that the addition of NaH₂PO₂·H₂O and the adoption of microwave irradiation are two significant factors which affect the reaction rate and the properties of Cu Nano-fluids.

A vacuum-SANSS (submerged arc Nanoparticle synthesis system) method has been employed by Lo⁵ et al. (2005) to prepare Cu-based Nano-fluids with different dielectric liquids such as de-ionized water, with 30%, 50%, 70% volume solutions of ethylene glycol and pure ethylene glycol. They found that the different morphologies that are obtained are mainly influenced and determined by the thermal conductivity of the dielectric liquids. CuO, Cu₂O, and Cu based Nano-fluids can also be efficiently prepared by this technique. An advantage of the one-step technique is that Nanoparticle agglomeration is minimized, while the disadvantage is that only low vapour pressure fluids are compatible with such a process. Recently, a Ni Nano-magnetic fluid and silver Nano fluid were also produced by Lo⁶ et al. (2006) using the SANSS method. The spherical silver Nanoparticle formed in the ethylene glycol and the mean particle size is about 12.5 nm, which more closely resembles Newtonian fluids.

The two-step method is extensively used in the synthesis of Nano-fluids considering the available commercial Nano powders supplied by several companies. In this method, Nanoparticles are first produced and then dispersed in the base fluids. Generally, ultrasonic equipment is used to intensively disperse the particles and reduce the agglomeration of particles. For example, Eastman et al. (1997), Lee et al. (1999), and Wang et al. (1999) used this method to produce Al₂O₃ Nano-fluids. Also, Murshed⁷ et al. (2005) prepared TiO₂ suspension in water using the two-step method. Other Nanoparticles reported in the literature are gold (Au), silver (Ag), silica and carbon Nanotubes. As compared to the single-step method, the two-step technique works well for oxide Nanoparticles, while it is less successful with metallic particles.

While most Nano fluid productions to date have used one of the above-described (one-step or two-step) techniques, other techniques are available depending on the particular combination of Nanoparticle material and fluid. For example, Nanoparticles with specific geometries, densities, porosities, charge, and surface chemistries can be fabricated by templating, electrolytic metal deposition, layer-by-layer assembly, micro droplet drying, and other colloid chemistry techniques. Another process, the chemical vapour condensation technique, appears to offer advantages in terms of control of particle size, ease of scalability, and the possibility of producing novel core-shell Nanostructures (Srdic⁸ et al, 2001). Still another technique is the shape- and size-

controlled synthesis of Nanoparticles at room temperature (CaO⁹ et al, 2006). The structural characteristics of Nanoparticles such as the mean particle size, particle size distribution, and shape depend on the synthesis method, and there is potential for good control. These characteristics for Nanoparticles in suspensions are not easily measured. This fact could account for some of the discrepancies in thermal properties reported in the literature among different experiments.

In addition to ultra sonification, some other techniques such as control of pH or addition of surface active agents are also used to attain stability of the suspension of the Nano-fluids against sedimentation. These methods change the surface properties of the suspended particles and thus suppress the tendency to form particle clusters. It should be noted that the selection of surfactants should depend mainly on the properties of the solutions and particles. Xuan and Li¹⁰ (2000) chose salt and oleic acid as the dispersant to enhance the stability of transformer oil-Cu and water-Cu Nano-fluids, respectively. Oleic acid and cetyltrimethylammonium bromide (CTAB) surfactants were used by Murshed et al. (2005) to ensure better stability and proper dispersion of TiO₂-water Nano-fluids. Sodium dodecyl sulphate (SDS) was used by Hwang¹¹ et al. (2005) during the preparation of water-based multi-walled carbon Nanotube (MWCNT) Nano-fluids since the fibres are entangled in the aqueous suspension.

By suspending Nano-particles in the base fluid heat transfer rate can be improved due to following reasons

- The suspended Nanoparticles increase the surface area and heat capacity of the fluid.
- The suspended Nanoparticles increase the effective thermal conductivity of the fluid.
- The interaction and collision among particles, fluids and the flow passage surface are intensified.
- The dispersion of Nano particles flattens the transverse temperature gradient of the fluid in its flow passage.
- The pumping power is low when compared to that of pure fluids to achieve equivalent heat transfer enhancements.
- There is reduced particle clogging when compared to conventional slurries.

II. MECHANISMS

2.1 Heat conduction Mechanisms in Nano fluids

Keblinski¹² presented four possible mechanisms in Nano fluids which may contribute to thermal conduction.

- (a) Brownian motion of Nano particles.
- (b) Liquid layering at the liquid/particle interface.
- (c) Ballistic nature of heat transport in Nanoparticles.
- (d) Nano particle clustering in Nano fluids.

Brownian motion is the random motion of particles suspended in a fluid (a liquid or a gas) resulting from their collision with the fast-moving atoms or molecules in the gas or liquid. The Brownian motion of Nano-particles could contribute to the thermal conduction enhancement through two ways, a direct contribution due to motion of Nano-particles that transport heat, and an indirect contribution due to micro-convection of fluid surrounding individual Nano-particles. In the second kind of modelling, the structure of the Nano fluid is considered analogous to the structure of a composite material. This composite material would present a core composed of the Nanoparticle, an interface layer containing intermediate properties surrounding this core, and a matrix composed of the base fluid that immerses these two regions. The composition of these regions could form a multiphase system, in which the phase superposition would be the main factor responsible for enhancing the thermal conductivity of the mixture. According to Ding et al. [30], at the interface between the solid particles and the base fluid, the liquid molecules could be significantly more ordered than along the rest of the base fluid. This can directly influence the thermal behaviour of the Nano-fluids, approaching the behaviour of crystalline solids, the conductivity of which is greater than that observed in liquids fig. 1, extracted from Keblinski¹² et al. shows that the rise of the interface layer results in an enhancement in the thermal conductivity proportional to the size of this layer. In this case, κ represents the dimensionless enhancement of the thermal conductivity. However, it is important to notice that the effect of the formation of an interface layer can deteriorate the thermal conductivity of a Nano fluid. In cases in which the interface presents a significant thermal resistance, (e.g., when the size of the Nano-particles is small as compared to a characteristic length of the flow), the use of Nano-fluids is not recommended. Several researchers used the interface layer concept in order to explain the great enhancement obtained in the thermal conductivity of Nano-fluids. Yu and Choi [31, 32] suggested models considering an interface layer of Nano metric dimensions formed by a base fluid around the Nano-particles.

A third kind of modelling is the study of the formation of particle clusters and of the distribution of these clusters. A study involving these concepts was presented by Wang and Mujumdar¹⁵. Ding et al. [30] also presented the use of a mechanism of structuring and clustering

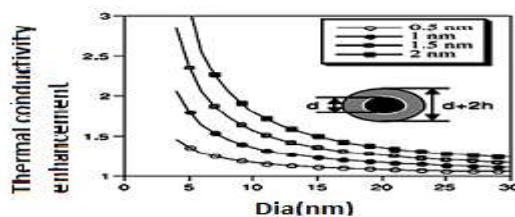


fig 1 effect of the thickness of the interface layer on thermal conductivity enhancement

This mechanism proposes the use of particle clusters with equivalent thermal conductivity. The results from the application of this model have good agreement with the experimental results. Several studies presented in Kakac and

Pramuanjaroenkij¹⁹ also reported that excessive particle clustering in Nano-fluids deteriorates the thermal conductivity so that an optimum level of clustering must be evaluated in order to achieve a maximum enhancement.

Fig. 2, reproduced from Koblinski¹² et al. shows that particle clusters with less compact structures allow a greater enhancement in heat transfer than compact arrangements. In this case, κ represents the dimensionless enhancement of thermal conductivity and ϕ represents the dimensionless particle clustering.

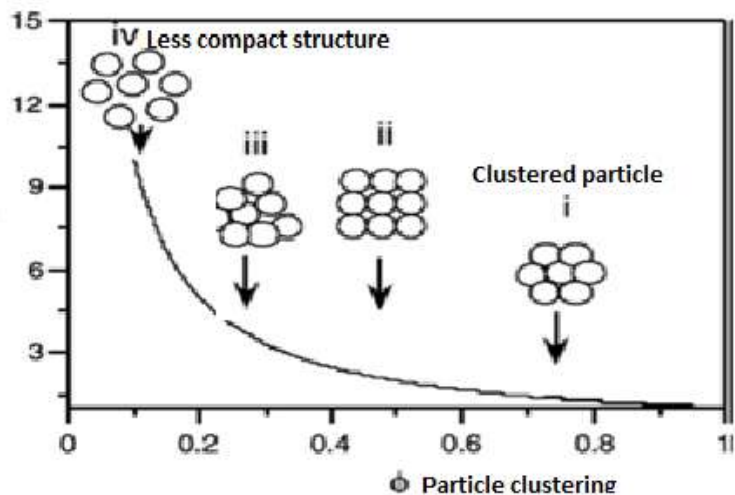


fig 2 effect of clustering of particles on thermal conductivity enhancement

Formation of Chain Structure

Studies of Nano-particles by Xinweiwang and Xianfausing transmission electron microscopy (TEM) show that the Al₂O₃ particles used in the work are spherical. Particles in the liquids are not separated completely. Using TEM, it is found that some particles adhere together to form a chain structure. According to Hamilton and Crosser,²⁰ heat transfers could be enhanced if the particles form chain structures because more heat is transported along those chains oriented along the direction of the heat flux. The effect of the particle size is not considered in their treatment. Assuming that an average chain consists of three particles, the thermal conductivity of particles is 10 times that of the base liquid, and there is 5 vol % particles in liquid, the thermal conductivity will increase 3% according to Hamilton and Crosser's equation²⁰ if the thermal conductivity ratio is taken as infinity, the increase of thermal conductivity is about 7%. Therefore, it is possible that the chain structure contributes to a thermal conductivity increase in Nanoparticle admixtures

A brief summary of previous research on thermal conductivity enhancement is as follows in the early phase of research period, the research group in Argonne National Laboratory made crucial contribution to start the study. Eastman²¹ et al. reported that they prepared stable water based CuO Nano-fluids of 5 volume%, and observed 60% thermal conductivity enhancement. Wang²² et al. measured thermal conductivity of water based CuO and Al₂O₃ Nano-fluids using a steady-state parallel plate method, and reported that their thermal conductivity was higher than those of conventional predictions.

Xian and Li prepared water based Cu Nano-fluids using two-step method, and investigated the effects of particle volume fraction, shape, size, and material properties on effective thermal conductivity. They reported that particle Brownian motion, sedimentation and dispersion would enhance convection heat transfer performance. Choi²³ et al. measured the thermal conductivity of oil based CNT Nano-fluids, and reported the large and non-linear increase of thermal conductivity with volume fraction. Eastman²⁴ et al. measured the thermal conductivity of ethylene glycol (EG) based Cu Nano-fluids of 0.3 volume%, and reported 40% thermal conductivity enhancement. Xie²⁵ et al. measured thermal conductivity of water/EG based SiC Nano-fluids using transient hot-wire method, and concluded that the thermal conductivity enhancement is independent of base fluid type, and it is a function of particle size and shape. Das²⁶ et al. measured thermal conductivity of Nano-fluids using temperature oscillation technique at different temperature and reported it increased linearly with temperature.

Findings report that particle size, nature of material, operating temperature Thermal conductivity and pH value of base fluid all have an influence on Thermal conductivity enhancement in Nano fluids.

III. Convective Heat transfer Enhancement with Nano Fluids:

The past decade has seen many research activities in the experimental heat transfer characteristics of various Nano-fluids. For forced convective heat transfer, Lee and Choi²⁷ (1996) studied the heat transfer behaviour in parallel channels using an unspecified Nano fluid and observed a reduction in thermal resistance by a factor of 2. Xian and Li²⁸ (2003) experimentally investigated flow and convective heat transfer characteristics for Cu-water based Nano-fluids through a straight tube with a constant heat flux at the wall. Results showed that the Nano-fluids give substantial enhancement of the heat transfer rate compared to pure water. They also claimed that the friction factor for the Nano-fluids at low volume fraction did not produce an extra penalty in the pumping power.

Wen and Ding²⁹ (2004b) reported experimental results for the convective heat transfer of γ -Al₂O₃ (27-56 nm)/water based Nano-fluids flowing through a copper tube (D = 4.5 mm, L = 970 mm) in laminar regime. They found that the inclusion of Al₂O₃ particles can significantly enhance the convective heat transfer coefficient, which increases with increasing Reynolds

number and particle concentrations. Furthermore, the improvement of the heat transfer coefficient was particularly large in the entrance region, and decreased with the axial distance. Apart from the improved effective thermal conductivity, they also attributed the improvement of heat transfer to particle migration, which caused a non-uniform distribution of thermal conductivity and viscosity field along the cross-section in the tube.

Li & Xuan³⁰ and Xuan & Li^[65] presented an experimental system to investigate the convective heat transfer coefficient and friction factor of Nano-fluids for laminar and turbulent flows in a tube. The working fluid used was 100nm Cu particles dispersed in de-ionized water. Experiments with different concentrations of Nano-particles were conducted. The Reynolds number of the Nano-fluids varied in the range of 800 – 25000. The experimental results concluded that the convective heat transfer coefficient of the Nano-fluids varied with the flow velocity and volume fraction. Also, the values were higher than those of the base fluid in the same conditions. The Nusselt number of the Nano-fluids with 2% volume fraction of Cu particles was 60% higher than that of water. The results are shown in fig. 3.

From the experimental data of Xuan & Li³⁰ the new heat transfer correlations for the prediction of the heat transfer coefficient of Nano-fluids flowing in a tube were given as follows:

- For laminar flow $Nu_{nf} = 0.4329(1.0 + 11.285\phi^{0.754}Pe_d^{0.218})Re_{nf}^{0.333}Pr_{nf}^{0.4}$
- For turbulent flow $Nu_{nf} = 0.0059(1.0 + 7.6286\phi^{0.688}Pe_d^{0.001})Re_{nf}^{0.923}Pr_{nf}^{0.4}$

Researchers have claimed that the heat transfer enhancement of Nano-fluids is not only caused by the thermal conductivity increase, but also attributed to other factors such as dispersion and chaotic movement of Nano-particles, Brownian motion and particle migration, shear-induced enhancement in flow, reduced boundary layer, particle re-arrangement, and high aspect ratio

The introduction of the Nano-particles directly can affect other physical properties of the base fluid, such as specific mass, specific heat, and dynamic viscosity. This causes the enhancement in the convection heat transfer coefficient to be even greater than the enhancement obtained due to the thermal conductivity. The enhancement obtained in the specific mass of the Nano-fluid can be represented by the mixture rule, defined for microscopic dispersions and widely spread among the literature. Experimental results by Pak and Cho³² and Ho³³ et al. show that the mixture rule can be also used for mixtures containing Nano-sized particles with an excellent agreement.

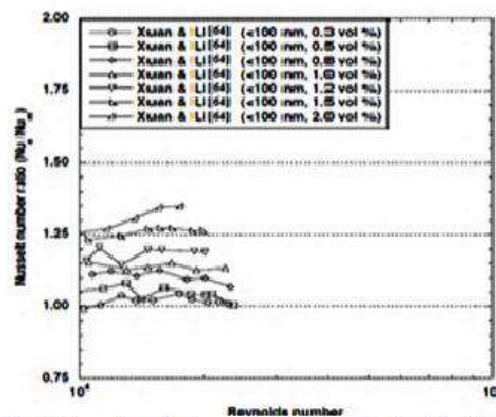


fig 3 nusselt number enhancement with different volume fraction for nano particles

The mixture rule can be represented as:

$$\rho_{nf} = \rho_{np} \phi + \rho_{bf} (1 - \phi)$$

Regarding the specific heat of Nano-fluids, O’Hanley³⁴ et al. studied the behaviour of the two main correlations used by the majority of the present works to describe this property of a Nano-fluid.

$$c_{p,nf} = \frac{\phi(\rho c_p)_{np} + (1-\phi)(\rho c_p)_{bf}}{\phi(\rho)_{np} + (1-\phi)(\rho)_{bf}}$$

Regarding the models used for evaluating the forced convection using Nano-fluids, besides the parameters usually used for determining the flow characteristics, such as the Reynolds number, and the thermal properties of the fluid, such as the Prandtl number, the use of Nano-fluids require additional parameters, so that the correlations take into account the physical phenomena that occur using Nano-fluids. Kakac and Pramuanjaroenkij³⁵ defined that the convection heat transfer coefficient of a Nano-fluid is expected to be related mainly to the following parameters:

- The thermal conductivities of the base fluid and of the Nanoparticle.
- The specific heat of the base fluid and of the Nanoparticle.
- The flow regime the Nano fluid is subjected to (through the Reynolds number).
- The temperature of the Nano fluid.
- The particle volume fraction of the Nano fluid.
- The dimensions and the geometry of the Nano-particles.

Buongiorno³⁶ discussed the influence of these and many other possible mechanisms responsible for the convective heat transfer enhancement using Nano-fluids. The main mechanisms studied were:

- Inertia
- Brownian diffusion



The irregular motion of small particles suspended in a liquid or a gas, caused by the bombardment of the particles by molecules of the medium: first observed by Robert Brown in 1827.

- Thermophoresis (Soret effect)

Thermophoresis (also thermo migration, thermo diffusion, the Soret effect, or the Ludwig-Soret effect) is a phenomenon observed in mixtures of mobile particles where the different particle types exhibit different responses to the force of a temperature gradient.

- Diffusophoresis:

Diffusophoresis is a spontaneous motion of dispersed particles in a fluid induced by a diffusion gradient (also called concentration gradient) of molecular substances that are dissolved in the fluid. This gradient affects structure of the particles in an interfacial double layer and causes sliding motion of the fluid relative to the particle surface.

- Magnus effect:

Magnus effect is generation of a sidewise force on a spinning cylindrical or spherical solid immersed in a fluid (liquid or gas) when there is relative motion between the spinning body and the fluid.

- Fluid drainage
- Gravity

From the effects presented, it was concluded that, for laminar flow and for the viscous sub layer of the turbulent flow, the effects whose relevance are more significant to the thermal behaviour of a Nano fluid are thermophoresis and Brownian diffusion. However, in the turbulent region, the Nano-particles are dragged by the vortexes without friction, making these mechanisms less relevant.

IV. CONCLUSIONS

Nano fluid, i.e., well-dispersed metallic Nano-particles at low volume fractions in liquids, enhances the mixture's thermal conductivity over the base-fluid values. Thus, they are potentially useful for advanced cooling of micro-systems. This paper presents an overview of the recent developments in the study of Nano-fluids, including the preparation methods, the evaluation methods for their stability, the ways to enhance their stability, the stability mechanisms, and their potential applications in heat transfer intensification, mass transfer enhancement, energy fields, and mechanical fields and so on. The performance of Nano fluid critically depends upon the size, quantity (volume percentage), shape and distribution of dispersoids, and their ability to remain suspended and chemically un-reacted in the fluid. In summary, the future scope in the Nano fluid research cycle are to concentrated on heat transfer enhancements and determine its physical mechanisms, taking into consideration such items as the optimum particle size and shape, particle volume concentration, fluid additive, particle coating, and base fluid. Precise measurement and documentation of the degree and scope of enhancement of thermal properties is extremely important. Better characterization of Nano-fluids is also important for developing engineering designs based on the work of multiple research groups, and fundamental theory to guide this effort should be improved. Finally, it is pertinent to suggest that Nano fluid research warrants a genuinely multidisciplinary approach with complementary efforts from material scientists (regarding synthesis and characterization), thermal engineers (for measuring thermal conductivity and heat transfer coefficient under various regimes and conditions), chemists (to study the agglomeration behaviour and stability of the dispersoid and liquid) and physicists (modelling the mechanism and interpretation of results).

At the end of this review, it becomes quite clear that the most significant mechanisms that influence the thermal transfer behaviour of a Nano fluid are the Brownian motion of Nano-particles, the particle clustering phenomenon and the formation of an interface layer around the Nano-particles. These parameters directly affect many of the correlations defined for the thermal conductivity of a Nano fluid. Also, these mechanisms are directly responsible for many of the practical problems observed with the use of Nano fluid in heat transfer applications. For the convection heat transfer coefficient, the enhancement obtained in some cases was even greater than the enhancement that would be obtained due to the thermal conductivity enhancement; that led the researchers to seek for alternative mechanisms to describe this phenomenon, such as thermal dispersion, particle migration, Brownian diffusion and thermophoresis.

REFERENCES

1. Akoh, H., Tsukasaki, Y., S.Yatsuya, and Tasaki, A. Magnetic properties of ferromagnetic ultrafine particles prepared by vacuum evaporation on running oil substrate. *Journal of Crystal Growth*, 45, 495–500 (1978).
2. Wagener, M., Murty, B. S., and Gunther, B. Preparation of metal Nano suspensions by high-pressure DC-sputtering on running liquids. In Komarnenl, S., Parker, J. C., and Wollenberger, H. J. (Editors), *Nano crystalline and Nano composite Materials II*, volume 457, 149–154. Materials Research Society, Pittsburgh PA (1997).
- 3 Eastman, J. A., Choi, U. S., Li, S., Thompson, L. J., and Lee, S. Enhanced thermal conductivity through the development of Nano-fluids. Volume 457 of *Materials Research Society Symposium - Proceedings*, 3–11. Materials Research Society, Pittsburgh, PA, USA, Boston, MA, USA (1997).
- 4 Zhu, H., Lin, Y., and Yin, Y. A novel one-step chemical method for preparation of copper Nano-fluids. *Journal of Colloid and Interface Science*, 227, 100–103 (2004).
5. Lo, C.-H., Tsung, T.-T., and Chen, L.-C. Shape-controlled synthesis of Cu-based Nano fluid using submerged arc Nanoparticle synthesis system (SANSS). *Journal of Crystal Growth*, 277, no. 1-4, 636–642 (2005).



6. Lo, C.-H., Tsung, T.-T., and Chen, L.-C. Ni Nano-magnetic fluid prepared by submerged arc Nano synthesis system (SANSS). *JSME International Journal, Series B: Fluids and Thermal Engineering*, 48, no. 4, 750–755 (2006).
7. Murshed, S. M. S., Leong, K. C., and Yang, C. Enhanced thermal conductivity of TiO₂ - Water based Nano-fluids. *International Journal of Thermal Sciences*, 44, no. 4, 367–373 (2005).
8. Srdic, V., Winterer, M., Moller, A., Mieke, G., and Hahn, H. Nano crystalline Zirconia surface-doped with alumina: chemical vapour synthesis, characterization, and properties. *Journal of the American Ceramic Society*, 84, 2771–2776 (2001).
9. Cao, H., Qian, X., Gong, Q., Du, W., Ma, X., and Zhu, Z. Shape- and size-controlled synthesis of Nanometre ZnO from a simple solution route at room temperature. *Nanotechnology*, 17, 3632–3636 (2006).
10. Xuan, Y. and Li, Q. Heat transfer enhancement of Nano-fluids. *International Journal of Heat and Fluid Transfer*, 21, 58–64 (2000).
11. Hwang, Y. J., Ahn, Y. C., Shin, H. S., Lee, C. G., Kim, G. T., Park, H. S., and Lee, J. K. Investigation on characteristics of thermal conductivity enhancement of Nano-fluids. *Current Applied Physics*, 6, no. 6, 1068–1071 (2005).
12. P. Keblinski, J.A. Eastman, D.G. Cahill, Nano-fluids for thermal transport, *Mater. Today* 8 (6)
13. Y. Ding, H. Chen, L. Wang, et al., Heat transfer intensification using Nano-fluids, *KONA* 25 (2007)
14. W. Yu, S.U.S. Choi, The role of interfacial layers in the enhanced thermal of Nano-fluids: a renovated Maxwell model, *J. Nano part. Res.* 5 (1–2) (2003)167–171
15. W. Yu, S.U.S. Choi, The role of interfacial layers in the enhanced thermal conductivity of Nano-fluids: a renovated Hamilton-Crosser model, *J. Nanopart.Res.* 6 (4) (2004) 355–361.
16. X.Q. Wang, A.S. Mujumdar, A review on Nano-fluids– Part I: theoretical and numerical investigations, *Braz. J. Chem. Eng.* 25 (2008) 613–630.
17. R. Prasher, W. Evans, P. Meakin, J. Fish, P. Phelan, P. Keblinski, Effect of aggregation on thermal conduction in colloidal Nano-fluids, *Appl. Phys.Lett.* 89 (2006) 1431–1438.
18. P. Keblinski, Nano-fluids for enhanced thermal transport: understanding and controversy, In: *Symposium II Nano scale Heat Transport – From Fundamentals to Devices*, Materials Research Society Spring Symposium. San Francisco, USA, 2007pp. 10–13
19. S. Kakac, A. Pramuanjaroenkij, Single-phase and two-phase treatments of convective heat transfer enhancement with Nano-fluids– a state-of-the-art review, *Int. J. Thermal. Sci.* 100 (2016) 75–97.
20. Hamilton, R. L., and Crosser, O. K., “Thermal Conductivity of Hetero-geneous Two-Component Systems,” *Industrial and Engineering Chemistry Fundamentals Vol. 1, No. 3, 1962*, pp. 187–19
21. J.A. Eastman, U.S. Choi, S. Li, L.J. Thompson, S. Lee, Enhanced thermal conductivity through the development of Nano-fluids, *MRS Proc.* 457 (1996)3–11.
22. X. Wang, X. Xu, S.U.S. Choi, Thermal conductivity of Nanoparticle–fluid mixture, *J. Thermo physics. Heat Transfer* 13 (4) (1999) 474–480. Y. Xuan, Q. Li, Heat transfer enhancement of Nano-fluids, *Int. J. Heat Fluid Flow* 21 (2000) 58–64.
23. S.U.S. Choi, Z.G. Zhang, W. Yu, F.E. Lockwood, E.A. Grulke, Anomalous thermal conductivity enhancement in Nanotube suspensions, *Appl. Phys. Lett.* 79 (14) (2001) 2252–2254.
24. J.A. Eastman, S.U.S. Choi, S. Li, W. Yu, L.J. Thompson, Anomalous increased effective thermal conductivities of ethylene glycol-based Nano-fluids containing copper Nano-particles, *Appl. Phys. Lett.* 78 (6) (2001) 718–720.
25. H.Xie, J. Wang, T. Xi, Y. Liu, Thermal conductivity of suspensions containing Nano sized SiC particles, *Int. J. Thermo physics.* 23 (2002) 571–580.
26. S.K. Das, N. Putra, P. Thiesen, W. Roetzel, Temperature dependence of thermal conductivity enhancement for Nano-fluids, *J. Heat Transfer* 125 (2003) 567–574.
27. Lee, S. and Choi, S. U. S. Application of metallic Nanoparticle suspensions in advanced cooling systems. In 1996 *International Mechanical Engineering Congress and Exhibition*. Atlanta, USA (1996).
28. Xuan, Y. and Li, Q. Investigation on convective heat transfer and flow features of Nano-fluids. *Journal of Heat Transfer*, 125, 151–155 (2003).
29. Wen, D. and Ding, Y. Experimental investigation into convective heat transfer of Nano-fluids at the entrance region under laminar flow conditions. *International Journal of Heat and Mass Transfer*, 47, no. 24, 5181 (2004b)
30. Xuan .Y, Li Q. “Investigation on Convective Heat Transfer and Flow Features of Nano-fluids” *ASME Journal of Heat Transfer*, 125(2003), pp. 151-155.
31. Li Q., Xuan .Y, “Convective Heat Transfer and Flow Characteristics of Cu- Water Nano fluid”, *Science in China (series E)*, 45 (2005), 4, pp. 408
32. B.C. Pak, Y.I. Cho, Hydrodynamic and heat transfer study of dispersed fluids with submicron metallic oxide particles, *Exp. Heat Transf.: J. Therm. Energy Generation, Transport, Storage, and Convers.* 11 (2) (1998) 151–170.
33. C.J. Ho, W.K. Liu, Y.S. Chang, C.C. Lin, Natural convection heat transfer of alumina-water Nano fluid in vertical square enclosures: an experimental study, *Int. J. Therm. Sci.* 49 (2010) 1345–1353.
34. H. O’Hanley, J. Buongiorno, T. McKrell, L.W. Hu, Measurement and model validation of Nano fluid specific heat capacity with differential scanning calorimetry, *Adv. Mech. Eng.* 2012 (181079) (2012) 1–6.
35. S. Kakac, A. Pramuanjaroenkij, Review of convective heat transfer enhancement with Nano-fluids, *Int. J. Heat Mass Transf.* 52 (2009) 3187–3196.
36. J. Buongiorno, Convective transport in Nano-fluids, *ASME J. Heat Transfer.* 128 (3) (2006) 240–250.



MATRUSRI ENGINEERING COLLEGE

(Approved by AICTE, Affiliated to Osmania University)

#16-1-486, Saidabad, Hyderabad - 500059



Sponsored by

MATRUSRI EDUCATION SOCIETY



ISBN: 97881-936274-0-2



1ST NATIONAL CONFERENCE ON TRENDS IN SCIENCE, ENGINEERING AND TECHNOLOGY

(NTSET - 2018)

February 2nd & 3rd - 2018

TECHNICAL PAPER ABSTRACTS



ORGANIZED BY

MATRUSRI ENGINEERING COLLEGE

(Approved by AICTE, Affiliated to Osmania University)

#16-1-486, Saidabad, Hyderabad - 500059



Sponsored by

MATRUSRI EDUCATION SOCIETY

ISBN: 97881-936274-0-2



NTSET 2018





EXTRACTION OF LIQUID HYDROCARBON FUEL FROM WASTE PLASTIC

Aditya Machiraju, V. Harinath, A. Kalyan Charan

*Assistant Professor, Assistant Professor, Assistant Professor.
Department of Mechanical Engineering,
Matrusri Engineering College, Hyderabad, India.*

Abstract: This Paper deals with the conversion of Plastic Wastes into alternative fuels. Waste Plastic from municipal solid waste were collected and were sorted based on their types like PET bottles, Polypropylene, Polystyrene, HDPE and LDPE. These Plastic wastes are graded and shredded and then heated in a closed chamber (Similar to a process called Pyrolysis) to attain temperatures up to 150-200^oC. The Plastic waste is melted and gases produced at this temperature are condensed to liquid state. Both, Condensed and Uncondensed gases can be used as fuel to engines. The Fuel produced is tested for Viscosity and Calorific Value, and is compared with Gasoline and Diesel Fuel and the results Obtained are tabulated.

Index Terms— Plastic wastes, Alternative Fuel, Polystyrene, Pyrolysis, Thermal Cracking and Calorific Value.

I. INTRODUCTION

Use of Plastics is increasing Day by Day and the disposal of waste generated from plastics has been a major concern. Plastics are processed from Crude Oil. The objective is to reverse the process and from flammable fuel from Plastic waste. Besides helping in removal of Tons of waste plastic, which makes a Tidy environment, the Pyrolysis of waste plastics also helps in generating an alternate fuel, a convenient from of fuel to replace Diesel or Gasoline. With the alarming levels of increase in consumption of Petrol, Diesel which are not only non-replenishable but also are the source for major hazardous pollutants that damage the environment, Innovation and search for Alternative fuels falls in its natural order and this Liquid Hydrocarbon obtained from waste plastics might as well save the day and meets the growing demand for Alternative fuels. This however requires a separate and well-planned set of Equipment that can serve the purpose and simultaneously present itself to be pocket-friendly.

The following are the requirements for a successful extraction of Liquid fuel from waste plastics:

- 1) Collection, Storage and shredding of Plastics
- 2) Develop/ Fabricate a Pyrolysis unit
- 3) Conduct different experiments to find the Thermo-Physical properties of the obtained liquid fuel.






II. METHODS AND PROCEDURES

In most of the situations, plastic waste recycling could also be economically viable, as it generates resources, which are in high demand. Plastic waste recycling also has a great potential for resource conservation and GHG emissions reduction, such as producing diesel fuel from plastic waste.

For many years, various methods are tried and tested for processing of waste plastic. The plastic materials are recycled and low value products are prepared. Plastic materials which cannot be recycled are usually dumped into undesirable landfill. Worldwide almost 20% of the waste stream is plastic, most of which still ends up in landfill or at worst it is incinerated.

This is a terrible waste of a valuable resource containing a high level of latent energy. In recent year this practice has become less and less desirable due to opposition from Government and environmentally conscious community groups. The value of plastics going to landfill is showing a marginal reduction despite extensive community awareness and education programs. Research Centre for Fuel Generation (RCFG) has conducted successful 300 successful pilot trials and commercial trials for conversion of waste plastic materials into high grade industrial fuel. The system uses liquefaction, Pyrolysis and the catalytic breakdown of plastic materials and conversion into industrial fuel and gases. The system can handle the majority of plastic materials that are currently being sent to landfill or which have a low recycle value. Catalytic conversion of waste plastic into high value product is a superior method of reusing this valuable resource.

The following table lists the types of Plastics that can be successfully used for Plastic Waste Recycling.

Symbol	Acronym	Full name and uses
	PET	Polyethylene terephthalate - Fizzy drink bottles and frozen ready meal packages.
	HDPE	High-density polyethylene - Milk and washing-up liquid bottles
	PVC	Polyvinyl chloride - Food trays, cling film, bottles for squash, mineral water and shampoo.
	LDPE	Low density polyethylene - Carrier bags and bin liners.
	PP	Polypropylene - Margarine tubs, microwaveable meal trays.
	PS	Polystyrene - Yoghurt pots, foam meat or fish trays, hamburger boxes and egg cartons, vending cups, plastic cutlery, protective packaging for electronic goods and toys.
	Other	Any other plastics that do not fall into any of the above categories. For example melamine, often used in plastic plates and cups.

“Table 2.1 – Classifications of Plastics:”

The following figure shows a typical Plastic-Landfill

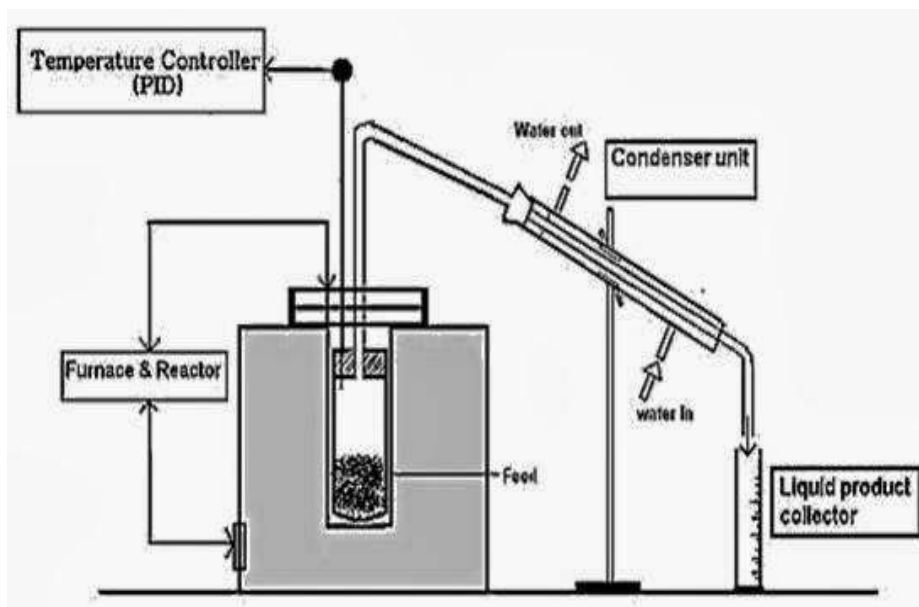


“Fig 2.1-Typical Plastic Landfill”

This is a terrible waste of a valuable resource containing a high level of latent energy. In recent year this practice has become less and less desirable due to opposition from Government and environmentally conscious community groups. The value of plastics going to landfill is showing a marginal reduction despite extensive community awareness and education programs. Research Centre for Fuel Generation (RCFG) has conducted successful 300 successful pilot trials and commercial trials for conversion of waste plastic materials into high grade industrial fuel. The system uses liquefaction, Pyrolysis and the catalytic breakdown of plastic materials and conversion into industrial fuel and gases. The system can handle the majority of plastic materials that are currently being sent to landfill or which have a low recycle value. Catalytic conversion of waste plastic into high value product is a superior method of reusing this valuable resource.

II.1 PYROLYSIS

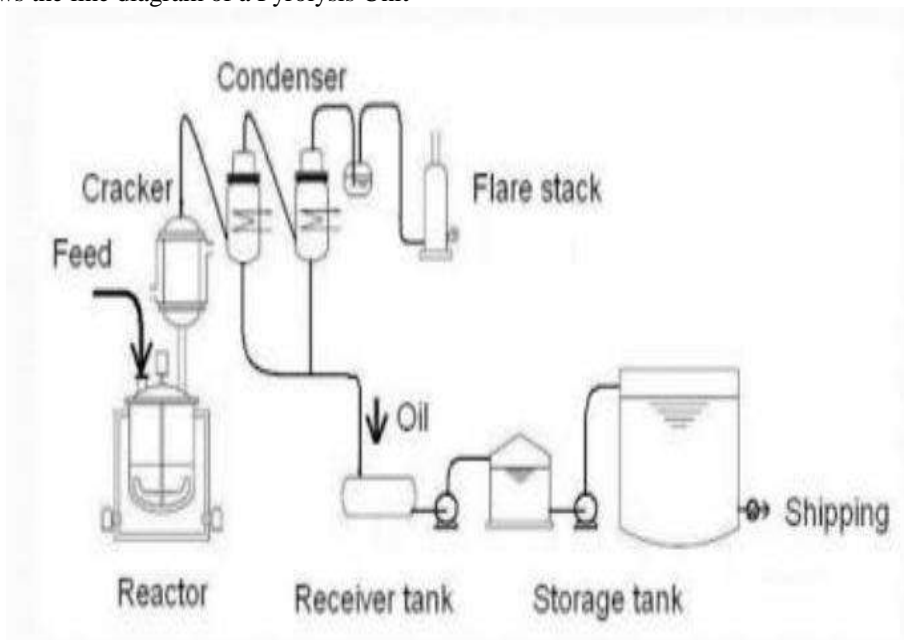
Pyrolysis is a process of thermal degradation in the absence of oxygen. Plastic & Rubber waste is continuously treated in a cylindrical chamber and the pyrolytic gases are condensed in a specially-designed condenser system. This yields a hydrocarbon distillate comprising straight and branched chain aliphatic, cyclic aliphatic and aromatic hydrocarbons. The resulting mixture is essentially the equivalent to petroleum distillate. The plastic / Rubber is pyrolyzed at 350-450^oC and the Pyrolysis gases are condensed in a series of condensers to give a low sulphur content distillate. Pyrolysis is a very promising and reliable technology for the chemical recycling of plastic wastes. Countries like UK, USA, and Germany etc have successfully implemented this technology and commercial production of monomers using Pyrolysis has already begun there.



“Fig 2.2- Schematic Diagram of Pyrolysis Unit”

Pyrolysis offers a great hope in generating fuel oils, which are heavily priced now. This reduces the economical burden on developing countries. The capital cost required to invest on Pyrolysis plant is low compared to other technologies. So, this technology may be an initiative to solve fuel crisis and the problems due to disposal of plastics.

The figure below shows the line diagram of a Pyrolysis Unit



“Fig 2.3 Line Diagram of a Pyrolysis Unit”



II.II PYROLYSIS PROCESS

Under controlled reaction conditions, plastics materials undergo random polymerization and are converted into three products:

- Coke.
- Combination of Gasoline, Kerosene, Diesel & Lube Oil
- LPG range gases.

The process consists of two steps:

- Random de-polymerization of Waste Plastics
- Fractional Distillation-Separation of various liquid fuels by virtue of the difference in their boiling points.

One important factor of the quality of the liquid fuel is that the sulphur content is less than 0.002 ppm which is much lower than the level found in regular fuel.

II.III ALTERNATIVE METHODS

Unfortunately, recycling plastics has proven difficult. The biggest problem with plastic recycling is that it is difficult to automate the sorting of plastic waste, and so it is labor intensive.

Typically, workers sort the plastic by looking at the resin identification code, though common containers like soda bottles can be sorted from memory. Other recyclable materials, such as metals, are easier to process mechanically. However, new mechanical sorting processes are being utilized to increase plastic recycling capacity and efficiency.

Developments are taking place in the field of active Disassembly, which may result in more consumer product components being re-used or recycled. Recycling certain types of plastics can be unprofitable, as well. For example, polystyrene is rarely recycled because it is usually not cost effective. These un-recycled wastes are typically disposed of in landfills, incinerated or used to produce electricity at waste-to-energy plants.

II.IV EXPERIMENTAL PROCEDURE

200g of weighed plastic granules are fed into the modified pressure cooker. The pressure cooker is modified by attaching a pressure gauge to maintain pressure and a thermocouple is attached to measure temperature.

Heat is provided by using Nichrome coil heater which may be between 150°C-200°C. It is the temperature at which plastic begins to melt and vaporize.

These vapors are passed through copper tubes which are connected to shell and tube heat exchanger. At the end of the heat exchanger, the distillate is collected. The amount of distillate obtained is measured.

The color of the distillate is noted. The time and temperature at which the distillate is obtained is also noted.

This experiment is repeated with different plastics such as LDPE, HDPE, PP, PS, plastic wastes (mainly plastic carry bags, CD case etc.)

The figure below shows the experimental set-up used to obtain the Liquid fuel from plastic waste



“Fig. 2.4- Experimental Setup”



The different polymers that are used as the feed for waste plastics are:

- High Density Polyethylene (HDPE)
- Polypropylene (PP)
- Polystyrene (PS)

The figure below shows Plastic samples used for Pyrolysis



“Fig. 2.5-Samples of Shredded Plastic Waste”

Steps involved in the Experimental Procedure

Feeding: Feed the feedstock's to reactor through feeder and closes the feeder inlet.

Heating: To increase the temperature of reactor, heat the product of reactor inside by using heating source.

Condensing: The plastic get evaporated at high temperature, this vapor is condensed to atmospheric temperature by using straight and spiral tube condensers.

Liquid collection: Out coming product from the condenser is collected at liquid collector. At the end of condenser provide a cyclone separator to separate the plastic liquid fuel and non-condensable gases. These non-condensable gases are reuses to heat the Pyrolysis unit.

III. RESULTS AND DISCUSSIONS

Pyrolysis process of shredded Polystyrene resulted in production of Bio-Oil obtained contained the following constituents by % Volume:

- Pyrolytic oil – 48.6%
- Wax- 40.7
- Pyrogas-10.1%
- Char- 0.6%.

The Operating Temperature during the entire process is 275^oC and was carried out in a modified pressure cooker of capacity 1 Liter (Approx 1.2Kg of Polystyrene by mass) without Catalyst. Use of Catalyst increases the yield of Pyrolytic Oil and Pyrolytic Gases.

The following figure shows Pyrolytic Oil collected after Pyrolysis of Polystyrene.



“Fig 3.1- Sample collected from Pyrolysis of Polystyrene”



III.I TEST FOR CHARACTERIZING OUTPUT

Different tests have been carried out to study and compare the fuel characteristics of different samples and those of petrol and diesel which are used as the standard reference.

The characteristics which are studied are:

CALORIFIC VALUE

INSTRUMENT USED: BOMB CALORIMETER

VALUE OBTAINED = 46,057 kJ/kg



“Fig 3.2 Bomb Calorimeter”

VISCOSITY

INSTRUMENT USED: SAYBOLT VISCOMETER

VALUE OBTAINED: 2.1 Centi-Stokes



“Fig. 3.3 Saybolt Viscometer”

FIRE POINT

INSTRUMENT USED: FIRE POINT APPARATUS

VALUE: FIRE POINT = 41°C.



“Fig3.4 Flash and Fire Point Test Apparatus”

DESINTY



INSTRUMENT USED: GRADUATED BEAKER

VALUE OBTAINED: 691.666 kg/m³



“Fig 3.5 Plastic fuel in a Graduated Beaker”

The Thermo-Physical properties are calculated and found using the mentioned Instruments and the results obtained are tabulated and compared with the conventional fuels like Gasoline and Diesel in Table 3.1

S.No	Properties	Plastic Oil	Gasoline	Diesel
1	Calorific Value(kJ/kg)	46,057	48,000	42,000
2	Density(kg/m3)	691.66	719.7	812
3	Viscosity(Centistokes)	2.1	0.71	3.05
4	Fire Point(^o C)	41	40	74

“Table 3.1- Comparison of Properties of Plastic Oil with conventional fuels”

IV. CONCLUSION

- Pyrolysis method is both Ecological and Economical
- 1Kg of Waste plastics is converted into 75% of useful liquid hydrocarbon fuels without emitting any pollutants.
- It would also take care of hazardous plastic waste and reduce the import of crude oil.
- The properties of produced plastic liquid fuel are almost similar to that of Diesel fuel, hence plastic fuel represents a good alternative fuel for diesel engine and therefore it can be used for diesel engine vehicles.

REFERENCES

- [1] A. Adrados, I. de Marco, B.M. Caballero, A. Lopez, M. F. Laresgoiti, A. Torres: - Pyrolysis of plastic packaging waste: A comparison of plastic residuals from material recovery facilities with simulated plastic waste.2007.
- [2] Achyut K. Panda, R.K. Singh, D.K. Mishra:-Thermolysis of waste plastics to liquid fuel. A suitable method for plastic waste management and manufacture of value added product a world prospective, 2009; 1-6: 10-11.
- [3] Alka Zadagaonkar (et al):- Conversion of waste plastic into liquid fuels. A major breakthrough in the arena of non-conventional sources of energy. Information Brochure and Technical.Write-2009.
- [4] A.G. Buekens, H. Huang: - Catalytic plastics cracking for recovery of gasoline-range Hydrocarbon liquid fuels municipal plastic wastes, Resources, Conservations and Recycling. 1998.
- [5] Bockhorn H (et al.): -Kinetic study on the thermal degradation or thermal pyrolysis of plastic wastes.
- [6] Miskolczia N, Bartha L, Deak G, JoverB:-Thermal degradation of plastic waste for production of fuel like Biodiesel. Polymer degradation and stability 2004. 2004; 84(1):123-7.
- [7] Sorum L (et al):- Pyrolysis characteristics and kinetics of municipal solid wastes. 2001; 80(9): 1217-1227.



MATRUSRI ENGINEERING COLLEGE

(Approved by AICTE, Affiliated to Osmania University)

#16-1-486, Saidabad, Hyderabad - 500059



Sponsored by

MATRUSRI EDUCATION SOCIETY



ISBN: 97881-936274-0-2



1ST NATIONAL CONFERENCE ON TRENDS IN SCIENCE, ENGINEERING AND TECHNOLOGY

(NTSET - 2018)

February 2nd & 3rd - 2018

TECHNICAL PAPER ABSTRACTS



ORGANIZED BY

MATRUSRI ENGINEERING COLLEGE

(Approved by AICTE, Affiliated to Osmania University)

#16-1-486, Saidabad, Hyderabad - 500059



Sponsored by

MATRUSRI EDUCATION SOCIETY

ISBN: 97881-936274-0-2



NTSET 2018



THERMAL ANALYSIS ON RECTANGULAR PLATE FIN WITH PERFORATIONS USING ANSYS

¹A.Kalyan Charan, ²G.Saikiran Srivastav, ³G.Krishna Teja Bharadwaj, ⁴G. Krishna Bharath,

¹Assistant Professor, ^{2,3,4}Students

¹Department of Mechanical Engineering

¹Matrusri Engineering College, Saidabad, Hyderabad, India

Email: ¹agirkalyan.mech@gmail.com, ²saikiranrivatsav005@gmail.com

Abstract: In this paper, analysis is carried on extended surfaces, which are commonly used to enhance convection heat transfer in a wide range of engineering applications. The conception of introducing perforations on the lateral surface of fin is to enhance heat transfer rate effectively. This analysis helps in deciding the optimal geometry and configuration of perforations on the surface of the fin. Finely perforated aluminum ($k=210\text{W/mK}$), copper ($k=410\text{W/mK}$) fins are selected for investigation because both has higher thermal conductivities and are predominantly used in heat transfer applications.

Key words: heat transfer, heat transfer coefficient, temperature, fins, and perforations.

1. Introduction:

There are numerous situations where heat is to be transferred between a fluid and a surface. In such cases, the heat flow depends on three factors namely [1] (i) area of the surface (ii) Temperature difference and (iii) the convective heat transfer coefficient.

The base surface area is limited by design of the system. The temperature difference depends on the process and cannot be altered. The only choice appears to be the convection heat transfer coefficient and this cannot be increased beyond a certain value. Any such increase will be at the expense of power for fans or pumps. Thus, the possible option is to increase the base area by the so-called extended surfaces or fins. Several shapes of fins are in use. These are (i) Plate fins of constant sectional area (ii) Plate fins of variable sectional area (iii) Annular or circumferential fins constant thickness (iv) Annular fins of variable thickness (v) Pin fins of constant sectional area and (vi) Pin fins of variable sectional area.

Fins are found more valuable when the convective heat transfer coefficient is low. The main aim is to design fins to optimize the heat transfer. For this purpose, it will be desirable that the use of materials of high thermal conductivity like copper or aluminum.

2. Present work:

The present simulation analysis investigates the heat transfer enhancement on rectangular lamina using two different materials copper and aluminum without perforations, with different perforation shapes on the above-mentioned two materials by keeping at constant Reynolds number and Power Input. Selecting one optimum perforation shape, material among the different perforation shapes after the analysis.

3. Experimental setup:

Figure 1 shows the schematic diagram of the experimental setup. It consists of a rectangular channel made up of metal sheet material. For experimentation different types of perforated fins are used which compared with the solid fins. Different types of perforated fins along with different materials are given in Table 1. Fins are heated uniformly at its base. A fan is used to produce airflow over the fins. The arrangement of fan and direction of airflow is as shown in Figure; thermocouples are used for the measurement of temperature of air at the inlet and outlet of channel. Mass flow rate of air is controlled by controlling the speed of fan. Mass flow rate is measured with the help of anemometer.

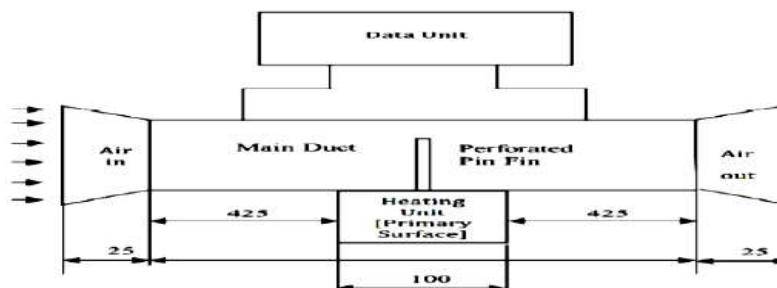


Figure 1: Pin Fin Apparatus

4. RESULTS AND DISCUSSIONS:

4.1 Input parameters:

- Ambient temperature 295 Kelvin
- Root temperature 773 Kelvin
- $H = 20 \text{ W/m}^2\text{K}$
- Materials used: Aluminum, Copper
- Time is equal to 500 seconds
- Common shear area is equal to 400 square mm
- Is equal to 150 mm
- Width is equal to 50 mm
- Thickness is equal to 5 mm

4.2 Output observations:

- Value of h
- Percentage increase of h over a blank fin
- Temperature

4.3 Formula correlations:

$$\frac{T_x - T_a}{T_o - T_a} = \frac{\cosh m(L - x)}{\cosh mL}$$

$$Re = \frac{\rho V L_c}{\vartheta}$$

$$Nu = 0.615 \times Re^{0.466} \quad \text{For } 40 < Re < 4000$$

$$Nu = \frac{h \times L_c}{K_{air}}$$

$$Q = \sqrt{h \times p \times K \times A} (\Delta T) \tanh mL$$

$$\eta = \frac{\tanh mL}{mL} \quad \phi_{fin} = \tanh mL \sqrt{\frac{p \times h}{K \times A}}$$

Where m is given by, $m = \sqrt{\frac{h \times p}{K \times A}}$

Where, h is the convective heat transfer coefficient,
P is the perimeter
K is the Thermal conductivity of the material,
A is the cross sectional area of the fin

Where, ρ = density of air,
 L_c = Characteristic length of the fin,
V = velocity of air,
 ϑ = Kinematic viscosity

$$Nu = 0.174 \times Re^{0.618} \quad \text{For } 4000 < Re < 40000$$

K_{air} = Thermal conductivity of air

T_x = Temperature at distance x from the root

T_a = Ambient temperature

T_o = Temperature at the root

L = Total length of the fin

4.4 Rectangular Lamina with Lateral Perforations:

The purpose of this analysis is to know the effects of lateral perforation [2] shapes on the thermal performance of fins in comparison with the solid fins. The rectangular lamina with different types of lateral perforations as shown in

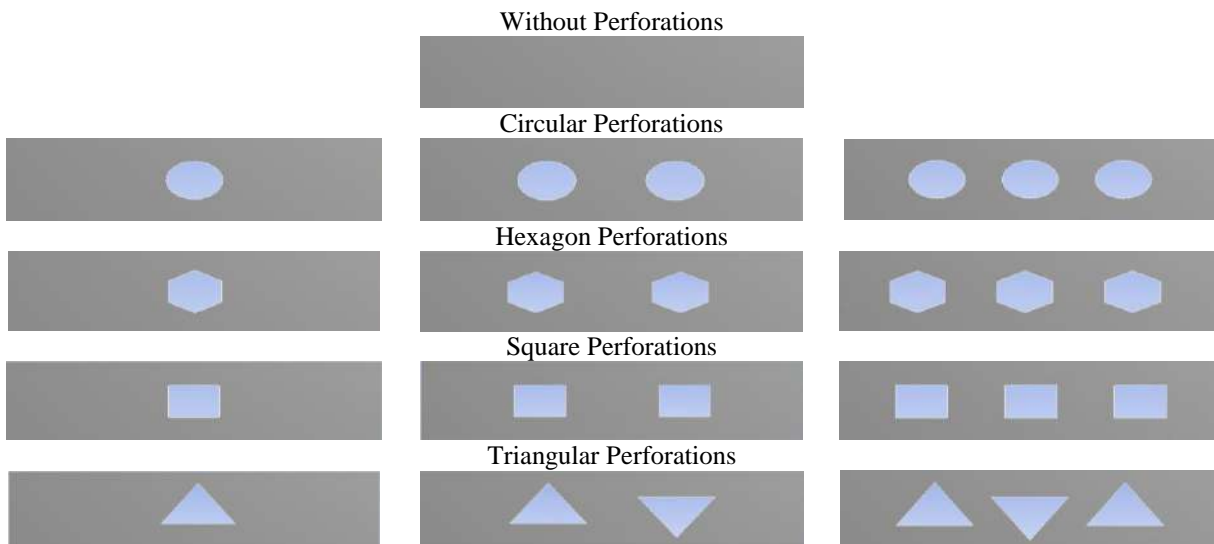


Figure 2: Rectangular Lamina with Lateral Perforations



Table 1: Rectangular Lamina with different types of Lateral Perforations

S.No	Material	With / Without Perforations	No of Perforations		
1	Aluminum	Without Perforations	0		
2	Aluminum	With Circular Perforations	1	2	3
3	Aluminum	With Square Perforations	1	2	3
4	Aluminum	With Hexagon Perforations	1	2	3
5	Aluminum	With Triangular Perforations	1	2	3
6	Copper	Without Perforations	0		
7	Copper	With Circular Perforations	1	2	3
8	Copper	With Square Perforations	1	2	3
9	Copper	With Hexagon Perforations	1	2	3
10	Copper	With Triangular Perforations	1	2	3

4.5 Analysis using ANSYS Software:

The purpose of this analysis is to know the effects of lateral perforation shapes on thermal performance when compared with the regular solid fins. In the present work first we perform analysis on non-perforated fin and then fins perforated by different shapes such as circle, square, hexagon and triangular but all these perforations have the same cross sectional area.

4.5.1 Non-Perforated:

A rectangular lamina of dimensions 150X50X5 mm is considered for the analysis with two materials viz., copper, aluminium as the reference and the following table gives the tip temperature, Convective Heat-Transfer Co-efficient.

Table 2: Non-perforated Rectangular Lamina with different materials

Temperature	Mat.\Type	Tip Temp	'h'(heat transfer coefficient) W/m ² K
Root 773 K	Aluminum	620 K	16.21
	Copper	671 K	17.64

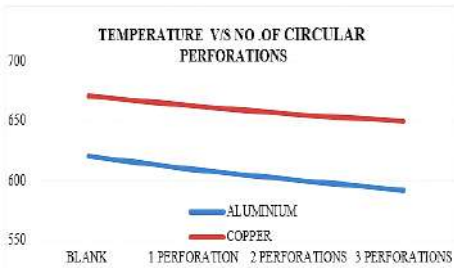
4.5.2 Perforated:

4.5.2.1 Circular Perforations:

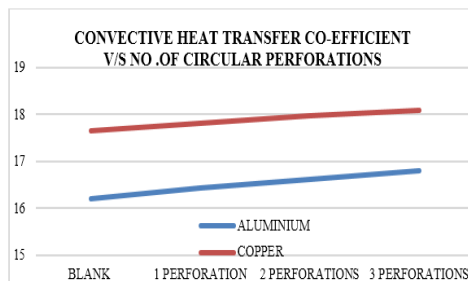
Circular perforations [3] with the shear area of 400mm² and increasing the perforations from 1 to 3 following is the data obtained from the ANSYS simulation. Plots of temperature v/s no. of perforations and Convective Heat-Transfer Co-efficient V/S No. of Circular Perforations, and Percentage increase of h over blank surface v/s no. of perforations.

Table 3: Circular -perforated Rectangular Lamina varying perforations with different materials

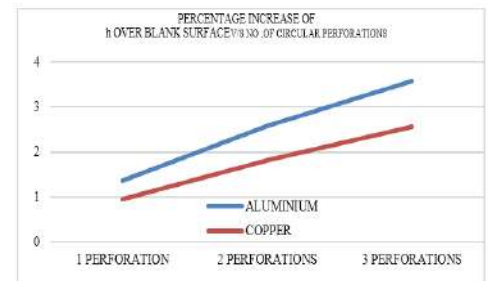
Temperature	Mat.\Type	No. Perforations	Tip Temp	'h'(heat transfer coefficient) W/m ² K	Percentage increase of 'h' over blank surface
Root 773 K	Aluminum	1	609.23 K	16.43	1.36
		2	599.77 K	16.62	2.59
		3	592.23 K	16.79	3.58
	Copper	1	663.07 K	17.81	0.94
		2	655.72 K	17.96	1.82
		3	649.66 K	18.09	2.56



Graph 1: Temperature V/S No. of Circular Perforations



Graph 2: Convective Heat-Transfer Co-efficient V/S No. of Circular Perforations



Graph 3: Percentage increase of 'h' over blank surface V/S No. of Circular Perforations



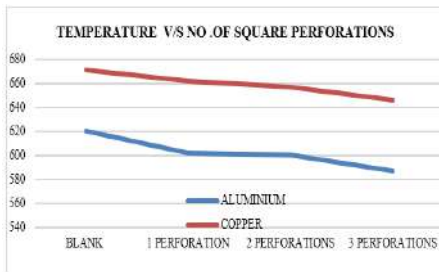
- From graph 1 it can be observed that aluminum has the lowest tip temperature with three perforations in it.
- From the graph 2 it can be noted that though initial copper has maximum ‘h’ value for three perforations, Aluminum has reached the close value of ‘h’ at third perforation.
- From the graph 3 it can be noted that aluminum has maximum percentage increase of ‘h’ over the blank fin for three perforated Aluminum.
- For circular perforation: Considering both temperature and ‘h’ it is better to select aluminum with three circular perforations in it.

4.5.2.2 Square Perforations:

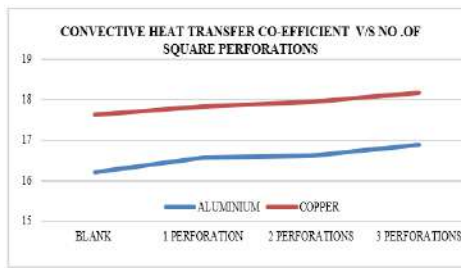
Square perforations [4, 5] with the shear area of 400 mm² and increasing the perforations from 1 to 3 following are the data obtained from the ANSYS simulation. Plots of Temperature V/S No. of Perforations and Convective Heat-Transfer Co-efficient V/S No. of Circular Perforations

Table 4: Square -perforated Rectangular Lamina varying perforations with different materials

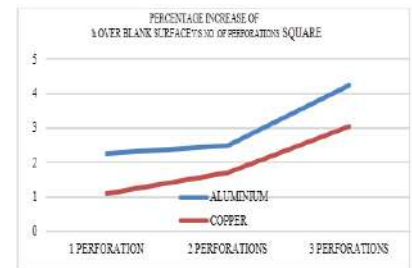
Temperature	Mat.\Type	No. Perforations	Tip Temp	‘h’(heat transfer coefficient) W/m ² K	Percentage increase of ‘h’ over blank surface
Root 773 K	Aluminum	1	602.30 K	16.57	2.25
		2	600.44 K	16.61	2.50
		3	587.39 K	16.89	4.23
	Copper	1	661.75 K	17.83	1.10
		2	656.71 K	17.94	1.70
		3	645.81 K	18.18	3.04



Graph 4: Temperature V/S No. of Square Perforations



Graph 5: Convective Heat-Transfer Co-efficient V/S No. of Square Perforations



Graph 6 : Percentage increase of ‘h’ over blank surface V/S No. of Square Perforations

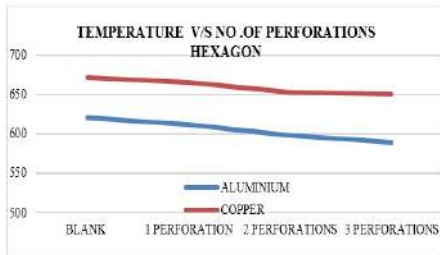
- From graph 4 it can be observed that aluminum has the lowest tip temperature with three perforations in it.
- From the graph 5 it can be noted that though initial copper has maximum ‘h’ value for three perforations, Aluminum has reached the close value of ‘h’ at third perforation.
- From the graph 6 it can be noted that aluminum has maximum percentage increase of ‘h’ over the blank fin for three perforated Aluminum.
- For Square perforation: Considering both temperature and ‘h’ it is better to select aluminum with three square perforations in it.

4.5.2.3 Hexagon Perforations:

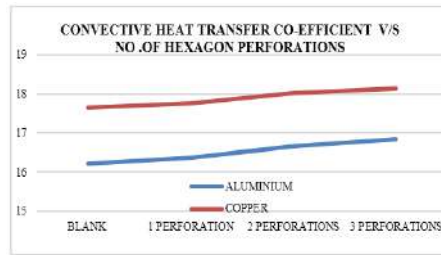
Hexagon perforations [3] with the shear area of 400 mm² and increasing the perforations from 1 to 3 following are the data obtained from the ANSYS simulation. Plots of Temperature V/S No. of Perforations and Convective Heat-Transfer Co-efficient V/S No. of Hexagon Perforations

Table 5: Hexagon -perforated Rectangular Lamina varying perforations with different materials

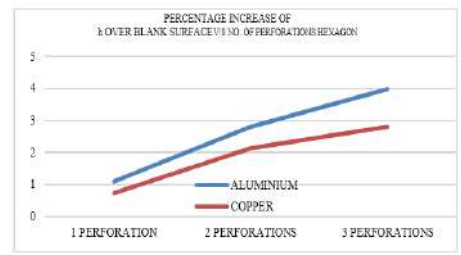
Temperature	Mat.\Type	No. Perforations	Tip Temp	‘h’(heat transfer coefficient) W/m ² K	Percentage increase of ‘h’ over blank surface
Root 773 K	Aluminum	1	611.21 K	16.38	1.11
		2	598.12 K	16.66	2.80
		3	589.09 K	16.85	4.00
	Copper	1	664.69 K	17.77	0.74
		2	653.12 K	18.02	2.14
		3	647.68 K	18.14	2.81



Graph 7: Temperature V/S No. of Hexagon Perforations



Graph 8: Convective Heat-Transfer Co-efficient V/S No. of Hexagon Perforations



Graph 9: Percentage increase of 'h' over blank surface V/S No. of Hexagon Perforations

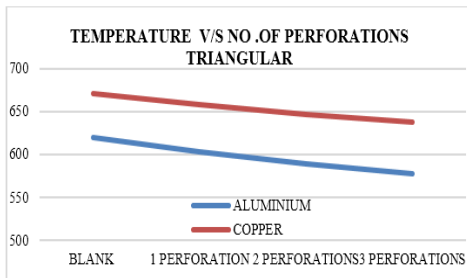
- From graph 7 it can be observed that aluminum has the lowest tip temperature with three perforations in it.
- From the graph 8 it can be noted that though initial copper has maximum 'h' value for three perforations, Aluminum has reached the close value of 'h' at third perforation.
- From the graph 9 it can be noted that aluminum has maximum percentage increase of 'h' over the blank fin for three perforated Aluminum.
- For Hexagon perforation: Considering both temperature and 'h' it is better to select aluminum with three hexagon perforations in it.

4.5.2.3 Triangular Perforations:

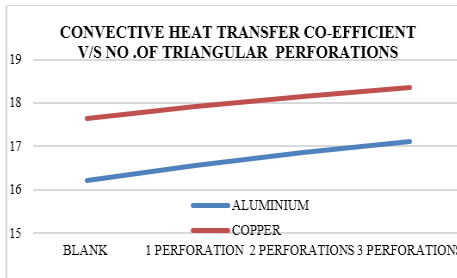
Triangular perforations [6] with the shear area of 400 mm² and increasing the perforations from 1 to 3 following are the data obtained from the ANSYS simulation. Plots of Temperature V/S No. of Perforations and Convective Heat-Transfer Co-efficient V/S No. of triangular Perforations

Table 5: Triangular -perforated Rectangular Lamina varying perforations with different materials

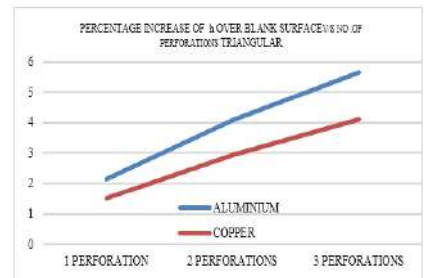
Temperature	Mat.\Type	No. Perforations	Tip Temp	'h'(heat transfer coefficient) W/m ² K	Percentage increase of 'h' over blank surface
Root 773 K	Aluminum	1	603.00 K	16.56	2.16
		2	588.62 K	16.86	4.07
		3	577.06 K	17.12	5.65
	Copper	1	658.18 K	17.91	1.52
		2	646.77 K	18.16	2.92
		3	637.35 K	18.36	4.10



Graph 10: Temperature V/S No. of Triangular Perforations



Graph 11: Convective Heat-Transfer Co-efficient V/S No. of Triangular Perforations



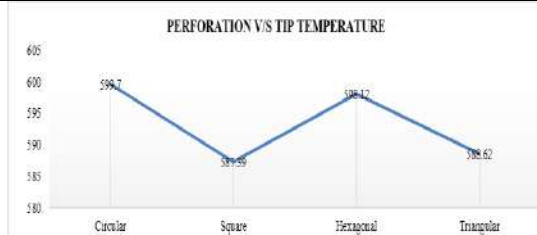
Graph 12: Percentage increase of 'h' over blank surface V/S No. of Triangular Perforations

- From graph 10 it can be observed that aluminum has the lowest tip temperature with three perforations in it.
- From the graph 11 it can be noted that though initial copper has maximum 'h' value for three perforations, Aluminum has reached the close value of 'h' at third perforation.
- From the graph 12 it can be noted that aluminum has maximum percentage increase of 'h' over the blank fin for three perforated Aluminum.
- For Triangular perforation: Considering both temperature and 'h' it is better to select aluminum with three triangular perforations in it.

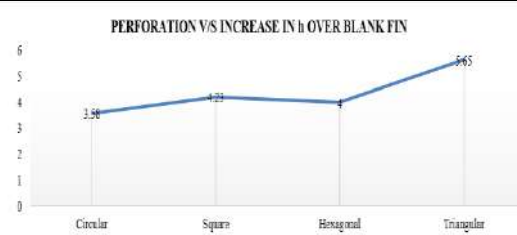


Table 6: Different Perforations of Aluminum Rectangular Lamina

Material	Perforation type	Root temperature	No. of perforations	Temperature	Increase of 'h' over blank fin
Aluminum	Circular	773K	3	599.7K	3.58
Aluminum	Square	773K	3	587.39K	4.23
Aluminum	Hexagonal	773K	3	598.12K	4
Aluminum	Triangular	773K	3	588.62K	5.65



Graph 13: Perforation V/S Tip Temperature.



Graph 14: Perforation V/S Increase in 'h' over blank fin.

5. CONCLUSION:

In circular perforation when we consider both temperature and 'h' it is better to select aluminum with three circular perforations in it when compared with copper. In Square perforation when we consider both temperature and 'h' it is better to select aluminum with three square perforations in it when compared with copper. In Hexagon perforation when we consider both temperature and 'h' it is better to select aluminum with three hexagon perforations in it when compared with copper. In Triangular, perforation when we consider both temperature and 'h' it is better to select aluminum with three triangular perforations in it when compared with copper. From the above research, it is evident that tip temperature is minimum for aluminum triangularly perforated with three perforations in it and h increase is maximum for triangularly perforated with three perforations of aluminum material. From the above research, we can say that convective heat transfer coefficient increases for perforated fin when compared with non-perforated fin. From the above research, we can say that Nusselt's numbers increases for perforated fin when compared with non-perforated fin. Therefore, a three triangle laterally perforated aluminum is most suitable for the fin applications.

REFERENCES:

- [1] Md. Farhad Ismail, Muhammad Noman Hasan, Suvash C. Sahac, "Numerical study of turbulent fluid flow and heat transfer in lateral perforated extended surfaces". Elsevier.
- [2] Raaid R. Jassem, "Effect the Form of Perforation on the Heat Transfer in the Perforated Fins", Academic Research International, ISSN-L: 2223-9553, ISSN: 2223-9944 Vol. 4 No. 3 May 2013.
- [3] Isam H. E. Qasem and Abdullah H. M. AlEssa, "One Dimensional Finite Element Analysis of Heat Dissipation from Rectangular Fin with Longitudinal Hexagonal Perforations", RRJET | Volume 4 | Issue 2 | April-June 2015.
- [4] H. M. AlEssa "Augmentation of Fin Natural Convection Heat Dissipation by Square Perforations", Journal of Mechanical Engineering and Automation 2012, 2(2): 1-5 DOI: 10.5923/j.jmea.20120202.01
- [5] Kavita H. Dhanawade, Vivek K. Sunnapwa and Hanamant S. Dhanawade, "Thermal Analysis of Square and Circular Perforated Fin Arrays by Forced Convection", International Journal of Current Engineering and Technology E-ISSN 2277 – 4106, P-ISSN 2347 – 5161
- [6] Abdullah H. AlEssa and Mohammed Q. Al-Odat, "Enhancement of Natural Convection Heat Transfer from A Fin by Triangular Perforations of Bases Parallel and Toward Its Base", the Arabian Journal for Science and Engineering, Volume 34, October 2009.



MATRUSRI ENGINEERING COLLEGE

(Approved by AICTE, Affiliated to Osmania University)

#16-1-486, Saidabad, Hyderabad - 500059



Sponsored by

MATRUSRI EDUCATION SOCIETY



ISBN: 97881-936274-0-2



1ST NATIONAL CONFERENCE ON TRENDS IN SCIENCE, ENGINEERING AND TECHNOLOGY

(NTSET - 2018)

February 2nd & 3rd - 2018

TECHNICAL PAPER ABSTRACTS



ORGANIZED BY

MATRUSRI ENGINEERING COLLEGE

(Approved by AICTE, Affiliated to Osmania University)

#16-1-486, Saidabad, Hyderabad - 500059



Sponsored by

MATRUSRI EDUCATION SOCIETY

ISBN: 97881-936274-0-2



NTSET 2018



REVIEW PAPER ON FRICTION STIR WELDING OF VARIOUS MATERIALS AND ALUMINIUM MATRIX COMPOSITES.

¹P.Naveen Kishore, ²Dr.D.Lingaraju

¹Assistant Professor, ²Assistant Professor

Dept of Mechanical engineering

Matrusri Engineering College, Saidabad, Hyd.

Abstract:

Objective: The comprehensive body of knowledge that has built up with respect to the friction stir welding (FSW) of aluminum alloys since the technique was invented in 1991 is reviewed on this paper. **Methods/Analysis:** The Friction Stir Welding of aluminum alloys with various other alloys and aluminium matrix composites are reviewed on this paper. The basic principles of FSW are described, followed by process parameters study which affects the weld strength. **Findings:** The microstructure and the likelihood of defects also reviewed. Tensile strength properties attained with different process parameters are discussed. **Conclusion:** It is demonstrated that FSW of aluminum and other material is becoming an emerging technology with numerous commercial applications.

Keywords: Aluminum Alloys, Tool design, Tool Wear, Friction-Stir Welding, Microstructure, Tensile Strength, and AMC.

I. INTRODUCTION

Friction Stir Welding (FSW) was invented at The Welding Institute (TWI) of the United Kingdom (Cambridge) in 1991 as a solid state joining technique and was initially applied to Aluminum Alloys (Dawes C and Thomas W, TWI Bull, 1995; Thomas W M, *et al.*, 1991). Friction Stir Welding is a solid state joining process combining deformation heating and mechanical work to obtain high quality, defect free joints. Friction Stir Welding is especially well suited to joining Aluminum Alloys in a large range of plate thickness and has particular advantages over fusion welding when joining of highly alloyed Aluminum is considered.[1]. The heat input into the material and the resulting welding temperature can be controlled by adapting process parameters like the down-force, rotational speed or welding speed as shown in Fig. 1.1

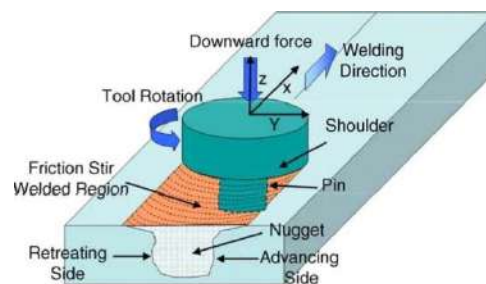


Fig. 1.1 Principle drawing of the FSW process for joints with indication of the main parameters

A method of solid state joining on a work piece offers a tool pin of material harder than the base metal's continuous surface which causes relative cyclic movement between the pin and the base metal. The frictional heat is generated as the pin stirs the work piece so as to create a plasticized region in the metal around the probe, stopping the relative cyclic movement, and allowing the plasticized material to solidify around the probe.[2]



The peak welding temperature can be limited to 80% of the melting temperature of the base metal (BM). Therefore, this process can be considered as a hot working process. As FSW has been widely used to join aluminium alloys, it may be developed as a viable route to join AMCs especially for high strength non-weldable series (AA2xxx, AA6xxx, and AA7xxx), which are susceptible to solidification cracking in the weld zone and liquation cracking in the heat affected zone (HAZ) [14]. Dissimilar joints of AMCs or with different metals can be manufactured by using FSW without concerns for composition compatibility, which is an important consideration in fusion welding to avoid solidification cracking [10].

FSW is an ideal process for producing low cost and high performance joints. The practical approach of FSW is to use a non-consumable rotating tool consisting of two parts including a shoulder and a pin. During FSW the pin is inserted into the faying surface of the plates and then moved horizontally in the direction of the joint line. The surface of the tool has dual actions for heat generation and mechanical sweeping of softened metal. The heat input through the frictional action between the tool and work piece leads to softening of the area around the pin. Meanwhile, the softened materials are swept in the form of severe plastic deformation from the advancing side (AS) to the retreating side (RS) to form a solid state joint. The advancing and retreating sides of the plates to be joined are defined by the direction of tool rotation (clockwise or anti-clockwise) and the traverse movement of the tool. Plate side is defined as advancing if the tool movement is in the same direction of the tool rotation, whilst it is retreating if the tool moves in the opposite direction (see Fig. 1). Different types of joint like butt, lap, and T-joints can be welded successfully by FSW [8, 10, and 15].

Moreover, FSW is considered as a green and environmentally friendly welding technology because of low energy consumption, no gas emission, and no need for consumable material such as electrodes, filler metals, and shielding gases (normally present in fusion welding processes). A survey carried out by the American Welding Society (AWS) in 2002 showed that \$34.4 billion per year is spent on arc welding including the use of consumables, repair, and energy consumption in the USA. The adoption of FSW has increased rapidly and 10% of joining processes have reportedly been replaced by FSW [16].

1.1 Principle of Operation

A non-consumable rotating tool with a specially designed pin and shoulder is inserted into the abutting edges of sheets or plates to be joined and subsequently traversed along the joint line. The FSW tool rotates in the counterclockwise direction and travels into the plunge (or left to right). The advancing side is on the right, where the tool rotation direction is the same as the tool travel direction (opposite the direction of metal flow), and the retreating side is on the left, where the tool rotation is opposite to the tool travel direction (parallel to the direction of metal flow). The tool serves three primary functions, that is, heating of the work piece, movement of material to produce the joint, and containment of the hot metal beneath the tool shoulder [1].

II. SUMMARY

2.1 Overview of MMC

In recent years, MMCs have attracted considerable attention for critical applications in industrial sectors such as spacecraft structures, deck panels, and automotive and railway brake discs. The global demand for MMCs is expected to increase from about 5496 tons to nearly 8000 tons in the period from 2012 to 2019, and it is continuously rising [17]. Light metals like aluminium, magnesium, and titanium alloys are considered as ideal base matrices to produce MMCs reinforced by carbide, nitride, boride, and oxide in the form of particles, whiskers, and fibres [18] [19]. MMCs can possess unique properties including good thermal conductivity, low coefficient of thermal expansion, low specific density, high specific stiffness, good dimensional stability, and excellent strength to weight ratio depending on the type of reinforcements used [20–22].

As a result of these desirable properties, MMCs have been used to withstand excessive environmental condition of substantial changes in temperature. For example, the International Space Station is exposed to varying temperatures from +125 °C to –125 °C as it orbits around the earth [23].

As a versatile material, AMCs may be selected as an alternative to high strength aluminium alloys in aeroengines and aerospace structures like fins, wings, and fuselage. In 2001 NASA used composite aluminium Al–Li 2195 rather than aluminium alloy Al 2219 for the external fuel tank of space shuttles leading to a reduction of weight by 3400 kg. This saving in weight increases the cargo capacity of space shuttles and enables it to transport more than one component in a single flight to the International Space Station [24]. Also, the use B/Al in truss and frame of aero planes saved 45% weight from an all aluminium design. Another application of AMCs is a 3.6 m antenna for Hubble Space Telescope manufactured from Gr/Al (P100/6061 Al). It offers high stiffness, superb electrical conductivity, and low coefficient of thermal expansion [23]. In addition, AMCs have found a wide range of applications in military sector such as armour, due to the combined static strength and high ballistic performance [10]



2.2 Weldability Of Aluminium Alloys And Amc's:

The strength of pure aluminium is inadequate for structural applications. Therefore, to eliminate this limitation it is alloyed with other metals like copper, manganese, magnesium, zinc, and silicon. Different mechanical properties can be achieved by controlling the amount of alloying elements and heat treatments. Aluminium and its alloys are often considered as formable and ductile due to their face-centered cubic crystal structure and are available in wrought and cast forms. The former can be produced, typically, by semi-continuous direct chill casting followed by rolling (hot or cold), extrusion, and forging, whilst the latter can be made from sand casting, lost wax casting, permanent steel mould casting, and die-casting. Wrought aluminium is classified into two types depending on the main alloying elements. Non heat treatable weldable aluminium alloys including AA1xxx, AA3xxx, and AA5xxx series are strengthened by cold working, whereas AA2xxx, AA6xxx and AA7xxx series are heat treatable, non-weldable alloys that can be strengthened by precipitation hardening [25,26].

In general, welding of aluminum and its alloys needs considerable attention. Problems may occur including the loss of strength and defect formation when fusion welding processes are used. Trapped porosity may also appear in the cross section, due to the dissolution of shielding gases (oxygen, nitrogen and hydrogen) or moisture in the electrode and flux in molten metal. Furthermore, lack of fusion occurs in part due to the high melting temperature up to 2060 °C of stable aluminium oxide on the surface. Centre-line or solidification cracking is also a serious problem in fusion welding of aluminium alloys. This failure occurs as a result of stresses induced by metal contraction in cooling and the often large difference between the liquidus temperature and eutectic or final solidification temperature. The variations in heating and cooling cycle in the HAZ normally result in lowered the strength of joint in heat treatable alloys [25, 27].

In addition to the aforementioned problems accompanied by welding of aluminium and its alloys, other difficulties come into view when AMCs are welded by fusion welding processes including:

(a) incomplete mixing between filler and BM, (b) the formation of excess eutectic, (c) the presence of large size porosity of more than 100 µm in the fusion zone, and (d) reaction between molten metal's and reinforcements resulting in undesirable phases such as Al₄C₃ [10]. A study was reported by Storjohann et al. [28] to compare three types of fusion welding (GTA, LBW, and EBW) with heat inputs of 165, 108, and 5.9 J/mm, respectively, with solid state welding (FSW) to fabricate similar AMC joints for AA6061/Al₂O₃/20p (20% volume of Al₂O₃ particles) and AA2124/SiC/20w (20% Volume of SiC whiskers). They found that in all fusion welding processes Al₂O₃ particles completely dissolved in molten aluminium leading to the reduction in the strength of joints. In the case of SiC whiskers, the formation of Al₄C₃ and precipitation of a Si-rich phase occurred as a result of fast reaction between the reinforcement and molten metal. In contrast, a good joint was achieved by FSW and there was no significant change in reinforcement volume fraction for both AMC joints. Therefore, the findings of this study gave a clear indication of the suitability of FSW to weld different types of AMCs.

2.3 Microstructure Of Fsw Joints In Amc's:

The heat generated through the rotation of FSW tool ideally reaches approximately 0.8 of the melting temperature of the joined AMCs. This leads to reinforcement redistribution and refinement, re-crystallization, and grain growth in the NZ. The microstructure of the AMC shows that the reinforcement materials are clustered and distributed heterogeneously in the matrix as a result of production processes (casting or powder metallurgy). The inhomogeneous distributions of reinforcement materials in the microstructure of the BM can affect the isotropy of mechanical properties. It is accepted that the stirring action during FSW causes a break up of clustered reinforcement and homogenous distribution in the weld zone due to the mixing of material and severe plastic deformation [29, 30]. In contrast, Periyasamy et reported that the NZ of AA6061/SiC/10p joints fabricated at a heat input below 1039 J/mm consisted of coarsely clustered SiC particles.

Meanwhile, the size of Al₂O₃ and SiC particles decreases obviously as compared to the original material and the particle edges can be rounded or blunted in the NZ. As a result, the aspect ratio of the particles decreases noticeably. This phenomenon may be explained by the abrasion and stirring effect between particles and tool pin circumference, shoulder surface during welding process [28, 29]. Ceschini et al. [30] pointed out that finer particles were formed closer to the shoulder of the tool than the tip of the pin. However, if the size of original reinforcement is small it is not exposed to the refinement process. For example, Storjohann et al. [28] reported that no change was noticed in the size of SiCw reinforcement with a diameter of 1–2 µm and length of 5–7 µm. Instead the whiskers were reoriented. Whilst 20 µm Al₂O₃ particles were subjected to refinement during FSW

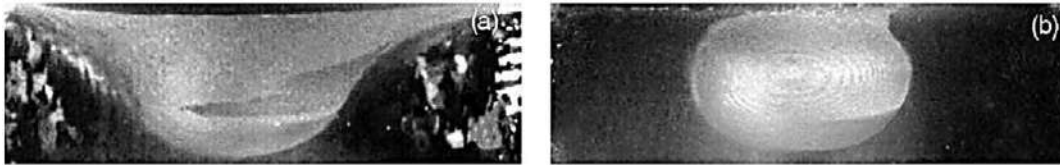


Fig 2.1 Nugget shape — (a) basin, (b) elliptical [10].

The NZ may be characterized by equiaxed grains much smaller than those in the BM. This indicated that new grains nucleated in the NZ during FSW as a result of dynamic re-crystallization. Feng et al. [32] reported that an obvious reduction in grain size of the NZ reached to about 5 μm in FSW of 8 mm thickness AA2009/SiC/15p plate. Grain growth occurs after PWHT to a T4 condition which leads to a grain size of 8 μm . Similar observations were made by Wang et al. [33]. They reported that the reduction of grain size from 10 μm to 6 μm taking place in the NZ of FSW 6 mm thick AA2009/SiC/15p plate. They believe that the high energy point on SiCp broken surface is the main location of the nucleation and growth of nano-size grains to decrease the aluminium matrix/reinforcement interface free energy. However, the growth of new grains in T4 PWHT was restricted by the presence of SiC particles. In addition, Periyasamy et al. [26] indicated that a fine grain structure, fine eutectic, and the elimination of dendritic structure in the NZ were achieved at high heat input through the increase of tool rotation speed. On the other hand, faster cooling rate due to low heat input leads to the formation of coarse grains because of incomplete recrystallization in the NZ of AA6061/SiC/10p FSW joint.

In summary, the evaluation of microstructure of AMCs welded by FSW showed an improvement in reinforcement distribution and refined particles due to the stirring action in FSW. Also the formation of new grains with equiaxed dimensions occurs as a result of dynamic re-crystallization process.

2.4 Tensile Strength Of AMC JOINTS:

The tensile strength of AMC joints fabricated by FSW was compared to that of the BM. The efficiency of joint produced by FSW is higher than that fabricated by conventional welding methods. Many factors influence the tensile strength of AMC joint including tool design, welding parameters, PWHT, and the formation of intermetallic compound.

2.5 Effect Of Tool Design:

The shape of tool shoulder and pin plays a significant role in the tensile strength of FSW joints. Vijay and Murugan [30] investigated the effect of different pin shapes (square, hexagonal, and octagon) in tapered and un-tapered profile on the tensile properties of FSW Al/TiB₂/10. The joint efficiency fabricated by un-tapered square pin exhibits a maximum tensile strength which reaches 99.47% of that of the BM in comparison to other profiles. This is attributed to the high ratios of static volume to dynamic volume of plasticized material, measured as 1.56 for square pin, 1.21 and 1.11 for hexagon and octagon profiles, respectively. This result was confirmed in a later study by Hassan et al. [31]. They used un-tapered (square, hexagonal, and octagon) pin profiles to join hybrid AMC (Al-4%Mg, 1% SiCp and 1% graphite particles). Wang et al. [32] found that the use of conical threaded pin at high traverse speed at 800 mm/min rather than a flat cylinder in joining AA2009/ SiC/17p led to an increase of the joint efficiency to 97% due to the improvement of the flowability of softened material. In a study reported by Yigezu et al. [19] in FSW 5 mm thick Al-12%Si/TiC/10 plates, three shoulder diameters (18, 20, and 22 mm) and threaded cylinder pin were used as FSW tool. They reported that the tensile strength of the weld joints varied from 124 MPa to 172 MPa depending on the tool type and process parameters. A 20 mm shoulder diameter is preferable for obtaining the maximum ultimate tensile strength (UTS). More recently, Kumar et al. [17] investigated the tensile strength of 5 mm rolled Al-4.5%Cu/TiC/10. In order to reveal the effect of three shoulder surface geometries on mechanical properties, full flat surface, 1 mm flat surface, and 2 mm flat surface shoulder with a 7° concave angle were used in FSW. Among the three surface shoulders, the second shoulder configuration resulted in the highest tensile strength. They concluded that the higher heat input as a result of higher contact area between the second shoulder surface and the work piece led to sufficient mixing in the stir-ring zone, as compared with the other two tool profiles.

2.6 Effect of welding parameters:

In FSW process, the welding parameters including tool rotation speed (ω , rpm), traverse speed (V , mm/min) and axial force (F , kN) affect the amount of friction heat generation and mixing process. Therefore, optimum welding parameters must be selected in order to produce the best joint strength. The efficiency of AMC weld joints is generally in the range from 60% to 97% of those of the BM. It is accepted that the UTS of FSW joints of AMCs increases by increasing the rotation speed until a specific limit [27]. The maximum strength was achieved by using a rotation speed ranging from

1000 to 1200 rpm depending on the types of AMC. This leads to the conclusion that there is insufficient heat input in welding joint if the rotation speed is below 1000 rpm, whilst excessive heat input is produced for the weld joint if the rotation speed is more than 1200 rpm. Either case of insufficient or excessive heat input produces inadequate mixing of soft metal. On the contrary, both Yigezu et al. [16] and Kumar et al. [18] reported that the tensile strength decreases linearly when the tool rotational speed increases in FSW rolled Al-12%Si/TiC/10 and rolled Al-4.5%Cu/TiC/10, respectively.

In addition to the tool rotation speed, another important parameter is the traverse speed of the tool along the weld line. A suitable traverse tool stirs the material efficiently from the AS to the RS. Three possible behaviours for the effects of the traverse speed on the tensile strength of AMC joints are discussed below.

Firstly, an unsteady behaviour of the traverse speed on the tensile strength for different types of AMC has been noted. For example, researches [20] on AA6061 composite aluminium as base matrices showed that the relation between the UTS and the traverse speed is not directly proportional. As traverse speed increases the tensile strength increases and reaches a maximum value before it decreases. They assert that the amount of heat input due to friction action between the tool and BM is mainly affected by tool rotation speed. On the other hand, the cooling rate is determined by the traverse speed. Therefore, at lower traverse speed an increase in frictional heat generation and slow cooling rate is accompanied by coarse grains (grain growth). Tunnel defects may occur due to excessive stirring resulting from slow traverse speed. In contrast, at higher traverse speeds insufficient heat input is generated into the joint, which leads to inadequate stirring action of softened material from the AS to the RS also causing tunnel defects. Therefore, reduced tensile strength can be resulted from both low and high traverse speeds.

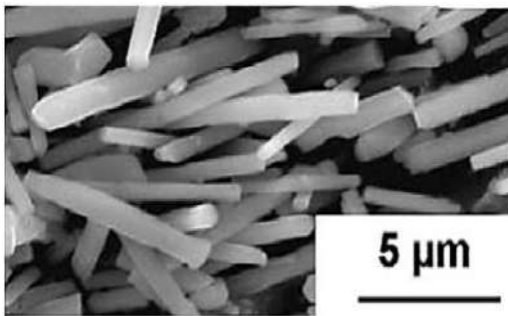


Fig. 2.2 Reorientation of reinforcement in FSW AA2124/SiC/20w [28]

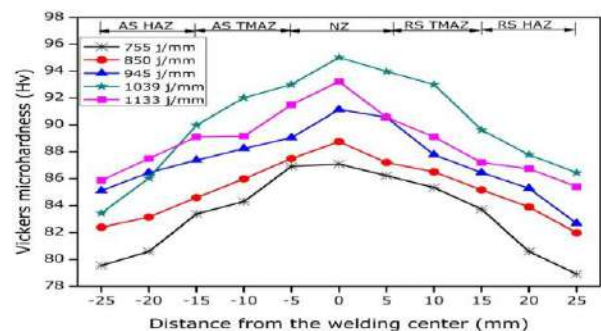


Fig. 2.3 Microhardness profile across the weld region of AA6061/SiC/10p at different heat inputs

Secondly, a linear behavior of traverse speed on the tensile strength for AA2009/SiC/17p was reported by Wang et al. [29]. The maximum joint efficiency was achieved to reach 97% of the BM at a higher traverse speed of 800 mm/min. They pointed out that at lower traverse speed failure of the joint happened in the HAZ which was characterized by lowered hardness due to dissolution and precipitates growth. This led to the reduction in tensile strength. On the other hand, as the traverse speed was increased the clusters were partially dissolved in the matrix in the HAZ owing to high cooling rate. Thus an increase in joint efficiency was achieved as a result of the increase of HAZ hardness and shift in fracture location from HAZ to NZ.

Thirdly, as reported by other researchers [24], the increase of the traverse speed slightly decreases the tensile strength of the joint (inversely proportional) for AMCs AA2124/SiC/25p, Al-4.5%Cu/TiC/10, and Al-12%Si/TiC/10, respectively. The best welding speeds are 40 mm/min for AA2124 and 20 mm/min for the other two AMCs. However, they mentioned that the influence of traverse speed on UTS is less obvious than the tool rotation speed and tool design.

Applied axial force is another important parameter in FSW. The heat generated by friction between the BM and tool depends on the friction coefficient which is specified by the applied force. Higher heat input is generated by a larger amount of applied force which causes sufficient flow. Defect free joint can be achieved if a sufficient axial force which is higher than the flow stress of the BM is applied. Thus higher tensile strength can be obtained when an adequate force is selected. In spite of the importance of the applied force on the amount of heat generation and the retention of the plasticized metal, few researchers have taken into account the effect of this parameter as one of the key welding variables on tensile strength.

Dinakaran and Murugan [21] reported that the maximum tensile strength of joint was obtained at 6 kN axial force when joining in-situ composite AA6061/ZrB₂. Further increment in hydrostatic pressure leads to a reduction in the tensile strength. The appearance of micro voids in the joint at lower force and excessive flash at larger force causes a reduction in the cross section of the joint and hence leads to a reduction in tensile strength of joint. Similarly, Murugan and Kumar [23] indicated that for the FSW joints of AA6061/AlN_p tunnel defects appeared in the cross section of joint due to the lack of heat generation when using lower axial forces. Therefore, a reduction in tensile strength happened when the applied force was lower than 5 kN. On



the other hand, if the applied force was more than 5 kN it led to thinning of the NZ and formation of worm hole, and therefore reduced the joint efficiency. A similar findings was reported by Kalaiselvan and Murugan [21] in FSW joints of AA6061/B4C with a different optimum axial force at 10 KN in their study.

In conclusion, welding parameters including tool rotation speed, traverse speed, and axial force affect significantly the UTS of AMC joints. Rotation speed has the greatest effect on joint efficiency, whilst traverse speed and axial force affect the tensile strength of AMC joints to a varying degree [33]. There is no general trend that can be related to welding parameters for all types of AMCs. Therefore, each material needs its own study to achieve its maximum tensile strength for the FSW joint.

2.7 Tool Wear in FSW of AMCs:

Wear of FSW tool is a critical issue particularly for AMC materials, which occurs as a result of friction, rotation, and movement of FSW tool along the base material. According to Rai et al. [7], plastic deformation, abrasion, diffusion, and reaction between the environment and the tool material are the major wear mechanisms that happen in FSW tools. Mishra and Ma [10] reported that FSW of soft metals such as aluminium and magnesium did not exhibit significant wear of the tool. However, tool life issue becomes more significant when hard metals of high melting temperature or MMCs are welded by FSW. This phenomenon is characterized by the deformation and reduction in the pin diameter.

The appearance of hard reinforcement particles in AMCs makes abrasion a dominating factor for tool wear in FSW. Prado et al. [12,13] studied the effect of welding parameters including rotation speed between 500 and 2000 rpm and traverse speed between 1 and 9 mm/s on threaded 1/4–20/01 AISI oil-hardened steel tool wear. Similar joints for AA6061/Al₂O₃/20p and monolithic aluminium AA6061-T6, were used in their studies. They pointed out that no wear was observed in the tool when welding a monolithic aluminium alloy, whilst severe wear started in joining AA6061/Al₂O₃/20p when reaching its maximum value at 1000 rpm then gradually becoming constant after a period of time (self-optimized tool shape). And thus the turbulent flow (vortex flow) of worn tool is less than the unworn tool due to the eroded threads. The rate of tool wear at various welds lengths and the relationship between weld speed and tool wear rate. However, from microstructure evaluation it was found that sound joint could be produced continuously by using tools with self-optimized shapes.

III. CONCLUSION:

FSW is the best process to welding of different alloys of aluminum for long lengths with an excellent quality. Considerable effort is being made to weld higher temperature materials such as alloys of magnesium, titanium and steels by using FSW. Extensive efforts are also required for joining of dissimilar aluminum alloy with various variables under consideration.

The mechanical properties of AMCs joined by FSW are largely dependent on the combined effect of both the composition of AMCs and the FSW processing conditions. Therefore, the mechanical performance of FSW joints should be evaluated accordingly. Early researches showed that FSW is a potential welding process to achieve defect free joints of AMCs. There is a clear need for more efforts to understand the effect of FSW on these materials in adequate depth to meet design and production requirements. For instance, there is a need for systematic studies which take into account the effects of reinforcement percentage and types of reinforcement on joint efficiency. More work is needed to understand the performance of FSW joint of such as AA2124 and AA6092 as base matrices for AMCs with different reinforcement percentages. Also there is a need for joining AMCs to other materials rather than monolithic aluminium alloys such as magnesium alloys, a new candidate material for aerospace application.

Furthermore, welding parameters such as tool rotation speed, traverse speed, and axial force have a significant effect on the amount of heat generation and strength of FSW joints. Macrostructural evaluation showed the formation of tunnel defects due to inappropriate flow of plasticized metal. Micro structural evaluation of FSW joints clearly shows the formation of new fine grains and refinement of reinforcement particles in the weld zone with different amount of heat input by controlling the welding parameters. However, there is no general trend between welding parameters and mechanical properties for different types of AMCs. Further work needs to be carried out to define the welding window of each composite metal for optimized mechanical properties. Also there is very limited data on fatigue strength and fracture toughness of friction stir welded AMCs. More effort is needed to study these properties in more depth to establish the full potential of FSW joints of AMCs.



REFERENCES:

- [1] G. Çam, M. Koçak, Progress in joining of advanced materials, *Int. Mater. Rev.* 43 (1) (1998) 1–44.
- [2] A.M. Hassan, M. Almomani, T. Qasim, A. Ghaithan, Effect of processing parameters on friction stir welded aluminum matrix composites wear behavior, *Mater. Manuf. Process.* 27 (12) (2012) 1419–1423.
- [3] K. Suryanarayanan, R. Praveen, S. Raghuraman, Silicon carbide reinforced aluminium metal matrix composites for aerospace applications: a literature review, *Int. J. Innov. Res. Sci. Eng. Technol.* 2 (11) (2013).
- [4] M.B.D. Ellis, Joining of aluminium based metal matrix composites, *Int. Mater. Rev.* 41 (2) (1996) 41–58.
- [5] W.M. Thomas, D.G. Staines, I.M. Norris, R. de Frias, Friction stir welding tools and developments, *Weld. World* 47 (2003) 10–17.
- [6] R. Rai, A. De, H.K.D.H. Bhadeshia, T. DebRoy, Review: friction stir welding tools, *Sci. Technol. Weld. Join.* 16 (4) (2011) 325–342.
- [7] Y.N. Zhang, X. Cao, S. Larose, P. Wanjara, Review of tools for friction stir welding and processing, *Can. Metall. Q.* 51 (3) (2012) 250–261.
- [8] P.L. Threadgill, A.J. Leonard, H.R. Shercliff, P.J. Withers, Friction stir welding of aluminium alloys, *Int. Mater. Rev.* 54 (2) (2009) 49–93.
- [9] R.S. Mishra, Z.Y. Ma, Friction stir welding and processing, *Mater. Sci. Eng. R Rep.* 50 (1–2) (2005) 1–78.
- [10] C.C. Tutum, J.H. Hattel, Numerical optimisation of friction stir welding: review of future challenges, *Sci. Technol. Weld. Join.* 16 (4) (2011) 318–324.
- [11] G. Cam, Friction stir welded structural materials: beyond Al-alloys, *Int. Mater. Rev.* 56 (1) (2011) 1–47.
- [12] P. Threadgill, A. Leonard, H. Shercliff, P. Withers, Friction stir welding of aluminium alloys, *Int. Mater. Rev.* 54 (2) (2009) 49–93.
- [13] Metal Matrix Composites (MMC) Market for Ground Transportation, Electronics/ Thermal Management, Aerospace and Other End-Users — Global Industry Analysis, Size, Share, Growth, Trends and Forecast, 2013–2019, <https://www.linkedin.com/pulse/20140605070839-173774513-metal-matrix-composites-market-review2014> (cited 2015; Available from:).
- [14] J. Kaczmar, K. Pietrzak, W. Włosiński, The production and application of metal matrix composite materials, *J. Mater. Process. Technol.* 106 (1) (2000) 58–67.
- [15] M. Rosso, Ceramic and metal matrix composites: routes and properties, *J. Mater. Process. Technol.* 175 (1–3) (2006) 364–375.
- [16] J.M. Kunze, C.C. Bampton, Challenges to developing and producing MMCs for space applications, *JOM* 53 (4) (2001) 22–25.
- [17] J. Pakkanen, A. Huetter, C. Poletti, N. Enzinger, C. Sommitsch, J.T. Niu, Friction stir welding of aluminum metal matrix composite containers for electric components, *Key Eng. Mater.* 611–612 (2014) 1445–1451.
- [18] G. Mathers, *The Welding of Aluminium and Its Alloys*, Woodhead Publishing Limited, Cambridge, England, 2002.
- [19] *Aluminum and Aluminum Alloys*, in: J.R. Davis (Ed.) ASM International, 1993. [27] S. Kou, *Welding Metallurgy*, Second ed. John Wiley & Sons, New Jersey, 2003.
- [20] D. Storjohann, O.M. Barabash, S.S. Babu, S.A. David, P.S. Sklad, E.E. Bloom, Fusion and friction stir welding of aluminum metal-matrix composites, *Metall. Mater. Trans. A* 36A (2005) 3237–3247.
- [21] D.R. Ni, D.L. Chen, D. Wang, B.L. Xiao, Z.Y. Ma, Influence of microstructural evolution on tensile properties of friction stir welded joint of rolled SiCp/AA2009-T351 sheet, *Mater. Des.* 51 (2013) 199–205.
- [22] K. Kalaiselvan, I. Dinaharan, N. Murugan, Characterization of friction stir welded boron carbide particulate reinforced AA6061 aluminum alloy stir cast composite, *Mater. Des.* 55 (2014) 176–182.
- [23] L. Ceschini, I. Boromei, G. Minak, A. Morri, F. Tarterini, Effect of friction stir welding on microstructure, tensile and fatigue properties of the AA7005/10 vol.% Al₂O₃p composite, *Compos. Sci. Technol.* 67 (3–4) (2007) 605–615.
- [24] A. Feng, B. Xiao, Z. Ma, Effect of microstructural evolution on mechanical properties of friction stir welded AA2009/SiCp composite, *Compos. Sci. Technol.* 68 (9) (2008) 2141–2148.
- [25] D. Wang, B.L. Xiao, Q.Z. Wang, Z.Y. Ma, Evolution of the microstructure and strength in the nugget zone of friction stir welded SiCp/Al–Cu–Mg composite, *J. Mater. Sci. Technol.* 30 (1) (2014) 54–60.
- [26] L. Ceschini, I. Boromei, G. Minak, A. Morri, F. Tarterini, Microstructure, tensile and fatigue properties of AA6061/20 vol.% Al₂O₃p friction stir welded joints, *Compos. A: Appl. Sci. Manuf.* 38 (4) (2007) 1200–1210.
- [27] Y. Bozkurt, H. Uzun, S. Salman, Microstructure and mechanical properties of friction stir welded particulate reinforced AA2124/SiC/25p-T4 composite, *J. Compos. Mater.* 45 (21) (2011) 2237–2245.
- [28] H. Nami, H. Adgi, M. Sharifitabar, H. Shamabadi, Microstructure and mechanical properties of friction stir welded



- Al/Mg₂Si metal matrix cast composite, *Mater. Des.* 32 (2) (2011) 976–983.
- [29] X.G. Chen, M. da Silva, P. Gougeon, L. St-Georges, Microstructure and mechanical properties of friction stir welded AA6063–B₄C metal matrix composites, *Mater. Sci. Eng. A* 518 (1–2) (2009) 174–184.
- [30] L.M. Marzoli, A.V. Strombeck, J.F. Dos Santos, C. Gambaro, L.M. Volpone, Friction stir welding of an AA6061/Al₂O₃/20p reinforced alloy, *Compos. Sci. Technol.* 66 (2) (2006) 363–371.
- [31] F. Cioffi, R. Fernández, D. Gesto, P. Rey, D. Verdera, G. González-Doncel, Friction stir welding of thick plates of aluminum alloy matrix composite with a high volume fraction of ceramic reinforcement, *Compos. A: Appl. Sci. Manuf.* 54 (2013) 117–123.
- [32] N. Murugan, B. Ashok Kumar, Prediction of tensile strength of friction stir welded stir cast AA6061-T6/AlNp composite, *Mater. Des.* 51 (2013) 998–1007.
- [33] P. Periyasamy, B. Mohan, V. Balasubramanian, Effect of heat input on mechanical and metallurgical properties of friction stir welded AA6061-10% SiCp MMCs, *J. Mater. Eng. Perform.* 21 (11) (2012) 2417–2428.



MATRUSRI ENGINEERING COLLEGE

(Approved by AICTE, Affiliated to Osmania University)

#16-1-486, Saidabad, Hyderabad - 500059



Sponsored by

MATRUSRI EDUCATION SOCIETY



ISBN: 97881-936274-0-2



1ST NATIONAL CONFERENCE ON TRENDS IN SCIENCE, ENGINEERING AND TECHNOLOGY

(NTSET - 2018)

February 2nd & 3rd - 2018

TECHNICAL PAPER ABSTRACTS



ORGANIZED BY

MATRUSRI ENGINEERING COLLEGE

(Approved by AICTE, Affiliated to Osmania University)

#16-1-486, Saidabad, Hyderabad - 500059



Sponsored by

MATRUSRI EDUCATION SOCIETY

ISBN: 97881-936274-0-2



NTSET 2018





REVIEW PAPER ON PROCESSING OF METAL MATRIX COMPOSITES & ITS PROPERTIES.

¹T.Somasekhar, ²P Niteesh Kumar

Assistant Professor, Mechanical Engineering, Matrusri Engineering College, Saidabad Hyderebad, India

Abstract: Several technical challenges exist with casting technology yet it can be used to overcome this problem. Achieving a uniform distribution of reinforcement within the matrix is one such challenge, which affects directly on the properties and quality of composite material. In the present study a modest attempt would be made to develop Aluminium based silicon carbide particulate MMCs with an objective to develop a conventional low cost method of producing MMCs and to obtain homogenous dispersion of ceramic material. To achieve these objectives two step-mixing method of stir casting technique has been proposed and subsequent property analysis has been made. Aluminium (98.41%) and SiC (320-grit) has been chosen as matrix and reinforcement material respectively. Aluminum alloys are widely used in aerospace and automobile industries due to their low density and good mechanical properties, better corrosion resistance and wear, low thermal coefficient of expansion as compared to conventional metals and alloys. The excellent mechanical properties of these materials and relatively low production cost make them a very attractive candidate for a variety of applications both from scientific and technological viewpoints. The aim involved in designing aluminum based metal matrix composite materials is to combine the desirable attributes of metals and Ceramics.

I. INTRODUCTION

From the last few years in industrial applications, the important parameters in material selection is specific strength, weight and cost. Before going study about the paper we must know the difference between the composite and MMC. The composite defined as the made of several part or element but only combined different material not a non-metal whereas the non-metal is mixed with material this called MMC. Clearly we had seen the review paper. the main mixed material most probably like aluminum alloy, silicon carbide, fly ash, graphite, boron carbide, fly ash chemosphere, silicon nitride, silicon carbide, etc, in this material we fabricated by using different method with respected to the grain size the generally we go for the stir and GPIT technique were check the material distribution by using SEM analyzed with FEA model. Finally we are going to study about the properties.

A more restrictive definition is used by industries and materials scientists: a composite is a material that consists of constituents produced via a physical combination of pre-existing ingredient materials to obtain a new material with unique properties when compared to the monolithic material properties. This definition distinguishes a composite from other multiphase materials which are produced by bulk processes where one or more phases result from phase transformation ("in-situ" composites).

Classification of the composite materials with metal matrix

Metal matrix composites can be classified in various ways. One classification is the consideration of type and contribution of reinforcement components in particle-, layer-, fiber- and penetration composite materials. Fiber composite materials can be further classified into continuous fiber composite materials (multi- and monofilament) and short fibers or, rather, whisker composite materials

The terms matrix and reinforcement are often used. The matrix is a percolating "soft" phase (with in general excellent ductility, formability and thermal conductivity) in which are embedded the "hard" reinforcements (high stiffness and low thermal expansion). The reinforcements can be continuous or discontinuous, orientated or disorientated. The composites are classified by: (1) their matrix (polymer, ceramic, metal), (2) their reinforcement, which includes the chemical nature (oxides, carbides, and nitrides), shape (continuous fibers, short fibers, whiskers, particulates) and orientation, (3) their processing routes.

Aluminum Matrix Composites (AMCs)



Aluminum is the most popular matrix for the metal matrix composites (MMCs). The Al alloys are quite attractive due to their low density, their capability to be strengthened by precipitation, their good corrosion resistance, high thermal and electrical conductivity, and their high damping capacity. Aluminum matrix composites (AMCs) have been widely studied since the 1920s and are now used in sporting goods, electronic packaging, amours and automotive industries. They offer a large variety of mechanical properties depending on the chemical composition of the Al-matrix. They are usually reinforced by Al₂O₃, SiC, C but SiO₂, B, BN, B₄C, AlN may also be considered. The aluminum matrices are in general Al-Si, Al-Cu, 2xxx or 6xxx alloys. As proposed by the American Aluminum Association the AMCs should be designated by their constituents: accepted designation of the matrix / abbreviation of the reinforcement's designation / arrangement and volume fraction in % with symbol of type (shape) of reinforcement. For example, an aluminum alloy AA6061 reinforced by particulates of alumina, 22 % volume fraction, is designated as "AA6061/Al₂O₃/22p".

In the 1980s, transportation industries began to develop discontinuously reinforced AMCs. They are very attractive for their isotropic mechanical properties (higher than their unreinforced alloys) and their low costs (cheap processing routes and low prices of some of the discontinuous reinforcement such as SiC particles or Al₂O₃ short fibers). Among the various and numerous applications [10, 11], a few arbitrary examples, are given in Fig. brake rotors for high speed train automotive braking systems automotive pushrods cors for HV electrical wires etc.

Some industrial AMCs applications: brake rotors for high speed train automotive braking systems automotive pushrods cors for HV electrical wires.

II. SUMMARY

Processing of MMCS

Accordingly to the temperature of the metallic matrix during processing the fabrication of MMCs can be classified into three categories: (a) Liquid phase processes, (b) solid state processes, and (c) Two phase (solid-liquid) processes

Stir Casting Process -Stir Casting is a liquid state method of composite materials fabrication, in which a dispersed phase (ceramic particles, short fibers) is mixed with a molten matrix metal by means of mechanical stirring. The liquid composite material is then cast by conventional casting methods and may also be processed by conventional Metal forming technologies.

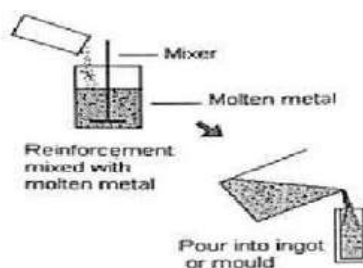


Fig-A: Stir Casting

Fabrication of the AMCs

There are many processes viable to fabricate AMCs; they can be classified in: solid-state, liquid-state and deposition processes. In solid-state processes, the most spread method is powder metallurgy PM; it is usually used for high melting point matrices and avoids segregation effects and brittle reaction product formation prone to occur in liquid state processes. This method permits to obtain discontinuously particle reinforced AMCs with the highest mechanical properties. These AMCs are used for military applications but remain limited for large scale productions. In liquid-state processes, one can distinguish the infiltration processes where the reinforcements form a perform which is infiltrated by the alloy melt (1) with pressure applied by a piston or by an inert gas (gas pressure infiltration GPI) and (2) without pressure. In the last case, one can distinguish (a) the reactive infiltration processes using the wetting between reinforcement and melt obtained by reactive atmosphere, elevated temperature, alloy modification or reinforcement coating (reactive infiltration) and (b) the dispersion processes, such as stir-casting, where the reinforcements are particles stirred into the liquid alloy. Process parameters and alloys are to be adjusted to avoid reaction with particles. In deposition processes, droplets of molten metal are sprayed together with the reinforcing phase and collected on a substrate where the metal solidification is completed. This technique has the main advantage that the matrix microstructure



exhibits very fine grain sizes and low segregation, but has several drawbacks: the technique can only be used with discontinuous reinforcements, the costs are high, and the products are limited to the simple shapes that by obtained by extrusion, rolling or forging

Comparison between MMC & AMMC:

The main concept of composite is that it contains matrix materials. In composite material the reinforcements can be fibers, particulates or whiskers, and the matrix materials can be metals, plastics, or ceramics. The reinforcements can be made from polymers, ceramics and metals. [1].

Some automotive companies using MMC for disc brakes also. Honda Company used AMMC for cylinder liners in some of their engines like F20C, F22C and H22A. In recent years considerable development has occurred in nonferrous composites and attention is now being given to make iron based composites. The paper [2] reviews the ongoing research and interaction between iron based materials and reinforcements including wetting and spreading of iron melts on ceramic materials. The paper provides insight into the evolution of the processes that are used to manufacture iron based composites, and the applications that benefit from their unique characteristics. In order for ferrous based composite materials to find applications in production environments, consistent and controlled mechanical and physical characteristics are required. Ultimately, industry standards need to be written defining the material design parameters. Over the past thirty years Metal Matrix Composites (MMCs) have [3] emerged as an important class of material within the engineering industry. At present, MMCs offer attractive performance or weight-saving alternatives for a wide range of applications within the sport industry, from Formula 1 racing components to golf club shafts. This paper briefly reviews the advantages of MMCs, and presents a study of the effects of additional treatments (heat and surface) which produce beneficial characteristics in monolithic and alloy materials, but whose effects become more complex when applied to composites. The material used for this study was 2124 Al alloy matrix, reinforced with particulate silicon carbide having a mean particle size of around 3 μm treatment. The influence of machining parameters [4] such as cutting forces and surface roughness on the machinability of LM6/ SiCp metal matrix composites at different weight fraction of SiCp discussed in this paper. It is observed that the depth of cut and the cutting speed at constant feed rate affects the surface roughness and the cutting forces during dry turning operation of cast MMCs. It is also observed that higher weight percentage of SiCp reinforcement imparts a higher surface roughness and needs high cutting forces. This experimental analysis and test results on the machinability of Al/SiC-MMC will provide essential guidelines to the manufacturers. A detailed study [5] on the processing of Al-metal matrix composites cites with the reinforcement of different particulates such as SiC, TiN and TiO₂ was carried out. The results of the present studies show that the Al based composites prepared through various techniques exhibits excellent mechanical, physical and tribological properties and could emerge as promising materials for defense, aerospace and other engineering applications. With concern [6] increasing over environmental issues, reduction in automobile weight has become more important and has been proved to be effective for improving fuel efficiency. Metal Matrix Composites (MMC) are expected to be useful to cope with these problems. The authors have developed a new aluminium engine block which has the cylinder bore surface structure reinforced with short hybrid fibers of alumina and carbon. The development of aluminum metal matrix composites (Al-MMC) brake rotor and pad was discussed [7]. The improvement in fuel consumption rate requires a reduction in vehicle weight. In this study, we developed aluminum metal matrix composites brake rotor and pads, which have equivalent braking effects and wear resistance to those of the conventional cast iron rotor, by optimization of the quantities and the particle diameter ratio of hard particles used for the rotor and the pad. Metal matrix composites [8] offer considerable potential for widespread application in most aerospace fields. The potential for the use of these materials in civil aircraft is largely dependent on costs and currently these are too high. However, by the use of appropriate design and manufacturing technology this intrinsic high cost can be overcome to unlock their potential.

Alumina as reinforcement

Aluminum oxide, commonly referred to as alumina, possesses strong ionic inter atomic bonding giving rise to its desirable material characteristics. It can exist in several crystalline phases which all revert to the most stable hexagonal alpha phase at elevated temperatures. Its high hardness, excellent dielectric properties, refractoriness and good thermal properties make it the material of choice for a wide range of applications.

Performance characteristics of Al/SiC-MMCs:

Hardness

The Brinell hardness test shall be carried out over Brinell hardness tester. Six samples of Al/SiC-MMC's for different sizes and weight fraction of SiC particles shall be prepared. After test and hardness value on dial, the Brinell hardness values with reference to scale HRB shall be taken for different samples



Impact Strength

Impact Test to be carried out over Charpy Impact Testing Machine and results to be recorded. According to size and weight fraction of SiC particles Twelve Specimens Al/SiC-MMC's of Square cross-section of size (10X10X55) with single V-notches are planned. The size of V-notches is 45° and 2mm depth.



Fig-B: Charpy impact testing machine

Microstructure

Metallographic samples are normally sectioned from the cylindrical cast bars. A 0.5 % HF solution is used to etch the samples wherever required. To see the difference in distribution of SiC particles in the aluminium matrix, microstructure of samples are developed on Inverted type Metallurgical Microscope (Make: Nikon, Range-X50 to X1500). Micrograph of Al/SiC-MMC's samples for different Sizes (2000 mesh, 250 mesh, 320 mesh) and weight fraction (2.5%, 4.5%, 12.5% & 17.5 %) of SiC particles. Optical micrographs show the distribution of SiC particles within the matrix.

III. CONCLUSION

Following direct improvements could be gained

- Impotent of the casting quality by minimizing the entrapped air during the shot sleeve process
- Minimizing set up time during the start of casting process.
- Optimization of the whole casting process by controlling filling with optimal plunger movement
- Shorter lead time during the tool designing process.
- Less scrap and waste production when new design is taken on the use.
- The results confirmed that stir formed Al alloy 6063 with Al₂O₃ reinforced composites is clearly superior to base Al alloy 6063 in the comparison of tensile strength, Impact strength as well as Hardness.
- Dispersion of Al₂O₃ particles in aluminum matrix improves the hardness of the matrix material.
- It is found that elongation tends to decrease with increasing particles wt. percentage, which confirms that alumina addition increases brittleness.
- Aluminum matrix composites have been successfully fabricated by stir casting.
- Technique with fairly uniform distribution of Al₂O₃ particles.
- It appears from this study that UTS and Yield.
- Strength trend starts increases with increase in weight percentage of Al₂O₃ in the matrix.
- The matrix hardening does not influence the stiffness of the alloy and therefore of the discontinuous AMCs, but significantly improves the yielding behavior and tensile properties.
- A fine precipitation homogeneously distributed in the matrix is required to obtain good mechanical properties for the matrix alloy and therefore also for the composite.



REFERENCES:

- [1] Saraev, S. Schmauder, (2003) "Finite element modelling of Al/SiCp metal matrix composites with particles aligned in stripes—a 2D–3D comparison" Staatliche Materialprüfungsanstalt (MPA), University of Stuttgart, Pfaffenwaldring 32, D-70569 Stuttgart, Germany, International Journal of Plasticity (19) 733– 747.
- [2] J. Hashim, L. Looney, M.S.J. Hashmi "Particle distribution in cast metal matrix composites—Part I" Journal of Materials Processing Technology, Volume 123, Issue 2, 30 April 2002, pp: 251–257
- [3] Sanjay K. Mazumdar, "Composites manufacturing", CRC Press, 2010.
- [4] D. Bacon, J. Moffatt, L. Edwards and M.E. Fitzpatrick, "Metal Matrix Composites: In the driving seat", Dept of Materials Engineering, The Open University, Walton Hall, Milton Keynes MK7 6AA A. D. Tarrant Aerospace Metal Composites Limited, REA Road, Farnborough, Hampshire GU14 6XE
- [5] Rabindra Behera, S. Kayal, N.R. Mohanta, G. Sutradharda, "Study on machinability of Aluminium Silicon Carbide Metal Matrix Composites", Journal of Minerals & Materials Characterization & Engineering, Vol. 10, No.10, pp.923-939, 2011
- [6] K. Venkateswarlu , A. K. Ray, S. K. Chaudhury and L. C. Pathak, "Development of aluminium based metal matrix composites", National metallurgical laboratory, Jamshedpur - 831007, India.
- [7] G.g. sozhamannan. S. Balasivanandha prabu, r. Paskaramoorthy. Failures analysis of particle reinforced metal matrix composites by microstructure based models, materials and design, 31(2010) 3785-3790
- [8] S.Rama rao. G. Padmanabhan, Fabrication and mechanical properties of aluminium-boron carbide composites, international journal of materials and biomaterials applications 2(2012) 15-18
- [9] M. Saravanan, R.M. Pillai, (2007) "Development of ultrafine grain aluminium–graphite metal matrix composite by equal channel angular pressing" Materials and Minerals Division, Regional Research laboratory (CSIR), Industrial Estate PO, Pappanamcode, Thriuvananthapuram 695 019, Kerala, India, Composites Science and Technology (67) 1275–1279.
- [10] Hiroaki Nakanishi, Kenji, Akinori, etc., "Development of aluminum metal matrix composites (Al-MMC) brake rotor and pad" , JSAE Review , Volume 23, Issue 3, July 2002, pp: 365–370.
- [11] David Charles , "Unlocking the potential of metal matrix composites for civil aircraft",Materials Science and Engineering: A Review, Volume 135, European Materials Research Society 1990 Spring Meeting on Metal Matrix Composites, 30 March 1991, pp: 295– 297
- [12] Mohamed A. Taha, (2001) "Practicalization of cast metal matrix composites MMCCs" Department of Design and Production Engineering, Faculty of Engineering, Ain-Shams University, P.O. Box 8022, Massaken Nasr-City, Materials and Design (22) 431 441
- [13] http://www.araifid.com/testing_validation_metallurgica1_testing.asp



MATRUSRI ENGINEERING COLLEGE

(Approved by AICTE, Affiliated to Osmania University)

#16-1-486, Saidabad, Hyderabad - 500059



Sponsored by

MATRUSRI EDUCATION SOCIETY



ISBN: 97881-936274-0-2



1ST NATIONAL CONFERENCE ON TRENDS IN SCIENCE, ENGINEERING AND TECHNOLOGY

(NTSET - 2018)

February 2nd & 3rd - 2018

TECHNICAL PAPER ABSTRACTS



ORGANIZED BY

MATRUSRI ENGINEERING COLLEGE

(Approved by AICTE, Affiliated to Osmania University)

#16-1-486, Saidabad, Hyderabad - 500059



Sponsored by

MATRUSRI EDUCATION SOCIETY

ISBN: 97881-936274-0-2

NTSET 2018





DESIGN AND ANALYSIS OF THERMO MECHANICAL LOADING FOR A TURBINE HOUSING USING FEA

¹Sampath Siddam, ²K Sridhar, ³M Sri Hari

^{1,2,3}Assistant Professor, ^{1,2,3}Mechanical Engineering Department,
¹Matrusri Engineering College, ²Malla Reddy Institutions, ³GNITC, Hyderabad, India.

Abstract: Turbochargers are the fastest and easiest way for an engine to increase its power. It increases engine's power up to 40% without any increase in the physical size of the engine and much extra weight. Turbochargers are also efficient in design because it utilizes the waste exhaust of the engine to power itself. A Turbocharger is a device that uses the energy of exhaust gases coming out from an engine to compress the air going into the engine. It must have at least four openings one for the engine exhaust gas to enter, second for the exhaust gas to exit, third is opening for intake air to enter the turbocharger, and fourth for the intake air to exit the turbocharger on its way to the engine intake. A turbocharger will also have one additional opening to vent excess air pressure. In this work an attempt is made to study the two important objectives firstly design of turbocharger in CATIA and finding out the critical thermal stresses in turbine housing of a turbocharger under thermo-mechanical loading using ANSYS. Secondly, to find out the Thermo-Mechanical fatigue life at different places of a turbocharger and finally computing the results.

Index Terms: Turbocharger, thermal stresses and thermo-mechanical fatigue life

I. INTRODUCTION

A Turbocharger is an air compressor used for forced-induction of an internal combustion engine. Like a supercharger, the purpose of a turbocharger is to increase the mass of air entering the engine to create more power. A turbocharger is a turbine driven supercharger. The turbine is driven by waste exhaust gas. Its benefit lies with the compressor increasing the pressure of air entering the engine thus resulting in greater performance. Popularly used with internal combustion engines. Turbochargers have also been found useful compounding external combustion engines

Turbocharger system are measured by the amount of pressure the compressor can output above ambient. This pressure is commonly called Boost pressure or Boost. Compressing the air increases its temperature, which lowers the density of the charge air and creates a less efficient cycle and loss of power. The temperatures can also have detrimental effects on the materials and structure of the engine. Increases the power of the engine because of the increased density of the air. Increased air density means more oxygen molecules, which means the engine can respond by increasing the amount of fuel it mixes with that oxygen. When the fuel and oxygen are burned, the result is a more powerful explosion with each piston stroke and thus more power coming out of the engine. This issues that the compressed air needs to be cooled in order to achieve maximum power and maintain the structural integrity of the pistons. A heat exchanger or intercooler is installed between the compressor and engine inlet to cool the charger air. Increasing the intake air pressure going into an engine can increase the engine's power, but too much air pressure can damage the engine increasing the pressure. The high temperature components of most industrial systems such as turbine components are exposed to large thermal fluctuations during operation. The combined effect of thermal and mechanical cyclic loading can produce very different results to the addition of the damage from the isothermal components of that exposure.

The purpose of this paper is to find out the critical thermal stresses in turbine housing under thermo-mechanical loading. And to find out the Thermo-Mechanical fatigue life of different duty cycles like lab test duty cycle and field data duty cycles and comparing the results.

Cristiana Delpretea [1] states that outlines of multi axial fatigue life calculation and qualification procedure of turbine housing subjected to various duty cycles in the field. Both analytical and experimental techniques are adopted in this work. Results of the analytical model were correlated to the experimental measurements for model verification. Analytical transient FEA analysis was utilized to understand the effect of thermal loading on the turbine housing. The model was calibrated against engine measurement during engine cyclic testing. After calibration the model is used to optimize the housing design. They compared different fatigue life models to calculate fatigue life and also the material properties.

Investigation of FaridAhdad, Carol Cai [2] states that the guidelines for determination of the thermo-mechanical behavior of the Turbine housing using Finite Element Analysis. This includes the steps of: 1) Geometry simplification 2) Meshing process 3) Transient thermal analysis 4) Static thermal stress analysis 5) Vibration analysis 6) Post processing Result.

FaridAhdad et al [3] have developed the fatigue model based on a cumulative damage approach (Chaboche model [1]) that is used to predict crack initiation. To determine the transient stress and temperature distributions due to the high rates of convection from

the gas, and the complexity of the design, conjugate heat transfer CFD simulation is performed. The tongue of the turbine housing is a critical region in which cracks initiate within a short time. Heat transfer coefficients (HTC) and bulk temperature predictions from CFD, in general, can be validated by thermal measurement. But because of the geometry and the location of the tongue, it is impossible to measure the metal temperature. For this work 2 methods were presented: HTC calibrated by thermal measurement and HTC from CFD heat transfer Conjugate method, steady state analysis. The design of turbine housing is optimized based on this TMF methodology and shows very good results in testing

The experimental investigation of FaridAhdadet.al [5] have developed an approach to perform quick TMF predictions for a complex duty cycle. To assess TMF failure, it is very critical to accurately estimate metal temperature of these components subjected to complex duty cycle where exhaust gas temperature vary significantly with time. The method was applied to evaluate the fatigue damage of turbine housing under actual condition. The transfer function for metal temperature and elastic stress are mainly function of material and heat transfer co-efficient. Thermal and elastic stress analytical methods were component with FE approach for complex geometry and duty cycle. From the comparison study result from analytical method are matching quite with FE results. The Elastic-plastic stress was determined by Glinka method which is based on strain energy density. Turbine Housing of turbocharger has been considered which a quite expensive component operating at a very high temperature. The life prediction show that the tongue region will start to fail only after 87000 kilometers.

II.FINITE ELEMENT MODEL GENERATION

The Finite element method is the dominant discretization technique in structural mechanics. The basic concept in the physical interpretation of the FEM is the subdivision of the mathematical modal into non-overlapping components of simple geometry called finite elements or elements for short. The response of each element is expressed in terms of a finite number of degrees of freedom characterized as the value of an unknown function at a set of nodal point.

The response of the mathematical model is then considered to be approximated by that of the discrete model obtained by connecting or assembling the collection of all elements. The disconnection-assembly concept occurs naturally when examining many artificial and natural systems

i)Element Type

Finite element method generation will generate a finite element mesh of node and geometric element type. These geometric element types are relative to the ANSYS element name via an element variant number. The element variant mapping for ANSYS may be displayed by using the FEMGEN.

a)Element used for Thermal Analysis

SOLID 87 (3-D 10-Node Tetrahedral Thermal Solid)

Figure 1 shows the element type SOLID 87 is well suited to irregular meshes the element has element has one degree of freedom, temperature, at each node. The element is applicable to 3-D, Steady-State or transient thermal analysis.

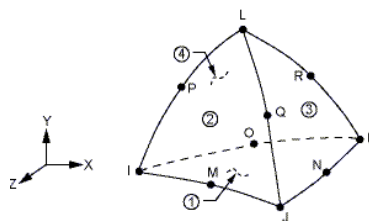


Figure1: SOLID 87 Element Type

b)Element used for Structural Analysis

SOLID 92 (3-D 10-Node Tetrahedral Structural Solid)

Figure 2 show the element type SOLID 92 have a quadratic displacement behavior and are well suited to model irregular meshes. The element is defined by ten nodes having three degrees of freedom at each node: translations in the x, y, and z directions. Temperature and fluencies may be input as element body loads at the nodes. The element also has plasticity, creep, swelling, stress stiffening, large deflection, and large strain capabilities.

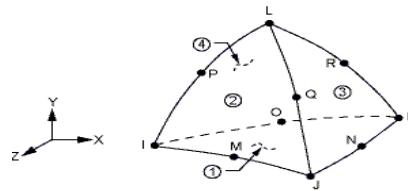


Figure 2: 3D 10-node Tetrahedral Solid Element Type

III. EXPERIMENTAL APPROACH

a) METHODOLOGY

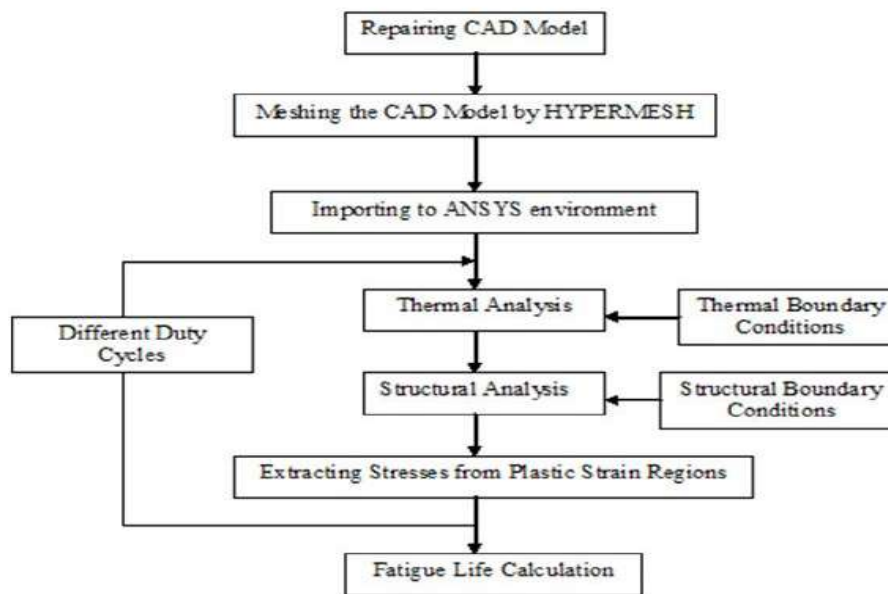


Figure 3: Methodology for thermo mechanical fatigue life

Figure 3 shows the methodology followed to find out the Thermo-Mechanical Fatigue life. This fatigue life is nothing but the number of cycles required to initiate the crack in the component.

b) THERMAL FATIGUE LIFE PREDICATION FOR TURBINE HOUSING

One of the root causes of the engine performance loss is failure of the turbine housing, which is mainly due to the transient thermal loading from the inlet exhaust gas. The cyclic stress generated under cyclic loading varies with temperature. In general, the traditional way to optimize the design of the turbine housing is based on FE Method

This involves: 3D FE Mesh generation of Turbine housing,

- Thermal Analysis with boundary conditions such as heat transfer coefficient and bulk temperature to predict metal temperatures under transient condition
- Transient Metal temperature is used as an input for elastic plastic analysis.

The turbine housing of turbocharger is mounted on Diesel Engine and is made up of Ductile Iron material. FE analysis carried out assuming under free conditions with no effect of the external load [6].

Material Properties

Changes in temperature can significantly vary the material properties. Therefore, both the high and low temperature extremes associated with the application should be considered. For applications subjected to large temperature variation, you'll need to take into account the dimensional change when assembled/bound with other materials of different coefficient of thermal expansion. Following factors that need to be considered when the operating temperatures are above normal room temperature. Part dimensions increase proportional to length, temperature increase, and coefficient of thermal expansion and contraction. Strength and modulus will be lower than at room temperature shows that strength decreases with increasing temperature. Material may

exhibit a rubber-like behavior with low modulus and high degree of drawing. The material properties are changes with the temperature such as yield stress, young's modules and poison ratio.

Thermal Analysis:

Finite element Model is imported to ANSYS to change element type from SOLID 92 to SOLID 87 for TETRA element with Thermal boundary conditions. The thermal boundary conditions applied at the different parts of the housing is tabulated in table 1. These data can be obtained from determined utilizing information regarding the flow velocities inside the volu11te as determined by computational fluid dynamics analysis or turbine gas temperatures measurements calibrated from tests.. The material properties utilized in this analysis were input as a function of temperature as shown in table

Sl.No	Component	Convection Coefficient(W/m ² °C)
1	Inlet Volute	900
2	Wheel Contour	500
3	Outlet Section	500
4	A-Surface	150
5	External	50

Table1: Thermal Boundary Conditions

The thermal simulation solutions enable to model thermal response including all the modes of heat transfer which could be affecting the response simultaneously. The object of the thermal study is often to understand thermal response of the structure. Meshing quality and density will have an influence on the final stress value and deformation. A refined mesh grid should be created in order to obtain an accurate result, especially in the following region:

- Regions of large stress gradient, such as the area around the tongue
- Stress concentration regions, such as at a locating pin hole
- Regions which cracked or failed during the testing or application process
- Other regions, such as on a contact surface.

If there is an external pressure load applied, it is better to use a mapped mesh. Once the loads are applied on the nodes, this will help to eliminate the extra moment caused by the force loads. Another important issue is to select the thermal component when doing the mesh. The ANSYS default requires that the maximum strain increment occurring within one load step not exceed 15%. Thus, during a large temperature or stress gradient time period, more load steps are recommended in order to aid the convergence. Time point density should be more concentrated during time periods when plasticity is likely to occur.

IV. RESULTS

4.1 Thermal Plots

Thermal results are presented with the following guidelines:

1. Temperature distribution at different time point and different angle of view, particularly to show the Maximum Temperature of the component.
2. Figure 4.1 shows temperature for lab test duty cycle.
3. Figure 4.2 shows temperature for City road duty cycle.
4. Figure 4.3 shows temperature for Motorway road duty cycle.
5. Figure 4.4 shows temperature for Country road duty cycle.
6. All the values have been scaled to 0-100.

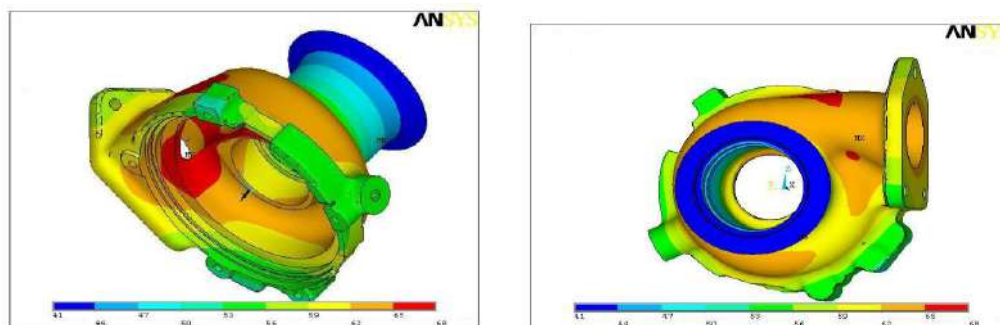


Figure 4.1: - Thermal Plot for Lab Test Duty Cycle

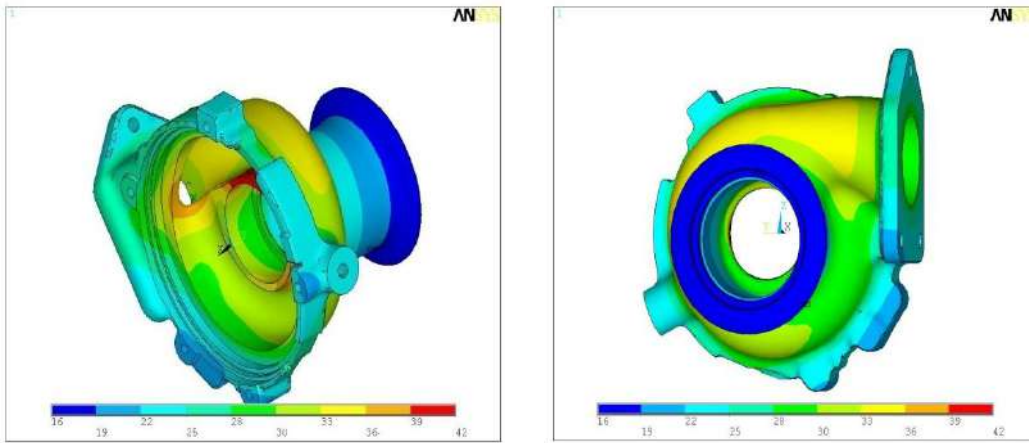


Figure 4.2: - Thermal Plot for City Road Duty Cycle

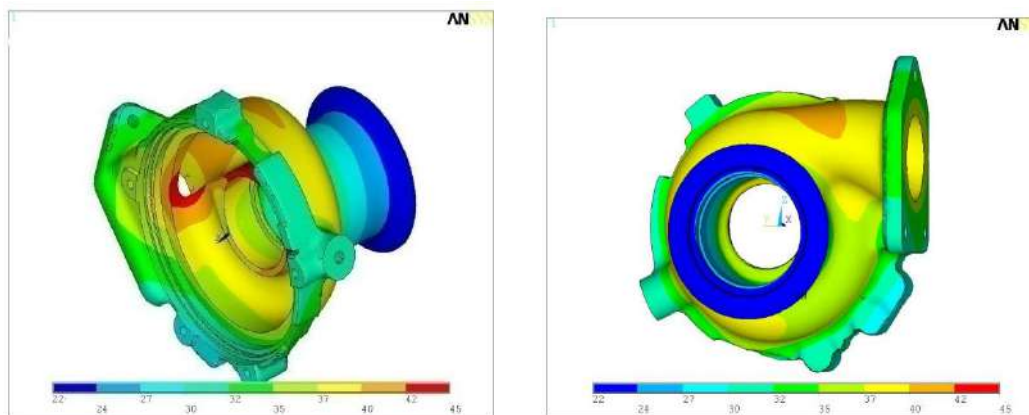


Figure 4.3: - Thermal Plot for Motorway Road duty Cycle

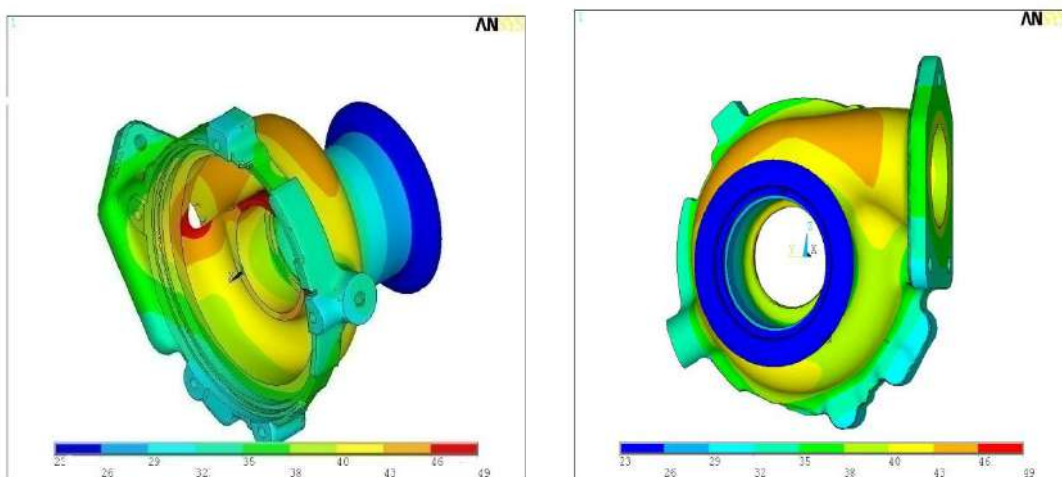


Figure 4.4: - Thermal Plot for Country Road duty Cycle

4. 2 Structural Analysis Plots:

Elasto-Plastic structural analysis results are presented with stress distribution plots for Von-Mises Stress and Plastic Strain. The views are taken with special care to clearly show critical regions that exceed material strength which are likely to fail due to TMF. For non-linear analysis, plastic strain intensity plots are generated.

4.3 Von-Mises Stress plots

Figure 4.5 shows the Von-Mises stress plots represents the beginning of yielding for material due to higher tensile stress the region represents in red color distribution is having higher values and blue color shows the lower yielding stress value. The maximum Von Mises generated in the Turbine housing at tongue region because the thickness of the housing is less at that section, and also as the temperature distribution was more. We can observe the temperature distribution in the Figure4.1 to Figure 4.4

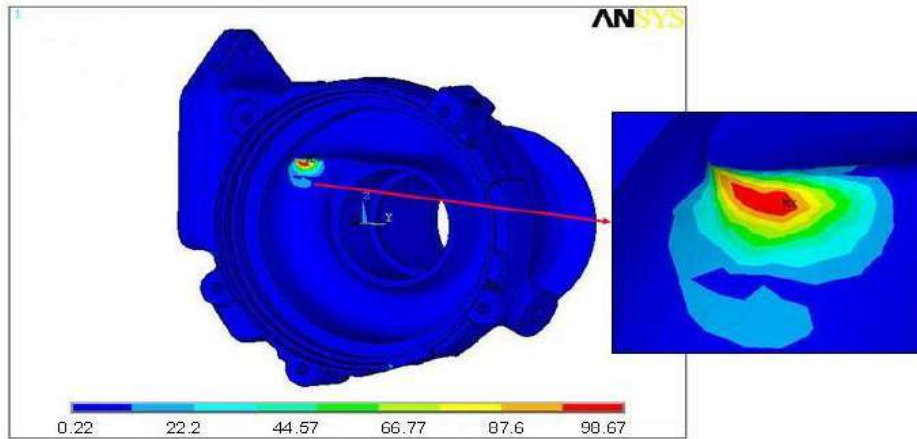


Figure 4.5: Von-Mises stress Plot

4.4 Plastic Strain Intensity Plot:

The figure 4.6 shows the plastic strain in the turbine housing due to thermo-mechanical fatigue. From the figure we can find the strain is max is at the tongue region, which is named as Location: 1. and also other regions where plastic strain may occur are also considered. Those locations are named as Location: 2 and Location: 3, which are considered at neck regions. As there is an abrupt change in geometry stresses may occur at these locations also.

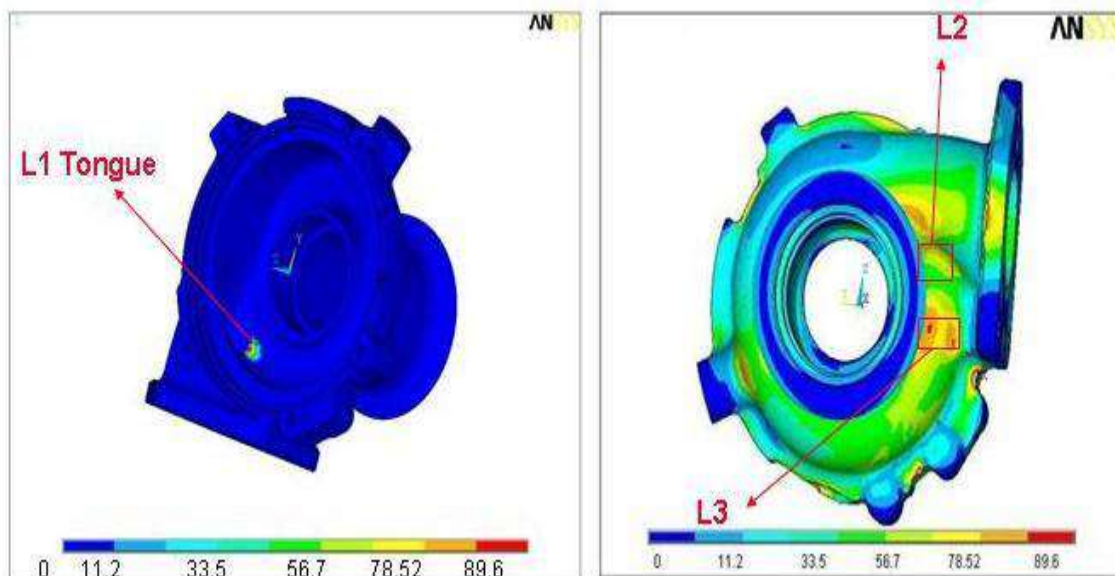


Figure 4.6: - Plastic Strain Plot

V. CONCLUSIONS

The fowling studies were performed on the turbine housingwith the objective to find the Thermo-Mechanical Fatigue life of different duty cycles and to find out the most severe duty cycle. In this study we mostly concentrated mostly on TMF life calculation not on optimization as it requires Computational Fluid Dynamic analysis over the flow of exhaust gas.

1. 3D Thermal, Elastic and Plastic FEA Analysis of the housing with different duty cycles.
2. Stress distribution over the component with comparison of temperature.
3. Thermo-Mechanical Fatigue life calculation by using Chaboche Model for all duty cycles.

5.1 Lab test duty cycle

The figure 4 has shown the comparison of stress distribution, temperature and time. It was obsorbed from the figure that the out-Phase type loading where, as the temperature increases the 3rd principal stress dominates compared to 1st principal stress. Signed Von-Mises stress was used to predict the life as there is a change in shift in between 1st principal stress and 3rd principal stress.

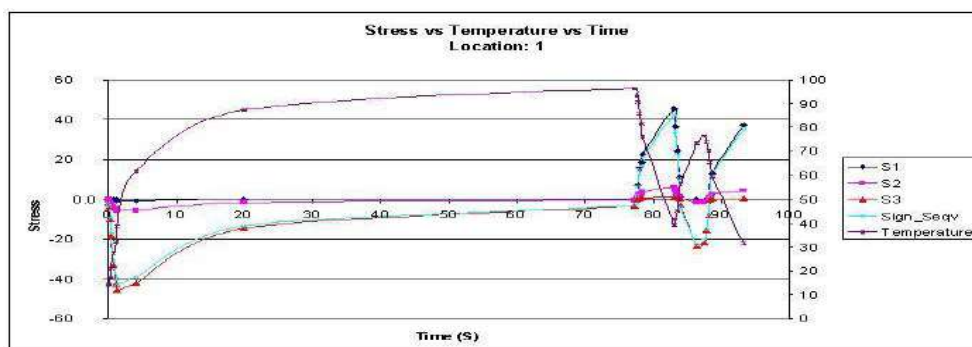


Figure 5.1: 1-Stress Distribution lab test duty cycle

City road duty cycle

The figure 5 has shown the comparison of stress distribution, temperature and time. It was obsorbed from the figure that the out-Phase where, as the temperature increases the 3rd principal stress dominates compared to 1st principal stress. Here all the values are scaled between 0-100 and the maximum temperature was 500⁰C.

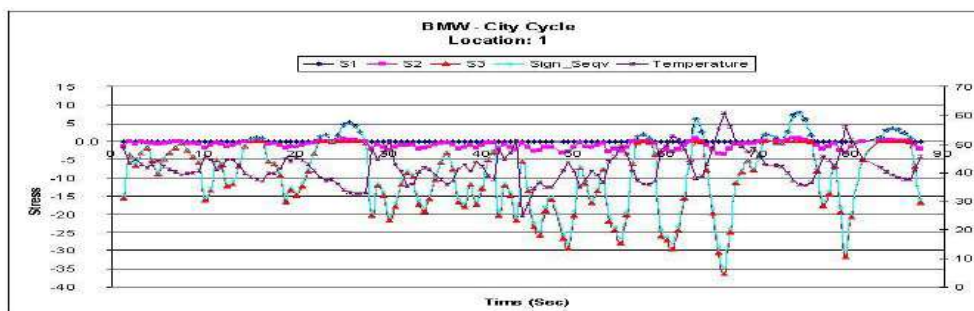


Figure 5.2: 2 Stress Distribution a City road cycle

Motorway road duty cycle

The figure 6 has shown the comparison of stress distribution, temperature and time. It was obsorbed from the figure that the observe Out-Phase where, as the temperature increases the 3rd principal stress dominates compared to 1st principal stress. Here all the values are Scaled between 0-100 and the maximum temperature was 500⁰ C.

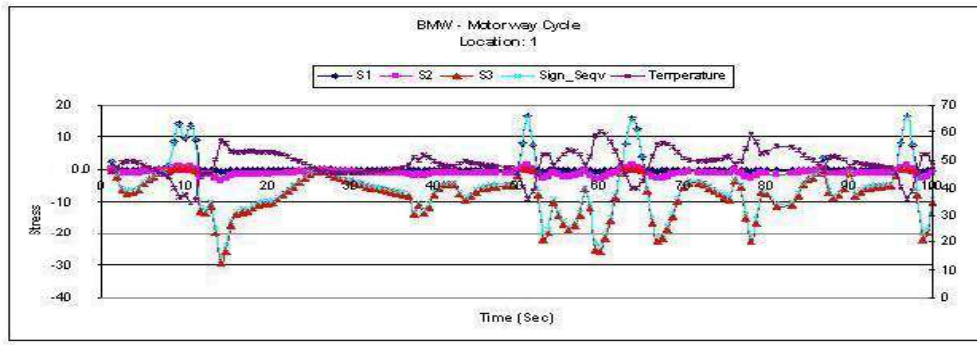
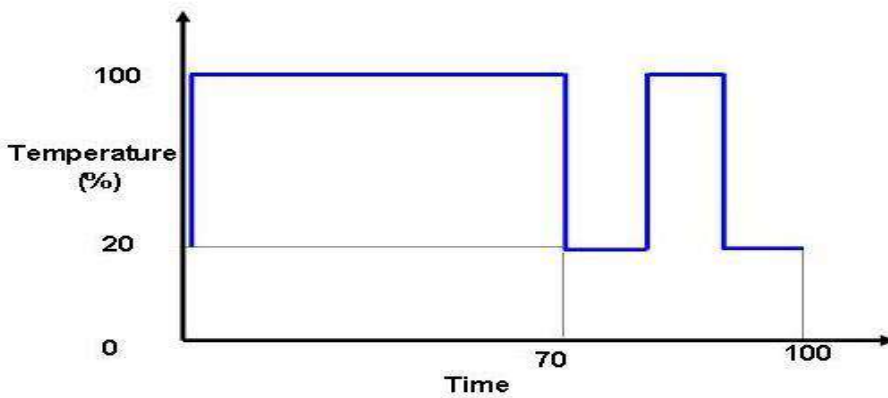


Figure 5.3: 3-Stress Distribution Motorway road cycle

5.2. Duty Cycles

Lab Test Duty Cycle: Graph: 5.1 shows the thermal duty cycle with respective time period. The total cycle time is 800 Sec. Out of that first 70% will be continuous heating then there will be sudden change i.e. cooling phase will happen. The remaining 30% will be alterations of the phases are applied. The maximum temperature of the heating phase is 800c and the minimum temperature at cooling phase is 200c. In order to get exact regions where plastic strain is occurring we considered this much phase

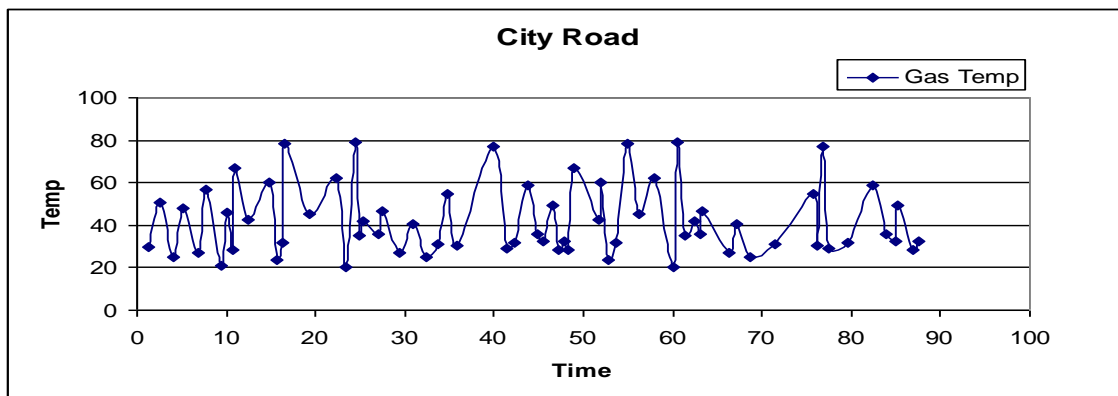


differ

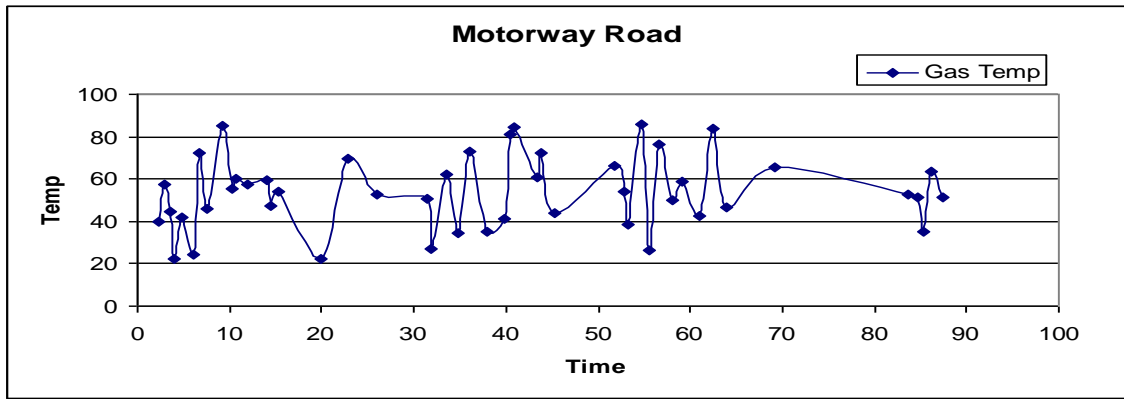
Graph: 5.4-Lab Test Duty Cycle

Field Data Duty Cycles:

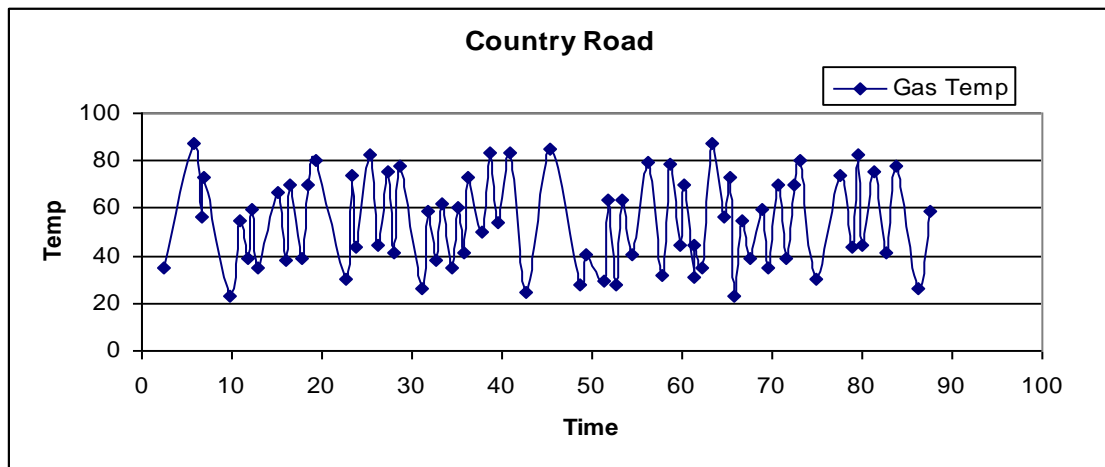
The following graphs shows the different field duty cycles which are obtained from different road conditions, like City road, Motorway road and Country road. The maximum time points in these graphs are 800Sec and the Temperature points also 800Deg C. Exhaust Gas Temperature over a period of time can be observe in the following Charts for various road conditions.



Graph: 5.5-Exhaust Gas temperature at City road



Graph: 5.6-Exhaust Gas temperature at Motorway road



Graph: 5.7-Exhaust Gas temperature at Country road

5.3 .FATIGUE LIFE CALCULATION

The life estimation of the components before crack initiation is calculated by Chaboche’s fatigue model. The causes of cracks during thermal shock testing are low cycle fatigue. If the plastic strain is not varying during the cycle, the material behavior is in the high cycle fatigue regime, where as if plastic strain varies through the cycle, the material behavior is in the low cycle fatigue regime. For design optimization the analyst and designer should minimize the plastic strain amplitude and the tensile stress, when it is occurred at high temperature, as much as possible. Hence we need to normalize or the Signed Von-mises the stress with the tensile strength, evaluated at the instantaneous metal temperature, throughout the thermal cycle. The Closer to UTS the elasto - plastic stress is, the shorter the expected life. But the Chaboche’s model is a stress based model, this bilinear kinematic property of material shows that, if there is a small change in stress creates large change in strain. That result would not be a realistic one.

Analytical Equation for Fatigue life calculation

Chaboche’s fatigue damage model is proposed with normalized stress concept of constant amplitude is given by

$$N_f = \frac{\langle S_u^* - S_{max} \rangle}{\alpha \langle S_{max} - S_l \rangle} \left[\frac{S_{max} - \bar{S}}{C_{nor}} \right]^{-\beta} \dots\dots\dots (1)$$

Where

$$\bar{S} = \frac{\bar{\sigma}}{SU(T)} \dots\dots\dots (2)$$

$$S_{max} = \frac{\sigma_{max}}{SU(T)} \dots\dots\dots (3)$$

$$S_l(\bar{S}) = S_{l0} (1 - b_{nor} \bar{S} / S_u)$$



..... (4)

$$C_{nor}(\bar{S}) = C_{nor0} \left(1 - b'_{nor} \frac{\bar{S}}{S_u} \right) \quad (5)$$

Equation 1 to Equation 5 represents the formulation to calculate fatigue life (Nf). In equation.2 SU(T) represents ultimate tensile strength at instantaneous temperature, as the material properties was changing with temperature mean stress was divided by ultimate tensile strength. Such as Lab Test duty cycle, City road duty cycle, Motorway road duty cycle . Out of all field data duty cycles Country road duty cycle was more severe. From these results we can say that the damage due to lab test duty cycle is the percentage distribution was 40% of Country road 30% of City road and 30% of Motorway road duty cycles

Sl.no	Duty Cycle	Location: 1	Location : 2	Location: 3
1.	Lab Test	2.54E03	1.52E04	2.68E04
2.	City Road	1.04E05	2.86E07	8.49E06
3.	Motorway Road	8.58E05	2.02E09	6.39E06

Table 2: Fatigue life results

Thermo-mechanical analysis on turbine housing of turbocharger suggested high thermal stresses occurring at tongue region of volute. Thermo-mechanical fatigue life was calculated and compared at the regions where plastic strain is occurring for different field data duty cycles.

Fatigue life results show Country road duty cycle is more severe than the other field data duty cycles like City road and Motorway road.

A lab test duty cycle was predicted in such a way that the sum of damage percentage of each field data duty cycle match to it. Study on change in material properties of turbine housing.

Shape optimization of tongue region to reduce stresses, but it is dependent on aerodynamic performance of the turbocharger.

VI. REFERENCES

- [1] Cristiana Delpretea, “Multi axial damage assessment and life estimation: application to an automotive exhaust manifold”.
- [2] Farid AHDAD, Carol CAI, “Finite Element Analysis of Turbine Housing”, Honeywell Turbo Technologies, NUMBER EDI004-23, REVISION 2, PP. 7-16, Date Published: 08-10-2007
- [3] Michal Vajdak, “Thermal Stress Analysis of Turbine Housing”, Honeywell Turbo Technologies, NUMBER 06-0854, REVISION A, Date Published: 12-11-2006
- [4] Mickael Cormerais, Pascal Chesse, Jean-Francois Hetet, “Turbocharger Heat Transfer Modeling Under Steady and Transient Conditions”, Int. J. of Thermodynamics, Vol. 12 (No. 4), PP. 193-202, Date Published: December 2009
- [5] Dr. Farid AHDAD, Ragupathy Kannusamy, Damodharan B., “Analytical Approach of TMF Prediction for Complex Loading”, Honeywell Turbo Technologies, NUMBER GT2010-23440, PP 3-10, Date Published: June 14-18, 2010
- [6] Dr. Farid AHDAD, Ragupathy Kannusamy, Damodharan B., “Analytical Approach of TMF Prediction for Complex Loading”, Honeywell Turbo Technologies, NUMBER GT2010-23440, PP. 3-10, Date Published: June 14-18, 2010



MATRUSRI ENGINEERING COLLEGE

(Approved by AICTE, Affiliated to Osmania University)

#16-1-486, Saidabad, Hyderabad - 500059



Sponsored by

MATRUSRI EDUCATION SOCIETY



ISBN: 97881-936274-0-2





NTSEET
2018



12.
1ST NATIONAL CONFERENCE ON TRENDS IN
SCIENCE, ENGINEERING AND TECHNOLOGY

(NTSEET - 2018)

February 2nd & 3rd - 2018

TECHNICAL PAPER ABSTRACTS



ORGANIZED BY

MATRUSRI ENGINEERING COLLEGE

(Approved by AICTE, Affiliated to Osmania University)

#16-1-486, Saidabad, Hyderabad - 500059



Sponsored by

MATRUSRI EDUCATION SOCIETY

ISBN: 97881-936274-0-2



NATIVITY LANGUAGE PREDICTION USING A DOCUMENT WEIGHTED APPROACH

P. Vijayapal Reddy¹, Raghunadha Reddy. T²

¹Professor, Department of CSE, Matrusri Engineering College, Saidabad, Hyderabad, drpvijayapalreddy@gmail.com

²Associate Professor, Dept of IT, Vardhaman College of Engineering, Hyderabad

Abstract: The task of analyzing an interested text to find demographic characteristics such as gender, age, country and nativity language of an unknown author based on the writing style of the text called Author Profiling. The writing style differences are very important in Author Profiling research. Different researchers proposed several stylistic features to differentiate the writing style of the authors. In this work, the experimentation carried out with content based features like most frequent terms in the corpus to predict the nativity language of the authors. A Profile specific Document Weighted approach is used with most frequent terms as features. In this approach, the document weights are used to represent the document vectors. Various classification algorithms were used to generate the classification model and to predict the nativity language of the authors. The achieved results were good when compared with exiting techniques for nativity language prediction in Author Profiling research area.

Index Terms: Author Profiling, Profile specific Document Weighted approach, Nativity Language Prediction, Term Weight Measure, Document Weight Measure.

I. INTRODUCTION

Author profiling is a text classification technique, which used to create a profile of an author of a text. Such a profile can include the gender, age, location, native language and the personality traits of the author. In author profiling, linguistic features are used to determine the profile of an author and the most common techniques that are used are different kind of machine learning techniques.

Author profiling is an important task in many different domains. For instance, from a marketing perspective, companies may be interested in knowing more about anonymous reviewers written on various product review sites. In forensic linguistics, author profiling can be used to determine the linguistic profile of an author of a suspicious text. This is something that can be valuable for evaluating suspects and as a support in investigations.

From an intelligence perspective author profiling is used to gain more information about a possible suspect - this could for example be a potential violent lone actor that reveals an intention of committing targeted violence in a online setting, something that research has shown is the case in previous attacks. Author Profiling is used to extract as much information as possible about an author may increase law enforcement's chances to advance in their investigations.

Machine learning is the most common approach for author profiling. However, there are some challenges when using these kind of techniques in realistic scenarios. First of all, the availability of labeled data that is used to train machine learning models on is limited. Secondly, the machine learning models may work well on the domain that they are trained and tested on but it is very difficult to predict how they will work on other domains. Therefore, it is very difficult to estimate the accuracy of the results when using author profiling in real-life scenarios. An important note here is to always involve human analysts in the usage of author profiling and only consider this kind of techniques as a support for humans in their analysis.

This paper is organized in 6 sections. The existing work in Author Profiling for nativity language prediction was explained in section 2. The corpus characteristics and performance evaluation measures were explained in section 3. The Profile specific Document Weighted model was described in section 4. The experimental results of PDW model represented in section 5. Section 6 concludes this paper with conclusions and future work.

II. RELATED WORK

Most of the researchers in Author Profiling proposed different types of stylistic features such as character, word, syntactic, content, structural, readability and information retrieval features for predicting the demographic characteristics of the authors[1]. Shlomo Argamon used [2] the corpus of International Corpus of Learner English (ICLE) which is a culmination of non-native English speakers from various countries and the corpus was tested to predict the age, gender and native language. He also used essays of 251 psychology undergraduates at the University of Texas at Austin for neurotism prediction. They considered five sub-corpora namely Russian, Czech Republic, Bulgaria, French and Spanish from ICLE. They used 258 authors writings from each sub corpus to avoid class imbalance problems. While predicting the age, gender, nativity language and neurotism they observed that style based features gave an accuracy of 65.1%, content based features gave an accuracy of 0.823 and both style based and content based features together gave an accuracy of 0.793.

Adamearcia et al., proposed [3] a simple classification method based on similarity among objects. They considered various features such as lemmas and grammatical category of lexical terms, tweets characteristics, subjectivity features and opinion mining analysis for document representation. They predicted gender and language variety from English language tweets.



It was observed that they got good results for gender prediction and low accuracy for language variety prediction. Basile et al., experimented [4] with a single model to predict gender and language variety of four language texts. They used linear support vector machines with a set of features like character 3 to 5 grams, word unigrams, POS tags, twitter handles and geographic entities for generating classification model. They obtained an accuracy of 82.53% for gender prediction and 91.84% for language variety prediction.

Martinc et al., proposed [5] a logistic regression classifier and experimented with different types of features such as character n-grams, word unigrams, word bigrams, word bound character tetragrams, punctuation trigrams, suffix character tetragrams, POS trigrams, character flooding count, document sentiment information, Emojis counts, wordlists specific to language variety. They experimented with different classifiers like Linear SVM, Logistic Regression, Random Forest and XGBoost. Among these classifiers Logistic Regression classifier obtained good accuracy of 86.63% for language variety prediction in English language. They got good accuracies in Portuguese language for gender and language variety prediction.

Ciobanu et al., used [6] character and word n-grams as features and multiple linear SVM as classifier for predicting gender and language variety of authors in different languages. they obtained 75% accuracy for language variety prediction in English language. ogaltsov et al., experimented [7] with high order character n-grams as features and Logistic Regression as classifier to predict gender and language variety of authors in different languages. they achieved 80.92% accuracy for language variety prediction in English language.

III. CORPUS CHARACTERISTICS AND EVALUATION MEASURES

In this section, the corpus characteristics and the measures for evaluating the performance of a classification model is discussed.

3.1 Dataset characteristics

In this work, PAN17-twitter corpus was used for experimentation which was released in 2017. This corpus consists of Twitter posts labeled with gender and their specific variation of their native language English (Australia (AS), Canada (CN), Great Britain (GB), Ireland (IL), New Zealand (NZ), United States (US)). The distribution of the classes is balanced. In total, PAN17-twitter consisted of 360 000 posts with a distribution of 60 000 posts for each class. Table 1 shows the characteristics of the corpus.

Table 1: The characteristics of PAN 17 Twitter English corpus for Nativity Language prediction

Number of Authors	Name	Labels	Number of posts	Label distribution	
3600	PAN17-twitter	Native Language	360000	Ireland	60000
				Canada	60000
				Great Britain	60000
				New Zealand	60000
				United States	60000
				Australia	60000

3.2 Performance measures

In general, when evaluating the results in the experiments in Author Profiling approaches the researchers used accuracy, precision, recall and F1-score was taken into consideration. Accuracy is the most commonly used performance measure which measures the proportion of all predictions that are correct. Using classification accuracy alone for evaluating the performance of the classification algorithm could be misleading, especially if the dataset is unbalanced or contains more than two classes. In this work, accuracy measure was used to evaluate the performance of the classifiers.

IV. PROFILE SPECIFIC DOCUMENT WEIGHTED APPROACH

The Profile specific Document Weighted (PDW) approach is proposed in [8]. The model of PDW approach is depicted in fig 1. In this approach, first the English corpus for nativity language prediction was collected from PAN 2017 competition. Then, preprocessing techniques were applied on the corpus to prepare the content for further analysis. The most frequent terms were extracted from the updated corpus. The term weight measure is used to compute the weights of the terms specific to each nativity language country of documents. The document weight measure is used to calculate the document weight specific to each nativity language country by using the weights of the terms in that document. The document vectors were represented with these document weights. Finally, these document vectors were given to different classification algorithms to generate the classification model and this model is used to predict the nativity language of unknown document.

In this approach, finding appropriate term weight measure and document weight measures are important to improve the accuracy prediction of nativity language prediction.

4.1 Term Weight Measure

The term weight measures assign suitable weights to the terms by considering different types of terms distribution information such inner-document (term distribution within a document), intra-class (term distribution within a positive class of documents) and inter-class distribution (term distribution across classes of documents) in the corpus of documents. In this work, a Supervised Unique Term Weight (SUTW) measure [9] is used to find the weight of the terms specific to every nativity language country. The SUTW measure is shown in equation (1).

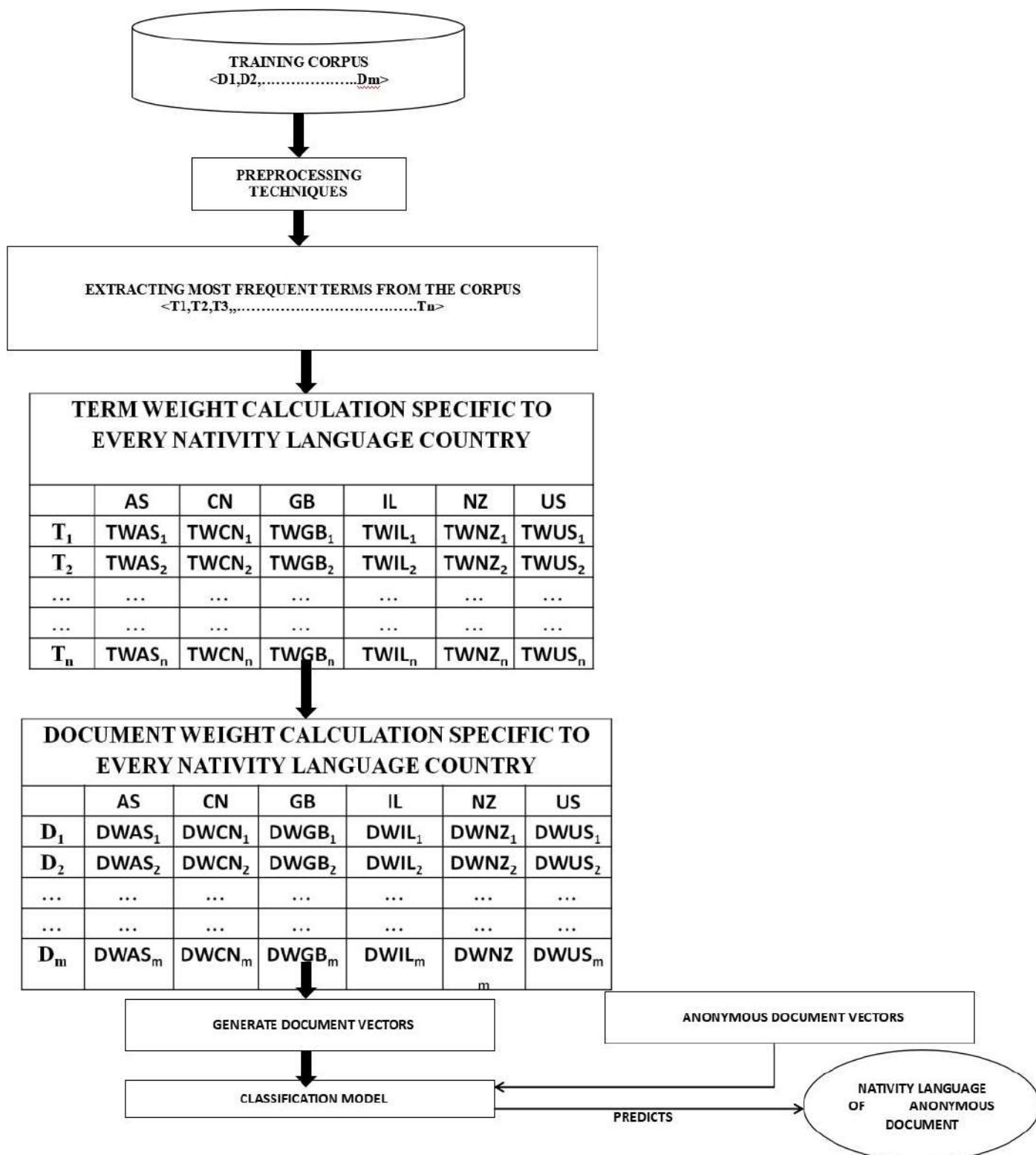


Fig. 1. The model of Profile specific Document Weighted approach



$$W(t_i, p_j) = \sum_{k=1, d_k \in p_j}^m \left(\frac{tf(t_i, d_k)}{tf(t_i, p_j)} \left[\frac{\log(d_{tk})}{0.8 * AVGUT_k + 0.2 * UT_k} \right] \right) \times \frac{a_{ij}}{(a_{ij} + b_{ij})} \times \frac{c_{ij}}{(c_{ij} + d_{ij})} \quad (1)$$

In this measure, $tf(t_i, d_k)$ is the number of times term t_i occurred in document d_k , $tf(t_i, p_j)$ is the number of times term t_i occurred in p_j , d_{tk} is the number of terms in document d_k , UT_k is the number of terms that occurred once in document d_k , $AVGUT_k$ is the average number of unique terms in document d_k , a_{ij} , b_{ij} is the number of documents in profile p_j which contain the term t_i and which does not contain term t_i respectively. c_{ij} , d_{ij} are the number of documents of other than profile p_j which contain the term t_i and which does not contain the term t_i respectively.

4.2 Document Weight Measure

The document weight measure computes the document by using the weights of the terms in that document. In this work, a document weight measure [10] is used to compute the document weight. Equation (2) shows the document weight d_k specific to profile p_j .

$$W_{d_{kj}} = \sum_{t_i \in d_k, d_k \in p_j} TFIDF(t_i, d_k) \cdot W_{t_{ij}} \quad (2)$$

Where, $TFIDF(t_i, d_k)$ is the term frequency and inverse document frequency of term t_i in document d_k and it is represented in equation (3). $TFIDF$ measure assigns more weight to the terms which are occurred in less number of documents. $W_{t_{ij}}$ is the weight of the term t_i in Profile p_j .

$$TFIDF(t_i, d_k) = tf(t_i, d_k) * \log \left(\frac{|D|}{|1 + DF_{t_i}|} \right) \quad (3)$$

Where, $|D|$ is the number of documents in the corpus, DF_{t_i} is the number of documents which contain the term t_i .

V. EXPERIMENTAL RESULTS

In this work, 8000 most frequent terms were extracted from the corpus. The experiment starts with 1000 terms and increased up to 8000 terms by adding 1000 terms in each iteration. By analyzing the corpus of language variety profile, it was observed that the content based features like the terms they used in their writings are different for different nativity language countries authors. It was understand that the selection of words to write a review is almost same for the users of one nativity language country. With this assumption most frequent 8000 terms were extracted from the corpus as features. Different classification algorithms such as Simple Logistic (SL), Logistic (LOG), Bagging (BAG), IBK, Naïve Bayes Multinomial (NBM) and Random Forest (RF) were used to generate the classification model. We obtained good results for nativity language prediction when compared with existing approaches of Author Profiling for nativity language prediction.

Table 2: The Accuracy of PDW model for nativity language of authors prediction using different Classifiers

Classifiers/ Number of Terms	SL	IBK	LOG	BAG	NBM	RF
1000	65.93	61.72	70.28	65.77	70.07	71.92
2000	66.14	62.57	71.11	68.59	74.54	75.89
3000	69.62	64.39	74.42	70.31	77.42	78.34
4000	71.38	65.74	75.20	71.72	78.21	81.71
5000	72.15	68.83	77.78	72.84	79.78	83.47
6000	72.08	70.24	78.46	74.27	81.46	85.41
7000	74.93	72.18	80.52	75.13	82.52	86.91
8000	75.74	73.92	81.14	77.22	84.63	88.57

The accuracies of nativity language prediction in PDW model using term weight measures are shown in Table 2. The Random Forest classifier obtained highest accuracy of 88.57% for nativity language prediction when compared with all other classifiers. The Naïve Bayes Multinomial classifier obtained an accuracy of 84.63% for nativity language prediction. It was observed that in all classifiers the accuracies of nativity language prediction was increased when the number of terms increases.

VI. CONCLUSION AND FUTURE SCOPE



This work was delimited to author profiling of native language on text written in English language. In addition, it was observed that how the PDW approach performed on different classifiers by comparing a number of different machine learning models for author profiling. Out of six evaluated classifiers, the results showed that the overall best performing classifier was the Random Forest classifier which outperformed the other classifiers. The Random Forest classifier obtained 88.57% accuracy for nativity language prediction when 8000 terms were used as features. How well each model performs on author profiling depends on many factors such as the size of the dataset, the balancing of the dataset is and the preprocessing techniques used to prepare the data for classification.

A potential extension would be to perform author profiling on text in other languages such as Spanish, Dutch and Arabic of PAN 2017 competition using similar models as used in this work. Also, another potential extension could be to discern information as personality traits, such information were for example included in the PAN 2015 dataset.

REFERENCES

- [1] T. Raghunadha Reddy, B.VishnuVardhan, and P.Vijaypal Reddy, "A Survey on Authorship Profiling Techniques", International Journal of Applied Engineering Research, Volume 11, Number 5 (2016), pp 3092-3102.
- [2] Argamon, S., Koppel, M., Pennebaker, J. W., and Schler, J. (2009). Automatically profiling the author of an anonymous text. Communications of the ACM, 52(2):119.(2009).
- [3] Yaritza Adame-Arcia, Daniel Castro-Castro, Reynier Ortega Bueno, Rafael Mu-ñoz, " Author Profiling, instance-based Similarity Classification", Proceedings of CLEF 2017 Evaluation Labs, 2017.
- [4] Angelo Basile, Gareth Dwyer, Maria Medvedeva, Josine Rawee, Hessel Haagsma, and Malvina Nissim, " N-GrAM: New Groningen Author-profiling Model Notebook for PAN at CLEF 2017", Proceedings of CLEF 2017 Evaluation Labs, 2017.
- [5] Matej Martinc, Iza Škrjanec, Katja Zupan, and Senja Pollak, " PAN 2017: Author Profiling - Gender and Language Variety Prediction", Proceedings of CLEF 2017 Evaluation Labs, 2017.
- [6] Alina Maria Ciobanu, Marcos Zampieri, Shervin Malmasi, Liviu P. Dinu, " Including Dialects and Language Varieties in Author Profiling", Proceedings of CLEF 2017 Evaluation Labs, 2017.
- [7] Alexander Ogaltsov and Alexey Romanov, " Language Variety and Gender Classification for Author Profiling in PAN 2017", Proceedings of CLEF 2017 Evaluation Labs, 2017.
- [8] Raghunadha Reddy T, Vishnu Vardhan B, Vijayapal Reddy P, "Profile specific Document Weighted approach using a New Term Weighting Measure for Author Profiling ", International Journal of Intelligent Engineering and Systems, Nov 2016, 9 (4), pp. 136-146. DOI: 10.22266/ijies2016.1231.15
- [9] Raghunadha Reddy T, Vishnu Vardhan B, Vijayapal Reddy P, "A Document weighted Approach for Gender and Age Prediction", International Journal of Engineering, Volume 30, No. 5, 2017, PP. 647-653.
- [10] Raghunadha Reddy T, Vishnu Vardhan B, Vijayapal Reddy P, "Author profile prediction using pivoted unique term normalization", Indian Journal of Science and Technology, Vol 9, Issue 46, Dec 2016.



MATRUSRI ENGINEERING COLLEGE

(Approved by AICTE, Affiliated to Osmania University)

#16-1-486, Saidabad, Hyderabad - 500059



Sponsored by

MATRUSRI EDUCATION SOCIETY



ISBN: 97881-936274-0-2





DYNAMIC EVALUATION OF EMBEDDED SYSTEMS

HARA GOPAL MANI PAKALA

Professor and Head

Electronics and Communication Engineering Department

Matrusri College of Engineering Saidabad Hyderabad Telangana 500059 India matrusri.hodece@gmail.com

Abstract: In the past decade, along with growing embedded systems complexity, the industry's perspective on the inadequacy of current system design methods and requirement of handling verification issues has gathered strengths due to economic reasons. This paper presents a practical application of *dynamic evaluation* method for handling the design verification issues in embedded system applications. This includes dedicated instrumentation for test case generation and evaluation. A practical case study of Signal Processing system describes the dynamic evaluation with the support of dedicated instrumentation and functional test case generation.

Index Terms — Embedded Systems, Design verification instrumentation, Dynamic evaluation, Input domain model

I. INTRODUCTION

Embedded systems, while becoming omnipresent and their complexity is growing at unprecedented rates in several market segments. The industry's perspective on the inadequacy of current system design methods and requirement of handling verification issues has gathered strengths mainly due to economic reasons [1]. The CES system design process is complex in a literary sense and in the initial phase of development the CES *uncertainty* is highest [2-3]. In the initial stages of development the cost of rectifying defects is relatively low. The introduction of system models and applying testing techniques much earlier in the lifecycle reduces the uncertainty and cost of development. Introduction of formality at higher levels, provide wider choices of model based tests to become a reality, viz., specification to design, to other levels of development. In [3] an incremental verification paradigm is proposed that introduces integration early in the design cycle and reduces uncertainty. Design verification is an essential step in the development of any system, especially for Complex Embedded Systems. Verification is the process of showing that system meets its specification. If specifications or test oracles are sufficiently precise and informative, verification can be a more objective technique than validation, which is used to validate user requirements.

This paper proposes *dynamic evaluation* method for design verification of an embedded system application. The section 2 describes related works. An overview of the *dynamic evaluation* method for design verification of embedded system applications is proposed in section 3. The section 4 briefly introduces functional tests and describes proposed procedure for Test case generation. The example case-study of Harbour Surveillance System described in section5 is used for illustrating the ideas proposed in this paper. Typical Test Sequence generated and expected outputs are shown.

II. Related Works

A great deal of effort was put in developing methodologies for all aspects of embedded systems product development life cycle [4, 5]. The authors [4] focus on product validation testing, combinatorial approaches and boundary conditions. Examining Complex and Embedded systems and software testing, it explains the use of simulation and emulation to complement testing. A practical overview of embedded software testing in a structured way is presented by the authors [5] along with ingredients of testing process and test design techniques. In [6] referring to the research directions for integration



in embedded and cyber-physical systems, the authors point deficiencies for high-quality and error-free systems integration. They suggest a relook on integration associated challenges and provide summary of current advances.

The verification and validation techniques that are reported can be categorized into (a) language dependent [7] (b) special tool / framework) [8-9], commercial tools [10] and also as instrumentation / environment [11]. Many different kinds of techniques and tools have been developed to answer specific testing concerns of embedded Systems [8-9]. The author in his thesis [8] proposes visual modelling of system along with its environment for complete verification of models and executable codes. UPPAAL [9] verifies embedded systems that can be modeled as networks of timed automata extended properly. Such approaches may work in the presence of the required specifications; they are not applicable in many cases in which appropriate specifications do not exist.

The author describes a commercially available tool “Test Weaver” used by automobile industry [10]. The tool approaches the task of system test and validation based on a combination of closed-loop system simulation and autonomous, intelligent exploration of the reachable system states. Published application reports indicate that the tool provides high test coverage with a relatively low work effort required for the test specification. In other example the authors present ESIDE [11], an integrated development environment for component-based embedded systems. Many researchers have created techniques for using dynamic execution information to verify system correctness [12] using program properties. In practice, a large percentage of faults involve problems with functional behavior, configuration errors, and misuse of resources in critical sections [13].

At present several researchers are pursuing verification issues of Embedded Systems. This paper is also is based on dynamic evaluation for design verification but uses dedicated instrumentation and functional tests for test case generation. This method is useful for verification complete system.

1. *Dynamic Evaluation Method*

The V-model constitutes the reference product development life cycle (PDLC) model for the development and testing of embedded systems in several application domains. System test can be broadly categorized as (i) development and (ii) operation tests. From specification to design to development tests fall under “verification category”. Verification is a process for determining the performance of a product design relative to the specifications on which the design was based upon [14]. More generally it is evaluation of whether or not a product, service, or system complies with a regulation, requirement, specification, or imposed condition. Though test generation techniques are being proposed for verification problems [15], testing alone as a means of verifying is rarely sufficient, and cannot guarantee correctness. Design verification starts with an implementation and confirms that the implementation meets its specifications. The basic principle behind verification consists of two steps: the first is a transformation (*verification transformation*) from specifications to an implementation; and in the second step, the result from the verification is compared with the result from the design for detecting any errors. Obviously, the more different the design and verification paths, the higher confidence the verification produce. In this paper *dynamic evaluation* is considered for achieving design verification of embedded system under development. Dynamic evaluation is defined very broadly [16]: in which either the object or the method of evaluation is changing and dynamic. However for this paper the more restricted definition, “Dynamic evaluation is the process of verifying a system (referred to as the target system) while it is executing” is being followed. A stepwise dynamic evaluation method for the verification of embedded system is illustrated in figure 1. The ‘design and prototype’ step indicates any general embedded system development method like [17-18] or rapid-prototype [19] may be used. The prototyping itself is a development methodology according to IEEE, with clear advantages [20]. Else rapid-prototype (temporary or limited design) may be used. Both approaches have their merits [20-21]. Alternately an adaptive design method [22] that supports step-wise design and verification can be adopted, if the requirements are hazy.

This includes parallel development of ‘target modular hardware architecture’ and application software. If the application (product) permits selection of ‘modular hardware architecture’ then the prototype will eventually become the final system design. Development of software involves plan and sequencing of implementing algorithms that are computationally intensive, require more resources, but also improve system performance. The prototype development, as mentioned earlier, will have *multiple levels of integration phases* [23] whatever may be the implementation architecture and technology; and they are to be supported during the dynamic evaluation. The focus of the paper is on design verification using dynamic evaluation method. For verification, detailed observations of the ES execution behaviour are checked at runtime against properties that specify the intended system behaviour. These properties are generally from the target application’s requirement specification, or sometimes the properties to be monitored may form the entire specification. The targets ES

itself must be instrumented to report events that are relevant for monitoring that the properties are satisfied on a particular execution. This instrumentation is based on the architecture of the Monitoring method.

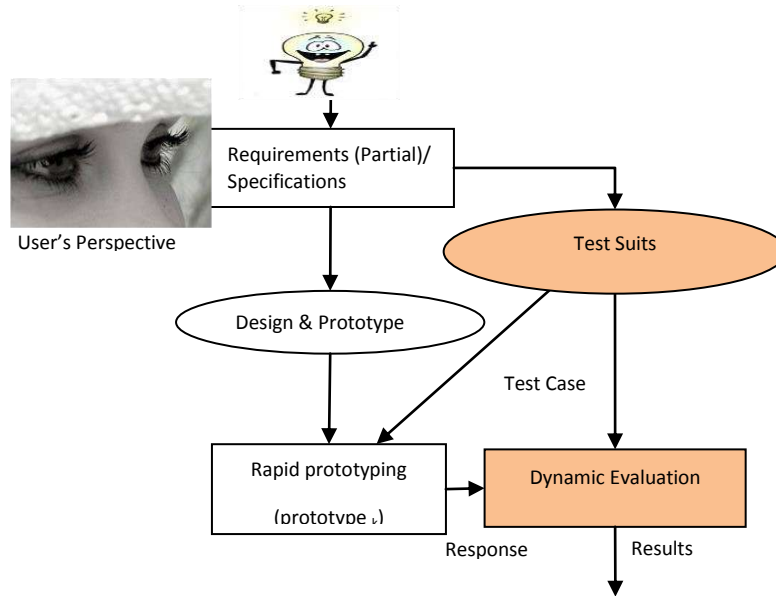


Figure 1: Dynamic Evaluation Method for Verification of Embedded System

The architectural requirements for evaluation, in addition to the target embedded system prototype are: (i) input test-sequences (ii) monitoring and (iii) verification mechanisms. The test case generator takes input from the Domain model of the of the application domain or can be directly generated based on a model. The model should further describe mapping from input values to properties: for each input element, the model defines what properties an execution on that input should satisfy. The test case generator generates input test-sequences and expected response for the application. These architectural elements of ES evaluation are depicted in figure 2.

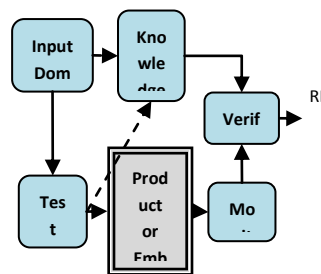


Figure 2: Architecture

A PC based dedicated real time *Verification Instrumentation for Test and Evaluation* with the following features is reported by the author(s) [24]:

1. Test case generation architecture simulates and generates Test case data off-line and inputs test sequence data in real time. Input domain model based on dynamic test scenarios is used for simulation in MATLAB.
2. The Hybrid Monitoring system architecture is distributed between the target-ES Boards and “separate and dedicated card-cage with separate mother board” as shown in figure3.

3. On separate mother board of target system card-cage, Monitoring and acquisition port (MAP1) and handshake signals are terminated. On the boards the Monitoring and acquisition port (MAP2) and handshake signals are terminated on a separate edge-connector located at the top of the board, which need not be used in the actual operation. Similarly on the mother-board. The software (code) does not interfere as the MAP's are not in use in the actual operation.
4. The Instrumentation can monitor/ acquire intermediate and other levels outputs of the prototype system under evaluation. The Instrument architecture is shown in figure 4.

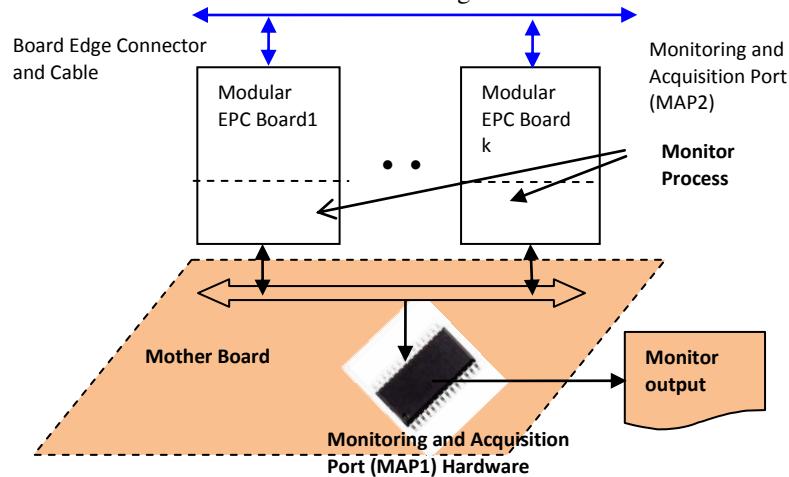


Figure 3: Hybrid Monitoring Architecture

Similar instrumentation is required for dynamic evaluation of prototype along with test case generation and expected output response by the based on input-domain. referred to [24] for of hardware and other data acquisition of data for evaluation. section an acoustic system case study used the functional test to complete the evaluation of ES.

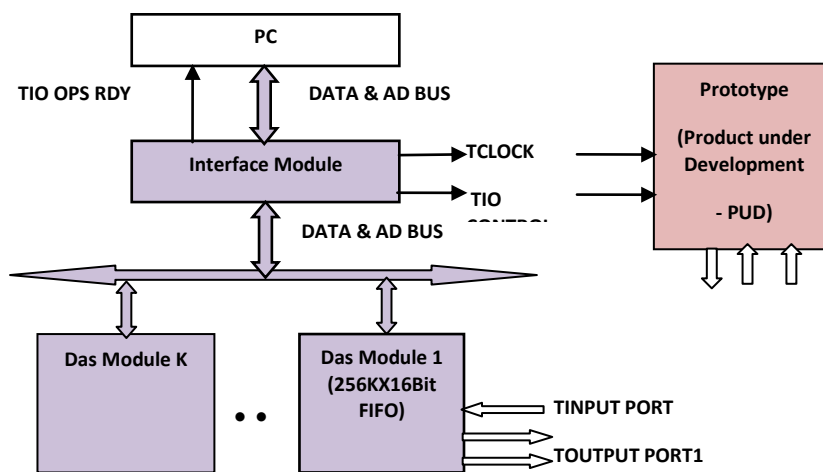


Figure 4: VITE Architecture]

prototype Readers more details software, and /monitoring In the next detection to describe methodology, dynamic

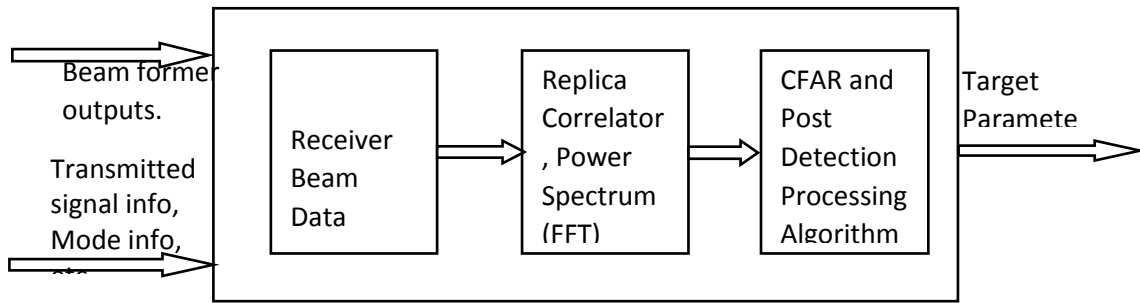


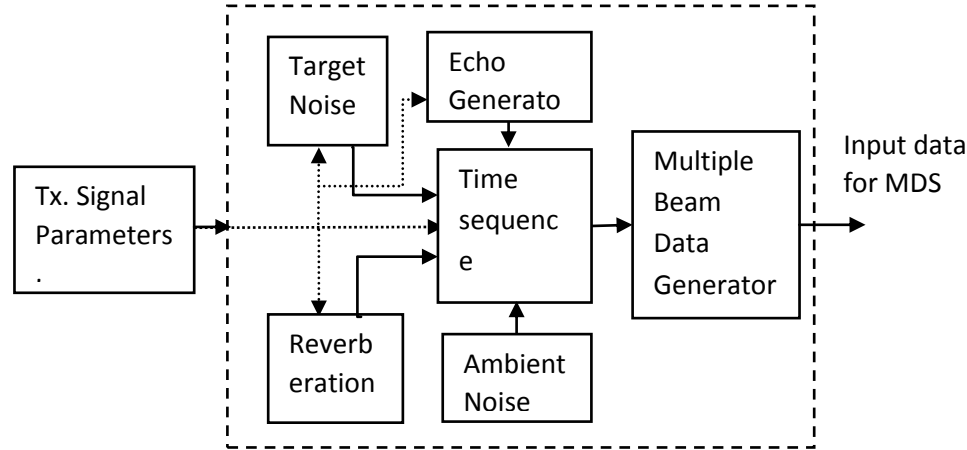
Figure.5 Multi-mode Detection Subsystem

2. CA
SE
ST
UD
Y -
MU
LTI
-
MO
DE
DE
TE

CTION SUBSYSTEM

In most Sonar systems, Harbour surveillance to Ship-systems [25-26], the all-important signal processing subsystem is Acoustic Detection Subsystem, which normally operates in several modes of operation and popularly called Multi-mode Detection System (MDS). As per selected mode of operation Sonar Transmitter transmits (if active) a selected type of signal. Otherwise the passive signal only is received by the Receiver. MDS operates on the data received from Digital Receiving Beam-former (DRB) for detecting target(s) and estimate target parameters. The main functions of MDS are (i) Acquire data from DRB (ii) Perform Detection Algorithm based on mode (iii) Perform Constant False Alarm Rate (CFAR) (selected) algorithm (iv) Perform Post Detection Processing(PDP) (v) Generate target parameters. MDS block diagram is given in figure 5. For more details on Sonars readers are referred to [26].

The mode subsystem



Multi-Detection functional

Figure 6: Input Domain Model for MDS

requirement, target detection problem can be written as binary hypothesis testing [27], where H_0 indicates absence of target and H_1 its presence.

$$\begin{aligned} H_0: \mathbf{x}(t) &= \mathbf{n}(t) + \mathbf{r}(t) \\ H_1: \mathbf{x}(t) &= \mathbf{e}(t) + \mathbf{n}(t) + \mathbf{r}(t); \end{aligned} \quad (1)$$

where $x(t)$ is the observed or received signal, $r(t)$ is the reverberation noise generated by the transmitted signal, and $n(t)$ represents white noise. The signal transmitted in the active mode $s(t)$ can be a PCW / LFM / any other signal and $e(t) = f\{s(t)\}$ is the reflected echo of $s(t)$. In passive mode $s(t) = 0$ and $r(t) = 0$; the signal of interest is self-generated noise-signature of the target that is buried in $n(t)$. The solution to this problem provides Detection algorithms [28], under given assumptions of noise and reverberation statistics. Interested readers may refer [29] for more information on models of noise and reverberation; and for some detection algorithms like Replica Correlation. The generation of signal $x(t)$ by modeling implies the complete input domain of the application [28-29].

The signal $y(t)$ at the input of Digital Receive Beam former is transformed into beam outputs $z(n, \zeta_m)$, where ζ_m is the pointing angle of main response axis of the beam; m is an integer indicating the number of parallel beams formed. The various beam outputs that are inputs to Multi-mode Detection subsystem are represented by $x_m(t)$ and $x(t)$ represents any of the beam outputs. For passive mode no active signal $s(t)$ transmission takes place. As $x(t)$ and $y(t)$ are related to each other linearly, the modelling and generation of $y(t)$ serves as test-sequence. However some components of $y(t)$ are characterized in a statistical sense only; e.g., noise or reverberation. The parameters of performance for Multi-mode Detection Subsystem are statistical quantities of the application context viz. ocean environment's physical phenomena characterized by the noise, reverberation and echo, during active mode. These models are required for generating the received signal $y(t)$ or $x(t)$. This requires modeling and generation of noise, reverberation and echo signals and several parameters are involved, giving rise to typically several sets of test cases whose parametric values range from minimum, typical, and maximum. The modelling issues are very similar and details are given in [29]. Figure 6 illustrates input data generation for MDS.

3. Case Study: Test-Data Sequences Generation:

The input model generates one beam, one PRI data belonging to single target and multi beam model generates single target multiple beams of data for storing in PC. The VITE [24] can input data to MDS or its (PROTO); and acquire output data, else, it can be stored in a file. This data can be taken as an input by application software for evaluating a detection algorithm and the output data can be observed. The data is generated offline using MATLAB. Examples of data sequence generated for typical operational conditions are shown in this section. Only Gaussian ambient noise input signal with TVG is shown in Figure 7(a). The x-axis is in time and the y-axis shows amplitude in numerical values. In Figure 7 (b) ambient noise plus reverberation for a PCW signal is shown. The axis markings are similar. The pulse width used is 60 ms and data is generated for one PRI of 3.75seconds.

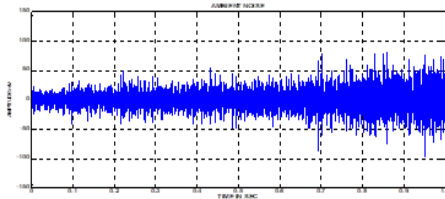
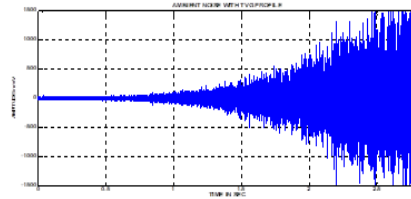


Figure 7(a): Ambient noise input;



(b) Ambient noise input signal with TVG.

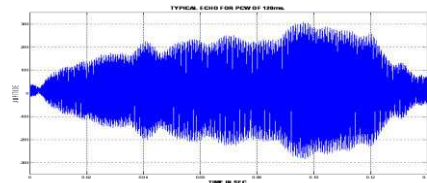
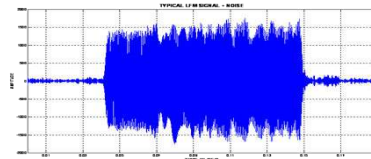


Figure 8 (a) PCW echo



(b) LFM echo with Noise.

Figure 8 shows typical echoes generated by transmitted PCW and LFM type of signals for a PW of 120 ms with additive noise. For the Ambient Noise plus Reverberation (LFM PW=120ms) with TVG data is given as an input to Correlator and Cell averaging constant false alarm rate (CA-CFAR) threshold computation algorithms. The input data and the Correlator output in blue color are shown in figure 9. The computed threshold is plotted in the same figure in red color. The expected data is on left side of the figure and the actual outputs are on the right side. It is to be noted that the input data is first generated using MATLAB and then later modified for giving as input to the



hardware.

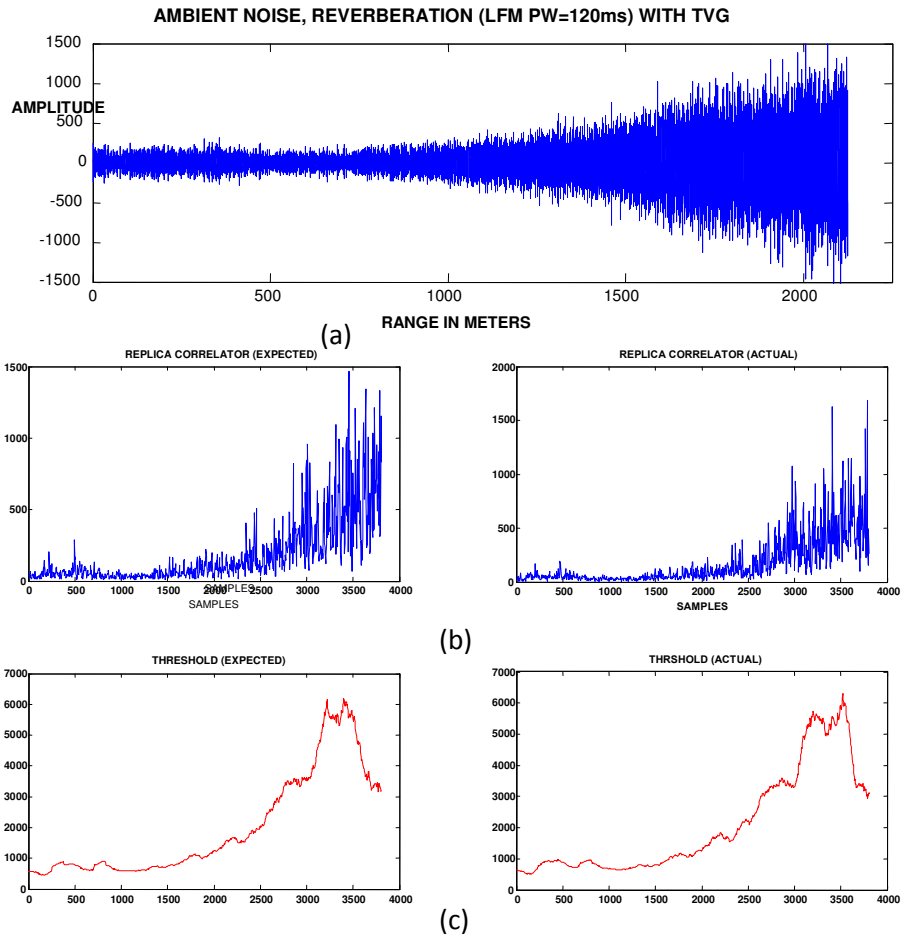


Figure 9: Expected (Left) vs. Actual (Right) outputs for the input data shown in (a) Replica Correlator Output (blue) (c) Threshold computed using CA-CFAR (Red)

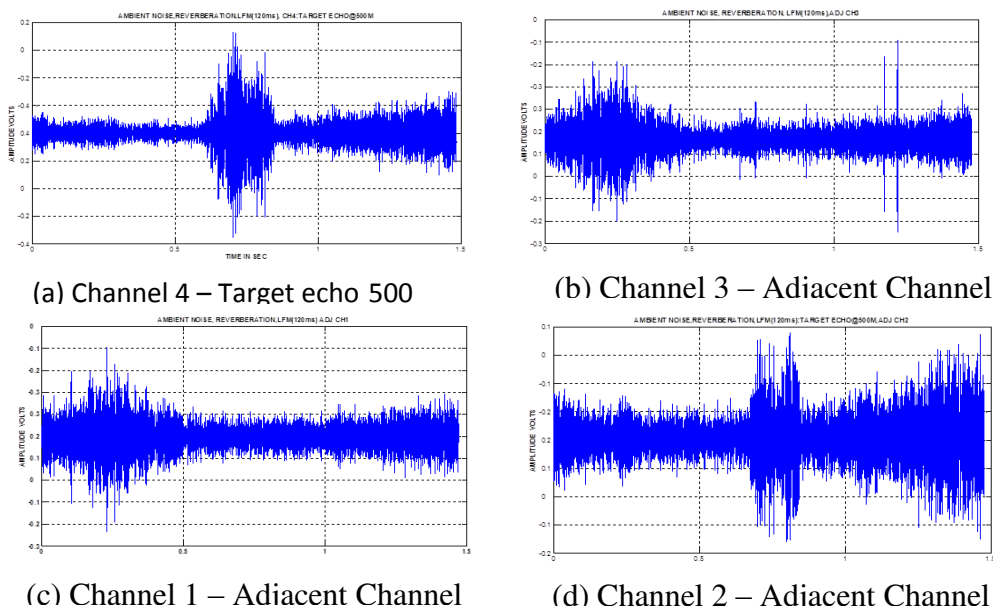


Figure 10: Adjacent Channel (beam) data generation



MDS requires beam former output data (beam /channel data) as input. Taking transmitted signal as LFM of 120 ms and target echo at 500M, simulated data generated for channel 4 (beam 4) is shown figure 9(a). Using this three adjacent channels data generated is shown in figure 10. (b) to (d). The Ambient Noise plus Reverberation (LFM PW=120ms) with TVG plus echo data generated via MATLAB is shown in figure 11(a). This data is converted to digital form and given as an input to target-board for computing Replica Correlator with exact reference and the output data is plotted in blue colour figure 11(b). On the Correlator output data CA-CFAR threshold computation algorithm is applied and threshold is computed. The threshold computed data is plotted in red colour are shown in figure 11 (c). Target echo presence at 1900M is clearly shown in the figure. Note the x-axis is in sample numbers and y-axis is the value in 16 bits.

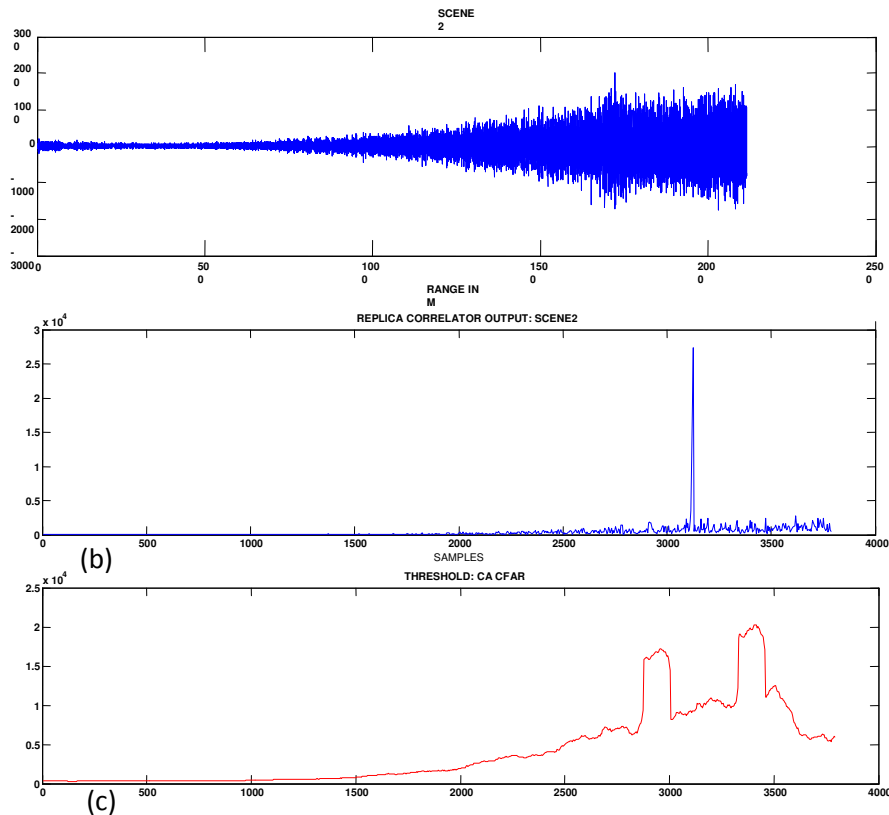


Figure 11: Target board output at level1 and level2 (a) Input data [(b) Correlator Output (Blue), (c) Threshold using CA-CFAR (Red)]

IV. CONCLUSION

This paper proposed *dynamic evaluation* method for design verification of an embedded system application. The dynamic evaluation architecture described and it involves test case generation based on functional testing. An overview of the basic steps of embedded system Test case generation is described. The example case-study of Harbour Surveillance System is used for illustrating the ideas presented. Test cases generated, design verification outputs for certain input data are presented.

REFERENCES

1. RTI. The Economic Impacts of Inadequate Infrastructure for Software Testing. Technical report, National Institute of Standards and Technology, May 2002
2. Zimmermann, Markus, et al. "On the design of large systems subject to uncertainty." *Journal of Engineering Design* 28.4 (2017): 233-254.
3. Hara Gopal Mani Pakala (2017)-An Incremental Verification Paradigm for Embedded Systems. 40-49. 10.1007/978-981-10-5427-3_5
4. Kim H. Pries, Jon M. Quigley, Testing complex and embedded systems. 2010 CRC Press Taylor & Francis Group.
5. Bart Broekman and Edwin Notenboom. Testing Embedded Software. Addison-Weseley, 2003



6. Feiler, Peter, et al. "Architecture-led Diagnosis and Verification of a Stepper Motor Controller." 8th European Congress on Embedded Real Time Software and Systems (ERTS 2016). 2016
7. Elshuber, Martin, Susanne Kandl, and Peter Puschner. "Improving System-Level Verification of SystemC Models with SPIN" 1st French Singaporean Workshop on Formal Methods and Applications (FSFMA 2013). Eds. Christine Choppy, and Jun Sun. Vol. 31. Schloss Dagstuhl--Leibniz-Zentrum fuer Informatik}, 2013.
8. Nokovic, Bojan. Verification and Implementation of Embedded Systems from High-Level Models. Diss. 2016
9. G. Behrmann, A. David, and K. G. Larson. A tutorial on UPPAAL. <http://www.uppaal.com>, 2004.
10. Tatar, Mugur, and Jakob Mauss. "Systematic Test and Validation of Complex Embedded Systems." ERTS-2014, Toulouse (2014): 05-07.
11. Nicholas T. Pilkington, Juncao Li, and Fei Xie, "ESIDE: An Integrated Development Environment for Component-Based Embedded Systems" 33rd Annual IEEE Intl. Conference COMPSAC 2009. <http://www.computer.org/portal/web/csdl/doi/10.1109/COMPSAC.2009.48>
12. Willem Visser, Klaus Havelund, Guillaume Brat, SeungJoon Park, and Flavio Lerda. Model checking programs. *Automated Software Engineering*, 10:203–232, 2003.
13. Nigel Jones. A taxonomy of bug types in embedded systems, October 2009. <http://embeddedgurus.com/stack-overflow/-2009/10/a-taxonomy-of-bugtypes-in-embedded-systems/>
14. System verification: proving the design solution satisfies the requirements, by Jeffrey O. Grady, 2007, Elsevier Inc.
15. Prab Varma, "Design Verification Problems: Test To The Rescue?" Proceedings of the IEEE International Test Conference 2003 (ITC'03).
16. Web Dictionary of Cybernetics and Systems: http://pespmc1.vub.ac.be/ASC/Dynami_Evalu.html
17. Xuan F Zha and Ram D Sriram "Platform-based product design and development: A knowledge-intensive support approach", Knowledge-Based Systems, Volume 19, Issue 7, November 2006, Pages 524-543
18. Lesley Shannon, Blair Fort, Samir Parikh, Arun Patel, Manuel Saldaña and Paul Chow, "A System Design Methodology For Reducing System Integration Time And Facilitating Modular Design Verification". FPL2006
19. Rui Wang and Shiyuan Yang, "The Design of a Rapid Prototype Platform for ARM Based Embedded System", IEEE Transactions on Consumer Electronics, Vol. 50, No. 2, MAY 2004, p746-751.
20. Fabrice Kordon and Luqi, "An Introduction to Rapid System Prototyping", IEEE Transactions On Software Engineering, Vol. 28, No. 9, September 2002, p817-821.
21. Baldwin, Carliss Y. and Kim B. Clark. "Modularity in the Design of Complex Engineering Systems." In Complex Engineered Systems: Science Meets Technology, edited by Ali Minaei, Dan Braha and Yaneer Bar Yam. Springer-Verlag, 2006.
22. Hara Gopal Mani Pakala, Dr PLH VaraPrasad , Dr. Raju KVSVN , and Dr. Ibrahim Khan, "An Adaptive Design Verification Methodology for Embedded Systems" International Journal of Ad hoc, Sensor & Ubiquitous Computing (IJASUC) Vol.2, No.3, September 2011.
23. Abel Marrero Pérez, Stefan Kaiser, "Integrating Test Levels for Embedded Systems", Proceedings TAIC-PART'09. 2009 Testing: Academic and Industrial Conference - Practice and Research Techniques, p184-193.
24. Hara Gopal Mani Pakala, Dr PLH VaraPrasad , Dr. Raju KVSVN , and Dr. Ibrahim Khan, "Development of Instrumentation for Test and Evaluation of a Signal Processing System". Journal of the Instrument Society of India, 40 (1) March 2012.
25. Harbor Surveillance Systems - <http://www.dsit.co.il/siteFiles/1/84/5379.asp>
26. Ashley Waite, "Sonar for Practising Engineers" 3rd edition , John Wiley & Sons Ltd, 2002.
27. Michael A. Ainslie, "Principles of Sonar Performance Modeling". Springer-Praxis Books, 2010.
28. PC Etter - Underwater acoustic modeling and simulation. Spon Press; 3 edition (April 4, 2003)
29. Pascal A.M. de Theije, Hans Groen, "Multi static Sonar Simulations with SIMONA" Proceedings of 9th International Conference on Information Fusion, July 2006, Florence, Italy.

1ST NATIONAL CONFERENCE ON TRENDS IN SCIENCE, ENGINEERING AND TECHNOLOGY (NTSET - 2018)

February 2nd & 3rd - 2018

TECHNICAL PAPER ABSTRACTS



ORGANIZED BY

MATRUSRI ENGINEERING COLLEGE

(Approved by AICTE, Affiliated to Osmania University)

#16-1-486, Saidabad, Hyderabad - 500059



Sponsored by

MATRUSRI EDUCATION SOCIETY

ISBN: 97881-936274-0-2

**NTSET
2018**





RASPBERRY PI BASED GLOBAL INDUSTRIAL PROCESS MONITORING THROUGH WIRELESS COMMUNICATION

¹A.Narmada, ²K.Praveen, ³Aswith Guntha

¹Assistant Professor, ²Assistant Professor, ³Student
Electronics and Communication Engineering,
Matrusri Engineering College, Hyderabad, India

Abstract – This paper proposes an advanced system for process management via a credit card sized single board computer called raspberry pi based multi parameter monitoring hardware system designed using RS232 and microcontroller that measures and controls various global parameters. Various kinds of sensors are utilized in order to control and monitor the various kinds of hazards that occur during industrial process. The system comprises of a single master and multiple slaves with wireless mode of communication and a raspberry pi system that can either operate on windows or Linux operating system. The parameters that can be tracked are current, voltage, temperature, light intensity and water level. The hardware design is done with the surface mount devices (SMD) on a double layer printed circuit board (PCB) to reduced the size and improve the power efficiency. The various interesting features are field device communication via USB-OTG enabled Android devices, on field firm ware update without any specific hardware and remote monitoring and control. Remote monitoring is also performed by connecting a web server to the raspberry kit and establishing a secure wireless connection to all the sensors used. With the updated security channels one can continuously track the process occurring in industries.

Index Terms – Raspberry pi, wireless industrial automation, PCB, SMD, wireless channels, sensors.

I. INTRODUCTION

The entire system is designed with the double layer SMD based embedded board with different sensors and a raspberry pi that can compile and communicate the data received from the sensors. The raspberry pi when operated on the Linux operating system can perform multi-tasking. The design of the embed board includes the interfacing of different sensors to two slave boards and connecting those slave to a master board through RF transmission. The master and slave boards use PIC 18F4550 Microcontroller, Encoder and Decoder ICs (HD12E & HD12D), LM35 & LDR Sensors, Water level sensor(IC CD4066) and RF Transceivers.

The RF transceivers present in slave and master boards uses the process of serial communication and as most of the computers have more than one serial port there is no need of any special hardware other than a cable. The effective baud rate is the main advantage of using RS232 and also the transmission is on both directions which mean the inverted logic is also handled with the same. RS232 uses MARK (negative voltage) and SPACE (positive voltage) as two voltage states. So the baud rate is identical to the maximum number of bits transmitted per second including the control bits. The transmission rate of this device is 9600 bandwidth. The duration of start bit and each subsequent bit is about 0.104ms. The complete character frame of 11 bits is transmitted in 1.146ms. MAX 232 IC mounted on the master board converts the 0's and 1's to TTL logic.

RF module uses Amplitude Shift Keying (ASK) modulation and the frequency range varies between 30 KHz and 300 GHz. Thw RF module is used in conjunction with a set of four channel encoder (HT12E)/decoder (HT12D) ICs. The Raspberry pi is a low cost credit card sized Linux computer which has the ability to interact with the outside world and has been used in a wide array of digital maker projects. An open source operating system that uses Linux kernel called Debian is used on the embedded Raspberry Pi device in an operating system called Raspberry. Linux kernel has been ported to variety of CPUs which are used not only for computers but also for ARC, ARM, AVR32, ETRAX CRIS, and FR – V, H8300, IP7000, m68k, PowerPC, SuperH and Xtensa processors.

A printed circuit board (PCB) uses conductive tracks, pads and other features etched from copper sheets to connect the electronic components laminated onto a non -conductive substrate. Surface – mount technology (SMT) is a technique where the components are placed directly onto the surface of printed circuit boards (PCBs). Both technologies can be used in a combination i.e. the components that cannot be mounted can be used with through whole technology.

In industrial automation, there are different manufactures producing their own PLCs. The PLCs in an industry is connected with distributed control system (DCS) by protocols such as RS232/485, USB and Ethernet. The DCS has multi-level hierarchical network structure for communication. Due to the hierarchical network, the communication becomes complex.

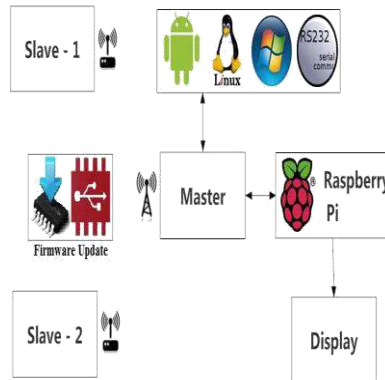


Fig.1. Block diagram of the process monitoring system using Raspberry pi

Complete network from field level to control level is not formed. The java simulators can be used as front end panel for monitoring and control. The java servers used to control the process in a field. Internet of Things (IoT) is a fast developing technology that connects all devices with internet. For soft real time systems TCP, UDP and IP protocols are efficient. Embedded web server and Linux based system is cost effective with high performance. The RS232 protocol is sufficient for parameter monitoring and control. The master slave architecture gives good performance in real time control applications. The graphical language is efficient for development of front end and back end panels for process monitoring and control.

II. SYSTEM DESCRIPTION

The Fig. 1 shows the system that is designed with both wireless slaves and wireless master where the communication is a half-duplex communication. The master module acts a bridge device between slaves and the raspberry pi computer. The master can also communicate with any android devices and compactable with all X86, X64 and ARM architectures that runs any operating system with RS232 functionality. The communication between the master and raspberry pi is wired and the raspberry pi can be operated through remote computing either wired or wireless.

The communication between the master and raspberry pi is wired and the raspberry pi can be operated through remote computing either wired or wireless. The on – field firmware up gradation of master and slave is possible without removing or disconnecting any devices from the module with the help of USB boot loader feature in PIC18F4550 microcontroller.

A. Master Module

The Fig. 2 shows the components of master module. Data acquired from slave 1 and slaves 2 are transmitted to the master which is in turn transmitted with the raspberry pi via UART serial communication. The master can also communicate with different platforms that execute serial communication.

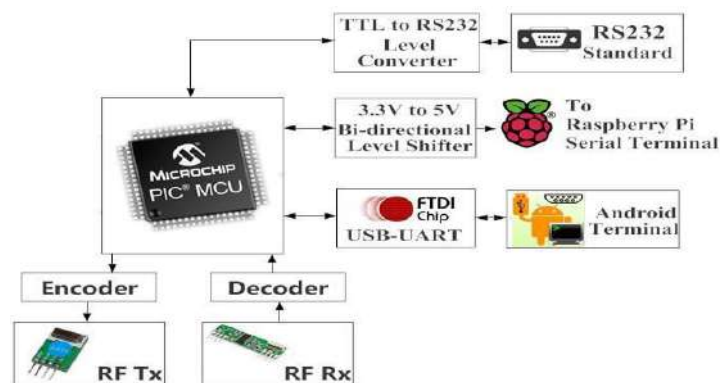


Fig. 2 Block diagram of master module.

The entire module functionality is controlled by the microcontroller. One of the major future enhancements of this master module is the in-built USB to UART converter which can directly communicate with the android devices that have USB-OTG functionality without using any other driver software or hardware.

The raspberry pi processor runs in 3.3V. So the master module has in-built MOSFET based 3.3V to 5V voltage level shifter circuit. No bridging hardware is required as the raspberry pi can directly communicate with the master module. A TTL to RS232 level shifter is used to communicate with any other hardware that accepts RS232 protocol.

B.Slave-1 Module

Fig. 3. Shows the interfacing of physical parameters like Temperature, Light intensity and Water level identifier in Slave-1 module. Data acquired from each parameter is collected in Slave -1 and sent to Master module through RF transmission. The relay and alarm are also connected to the microcontroller for controlling purpose. The encoder and decoder are responsible for converting parallel data into addressed serial data and vice versa. This serial data is transmitted or received over RF wireless modules.

C.Slave-2 Module

The Fig. 4, Shows the interfacing of physical parameters like voltage and current in Slave-2 module. Data acquired from each parameter is collected in Slave -2 and sent to Master through RF transmission. The relay and alarm are also connected to the microcontroller for controlling purpose. The in-built analog to digital (ADC) converter is used to measure the voltage and current. The encoder and decoder serve the same purpose as in the Slave-1.

III. SOFTWARE SPECIFICATION

The following software tools are required for designing, compiling and debugging.

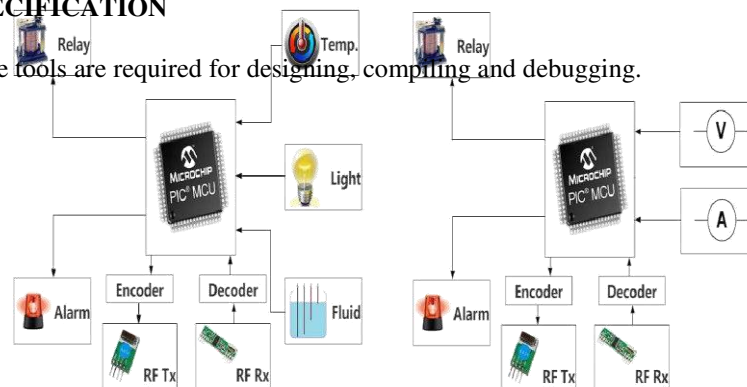


Fig. 3 Block diagram of Slave-1 module. Fig. 4 Block diagram of Slave-2 module.

A. MikroC Pro for PIC

MikroC PRO is an ANSI C compiler for PIC devices from Microchip. The main features are intuitive IDE, powerful compiler with advanced optimizations, lots of hardware and software library. Some of the tools that is integrated with this compiler are active comment editor, ASCII chart, EEPROM editor, GLCD bitmap editor, HID terminal, LCD custom character, Mikro boot loader, UDP terminal and USART terminal. Software simulator simulates the code flow in PC and supports all debugging modes s MikroICD.

B. Diptrace

Diptrace is quality schematic capture and PCB design software that is used to create simple and complex multi-layer board from the schematic to the state of ready manufacturing files. Direct3D mode is the fastest mode and so recommended for usage for most typical Windows PC. OpenGL mode is bit slower than Diect3D but it is less dependent on hardware and so it is preferred for different operating systems.

C. Raspbian operating system

Raspbian is a free operating system based on Debian optimized for the Raspberry Pi hardware. Raspbian comes with over 35,000 packages and pre-compiled software bundled in a nice format for easy installation on Raspberry Pi. Raspbian is still under development to improve stability and performance of as many Debian packages as possible.

IV. HARDWARE SPECIFICATION

The following are the hardware requirements for this process monitoring system.

A. Raspberry Pi Model B+

Raspberry Pi is based on the Broadcom BCM2835 system on a chip (SoC) that includes an ARM1176JZF-S 700 MHz processor, Video Core 4 GPU, and was originally designed with 256 megabytes of RAM and later upgraded to 512 MB. The system has either Secure Digital (SD) or Micro SD sockets for boot media and persistent storage. The other features of Raspberry Pi Model B+ are 700 MHz clock speed, four individual USB host ports, 10/100 Base T Ethernet port and HDMI audio and video output.

B. PIC 18F4550

PIC18F4550 is ideal for low power and connectivity applications because of availability of three serial ports: FS-USB (12 Mbit/s), I²C and SPI (up to 10Mbit/s) and an asynchronous serial port (EUSART). The features of PIC18F4550 microcontroller are 32Kbyte program memory, 2Kbyte data memory, 35 I/O lines, 13 channels 10-Bit analog to digital converter, USB V2.0 compliant, two external clock modes, 8* 8 Single-Cycle hardware multiplier, Single-Supply 5V In-Circuit Serial Programming (ICSP), In-Circuit Debug via two pins and wide operating voltage range (2.0V to 5.5V).

V. HARDWARE DESCRIPTION

A. Master module

Master module is fully equipped with in-built peripherals and there is no need of any bridging devices for communicating with Raspberry Pi or other platform. Module operates in 5 volt and 500mA of current and also circuit has reverse voltage protection for safe operation. 20 MHz of clock frequency is fed as oscillator input to microcontroller.

1. FT232R is a USB to serial UART interface with optional clock generator which has asynchronous and Synchronous bit bang interface modes.



Fig. 5. Top side of master hardware

2. MAX232 level converter is an IC that converts signals from an RS-232 serial port to signals suitable for use in TTL compatible digital logic circuits.
3. V to 5V voltage level shifter is used to connect with the master with Raspberry Pi as it can operate with a minimum of 3.3V.

The hardware is made by double layer PCB that is fabricated in laboratory by using toner transfer method. The design is done using Diptrace EDA CAD tool and SMD components are used to reduce the hardware size and power consumption.

The design information includes the following

- 1) Width – 79.12 mm
- 2) Height – 65.85 mm

- 3) Trace width – 0.4 mm
- 4) Number of holes – 172
- 5) Number of vias – 72

B. Slave-1 Module

Slave-1 module uses the same microcontroller configuration as that of the master module. The slave-1 address is manually set using the address switch and the address is also known to the master module by its program.

The design information includes the following

- 1) Width – 81.74 mm
- 2) Height – 75.5 mm
- 3) Trace width – 0.4 mm



Fig. 6 Top side of slave-1 hardware

The main functionality of the Slave-1 module is as follows.

1. Temperature measurement

The current temperature is converted to an appropriate voltage level using a 3 pin integrated circuit temperature sensor unit (IC LM35DZ). The three pins are ground (GND), voltage source (Vs) and output voltage (V out). Analog to Digital converter (ADC) converts the signal into digital value that is fed as input to the microcontroller. LM35 series is precision integrated circuit temperature sensor whose output voltage can be linearly calibrated in degree Celsius i.e. Linear + 10.0 mV/°C scale factor with 0.5°C accuracy guarantee and rated for full -55°C to +150°C range. It operates in 4 to 30 volts and draws less than 60 μ A.

2. Light Intensity measurement

A light/dark activated switch that is present in the Slave-1 is used to measure the light level which will turn on and off accordingly. A Light Dependent Resistor (LDR) is used to measure the light level. The circuit has a transistor switch with the base connected to a voltage divider. The voltage divider has 50K potentiometer plus the protective resistor and LDR. When the light falls on the surface of LDR, the resistance of the LDR is changed. The more the light, the less the resistance, the less the voltage drop across it and vice versa. As the voltage drop increases, the V_B of the BC547 transistor and I_{CE} will also increase.

3. Water Level identifier

IC CD4066 bilateral switch CMOS IC is used to identify the water level through LEDs. When the water is empty in the tank the circuit is open and 180K resistor pulls the switch to open and so the switches and LEDs are off. When the water begins to fill the first wire is connected to the reservoir in the S1 and the positive supply is shortened by the water. This closes the S1 and turns on the LED. As the water level increases in the tank, LEDs 2, 3 and 4 are Switched on in sequence.



Fig. 7 Top side of slave-2 hardware

C. Slave-2 Module

Slave-2 module uses the same microcontroller configuration as that of the master module. The slave-2 address is manually set using the address switch and the address is also known to the master module by its program.

The design information includes the following

1. Width – 80.32 mm
2. Height – 75.72 mm
3. Trace width – 0.4 mm
4. Number of holes – 152
5. Number of vias – 52

The main functionality of the Slave-1 module is as follows.

(1) Voltage measurement

Voltage measures the potential energy of an electric field to cause an electric current in an electrical conductor and most of the measurement devices can measure voltage. The two types of voltage measurements are direct current (DC) and alternating current (AC). The main challenge in measuring the voltage is noise. The potentiometer is used to measure the variable voltage in Slave-2 module.

(2) Current measurement

The current is measured with ammeter that contains the external resistors that is added to extend the usable range of the movement connected in parallel. The current divider circuits are formed with parallel resistances.

D. RF Module

RF module is used for making a wireless remote communication via radio frequency signals. A receiver configured for the same frequency as the sender can only receive the signals. Here the operating frequency is 434 MHz

1) Encoder IC

HT12E IC is used as the encoder IC that receives the parallel data in the form of addresses and control bits. The control signals from the remote switches with 8 address bits that constitute a set of 12 parallel signals. The encoder encodes these parallel signals to serial bits. In the encoder IC ground is pin 14 and control signals are given from pin 10-13 and serial data is fed to the transmitter through pin 17 RF transmitter transmits the signal that is fed from the IC to the receiver in a wireless mode.

2) Decoder IC

HT12D is used as the decoder IC. The receiver sends the signals to decoder IC that retrieves the serial data. When there is no signal received, then the IC remains in the standby mode that consumes very less current for a voltage of 5V. On receiving the signal oscillator of HT12D IC gets activated and decodes the serial data and checks the address bits three times. If these bits match with the local address pins (pins 1 – 8) of HT12D, then data bits are put into the data pins (pins 10 – 13) and makes the VT pin high. The LED connected to the VT pin acts an indicator to indicate a valid transmission. For a successful communication, address bits of encoder and decoder ICs must be identical. By configuring the address bits properly, same RF transmitter can be used to control different RF receivers of the same frequency.



E. Relay and Alarm Driver Circuit

Relay and alarm driver circuit is a simple transistor switching driver using NPN transistor. Since the relay and alarm consume more power than a microcontroller, driver is essential.

F. Firmware Update

USB HID boot loader firmware is a free tool that can be downloaded from microelectronics website. Also no additional OS drivers are required for this firmware update. The five basic steps to boot load the program in PIC 18F4550 are as follows.

- 1) The board is connected to PC and once the device is recognized by the OS the grey USB will turn red which indicates that the USB link is established successfully.
- 2) The connect button is clicked within 5 seconds and the chip enters the boot loader mode.
- 3) The HEX file load is chosen to load the program into the chip after browsing the file using browse for HEX button.
- 4) Boot loader is started by clicking on the begin upload button. THE show activity button can be used to view the boot loader operation.
- 5) Reset chip boot loader firmware will automatically reset the MCU, after which the newly loaded program will start in 5 seconds.

VI. FUTURE WORK

The system can be enhanced for wave form representation of data in an excel sheet using raspberry pi. The additional slaves can be added for measures various other parameters. Also controlling action can be set for some predefined cases in the master module which enables the automatic operation at certain cases. A dedicated video processor can be used in raspberry pi to display graphical and three dimensional view of the industry. An additional camera can be attached to the slave module in order for live tracking. Apart from this an infrared sensor that senses the human movements even at the night times can be utilized effectively in a way to track the thefts. Various other sensors can be attached in order to monitor the various defects in the functionality of the machines through wireless communication. An automatic control gate can be operated by wireless channel such that the gate operates as the safety measures for the workers in the industry during critical conditions. So in many ways we can enhance the working of the kit in effective way.

REFERENCES

- [1] Alfredo Gardel Vicente, Ignacio Bravo Munoz Jose Luis Lazaro Galilea and Pedro A. Revenga del Toro, "Remote Automation Laboratory Using a Cluster of Virtual Machines," IEEE Transactions on Industrial Electronics, vol. 57, no. 10, pp. 3276–3283, 2010.
- [2] Amiya Ranjan Panda, Utpal Mandal and Hare Krishna Ratha, "Integrated Monitoring of Encoder Status Parameters and GUI based Remote Control Panel Using Lab view," IJCA., vol. 43, no. 3, pp. 21–26, 2012.
- [3] Arkadiusz Jestratjew and Andrzej Kwiecien, "Performance of HTTP Protocol in Networked Control Systems," IEEE Transaction on Industrial Informatics, vol. 9, no. 1, pp. 271–276, 2013.
- [4] Baosheng Yanga, Jianxin Lia, and Qian Zhangb, "G Language Based Design of Virtual Experiment Platform for Communication with Measurement and Control," Elsevier-International Journal of Procedia Engineering, vol. 29, pp. 1549-1553, 2012.
- [5] Eva Besada-Portas, Jose A. Lopez-Orozco, Luis de la Torre, and Jesus M. de la Cruz, "Remote Control Laboratory Using EJS Applets and Twin CAT Programmable Logic Controllers," IEEE Transaction on Education, vol. 56, no. 2, pp. 156–164, 2013.
- [6] Md. Nasimuzzaman Chowdhury, Md. Shiblee Nooman and Srijon Sarker, "Access Control of Door and Home Security by Raspberry Pi through Internet," IJSER, vol. 4, issue. 11, pp. 550–558, 2013.
- [7] Mukesh Kumar, Sanjeev Sharma, and Mansav Joshi, "Design of Real Time Data Acquisition with Multi Node Embedded Systems,IJCA" vol. 42, no. 11, pp. 6– 12, 2012.



- [8] Su Chunli and Zhao Xiangmei, "Comparison on Application of DCS and FCS," IEEE Conference on ICDMA, pp. 358–360, 2013.
- [9] Wan Xining, & Zhao Cheng, "Design and Simulation of Voltage Fluctuation Rate Monitor System Based on Virtual Instrument Technology," Elsevier-International Journal of Energy Procedia, vol. 17, pp. 450–455, 2012.
- [10] Dip Trace - Schematic and PCB design software.
- [11] Embedded Linux Wiki.
- [12] Linux on embedded systems.
- [13] Raspberry Pi.
- [14] Surface Mount Device.
- [15] Surface Mount Technology.
- [16] Embedded Linux training.
- [17] Embedded Linux development
- [18] Basic Homemade PCB.
- [19] [.com/community/community/raspberry y-pi/](http://www.raspberrypi.org/community/community/raspberry-pi/)
- [20] Learning Linux for embedded systems.



MATRUSRI ENGINEERING COLLEGE

(Approved by AICTE, Affiliated to Osmania University)

#16-1-486, Saidabad, Hyderabad - 500059



Sponsored by

MATRUSRI EDUCATION SOCIETY



ISBN: 97881-936274-0-2



1ST NATIONAL CONFERENCE ON TRENDS IN SCIENCE, ENGINEERING AND TECHNOLOGY (NTSET - 2018)

February 2nd & 3rd - 2018

TECHNICAL PAPER ABSTRACTS



ORGANIZED BY

MATRUSRI ENGINEERING COLLEGE

(Approved by AICTE, Affiliated to Osmania University)

#16-1-486, Saidabad, Hyderabad - 500059



Sponsored by

MATRUSRI EDUCATION SOCIETY

ISBN: 97881-936274-0-2

**NTSET
2018**





EFFECTIVE FOOD GRAIN LOSS REDUCTION TECHNIQUE USING IOT

¹A S Keerthi Nayani, ²CH.Sekhar, ³Aruna Kokkula

^{1,2,3}Assistant Professor,

^{1,3}Dept. of ECE, Matrusri Engineering College, Hyderabad, India.

²Dept. of CSE, Vignan's institute of information technology(Auto.)Vishakhapatnam(A.P)

Abstract: Internet of Things (IoT) is one of the affirmative platforms to implement a large data analytics task which comprises the way to exploits networking, detecting, huge information, and computerized reasoning innovation to convey finish frameworks for an item or administration. These frameworks permit more prominent straightforwardness, control, and execution when connected to any industry or fr. In this paper, we are going to discuss about loss due to atmospheric moisture beyond threshold results in infestation etc and hence damages the food grain. Those losses can be reduced effectively with support of various sensors to detecting the status of food grains stored in the Central Warehousing. Based on moisture and temperature data captured, the software should do appropriate data analytics and send timely alert to concern officials of CWC for mitigation and remedial actions arising due to moisture and temperature inside the warehouse. This paper emphasizes the usage of IoT which enables the Central warehouse centers to avoid the losses of food grains.

Index Terms- *Moister, Temperature, Sensors, IoT Technology.*

I. INTRODUCTION

Taking care of the sustenance demand of a quickly expanding worldwide populace is developing as a major test to humanity. The populace is relied upon to develop to 9.1 billion individuals by the year 2050, and around 70% additional nourishment creation will be required to encourage them [1]. A large portion of this populace rise is relied upon to be credited to creating nations, a few of which are now confronting issues of yearning and sustenance uncertainty. Expanding urbanization, environmental change and land use for non-sustenance edit generation, heighten these worries of expanding nourishment requests. Over the most recent couple of decades, a large portion of the nations have concentrated on enhancing their rural generation, arrive utilize, and populace control as their arrangements to adapt to this expanding sustenance request. In any case, postharvest misfortune (PHL), a basic issue, does not get the required consideration and under 5% look into subsidizing has been assigned for this issue in earlier years . Around 33% of the nourishment delivered (around 1.3 billion ton), worth about US \$1 trillion, is lost all around amid postharvest operations consistently. "Sustenance misfortune" is characterized as nourishment that is accessible for human utilization however goes unconsumed. The answers for diminish postharvest misfortunes require generally humble speculation and can bring about significant yields contrasted with expanding the harvest creation to take care of the sustenance demand.

CWC (Central Warehousing Corporation) is a warehousing agency. It offers services like storage and handling of goods, transportation of goods. This project benefits the government as there is difficulty in handling large number of goods from different sectors of industries. As we know there are huge numbers of commodities that include Agricultural produce, Industrial raw materials, finished goods and variety of perishable items where we can observe storage loss at huge amount. This sort of storage loss of quality outcome of food grains and perishable goods can be controlled through quality control practices that include chemical treatment, sanitation, age analysis, regular inspection and many more. Sometimes storage loss can also be observed due to atmospheric moisture beyond threshold results. So, a preferable low cost IT solution is around Internet Of Things (IOT) Sensor and IOT data integration. As a part of solution we are creating an IOT dashboard that includes all information related to moisture, temperature, fire and earthquake.

II. PROBLEM STATEMENT

Post-harvest losses:



Seeds of low quality, deficient cultivating practices, or creepy crawly assaults in the field can incite misfortunes of items even before their reap. Be that as it may, we are worried here just with counteractive action of misfortunes after the collect.

Losses in quality

Criteria of value fluctuate broadly and include the outside angle, shape and size, as much as the odor and taste. In such manner, the social contemplations with which weight control plans and dietary patterns are instilled can't be disregarded. A clean healthy item is of essential significance in advertising. By grasping a modest bunch of grain from a pack, for instance, a tradesman can rapidly check whether it emits a floury tidy and can thusly reason regardless of whether it originates from an invasion by creepy crawlies. Similarly, a terrible stench can lead him to presume rat assaults, which can be affirmed by the nearness of rodent or mouse dung or hairs. Misfortunes in quality are in this way confirmed by a decline in the market estimation of the item. These misfortunes are quantifiable just on condition that criteria or benchmarks of value have been already settled. Based on target criteria, the nature of the items can be assessed by genuinely confounded tests, estimations and research facility examinations. A considerable lot of the criteria embraced depend on assessment of principles identified with the physical state of the grain and to its sustenance, nutritive and germinative esteems. In different nations, quality evaluations depend on the general chief as per which grain must be "healthy, sound, of market quality and unscented".

Certain in this definition are the central criteria for assessing the nature of a given cluster of grain; these include:

- Moisture Content: reasonable for the capacity or further treatment of the item;
- Colour: homogeneous and fitting to the sort of item under thought;
- Odour: it must not indicate that any biochemical change is going on;
- Cleanness: the quantity of debasements must fit in with set up models of value;
- Infestation: the nonattendance of bugs or other living life forms must be discovered.

For the most part, numerous criteria join to characterize the nature of the items, and they likewise consider social perspectives identified with group dietary patterns. In Senegal, for instance, broken rice is very prized by customers; hence, the level of breakage, as a standard of rice quality, clearly has less significance than in different settings.

Loss in quality are for the most part the aftereffect of mechanical requirements experienced by the item, the activity of bugs (creepy crawlies, rodents) and small scale creatures (molds), or the concoction changes delivered inside the grains under the impact of natural conditions (temperature, mugginess, length of capacity).

Problem Identified

1. Central Warehousing Corporation (CWC) is into scientific storage and handling services for more than 400 commodities include Agricultural produce, Industrial raw-materials, finished goods and variety of hygroscopic and perishable items.
2. Storage loss of food grains and perishables goods are being controlled through quality control practices including periodic chemical treatment , recording of moisture and other parameters, proper documentation , regular inspection , age analysis , sanitation , physical condition of warehouse.
3. Further storage loss due to atmospheric moisture beyond threshold results in infestation etc and hence damages the food grains/perishables.

III. PROPOSED SOLUTIONS AND METHODOLOGY

Expected deliverables:

- Low cost IT solution preferably around Internet of the things (IoT) sensor and IoT data integration to existing application software. The sensor is expected to auto capture the atmospheric moisture and temperature inside the warehouse.

- Based on moisture and temperature data so captured, the software should do appropriate data analytics and send timely alert to concern officials of CWC for mitigation and remedial actions arising due to moisture and temperature inside the warehouse.
- Additionally, IoT sensor can also capture fire, earthquake etc and can alert the respective nearest authority like Fire Station, Hospital, and Police besides alerting CWC officials for mitigation. Sample data: Data to either simulated participants or can visit warehouses for sampling.

The following are the various sensors can be used to detect and monitor the status of food grains stored in the central warehouse.

Sensor to Detect Moisture Level in Room:

Stickiness is the nearness of water in air. The measure of water vapor in air can influence nourishment grains in the event that it is more than the required level. The nearness of water vapor additionally impacts different physical, synthetic, and natural procedures. Thus, stickiness detecting is essential, particularly in the focal stockpiles' of nourishment grains.

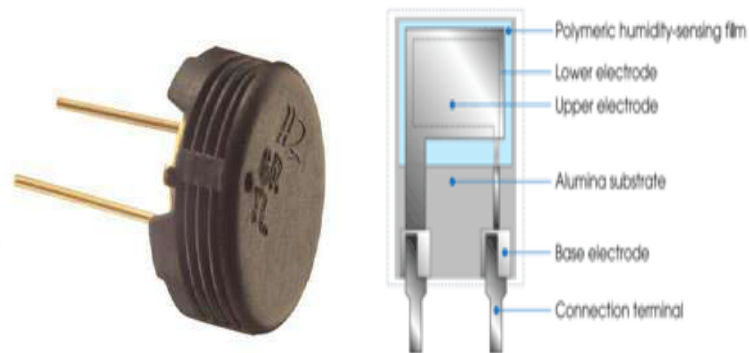


Fig1. Humidity Sensor and capacitive type humidity

Sensor to detect temperature(IC LM 34/35)

Temperature sensor IC LM34/35, are used in various applications to detect temperature variations. These devices can switch off / on circuits when the temperature varies from the normal set level. LM 34 and LM 35 Integrated Circuits are precision temperature sensors widely used in temperature sensing applications. LM 34 senses temperature in Fahrenheit range while LM 35 senses temperature in Celsius (Centigrade) range. The output voltage of these sensors is linearly proportional to the temperature.

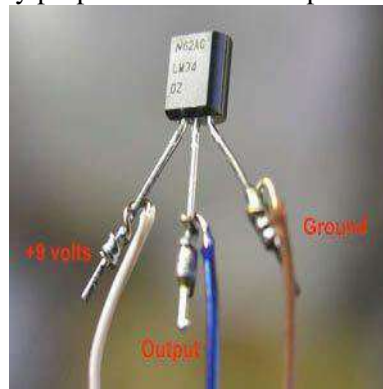


Fig3. Temperature Sensor

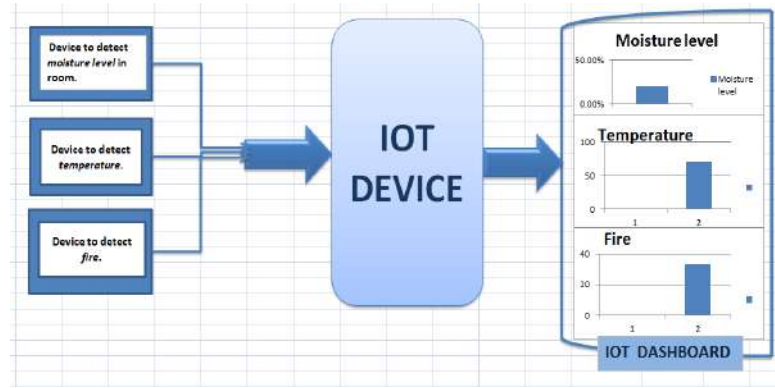


Fig 4: Working Model

IV. WORKING MECHANISM

The accompanying table demonstrates the degrees of dampness content considered fitting for good collect conditions and the attributes allowing affirmation of physiological development[2].

Table -1

GRAINS	MOISTURE	PHYSICAL CHARACTERISTICS
Rice	22-28%	The panicles bend with their own weight, yellowed hulls, full grains, neither too ripe (cracked), nor too green.
Maize	23-28%	Cobs almost dry, hard and glassy kernels resistant to scoring with the thumbnail, black dot in the caryopsis.
Sorghum	20-25%	Dried stems and leaves, hard grains resistant to the thumbnail, glassiness depending on variety.
Beans	30-40%	Pods ripe and yellow, shells dried, skins of kernels easily detached.
Groundnuts	30-35%	Leaves yellow, shells dried, skins of kemels easily detached.
Sunflower	9-10%	Upper leaves dry and flower faded.

As mentioned above sample scenario, the following process need to implement to achieve the desired level of room temperature.

Considering the need of modern technology the smart central warehouse need to ready to store the food grains and to reduce the losses due to various atmospheric conditions To avoid the losses due to normal storage places such problems in above existing system we are planning to design IOT based Smart Warehouse and Monitoring System. This system monitors the various things such as temperature, humidity etc. Time to time levels of respective measures collected and sends to the central control system via a webpage.

For this the system uses various sensors mentioned above placed over the all the rooms to detect the levels and compare it with the required. Once when the level reaches the threshold limit the system puts on the buzzer/ alarms the employees working in that particular region. Thus this system helps to keep the roomat desired levels.

- Real time information of the room's level will be displayed in web browser.
- Intelligent sensors placed at the rooms which notify about the temperature, humidity content in the bins.
- The web application can also be operated using any devices.
- This system is adaptive and hence can adapt to various new technologies.
- This process reduces cost and resource optimization.
- Improves quality and effective usage of rooms.

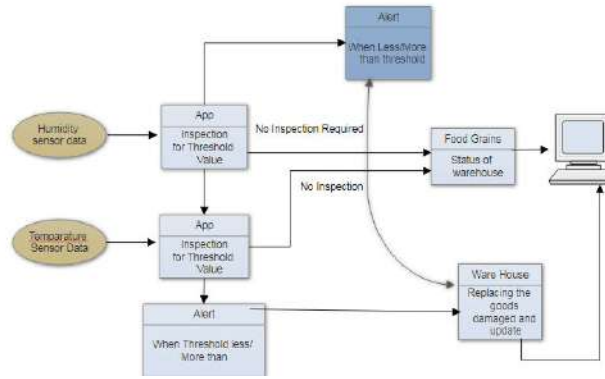


Fig5: Work Flow of Detecting and Monitoring the Warehouse

V. RESULTS DISCUSSION

Warehouse monitoring system is designed and implementation is done on IC LM 34/35 development board .The communication between controllers and interference are designed accurately done. Monitoring System is done to meet all the requirement and specification as mentioned in the objective. An embedded application is created using Python and R Programming. The predict results of the monitor model proposed are shown in table below.

Table 2

Temperature	25	>35	>40
Relative Moisture	44	60	75
Co ₂ Concentration(1000ppm)	<50	>110	>130
Status	Good	Critical	Risk/Danger

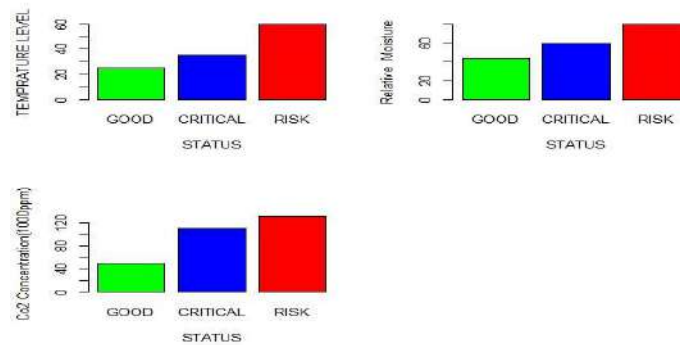


Fig6: Warehouse Status based on the Various Factors

VI. CONCLUSION

In this Paper Monitoring system is designed for monitor and controlling of the Food granule losses based on the various temperature level conditions. The grain system design is done to meet all the requirement and specification as mentioned in the objective. It is shown from the design implemented in the current work provides flexibility, scalability, portability and security/integrity of the data transmission over long networks with lower power consumption.

There are certain aspects in this work that can be investigated in future design should GPRS network is used to transferring data to all the warehouses. That will help to getting centralized data at one location and able monitor by authority to take necessary measure to reduce as much as possible.

There are certain aspects in this work that can be investigated in future, such as Environmental factors influencing the Grain quality, we are considered only major parameters Temperature, Humidity and Carbon Dioxide concentration for early



detection of deterioration of Food Grains and Good Control actions like Reducing Temperature in the Grain depot if Temperature is High i.e. keeping parameters at nominal level by an Automatic system irrespective of condition.

REFERENCES

- [1] Deepak Kumar AndPrasantaKalita. Reducing Postharvest Losses during Storage of Grain Crops to Strengthen Food Security in Developing Countries
- [2] <http://www.fao.org/docrep/t0522e/T0522E04.htm>
- [3] Xiaodong Zhang, Xiujuan Li, Jie Zhang (2010). Design and implementation of embedded monitoring system for grain storage: IEEE Conference.
- [4].Ch.Chandra Sekhar, et.allBig Data Analytics on Indian Crop Planning to Increase Agricultural Production, ASTL -Research on Smart Technologies in Data Science and Communications.
- [5]Ch Sudhakar,et..allAn IoT Application-Weather Reporting System, ASTL -Research on Smart Technologies in Data Science and Communications. Vol.147
- [6]Maier, Channaiah, Martinez-Kawas, (2010).Monitoring carbon dioxide concentration for early detection of spoilage in stored grain: Department of Grain Science and Industry, Manhattan, Kansas



MATRUSRI ENGINEERING COLLEGE

(Approved by AICTE, Affiliated to Osmania University)

#16-1-486, Saidabad, Hyderabad - 500059



Sponsored by

MATRUSRI EDUCATION SOCIETY



ISBN: 97881-936274-0-2



1ST NATIONAL CONFERENCE ON TRENDS IN SCIENCE, ENGINEERING AND TECHNOLOGY (NTSET - 2018)

February 2nd & 3rd - 2018

TECHNICAL PAPER ABSTRACTS



ORGANIZED BY

MATRUSRI ENGINEERING COLLEGE

(Approved by AICTE, Affiliated to Osmania University)

#16-1-486, Saidabad, Hyderabad - 500059



Sponsored by

MATRUSRI EDUCATION SOCIETY

ISBN: 97881-936274-0-2

NTSET 2018





DESIGN AND IMPLEMENTATION OF ALL DIGITAL PHASE LOCKED LOOP ON FPGA

¹Mrs. K. Aruna, ²K. Rohith, ³A. Mahendar

¹Assistant Professor, ^{2,3}Student,
^{1,2,3} Electronics and Communication Engineering
^{1,2,3}Matrusri Engineering College, Saidabad, India.

Abstract : Phase Locked Loops (PLLs) are widely used in clock recovery and frequency synthesis. Fully Digital PLLs are more suitable for the monolithic implementation with other circuits compared to the traditional implementations of the PLLs. The All Digital PLLs are also independent of process variation and can be easily ported to different technologies. This paper presents the design of an All Digital Phase Locked Loop (ADPLL) and implemented on FPGA as ALL DIGITAL FM receiver. General design criteria are summarized for the all digital implementation in comparison to the traditional approaches and analog implementations. The ADPLL has 8-bit binary control and can operate in the frequency range between 1MHz and 500 MHz. The ADPLL has 50-cycles lock time and a duty cycle distortion of less than 2%. The simulation and test results of the ADPLL are also presented to verify its operation.

IndexTerms – Phased Locked Loop, All Digital Phased Locked Loop, Field Programmable Gate Array.

I. INTRODUCTION

Phase Locked Loops (PLLs) are feedback systems that generate signals that are phase locked with external input signals. PLLs are used to generate an output signal whose frequency is a programmable, rational multiple of a fixed input frequency. In other words, PLLs are used to lock or track input signals in frequency and phase. When the phase and frequency of the input signals are synchronized, the PLL is said to be in the locked condition. The phase difference between the output signal and the reference is a known value when the loop is locked. Phase Locked Loops are used for applications such as clock recovery, motor speed control and frequency control of communications equipment. PLLs are widely used in modern communication systems and high performance microprocessors because of their remarkable versatility. PLLs are also used in frequency modulation, demodulation as well as to regenerate the carrier from an input signal in which the carrier has been suppressed. In communication applications, PLLs are used to make local clocks synchronous with other signals. Currently, PLL design techniques are trying to achieve the following using state of the art design methodologies such as Faster lock time, Improved jitter performance and Robust performance and enhanced stability.

The complex nonlinear PLL feedback system is made up of the following blocks: Phase Detector (PD), Low Pass Filter (LPF) and Voltage Controlled Oscillator (VCO). A Divide by N Counter is inserted between the VCO and the PD in frequency synthesis applications. When the counter is used, the VCO generates a frequency that is N times the reference frequency. The working of a basic PLL can be summarized as follows; the Phase Detector (PD) compares the frequencies and phases of the input signal ($v_s(t)$) and the output of the Voltage Controlled Oscillator (VCO) ($v_o(t)$). The PD generates an error signal that is proportional to the phase difference between the two signals. The Low Pass Filter (LPF) is used to suppress the sum or the high-frequency component of the error signal. The VCO is a free-running multivibrator and operates at a frequency called the free running frequency (f_0). It can be shifted to either side by applying a decontrol voltage to the VCO. The low-frequency component from the LPF is applied as the control signal to the VCO. The VCO generates an output signal whose frequency is a linear function of the control voltage. This signal is then fed back to the Phase Detector to achieve zero or constant phase difference between the input signal and the output of the VCO. Once locked, the PLL tracks the frequency changes of the input signal.

II. Architecture of All Digital Phase Locked Loop (ADPLL)

The All Digital Phase Locked Loop (ADPLL) aims at eliminating all the analog circuitry. In contrast to the Digital Phase Locked Loop (DPLL), it is "fully digital". The all digital phase locked loops offer better scalability and portability. Existing standard cell implementations can be used for the all digital PLL blocks. The term "digital" in an ADPLL signifies two things: Firstly, the components of an ADPLL are entirely digital. Secondly, the signals associated with the different blocks are also digital and could be binary or bit signals or word signals such as the digital code word output of

a data register or n-bit output word of a counter. ADPLLs offer some advantages compared to Analog or Charge Pump Phase Locked Loops with respect to simplicity and flexibility of the design. But these loops also have some limitations when it comes to characteristics such as jitter performance or locking range.

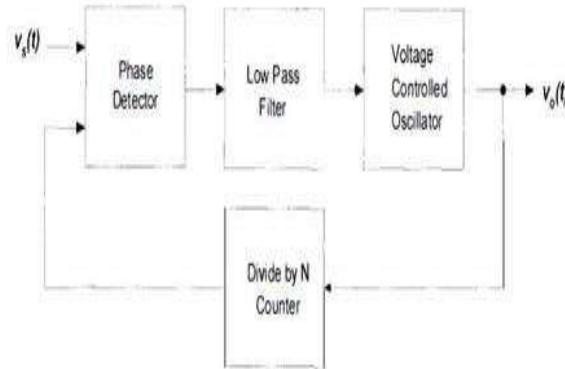


Figure 1: Block Diagram of a basic Phase Locked Loop (PLL)

The goal of this work was to design a fully Digital Phase Locked Loop that can match or exceed the performance of the Analog PLLs. Some ADPLLs may also use a Number Controlled Oscillator (NCO) in contrast to its analog counterpart: the Voltage Controlled Oscillator (VCO). The following section explores some of the possible digitized phase detectors, loop filters and NCO implementations used in ADPLLs.

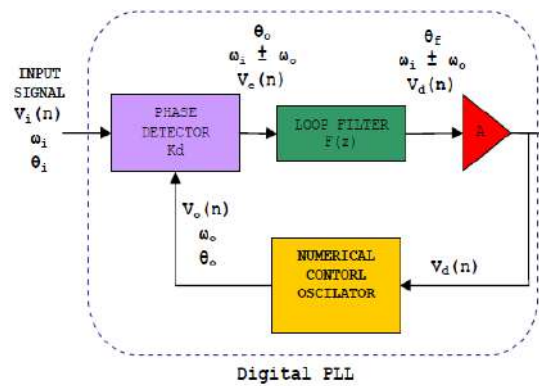


Figure 2: Block Diagram of ADPLL

A. Nyquist rate and phase detector:

Phase Detector (PD) detects phase error between input signal and output signal from NCO. This operation employs a multiplier module. The input signal is frequency modulated, so the input signal $V_i(n)$ can be expressed as follows,

$$V_i(n) = \sin(\omega_i n + \theta_i)$$

Feedback loop mechanism of the PLL will force NCO to generate sinusoidal signal $V_o(n)$ with the same frequency of $V_i(n)$, then

$$V_o(n) = \cos(\omega_i n + \theta_o) \quad (1)$$

Output of phase detector is product of these two signals, using familiar trigonometric identity we obtain

$$\begin{aligned} V_d(n) &= K_d \sin(\omega_i n + \theta_i) \cos(\omega_i n + \theta_o) \\ &= \frac{K_d}{2} [\sin(2\omega_i n + \theta_i + \theta_o) + \sin(\theta_i - \theta_o)] \end{aligned} \quad (2)$$

K_d is the gain of the phase detector. The first term in (3) corresponds to high frequency component. The second term corresponds to the phase difference between $V_i(n)$ and $V_o(n)$. By removing the first term thru loop filtering, the phase difference can be obtained.

B. Multiplier

For multiplier, we use *Booth's Multiplication algorithm* instead of simple signed arithmetic multiplier operation. Arithmetic multiplier will consume large area, while Booth's multiplication algorithm for 8-bit multiplication only needs eight 8-bit adders which is much save in area consumption. For this algorithm, as shown in Figure 3, the individual partial products determined from the multiplicand may be: added to, subtracted to, or may not change the final product at all based on the following rules:

- The multiplicand is subtracted from the partial product upon encountering the first 1 in a string of 1's in the multiplier.

- The multiplicand is added to the partial product upon encountering the first 0 provided that there was no previous 1 in a string of 0's in the multiplier,
- The partial product does not change when the bit is identical to the previous multiplier bit.

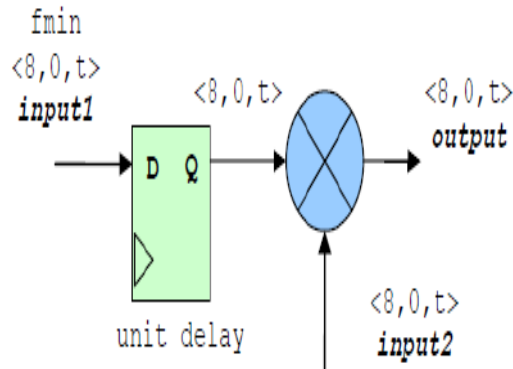


Figure 3: The Block Diagram of Phase Detector is a Multiplier

C. Loop filter

Loop filter will remove the high frequency component .the block diagram shows a first order loop filter used in the receiver system.

Summary of operation:

- input C is multiplier's output in $\langle 8,0,t \rangle$ format. Output is $D1 \langle 12,4,t \rangle$. $D1$ will be multiplied by $15/16$ and then the product is summed back to C
- $d_{temp} \langle 12,4,t \rangle$ is internal signal which is the summing result of C and $D1$. C must be changed to $\langle 12,4,t \rangle$ before summation, hence,

	$\langle 8, 0, t \rangle$	$\langle 12, 4, t \rangle$
C	$C(7 \text{ downto } 0)$	$C(7) \& C(7) \& C(7) \& C(7) \& C(7 \text{ downto } 0)$

- d_{temp} will be assigned to $D1$. Then $d_{temp} \times 15/16 = d_{temp} \times (1 - 1/16) = d_{temp} - (d_{temp} \times 1/16) = d_{temp} - E$
- $E = d_{temp} \times 1/16$, in reality $1/16$ multiply can be implemented by just 4 bit right shift operation. Then no multiplier is required.

First order loop filter as shown in Fig. 4 is a low pass filter with the transfer function

$$H(z) \equiv \frac{Y(z)}{X(z)} = \left(\frac{1}{z - 0.9375} \right)$$

Which has a pole on the real axis at $z = 0.9375$. From stability property of discrete time filter, we know that $H(z)$ is stable since its pole is located within the unit circle

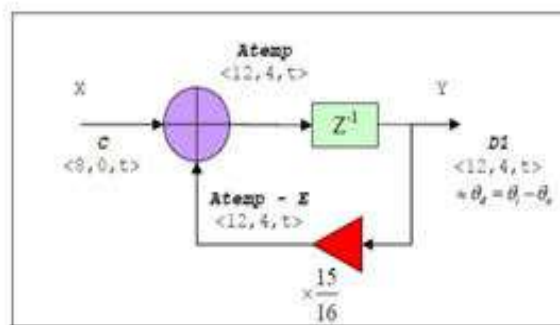


Figure 4: Block Diagram of First Order Loop Filter

D. Numerical controlled oscillator

Numerical Controlled Oscillator (NCO) will take the corrective error voltage, and then shift its output frequency from its free-running value to the input signal frequency and thus keep the PLL in lock. Here we assume the NCO free running frequency is 1 MHz and the system clock frequency is 16 MHz; there are 16 sampling points in one cycle of 1 MHz free running frequency. When input is zero, NCO has to generate output equal to free running frequency. Since there are 16 sampling points in one cycle of free running frequency, so the offset must be $1/16$. The greater input will produce greater frequency, and vice versa. The system is a simple integrator which accumulates the input value and maps it into

predefined cosine ROM. All 1024 values were given (*file: cos.txt*) to define one cycle of cosine signal, but we actually don't need to use all of these values. Since one cycle can be divided to four quarter, we only need to define the first quarter with 257 values. The remains quarters are duplicated form the first quarter, where the opposite sign is applied to second and third quarter.

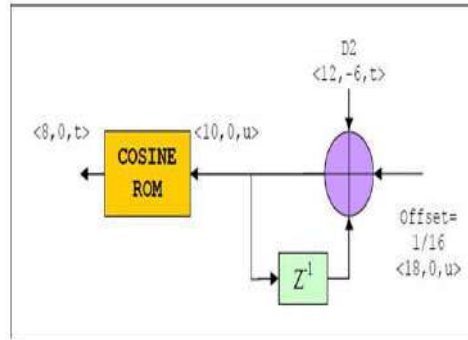


Figure 5: Block Diagram of NCO

E. FIR Filter

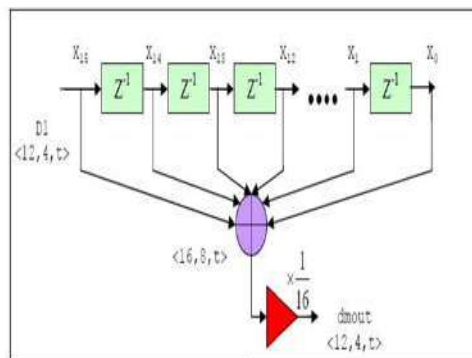


Figure 6: Block Diagram of FIR Filter

The last stage of the receiver system is to perform signal shaping. Here we use 16 tap Finite Impulse Response (FIR) filter to perform digital low pass filter. This filter is essentially average filter since its output is equal to the average value of its input over the last n -tap samples, where n is number of tap used [4]. This configuration needs 16 coefficients, but simplification is taken by assuming all of the coefficients are the same, $1/16$. In reality $1/16$ multiply can be implemented by just 4 bit right shift operation. Then no multiplier is required.

III. Results and Simulations

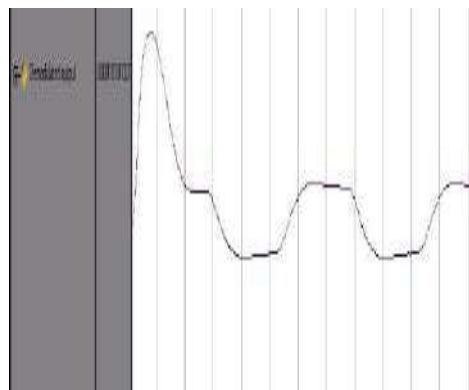


Figure 7: Demodulated Output

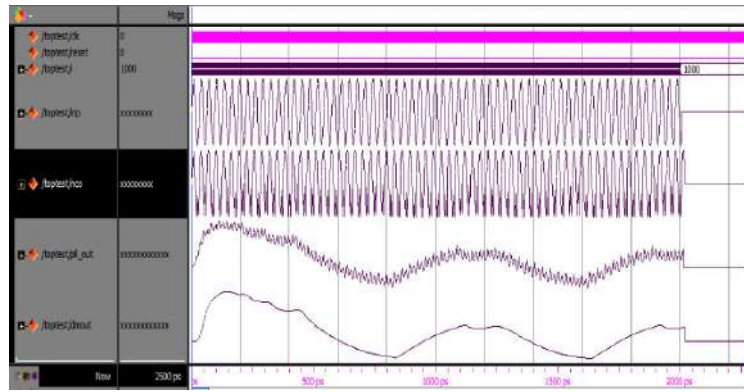


Figure 8: Top test of Numerically Controlled Oscillator

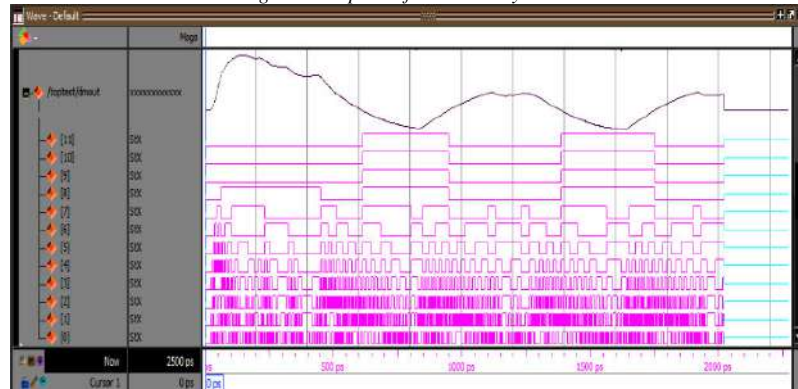


Figure 9: Top test of Demodulated Output for Each Bit

On Chip Utilization:

1. Slice Logic

Site Type	Used	Fixed	Available	Util%
Slice LUTs*	355	0	63400	0.56
LUT as Logic	355	0	63400	0.56
LUT as Memory	0	0	19000	0.00
Slice Registers	301	0	126800	0.24
Register as Flip Flop	301	0	126800	0.24
Register as Latch	0	0	126800	0.00
F7 Muxes	20	0	31700	0.06
F8 Muxes	10	0	15850	0.06

Power:



1.1 On-Chip Components

On-Chip	Power (W)	Used	Available	Utilization (%)
Slice Logic	7.126	866	---	---
LUT as Logic	6.373	355	63400	0.56
CARRY4	0.354	52	15850	0.33
Register	0.337	301	126800	0.24
F7/F8 Muxes	0.048	30	63400	0.05
BUFG	0.014	2	32	6.25
Others	0.000	9	---	---
Signals	6.684	744	---	---
I/O	34.664	22	210	10.48
Static Power	0.797			
Total	49.270			

Clocking:

Slack: inf
Source: f1/d_reg[11][4]/C
(rising edge-triggered cell FDCE)
Destination: f1/out_reg[10]/D
Path Group: (none)
Path Type: Max at Slow Process Corner
Data Path Delay: 7.923ns (logic 3.013ns (38.028%) route 4.910ns (61.972%))
Logic Levels: 12 (CARRY4=4 FDCE=1 LUT3=3 LUT4=2 LUT5=1 LUT6=1)

REFERENCES

- [1] Samir Palnitkar, "VERILOG HDL : a guide to digital design and synthesis," Pearson, 2016.
- [2] Roland E. Best, "Phase Locked Loop, Theory, Design, and Applications," McGraw – Hill, 2003.
- [3] NursaniRahmatullah "Design of All Digital FM Receiver Circuit", Institute Technology Bandung, Indonesia, March 2005.
- [4] MartinKumm, HaraldKlingbeil, Peter Zipf, "An FPGABased Linear All-Digital Phase-Locked Loop", IEEE Trans. on Circuits and Systems 57-I(9): 2487-2497 (2010).
- [5] AnithaBabu, BhavyaDaya, BanuNagasundaram, NivethaVeluchamy "All Digital Phase Locked Loop Design and Implementation," University of Florida, Gainesville, FL, 32608, USA



MATRUSRI ENGINEERING COLLEGE

(Approved by AICTE, Affiliated to Osmania University)

#16-1-486, Saidabad, Hyderabad - 500059



Sponsored by

MATRUSRI EDUCATION SOCIETY



ISBN: 97881-936274-0-2



1ST NATIONAL CONFERENCE ON TRENDS IN SCIENCE, ENGINEERING AND TECHNOLOGY

(NTSET - 2018)

February 2nd & 3rd - 2018

TECHNICAL PAPER ABSTRACTS



ORGANIZED BY

MATRUSRI ENGINEERING COLLEGE

(Approved by AICTE, Affiliated to Osmania University)

#16-1-486, Saidabad, Hyderabad - 500059



Sponsored by

MATRUSRI EDUCATION SOCIETY

ISBN: 97881-936274-0-2

NTSET 2018





RTL GENERATION USING A HIGH PERFORMANCE DIF ALGORITHM USING ‘C’

¹Mr.Upendar Sapati, ²Mrs. B.Indira Priyadarshini, ³Dr. Pallavi Khare

¹Associate professor, ^{2,3}Assistant professor

^{1,2,3}Dept. of ECE,

¹Vjit, Aziz nagar, Hyd., ^{2,3}Matrusri Engg College, Hyd.

Abstract: Powerful high-level languages to RTL generators are now emerging. One of the use of these tools is to allow software engineers to implement algorithms quickly in a familiar language and target the design to a programmable device. The generators available today support syntaxes with varying degrees of fidelity to the original language. This paper focuses on the efficient use of C to RTL generators that have a high degree of fidelity to the original C language. However, coding algorithms without regard for the capabilities of the target programmable logic can lead to low-performance realizations of the algorithm that are several times slower than what could be achieved with a DSP. This paper presents the architecture of a high-performance radix-2 FFT written in ANSI C that is similar in composition to the classic C implementation that is familiar to most engineers. First, methods to organize memory elements and arrays for maximum data accesses per clock cycle are discussed. Next, the exploitation of the natural parallelism of a radix-2 decimation in frequency algorithm is discussed. Finally, the performance improvement by hiding the first and last of the $\log_2(n)$ butterfly stages is discussed. The resulting RTL outperforms hand optimized DSP assembly code by a factor of three while using less effective area than a DSP solution.

Index Terms: C Language, Code Converters, Discrete Fourier Transforms, Field programmable gate arrays, Hardware Design Languages, Logic Design

I. INTRODUCTION

THE ability to describe digital logic in a high-level language (HLL) such as C is attractive for several reasons. First, the development time and source lines of code (SLOC) for the logic can be reduced if the level of abstraction is raised. This also results in lower maintenance costs and improves the reusability of the code. Secondly, the available developer pool for intellectual property (IP) blocks increases to include a large pool of embedded software engineers. Finally, if the language used has a high degree of fidelity to the original language, the code describing the IP may be used in both hardware and software targets with only small source code modifications required. Therefore, we attempted to develop an IP block with the following goals:

- Implement the code as it would be implemented in a software environment by a software engineer
 - Show a dramatic improvement in development time
 - For the chosen IP block (an FFT), beat the performance of a DSP while maintaining the power consumption.
- The IP chosen was the complex FFT. The FFT is a standard DSP benchmark and has classic Radix-2 implementation in C [1].

II. C to RTL GENERATOR

A number of C to RTL tools are currently available. Some use extensions to the C language to allow control of the generated RTL down to the wire and register level. While use of a language with this level of control can result in performance that approaches that of an HDL [2], it also requires a larger time investment to learn the language and requires a larger number SLOC to implement the algorithm.

This IP development was done as part of a larger effort in a hardware/software runtime partitioning project [7]. Therefore, to allow reuse of our source code, we chose an RTL generator that has a high degree of fidelity to the C language. Impulse C [2] is largely a subset of the ANSI-C language with support for pointers and arrays. While function calls are not supported, methods for constructing complex applications that will be familiar to software engineers are available: processes and signals. Some control over the pipelining of the generated logic is available via a C #pragma directive. Since the compiler will try to implement large blocks of combinatorial logic, this #pragma can be used to tell the compiler the maximum allowable gate delay permitted in the generated logic. With this tool, the designer can trade latency in clock cycles for clock frequency.

ImpulseC comes with a development environment called CoDeveloper. This tool will compile the C code for execution on a desktop machine in order to debug and verify the algorithm. CoDeveloper allows simulation of the software and hardware components of a design and the development of test benches in C. This environment is very

familiar to a software engineer, does not require learning an HDL simulation tool, and results in fast development and verification of new IP. The tool also has direct support for some common bus protocols that would enhance the portability of the IP blocks in embedded systems. For example, the tool can automatically place a CoreConnect PLB or OPB bus wrapper around the generated IP and also generate the required metadata required for incorporation into the Xilinx EDK environment [5].

III. DEVELOPMENT ENVIRONMENT:

A. IP Creation

A standard fixed-point 1024 point complex FFT was written in ImpulseC and debugged in the product's CoDeveloper environment. Once debugged, the RTL generator was run on the C code and VHDL output was collected.

A simple bus wrapper was placed around the generated VHDL to place the IP on to the local bus supported by the FPGA card. The IP was then synthesized using Synplicity's Synplify and implemented using the Xilinx tool chain. The bus-wrapper also included a counter to time the last-data-in to first-data-out latency of the algorithm in clock cycles.

I. Hardware

To allow fast evaluation of the developed IP and a rich programming and visualization environment for analyzing the performance of the algorithms, an Alpha-Data card with a VirtexII Pro FPGA on a PCI carrier card was chosen. In these experiments, the on-chip Power PC was not used. The card comes with supporting software library to handle the configuration of the FPGA. A standard PC running Windows XP was used for the IP test bench.

II. Software

The FPGA test bench was written on a PC using C in Visual Studio .NET. The core of the test bench was taken from the test bench used within the CoDeveloper environment. Additional code was added to perform the Alpha Data card initialization and FPGA configuration bit stream load.

B. basic radix-2 fft in c

The classic software implementation of an FFT is a radix-2 version. The calculations consist of a series of butterfly calculations performed by three nested loops. In a decimation in time implementation, the inputs are supplied to the input butterfly stage in "bit-reversed order" and the outputs are in "natural order." Conversely, in decimation in frequency implementation, the inputs are in natural order and the outputs are in bit-reversed order. The two implementations are very similar and require the same computational power.

In this paper, we adopt the graphical notation for a butterfly presented in [4]. Figure 1 shows a 16-point decimation in time algorithm with the three software loops highlighted. In the figure, the wing tips of a butterfly (black dots) represent data storage while the bodies of a butterfly (blue dots) represent the complex multiplies and adds that define an FFT butterfly.

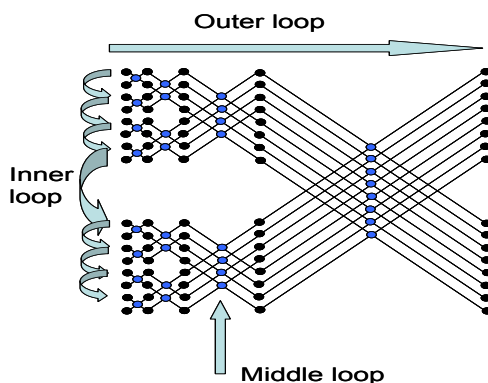


Figure 1. Classic decimation in time FFT

A radix-2 FFT requires $\log_2(N)$ stages where N is the number of sample points. In Figure 1, the stages are indicated by columns of the butterfly bodies and for our 16-point illustration, there are four stages. In this paper, we'll say that each stage is made up of a number of branches and the number of branches in this case decreases with each stage. For example, the first stage has 8 branches and the second stage has four stages. The middle loop in our software implementation walks the butterflies in each of these branches. Finally, the innermost loop in our algorithm walks the branches themselves.

Note that this implementation stores complex data in the "data" array as sequential real/imaginary pairs. It should also be noted that this implementation is a floating point version; we will not have floating point support in our C to RTL tool or in the FPGA so we will implement a fixed-point version.

The outer loop, in addition to the logic to walk the stages also contains the initialization of FFT "twiddle" factors for each stage. Likewise, the middle loop contains logic to update the twiddle factors for each butterfly. Variations on this classic software approach may include table look-ups of twiddle factors to speed up the code.



C. C to RTL Implementations of the FFT:

To examine the performance of a flow mapping a software implementation of an algorithm to a hardware target, we begin with the classic FFT in C algorithm. Other options are available, e.g. Radix-4 and pipelined approaches, but these are left for future study. The general I/O flow of our implementation is to write the data input to the FPGA, wait until the first data out is available, and then read all the resulting data.

The DSP benchmark used for a comparison of our results is the data given for the TI TMS320C55x processor [6]. The data is given as the number of clock cycles from last-data-in to first-data-available with no overflow scaling and is reported to be 23,848 clock cycles.

- Implementation A: Direct Mapping of the FFT

The first implementation of the FFT algorithm is virtually a direct port of the classic algorithm to Impulse. The following is the code for the innermost loop.

```
j = i+mmax;
CMPLX_RD( i, cmplxI );
CMPLX_RD( j, cmplxJ );
tempR = (wr*cmplxJ[REAL] - wi*cmplxJ[IMAG]) >> FAC_SHIFT;
tempI = (wr*cmplxJ[IMAG] + wi*cmplxJ[REAL]) >> FAC_SHIFT;
cmplxJ[REAL] = cmplxI[REAL] - tempR;
cmplxJ[IMAG] = cmplxI[IMAG] - tempI;
cmplxI[REAL] += tempR;
cmplxI[IMAG] += tempI;
CMPLX_WR( i, cmplxI );
CMPLX_WR( j, cmplxJ );
```

Comparing the code to the original code in **Error! Reference source not found.**, we note the following differences:

- The direct mapped version reads the butterfly inputs into the temporary variables cmplxI and cmplxJ. These variables are two element arrays used to represent complex numbers.
- The direct mapped version implements a scale factor by right shifting the result of multiply operations

This implementation of the FFT required about 1 week to develop and test in the CoDeveloper environment and required about 100 SLOC. We note also that the size of the FFT can be changed by changing a single #define in the source module. Table 1 shows that it requires 48,162 clocks to complete; about twice the number required by our benchmark DSP.

- Implementation B: Optimized complex number working variables

A simple first optimization to the algorithm is obtained when we realize that an FPGA and implements (within practical limits) as many memories as we need and bottlenecks in our code due to memory accesses can be reduced. Thus, in this implementation, we change the definition of cmplxI and cmplxJ from two element arrays to four individual integer variables: cmplxIReal, cmplxJImag, cmplxJReal, cmplxJImag. And, we redefine the CMPLX_RD and CMPLX_WR macros. This scheme allows simultaneous reading and writing of the working complex variables and, as Table 1 shows, reduces the inner-loop computation time from 9 to 6 clock cycles. These 3 clock cycles are saved for each of 5120 butterfly calculations, reducing the overall calculation time to 32802 clock cycles, about 1.4 times that of our benchmark DSP.

- Implementation C: Input buffer optimization

The optimization implemented in the previous version can also be applied to the input data buffer; it too can be composed of two distinct memories in order to improve the parallelism of our memory accesses. Thus, our input data buffer is replaced with imaginary and real arrays and the input data is directed to the appropriate array during the data load period.

This implementation again drops three clock cycles from our inner loop computation time and results in a total calculation time of 17,442 clock cycles, or, about 0.7 times that of a DSP. With this optimization, we are now beating the DSP performance in terms of clock cycles to complete the job.

- Implementation D: Further Parallelization

Examination of Figure 1, shows that the two main branches of the FFT could execute in parallel until the last stage where the results would be combined. Likewise, this could be achieved with a decimation in frequency approach where after the first stage; two engines could run in parallel to produce the output data.

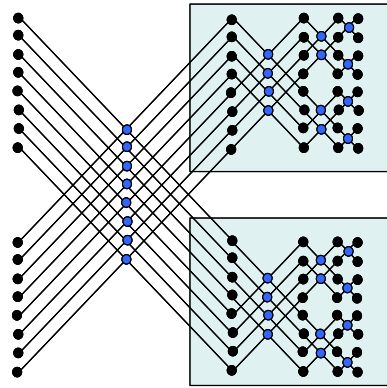


Figure 2. DIF FFT with two butterfly engines

Since ImpulseC will attempt to generate the fewest possible pipeline stages for our logic and create as much parallelism as possible, we only need to create two sets of variables and calculations within our main butterfly engine to effectively get two parallel machines. A more elegant solution here would have been to use the ImpulseC concept of processes, but the “cut and paste” code approach allows us to keep a structure for the code that resembles the original software implementation.

Further, since the data in the DIF arrives in order, we could be processing the first stage of butterflies as the second half of the input data arrives. The I/O for the output phase can also be overlapped with the butterfly calculations by indicating that data is ready to the host processor after completion of the penultimate butterfly stage. If we do this, we can complete each of the last butterfly stages as the host processor reads back the data. Effectively, we are “hiding” the first and last butterfly stages. Again, similar logic applies to a decimation in time implementation. But, here we used DIF because the multiplies on the output stage turn out to be “trivial” (by one) and make it more likely that we will get the data out as fast as the host can consume it. We took the tact here that there is more likely to be delay in the arrival of new data points than there is in the ability of the host to consume the output data. Figure shows the DIF algorithms with the input and output stages highlighted.

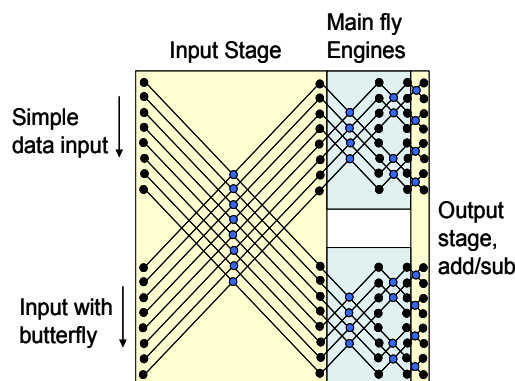


Figure 3. DIF implementation with stage hiding.

Since there is no way in ImpulseC to directly specify the reuse of multipliers within the FPGA and our input stage and second main butterfly engine result in four additional multipliers each, we looked for a way to reduce the total number of multipliers. This was achieved by moving the twiddle factor updates into ROM instead of calculating them in the middle loop using multiplies. The number of block rams on a device tends to equal the number of multipliers available and thus we traded block RAMs for multipliers in an attempt to keep their usage equal. Implementation D uses 12 multipliers and 8 block RAMs.

The total execution time for implementation D is 7186 clock cycles, about 0.3 times that of our DSP benchmark. Let’s examine where the savings come from (vs. Implementation C). First, we have implemented two main engines in parallel and each stage thus only has to run half as many butterflies, so the savings is:

$$8 \text{ stages} * (512/2 \text{ flies per stage}) * (3 \text{ clocks per fly}) = 6144 \text{ clocks} \quad (1)$$

Next, we note that the overhead of running the outer and middle loops is also saved by running the processes in parallel. The overhead for the outer loop has been further reduced by a single clock cycle by moving the twiddle factors to ROM, but the overall savings of the outer loop is negligible. The overhead of running the inner-loop is reported by the ImpulseC compiler output to be 2 clock cycles per execution of the loop, and the net savings is:

$$2 \text{ clocks} * (\sum 2^n, n=1,2,\dots,8) \text{ loop iterations} = 1024 \text{ clocks} \quad (2)$$

Finally, the savings due to the hiding of the first and last stages is:

$$2 \text{ stages} * 512 \text{ flies} * 3 \text{ clocks} = 3072 \text{ clocks} \quad (3)$$



- **On Speed, Size, and Power**

This design is capable of running at 76MHz on a VirtexII Pro FPGA. This rate includes the penalty of moving data on and off the FPGA and no explorations were done into methods to improve the clock rate. The DSP for considered for our benchmark can operate at about twice our max frequency.

Power and energy estimates were performed for the FPGA and DSP options using the power estimation tools available from each vendor. The estimates were done separately for the data input/output phases and the butterfly calculation phases. The estimated power consumption for the DSP with 150MHz clock was about 165mW in both cases. Using an appropriate Virtex4 FPGA, the estimates came to about 400mW for the I/O phase and 800mW for the butterfly phase. The respective energy consumptions for the DSP and FPGA were 32 and 42 μ J.

IV. Results and Conclusions

Our DSP benchmark takes 23848 clock cycles to complete the FFT. While we can beat this by a factor of three, our maximum clock rate was only half that of the DSP and ways of improving the maximum clock rate of our design should be explored.

Table 1: implementation results

	A	B	C	D
Inner loop Clocks	9	6	3	3
Total clocks	48162	32802	17442	7186
Slices	536	398	425	859
Multipliers	8	8	8	12
Block RAMs	2	2	2	8

Our energy and size estimates show that the implementation offers an area improvement over a DSP solution but can not match the energy efficiency of the DSP solution.

This FFT began with a classic Radix2 software routine that took only a week to implement and we made simple variations on that design to explore the performance possibilities of implementations that maintain much of the structure of the original design. Parallelism was implemented here by “doubling-up” the software in our butterfly loop and overlapping the first and last butterfly stages with the I/O operations. Additional approaches to creating more parallelism that should be investigated include higher radix implementations, e.g. Radix4, and implementations that use Impulse C processes.

REFERENCES

- [1] W. H. Press et al., “Numerical Recipes in C,” 2nd ed., Cambridge: Cambridge University Press, 1992, p. 507.
- [2] Impulse Accelerated Technologies,
- [3] S. Sukhsawas and K. Benkrid, “A High-level Implementation of a High Performance Pipeline FFT on Virtex-E FPGAs,” in Proc 2004 IEEE Computer Society Annual Symposium on VLSI Emerging Trends in VLSI Systems Design.
- [4] L. R. Rabiner and B. Gold, “Theory and Application of Digital Signal Processing,” Englewood Cliffs: Prentice-Hall, 1975, pp. 360-362.
- [5] Xilinx Embedded Development Kit (EDK), <http://www.xilinx.com>.
- [6] Texas Instruments TMS320C55x DSP core, <http://www.ti.com>.
- [7] J. Ardini, “Demand and Penalty-Based Resource Allocation for Reconfigurable Systems with Runtime Partitioning,” to be presented at the *MAPLD 2005 International Conference*, Sept. 7-9 2005, Washington, D.C.



MATRUSRI ENGINEERING COLLEGE

(Approved by AICTE, Affiliated to Osmania University)

#16-1-486, Saidabad, Hyderabad - 500059



Sponsored by

MATRUSRI EDUCATION SOCIETY



ISBN: 97881-936274-0-2



1ST NATIONAL CONFERENCE ON TRENDS IN SCIENCE, ENGINEERING AND TECHNOLOGY (NTSET - 2018)

February 2nd & 3rd - 2018

TECHNICAL PAPER ABSTRACTS



ORGANIZED BY

MATRUSRI ENGINEERING COLLEGE

(Approved by AICTE, Affiliated to Osmania University)

#16-1-486, Saidabad, Hyderabad - 500059



Sponsored by

MATRUSRI EDUCATION SOCIETY

ISBN: 97881-936274-0-2

**NTSET
2018**





A 64 BIT MAC UNIT DESIGN USING REVERSIBLE LOGIC GATE AND VEDIC MULTIPLIER

¹Mrs. B. Indira Priyadarshini, ²D.Niharika, ³ G.Pranaya

¹Assistant Professor, ^{2,3}Student

^{1,2,3}Department of Electronics and Communication Engg

^{1,2,3}Matrusri Engineering College, Saidabad, Hyd. India.

Abstract: A Vedic Multiplier and the reversible Logic Gates has designed and implemented in the multiply and Accumulate Unit (MAC) and that is shown in this project. A Vedic multiplier is designed by using Urdhva Triyakbhayam sutra and the adder design is done by using reversible logic gate. Reversible logics are also the fundamental requirement for the emerging field of quantum computing. The Vedic multiplier is used for the multiplication Unit so as to reduce partial products and to get high performance and lesser area. A reversible Logic Gate is used to get less power. The MAC is designed in Verilog HDL and the simulation is done in Xilinx 10.1. The FPGA implementation is done on Spartan3.

Index Terms: Vedic Multiplier, Reversible logic gate, Urdhva Triyakbhayam

I. INTRODUCTION

The MAC unit is to provide a physically compact, good speed and a low power consumption chip. The MAC unit has been extensively used in DSP, high speed processors for applications like filtering, signal conditioning etc. In order to improve the MAC unit speed, the partial product generation has to be reduced and the accumulator block usage has to be limited. The Vedic multiplication technique is used for the fastest operation with less partial propagation. Vedic maths tricks enhance the calculation 10 to 15 times than the usual method. Among the Vedic arithmetic the Vedic multiplication is used in the design of MAC. Reversible computing was started when the basis of thermodynamics of information processing was shown that conventional irreversible circuits unavoidably generate heat because of losses of information during the computation. The different physical phenomena can be exploited to construct reversible circuits avoiding the energy losses. One of the most attractive architecture requirements is to build energy lossless small and fast quantum computers. Most of the gates used in digital design are not reversible for example NAND, OR and EXOR gates. A Reversible circuit/gate can generate unique output vector from each input vector, and vice versa, i.e., there is a one to one correspondence between the input and output vectors. Thus, the number of outputs in a reversible gate or circuit has the same as the number of inputs, and commonly used traditional NOT gate is the only reversible gate. Each Reversible gate has a cost associated with it called Quantum cost. The Quantum cost of a Reversible gate is the number of 2*2 Reversible gates or Quantum logic gates required in designing. One of the most important features of a Reversible gate is its garbage output i.e., every input of the gate which is not used as input to other gate or as a primary output is called garbage output.

II. LITERATURE REVIEW

Jayakumar.S et.al. proposed that multiplication is an important essential characteristic in arithmetic operations. Multiplication-based operations such as multiply and Accumulate (MAC) and inner product are among some of the regularly used Computation. Tapsavi.B et.al. Described that carry choose adder is one of the speedy computing adder design. The pace of the multiplication operation of such an adder is reduced by lift propagation from enter to output. Neha Deshmukh et.al. Stated that array Multiplier requires more powerconsumption and offers top of the line quantity of elements required. Ponni.M et.al. The setup of the prefix network denotes the type of the Parallel Prefix Adder. The elevate pick out adder consists of two ripple lift adder and a multiplexer block.

III. PROPOSED METHOD:

The MAC unit is the hardware that performs the product of two numbers and stores the end result in the accumulator register. The 32 bit multiplier and 32 bit multiplicand are improved together to provide 64 bit output. The main objective is to

Design A 64 BIT MAC Unit Design Using Vedic Multiplier and Reversible Logic Gate Implementation of Testable Reversible Sequential Circuit on FPGA. To design and implement the multiply and Accumulate Unit (MAC) in Verilog HDL and the simulation and synthesis is done in both RTL compiler using Xilinx 14.2.

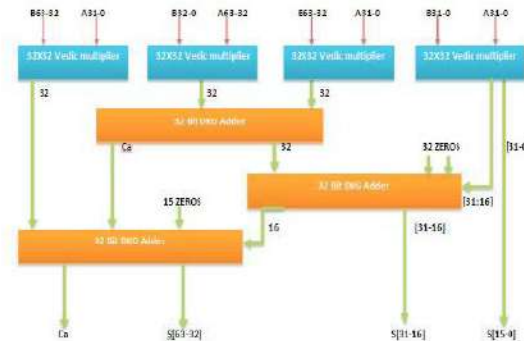


Figure1. Block diagram of 64*64 bit Vedic multiplier

Figure shows the 64*64 Vedic multiplier. The Vedic multiplier has to be designed by hierarchical method. The design of the Vedic multiplier requires the lower level bit multiplier say 32*32 bit for the design of 64*64 bit Vedic multiplier. The design requires the intermediate adder stage. The adder stage of the reversible logic adder is designed using one of the most popular reversible DKG gate. The two numbers A,B are applied in the crosswise order. The inputs are of 64 bit and final result will be maximum of 128 bit. The logic behind the operation of the architecture is given number which is of 64 bit and is sub divided into two halves each of 32 bit. The input to the first stage of multiplier will be lower half of both the numbers, second and third stage will be swapped halves of the two and final and fourth stage will be the upper half of the numbers. The multiplication operation is followed by the addition operation which can add 64 bit numbers and the sum will be saved, the carry if generated will be added to the next successive stages and so on. The adder will be appended with zeros to one of the input in order to equate the number of bits so as the addition operation can be performed without any error. Three DKG adder stage can be rectified by inspecting the architecture of the 64 bit multiplier. The adder is responsible to provide the carry of the last stage where the output of the last stage adder is considered as the sum. The LSB bits will be directly taken from the last stage of the multiplier. The architecture has the 32 bit multiplier whose architecture is the photocopy of the 64 bit multiplier except the difference is the 32 bit architecture consists of the inputs to be 32 bits and the reversible DKG adder of 32 bit.

I. MAC unit Implementation:

Multiply-accumulate operation is one of the basic arithmetic operations extensively used in modern digital signal processing (DSP). The MAC unit provides high speed multiplication, multiplication with cumulative addition, multiplication with cumulative subtraction, saturation, and clear-to-zero functions. Therefore, the main motivation is to investigate various pipelined MAC architectures and circuit and the design techniques which are suitable for the implementation of high through put signal processing algorithms. Hence, a high-speed MAC is capable of supporting multiple precisions and parallel operations is highly desirable. MAC is composed of an adder, multiplier and an accumulator. The implementation of the multiplier is in the form of Booth Multiplier. The adder used is Ripple Carry Adder.

The Parallel in Parallel out (PIPO) shift register is used as the accumulator. The inputs for the MAC are to be fetched from memory location and fed to the multiplier block of the MAC, which will perform multiplication and give the result to the adder which will accumulate the result and then will store the result into a memory location. Entire process is to be achieved in a single clock cycle in the architecture of the MAC unit. The MAC design consists of one 8-bit booth multiplier, one 16-bit ripple carry adder & a 17-bit accumulator using PIPO shift register. To multiply the values of A and B, Booth multiplier is used instead of conventional multiplier because it is simple to design. However to gain better performance, parallel multipliers are used as they are the fastest but the designs are much more complex. Hence, when regularity, high performance & low power are primary concerns, Booth Multipliers tend to be the primary choice. MAC architecture is demonstrated as figure below.

A multiplying function can be carried out in three ways: partial product Generation (PPG), partial product addition (PPA), and final conventional addition. The two bottle necks should be considered are increasing the speed of MAC are partial product reduction and accumulator block. The 32 bit Mac design by using Vedic multiplier and reversible logic gate can be done in two parts. First, multiplier unit, where a conventional multiplier is replaced by Vedic multiplier using UrdhavaTriyagbhayam sutra. Multiplication is the fundamental operation of MAC unit. Power consumption, dissipation,



area, speed and latency are the major issues in the multiplier unit. So, to avoid them, prefer for fast multipliers in various applications of DSP, networking, etc. There are two major criterion improve the speed of the MAC units are reducing the partial products and because of accumulator burden is getting reduced. The basic operational blocks in digital system in which the multiplier determines the critical path and the delay. The partial products are produced by $2N-1$ cross products of different widths for $N*N$. The partial products are generated by Urdhava sutra is by Criss Cross Method. The maximum number of bits in partial products will lead to Critical path. The second part of MAC is Reversible logic gate. In modern VLSI, fast switching of signals leads to more power dissipation. Loss of every bit of information in the computations are not reversible is $kT\log(2)$ joules of heat energy is generated, where k is Boltzmann's constant and T the absolute temperature at which computation is performed. In recent years, reversible logic functions has emerged and played a vital role in several fields such as Optical, Nano, Cryptography, etc. The design of MAC architecture consists of 3 sub designs.

- Design of 64 bit Vedic multiplier.
- Design of adder using DKG gate reversible logic.
- Design of accumulator which integrates both multiplier and adder stages.

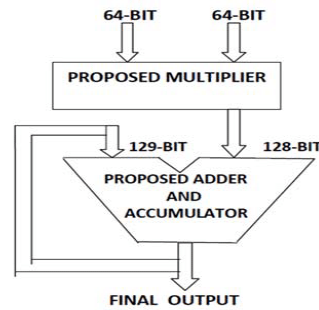


Figure2: Proposed MAC unit

II. Using Vedic Multiplier (Urdhava Triyagbhayam Sutra):

Digital multipliers are the core components of all Digital signal processors. The speed of DSP is largely determined by the speed of its multipliers. Multiply Accumulate (MAC) operation is a commonly used operation in various Digital Signal Processing Applications. Use of a Digital Signal processor can significantly increase the performance of a MAC. Normally a multiply accumulate unit consists of a multiplier along with an accumulator which stores previous multiplication products. Since system performance widely depends on time needed to execute the instruction and multiplication being the most time consuming, any improvement to multiplication will inherently improve the system performance. Multiplication can be designed using several algorithms such as array, Booth, carry save, Modified Booth algorithm and Wallace tree. In array multiplier multiplication of two numbers can be obtained with one micro operation. It is a fast method of multiplication since the only delay is time for the signals to propagate through the gates. But it requires larger number of gates and so it is less economical. Here we use Urdhva Tiryagbhyam of Vedic mathematics. This sutra was traditionally used in ancient for the multiplication of two decimal numbers in relatively less time. The architecture of urdhva tiryagbhyam is explained that any $N \times N$ multiplication can be efficiently designed by breaking it into smaller numbers of size $(N/2=n)$ and these smaller numbers can again broken into smaller numbers $(n/2)$ till we reach multiplicand size of (2×2) . Thus simplifying the whole multiplication process. This work present a systematic design methodology for fast and area efficient digital multiplier based on Vedic mathematics and then a MAC unit has been made which uses this multiplier. The main purpose of Vedic Mathematics is to able to solve complex calculations by simple techniques. The formula being very short makes them practically simple in implementation. urdhva triyagbhayam is also known as vertically-cross wise sutra. This sutra is general formula applicable to multiplication operation.

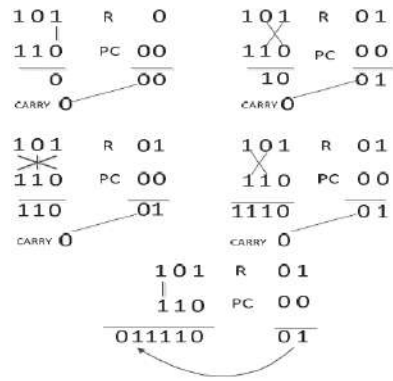


Figure3. Multiplication of two numbers Using Urdhva Triyakbhyam Sutra

III. Adders using reversible logic:

A gate is considered to be reversible only if for each distinct input there is a distinct output assignment. Thus inputs to reversible gates can be uniquely determined from its outputs. A reversible gate must have same no of inputs and outputs.

Basic gates:

In classical computers, only NOT gate performs reversible operation since it has an equal number of inputs and outputs with their unique one to one mapping. Some reversible gates have already been proposed in literature like the controlled-not (CNOT) (proposed by Feynman), Toffoli and Fredkin gates, IG Gate and MIG gate. Reversible gates have various application in the designing of adders, subtractors, multipliers etc, same like classical computers.

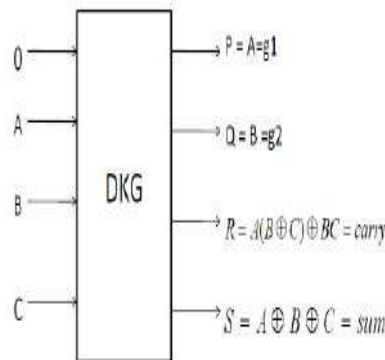
Truth Table:

A	P
0	1
1	0

AB	PQ
00	00
01	01
10	11
11	10

ABC	PQR
000	000
001	001
010	010
011	011
100	100
101	101
110	111
111	110

DKG as Full Adder:



The adder used in the 64 bit Vedic multiplier is the reversible adder called DKG gate. The design of adder is based on the property of the reversibility. The DKG gate consists of four inputs and four outputs among which two are garbage outputs. The ancillary bits which are also called the garbage bits are required to obtain the balancing between the input and output to satisfy the condition of equal number of input and output. The DKG gate which is 4*4 reversible logic is shown in the figure.

- The DKG gate works as both full adder and full subtractor.
- By setting the ancillary bit to the first input the adder or subtractor is selected.
- If input A=0, the gate works as full adder and if input A=1, the gate works as full subtractor.



Once the sum has been determined, it is written to the main memory or to another register. In computing, especially digital signal processing, the multiply–accumulate operation is a common step computes the product of two numbers and adds product to an accumulator. The hardware unit performs the operation is known as a multiplier–accumulator (MAC, or MAC unit); the operation itself is also often called a MAC or a MAC operation. The MAC operation modifies an accumulator a :

$$a \leftarrow a + (b \times c)$$

(1)

When done with floating point numbers, it might be performed with two rounding's (typical in many DSPs), or with a single rounding. When performed with a single rounding, it is called a fused multiply–add (FMA) or fused multiply–accumulate (FMAC).

Modern computers may contain a dedicated MAC, consisting of a multiplier implemented in combinational logic followed by an adder and an accumulator register stores the result. The output of the register is fed back to one input of the adder, so on each clock cycle, the output of the multiplier is added to the register. Combinational multipliers require a large amount of logic, but can compute a product much more quickly than the method of shifting and adding typical of earlier computers. The first processors to be equipped with MAC units were digital signal processors, but the technique is now also common in general-purpose processors.

III. CONCLUSION

The design of Vedic multiplier with 64 bits and reversible logic are quite good. MAC unit is designed using basic building blocks and its performance has been analyzed for all the blocks. Therefore, the Urdhava Triyagbhayamsutra with 64-bit Multiplier and reversible logic is the best in all aspects like speed, delay, area and complexity as compared to other architectures.

REFERENCES

- [1] Vaijyanath Kunchigi ,Linganagouda Kulkarni, Subhash Kulkarni, "32-bit MAC unit design using Vedic multiplier International Journal of Scientific and Research Publications", Volume3, Issue 2, February 2013
- [2] Ramalatha, M.Dayalan, K D Dharani, P Priya, and S Deoborah, "High Speed Energy Efficient ALU design using Vedic multiplication techniques, International Conference on Advances in Computational Tools for Engineering Applications", 2009. ACTEA '09.pp. 600 -3, Jul 15-17, 2009.
- [3] SreeNivas A and Kayalvizhi N. Article: "Implementation of Power Efficient Vedic Multiplier. International Journal of Computer Applications" 43(16):21-24, April 2012. Published by Foundation of Computer Science, New York, USA
- [4] Vaijyanath Kunchigi, Linganaagouda Kulkarni, Subhash Kulkarni, "High Speed and Area Efficient Vedic Multiplier, International Conference on Devices, Circuits and Systems" (ICDCS), 2012.
- [5] D.P.Vasudevan, P.K.Lala, J.Di and J.P.Parkerson, "Reversible logic design with online testability", IEEE Trans. On Instrumentation and Measurement, vol.55, no.2, pp.406-414, April 2006.
- [6] RaghavaGaripelly , P.MadhuKiran , A.Santhosh Kumar, "A Review on Reversible Logic Gates and their Implementation International Journal of Emerging Technology and Advanced" Engineering Website: www.ijetae.com (ISSN 2250-2459, ISO 9001:2008 Certified Journal, Volume 3, Issue 3, March 2013.



MATRUSRI ENGINEERING COLLEGE

(Approved by AICTE, Affiliated to Osmania University)

#16-1-486, Saidabad, Hyderabad - 500059



Sponsored by

MATRUSRI EDUCATION SOCIETY



ISBN: 97881-936274-0-2



1ST NATIONAL CONFERENCE ON TRENDS IN SCIENCE, ENGINEERING AND TECHNOLOGY (NTSET - 2018)

February 2nd & 3rd - 2018

TECHNICAL PAPER ABSTRACTS



ORGANIZED BY

MATRUSRI ENGINEERING COLLEGE

(Approved by AICTE, Affiliated to Osmania University)

#16-1-486, Saidabad, Hyderabad - 500059



Sponsored by

MATRUSRI EDUCATION SOCIETY

ISBN: 97881-936274-0-2

**NTSET
2018**





IMPROVED DESIGN OF LOW POWER TPG USING LP LFSR

¹Mrs.Indira Priyadarshini, ²B.Navaneetha, ³M.Akhila

¹Assistant Professor, ^{2,3} Student

^{1,2,3}Department of Electronics and Communication Engineering

^{1,2,3}Matrusri Engineering College, Saidabad, India.

Abstract: This paper presents a novel test pattern generator which is more suitable for built in self test (BIST) structures used for testing of VLSI circuits. The purpose of the BIST is to reduce power dissipation without affecting the fault coverage. The demonstrated test pattern generator reduces the switching activity among the test patterns at the most. In this method, the single input change patterns generated by a counter and a gray code generator are Exclusive-ORed with the seed generated by the low power linear feedback shift register [LPLFSR]. The proposed scheme is evaluated by using a 4x4 Braun array multiplier. The System-On-Chip (SOC) approach is adopted for implementation on Altera Field Programmable Gate Arrays (FPGAs) based SOC kits with Nios II soft-core processor. From the implementation results, it is verified that the testing power for the proposed method is reduced by a significant percentage

Index Terms – FPGA, BIST, LP-LFSR, Switching Activity.

I. INTRODUCTION

In VLSI circuits, built in self test (BIST) are used for testing. The objective of the BIST is to reduce power dissipation without affecting the fault coverage[1]. The main challenging areas in VLSI circuits are cost, performance, reliability, power, testing and area. The demand for portable computing devices and communication system are rapidly increasing. These applications require low power dissipation for VLSI circuits[2]. The ability to design, fabricate and test Application Specific Integrated Circuits (ASICs) as well as FPGAs with gate count of the order of a few tens of millions has led to the development of complex embedded SOC. Hardware components in a SOC may include one or more processors, memories and dedicated components for accelerating critical tasks and interfaces to various peripherals. One of the approaches for SOC design is the platform based approach. For example, the platform FPGAs such as Xilinx Virtex II Pro and Altera Excalibur include custom designed fixed programmable processor cores together with millions of gates of reconfigurable logic devices. In addition to this, the development of Intellectual Property (IP) cores for the FPGA's for a variety of standard functions including processor's, enables a multimillion gate FPGA to be configured to contain all the hard-core processors and they can be enhanced with custom hardware to optimize them for specific application. Power dissipation is a challenging problem for today's System-onChips (SOCs) design and test.

II. LITERATURE SURVEY

Y.Zorian[3] presented that the power dissipation of a system in test mode is more than in normal mode. P.Girard[4] demonstrated that four reasons are blamed for power increase during test. Due to nature of test patterns, high switching activity occurs. During test mode, parallel activation of internal cores happens. Extra design-for-test (DFT) circuitry consumes power. Low correlation among test vectors.

MechrdadNourani[5] explained that this extra average power consumption and peak power consumption can create problems such as instantaneous power surge that cause formation of hot spots, circuit damage, difficulty in performance verification and reduction of the product field and life time. Thus, special care must be taken to ensure that the power rating of circuits is not exceeded during test application. Different types of methods are stated to control the power consumption. These methods mainly includes algorithms for test scheduling with minimum power, techniques to reduce peak power and average power, techniques for reducing power during scan testing and BIST (built-in-self-test) technique. In order to minimize the time required for adjustment of the parameters, off-chip communication between a processor and the FPGA is bound to be slower than on-chip communication. The BIST (built-in-self-test) approach using design for testability technique is presented for this case. Different techniques are available to reduce the switching activities of test pattern, which reduces the power in test mode. P .Giard[6] proposed a modified clock scheme for linear feedback shift register (LFSR), in which only half of the D flip-flops works. Thus, only half of the test pattern can be switched. S.K.Guptha[7] determined a BIST TPG for low switching activity in which there is d-times clock frequency between slow LFSR and normal LFSR and thus, the test pattern generated by original LFSR is re-arranged to reduce the switch frequency. MechrddadNourani[5] presented low transition test pattern generator (LT-TPG) which reduces the average and peak power of a circuit during test. The above said techniques can reduce the average power compared to

traditional linear feedback shift register (LFSR). A better low power can be achieved by using single input change pattern generators.

III. POWER ANALYSIS FOR TESTING:

In CMOS technology, the power dissipation can be classified into static and dynamic. Static power dissipation is mainly due to the leakage current. Dynamic power dissipation is due to switching transient current and charging and discharging of load capacitances. Some significant parameters for evaluating the power consumption of CMOS circuits are discussed below.

$$E_i = V_d 2C_0 F_i S_i \quad (1)$$

Where V_d is the supply voltage, C_0 is the load capacitance. The product of F_i and S_i is called weighted switching activity of internal circuit node i . The average power consumption of internal circuit node i can be given by,

$$P_i = V_d 2CFS f \quad (2)$$

f is the clock frequency. The summary of P_i of all the nodes is named as average power consumption. It can be observed from (1) and (2) that the energy and power consumption mainly depends on the supply voltage, switching activities and clock frequency. This paper reduces the switching activity as low as possible at the inputs of the circuit which is under test

A. BIST Approach:

BIST is a design for testability (DFT) technique in which testing is carried out using built-in hardware features. Since testing is built into the hardware, it is faster and efficient. The BIST architecture shown in fig.1 needs three additional hardware blocks such as a test controller, a test pattern generator and output response analyzer.

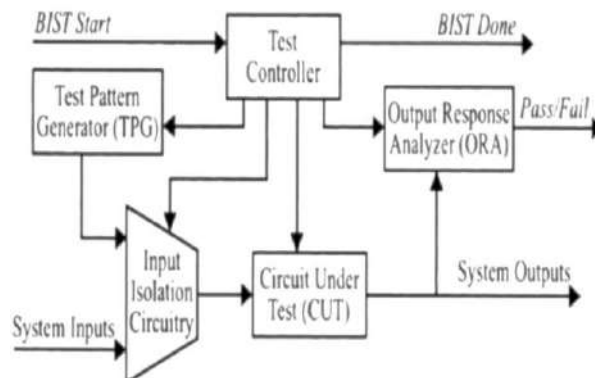


Figure1: BIST Architecture

A test controller provides a control signal to activate all the blocks. For test pattern generators, we can use either a ROM with stored patterns, or a counter or a linear feedback shift register (LFSR). A response analyzer is a compactor with stored responses or an LFSR used as a signature analyzer. BIST has some major drawbacks where architecture is based on the linear feedback shift register [LFSR]. The circuit introduces more switching activities in the circuit under test (CUT) during operation test than that during normal operation. R.S.Katti et al., [12] proposed that it causes excessive power dissipation and results in delay penalty into the design

IV. PROPOSED METHOD

Linear feedback shift register [LFSR] is used due to the simplicity of the circuit and less area occupation, for generating test patterns. In this paper, we determined a novel architecture which generates the test patterns with reduced switching activities. Figure3 shows the Low power test pattern generator (LP-TPG) structure consists of modified low power linear feedback shift register (LP-LFSR), m-bit counter, gray code generator, NOR-gate structure and XOR array. The m-bit counter is initialized with Zeros and which generates 2^m test patterns in sequence. A gray code generator and m-bit counter are controlled by common clock signal [CLK]. The output of m-bit counter is applied as input to a NOR-gate structure and a gray code generator. When all the bits of counter output are Zero, the NOR-gate output is one. Only when the NOR-gate output is one, the clock signal is applied to activate the LP-LFSR which generates the next sequence. The sequence generated from LP-LFSR is Exclusive-ORed with the sequence generated from gray code generator. The patterns generated from the Exclusive-OR array are the final output patterns.

A. V. LP-LFSR ALGORITHM

the LP-LFSR algorithm is given below:



- Consider a N-bit internal (or) external linear feedback shift register [$n > 2$].
- For example n-bit, external LFSR is considered which consists of n-flip flops in series. A common clock signal is applied for all flip flops as control signal.
- For exchanging the output of adjacent flip flops, multiplexers are used. The output of the last stage flip flop is taken as a select line.
- If the output of last stage flip flop is Zero, swapping will not be carried out.
- If the output of last stage flip flop is one, any one of the flip flop output is swapped with its adjacent flip flop output value.
- From other flip flops, the output will be taken as such.
- If the LFSR is moved through a complete cycle of 2^n states then expected transitions are 2^{n-1} . When the output of the adjacent flip flops are swapped, the expected transitions are 2^{n-2} . Thus, the transitions produced are reduced by 50% compared with original LFSR. The transition reduction is concentrated mainly on any one of the multiplexer output.
- Gray converter modifies the counter output such that two successive values of its output are differing in only one bit.
- Thus, the XOR result of the sequences is single input changing sequence. In turn reduces the switching activity and hence, the power dissipation is very less compared with conventional LFSR. The below patterns shows the counter and its respective gray value. It is shown that all values of $g[2:0]$ are single input changing patterns.

Patterns:

K [2:0] g [2:0]
 K0= 000 g0= 000
 K1= 001 g1= 001
 K2= 010 g2= 011
 K3= 011 g3= 010
 K4= 100 g4= 110
 K5= 101 g5= 111
 K6= 110 g6= 101
 K7= 111 g7= 100

V. IMPLIMENTATION DETAILS:

To validate the effectiveness of the proposed method, we select test pattern generator (TPG) using conventional linear feedback shift register [LFSR] for comparison with proposed system. Table 1 shows the power consumption comparison between TPG using conventional LFSR and the proposed LPLFSR after applying the generated patterns to the 4x4 braun array multiplier. The static power dissipation from conventional LFSR and proposed LP-LFSR are shown.

Table1: Comparison of power dissipation

	Conventional LFSR with 4x4	Proposed LP-LFSR With 4x4
Registers	81	---
Frequency (MHz)	132.33	107.7
Static power dissipation (mV)	80.03	59.84

From the implementation details, it is verified that the presented method gives better power reduction compared to the existing method.

VII. CONCLUSION

A low power test pattern generator has been proposed which consists of a modified low power linear feedback shift register (LP-LFSR). The sequence generated from LPLFSR is Ex-ORed with the single input changing sequences generated from gray code generator, which effectively reduces the switching activities between the test patterns. Thus, the proposed method reduces the power consumption during testing mode with minimum number of switching activities using LP-LFSR instead of conventional LFSR.

REFERENCES

[1] A.Kavitha, G.Seetharaman, T.N.Prabhakar and Shrinithi.S “Design of Low Power TPG Using LP-LFSR”, 2012 third international conference on intelligent systems modeling and simulation.



- [2] BalwinderSingh, Arunkhosla and SukhleenBindra “Power Optimization of linear feedback shift register(LFSR) for low power BIST”, 2009 IEEE international Advance computing conference(IACC 2009) Patiala,India 6-7 March 2009.
- [3] Y.Zorian, “A Distributed BIST control scheme for complex VLSI devices,” Proc. VLSI Test Symp., P.4-9, 1993.
- [4] P.Girard, ”survey of low-power testing of VLSI circuits,” IEEE design and test of computers, Vol. 19,no.3,PP 80-90,May-June 2002.
- [5] MechrdadNourani, ”Low-transition test pattern generation for BISTBased Applications”, IEEE TRANSACTIONS ON COMPUTERS, Vol 57,No.3 ,March 2008.
- [6]P.Girard, L.Guiller, C.Landrault, S.Pravossoudovitch,andH.J.Wunderlich, ” A modified clock scheme for a low power BIST test pattern generator,” 19th IEEE proc. VLSI test Symp.,CA,pp-306- 311,Apr-May 2001.
- [7] S.Wang and S.K.Gupta, ”DS-LFSR: a BIST TPG for low switching activity,” IEEE Trans.computer-aided design of Integrated circuits and systems, Vol. 21,No.7,pp.842-851,July 2002.
- [8] I.Voyiatzis,A.paschalis,D.Nikolos and C.Halatsis, ”An efficient built-in self test method for robust path delay fault testing,” Journal of electronic testing: Theory and applications Vol.8,No.2,pp-219- 222,Apr- 1996.
- [9] S.C.Lei, J.Guo, L.Cao, Z.Ye.Liu, and X.M.Wang, ”SACSR: A low power BIST method for sequential circuits”, Academic Journal of XI’AN jiaotong university(English Edition),Vol.20,no.3,pp.155- 159,2008.
- [10]R.H.He,X.W.Li and Y.Z.Gong, ” A scheme for low power BIST test pattern generator”, micro electronics& computer,no.2,pp.36-39 Feb.2003.



MATRUSRI ENGINEERING COLLEGE

(Approved by AICTE, Affiliated to Osmania University)

#16-1-486, Saidabad, Hyderabad - 500059



Sponsored by

MATRUSRI EDUCATION SOCIETY



ISBN: 97881-936274-0-2



Defects Detection in Printed Circuit Board using Integrated Framework

¹Dr. Pallavi Khare²Mrs. B. Indira Priyadarshini³ Mrs. Anjali VermaMatrusri Engineering College, Hyderabad Telangana, India⁽¹⁾⁽²⁾Maharaja Agrasen International College, Raipur (C.G), India⁽³⁾

Abstract: This paper was inspired for the most part by the need for more effective strategies in assessment of the PCB in creation handle. The goals of this venture are to give an economical and complete deformity system, by presenting and executing a PCB review framework utilizing Image preparing and Installed framework to evacuate the subjective parts of manual review. In the meantime, this framework gives constant evaluation of the PCB. The procedure of this proposed framework is to identify the deformity in view of the advanced picture of the PCB utilizing picture preparing strategies. There are a couple of steps taken after to distinguish imperfection of uncovered PCB, i.e. framework should gather PCB pictures through camera, from that point by picture acknowledgment also, examination handle, the pictures ought to be looked at with the layouts. The normal deformities, for example, short circuit, open circuit, shorts, missing gaps and other imperfections can be discovered accurately. To get the subtle elements about the imperfections, extricating the auxiliary components in light of the provincial properties, for example, edge, local territories, introduction and so on. At long last the acknowledgment results will be gained and announced. Under the control of the Controller, the PCB conveying segments like transport line, DC engine naturally move the given PCBs. Moving and controlling of the subsystem can be accomplished by getting the focal PC's control charges and handling is finished utilizing MATLAB. The resultant information will be sent to the focal PC and shown on GUI.

Keywords: Efficient technique, Image processing, Manual Inspection, Structural features, Subsystems.

1. INTRODUCTION

The PCB (printed circuit board) fabricating is winding up plainly more vital as the electronic buyer items, for example, cell phones, tablet PCs, programmed clothes washers et cetera, are essential for our regular daily existence. An uncovered printed circuit board is a PCB that is utilized before the placement of parts and the patching procedure. It is utilized alongside different segments to deliver electronic merchandise. Amid the assembling of printed circuit sheets, widths of covers and conduits can change due to assembling imperfections, for example, tidy, over drawing, under carving, and spurious metals. Drawing is the procedure, where the copper board will experience peeling process, where the circuit format will be saved while whatever is left of the copper foundation will be washed out. So as to limit scrap caused by the wrongly carved PCB board, assessment must be done in early stage.

To diminish producing costs related with defected uncovered PCBs, the examination of exposed PCBs is required as the first step of the assembling procedure. It is vital to create the PCB with zero-abandons. This is to guarantee an amazing PCB that means dependable and quality advanced finished results. At first, the uncovered PCBs were inspected haphazardly utilizing manual assessment framework, which includes human administrators. This system is very exorbitant since it is profoundly blunder inclined due to human mistake. A more modern method for doing the assessment is the utilization of in-house circuit testing (ICT) system. This system utilizes an extremely costly machine that checks the conductivity of the PCB utilizing tests. In any case, the impediment of this system is it can just distinguish surrenders that depend on either shorts or open. This strategy is not economical in a long keep running as it takes many worker hours. Any misalignment can make the test fall flat completely. Additionally, it is difficult to check the whole PCBboards at each area immediately. Rather, the printed overlay is tested a specific interim of amount for manual investigation. As the electronic hardware innovation propels, the PCBpattern winds up noticeably denser and confused to facilitate littler finished results. In this manner, manual inspection is not appropriate any longer

There are three principle forms in PCB investigation: imperfection recognition, deformity characterization and deformity area. Right now there are numerous calculations created for PCB imperfection recognition and arrangement utilizing contact or noncontact strategies. PCB imperfections can be classified into two gatherings: Functional deformities and restorative deformities. Execution of the PCB gets influenced by the useful deformities. Corrective deformities influence the presence of the PCB, yet can likewise imperil its execution over the long haul because of unusual warmth scattering and dispersion of current. In the interim, the advances in PCs in term of rapid, huge memory with minimal effort have brought about better and less expensive gear for picture handling. In the meantime, the computerized PCB investigation framework gives continuous appraisal of the PCB board. Subsequently, it is pivotal to distinguish these two sorts of defects in the examination stage. Figure 1.1 demonstrates a simulated deformity free PCB picture design, while Figure 1.2 demonstrates a similar picture design with a variety of imperfections on it.

2. PROBLEM DEFINITION

The Fig 1.3 shows an image of practical PCB by which we cannot manually guess that it consists of defects or not. These kind manual inspection techniques can be helpful to extinct in the detection of error but not all the errors can be detected. For this reason an user friendly technique is required.

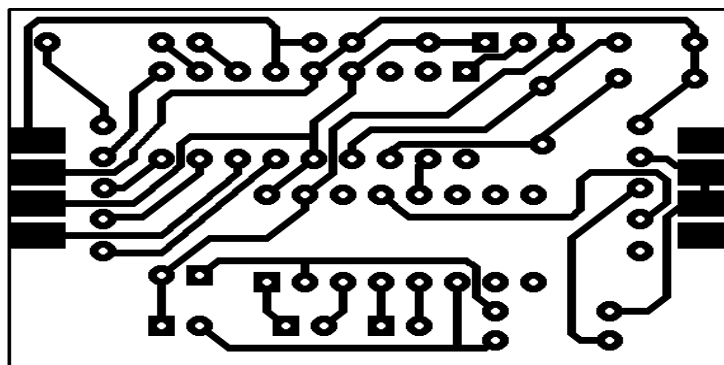


Figure 1.1 PCB without Defects

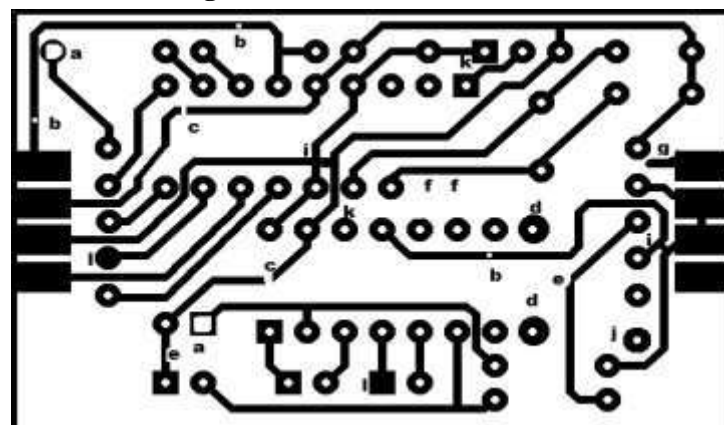


Figure 1.2 PCB with Defects

(a) breakouts, (b) Pin hole, (c) open-circuit, (d) under etch, (e) mouse bite, (f) missing conductor, (g) spurious copper, (i) short-circuit, (j) wrong side hole, (K) conductors too close, (l) missing hole, (m) over etch.

It is essential to create the PCB with zero-surrenders. This is to guarantee a top notch PCB that means solid and quality advanced end push. At first, the exposed PCBs (PCB without components connected to it) were investigated haphazardly utilizing manual examination framework, which includes human administrators.

This system is very expensive since it is exceedingly blunder inclined because of human mistake. An all the more sophisticated method for doing the review is the utilization of in-house circuit testing (ICT) strategy.

This technique uses a very expensive machine that checks the conductivity of the PCB using probes. However, the limitation of this technique is it can only detect defects that are based on either shorts or open. So it is essential to provide an alternative inexpensive and comprehensive defect detection technique.

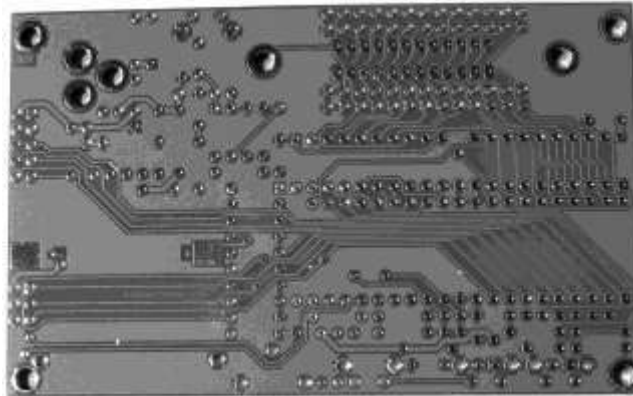


Figure 1.3: Image of practical PCB

3. LITERATURE SURVEY

Research on PCB mistakes detection and correction has received a renewed attention in recent years which has added a growth inside the industry issues. Many detection strategies were evolved and are being advanced, with maximum of them implemented in ultra-modern industry. Detection strategies encompass several methodologies out of them, detection the use of image processing is taken into consideration to be the maximum widely desired approach for utmost detection and correction. Advances in era and an increasing call for PCB's are driving a burgeoning for electronic industries to increase new strategies. This chapter evaluations some factors on how a PCB identification synthetic, its classifications, inspection techniques which had been used earlier and gives emphasis on how image processing got here into picture.

3.1 PCB Inspection Techniques

Within the early days of PCB manufacture, or the manufacture of any electronics gadget, all inspection changed into undertaken manually. This changed into the best alternative, but turned into recognized as having handiest limited cost. The repetitive nature of the procedure meant that many faults have been no longer noticed and handed on into the subsequent level of production undetected.

3.2 Various method of PCB Inspection

There are different techniques by which PCB assessment can be accomplished. They are as per the following,

GUI PCB investigation: as the call infers, (manual inspection[2]) incorporates man or lady assessors taking a gander at gatherings or different congregations to investigate them for inconveniences. This approach has been ended up being expensive and yielding terrible impacts before automation, it changed into the handiest way that examination may be done.

AOI PCB investigation: modernized or automatic (optical inspection[1]) is the favored approach of PCB assessment. It makes utilization of an optical contraption that takes aimage of a marvelous get together and looks at the 2 pics to hit upon any flaws or problems. This type of PCB assessment is broadly utilized and has been consummated with the goal that it works dependably.

AXI PCB review: with thickness on PCBs expanding and new IC mounting innovation getting utilized, no longer all patch joints might be unmistakable. Specifically while new gatherings are being engineered and new set up is being utilized, it is extremely fundamental to test that bond joints on programs which incorporate BGA's (ball framework clusters) are as a rule effectively welded. Optical examination can't get this on the

grounds that the more established joints aren't seen. regardless of the way that expensive and least difficult utilized for a little offer of the bind joints, and numerous others, they might be fundamental frequently.

PC supported turmoil recognition is an ex-pressure of computerized optical review structures expressed inside the past device are utilized the in-spection and gathering strategies of PCB. The primary issue of these systems lies in acquiring particular arrangements and uniform lighting apparatuses situations on depictions. by utilizing the option hand, the non-referential approach is uncommonly based at the outline lead checking (DRC) technique for uncovered PCBs.

3.3 Mathematical Morphology for Image Segmentation

A format picture is a grayscale picture of an awesome PCB design with no imperfections or twisting that is utilized as reference which is contains all deformities. each the pictures are divided into four portions each; rectangular stage, gap fragment, thick line area and thin-line segment as in figure 2.2. The square stage incorporates the images of square

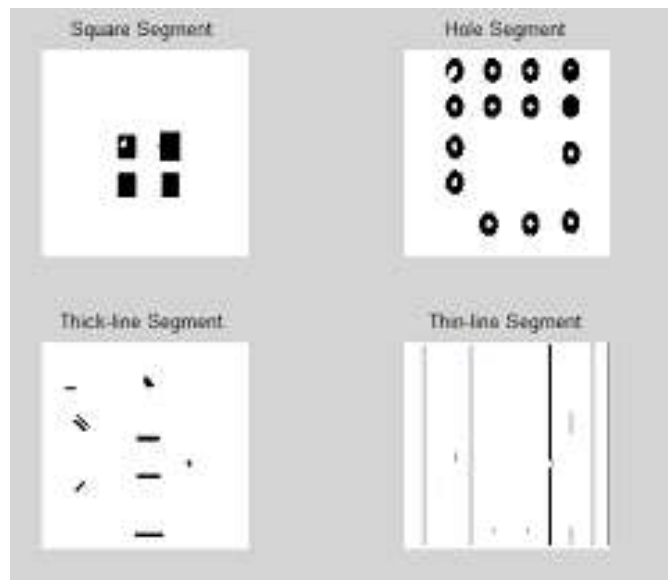


Figure 2.2 Segmentation of PCB Image.

pads, the empty segment incorporates the images of empty cushions, the thick-line area comprises of the images of thick conductors and the thin-line segment conveys the previews of thin conductors. a few imperfections best emerge on particular sections of test image alongside off base length gap, breakout and lacking empty for gap stage or lacking conductor and open circuit for thin line fragment. different deformities may exist in more than one sections. Mousechomp and beneath engraving may exist in each hollow and square sections. by methods for breaking the images into groups, a portion of the imperfections related with positive sections can without trouble be perceived and sorted. after this then musical show such has image expansion, picture subtraction, picture refinement administrator and now not musical show tor are finished and the yields obtained comprises of the previews assembled in this sort of path that from the ones pix imperfections can be marked and detected.

3.4 Image Processing

Primarily based on critiques of previous works, heriansyah et al developed a PCB picture segmentation algorithm by clustering primitive styles of a PCB images into 4 fundamental segments using mathematical morphology and windowing technique. Laterheriansyah classifies 12 out of the 14 recognized PCB defects by means of combining the image segmentation with synthetic neural network (ANN). lately, khalid produced an image processing set of rules using MATLAB with the aid of subtracting the snap shots and performing x-or operation. the 14 defects are then grouped into five categories.

4. PROPOSED SYSTEM

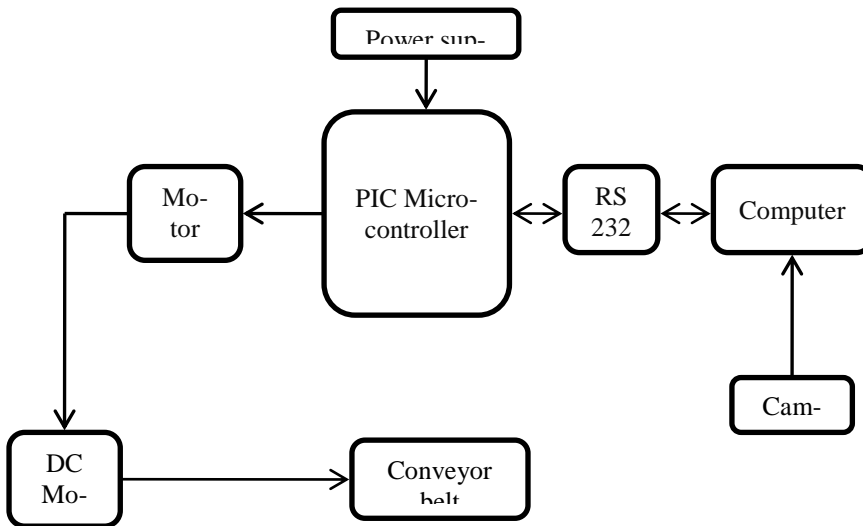


Figure 3.1 Block Diagram

4.1 Embedded System

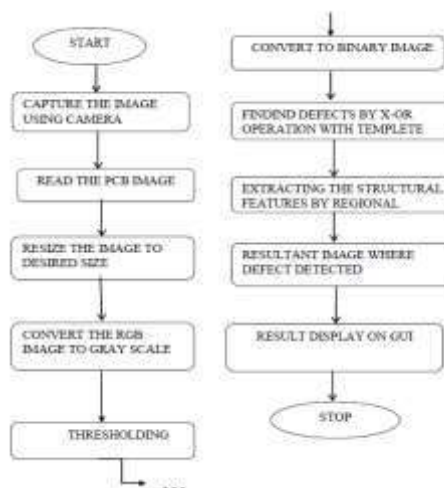
An embedded device is a mixture of each hardware and software program. the PIC microcontroller used is the heart of this device. by means of the aid of the module we're going to reap a communication link between the digital camera and GUI by the use of a PIC microcontroller, which scans the take a look at image with the assist of motor and conveyor belt. the PIC controller is interfaced with dc motor and personal pc by means of a motor driving force L293D and max 232 serial IC's as peripheral gadgets.

4.2 Image Subtraction Method

Image subtraction operation is carried out with the intention to get the variations between two images. the pictures are the reference images and the inspected images. The method compares each pictures pixel-by-pixel using xor logic operator. The subtraction operation will produce both negative or advantageous image, '1' represents white pixel and '0' represents black pixel in a binary picture. Policies exists for images subtraction operation

Rule 1: If $1-0 = 1$ then it gives positive pixel image Rule 2: If $0-1 = -1$ then it gives negative pixel image

4.3 Flow Chart



4.4 Implementation

The method of selecting the images and giving to system as an input is known as picture acquisition. Fine of obtaining image is one among key generation depends on camera. Whilst the digital camera gadgets are determined, it's far essential to provide proper illumination procedures to ensure picture excellent. When extracting images, the luminary depth and the stability of the auxiliary mild source have outstanding influences at the picture excellent. too weak or too robust light will cause the acute deterioration of the picture pleasant. moreover the PCB has excessive light reflection; it acts like a mirror, on the way to motive shadows of the object images whilst the images come into being by using the top light source, which affects the picture excellent significantly. secondly, the effect of envi-ronment light must be decreased in order that the objective capabilities of pictures captured have less distortion and the computing complexity of images processing algorithms may be decreased.

The surroundings light in laboratories is normally uniform, however the time various noise can make a high-quality effect on the surroundings mild in factories. so, we need shield the environ-mental light or beautify the mild depth to take away or weaken the impact of environmental light. while precise illumination conditions are glad, our layout is strong. on this device, actual PCB snap shots could be captured using a excessive decision pixels it 306wc computer webcam camera. the camera's resolution is carefully associated with the camera's price and additionally immediately affects the de-vice accuracy. in standard, excessive decision means better dimension accuracy, however the gadget's consistent with performance ratio also must be taken into consideration height in between the camera. there are 3 kinds of camera information transmitting modes: USB, camera link, gigabit ethernet ports we've used USB cable.

From the glide chart we get to realize overall go with the flow of the software program element which get execute in MATLAB. procedure get begin by way of urgent the button of start on GUI, so motor starts offevolved to run and PCB begins to transport closer to camera. as soon as PCB comes just under the camera it captures the image of it. computer reads the PCB image. Pre-processing part get finished as a way to make picture suitable for the similarly processing. it first off resizes the images on the way to make it appropriate to examine with template picture. then it converts of RGB image into grey scale for that it uses the thresholding technique to set the threshold value so that sooner or later image get converted into binary format. due to binary layout of the images processing will be easy as properly because it wishes less computational reminiscence in comparison to different codecs of images.

After preprocessing part is completed, it in step with-forms the difference operation with the given actual time image and saved template image, so defects get discover. then it extracts structural capabilities using local homes such as vicinity, eccentricity, principal axis duration, minor axis period, orientation and so on .from these houses it identifies hollow and line defects.

5. RESULTS AND DISCUSSIONS

On this device, we are displaying consequences on GUI due to the fact in this person can load the images, starts the processing on it via selecting given graphical elements for it .so t is well known that GUI could be very clean to apply because it does no longer need greater experience or training to use. Following images indicates final output displayed on GUI. We have developed our model on a real time device and its end result is getting displayed on GUI. Experimental end result indicates that the test image is grabbed and processed with the aid of the seasoned-posed set of rules Determine end result picture displaying line and one hole defects. Determine experimental setup of the machine

6. CONCLUSION

This research computerized PCB inspection gadget for detecting defects on naked printed circuit board. Within the technique of imposing the system, we found out that careful plans are required in each steps which includes image acquisition, picture processing, images aspect extraction and illness reputation. at gift, the completed designed machine can locate common PCB defects consisting of: lacking hollow, open circuit

and so on. after image had been captured images subtraction operation, minimum thresholding and noise elimination operations are used to get noise-unfastened tremendous and terrible pictures. then structural functions have extracted the usage of nearby houses to get the element statistics of the defects. even though, this gadget isn't being able to obtain GPS indicators in indoor areas and also delays in replying due to GPS. in view that GPS delays in receiving information from satellite TV for pc facet.

REFERENCES

- [1]. Moganti M., Dagli, C. H. and ShouTsunekawa, “**Automatic PCB Inspection Algorithms A Survey**”, Computer Vision and Image Understanding Vol. 63, No. 2, pp 287 – 313, 1996
- [2]. Eduardo Bayro-Corrochano, “**Review of Automated Visual Inspection 1983 to 1993 - Part I &11,**” SPIEIntelligent Robots and Cornpiiter Vision
- [3]. HisashiTsunekawa, “**Latest Image Evaluation Systems Aid Efforts for Product Quality,**” *Journal of Electronic Engineering*, No. 306, **Vol. 29**, pp. 72-77, June 1992. *XII*, Vol. 2055, pp. 128-172, 1993.
- [4]. Ajay Pal Singh Chauhan, Sharat Chandra Bhardwaj, “**Detection Of Bare PCB Defects By Image Subtraction Method Using Machine Vision**” IEEE World Congress On Engineering, Vol 2 WCE, July 6 - 8, 2011.
- [5]. SonalKaushik, Javed Ashraf, “**Automatic PCB Defect Detection Using Image Subtraction Method**”, International Journal Of Computer Science And Network (IJCSN), Volume 1, Issue 5, October 2012
- [6]. B. Kaur and J. Kaur, “**Applications of Image Processing: A Review**”, Proceedings of 25th International Conference on Electrical, Electronics and Computer Engineering, August 2013.
- [7]. Malge P.S., “**A Survey: Automated PCB Inspection Algorithm**”, International Journal Of Engineering Research And Technology, Vol 3, 2278-0181, January 2014.
- [8]. Malge P.S.” **Printed Circuit Board Defect Detection Using Mathematical Morphology and MATLAB Image Processing Tools**”, 2nd International Conference on Education Technology and Computer (ICETC), Vol 87, Feb 2014.
- [9]. Hara, Y., Akiyama, N. and Karasaki, K, “**Automatic Inspection System for Printed Circuit Boards**” IEEE Transactions on Pattern Analysis and Machine Intelligence”. Vol. PAMI-5. No.6,623 – 630.

Defects Detection in Printed Circuit Board using Integrated Framework

¹Dr. Pallavi Khare²Mrs. B. Indira Priyadarshini³ Mrs. Anjali VermaMatrusri Engineering College, Hyderabad Telangana, India⁽¹⁾⁽²⁾Maharaja Agrasen International College, Raipur (C.G), India⁽³⁾

Abstract: This paper was inspired for the most part by the need for more effective strategies in assessment of the PCB in creation handle. The goals of this venture are to give an economical and complete deformity system, by presenting and executing a PCB review framework utilizing Image preparing and Installed framework to evacuate the subjective parts of manual review. In the meantime, this framework gives constant evaluation of the PCB. The procedure of this proposed framework is to identify the deformity in view of the advanced picture of the PCB utilizing picture preparing strategies. There are a couple of steps taken after to distinguish imperfection of uncovered PCB, i.e. framework should gather PCB pictures through camera, from that point by picture acknowledgment also, examination handle, the pictures ought to be looked at with the layouts. The normal deformities, for example, short circuit, open circuit, shorts, missing gaps and other imperfections can be discovered accurately. To get the subtle elements about the imperfections, extricating the auxiliary components in light of the provincial properties, for example, edge, local territories, introduction and so on. At long last the acknowledgment results will be gained and announced. Under the control of the Controller, the PCB conveying segments like transport line, DC engine naturally move the given PCBs. Moving and controlling of the subsystem can be accomplished by getting the focal PC's control charges and handling is finished utilizing MATLAB. The resultant information will be sent to the focal PC and shown on GUI.

Keywords: Efficient technique, Image processing, Manual Inspection, Structural features, Subsystems.

1. INTRODUCTION

The PCB (printed circuit board) fabricating is winding up plainly more vital as the electronic buyer items, for example, cell phones, tablet PCs, programmed clothes washers et cetera, are essential for our regular daily existence. An uncovered printed circuit board is a PCB that is utilized before the placement of parts and the patching procedure. It is utilized alongside different segments to deliver electronic merchandise. Amid the assembling of printed circuit sheets, widths of covers and conduits can change due to assembling imperfections, for example, tidy, over drawing, under carving, and spurious metals. Drawing is the procedure, where the copper board will experience peeling process, where the circuit format will be saved while whatever is left of the copper foundation will be washed out. So as to limit scrap caused by the wrongly carved PCB board, assessment must be done in early stage.

To diminish producing costs related with defected uncovered PCBs, the examination of exposed PCBs is required as the first step of the assembling procedure. It is vital to create the PCB with zero-abandons. This is to guarantee an amazing PCB that means dependable and quality advanced finished results. At first, the uncovered PCBs were inspected haphazardly utilizing manual assessment framework, which includes human administrators. This system is very exorbitant since it is profoundly blunder inclined due to human mistake. A more modern method for doing the assessment is the utilization of in-house circuit testing (ICT) system. This system utilizes an extremely costly machine that checks the conductivity of the PCB utilizing tests. In any case, the impediment of this system is it can just distinguish surrenders that depend on either shorts or open. This strategy is not economical in a long keep running as it takes many worker hours. Any misalignment can make the test fall flat completely. Additionally, it is difficult to check the whole PCBboards at each area immediately. Rather, the printed overlay is tested a specific interim of amount for manual investigation. As the electronic hardware innovation propels, the PCBpattern winds up noticeably denser and confused to facilitate littler finished results. In this manner, manual inspection is not appropriate any longer

There are three principle forms in PCB investigation: imperfection recognition, deformity characterization and deformity area. Right now there are numerous calculations created for PCB imperfection recognition and arrangement utilizing contact or noncontact strategies. PCB imperfections can be classified into two gatherings: Functional deformities and restorative deformities. Execution of the PCB gets influenced by the useful deformities. Corrective deformities influence the presence of the PCB, yet can likewise imperil its execution over the long haul because of unusual warmth scattering and dispersion of current. In the interim, the advances in PCs in term of rapid, huge memory with minimal effort have brought about better and less expensive gear for picture handling. In the meantime, the computerized PCB investigation framework gives continuous appraisal of the PCB board. Subsequently, it is pivotal to distinguish these two sorts of defects in the examination stage. Figure 1.1 demonstrates a simulated deformity free PCB picture design, while Figure 1.2 demonstrates a similar picture design with a variety of imperfections on it.

2. PROBLEM DEFINITION

The Fig 1.3 shows an image of practical PCB by which we cannot manually guess that it consists of defects or not. These kind manual inspection techniques can be helpful to extinct in the detection of error but not all the errors can be detected. For this reason an user friendly technique is required.

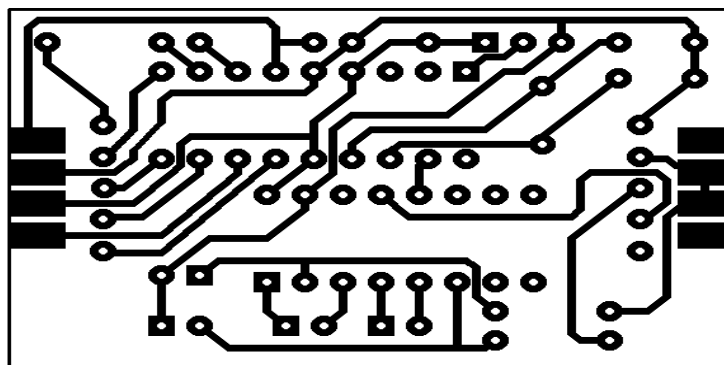


Figure 1.1 PCB without Defects

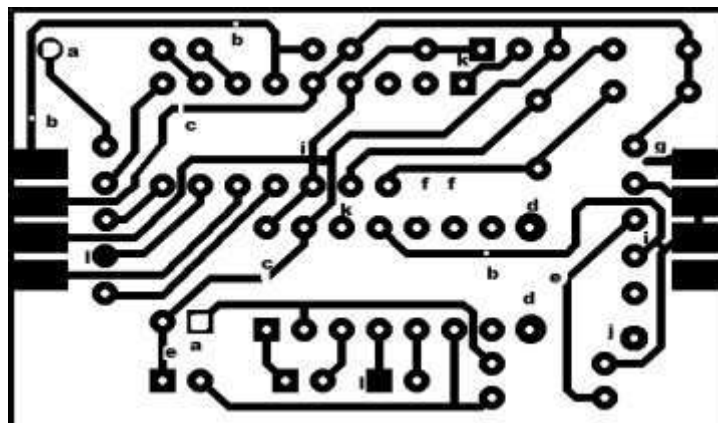


Figure 1.2 PCB with Defects

(a) breakouts, (b) Pin hole, (c) open-circuit, (d) under etch, (e) mouse bite, (f) missing conductor, (g) spurious copper, (i) short-circuit, (j) wrong side hole, (K) conductors too close, (l) missing hole, (m) over etch.

It is essential to create the PCB with zero-surrenders. This is to guarantee a top notch PCB that means solid and quality advanced end push. At first, the exposed PCBs (PCB without components connected to it) were investigated haphazardly utilizing manual examination framework, which includes human administrators.

This system is very expensive since it is exceedingly blunder inclined because of human mistake. An all the more sophisticated method for doing the review is the utilization of in-house circuit testing (ICT) strategy.

This technique uses a very expensive machine that checks the conductivity of the PCB using probes. However, the limitation of this technique is it can only detect defects that are based on either shorts or open. So it is essential to provide an alternative inexpensive and comprehensive defect detection technique.

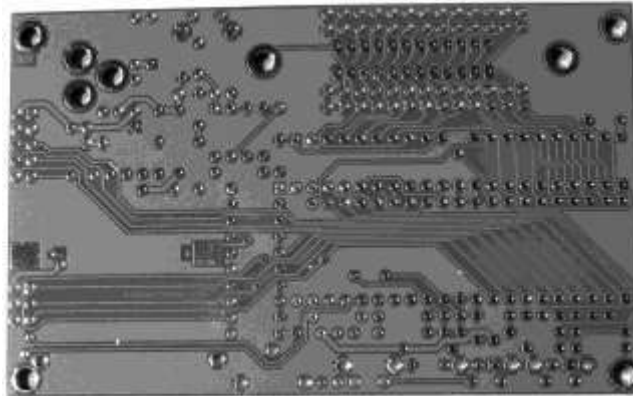


Figure 1.3: Image of practical PCB

3. LITERATURE SURVEY

Research on PCB mistakes detection and correction has received a renewed attention in recent years which has added a growth inside the industry issues. Many detection strategies were evolved and are being advanced, with maximum of them implemented in ultra-modern industry. Detection strategies encompass several methodologies out of them, detection the use of image processing is taken into consideration to be the maximum widely desired approach for utmost detection and correction. Advances in era and an increasing call for PCB's are driving a burgeoning for electronic industries to increase new strategies. This chapter evaluations some factors on how a PCB identification synthetic, its classifications, inspection techniques which had been used earlier and gives emphasis on how image processing got here into picture.

3.1 PCB Inspection Techniques

Within the early days of PCB manufacture, or the manufacture of any electronics gadget, all inspection changed into undertaken manually. This changed into the best alternative, but turned into recognized as having handiest limited cost. The repetitive nature of the procedure meant that many faults have been no longer noticed and handed on into the subsequent level of production undetected.

3.2 Various method of PCB Inspection

There are different techniques by which PCB assessment can be accomplished. They are as per the following,

GUI PCB investigation: as the call infers, (manual inspection[2]) incorporates man or lady assessors taking a gander at gatherings or different congregations to investigate them for inconveniences. This approach has been ended up being expensive and yielding terrible impacts before automation, it changed into the handiest way that examination may be done.

AOI PCB investigation: modernized or automatic (optical inspection[1]) is the favored approach of PCB assessment. It makes utilization of an optical contraption that takes aimage of a marvelous get together and looks at the 2 pics to hit upon any flaws or problems. This type of PCB assessment is broadly utilized and has been consummated with the goal that it works dependably.

AXI PCB review: with thickness on PCBs expanding and new IC mounting innovation getting utilized, no longer all patch joints might be unmistakable. Specifically while new gatherings are being engineered and new set up is being utilized, it is extremely fundamental to test that bond joints on programs which incorporate BGA's (ball framework clusters) are as a rule effectively welded. Optical examination can't get this on the

grounds that the more established joints aren't seen. regardless of the way that expensive and least difficult utilized for a little offer of the bind joints, and numerous others, they might be fundamental frequently.

PC supported turmoil recognition is an ex-pression of computerized optical review structures expressed inside the past device are utilized the in-spection and gathering strategies of PCB. The primary issue of these systems lies in acquiring particular arrangements and uniform lighting apparatuses situations on depictions. by utilizing the option hand, the non-referential approach is uncommonly based at the outline lead checking (DRC) technique for uncovered PCBs.

3.3 Mathematical Morphology for Image Segmentation

A format picture is a grayscale picture of an awesome PCB design with no imperfections or twisting that is utilized as reference which is contains all deformities. each the pictures are divided into four portions each; rectangular stage, gap fragment, thick line area and thin-line segment as in figure 2.2. The square stage incorporates the images of square

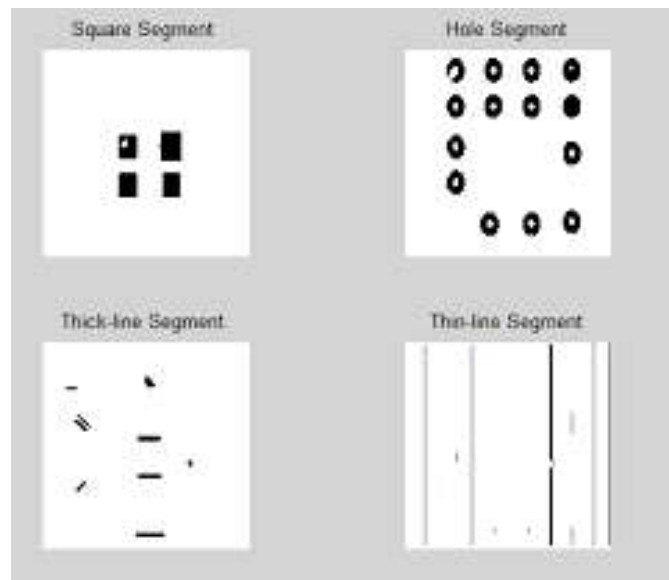


Figure 2.2 Segmentation of PCB Image.

pads, the empty segment incorporates the images of empty cushions, the thick-line area comprises of the images of thick conductors and the thin-line segment conveys the previews of thin conductors. a few imperfections best emerge on particular sections of test image alongside off base length gap, breakout and lacking empty for gap stage or lacking conductor and open circuit for thin line fragment. different deformities may exist in more than one sections. Mousechomp and beneath engraving may exist in each hollow and square sections. by methods for breaking the images into groups, a portion of the imperfections related with positive sections can without trouble be perceived and sorted. after this then musical show such has image expansion, picture subtraction, picture refinement administrator and now not musical show tor are finished and the yields obtained comprises of the previews assembled in this sort of path that from the ones pix imperfections can be marked and detected.

3.4 Image Processing

Primarily based on critiques of previous works, heriansyah et al developed a PCB picture segmentation algorithm by clustering primitive styles of a PCB images into 4 fundamental segments using mathematical morphology and windowing technique. Laterheriansyah classifies 12 out of the 14 recognized PCB defects by means of combining the image segmentation with synthetic neural network (ANN). lately, khalid produced an image processing set of rules using MATLAB with the aid of subtracting the snap shots and performing x-or operation. the 14 defects are then grouped into five categories.

4. PROPOSED SYSTEM

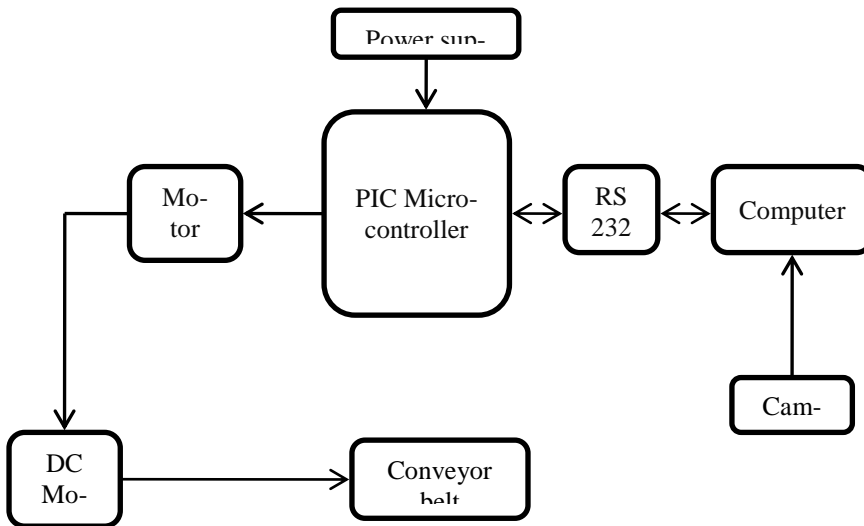


Figure 3.1 Block Diagram

4.1 Embedded System

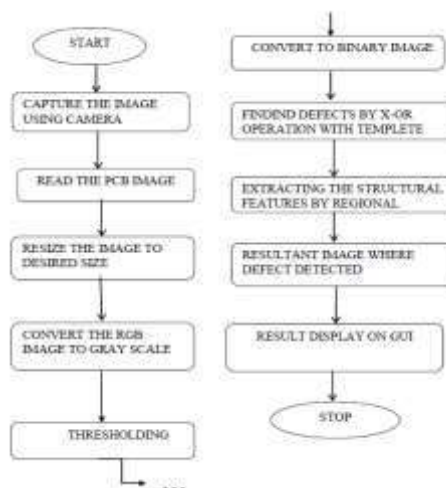
An embedded device is a mixture of each hardware and software program. the PIC microcontroller used is the heart of this device. by means of the aid of the module we're going to reap a communication link between the digital camera and GUI by the use of a PIC microcontroller, which scans the take a look at image with the assist of motor and conveyor belt. the PIC controller is interfaced with dc motor and personal pc by means of a motor driving force L293D and max 232 serial IC's as peripheral gadgets.

4.2 Image Subtraction Method

Image subtraction operation is carried out with the intention to get the variations between two images. the pictures are the reference images and the inspected images. The method compares each pictures pixel-by-pixel using xor logic operator. The subtraction operation will produce both negative or advantageous image, '1' represents white pixel and '0' represents black pixel in a binary picture. Policies exists for images subtraction operation

Rule 1: If $1-0 = 1$ then it gives positive pixel image Rule 2: If $0-1 = -1$ then it gives negative pixel image

4.3 Flow Chart



4.4 Implementation

The method of selecting the images and giving to system as an input is known as picture acquisition. Fine of obtaining image is one among key generation depends on camera. Whilst the digital camera gadgets are determined, it's far essential to provide proper illumination procedures to ensure picture excellent. When extracting images, the luminary depth and the stability of the auxiliary mild source have outstanding influences at the picture excellent. too weak or too robust light will cause the acute deterioration of the picture pleasant. moreover the PCB has excessive light reflection; it acts like a mirror, on the way to motive shadows of the object images whilst the images come into being by using the top light source, which affects the picture excellent significantly. secondly, the effect of envi-ronment light must be decreased in order that the objective capabilities of pictures captured have less distortion and the computing complexity of images processing algorithms may be decreased.

The surroundings light in laboratories is normally uniform, however the time various noise can make a high-quality effect on the surroundings mild in factories. so, we need shield the environ-mental light or beautify the mild depth to take away or weaken the impact of environmental light. while precise illumination conditions are glad, our layout is strong. on this device, actual PCB snap shots could be captured using a excessive decision pixels it 306wc computer webcam camera. the camera's resolution is carefully associated with the camera's price and additionally immediately affects the de-vice accuracy. in standard, excessive decision means better dimension accuracy, however the gadget's consistent with performance ratio also must be taken into consideration height in between the camera. there are 3 kinds of camera information transmitting modes: USB, camera link, gigabit ethernet ports we've used USB cable.

From the glide chart we get to realize overall go with the flow of the software program element which get execute in MATLAB. procedure get begin by way of urgent the button of start on GUI, so motor starts offevolled to run and PCB begins to transport closer to camera. as soon as PCB comes just under the camera it captures the image of it. computer reads the PCB image. Pre-processing part get finished as a way to make picture suitable for the similarly processing. it first off resizes the imageson the way to make it appropriate to examine with template picture. then it converts of RGB image into grey scale for that it uses the thresholding technique to set the threshold value so that sooner or later image get converted into binary format. due to binary layout of the images processing will be easy as properly because it wishes less computational reminiscence in comparison to different codecs of images.

After preprocessing part is completed, it in step with-forms the difference operation with the given actual time image and saved template image, so defects get discover. then it extracts structural capabilities using local homes such as vicinity, eccentricity, principal axis duration, minor axis period, orientation and so on .from these houses it identifies hollow and line defects.

5. RESULTS AND DISCUSSIONS

On this device, we are displaying consequences on GUI due to the fact in this person can load the images, starts the processing on it via selecting given graphical elements for it .so t is well known that GUI could be very clean to apply because it does no longer need greater experience or training to use. Followingimages indicates final output displayed on GUI. We have developed our model on a real time device and its end result is getting displayed on GUI. Experimental end result indicates that the test image is grabbed and processed with the aid of the seasoned-posed set of rules Determineend result picture displaying line and one hole defects. Determine experimental setup of the machine

6. CONCLUSION

This research computerized PCB inspection gadget for detecting defects on naked printed circuit board. Within the technique of imposing the system, we found out that careful plans are required in each steps which includes image acquisition, picture processing, images aspect extraction and illness reputation. at gift, the completed designed machine can locate common PCB defects consisting of: lacking hollow, open circuit

and so on. after image had been captured images subtraction operation, minimum thresholding and noise elimination operations are used to get noise-unfastened tremendous and terrible pictures. then structural functions have extracted the usage of nearby houses to get the element statistics of the defects. even though, this gadget isn't being able to obtain GPS indicators in indoor areas and also delays in replying due to GPS. in view that GPS delays in receiving information from satellite TV for pc facet.

REFERENCES

- [1]. Moganti M., Dagli, C. H. and ShouTsunekawa, “**Automatic PCB Inspection Algorithms A Survey**”, Computer Vision and Image Understanding Vol. 63, No. 2, pp 287 – 313, 1996
- [2]. Eduardo Bayro-Corrochano, “**Review of Automated Visual Inspection 1983 to 1993 - Part I &11,**” SPIEIntelligent Robots and Cornpiiter Vision
- [3]. HisashiTsunekawa, “**Latest Image Evaluation Systems Aid Efforts for Product Quality,**” *Journal of Electronic Engineering*, No. 306, **Vol. 29**, pp. 72-77, June 1992. *XII*, Vol. 2055, pp. 128-172, 1993.
- [4]. Ajay Pal Singh Chauhan, Sharat Chandra Bhardwaj, “**Detection Of Bare PCB Defects By Image Subtraction Method Using Machine Vision**” IEEE World Congress On Engineering, Vol 2 WCE, July 6 - 8, 2011.
- [5]. SonalKaushik, Javed Ashraf, “**Automatic PCB Defect Detection Using Image Subtraction Method**”, International Journal Of Computer Science And Network (IJCSN), Volume 1, Issue 5, October 2012
- [6]. B. Kaur and J. Kaur, “**Applications of Image Processing: A Review**”, Proceedings of 25th International Conference on Electrical, Electronics and Computer Engineering, August 2013.
- [7]. Malge P.S., “**A Survey: Automated PCB Inspection Algorithm**”, International Journal Of Engineering Research And Technology, Vol 3, 2278-0181, January 2014.
- [8]. Malge P.S.” **Printed Circuit Board Defect Detection Using Mathematical Morphology and MATLAB Image Processing Tools**”, 2nd International Conference on Education Technology and Computer (ICETC), Vol 87, Feb 2014.
- [9]. Hara, Y., Akiyama, N. and Karasaki, K, “**Automatic Inspection System for Printed Circuit Boards**” IEEE Transactions on Pattern Analysis and Machine Intelligence”. Vol. PAMI-5. No.6,623 – 630.

OPTIMAL SOLUTION OF LINEAR PROGRAMMING PROBLEMS WITH FUZZY VARIABLES

¹M. Ramesh and ²G. Ravindra Babu

¹Department of Mathematics, ²Department of Computer Science and Engineering

¹Matrusri Engineering College, Hyderabad, Telangana, India, ²Trinity College of Engineering and Technology, Karimnagar, India

Abstract: This paper presents to find the Optimal Solution of Fuzzy Linear Programming problems with inequality constraints by representing all the parameters as fuzzy numbers. By using the proposed method the fuzzy Optimal Solution of Linear Programming problems, occurring in real life situation, can be easily obtained.

Key words - Fuzzy Linear Programming problems, Fuzzy Optimal Solution, Fuzzy numbers, membership function, ranking function.

I. INTRODUCTION

Through knowledge, Science and Specialization, man has recognized many of the relationships of his environmental systems. Due to the nature of real world problems, the collected data usually involve some kind of uncertainty. As a matter of fact, many pieces of information cannot be quantified due to their nature. Incomplete information is also another cause for resorting to fuzziness.

This new knowledge has provided man with the opportunity to manipulate environmental conditions to produce desired consequences. Man attempts to select the courses of action, from a set of alternative courses of action, that will achieve his objectives. Decision analysis is a formalized process for increasing man's understanding and control over environmental conditions. In real world any linear programming model involves Parameters whose values are assigned by experts. They usually cannot assign exact values to these important parameters. The decision maker has to deal with uncertainty. In contrast with crisp logic, where binary sets have two valued logic, fuzzy logic variables many have a truth value that ranges in degree between '0' and '1'. Fuzzy logic concept is used widely in many implementations like automatic gear control systems, air conditioners, TV sets, mobile robots and so on.

Fuzzy Linear Programming problem was introduced by Zimmermann. The concept of Fuzzy logic was first conceived by Loft ZADEH. NASSERI et al [1] proposed for solving Fuzzy Linear Programming by using Tsao's method. EBRAHIMMEJAD et al [2] have developed using complementary slackness property to solve L.P.P with Fuzzy parameters. MALEKI et al [3] proposed to solve Linear Programming with Fuzzy variables. BEAULA et al [4] have developed solving Fully Fuzzy Linear Programming using Breaking Points Method. BELLMAN et al [10] proposed the concept of decision making in fuzzy environment. AMITKUMAR et al [11] proposed a new method for solving fuzzy Linear Programming. Li XIAOZHONG et al have developed fuzzy linear programming problems with fuzzy variables.

II. FUZZY LINEAR PROGRAMMING PROBLEM

Definition

A ranking function is a function $f: F(R) \rightarrow R$, where $F(R)$ is a set of fuzzy numbers defined on set of real numbers, which maps each fuzzy number into a real line.

Let $A = (a, b, c)$ be a triangular fuzzy number then

$$f(A) = \frac{a+2b+c}{4}$$

The Objective Function of each LP problem is expressed in terms of decision variables to optimize the criterion of Optimality, it is represented as:

Maximize (or) Minimize = $C^T \cdot X$

Subject to $A \cdot X \leq, =, \geq b$, X is a non-negative fuzzy number,

where $A = (a_{ij})_{m \times n}$, $C^T = (c_j)_{1 \times n}$, $b = (b_i)_{m \times 1}$, $x = (x_j)_{n \times 1}$ and $a_{ij}, c_j, b_i, x_j \in F(R)$ is said to be multi objective FLP problem with fuzzy variable and fuzzy constraints.

III. CONVERSION OF INEQUALITY CONSTRAINTS INTO EQUALITY CONSTRAINTS

Check type of all constraints

$$\sum_{j=1}^n a_{ij} \cdot X_j = b_i \quad \text{or} \quad \sum_{j=1}^n a_{ij} \cdot X_j \neq b_i$$

for all $i=1, 2, \dots, m$

Case I : If

$$\sum_{j=1}^n a_{ij}.X_j \leq b_i$$

for some i, then convert inequality constraints into equality constraints by introducing non-negative variables S_i to the left side of the constraints i.e.

$$\sum_{j=1}^n a_{ij}.X_j + S_i = b_i$$

for some i, where S_i is a non- negative fuzzy number.

Case II : If

$$\sum_{j=1}^n a_{ij}.X_j \geq b_i$$

for some i, then convert inequality constraints into equality constraints by introducing non-negative variables S_i to the right side of the constraints i.e.

$$\sum_{j=1}^n a_{ij}.X_j = b_i + S_i,$$

for some i, where S_i is a non- negative fuzzy number.

IV. METHOD TO FIND THE FUZZY OPTIMAL SOLUTION OF FLP PROBLEMS

Maximize (or Minimize) $C^T.X$ subject to $A.X \leq, =, \geq b$,
where $A = (a_{ij})_{m \times n}$, $C^T = (c_j)_{1 \times n}$, $b = (b_i)_{m \times 1}$, $x = (x_j)_{n \times 1}$

Step 1 Convert all the inequalities of the constraints into equations.

Step 2 Now the FLP may be written as:

Maximize (or Minimize)

$$\sum_{j=1}^n C_j . X_j$$

Subject to

$$\sum_{j=1}^n a_{ij}.X_j = b_i$$

for all $i=1,2,\dots,m$, X_j is a non-negative triangular fuzzy number.

Step 3 If all the parameters are represented by triangular fuzzy number then FLP can be written as:

Maximize (or Minimize)

$$\sum_{j=1}^n .(p_j, q_j, r_j) . (x_j, y_j, z_j)$$

Subject to $(a_{ij}, b_{ij}, c_{ij}) . (x_j, y_j, z_j) = (b_i, g_i, h_i)$ for all $i=1,2,\dots,m$

(x_j, y_j, z_j) is a non-negative triangular fuzzy number

Step 4 Assuming $(a_{ij}, b_{ij}, c_{ij}) . (x_j, y_j, z_j) = (m_{ij}, n_{ij}, o_{ij})$ then the FLP obtained in step 3 may be written as:

Maximize (or Minimize)

$$f\left(\sum_{j=1}^n .(p_j, q_j, r_j) . (x_j, y_j, z_j)\right)$$

Subject to

$$\sum_{j=1}^n : (m_{ij}, n_{ij}, o_{ij}) = (b_i, g_i, h_i)$$

for all $i=1,2, \dots,m$

(x_j, y_j, z_j) is a non-negative triangular fuzzy number

Step 5 Using arithmetic operations, FLP obtained in step 4 is converted into following LP problem:

Maximize (or Minimize)

322

$$f\left(\sum_{j=1}^n \cdot (p_j, q_j, r_j) \cdot (x_j, y_j, z_j)\right)$$

Subject to

$$\sum_{j=1}^n \cdot m_{ij} = b_i,$$

$$\sum_{j=1}^n \cdot n_{ij} = g_i,$$

$$\sum_{j=1}^n \cdot o_{ij} = h_i,$$

$$y_j - x_j \geq 0, z_j - y_j \geq 0, \text{ for all } i=1,2,\dots,m$$

Step 6 Find the optimal solution x_j, y_j, z_j by solving the LP problem obtained in step 5 .

Step 7 Find the fuzzy optimal solution by putting the values of x_j, y_j, z_j in $X_j=(x_j, y_j, z_j)$.

Step 8 Find the fuzzy optimal value by putting X_i in X_j .

V. PROPOSED METHOD IS ILLUSTRATED WITH THE HELP OF NUMERICAL EXAMPLES

Example 1: Let us consider the following FLP, problem and solve by the proposed method.

$$\text{Maximize} = (2,2,3).x_1+(3,3,4).x_2$$

Subjected to

$$(2,3,0).x_1 + (3,2,1).x_2 \leq (3,6,9)$$

$$(1,3,2).x_1+(0,2,3).x_2 \leq (3,4,26)$$

x_1, x_2 are non-negative triangular fuzzy numbers.

Solution: Converting all the inequalities of the constraints into equation by adding non-negative fuzzy number FLP problem may be written as:

$$\text{Maximize} = (2,2,3).x_1+(3,3,4).x_2$$

Subjected to

$$(2,3,0).x_1 + (3,2,1).x_2 + (1,1,1).s_1 = (3,6,9)$$

$$(1,3,2).x_1+(0,2,3).x_2 + (1,1,1).s_2 = (3,4,26)$$

x_1, x_2, s_1, s_2 are non-negative triangular fuzzy numbers.

Let $x_1=(x_1, y_1, z_1)$, $x_2=(x_2, y_2, z_2)$, $s_1=(s_1, t_1, u_1)$, $s_2=(s_2, t_2, u_2)$ then given FLPP may be written as:

$$\text{Maximize} = ((2,2,3).x_1+(3,3,4).x_2)$$

$$\text{Subjected to} \quad (2,3,0) (x_1, y_1, z_1) + (3,2,1) (x_2, y_2, z_2) + (1,1,1) (s_1, t_1, u_1) = (3,6,9)$$

$$(1,3,2) (x_1, y_1, z_1) + (0,2,3) (x_2, y_2, z_2) + (1,1,1) (s_2, t_2, u_2) = (3,4,26)$$

Where (x_1, y_1, z_1) , (x_2, y_2, z_2) , (s_1, t_1, u_1) and (s_2, t_2, u_2) are non-negative triangular fuzzy numbers

$$\text{Maximize} = f(2x_1+3x_2, 2y_1+3y_2, 3z_1+4z_2)$$

Subjected to

$$(2x_1+3x_2+s_1, 3y_1+2y_2+t_1, 0.z_1+2z_1+u_1) = (3,6,9)$$

$$(x_1+0.x_2+s_2, 3y_1+2y_2+t_2, 2z_1+3z_2+u_2) = (3,4,26)$$

Now by using step 5 the above FLP problem is converted into the following problem.

$$\text{Maximize} = (1/4 (2x_1+3x_2+4y_1+6y_2+3z_1+4z_2))$$

Subjected to

$$2x_1+3x_2+s_1 = 3$$

$$3y_1+2y_2+t_1 = 6$$

$$0.z_1+2z_2+u_1 = 9$$

$$x_1+0.x_2+s_2 = 3$$

$$3.y_1+2.y_2+t_2 =4$$

$$2z_1+3.z_2+u_2 =2$$

The optimal solution of the above L.P. problem is

$$x_1=2$$

$$x_2=0$$

$$y_1=2.5$$

$$y_2=0$$

$$z_1=6$$

$$z_2=5$$

Using step 7, the fuzzy optimal solution is given by

$$x_1=(2,2.5,6)$$

$$x_2=(0,0,5)$$

Hence, using step 8, the fuzzy optimal value of the given FLP problem is=(2,2.5,32)

Example2: Maximize = (2,4,4).x₁ + (4,6,6).x₂

Subjected to

$$(0,2,4).x_1 + (2,4,0).x_2 \leq (2,16,24)$$

$$(2,4,6).x_2 + (0,4,8).x_2 \leq (4,24,60)$$

x₁, x₂ are non-negative triangular fuzzy numbers.

Solution: Converting all the inequalities of the constraints into equation by adding non-negative fuzzy number FLP problem may be written as:

$$\text{Maximize} = (2,4,4).x_1 + (4,6,6).x_2$$

Subjected to

$$(0,2,4).x_1 + (2,4,0).x_2 + (1,1,1) s_1 = (2,16,24)$$

$$(2,4,6).x_1 + (0,4,8).x_2 + (1,1,1) s_2 = (4,24,60)$$

Let x₁, x₂, s₁, s₂ are non-negative triangular fuzzy numbers.

Let x₁=(x₁,y₁,z₁), x₂=(x₂,y₂,z₂), s₁=(s₁,t₁,u₁) and s₂=(s₂,t₂,u₂) then given FLP problem may be written as :

$$\text{Maximize} = (2,4,4).x_1 + (4,6,6).x_2$$

Subjected to

$$(0,2,4). (x_1,y_1,z_1) + (2,4,0). (x_2,y_2,z_2) + (1,1,1) (s_1,t_1,u_1) = (2,16,24)$$

$$(2,4,6). (x_1,y_1,z_1) + (0,4,8). (x_2,y_2,z_2) + (1,1,1) (s_2,t_2,u_2) = (4,24,60)$$

$$\text{Maximize} = f(2x_1+4x_2, 4y_1+6y_2, 4z_1+6z_2)$$

Subjected to

$$(0.x_1+2.x_2+s_1, 2y_1+4y_2+t_1, 4z_1+0.z_2+u_1) = (2, 16,24)$$

$$(2.x_1+0.x_2+s_2, 4y_1+4y_2+t_2, 6z_1+8z_2+u_2) = (4, 24,60)$$

(x₁,y₁,z₁),(x₂,y₂,z₂),(s₁,t₁,u₁) and (s₂,t₂,u₂) are non-negative triangular fuzzy numbers.

Now by using step 5 the above FLP problem is converted into the following problem.

$$\text{Maximize} = 1/4 (2x_1+4x_2+8y_1+12y_2+4z_1+6z_2)$$

Subjected to

$$0.x_1+2x_2+s_1 = 2$$

$$2.y_2+4y_2+t_1 = 16$$

$$4z_1+0.z_1+u_1 = 24$$

$$2.x_1+0.x_2+s_2 = 4$$

$$4.y_1+4y_2+t_2 = 24$$

$$6z_1+8z_2+u_2 = 60$$

The optimal solution of the above L.P. problem is

$$x_1=2$$

$$x_2=1$$

$$y_1=0$$

$$y_2=4$$

$$z_1=0$$

$$z_2=7.5$$

Using step 7, the fuzzy optimal solution is given by

324

$$x_1=(2,0,0)$$

$$x_2=(1,4,7.5)$$

Hence, using step 8, the fuzzy optimal value of the given FLP problem is (4,12,22.5)

VI. CONCLUSION

In this method we proposed a method to find the Fuzzy Optimal Solution of Fuzzy Linear Programming Problem with inequality constraints by representing all the parameters as triangular fuzzy members. Two examples were solved and results are discussed to illustrate our proposed method.

REFERENCES

- [1] S.H. Nasser, M. Sohrabi “ Solving Fuzzy Linear Programming by using Tsao’s Method”, Australian Journal of Basic and Applied Sciences,4(10)(2010), 4592-4600.
- [2] A. Ebrahimnejad, S.H. Nasser, “Using Complementary Slackness Property to solve Linear Programming with Fuzzy Parameters”, Fuzzy Information and Engineering ,vol.1,2009,pp.233-245.
- [3] H R Maleki et al., “Linear Programming with Fuzzy variables,” Fuzzy sets and systems .109(2000)21-33.
- [4] T. Beaula, S. Rajalakshmi, “Solving Fully Fuzzy Linear Programming using Breaking point method” International Journal Of applied Operations Research, 2 (3) (2012),11-20.
- [5] Nuran Guzel “Fuzzy Transportation problem with the fuzzy Amount and the Fuzzy costs”, Word Applied Science Journal 8(5) (2010)543-549.
- [6] H. Tanaka and K. Asai, “ Fuzzy Linear Programming problems with fuzzy Numbers”, Fuzzy Sets and system 13(1984) 1-10.
- [7] Li Xiaozhong. Fuzzy Linear Programming problems with fuzzy variables and fuzzy coefficients.BUSEFAL,1998,73.
- [8] L. Campos and J.L. Verdegay. Linear programming problems and ranking of Fuzzy numbers. Fuzzy Sets and systems, 1989, 32:1-12.
- [9] H. Tanaka, T. Okuda and K. Asai on fuzzy mathematical programming. J. Cybernet, 1974, 3:37-46.
- [10] Amitkumar and Jagdeep kaur,(2011),A new method for solving fuzzy linear Programs with Trapezoidal fuzzy numbers, International Journal of fuzzy Set valued Analysis, (2011),1-12.
- [11] Bellman, R.E and Zadeh, L.A.(1970),Decision making in a fuzzy environment, management Science, 17,141-164.





Institutional Sign In

All



ADVANCED SEARCH

Conferences > 2017 International Conference... ?

High speed architecture for orthogonal code convolution

Publisher: IEEE

Cite This

Cite This

PDF

Sudhakar Ajmera ; Mahendra Vucha ; Aruna Kokkula **All Authors**

27 Full Text Views



Export to

Collabratec

Alerts

Manage

Content Alerts

Add to Citation

Alerts

More Like This

Design and implementation of LDPC(Low Density Parity Check) coding technique on FPGA (Field Programmable Gate Array) for DVB-S2 (Digital Video Broadcasting-Satellite)

2014 IEEE International Conference on Aerospace Electronics and Remote Sensing Technology
Published: 2014

Field-programmable gate-array-based investigation of the error floor of low-density parity check codes for magnetic recording channels

IEEE Transactions on Magnetics
Published: 2005

Show More

Abstract

Downl

PDF

Document Sections

1. Introduction
2. Literature Survey
3. Orthogonal Codes
4. Results and Discussion
5. Conclusion and Future Scope

Abstract:The orthogonal code is one of the error correction and detection codes and it can detect errors and correct corrupted data. An n-bit orthogonal code would haven/2 1's and... **View more**

Metadata

Abstract:

The orthogonal code is one of the error correction and detection codes and it can detect errors and correct corrupted data. An n-bit orthogonal code would haven/2 1's and n/2 0's and these properties can effectively participate in detecting and correcting the errors. Thus this article presents a new methodology to enable error detection capabilities using the orthogonal code. The orthogonal codes has been verified experimentally and proved their physical reliability by implementing on Field Programmable Gate Arrays (FPGA). The experimental results shows that the proposed orthogonal code can improve the detection capabilities of the transmitted information up to 99.9% and also it corrects errors up to (n/2 - 1) bits in the received information with bandwidth efficiency.

Published in: 2017 International Conference on Intelligent Sustainable Systems (ICISS)

Date of Conference: 7-8 Dec. 2017

INSPEC Accession Number: 17858403

Date Added to IEEE Xplore: 21 June 2018 **DOI:** 10.1109/ISS1.2017.8389368

ISBN Information:

Publisher: IEEE

 Contents

1. Introduction

Whenever useful data is stored, compressed and transmitted through a wired or wireless communication channel, the noise sources like Electromagnetic Interference (EMI), crosstalk, and distance can affect the quality and reliability of data. So, there is need of Error detection and correction techniques to detect and nullify the errors occurred during transmission. There were some codes which can only detect errors like Cyclic Redundancy Check [2], [3], and there are codes like Solomon Codes [4] which were designed to detect errors and correct as well. However, the existing techniques in literature cannot achieve high efficiency and meet bandwidth requirements, especially enhancement in quantity of data transmission. The Orthogonal Code is an efficient code technique that can detect errors and correct the corrupted data.

Sign in to Continue Reading

Authors	▼
Figures	▼
References	▼
Keywords	▼
Metrics	▼

IEEE Personal Account

CHANGE USERNAME/PASSWORD

Purchase Details

PAYMENT OPTIONS
VIEW PURCHASED DOCUMENTS

Profile Information

COMMUNICATIONS PREFERENCES
PROFESSION AND EDUCATION
TECHNICAL INTERESTS

Need Help?

US & CANADA: +1 800 678 4333
WORLDWIDE: +1 732 981 0060
CONTACT & SUPPORT

Follow



[About IEEE Xplore](#) | [Contact Us](#) | [Help](#) | [Accessibility](#) | [Terms of Use](#) | [Nondiscrimination Policy](#) | [Sitemap](#) | [Privacy & Opting Out of Cookies](#)

A not-for-profit organization, IEEE is the world's largest technical professional organization dedicated to advancing technology for the benefit of humanity.

© Copyright 2021 IEEE - All rights reserved. Use of this web site signifies your agreement to the terms and conditions.

IEEE Account

» Change Username/Password
» Update Address

Purchase Details

» Payment Options
» Order History
» View Purchased Documents

Profile Information

» Communications Preferences
» Profession and Education
» Technical Interests

Need Help?

» **US & Canada:** +1 800 678 4333
» **Worldwide:** +1 732 981 0060
» Contact & Support

[About IEEE Xplore](#) | [Contact Us](#) | [Help](#) | [Accessibility](#) | [Terms of Use](#) | [Nondiscrimination Policy](#) | [Sitemap](#) | [Privacy & Opting Out of Cookies](#)

A not-for-profit organization, IEEE is the world's largest technical professional organization dedicated to advancing technology for the benefit of humanity.

© Copyright 2021 IEEE - All rights reserved. Use of this web site signifies your agreement to the terms and conditions.

HIGH SPEED ARCHITECTURE FOR ORTHOGONAL CODE CONVOLUTION

Sudhakar Ajmera¹, Mahendra Vucha¹

¹Department of Electronics and Communication Engineering
MLR Institute of Technology,
Hyderabad, India.

Aruna Kokkula²

²Dept. of ECE
Matrusri Engineering College
Hyderabad, India.

Abstract: The orthogonal code is one of the error correction and detection codes and it can detect errors and correct corrupted data. An n -bit orthogonal code would have $n/2$ 1's and $n/2$ 0's and these properties can effectively participate in detecting and correcting the errors. Thus this article presents a new methodology to enable error detection capabilities using the orthogonal code. The orthogonal codes has been verified experimentally and proved their physical reliability by implementing on Field Programmable Gate Arrays (FPGA). The experimental results shows that the proposed orthogonal code can improve the detection capabilities of the transmitted information up to 99.9% and also it corrects errors up to $(n/2 - 1)$ bits in the received information with bandwidth efficiency.

Keywords: Orthogonal Code, Cyclic Redundancy Check, Field Programmable Gate Array.

1. INTRODUCTION

Whenever useful data is stored, compressed and transmitted through a wired or wireless communication channel, the noise sources like Electromagnetic Interference (EMI), crosstalk, and distance can affect the quality and reliability of data. So, there is need of Error detection and correction techniques to detect and nullify the errors occurred during transmission. There were some codes which can only detect errors like Cyclic Redundancy Check [2, 3], and there are codes like Solomon Codes [4] which were designed to detect errors and correct as well. However, the existing techniques in literature cannot achieve high efficiency and meet bandwidth requirements, especially enhancement in quantity of data transmission. The Orthogonal Code is an efficient code technique that can detect errors and correct the corrupted data.

A. Cyclic Redundancy Check

The Cyclic Redundancy Check (CRC) used to detect errors present in a message. The CRC has two types of implementation schemes.

- Table driven CRC method
- Loop driven CRC method

The CRC is polynomial technique that describes several implementations like CRC-16, CRC-

CCITT, and CRC-32. The CRC is a very common and simple implementation for detecting errors in transmitted messages or stored information and it is powerful in error detection but easily implemented to achieve data reliability.

The CRC generation provides many enhancements as compared to simple sum or parity check error correction and detection techniques. The CRC techniques can detect single bit errors, double bit errors and bundled bit errors but the parity bit check techniques detect only single bit errors. The CRC error correction technique is always used for large data packages involved in transmission through local area networks.

B. Reed-Solomon Error Correction code

The Reed-Solomon (RS) techniques are non-binary cyclic error correcting codes and they describe systematic ways to build codes to detect and correct multiple errors. Up on appending of ' t ' check symbols to the data, the RS code can detect errors up to ' t ' symbols, and correct up to $t/2$ symbols. So, the RS codes can be used as multiple-burst bit-error correcting codes and the sequence of $b+1$ consecutive bit errors can affect at most two symbols of size b . In Reed-Solomon coding, the symbols are the coefficients of polynomial $p(x)$ over a finite field. The objective of RS code is to generate n code symbols from k source symbols by over sampling $p(x)$ at $n > k$ distinct points and then the sampled points are transmitted by using interpolation techniques at the receiver. The RS codes are also represented as cyclic BCH codes by deriving the encoding symbols from the coefficients of polynomial constructed by multiplying $p(x)$ with a cyclic generator polynomial. Reed-Solomon codes play very important role in space communication, computer based data transmission applications like DSL & Wi-MAX and also in consumer electronics such as CDs, DVDs, Blu-ray Discs.

2. LITERATURE SURVEY

The CRC identification is very straight forward theory. The CRC algorithm considers the binary numbers as input data. This input binary data is divided by polynomial numbers represented in

binary data. The quotient of division represents CRC checksum and the remainder is then appended into transmitter buffer as the transmitted message. At the receiver end, the received data is divided by the polynomial used at the transmitter end. If the result of the division at the receiver end is zero, then the transmission was successful. However, if the result of the division at the receiver is not equal to zero then there would be an error occurred during the transmission. The CRC polynomial of order 16 is shown in Equation 1. The coefficients of the polynomial are represented in binary form in order to perform division operation on input binary data. For example, the CRC polynomial of order 16 shown in equation 1 can be represented as 110000000000101b. The division uses the Modulo-2 arithmetic and the Modulo-2 arithmetic is realized by using XOR two numbers. The CRC polynomial with order 16 is

$$P(x) = x^{16} + x^{15} + x^2 + 1$$

The CRC generation techniques bring many advantages as compared to sum or parity check techniques. The CRC codes detects following errors:

1. Single bit
2. Double bit
3. Bundled bit (bits next to each other)

The method of parity bit check supports in detecting single bit errors only. Unlike parity bit check, the CRC error correction is used to identify multiple errors in order to transmit large data packages over local area networks such as Ethernet.

In Reed-Solomon coding, the symbols are the coefficients of polynomial $p(x)$ over a finite field. The objective of RS code is to generate n code symbols from k source symbols by over sampling $p(x)$ at $n > k$ distinct points and then the sampled points are transmitted by using interpolation techniques at the receiver. The RS codes are also represented as cyclic BCH codes by deriving the encoding symbols from the coefficients of polynomial constructed by multiplying $p(x)$ with a cyclic generator polynomial. Reed-Solomon codes play very important role in space communication, computer based data transmission applications like DSL & WiMAX and also in consumer electronics such as CDs, DVDs, Blu-ray Discs.

The orthogonal codes consists equal number of binary values 1's and 0's i.e. n -bit orthogonal code would have $\frac{n}{2}$ 1's and $\frac{n}{2}$ 0's. So, the orthogonal codes and its antipodal code generate zero parity bits. In orthogonal codes, the transmitter no needs

to send parity bit because of the parity bit is always zero [5]. The orthogonal codes enable the receiver to detect the transmission error by generating parity bit from the received data at the receiver end. The transmitting k -bit data can be converted into a unique n -bit set and the unique n -bit data sets are transmitted.

At the receiver end, the received data is decoded based on code correlation and the threshold value set between two orthogonal codes. The threshold is described by the following equation

$$d_{th} = \frac{n}{4}$$

Where n represents code length and d_{th} represents threshold which describes middle of two orthogonal codes.

$$t = \frac{n}{4} - 1$$

In the above equation, the t represents number of errors presented in received code and corrected by using n -bit orthogonal codes. For example, 8-bit orthogonal code ($n = 8$) can correct single error and 16-bit orthogonal code ($n = 16$) can correct three-errors and so on.

At the receiver end, the received data would be compared with codes exists in the lookup table in order to detect the error. This is achieved by counting the number of ones generated by performing 'XOR' operation between the received data and each combination of the orthogonal codes defined in the lookup table. Arithmetic counter is used for counting the number of ones presented in n -bit signals produced by comparison and also it search for minimum count. However positive value rather than zero represents an error present in the received data. The orthogonal code presented in the lookup table associated with the minimum count is determines corrupted received data. The matched orthogonal code in the lookup table would be the corrected code and which can be decoded into k -bit data. The orthogonal code supports the

receiver to correct up to $(\frac{n}{4} - 1)$ bits of received code.

3. ORTHOGONAL CODES

The orthogonal codes are formed with equal number of 1's and 0's binary values. The n -bit

orthogonal code would have $\frac{n}{2}$ 1's and $\frac{n}{2}$ 0's.

All orthogonal codes can generate zero parity bits and it is demonstrated, in figure 3, for 16-bit orthogonal code. The figure 3 demonstrates 16-orthogonal codes and 16-antipodal codes and the antipodal codes are inverse codes of orthogonal

codes. The antipodal codes are orthogonal among themselves.

A. Theory of Operation

Since the orthogonal codes could have equal number of 1's and 0's, each orthogonal code can generate a zero parity bit and the antipodal codes also can generate a zero parity bit. The nature of self-generating zero parity bit in orthogonal codes helps the transmitter not to include parity bit in their transmitted data [7].

At the receiver end, the transmission error can be detected by generating a parity bit in received data. At the transmitter end, the transmitting k-bit data set can be mapped into a unique code of n-bit. For example, a 5-bit transmission data set can be represented as a 16-bit orthogonal code and the 16-bit orthogonal code can be transmitted without including parity bit.

At the receiver end, the received data can be decoded using the concept of correlation and it is achieved by setting a threshold value which is between the two orthogonal code and it is achieved by using following equation

$$d_{th} = \frac{n}{4}$$

Where n describes code length and d_{th} describes threshold of orthogonal code. The 16-bit orthogonal codes shown in figure 4 can have threshold $d_{th} = \frac{16}{4} = 4$. The threshold

mechanism helps in examining the received orthogonal code for comparing with neighbouring codes for a possible match. A valid code is obtained when an n-bit autocorrelation value is produced; otherwise a false code is obtained. This is achieved by the correlation process described below.

In this processes the n-bit codes $x_1, x_2, x_3, \dots, x_n$ and $y_1, y_2, y_3, \dots, y_n$ are compared by using the equation stated below.

$$R(x, y) = \sum_{i=1}^n x_i y_i \leq \frac{n}{4} - 1$$

In the above equation, $R(x, y)$ describes result of autocorrelation of two codes and the n is length of the codes and d_{th} is the threshold defined between two valid codes. The number of errors corrected by using process can be estimated by using the

following equation. $t = n - R(x, y) = \frac{n}{4} - 1$

In the above equation, t is the number of errors that can be corrected by using an n-bit orthogonal code.

Table 1: Orthogonal codes and the corresponding chip Error Control capabilities

Length of orthogonal code (n)	Number errors which can be corrected
8	1
16	3
32	7
64	15

For example, single error correcting orthogonal code is constructed by using an 8-bit orthogonal code. Similarly, a three error correcting orthogonal code is constructed by using a 16-bit orthogonal code. The error correcting capabilities of various orthogonal codes is stated in the table 1.

B. Architecture of receiver to process Orthogonal Codes

At the receiver, the received code can be processed through the sequence of steps shown in Figure 5. Initially, the received serial bits are converted into n-bit parallel code and the received code is then compared with predefined orthogonal codes in the lookup table in order to detect errors. The comparison is performed by counting the number of ones generated by performing the 'XOR' operation on the received code and each combination of the orthogonal codes stored in the lookup table. A 4-bit counter is designed and used to count the number of ones after comparison. If the count is non zero indicates an error in the received code. The minimum count describes the closest match for received corrupted data. The matched received codes are the corrected code which needs to be decoded back to k-bit data. The proposed receiver is capable of correcting received bits of size up to $(n/4)-1$. Whenever, minimum count is identified with more than one combination of predefined orthogonal code then a signal REQ in receiver goes high.

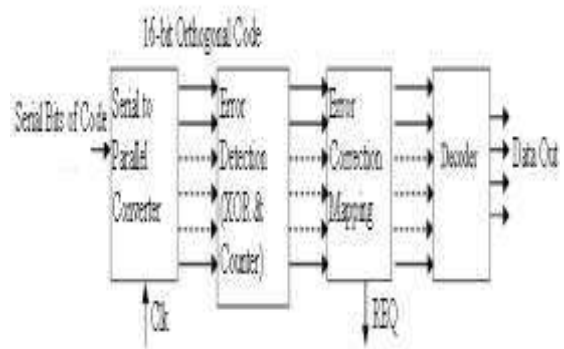


Figure 5: Block diagram of the Receiver

Orthogonal Code																	
0	0	0	0	0	0	0	0	0	0	0	0	0	0	0	0	0	
0	1	0	1	0	1	0	1	0	1	0	1	0	1	0	1	0	
0	0	1	1	0	0	1	1	0	0	1	1	0	0	1	1	0	
0	1	1	0	0	1	1	0	0	1	1	0	0	1	1	0	0	
0	0	0	0	1	1	1	1	0	0	0	0	1	1	1	1	1	
0	1	0	1	1	0	1	0	0	1	0	1	1	0	1	0	0	
0	0	1	1	1	1	0	0	0	0	1	1	1	1	0	0	0	
0	1	1	0	1	0	0	1	0	1	1	0	1	0	0	0	1	
1	1	1	1	1	1	1	1	1	1	1	1	1	1	1	1	1	
1	0	1	0	1	0	1	0	1	0	1	0	1	0	1	0	0	
1	1	0	0	1	1	0	0	1	1	0	0	1	1	0	0	0	
1	0	0	1	1	0	0	1	1	0	0	1	1	0	0	0	1	
1	1	1	1	0	0	0	0	1	1	1	1	0	0	0	0	0	
1	0	1	0	0	1	0	1	1	0	1	0	0	1	0	1	0	
1	1	0	0	0	0	1	1	1	1	0	0	0	0	1	1	0	
1	0	0	1	0	1	1	0	1	0	0	1	0	1	1	0	0	
0	0	0	0	0	0	0	0	0	0	0	0	0	0	0	0	0	P

Antipodal Code																	
0	0	0	0	0	0	0	0	1	1	1	1	1	1	1	1	0	
0	1	0	1	0	1	0	1	1	0	1	0	1	0	1	0	0	
0	0	1	1	0	0	1	1	1	1	0	0	1	1	0	0	0	
0	1	1	0	0	1	1	0	1	0	0	1	1	0	0	1	0	
0	0	0	0	1	1	1	1	1	1	1	1	0	0	0	0	0	
0	1	0	1	1	0	1	0	1	0	1	0	0	1	0	1	0	
0	0	1	1	1	1	0	0	1	1	0	0	0	0	0	1	1	
0	1	1	0	1	0	0	1	1	0	0	1	0	1	1	0	0	
1	1	1	1	1	1	1	1	0	0	0	0	0	0	0	0	0	
1	0	1	0	1	0	1	0	0	1	0	1	0	1	0	1	0	
1	1	0	0	1	1	0	0	0	0	1	1	0	0	1	1	0	
1	0	0	1	1	0	0	1	0	1	1	0	0	1	1	0	0	
1	1	1	1	0	0	0	0	0	0	0	0	1	1	1	1	0	
1	0	1	0	0	1	0	1	0	1	0	1	1	0	1	0	0	
1	1	0	0	0	0	1	1	0	0	1	1	1	1	0	0	0	
1	0	0	1	0	1	1	0	0	1	1	0	1	0	0	1	0	
0	0	0	0	0	0	0	0	0	0	0	0	0	0	0	0	0	P

Figure 3: 16-bit orthogonal code and their parity

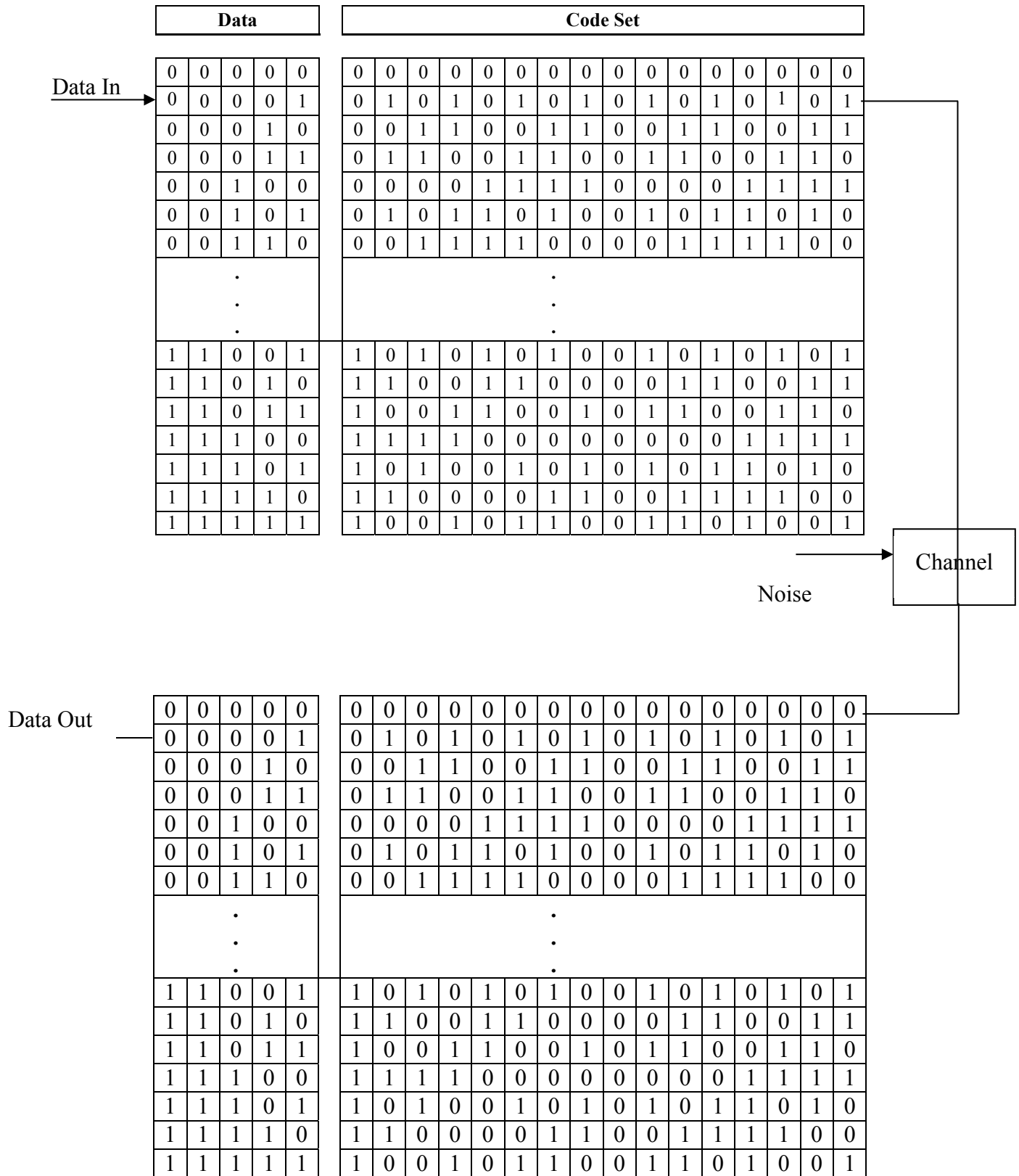


Figure 4: The Encoding and Decoding

4. RESULTS AND DISCUSSION

This section presents the simulation results of the proposed architecture for orthogonal codes. The proposed block diagram has various modules like Encoder, Parallel - Serial Converter, Transmitter, Serial - Parallel Converter, and Receiver. Architecture is created by writing HDL codes for modules like transmitter and receiver which are the main functional blocks in the orthogonal codes for error detection and correction. The synthesizable HDL written for the design ensures feasibility of implementing them on programmable devices. The behaviour of the orthogonal codes is described in VHDL and then synthesized to produce gate level net list. The gate level net list is then implemented on Spartan-3 FPGA device for function verification of the proposed architecture. The schematic of the orthogonal codes in a receiver of communication system is shown in figure 5.

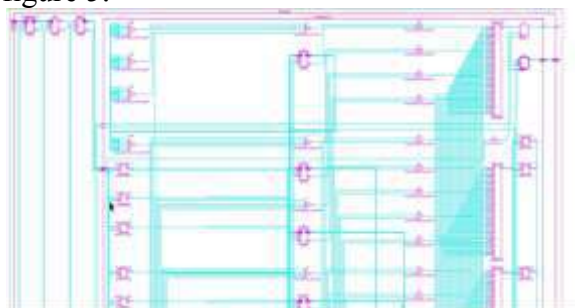


Figure 5: Schematic of Orthogonal code in Receiver Architecture

The designed architecture is verified through series of test vectors and found detection rate is computed corresponding to 8-bit and 16-bit orthogonal codes and summarized in table 2.

Table 2: Detection Rate corresponding to 8-bit and 16-bit Orthogonal Codes

Size of Orthogonal code	Number of combinations (2^n)	Number of undetected combinations ($N_f = 2n$)	Detection rate $(2^n - N_f) / 2^n\%$
8-bit	256	16	93.57%
16-bit	65536	32	99.95%
N-bit	2^N	2N	$(2^N - N_f) / 2^N$

The results summary in table 2 demonstrated that whenever a 5-bit data is translated into 16-bit orthogonal code and the translated orthogonal code will have total i.e. $2^5 = 32$ combinations. So, 16-bit received data produces 65,536 possible combinations of orthogonal codes and hence the receiver cannot guarantee the detection of all the error in orthogonal code combinations. The percentage of error detection for 16-bit orthogonal code has been identified from the formula $(2^{16} - 2^5) / 2^{16} = 99.95\%$. The orthogonal codes are very effective in detection of multiple errors but they can correct single bit error only. Therefore, the k-bit information generates n-bit orthogonal code which can detect faulty combinations which are other than the orthogonal code combinations generated by k bit information. The numbers of orthogonal code combinations generated by k-bit information is 2^k , and the percentage of detection is $(2^n - 2^k) / 2^n\%$. The orthogonal code can correct errors up to $(\frac{n}{4} - 1)$ bit.

The orthogonal codes require $2n+2$ clock cycles to process the received successfully. The experimental results shown that the orthogonal code technique could improve the error detection percentage up to 93% when 8-bit orthogonal code is used and up to 99.9% when 16-bit orthogonal code used.

5. CONCLUSION AND FUTURE SCOPE

The orthogonal code architecture for error detection and correction can enhance the error detection percentage up to 93% and up to 99.9% for 8-bit and 16-bit orthogonal codes respectively. The clock cycles required for 16-bit orthogonal code is 34 and it is 18 for the 8-bit orthogonal code. Similarly, an n-bit orthogonal code requires $2n+2$ clock cycles to detect and correct information. In future, there is need to enhance the orthogonal code correction capabilities and also introduce parallel processing techniques to speed up the processing of data.

REFERENCES

- [1] NaimaKaabouch, AparnaDhirde, and SalehFaruque, "Improvement of the Orthogonal Code Convolution Capabilities Using FPGA Implementation," IEEE Proceedings, Nov. 2007.
- [2] Baicheva, T., S. Dodunekov, and P. Kazakov, "Undetected error probability performance of cyclic redundancy- check codes of 16-bit redundancy," IEEE Proc. Comms., Vol. 147, No. 5, Oct. 2000, pp. 253- 256.
- [3] A. Hokanin, H. Delic, S. Sarin, "Two dimensional CRC for efficient transmission of ATM Cells over CDMA," IEEE Communications Letters, Vol. 4, No. 4, April 2000.
- [4] StylianakisV, Toptchiyski S, "A Reed-Solomon coding/decoding structure for an ADS modem," Electronics, Circuits and Systems, 1999. Proceedings of ICECS apos; 99. The 6th IEEE International Conference, Volume 1, Issue, 1999, pp. 473 - 476.
- [5] SalehFaruque, "Error Control Coding Based on Orthogonal Codes," Wireless Proceedings, Vol. 2, pp. 608-615, 2004.

- [6] S.Faruque, A.Dhirde ,N.Kaabouch, “Forward error control coding based on orthogonal code and its implementation using FPGA,” 7th IASTED International Conference, Montreal, Quebec, Canada, May 30 – June 1, 2007, Unpublished.
- [7] B. Sklar, “Digital Communications Fundamentals and Applications,” Prentice Hall, 1998.
- [8] J.G. Proakis., “Digital Communications,” McGraw-Hill, second edition, 1989.
- [9] RanjanBose ,“Information theory coding and Cryptography,” McGraw-Hill.

Performance Comparison of Weighted Modulo ($2^n + 1$) Adder using Different Prefix Structures

Aruna Kokkula

Electronics and Communication Engineering
Matrusri Engineering College, Saidabad
Hyderabad, India

A.S. Keerthi Nayani

Electronics and Communication Engineering
Matrusri Engineering College, Saidabad
Hyderabad, India

Abstract -- Arithmetic modulo $2^n + 1$ computation is one of the most common Residue Number System (RNS) operations that are used in Pseudo random number generation and Cryptography. The RNS has been employed for efficient parallel carry-free arithmetic computations, such as addition, subtraction, and multiplication, in DSP applications. As the computations for each residue channel can independently be done without carry propagation. Since RNS based computations can achieve significant speedup over the binary-system-based computation, they are widely used in DSP processors, FIR filters, and communication components. Modulo $2^n + 1$ adder provides the computation of the arithmetic addition by using a system called RNS. RNS speeds up the arithmetic operations by dividing into smaller parallel operations. This paper proposes improved area efficient weighted modulo $2^n + 1$ adders. This is achieved by modifying existing diminished-1 modulo $2^n + 1$ adders to incorporate simple correction schemes. Our proposed adders can produce modulo sums within the range $\{0, 2^n\}$, which is more than the range $\{0, 2^n - 1\}$ produced by existing diminished-1 modulo $2^n + 1$ adders using different prefix structures. Different prefix structures are used for comparing the adder in Area, Delay, Speed. This paper is implemented in Xilinx 10.1 using Verilog and it is simulated in ISE simulator.

Keywords -- Weighted Modulo Adder, Residue Number System and Arithmetic modulo.

I. INTRODUCTION

Arithmetic modulo $2^n + 1$ computation is one of the most common Residue Number System (RNS) operations. The RNS has been employed for efficient parallel carry-free arithmetic computations. RNS based computations can achieve significant speedup over the binary-system-based computation. RNS is widely used in DSP processors, FIR filters and communication components. Modulo $2^n + 1$

adder are also utilized as the last stage adder of modulo $2^n + 1$ multipliers. The modulo $2^n + 1$ addition is the most crucial step among the commonly used moduli sets.

The modulo arithmetic: Two numbers a and b are said to be equal or congruent modulo N if $N \mid (a-b)$, i.e. if their difference is exactly divisible by N . Usually a, b , are non negative and N is a positive integer. $a \equiv b \pmod{N}$. The word 'modulo' means 'to the modulus'. For any positive integer n , let S be the complete set of residues $\{0, 1, 2, 3, \dots, n-1\}$. Then addition modulo n on s is defined as for a and b in S , take the usual sum of a and b as integers, and let r be the element of S to which the result is congruent (modulo n); the sum $a+b \pmod{N}$ is equal to r . Similarly, multiplication modulo n is defined by taking $ab \pmod{n}$ to be equal to s , where s is the element of S to which the usual product of a and b is congruent modulo n . The set of numbers congruent to a modulo N is denoted $[a]_N$. If $b \in [a]_N$ then, by definition, $N \mid (a-b)$, or, in other words, a and b have the same remainder of division by N . Since there are exactly N possible remainders of division by N , there are exactly N different sets $[a]_N$. Quite often these N sets are simply identified with the corresponding remainders: $[0]_N=0, [1]_N=1, \dots, [N-1]_N=N-1$. Remainders are often called *residues* accordingly, $[a]_N$'s are also known as the *residue classes*. It's easy to see that if $a \equiv b \pmod{N}$ and if $c \equiv d \pmod{N}$ then $(a+c) \equiv (b+d) \pmod{N}$. The same is true for multiplication. These allow us to introduce an algebraic structure into the set $\{[a]_N: a=0, 1, \dots, n-1\}$. A first application field is in Residue Number Systems (RNS). In an RNS based application, every number X is represented by a sequence of residues (X_1, X_2, \dots, X_M) , where $X_i = X$

mod p_i , where p_i = prime integers. Every RNS operation on two operands is defined as.

$$(Z_1; Z_2; \dots; Z_M) = (X_1; X_2; \dots; X_M) \diamond (Y_1; Y_2; \dots; Y_M)$$

For most RNS applications, \diamond denotes addition, subtraction, or multiplication. Significant speedup over the corresponding binary operations can be therefore achieved because each Z_i is computed in parallel in a separate arithmetic unit (channel) since its computation depends only on X_i , Y_i , and p_i . Addition in such systems is performed using three channels that, in fact, are a modulo 2^n-1 (equivalently, one's complement), a modulo 2^n , and a modulo 2^n+1 adder. The addition delay in an RNS application which uses the above modulo is dictated by the modulo 2^n+1 channel. Modulo 2^n+1 adder are also utilized as the last stage adder of modulo 2^n+1 multipliers. Modulo 2^n+1 multipliers find applicability in many applications such as cryptography, fermat numbers etc.

II. LITERATURE SURVEY

A number of different architectures can be followed for the design of a modulo 2^n+1 weighted adder; some of them stem from the general residue adder case, whereas others are dedicated architectures for this particular modulus. For the modulo 2^n+1 addition of A and B , here after denoted by $|A+B|_{2^n+1}$, where $A = a_n a_{n-1} a_{n-2} \dots a_1 a_0$ and $B = b_n b_{n-1} b_{n-2} \dots b_1 b_0$ are two $(n+1)$ -bit binary numbers in the range $[0, 2^n]$, we have that :

$$|A+B|_{2^n+1} = A+B - (2^n+1), \text{ if } A+B \geq 2^n+1 \\ = A+B, \text{ otherwise.}$$

Following the general residue adder architecture, implementation by using two binary adders connected in series and a multiplexer. A $(n+1)$ bit adder is used to compute $A+B$, while a $-(2^n+1)$ correction is added to its output by the second $(n+2)$ -bit adder. The multiplexer is then used to select between the two adders' results depending on the value of the carry output of the second adder. Dugdale has reduced the width of the second adder to $(n+1)$ bits and has shown that the multiplexers can be controlled by the logical OR of the two adders carry outputs. She has also presented an area efficient architecture that performs the modular addition using just one adder in two addition cycles. Both these architectures are very slow. An obvious solution for decreasing the delay of the above architectures is to have both cases is computed in

parallel. This solution however, apart from the two adders requires the addition of a Carry-Save Adder (CSA) stage. A more area effective solution was proposed, by observing that most carry propagate and generate signals for both cases are common and therefore an augmented single Carry Look-Ahead (CLA) unit is sufficient. Finally, parallel-prefix weighted adders have been presented. These have been shown to be the fastest available and more efficient than the others. From the estimates it becomes obvious that, considering the current state of the art, a diminished-1 adder is both a smaller and faster circuit than a weighted modulo 2^n+1 adder. Therefore, if we could use a diminished-1 adder with minor modifications also perform weighted modulo 2^n+1 addition, by reducing both the area and the delay of the resulting components.

(a) Vergos and Efstathiou

Given two $(n+1)$ -bit numbers A and B , where $0 \leq A, B \leq 2^n$, the values of diminished-1 of A and B are denoted by $A^* = A-1$ and $B^* = B-1$, respectively. The diminished-1 sum S^* can be computed by

$$S^* = |S-1|_{2^n+1} = |A+B-1|_{2^n+1} = |A^* + B^*|_{2^n} + c_{out}$$

Where $|X|_Z$ is defined as modulo Z of X , and c_{out} is denoted as the inverted end-around carry of the diminished-1 modulo 2^n sum of n -bit A^* and B^* . Suppose that $A = a_n a_{n-1} a_{n-2} \dots a_1 a_0$ and $B = b_n b_{n-1} b_{n-2} \dots b_1 b_0$ denote two operands in the composed of the least significant bits of A and B , respectively. Equivalently, we have that $A = a_n \times 2^n + A_n$ and $B = b_n \times 2^n + B_n$. weighted representation. Let A_n and B_n denote the n -bit vectors composed of the least significant bits of A and B , respectively. Equivalently, we have that $A = a_n \times 2^n + A_n$ and $B = b_n \times 2^n + B_n$.

The previous analysis indicates that the A_n , B_n vectors, and D can be added by the inverted end-around carry save adder stage presented in Fig. 4. We can then drive its outputs Y and U to a diminished-1 adder, that will provide at its output $Y+U+1 \pmod{2^n+1}$, that is, it will provide the n least significant bits of the weighted modulo addition of A and B . The most significant bit of the weighted sum should be at 1, only when $A+B \pmod{2^n+1}$ is equal to 2^n , or equivalently when $Y+U+1 \pmod{2^n+1}$ equal to 2^n , or equivalently (since) when $Y+U = 2^n-1$, that is, when Y and U are bitwise complementary.

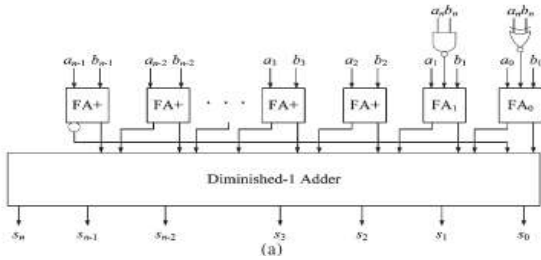


Figure 1: Architecture of the weighed modulo 2^n+1 adder for Vergos and Efstathiou

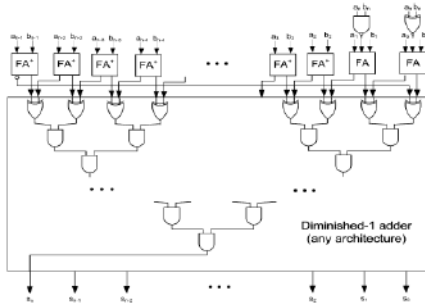


Figure 2: Modulo 2^n+1 adder for weighted operands built using a diminished-1 adder.

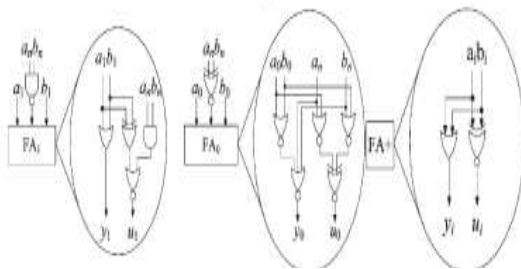


Figure 3: Architecture of FA1, FA0, and FA+.

This condition can be easily detected as the logical AND of the XOR of the bits of Y and U with the same weight. Since in every fast adder architecture there is a preprocessing stage that apart from the generate and propagate terms also computes the half-sum term, that is the XOR of the corresponding input operands bits, the extra hardware required for the most significant bit of the weighted addition is small; just AND ing the half-sum terms together. It should be noted that this operation will not add any delay on the critical path of the adder. The figure presents the implementation that results from the previous analysis for a modulo 2^n+1 adder for operands in the weighted representation. It is composed of a diminished-1 adder and an inverted end-around-carry CSA stage. The full adders of the CSA stage perform the $|A_n + B_n + D|_{2^n+1}$ addition. The FAs at bit positions 2 up to (n-1) are denoted as FA s since one of their operands coming

from vector is 1. Therefore, they have hardware and delay complexity equal to that of a half adder. Several simplifications can also be performed to the two rightmost FAs along with the accompanying NAND and XNOR gates by considering that $a_n(b_n)$ and a_1 or a_0 (and b_1 or b_0) cannot be simultaneously at 1. Fig. 6 presents examples of simplified circuits at these least significant bit positions. However, even more aggressive simplification is possible within the pre-processing stage of the diminished-1 adder by considering that the propagate and generate signals at bit position 1 depend on signals y_0 and u_1 that are both dependent on a_n and b_n . The most significant carry bit produced by the CSA is inverted and then driven to the least significant position. The sum and carry bits of equal weight produced by the CSA stage are then driven to the diminished-1 adder. Obviously, any architecture proposed, can be used for the latter. The diminished-1 adder's result forms the n least significant bits of the weighted sum. The indication of complementary input vectors at the diminished-1 adder is the most significant bit of the weighted sum.

(b) *Vergos and Bakalis (Using a Diminished-1 Adder for Weighted Addition:*

Let A and B represent two n-bit operands in the $[0, 2^n - 1]$ range. Let A^* and B^* denote two n-bit vectors such $A^* + B^* = A + B - 1$. According to (9), we then have that :

$$|A + B|_{2^n+1} = A + B - (2^n + 1), \text{ if } A + B \geq 2^n + 1$$

$$= A + B, \text{ otherwise.}$$

or equivalently that :

$$|A + B|_{2^n+1} = (A + B - 1) - 2^n, \text{ if } A + B - 1 \geq 2^n$$

$$= (A + B - 1) + 1, \text{ otherwise.}$$

Taking the modulo 2^n of (2) and using A^* and B^* we then get :

$$(|A + B|_{2^n+1})_{2^n} = (A^* + B^*), \text{ if } (A^* + B^*) \geq 2^n$$

$$= (A^* + B^*) + 1, \text{ otherwise.}$$

Let c_{out} denote the carry output of the $(A^* + B^*)$ n-bit integer addition. Using it, we can unify the two cases

$$\text{as : } |A + B|_{2^n+1} \cdot 2^n = |A^* + B^*|_{2^n} + c_{out}$$

Relation 12 indicates that we can derive the n-least significant bits of the weighted modulo 2^n+1 addition of A and B by using an inverted end-around carry adder (equivalently, a diminished-1

adder) provided that the sum of its inputs is decreased by 1, that is, if we use as inputs the A^* and B^* vectors. The most significant bit of the weighted addition of A and B should be 1, only when $|A + B|_{2^{n+1}} = 2^n$, which since $0 \leq A, B \leq 2^n - 1$ reduces to $A^* + B^* = 2^n - 1$, that is, when A^* and B^* are bit-wise complementary. This condition can be easily detected as the logical AND of the XOR of the bits of A^* and B^* with the same weight. Since in every fast adder architecture there is a pre-processing stage that computes the half-sum terms, that is, the XOR of the corresponding input operands bits, the extra hardware required for deriving the most significant bit of the weighted addition is small. Since this operation, according to the unit gate model, can be completed by a tree of two-input gates in $\log n + 2$ time units, while the diminished-1 adder computes the rest bits in $2 \log n + 3$ time units, it does not add any delay on the critical path of the diminished-1 adder. In some adder cases (known as XOR adders) the half sum term is also used as the carry propagate term. The group propagate terms in these adders are the logical AND of the half-sum terms and therefore no extra hardware is required for the derivation of the most significant bit. Figure 1 presents the architecture that result from the previous analysis. A translator circuit accepts the n -bit vectors A and B and provides the vectors A^* and B^* . These are driven to an augmented diminished-1 adder that is capable of providing the $(n + 1)$ -bit sum of the weighted modulo $(2^n + 1)$ addition of A and B . The augmented diminished-1 adder also offers implementation area and execution delay savings over every architecture proposed for weighted addition. We therefore conclude that its use is very attractive if the translator circuit of Figure 1 can be designed efficiently.

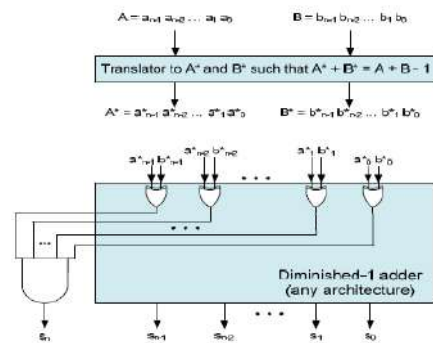
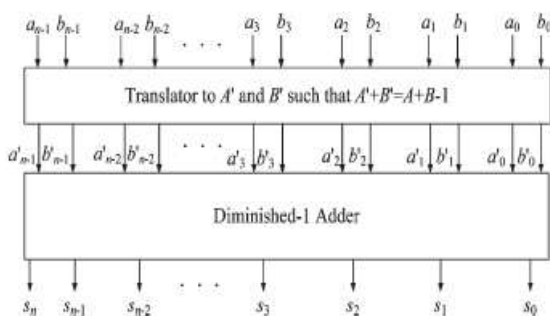


Figure 4: Architectures of the weighed modulo 2^{n+1} adder for proposal

The architecture proposed in [1] makes use of a constant time operator, which is composed of a simplified carry-save adder stage, leading to efficient modulo $2^n + 1$ adder. The architecture proposed in [2] can be applied in the design of area-efficient residue generators and multi operand modulo adders. However, it should be noted that, in [1], the values that are subtracted by the inputs A and B are not constants. In [2], the way to implement the translator for decreasing the sum of two inputs by 1 was not mentioned. Furthermore, in [2], the ranges of two inputs A and B are less than the one proposed in [1] (i.e., $\{0, 2^n - 1\}$ versus $\{0, 2^n\}$). To remedy these problems, we will propose our area-efficient weighted modulo $2^n + 1$ adder design.

III. AREA-EFFICIENT WEIGHTED MODULO $2^N + 1$ ADDER DESIGN

Instead of subtracting the sum of A and B by D , which is not a constant, we use the constant value $-(2^n + 1)$ to be added by the sum of A and B . In addition, we make the two inputs A and B to be in the range $\{0, 2^n\}$, which is 1 more than $\{0, 2^n - 1\}$ as proposed. In the following, we present the designs of our proposed weighted modulo $2^n + 1$ adder.

Given two $(n+1)$ -bit inputs $A = a_n a_{n-1} \dots a_0$ and $B = b_n b_{n-1}, \dots, b_0$, where $0 \leq A, B \leq 2^n$. The weighted modulo $2^n + 1$ of $A+B$ can be represented as follows:

$$|A+B|_{2^{n+1}} = \begin{cases} A+B - (2^n + 1), & \text{if } (A+B) > 2^n \\ A+B, & \text{otherwise.} \end{cases}$$

Equation (1) can be stated as

$$||A + B|_{2^{n+1}}|_{2^n} = |A+B - (2^n + 1)|_{2^n}, \text{ if } (A+B) > 2^n$$

$= |A+B-(2^n+1)|_{2^n} + |(2^n+1)|_{2^n}$,
otherwise.

This can then be expressed as

$$\|A + B\|_{2^{n+1}}|_{2^n} = |A+B - (2^n+1)|_{2^n}, \text{ if } (A + B) > 2^n$$

$$= |A+B - (2^n+1)|_{2^n} + 1, \text{ otherwise.}$$

From (3), it can easily be seen that the value of the weighted modulo 2^n+1 addition can be obtained by first subtracting the value of the sum of A and B by (2^n+1) (i.e., 0111, . . . , 1) and then using the diminished-1 adder to get the final modulo sum by making the inverted end-around carry as the carry-in. Now, we present the method of weighted modulo 2^n+1 addition of A and B as follows. Denoting Y' and U' as the carry and sum vectors of the summation of A, B and $-(2^n + 1)$, where $Y' = y'_{n-2} y'_{n-3}, \dots, y'_0 y'_{n-1}$ and $U' = u'_{n-1} u'_{n-2}, \dots, u'_0$, the modulo addition can be expressed as follows:

$$\begin{aligned} |A+B-(2^n+1)|_{2^n} &= |A + B - (2^n + 1)|_{2^n} \\ &= \left| \sum_{i=0}^{n-2} (2^i \times (a_i + b_i)) + 2^{n-1} \right. \\ &\quad \left. \times (2a_n + 2b_n + a_{n-1} + b_{n-1}) + \underbrace{011\dots11}_{n \text{ bits}} \right|_{2^n} \\ &= \left| \sum_{i=0}^{n-2} (2^i \times (a_i + b_i + 1)) + 2^{n-1} \right. \\ &\quad \left. \times (2a_n + 2b_n + a_{n-1} + b_{n-1} + 1) \right|_{2^n} \\ &= \left| \sum_{i=0}^{n-2} (2^i \times (2y'_i + u'_i)) + 2^{n-1} \right. \\ &\quad \left. \times (2a_n + 2b_n + a_{n-1} + b_{n-1} + 1) \right|_{2^n} \end{aligned}$$

For $i=0$ to $n - 2$, the values of y'_i and u'_i can be expressed as $y'_i = a_i \vee b_i$ and $u'_i = a_i \oplus b_i$, respectively (\vee is denoted as logic OR operation). Since the bit widths of Y' and U' are only n bits, the values of y'_{n-1} and u'_{n-1} are required to be computed taking the values of a_n, b_n, a_{n-1} , and b_{n-1} into consideration (i.e., y'_{n-1} and u'_{n-1} are the values of the carry and the sum produced by $2a_n + 2b_n + a_{n-1} + b_{n-1} + 1$, respectively). It should be noted that $0 \leq A, B \leq 2^n$, which means $a_n = a_{n-1} = 1$ or $b_n = b_{n-1} = 1$ will cause the value of A or B to exceed the range of $\{0, 2^n\}$. Thus, these input combinations (i.e., $a_n = a_{n-1} = 1$ or $b_n = b_{n-1} = 1$) are not allowed and can be viewed as don't care conditions, which can help us

simplify the circuits for generating y'_{n-1} and u'_{n-1} . That is, the maximum value of $2a_n + 2b_n + a_{n-1} + b_{n-1} + 1$ is 5, which occurs at $a_n = b_n = 1$ (i.e., the maximum value of y'_{n-1} is 2). The truth table for generating y'_{n-1}, u'_{n-1} and FIX is given in Table I, where \times is denoted as don't care. The reason for FIX is that, under some conditions, $y'_{n-1} = 2$ (e.g., $a_n = b_n = 1$ and $a_{n-1} = b_{n-1} = 0$), which cannot be represented by 1-bit line (marked as "*" in Table I); therefore, the value of y'_{n-1} is set to 1, and the remaining value of carry (i.e., 1) is set to FIX. Notice that FIX is wired-OR with the carry-out of $Y' + U'$ (i.e., c_{out}) to be the inverted end around carry (denoted by $c_{out} \vee \text{FIX}$) as the carry-in for the diminished-1 addition stage later on. When $y'_{n-1} = 2$, $\text{FIX} = 1$; otherwise, $\text{FIX} = 0$.

TABLE 1. Truth Table For Generating y'_{n-1}, u'_{n-1} AND FIX (*: CONDITIONS WHEN $y'_{n-1} = 2$)

a_n	b_n	a_{n-1}	b_{n-1}	u'_{n-1}	y'_{n-1}	FIX
0	0	0	0	1	0	0
0	0	0	1	0	1	0
0	0	1	0	0	1	0
0	0	1	1	1	1	0
0	1	0	0	1	1	0
0	1	0	1	\times	\times	\times
0	1	1	0	0	1*	1
0	1	1	1	\times	\times	\times
1	0	0	0	1	1	0
1	0	0	1	0	1*	1
1	0	1	0	\times	\times	\times
1	0	1	1	\times	\times	\times
1	1	0	0	1	1*	1
1	1	0	1	\times	\times	\times
1	1	1	0	\times	\times	\times
1	1	1	1	\times	\times	\times
1	1	1	1	\times	\times	\times

According to Table 1, we can have $y'_{n-1} = (a_n \vee b_n \vee a_{n-1} \vee b_{n-1})$, $u'_{n-1} = a_{n-1} \oplus b_{n-1}$, and $\text{FIX} = a_n b_n \vee b_n a_{n-1} \vee a_n b_{n-1}$, respectively.

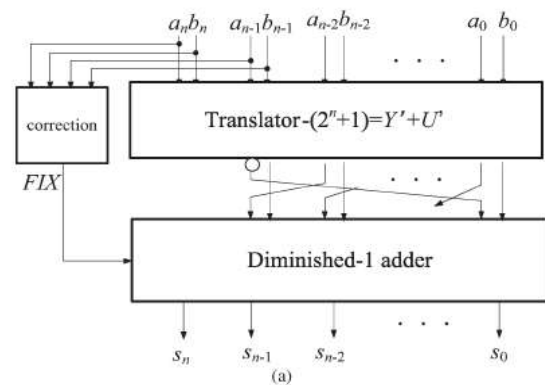


Figure 5: Architecture of proposed weighted modulo 2^n+1 adder with the correction

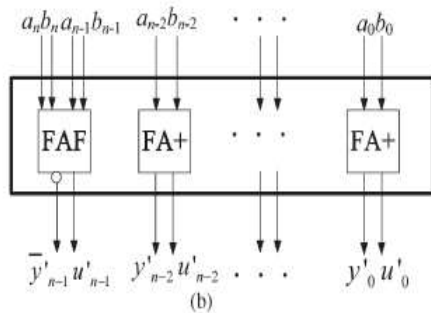


Figure 6: Architecture of the translator – $(2^n + 1)$

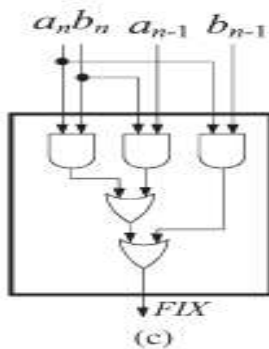


Figure 7: Architecture of the correction scheme

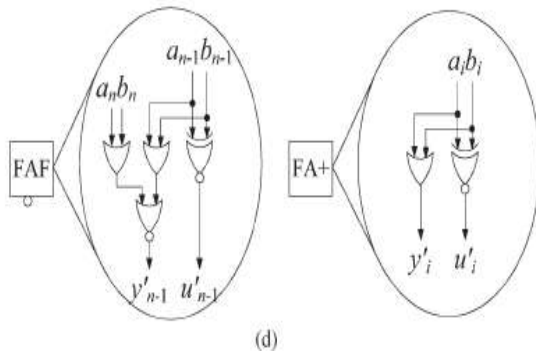


Figure 8: Architecture of FAF and FA+

From Fig. 3, the signal of FIX can be computed in parallel with the translation to $Y'+U'$, leading to efficient correction. In addition, the hardware cost for our correction scheme and FAF are less than the one proposed in [1], due to the fact that there are two inconstant numbers that should be processed [i.e., FA1 and FA0, as shown in Fig. 1(b)] in the translation stage. We used Sklansky-style and Brent-Kung style parallel-prefix structures for the diminished-1 adder implementations. The diminished-1 adder based on the Sklansky-style parallel-prefix structure with correction circuits for our proposed weighted modulo 2^8+1 adder is shown in Fig. 4(a). The square () and diamond (♦) nodes

denote the pre- and post processing stages of the operands, respectively. The black nodes (●) evaluate the prefix operator, and the white nodes (○) pass the unchanged signals to the next prefix level. The four nodes with detailed implementations are given in Fig. 4(b). It should be noted that the value of s_n (i.e., c_{out}) can be computed by wiring-AND all propagate signals (i.e., $s_n = \prod_{i=0}^{n-1} p_i$).

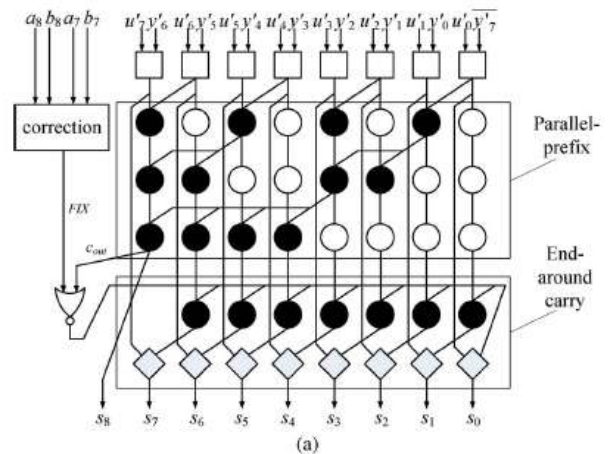


Figure 9: Diminished-1 adder based on the Sklansky-style parallel-prefix Structure

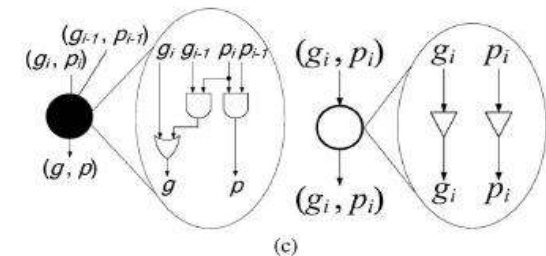
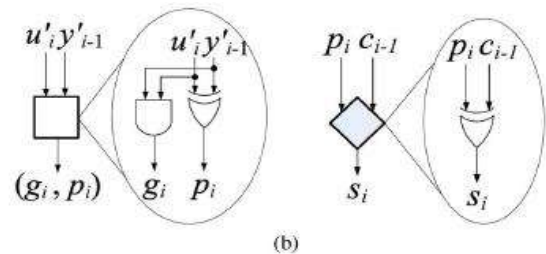


Figure 10: Square and (♦) diamond nodes, respectively

(●) Black and (○) white nodes, respectively

3.3 Parallel Prefix Structures:

The different prefix structures are provided for the implementation of the modulo addition.

- **Sklansky prefix structure:** This structure provided the basic prefix operations in the modulo performance. This requires the less number of the

gates when compared to the other structures. These are 4 layered structures.

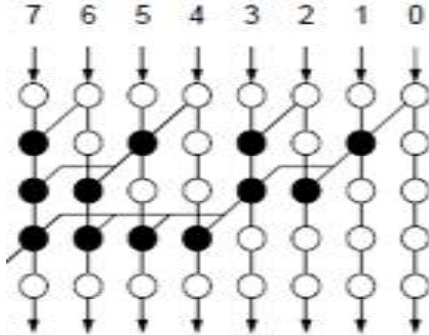


Figure 11: Sklansky prefix structure

Koggestone prefix structure: This structure requires the more number of the gates when compared to the other structures. These are also 4 layered structures.

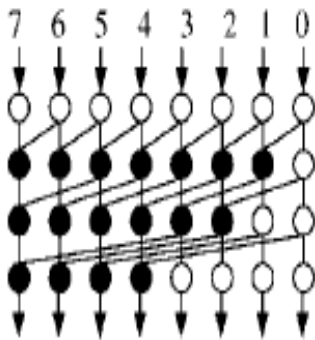


Figure 12: Koggestone structure

Lander-Fisher prefix structure: This structure is similar to the Sklansky prefix structure. This structure requires the more number of the gates when compared to the other structures. These are also 4 layered structures

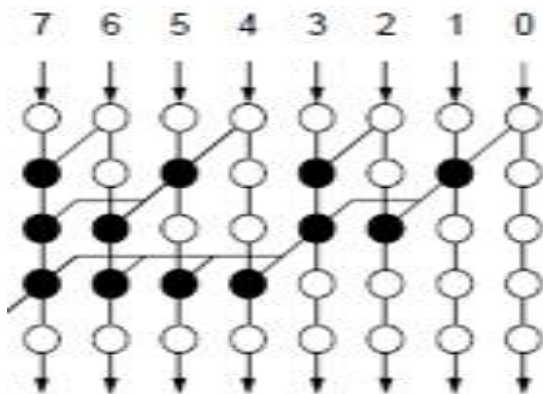


Figure 13: Lander-Fisher structure

Brent-Kung Structure: The Brent-Kung adder is a parallel prefix adder that requires $2(\log_2 N) - 1$ stages. It was originally proposed as a simple and regular design of a parallel adder that addresses the problems of connecting gates in a way to minimize chip area. Accordingly, it is considered one of the better tree adders for minimizing wiring tracks, fan out, and gate count and is used as a basis for many other networks.

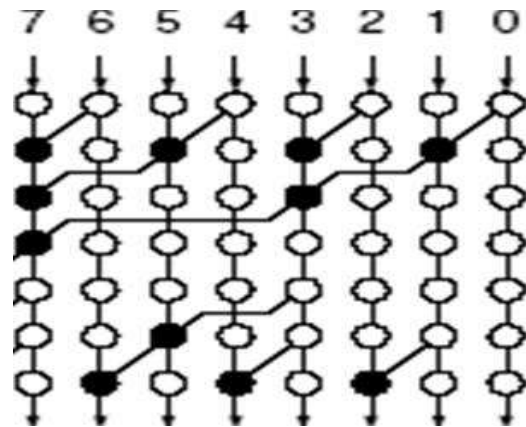


Figure 14: Brent-Kung parallel-prefix structure:

Example 1: Suppose $n = 4$, $A = 16_{10} = 10000_2$, and $B = 15_{10} = 01111_2$.

Step 1: $(A + B) - (2^n + 1) \Rightarrow Y' = 1110_2$, $U' = 0000_2$, $FIX = 1$.

Step 2: $Y' + U' = 1110_2$, $c_{out} = 0$,

$\Rightarrow Y' + U' + c_{out} \vee FIX = 1110_2 = |16 + 15|_{17} = 14_{10}$.

Example 2: Suppose $n = 4$, $A = 11_{10} = 01011_2$, and $B = 5_{10} = 00101_2$.

Step 1: $(A + B) - (2^n + 1) \Rightarrow Y' = 1110_2$, $U' = 0001_2$, $FIX = 0$.

Step 2: $Y' + U' = 1111_2$, $c_{out} = 0$,

$\Rightarrow Y' + U' + c_{out} \vee FIX = 10000_2 = |11 + 5|_{17} = 16_{10}$

IV. RESULTS DISCUSSIONS

This section presents the evaluation parameters such as area, delay and these parameters can be utilized to select the efficient design for real time applications.

Table 2: Comparison of area (8-bit)

Parameter	SKLANSKY	KOGGESTONE	BRENTKUNG
No of Slices	15	48	15
No of 4 i/p LUT's	26	85	26
No of I/O's	27	51	27
No of bounded I/O's	27	51	27

Table 3: Comparison of area (16-bit)

Parameter	SKLANSKY	KOGGESTONE	BRENTKUNG
No of Slices	48	119	49
No of 4 i/p LUT's	85	210	85
No of I/O's	51	27	51
No of bounded I/O's	51	27	51

Table 4: Comparison of Delay(8-bit)

Prefix Structures Model	8 BIT	16 BIT
SKLAN SKY	7.132 ns	32.250 ns
KOGGEESTONE	9.347 ns	25.139 ns
BRENTKUNG	18.863ns	30.710

V.CONCLUSION & FUTURE SCOPE

Conclusion: In this brief, an improved area-efficient weighted modulo $2^n + 1$ adder has been proposed. This has been achieved by modifying the existing diminished-1 modulo adders to incorporate simple correction schemes. The proposed adders can perform weighted modulo $2^n + 1$ addition and

produce sums that are within the range $\{0, 2^n\}$. Synthesis results show that our proposed adders can outperform previously reported weighted modulo adder in terms of area and delay constraints.

Future scope: The design can be extended to applications where the area and delay are the major parameters. The design can also be implemented in 32 and 64 bits to improve area and delay and it can be used for low power CMOS applications like digital signal processing and nanotechnology.

REFERENCES

- [1] .R. Zimmermann, "Efficient VLSI implementation of modulo $2n \pm 1$ addition and multiplication," in Proc. 14th IEEE Symp. Comput. Arithmetic, Apr. 1999, pp.158–167.
- [2] . H. T. Vergos, C. Efstathiou, and D. Nikolos, "Diminished-one modulo $2n + 1$ adder design," IEEE Trans. Comput., vol. 51, no. 12, pp. 1389–1399, Dec. 2002.
- [3] . C. Efstathiou, H. T. Vergos, and D. Nikolos, "Modulo $2n \pm 1$ adder design using select-prefix blocks," IEEE Trans. Comput., vol. 52, no. 11, pp. 1399–1406, Nov. 2003.
- [4] . S.-H. Lin and M.-H. Sheu, "VLSI design of diminished-one modulo $2n + 1$ adder using circular carry selection," IEEE Trans. Circuits Syst. II, Exp. Briefs, vol. 55, no. 9, pp. 897–901, Sep. 2008.
- [5] . T.-B. Juang, M.-Y. Tsai, and C.-C. Chiu, "Corrections on 'VLSI design of diminished-one modulo $2n + 1$ adder using circular carry selection'," IEEE Trans. Circuits Syst. II, Exp. Briefs, vol. 56, no. 3, pp. 260–261, Mar. 2009.
- [6] . H. T. Vergos and C. Efstathiou, "A unifying approach for weighted and diminished-1 modulo $2n + 1$ addition," IEEE Trans. Circuits Syst. II, Exp. Briefs, vol. 55, no. 10, pp. 1041–1045, Oct. 2008.
- [7] . H. T. Vergos and D. Bakalis, "On the use of diminished-1 adders for weighted modulo $2n + 1$ arithmetic components," in Proc. 11th EUROMICRO Conf. Digit. Syst. Des. Archit., Methods Tools, Sep. 2008, pp. 752–759.

1ST NATIONAL CONFERENCE ON TRENDS IN SCIENCE, ENGINEERING AND TECHNOLOGY (NTSET - 2018)

February 2nd & 3rd - 2018

TECHNICAL PAPER ABSTRACTS



ORGANIZED BY

MATRUSRI ENGINEERING COLLEGE

(Approved by AICTE, Affiliated to Osmania University)

#16-1-486, Saidabad, Hyderabad - 500059



Sponsored by

MATRUSRI EDUCATION SOCIETY

ISBN: 97881-936274-0-2

**NTSET
2018**





EFFECTIVE FOOD GRAIN LOSS REDUCTION TECHNIQUE USING IOT

¹A S Keerthi Nayani, ²CH.Sekhar, ³Aruna Kokkula

^{1,2,3}Assistant Professor,

^{1,3}Dept. of ECE, Matrusri Engineering College, Hyderabad, India.

²Dept. of CSE, Vignan's institute of information technology(Auto.)Vishakhapatnam(A.P)

Abstract: Internet of Things (IoT) is one of the affirmative platforms to implement a large data analytics task which comprises the way to exploits networking, detecting, huge information, and computerized reasoning innovation to convey finish frameworks for an item or administration. These frameworks permit more prominent straightforwardness, control, and execution when connected to any industry or fr. In this paper, we are going to discuss about loss due to atmospheric moisture beyond threshold results in infestation etc and hence damages the food grain. Those losses can be reduced effectively with support of various sensors to detecting the status of food grains stored in the Central Warehousing. Based on moisture and temperature data captured, the software should do appropriate data analytics and send timely alert to concern officials of CWC for mitigation and remedial actions arising due to moisture and temperature inside the warehouse. This paper emphasizes the usage of IoT which enables the Central warehouse centers to avoid the losses of food grains.

Index Terms- *Moister, Temperature, Sensors, IoT Technology.*

I. INTRODUCTION

Taking care of the sustenance demand of a quickly expanding worldwide populace is developing as a major test to humanity. The populace is relied upon to develop to 9.1 billion individuals by the year 2050, and around 70% additional nourishment creation will be required to encourage them [1]. A large portion of this populace rise is relied upon to be credited to creating nations, a few of which are now confronting issues of yearning and sustenance uncertainty. Expanding urbanization, environmental change and land use for non-sustenance edit generation, heighten these worries of expanding nourishment requests. Over the most recent couple of decades, a large portion of the nations have concentrated on enhancing their rural generation, arrive utilize, and populace control as their arrangements to adapt to this expanding sustenance request. In any case, postharvest misfortune (PHL), a basic issue, does not get the required consideration and under 5% look into subsidizing has been assigned for this issue in earlier years . Around 33% of the nourishment delivered (around 1.3 billion ton), worth about US \$1 trillion, is lost all around amid postharvest operations consistently. "Sustenance misfortune" is characterized as nourishment that is accessible for human utilization however goes unconsumed. The answers for diminish postharvest misfortunes require generally humble speculation and can bring about significant yields contrasted with expanding the harvest creation to take care of the sustenance demand.

CWC (Central Warehousing Corporation) is a warehousing agency. It offers services like storage and handling of goods, transportation of goods. This project benefits the government as there is difficulty in handling large number of goods from different sectors of industries. As we know there are huge numbers of commodities that include Agricultural produce, Industrial raw materials, finished goods and variety of perishable items where we can observe storage loss at huge amount. This sort of storage loss of quality outcome of food grains and perishable goods can be controlled through quality control practices that include chemical treatment, sanitation, age analysis, regular inspection and many more. Sometimes storage loss can also be observed due to atmospheric moisture beyond threshold results. So, a preferable low cost IT solution is around Internet Of Things (IOT) Sensor and IOT data integration. As a part of solution we are creating an IOT dashboard that includes all information related to moisture, temperature, fire and earthquake.

II. PROBLEM STATEMENT

Post-harvest losses:



Seeds of low quality, deficient cultivating practices, or creepy crawly assaults in the field can incite misfortunes of items even before their reap. Be that as it may, we are worried here just with counteractive action of misfortunes after the collect.

Losses in quality

Criteria of value fluctuate broadly and include the outside angle, shape and size, as much as the odor and taste. In such manner, the social contemplations with which weight control plans and dietary patterns are instilled can't be disregarded. A clean healthy item is of essential significance in advertising. By grasping a modest bunch of grain from a pack, for instance, a tradesman can rapidly check whether it emits a floury tidy and can thusly reason regardless of whether it originates from an invasion by creepy crawlies. Similarly, a terrible stench can lead him to presume rat assaults, which can be affirmed by the nearness of rodent or mouse dung or hairs. Misfortunes in quality are in this way confirmed by a decline in the market estimation of the item. These misfortunes are quantifiable just on condition that criteria or benchmarks of value have been already settled. Based on target criteria, the nature of the items can be assessed by genuinely confounded tests, estimations and research facility examinations. A considerable lot of the criteria embraced depend on assessment of principles identified with the physical state of the grain and to its sustenance, nutritive and germinative esteems. In different nations, quality evaluations depend on the general chief as per which grain must be "healthy, sound, of market quality and unscented".

Certain in this definition are the central criteria for assessing the nature of a given cluster of grain; these include:

- Moisture Content: reasonable for the capacity or further treatment of the item;
- Colour: homogeneous and fitting to the sort of item under thought;
- Odour: it must not indicate that any biochemical change is going on;
- Cleanness: the quantity of debasements must fit in with set up models of value;
- Infestation: the nonattendance of bugs or other living life forms must be discovered.

For the most part, numerous criteria join to characterize the nature of the items, and they likewise consider social perspectives identified with group dietary patterns. In Senegal, for instance, broken rice is very prized by customers; hence, the level of breakage, as a standard of rice quality, clearly has less significance than in different settings.

Loss in quality are for the most part the aftereffect of mechanical requirements experienced by the item, the activity of bugs (creepy crawlies, rodents) and small scale creatures (molds), or the concoction changes delivered inside the grains under the impact of natural conditions (temperature, mugginess, length of capacity).

Problem Identified

1. Central Warehousing Corporation (CWC) is into scientific storage and handling services for more than 400 commodities include Agricultural produce, Industrial raw-materials, finished goods and variety of hygroscopic and perishable items.
2. Storage loss of food grains and perishables goods are being controlled through quality control practices including periodic chemical treatment , recording of moisture and other parameters, proper documentation , regular inspection , age analysis , sanitation , physical condition of warehouse.
3. Further storage loss due to atmospheric moisture beyond threshold results in infestation etc and hence damages the food grains/perishables.

III. PROPOSED SOLUTIONS AND METHODOLOGY

Expected deliverables:

- Low cost IT solution preferably around Internet of the things (IoT) sensor and IoT data integration to existing application software. The sensor is expected to auto capture the atmospheric moisture and temperature inside the warehouse.

- Based on moisture and temperature data so captured, the software should do appropriate data analytics and send timely alert to concern officials of CWC for mitigation and remedial actions arising due to moisture and temperature inside the warehouse.
- Additionally, IoT sensor can also capture fire, earthquake etc and can alert the respective nearest authority like Fire Station, Hospital, and Police besides alerting CWC officials for mitigation. Sample data: Data to either simulated participants or can visit warehouses for sampling.

The following are the various sensors can be used to detect and monitor the status of food grains stored in the central warehouse.

Sensor to Detect Moisture Level in Room:

Stickiness is the nearness of water in air. The measure of water vapor in air can influence nourishment grains in the event that it is more than the required level. The nearness of water vapor additionally impacts different physical, synthetic, and natural procedures. Thus, stickiness detecting is essential, particularly in the focal stockpiles' of nourishment grains.

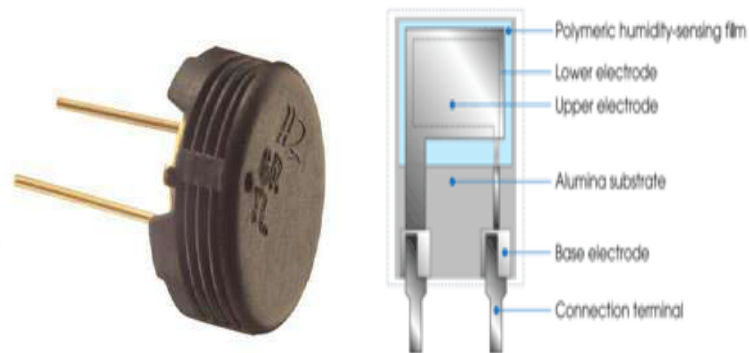


Fig1. Humidity Sensor and capacitive type humidity

Sensor to detect temperature(IC LM 34/35)

Temperature sensor IC LM34/35, are used in various applications to detect temperature variations. These devices can switch off / on circuits when the temperature varies from the normal set level. LM 34 and LM 35 Integrated Circuits are precision temperature sensors widely used in temperature sensing applications. LM 34 senses temperature in Fahrenheit range while LM 35 senses temperature in Celsius (Centigrade) range. The output voltage of these sensors is linearly proportional to the temperature.

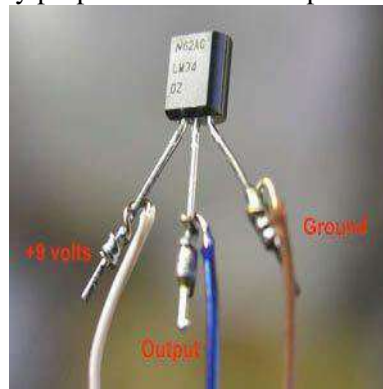


Fig3. Temperature Sensor

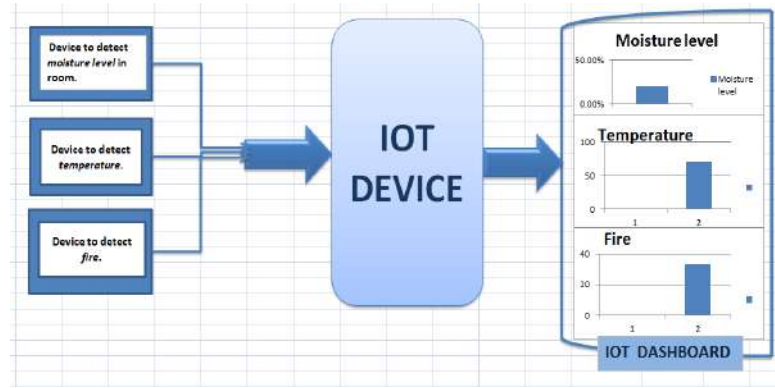


Fig 4: Working Model

IV. WORKING MECHANISM

The accompanying table demonstrates the degrees of dampness content considered fitting for good collect conditions and the attributes allowing affirmation of physiological development[2].

Table -1

GRAINS	MOISTURE	PHYSICAL CHARACTERISTICS
Rice	22-28%	The panicles bend with their own weight, yellowed hulls, full grains, neither too ripe (cracked), nor too green.
Maize	23-28%	Cobs almost dry, hard and glassy kernels resistant to scoring with the thumbnail, black dot in the caryopsis.
Sorghum	20-25%	Dried stems and leaves, hard grains resistant to the thumbnail, glassiness depending on variety.
Beans	30-40%	Pods ripe and yellow, shells dried, skins of kernels easily detached.
Groundnuts	30-35%	Leaves yellow, shells dried, skins of kemels easily detached.
Sunflower	9-10%	Upper leaves dry and flower faded.

As mentioned above sample scenario, the following process need to implement to achieve the desired level of room temperature.

Considering the need of modern technology the smart central warehouse need to ready to store the food grains and to reduce the losses due to various atmospheric conditions To avoid the losses due to normal storage places such problems in above existing system we are planning to design IOT based Smart Warehouse and Monitoring System. This system monitors the various things such as temperature, humidity etc. Time to time levels of respective measures collected and sends to the central control system via a webpage.

For this the system uses various sensors mentioned above placed over the all the rooms to detect the levels and compare it with the required. Once when the level reaches the threshold limit the system puts on the buzzer/ alarms the employees working in that particular region. Thus this system helps to keep the roomat desired levels.

- Real time information of the room's level will be displayed in web browser.
- Intelligent sensors placed at the rooms which notify about the temperature, humidity content in the bins.
- The web application can also be operated using any devices.
- This system is adaptive and hence can adapt to various new technologies.
- This process reduces cost and resource optimization.
- Improves quality and effective usage of rooms.

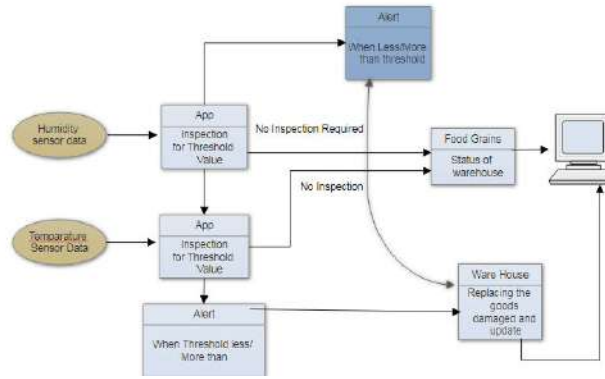


Fig5: Work Flow of Detecting and Monitoring the Warehouse

V. RESULTS DISCUSSION

Warehouse monitoring system is designed and implementation is done on IC LM 34/35 development board .The communication between controllers and interference are designed accurately done. Monitoring System is done to meet all the requirement and specification as mentioned in the objective. An embedded application is created using Python and R Programming. The predict results of the monitor model proposed are shown in table below.

Table 2

Temperature	25	>35	>40
Relative Moisture	44	60	75
Co ₂ Concentration(1000ppm)	<50	>110	>130
Status	Good	Critical	Risk/Danger

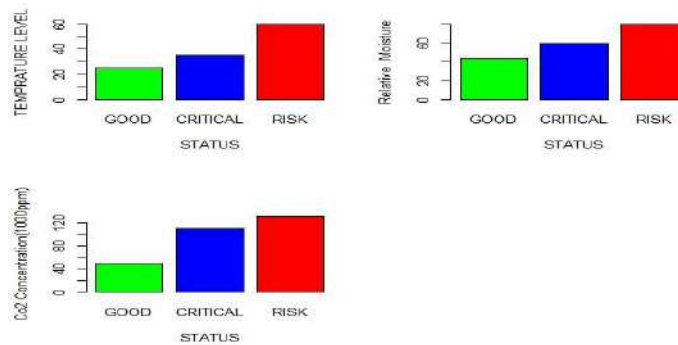


Fig6: Warehouse Status based on the Various Factors

VI. CONCLUSION

In this Paper Monitoring system is designed for monitor and controlling of the Food granule losses based on the various temperature level conditions. The grain system design is done to meet all the requirement and specification as mentioned in the objective. It is shown from the design implemented in the current work provides flexibility, scalability, portability and security/integrity of the data transmission over long networks with lower power consumption.

There are certain aspects in this work that can be investigated in future design should GPRS network is used to transferring data to all the warehouses. That will help to getting centralized data at one location and able monitor by authority to take necessary measure to reduce as much as possible.

There are certain aspects in this work that can be investigated in future, such as Environmental factors influencing the Grain quality, we are considered only major parameters Temperature, Humidity and Carbon Dioxide concentration for early



detection of deterioration of Food Grains and Good Control actions like Reducing Temperature in the Grain depot if Temperature is High i.e. keeping parameters at nominal level by an Automatic system irrespective of condition.

REFERENCES

- [1] Deepak Kumar AndPrasantaKalita. Reducing Postharvest Losses during Storage of Grain Crops to Strengthen Food Security in Developing Countries
- [2] <http://www.fao.org/docrep/t0522e/T0522E04.htm>
- [3] Xiaodong Zhang, Xiujuan Li, Jie Zhang (2010). Design and implementation of embedded monitoring system for grain storage: IEEE Conference.
- [4].Ch.Chandra Sekhar, et.allBig Data Analytics on Indian Crop Planning to Increase Agricultural Production, ASTL -Research on Smart Technologies in Data Science and Communications.
- [5]Ch Sudhakar,et..allAn IoT Application-Weather Reporting System, ASTL -Research on Smart Technologies in Data Science and Communications. Vol.147
- [6]Maier, Channaiah, Martinez-Kawas, (2010).Monitoring carbon dioxide concentration for early detection of spoilage in stored grain: Department of Grain Science and Industry, Manhattan, Kansas



MATRUSRI ENGINEERING COLLEGE

(Approved by AICTE, Affiliated to Osmania University)

#16-1-486, Saidabad, Hyderabad - 500059



Sponsored by

MATRUSRI EDUCATION SOCIETY



ISBN: 97881-936274-0-2



Performance Comparison of Weighted Modulo ($2^n + 1$) Adder using Different Prefix Structures

Aruna Kokkula

Electronics and Communication Engineering
Matrusri Engineering College, Saidabad
Hyderabad, India

A.S. Keerthi Nayani

Electronics and Communication Engineering
Matrusri Engineering College, Saidabad
Hyderabad, India

Abstract -- Arithmetic modulo $2^n + 1$ computation is one of the most common Residue Number System (RNS) operations that are used in Pseudo random number generation and Cryptography. The RNS has been employed for efficient parallel carry-free arithmetic computations, such as addition, subtraction, and multiplication, in DSP applications. As the computations for each residue channel can independently be done without carry propagation. Since RNS based computations can achieve significant speedup over the binary-system-based computation, they are widely used in DSP processors, FIR filters, and communication components. Modulo $2^n + 1$ adder provides the computation of the arithmetic addition by using a system called RNS. RNS speeds up the arithmetic operations by dividing into smaller parallel operations. This paper proposes improved area efficient weighted modulo $2^n + 1$ adders. This is achieved by modifying existing diminished-1 modulo $2^n + 1$ adders to incorporate simple correction schemes. Our proposed adders can produce modulo sums within the range $\{0, 2^n\}$, which is more than the range $\{0, 2^n - 1\}$ produced by existing diminished-1 modulo $2^n + 1$ adders using different prefix structures. Different prefix structures are used for comparing the adder in Area, Delay, Speed. This paper is implemented in Xilinx 10.1 using Verilog and it is simulated in ISE simulator.

Keywords -- Weighted Modulo Adder, Residue Number System and Arithmetic modulo.

I. INTRODUCTION

Arithmetic modulo $2^n + 1$ computation is one of the most common Residue Number System (RNS) operations. The RNS has been employed for efficient parallel carry-free arithmetic computations. RNS based computations can achieve significant speedup over the binary-system-based computation. RNS is widely used in DSP processors, FIR filters and communication components. Modulo $2^n + 1$

adder are also utilized as the last stage adder of modulo $2^n + 1$ multipliers. The modulo $2^n + 1$ addition is the most crucial step among the commonly used moduli sets.

The modulo arithmetic: Two numbers a and b are said to be equal or congruent modulo N if $N \mid (a-b)$, i.e. if their difference is exactly divisible by N . Usually a, b , are non negative and N is a positive integer. $a \equiv b \pmod{N}$. The word 'modulo' means 'to the modulus'. For any positive integer n , let S be the complete set of residues $\{0, 1, 2, 3, \dots, n-1\}$. Then addition modulo n on s is defined as for a and b in S , take the usual sum of a and b as integers, and let r be the element of S to which the result is congruent (modulo n); the sum $a+b \pmod{N}$ is equal to r . Similarly, multiplication modulo n is defined by taking $ab \pmod{n}$ to be equal to s , where s is the element of S to which the usual product of a and b is congruent modulo n . The set of numbers congruent to a modulo N is denoted $[a]_N$. If $b \in [a]_N$ then, by definition, $N \mid (a-b)$, or, in other words, a and b have the same remainder of division by N . Since there are exactly N possible remainders of division by N , there are exactly N different sets $[a]_N$. Quite often these N sets are simply identified with the corresponding remainders: $[0]_N=0, [1]_N=1, \dots, [N-1]_N=N-1$. Remainders are often called *residues* accordingly, $[a]_N$'s are also known as the *residue classes*. It's easy to see that if $a \equiv b \pmod{N}$ and if $c \equiv d \pmod{N}$ then $(a+c) \equiv (b+d) \pmod{N}$. The same is true for multiplication. These allow us to introduce an algebraic structure into the set $\{[a]_N: a=0, 1, \dots, n-1\}$. A first application field is in Residue Number Systems (RNS). In an RNS based application, every number X is represented by a sequence of residues (X_1, X_2, \dots, X_M) , where $X_i = X$

mod p_i , where p_i = prime integers. Every RNS operation on two operands is defined as.

$$(Z_1; Z_2; \dots; Z_M) = (X_1; X_2; \dots; X_M) \diamond (Y_1; Y_2; \dots; Y_M)$$

For most RNS applications, \diamond denotes addition, subtraction, or multiplication. Significant speedup over the corresponding binary operations can be therefore achieved because each Z_i is computed in parallel in a separate arithmetic unit (channel) since its computation depends only on X_i , Y_i , and p_i . Addition in such systems is performed using three channels that, in fact, are a modulo 2^n-1 (equivalently, one's complement), a modulo 2^n , and a modulo 2^n+1 adder. The addition delay in an RNS application which uses the above modulo is dictated by the modulo 2^n+1 channel. Modulo 2^n+1 adder are also utilized as the last stage adder of modulo 2^n+1 multipliers. Modulo 2^n+1 multipliers find applicability in many applications such as cryptography, fermat numbers etc.

II. LITERATURE SURVEY

A number of different architectures can be followed for the design of a modulo 2^n+1 weighted adder; some of them stem from the general residue adder case, whereas others are dedicated architectures for this particular modulus. For the modulo 2^n+1 addition of A and B , here after denoted by $|A+B|_{2^n+1}$, where $A = a_n a_{n-1} a_{n-2} \dots a_1 a_0$ and $B = b_n b_{n-1} b_{n-2} \dots b_1 b_0$ are two $(n+1)$ -bit binary numbers in the range $[0, 2^n]$, we have that :

$$|A+B|_{2^n+1} = A+B - (2^n+1), \text{ if } A+B \geq 2^n+1 \\ = A+B, \text{ otherwise.}$$

Following the general residue adder architecture, implementation by using two binary adders connected in series and a multiplexer. A $(n+1)$ bit adder is used to compute $A+B$, while a $-(2^n+1)$ correction is added to its output by the second $(n+2)$ -bit adder. The multiplexer is then used to select between the two adders' results depending on the value of the carry output of the second adder. Dugdale has reduced the width of the second adder to $(n+1)$ bits and has shown that the multiplexers can be controlled by the logical OR of the two adders carry outputs. She has also presented an area efficient architecture that performs the modular addition using just one adder in two addition cycles. Both these architectures are very slow. An obvious solution for decreasing the delay of the above architectures is to have both cases is computed in

parallel. This solution however, apart from the two adders requires the addition of a Carry-Save Adder (CSA) stage. A more area effective solution was proposed, by observing that most carry propagate and generate signals for both cases are common and therefore an augmented single Carry Look-Ahead (CLA) unit is sufficient. Finally, parallel-prefix weighted adders have been presented. These have been shown to be the fastest available and more efficient than the others. From the estimates it becomes obvious that, considering the current state of the art, a diminished-1 adder is both a smaller and faster circuit than a weighted modulo 2^n+1 adder. Therefore, if we could use a diminished-1 adder with minor modifications also perform weighted modulo 2^n+1 addition, by reducing both the area and the delay of the resulting components.

(a) Vergos and Efstathiou

Given two $(n+1)$ -bit numbers A and B , where $0 \leq A, B \leq 2^n$, the values of diminished-1 of A and B are denoted by $A^* = A-1$ and $B^* = B-1$, respectively. The diminished-1 sum S^* can be computed by

$$S^* = |S-1|_{2^n+1} = |A+B-1|_{2^n+1} = |A^* + B^*|_{2^n} + c_{out}$$

Where $|X|_Z$ is defined as modulo Z of X , and c_{out} is denoted as the inverted end-around carry of the diminished-1 modulo 2^n sum of n -bit A^* and B^* . Suppose that $A = a_n a_{n-1} a_{n-2} \dots a_1 a_0$ and $B = b_n b_{n-1} b_{n-2} \dots b_1 b_0$ denote two operands in the composed of the least significant bits of A and B , respectively. Equivalently, we have that $A = a_n \times 2^n + A_n$ and $B = b_n \times 2^n + B_n$. weighted representation. Let A_n and B_n denote the n -bit vectors composed of the least significant bits of A and B , respectively. Equivalently, we have that $A = a_n \times 2^n + A_n$ and $B = b_n \times 2^n + B_n$.

The previous analysis indicates that the A_n , B_n vectors, and D can be added by the inverted end-around carry save adder stage presented in Fig. 4. We can then drive its outputs Y and U to a diminished-1 adder, that will provide at its output $Y+U+1 \text{ mod } 2^n+1$, that is, it will provide the n least significant bits of the weighted modulo addition of A and B . The most significant bit of the weighted sum should be at 1, only when $A+B \text{ mod } 2^n+1$ is equal to 2^n , or equivalently when $Y+U+1 \text{ mod } 2^n+1$ equal to 2^n , or equivalently (since) when $Y+U = 2^n-1$, that is, when Y and U are bitwise complementary.

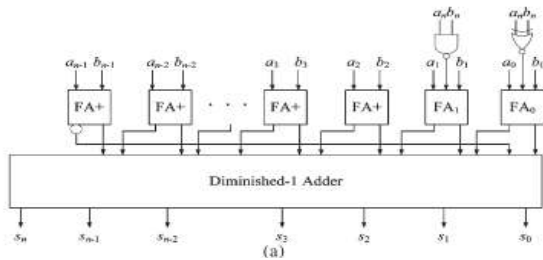


Figure 1: Architecture of the weighed modulo 2^n+1 adder for Vergos and Efstathiou

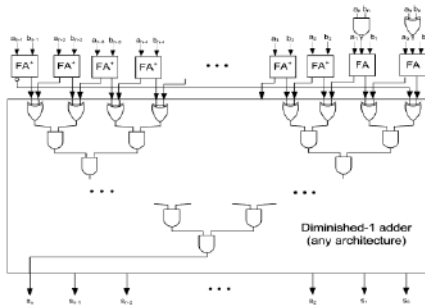


Figure 2: Modulo 2^n+1 adder for weighted operands built using a diminished-1 adder.

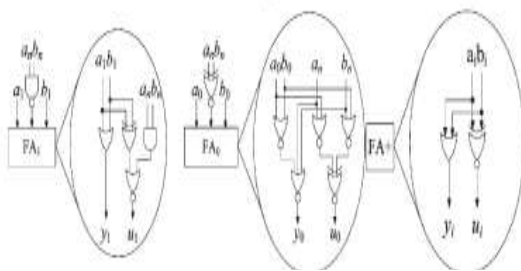


Figure 3: Architecture of FA1, FA0, and FA+.

This condition can be easily detected as the logical AND of the XOR of the bits of Y and U with the same weight. Since in every fast adder architecture there is a preprocessing stage that apart from the generate and propagate terms also computes the half-sum term, that is the XOR of the corresponding input operands bits, the extra hardware required for the most significant bit of the weighted addition is small; just AND ing the half-sum terms together. It should be noted that this operation will not add any delay on the critical path of the adder. The figure presents the implementation that results from the previous analysis for a modulo 2^n+1 adder for operands in the weighted representation. It is composed of a diminished-1 adder and an inverted end-around-carry CSA stage. The full adders of the CSA stage perform the $|A_n + B_n + D|_{2^n+1}$ addition. The FAs at bit positions 2 up to (n-1) are denoted as FAs since one of their operands coming

from vector is 1. Therefore, they have hardware and delay complexity equal to that of a half adder. Several simplifications can also be performed to the two rightmost FAs along with the accompanying NAND and XNOR gates by considering that $a_n(b_n)$ and a_1 or a_0 (and b_1 or b_0) cannot be simultaneously at 1. Fig. 6 presents examples of simplified circuits at these least significant bit positions. However, even more aggressive simplification is possible within the pre-processing stage of the diminished-1 adder by considering that the propagate and generate signals at bit position 1 depend on signals y_0 and u_1 that are both dependent on a_n and b_n . The most significant carry bit produced by the CSA is inverted and then driven to the least significant position. The sum and carry bits of equal weight produced by the CSA stage are then driven to the diminished-1 adder. Obviously, any architecture proposed, can be used for the latter. The diminished-1 adder's result forms the n least significant bits of the weighted sum. The indication of complementary input vectors at the diminished-1 adder is the most significant bit of the weighted sum.

(b) *Vergos and Bakalis (Using a Diminished-1 Adder for Weighted Addition:*

Let A and B represent two n-bit operands in the $[0, 2^n - 1]$ range. Let A^* and B^* denote two n-bit vectors such $A^* + B^* = A + B - 1$. According to (9), we then have that :

$$|A + B|_{2^n+1} = A + B - (2^n + 1), \text{ if } A + B \geq 2^n + 1$$

$$= A + B, \text{ otherwise.}$$

or equivalently that :

$$|A + B|_{2^n+1} = (A + B - 1) - 2^n, \text{ if } A + B - 1 \geq 2^n$$

$$= (A + B - 1) + 1, \text{ otherwise.}$$

Taking the modulo 2^n of (2) and using A^* and B^* we then get :

$$(|A + B|_{2^n+1})_{2^n} = (A^* + B^*), \text{ if } (A^* + B^*) \geq 2^n$$

$$= (A^* + B^*) + 1, \text{ otherwise.}$$

Let c_{out} denote the carry output of the $(A^* + B^*)$ n-bit integer addition. Using it, we can unify the two cases

$$\text{as : } |A + B|_{2^n+1} \cdot 2^n = |A^* + B^*|_{2^n} + c_{out}$$

Relation 12 indicates that we can derive the n-least significant bits of the weighted modulo 2^n+1 addition of A and B by using an inverted end-around carry adder (equivalently, a diminished-1

adder) provided that the sum of its inputs is decreased by 1, that is, if we use as inputs the A^* and B^* vectors. The most significant bit of the weighted addition of A and B should be 1, only when $|A + B|_{2^{n+1}} = 2^n$, which since $0 \leq A, B \leq 2^n - 1$ reduces to $A^* + B^* = 2^n - 1$, that is, when A^* and B^* are bit-wise complementary. This condition can be easily detected as the logical AND of the XOR of the bits of A^* and B^* with the same weight. Since in every fast adder architecture there is a pre-processing stage that computes the half-sum terms, that is, the XOR of the corresponding input operands bits, the extra hardware required for deriving the most significant bit of the weighted addition is small. Since this operation, according to the unit gate model, can be completed by a tree of two-input gates in $\log n + 2$ time units, while the diminished-1 adder computes the rest bits in $2 \log n + 3$ time units, it does not add any delay on the critical path of the diminished-1 adder. In some adder cases (known as XOR adders) the half sum term is also used as the carry propagate term. The group propagate terms in these adders are the logical AND of the half-sum terms and therefore no extra hardware is required for the derivation of the most significant bit. Figure 1 presents the architecture that result from the previous analysis. A translator circuit accepts the n -bit vectors A and B and provides the vectors A^* and B^* . These are driven to an augmented diminished-1 adder that is capable of providing the $(n + 1)$ -bit sum of the weighted modulo $(2^n + 1)$ addition of A and B . The augmented diminished-1 adder also offers implementation area and execution delay savings over every architecture proposed for weighted addition. We therefore conclude that its use is very attractive if the translator circuit of Figure 1 can be designed efficiently.

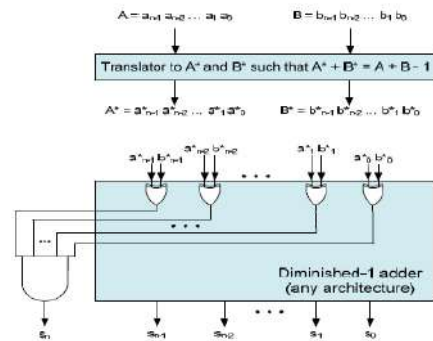
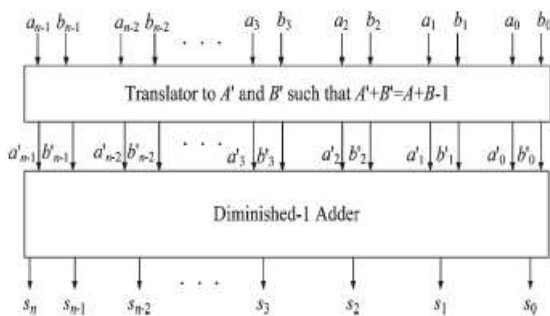


Figure 4: Architectures of the weighed modulo $2^n + 1$ adder for proposal

The architecture proposed in [1] makes use of a constant time operator, which is composed of a simplified carry-save adder stage, leading to efficient modulo $2^n + 1$ adder. The architecture proposed in [2] can be applied in the design of area-efficient residue generators and multi operand modulo adders. However, it should be noted that, in [1], the values that are subtracted by the inputs A and B are not constants. In [2], the way to implement the translator for decreasing the sum of two inputs by 1 was not mentioned. Furthermore, in [2], the ranges of two inputs A and B are less than the one proposed in [1] (i.e., $\{0, 2^n - 1\}$ versus $\{0, 2^n\}$). To remedy these problems, we will propose our area-efficient weighted modulo $2^n + 1$ adder design.

III. AREA-EFFICIENT WEIGHTED MODULO $2^N + 1$ ADDER DESIGN

Instead of subtracting the sum of A and B by D , which is not a constant, we use the constant value $-(2^n + 1)$ to be added by the sum of A and B . In addition, we make the two inputs A and B to be in the range $\{0, 2^n\}$, which is 1 more than $\{0, 2^n - 1\}$ as proposed. In the following, we present the designs of our proposed weighted modulo $2^n + 1$ adder.

Given two $(n+1)$ -bit inputs $A = a_n a_{n-1} \dots a_0$ and $B = b_n b_{n-1}, \dots, b_0$, where $0 \leq A, B \leq 2^n$. The weighted modulo $2^n + 1$ of $A+B$ can be represented as follows:

$$|A+B|_{2^n+1} = \begin{cases} A+B - (2^n+1), & \text{if } (A+B) > 2^n \\ A+B, & \text{otherwise.} \end{cases}$$

Equation (1) can be stated as

$$||A + B|_{2^n+1}|_{2^n} = |A+B - (2^n+1)|_{2^n}, \text{ if } (A+B) > 2^n$$

$= |A+B-(2^n+1)|_{2^n} + |(2^n+1)|_{2^n}$,
otherwise.

This can then be expressed as

$$\|A + B\|_{2^{n+1}}|_{2^n} = |A+B - (2^n+1)|_{2^n}, \text{ if } (A + B) > 2^n$$

$$= |A+B - (2^n+1)|_{2^n} + 1, \text{ otherwise.}$$

From (3), it can easily be seen that the value of the weighted modulo 2^n+1 addition can be obtained by first subtracting the value of the sum of A and B by (2^n+1) (i.e., 0111, . . . , 1) and then using the diminished-1 adder to get the final modulo sum by making the inverted end-around carry as the carry-in. Now, we present the method of weighted modulo 2^n+1 addition of A and B as follows. Denoting Y' and U' as the carry and sum vectors of the summation of A, B and $-(2^n + 1)$, where $Y' = y'_{n-2} y'_{n-3}, \dots, y'_0 y'_{n-1}$ and $U' = u'_{n-1} u'_{n-2}, \dots, u'_0$, the modulo addition can be expressed as follows:

$$\begin{aligned} |A+B-(2^n+1)|_{2^n} &= |A + B - (2^n + 1)|_{2^n} \\ &= \left| \sum_{i=0}^{n-2} (2^i \times (a_i + b_i)) + 2^{n-1} \right. \\ &\quad \left. \times (2a_n + 2b_n + a_{n-1} + b_{n-1}) + \underbrace{011\dots11}_{n \text{ bits}} \right|_{2^n} \\ &= \left| \sum_{i=0}^{n-2} (2^i \times (a_i + b_i + 1)) + 2^{n-1} \right. \\ &\quad \left. \times (2a_n + 2b_n + a_{n-1} + b_{n-1} + 1) \right|_{2^n} \\ &= \left| \sum_{i=0}^{n-2} (2^i \times (2y'_i + u'_i)) + 2^{n-1} \right. \\ &\quad \left. \times (2a_n + 2b_n + a_{n-1} + b_{n-1} + 1) \right|_{2^n} \end{aligned}$$

For $i=0$ to $n - 2$, the values of y'_i and u'_i can be expressed as $y'_i = a_i \vee b_i$ and $u'_i = a_i \oplus b_i$, respectively (\vee is denoted as logic OR operation). Since the bit widths of Y' and U' are only n bits, the values of y'_{n-1} and u'_{n-1} are required to be computed taking the values of a_n, b_n, a_{n-1} , and b_{n-1} into consideration (i.e., y'_{n-1} and u'_{n-1} are the values of the carry and the sum produced by $2a_n + 2b_n + a_{n-1} + b_{n-1} + 1$, respectively). It should be noted that $0 \leq A, B \leq 2^n$, which means $a_n = a_{n-1} = 1$ or $b_n = b_{n-1} = 1$ will cause the value of A or B to exceed the range of $\{0, 2^n\}$. Thus, these input combinations (i.e., $a_n = a_{n-1} = 1$ or $b_n = b_{n-1} = 1$) are not allowed and can be viewed as don't care conditions, which can help us

simplify the circuits for generating y'_{n-1} and u'_{n-1} . That is, the maximum value of $2a_n + 2b_n + a_{n-1} + b_{n-1} + 1$ is 5, which occurs at $a_n = b_n = 1$ (i.e., the maximum value of y'_{n-1} is 2). The truth table for generating y'_{n-1}, u'_{n-1} and FIX is given in Table I, where \times is denoted as don't care. The reason for FIX is that, under some conditions, $y'_{n-1} = 2$ (e.g., $a_n = b_n = 1$ and $a_{n-1} = b_{n-1} = 0$), which cannot be represented by 1-bit line (marked as "*" in Table I); therefore, the value of y'_{n-1} is set to 1, and the remaining value of carry (i.e., 1) is set to FIX. Notice that FIX is wired-OR with the carry-out of $Y' + U'$ (i.e., c_{out}) to be the inverted end around carry (denoted by $c_{out} \vee \text{FIX}$) as the carry-in for the diminished-1 addition stage later on. When $y'_{n-1} = 2$, $\text{FIX} = 1$; otherwise, $\text{FIX} = 0$.

TABLE 1. Truth Table For Generating y'_{n-1}, u'_{n-1} AND FIX (*: CONDITIONS WHEN $y'_{n-1} = 2$)

a_n	b_n	a_{n-1}	b_{n-1}	u'_{n-1}	y'_{n-1}	<i>FIX</i>
0	0	0	0	1	0	0
0	0	0	1	0	1	0
0	0	1	0	0	1	0
0	0	1	1	1	1	0
0	1	0	0	1	1	0
0	1	0	1	\times	\times	\times
0	1	1	0	0	1*	1
0	1	1	1	\times	\times	\times
1	0	0	0	1	1	0
1	0	0	1	0	1*	1
1	0	1	0	\times	\times	\times
1	0	1	1	\times	\times	\times
1	1	0	0	1	1*	1
1	1	0	1	\times	\times	\times
1	1	1	0	\times	\times	\times
1	1	1	1	\times	\times	\times
1	1	1	1	\times	\times	\times

According to Table 1, we can have $y'_{n-1} = (a_n \vee b_n \vee a_{n-1} \vee b_{n-1})$, $u'_{n-1} = a_{n-1} \oplus b_{n-1}$, and $\text{FIX} = a_n b_n \vee b_n a_{n-1} \vee a_n b_{n-1}$, respectively.

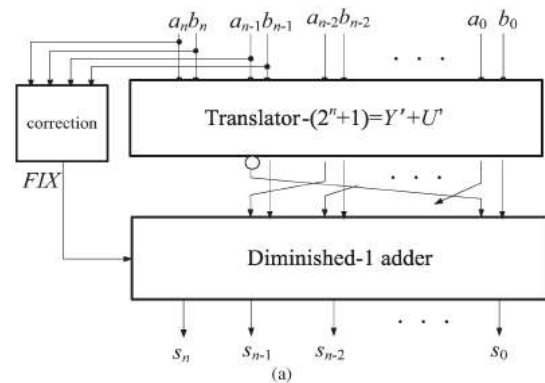


Figure 5: Architecture of proposed weighted modulo 2^n+1 adder with the correction

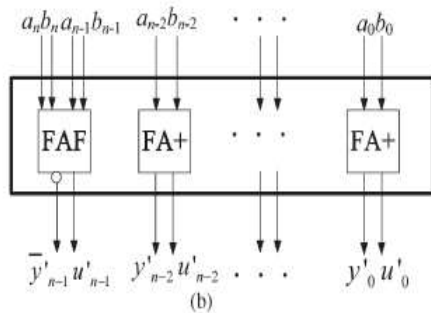


Figure 6: Architecture of the translator – $(2^n + 1)$

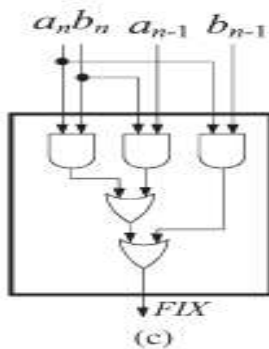


Figure 7: Architecture of the correction scheme

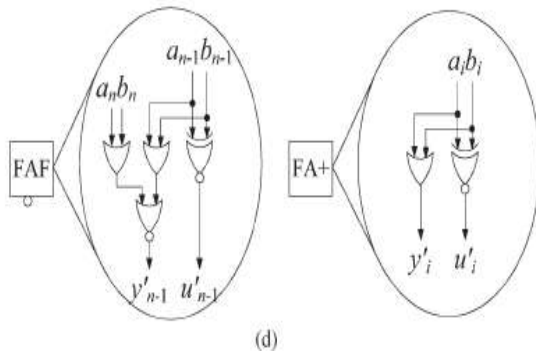


Figure 8: Architecture of FAF and FA+

From Fig. 3, the signal of FIX can be computed in parallel with the translation to $Y'+U'$, leading to efficient correction. In addition, the hardware cost for our correction scheme and FAF are less than the one proposed in [1], due to the fact that there are two inconstant numbers that should be processed [i.e., FA1 and FA0, as shown in Fig. 1(b)] in the translation stage. We used Sklansky-style and Brent-Kung style parallel-prefix structures for the diminished-1 adder implementations. The diminished-1 adder based on the Sklansky-style parallel-prefix structure with correction circuits for our proposed weighted modulo 2^8+1 adder is shown in Fig. 4(a). The square () and diamond (♦) nodes

denote the pre- and post processing stages of the operands, respectively. The black nodes (●) evaluate the prefix operator, and the white nodes (○) pass the unchanged signals to the next prefix level. The four nodes with detailed implementations are given in Fig. 4(b). It should be noted that the value of s_n (i.e., c_{out}) can be computed by wiring-AND all propagate signals (i.e., $s_n = \prod_{i=0}^{n-1} p_i$).

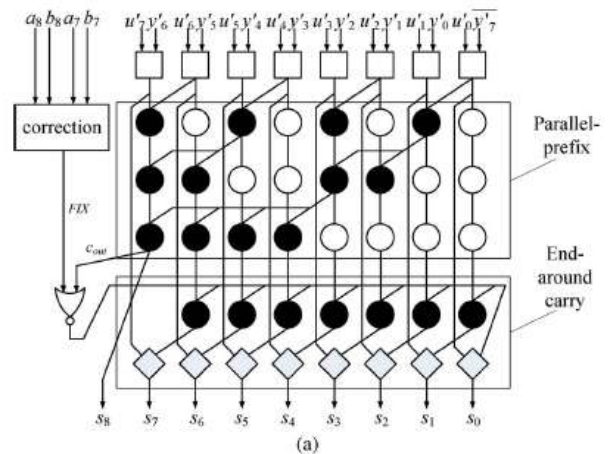


Figure 9: Diminished-1 adder based on the Sklansky-style parallel-prefix Structure

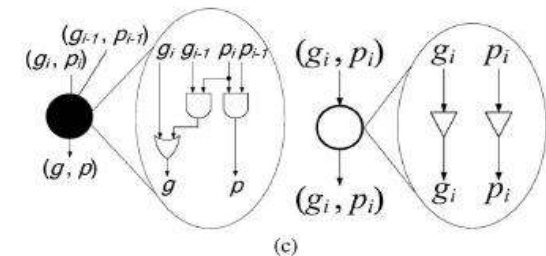
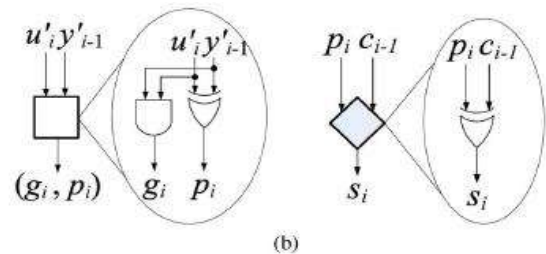


Figure 10: Square and (♦) diamond nodes, respectively

(●) Black and (○) white nodes, respectively

3.3 Parallel Prefix Structures:

The different prefix structures are provided for the implementation of the modulo addition.

- **Sklansky prefix structure:** This structure provided the basic prefix operations in the modulo performance. This requires the less number of the

gates when compared to the other structures. These are 4 layered structures.

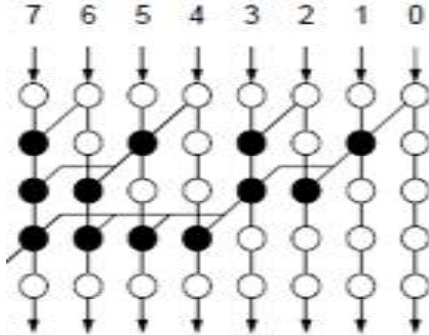


Figure 11: Sklansky prefix structure

Koggestone prefix structure: This structure requires the more number of the gates when compared to the other structures. These are also 4 layered structures.

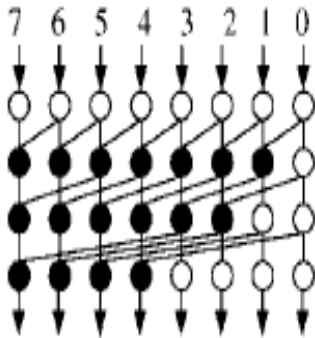


Figure 12: Koggestone structure

Lander-Fisher prefix structure: This structure is similar to the Sklansky prefix structure. This structure requires the more number of the gates when compared to the other structures. These are also 4 layered structures

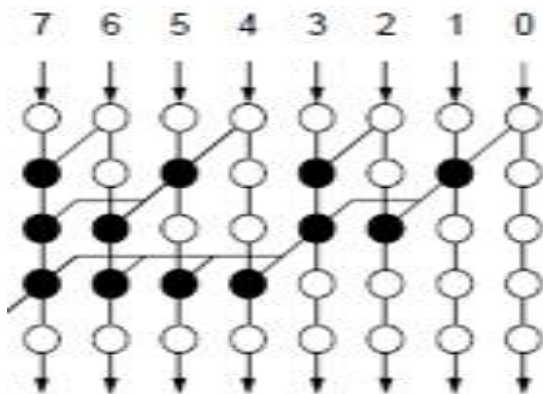


Figure 13: Lander-Fisher structure

Brent-Kung Structure: The Brent-Kung adder is a parallel prefix adder that requires $2(\log_2 N) - 1$ stages. It was originally proposed as a simple and regular design of a parallel adder that addresses the problems of connecting gates in a way to minimize chip area. Accordingly, it is considered one of the better tree adders for minimizing wiring tracks, fan out, and gate count and is used as a basis for many other networks.

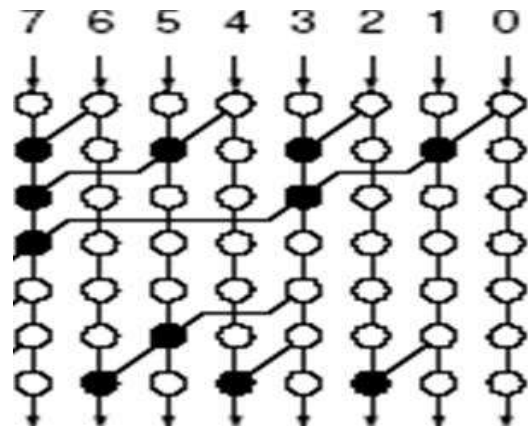


Figure 14: Brent-Kung parallel-prefix structure:

Example 1: Suppose $n = 4$, $A = 16_{10} = 10000_2$, and $B = 15_{10} = 01111_2$.

Step 1: $(A + B) - (2^n + 1) \Rightarrow Y' = 1110_2, U' = 0000_2, \text{FIX} = 1.$

Step 2: $Y' + U' = 1110_2, c_{out} = 0,$

$\Rightarrow Y' + U' + c_{out} \vee \text{FIX} = 1110_2 = |16 + 15|_{17} = 14_{10}.$

Example 2: Suppose $n = 4$, $A = 11_{10} = 01011_2$, and $B = 5_{10} = 00101_2.$

Step 1: $(A + B) - (2^n + 1) \Rightarrow Y' = 1110_2, U' = 0001_2, \text{FIX} = 0.$

Step 2: $Y' + U' = 1111_2, c_{out} = 0,$

$\Rightarrow Y' + U' + c_{out} \vee \text{FIX} = 10000_2 = |11 + 5|_{17} = 16_{10}$

IV. RESULTS DISCUSSIONS

This section presents the evaluation parameters such as area, delay and these parameters can be utilized to select the efficient design for real time applications.

Table 2: Comparison of area (8-bit)

Parameter	SKLANSKY	KOGGESTONE	BRENTKUNG
No of Slices	15	48	15
No of 4 i/p LUT's	26	85	26
No of I/O's	27	51	27
No of bounded I/O's	27	51	27

Table 3: Comparison of area (16-bit)

Parameter	SKLANSKY	KOGGESTONE	BRENTKUNG
No of Slices	48	119	49
No of 4 i/p LUT's	85	210	85
No of I/O's	51	27	51
No of bounded I/O's	51	27	51

Table 4: Comparison of Delay(8-bit)

Prefix Structures Model	8 BIT	16 BIT
SKLAN SKY	7.132 ns	32.250 ns
KOGGEESTONE	9.347 ns	25.139 ns
BRENTKUNG	18.863ns	30.710

V.CONCLUSION & FUTURE SCOPE

Conclusion: In this brief, an improved area-efficient weighted modulo $2^n + 1$ adder has been proposed. This has been achieved by modifying the existing diminished-1 modulo adders to incorporate simple correction schemes. The proposed adders can perform weighted modulo $2^n + 1$ addition and

produce sums that are within the range $\{0, 2^n\}$. Synthesis results show that our proposed adders can outperform previously reported weighted modulo adder in terms of area and delay constraints.

Future scope: The design can be extended to applications where the area and delay are the major parameters. The design can also be implemented in 32 and 64 bits to improve area and delay and it can be used for low power CMOS applications like digital signal processing and nanotechnology.

REFERENCES

- [1] .R. Zimmermann, "Efficient VLSI implementation of modulo $2n \pm 1$ addition and multiplication," in Proc. 14th IEEE Symp. Comput. Arithmetic, Apr. 1999, pp.158–167.
- [2] . H. T. Vergos, C. Efstathiou, and D. Nikolos, "Diminished-one modulo $2n + 1$ adder design," IEEE Trans. Comput., vol. 51, no. 12, pp. 1389–1399, Dec. 2002.
- [3] . C. Efstathiou, H. T. Vergos, and D. Nikolos, "Modulo $2n \pm 1$ adder design using select-prefix blocks," IEEE Trans. Comput., vol. 52, no. 11, pp. 1399–1406, Nov. 2003.
- [4] . S.-H. Lin and M.-H. Sheu, "VLSI design of diminished-one modulo $2n + 1$ adder using circular carry selection," IEEE Trans. Circuits Syst. II, Exp. Briefs, vol. 55, no. 9, pp. 897–901, Sep. 2008.
- [5] . T.-B. Juang, M.-Y. Tsai, and C.-C. Chiu, "Corrections on 'VLSI design of diminished-one modulo $2n + 1$ adder using circular carry selection'," IEEE Trans. Circuits Syst. II, Exp. Briefs, vol. 56, no. 3, pp. 260–261, Mar. 2009.
- [6] . H. T. Vergos and C. Efstathiou, "A unifying approach for weighted and diminished-1 modulo $2n + 1$ addition," IEEE Trans. Circuits Syst. II, Exp. Briefs, vol. 55, no. 10, pp. 1041–1045, Oct. 2008.
- [7] . H. T. Vergos and D. Bakalis, "On the use of diminished-1 adders for weighted modulo $2n + 1$ arithmetic components," in Proc. 11th EUROMICRO Conf. Digit. Syst. Des. Archit., Methods Tools, Sep. 2008, pp. 752–759.

1ST NATIONAL CONFERENCE ON TRENDS IN SCIENCE, ENGINEERING AND TECHNOLOGY (NTSET - 2018)

February 2nd & 3rd - 2018

TECHNICAL PAPER ABSTRACTS



ORGANIZED BY

MATRUSRI ENGINEERING COLLEGE

(Approved by AICTE, Affiliated to Osmania University)

#16-1-486, Saidabad, Hyderabad - 500059



Sponsored by

MATRUSRI EDUCATION SOCIETY

ISBN: 97881-936274-0-2

**NTSET
2018**



A REVIEW ON MIXED IRIS SPOOFING ATTACKS DETECTION

¹Dr.PallaviKhare, ²Vinithakotla, ³SaiAkhil , ⁴V.Pravalika

¹Assistant professor, ^{2,3,4}Student
^{1,2,3,4} Department of Electronics and Communication
^{1,2,3,4} Matrusri Engineering College, Hyderabad
Telangana, India.

Abstract: Human iris is viewed as a dependable and exact methodology for biometric acknowledgment because of its one of a kind surface data. All known biometric frameworks are helpless against introduction assaults (usually called ridiculing) that endeavor to cover or imitate character. Image based biometric modalities (e.g. confront, finger, iris) are especially helpless at the image obtaining step. Cases of run of the mill iris parodying assaults are printed iris images, finished contact focal points, and engineered formation of iris images. It is basic to take note of that greater part of the calculations proposed in the writing are prepared to deal with a particular kind of parodying assault. These calculations as a rule perform exceptionally well on that specific assault. Notwithstanding, in genuine applications, an assailant may perform distinctive parodying assaults. In such a case, the issue turns out to be all the more difficult because of natural varieties in various assaults. In this paper, we concentrate on a mixture of iris mocking assaults and present a bound together structure for distinguishing such assaults. We propose a novel basic and textural include based iris mocking recognition structure (DESIST). Multi-arrange thick Zernike minutes are ascertained over the iris image which encode varieties in structure of the iris image. Neighborhood Binary Pattern with Variance (LBPV) is used for speaking to textural changes in a caricature iris image. The most noteworthy characterization precision is seen by the proposed structure for recognizing ordinary and parodied iris images on a joined iris caricaturing database.

Index Terms: Iris recognition, Iris, Databases, Lenses, Feature extraction, Algorithm design and analysis, Training

I. INTRODUCTION

Iris is a standout amongst the most solid and exact biometric modalities because of the exceedingly exceptional character of iris tissue structure. John Daugman protected the primary effective iris acknowledgment calculation in 1994; it depended on a trial of measurable freedom of the period of Gabor wavelets fit-(a) (b) (c) (d) Figure 1. Cases of iris mocking. (a) Contact Lens , (b) Synthetic Iris, (c) Print+Capture Attack , and (d) Print+Scan Attack . ted on a lattice of areas superimposed on a pseudo-polar change of the iris surface. That fundamental outline remains the predominant iris acknowledgment strategy in 2016. It has been utilized effectively in various applications including national ID undertakings and outskirt security. The achievement of vast scale personality applications utilizing iris acknowledgment, thusly, implies there are presently people who can pick up advantage by crushing these applications to increase unapproved access to areas or assets or to escape acknowledgment as a person of intrigue. Relief of such introduction/mocking assaults has turned into a key goal in the plan of such frameworks and is the theme of progressing guidelines endeavors, e.g. ISO/IEC 30107-1:2016. Some average iris introduction assault strategies are delineated in Fig. 1 and quickly portrayed herewith:

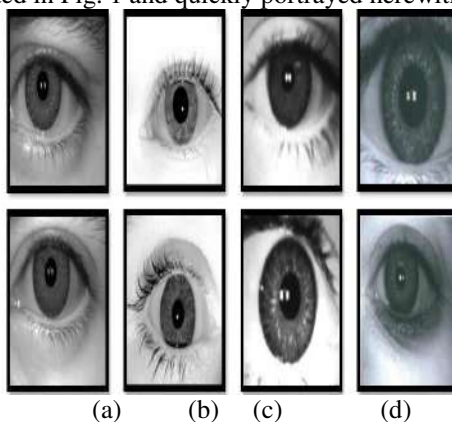


Figure 1.Examples of iris spoofing. (a) Contact Lens , (b) Synthetic Iris , (c) Print+Capture Attack , and (d) Print+Scan Attack

• **Fake/Printed Iris Images:** This assault is most straightforward to prompt as it includes showing aimage of an iris to the sensor. The image could be a checked or printed duplicate of the first iris image can be utilized with the aim of mimicking someone else's personality. Utilizing a decent quality paper, printer and high determination iris images, parodied iris images can be produced to misuse acknowledgment frameworks. The examination by Gupta et al. demonstrated that both print+scan



and print+capture assaults can decrease the confirmation precision to under 10% at 0.01% FAR. Raghavendra and Busch proposed a multi-scale binarized factual image include (m-BSIF) on iris and periocular images alongside straight help vector machines to identify image print assault and screen assault. Akhtar et al. proposed LUCID descriptor and assessed its adequacy on ATVS-FIR database of printed iris images.

- **Synthetic Iris Images:** Venugopalan and Savvides portrayed a novel caricaturing assault by making engineered "common" iris images that can trick iris acknowledgment frameworks. They implanted highlights in iris to parody someone else's iris and expected that the component extraction instrument of the iris framework is known. Galbally et al proposed a hereditary calculation based engineered iris creation method. Their probabilistic approach created iris-like example whose comparing iriscodes coordinated with a certifiable client.

- **Textured Contact Lenses:** With progresses in innovation and low costs, contact focal points are picking up prevalence around the globe. Aside from being utilized for visual perception amendment, they are progressively being utilized for restorative purposes also. These finished (restorative) focal points cover the first surface of the iris with a thin finished focal point which can extremely corrupt the execution of iris acknowledgment frameworks. A few examinations exhibited the requirement for distinguishing contact focal points as both straightforward (delicate) and finished (corrective) focal points have been appeared to influence iris acknowledgment frameworks precision. Zhang et al proposed using improved LBP for grouping bona fide and mock iris images. Filter descriptor figured at each pixel is utilized to process weighted LBP (wLBP) outline with factual highlights.

In the writing, specialists have concentrated on one specific kind of iris satirizing assault and have exhibited calculations to address it. Be that as it may, in genuine situations, iris acknowledgment frameworks need to deal with and recognize a wide range of satirizing assault. The key inspiration of this paper is to recreate this genuine ridiculing assault situation for which, we evaluate print assaults, manufactured iris images, and contact focal points exhaustively. The real commitments of this paper are:

- Combining diverse kinds of mocking assaults trying to recreate true situations, and
 - Proposing a novel system using auxiliary and textural highlights to distinguish such numerous complex ridiculing assaults.
- In the consequent areas, we clarify the proposed system took after by the databases utilized as a part of this paper, exploratory convention took after, and the outcomes acquired.

II. Proposed Detection of Iris Spoofing utilizing Structural and Textural Feature Framework

Fig. 2 demonstrates the proposed DEtection of iriSspoofIng utilizing Structural and Textural include (DESIST) system for identifying parodied iris images. The proposed system includes two sections: auxiliary decay of images to investigate nearby locales of the images, and a textural examination to watch the adjustments conversely of the info iris image. We depict both the parts in detail beneath.

2.1. Auxiliary Decomposition of Images utilizing Zernike Moments

Zernike moments (ZMs) are known for their invariance crosswise over scale, turn, and interpretation; and have been effectively connected in iris division and iris acknowledgment at a separation. The inspiration driving separating these Zernike minutes is to catch the adjustments in the shape between a caricature and a typical iris image. ZMs of a image are characterized over an orthogonal arrangement of polynomials and include calculation of the outspread polynomial $R_{n,m}$. Zernike premise capacities can be ascertained after the polynomial is registered and projection of the info image over these premise capacities is resolved. The spiral polynomial R is characterized as:

$$R_n^m(\rho) = \sum_{i=0}^{\frac{n-|m|}{2}} \frac{(-1)^i \rho^{n-2i} (n-i)!}{i! \left(\frac{n+|m|}{2}-i\right)! \left(\frac{n-|m|}{2}-i\right)!} \quad (1)$$

where, ρ is the separation between the focal point of the image and a comparing point (x, y) on the image, n is known as the request of the polynomial and m are the reiterations with the end goal that $|m| < n$ and $|n-m|$ is even. Zernike premise capacity can be straightforwardly processed in the Cartesian organize space as characterized beneath:

$$Z_{n,m}(x, y) = R_n^m(\rho_{x,y}) e^{-jm\theta_{x,y}} \quad (2)$$

where $N \times N$ is the extent of the image,

$$\rho_{x,y} = \frac{1}{N} \times \sqrt{(2x - N + 1)^2 + (N - 1 - 2y)^2} \quad (3)$$

And

$$\theta_{x,y} = \tan^{-1} \left(\frac{N-1-2y}{2x-N+1} \right) \quad (4)$$

Given an iris image I , thick Zernike minutes are ascertained for a given match of (n, m) crosswise over non-covering windows of size $P \times P$. Numerous sets of (n, m) are chosen to figure the abundancy of multi-arrange Zernike moments. This will help in improving the portrayal of the information iris image.

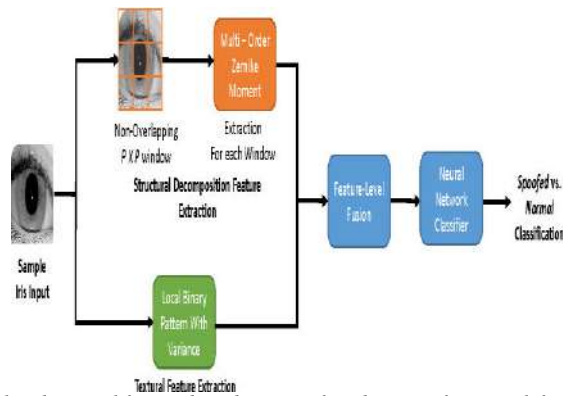


Figure 2. Proposed structural and textural feature based iris spoofing detection framework for detecting spoofed iris images.

2.2. Textural Analysis utilizing LBPV Descriptor

Through prior examinations it is referred to that satirize iris assaults, for example, contact focal point iris images, printed iris images have varieties in surface as for the standard iris images. Thusly, the inspiration driving using surface methods is to distinguish the changed surface of the ridiculed iris image. For this reason, Local Binary Pattern Variance (LBPV) descriptor is used. LBPV descriptor represents the difference in the information images by adaptively measuring the LBP vectors by their fluctuation of the locale. It is likewise more powerful to light variety which is helpful as the obtained iris images may have diverse enlightenment sources. In this way, LBPV descriptor is ascertained for the info iris image and gave to the classifier.

2.3. Feature Fusion and Classification

Multi-arrange Zernike and LBPV highlights give corresponding data in regards to the info iris image. In this way, highlight level combination is performed by connecting them. The connected (combined) highlight vector is then utilized as contribution for a fake neural system (ANN) to decide if the iris is ridiculed or not. A three layer ANN is prepared with H shrouded hubs and scaled conjugate slope calculation is used for back-proliferation.

III. Exploratory Setup

To assess the execution of the proposed DESIST structure; images from the joined caricaturing database (CSD) are resized to a typical size of 256×256 pixels. Following the convention portrayed in two folds are made for every database where half of the subjects are allocated to crease one and the staying half of the subjects are allotted to the next overlap. Utilizing these inconspicuous preparing and testing folds, five times arbitrary two overlap cross-approval is performed.

Multi-arrange neighborhood Zernike minutes are processed from non-covering windows of size $P \times P$ of the images. The abundancy of the Zernike minutes is processed for request of the Zernike minutes $(n) = (0, 1, 2, 3, 4, 5, 6, 7, 8, 9, 10)$ and comparing reiteration number of Zernike minute $(m) = (0, 1, 0, 1, 0, 1, 0, 1, 0, 1, 0)$. LBPV highlights are likewise registered for the entire iris image and highlight level combination is performed utilizing the Zernike and LBVP highlights. These highlights are utilized for the last order of the info image as ridiculed or ordinary. A three layer neural system is prepared utilizing melded includes and scaled conjugate slope calculation is used for back-engendering. Alongside the proposed calculation, we have assessed the execution of a few existing descriptors too.

IV. CONCLUSION

In the writing of iris satirizing discovery, specialists have commonly centered around a specific sort of iris parodying assault and have given answers for give them. In any case, in certifiable situations, iris acknowledgment frameworks need to deal with an introduction mocking assault. In this paper, we display a certifiable situation, where diverse kinds of satirize iris images can be exhibited at the securing step. We have used a joined database containing satirize iris images having a place with contact focal point, print-catch, print-sweep and manufactured iris images. We propose DESIST, a system to recognize parodied iris images crosswise over genuine assault situations. The proposed DESIST system identifies mock iris images with a good precision when connected to a joined iris caricaturing database of ordinary and satirize iris images.

REFERENCES

- [1] Z. Akhtar, C. Micheloni, C. Piciarelli, and G. L. Foresti. *Mobiolidvet: Mobile biometric liveness location*. In Conference on Advanced Video and Signal Based Surveillance, pages 187–192, 2014.
- [2] K. W. Bowyer and J. S. Doyle. *Restorative contact focal points and iris acknowledgment ridiculing*. PC, 47(5):96–98, 2014.
- [3] J. Daugman. *How iris acknowledgment functions*. Procedures of the IEEE, 14(1):21–30, 2000.
- [4] N. Evans, S. Z. Li, S. Marcel, and A. Ross. *Visitor publication: Special issue on biometric mocking and countermeasures*. IEEE Transactions on Information Forensics and Security, 10(4):699–702, 2015.



- [5] J. Galbally, A. Ross, M. Gomez-Barrero, J. Fierrez, and J. Ortega-Garcia. Iris image reproduction from twofold layouts: A proficient probabilistic approach in light of hereditary calculations. *PC Vision and Image Understanding*, 117(10):1512– 1525, 2013.
- [6] Z. Guo, L. Zhang, and D. Zhang. Pivot invariant surface grouping utilizing LBP change (LBPV) with worldwide coordinating. *Example acknowledgment*, 43(3):706– 719, 2010.
- [7] P. Gupta, S. Behera, M. Vatsa, and R. Singh. On iris caricaturing utilizing print assault. In *Proceedings of International Conference on Pattern Recognition*, pages 1681– 1686, 2014.
- [8] N. Kohli, D. Yadav, M. Vatsa, and R. Singh. Returning to iris acknowledgment with shading restorative contact focal points. In *International Conference on Biometrics*, pages 1– 7, June 2013.
- [9] A. Kumar and A. Passi. Examination and mix of iris matchers for dependable individual confirmation. *Example acknowledgment*, 43(3):1016– 1026, 2010.
- [10] D. Menotti, G. Chiachia, A. Pinto, W. Robson Schwartz, H. Pedrini, A. Xavier Falcao, and A. Rocha. Profound portrayals for iris, face, and unique mark parodying discovery. *IEEE Transactions on Information Forensics and Security*, 10(4):864– 879, 2015.
- [11] R. Raghavendra and C. Busch. Strong plan for iris introduction assault recognition utilizing multiscale binarized factual image **highlights**. *IEEE Transactions on Information Forensics and Security*, 10(4):703– 715, 2015.



MATRUSRI ENGINEERING COLLEGE

(Approved by AICTE, Affiliated to Osmania University)

#16-1-486, Saidabad, Hyderabad - 500059



Sponsored by

MATRUSRI EDUCATION SOCIETY



ISBN: 97881-936274-0-2



1ST NATIONAL CONFERENCE ON TRENDS IN SCIENCE, ENGINEERING AND TECHNOLOGY (NTSET - 2018)

February 2nd & 3rd - 2018

TECHNICAL PAPER ABSTRACTS



ORGANIZED BY

MATRUSRI ENGINEERING COLLEGE

(Approved by AICTE, Affiliated to Osmania University)

#16-1-486, Saidabad, Hyderabad - 500059



Sponsored by

MATRUSRI EDUCATION SOCIETY

ISBN: 97881-936274-0-2

**NTSET
2018**





A SMART INTEGRATED SYSTEM FOR BIKE RIDERS: A REVIEW

¹Dr.Pallavi Khare, ²Ch Sri Krishna Mohan, ³ K. Sai Bharath, ⁴T Vamshi Krishna

¹Assistant professor, ^{2,3,4} Student
^{1,2,3,4} Department of Electronics and Communication
^{1,2,3,4} Matrusri Engineering College, Hyderabad
Telangana, India.

Abstract -A smart helmet is a form of protecting headgear used by the rider which makes motorbike driving more secure than earlier than. the principle reason of this smart helmet to provide safety for rider . This put into effect with the aid of the use of develop feature like alcohol detection, accident identification, area tracking, use as a hands loose tool, sun powered, fall detection. This makes now not most effective smart helmet however additionally function of smart bike. Its compulsory to wear helmet, without helmet ignition switch can't ON. A RF Module as wireless link which capable of talk between transmitter and receiver. If rider getting inebriated it receives robotically ignition transfer is locked, and ship message robotically to their register range with their cutting-edge area. So when twist of fate occurs, it'll send message by using GSM to sign up numbers with their modern region by using GPS module. it is able to use to obtain call at the same time as using. The special software of project is fall detection, if the motorbike rider fall from motorbike it will ship message robotically.

Index terms: Biker's safety, twist of fate detection and alert system, smart helmet, Alcohol detection,

I. INTRODUCTION:

Human beings select motorcycle over automobiles as its miles a great deal simpler to pressure In India around 41 % of population are the usage of two wheelers than four wheelers. because the usage is excessive, the accident percentage is also higher than 4 wheelers. Accidents regarding wheelers are greater dangerous than 4 wheelers. These are the three most important troubles which motivates us for developing this mission. step one is to discover the helmet is wear or not. If helmet is wear then ignition will start in any other case it's going to stays off till helmet isn't always put on. For these we use FSR sensor. the second step is alcohol detection. Alcohol sensor is use as breath analyzer which stumble on the presence of alcohol in rider breathe if it is exceeds permissible range ignition can't begin. it's going to ship the message to register number. MQ-3 sensor is used for those. While these situations are glad then ignition will start. The 1/3 essential trouble is twist of fate and past due medical assist. If the rider met twist of fate with him he can not obtain medical assist immediately, its large reason for deaths. Around each second humans die due to overdue clinical assist or the accident vicinity is unmanned. In fall detection, we location accelerometer at the bike unit. Because of these mechanism we locate the twist of fate occurs or not. The purpose of this project is to make a protection gadget in a helmet for an excellent safety of motorcycle rider. The smart helmet that we made is fixed with sensors which act as to detect put on helmet or not. There are two distinct microcontroller is used in this task. Each unit has used a separate microcontroller, for motorcycle unit we use Arduino Lilypad and for helmet unit we use ARM7 lpc2148. Sign transmission among the helmet unit and motorbike unit is the use of a RF idea.

II. LITERATURE SURVEY

2.1 Force Sensing Resistor (FSR)

force Sensing Resistor is placed at in the helmet wherein the real human touch is sensed. It determines by using helmet unit that whether or not helmet is worn or not. If this situation will fulfill or not satisfied then it sends the sign to motorcycle unit. force Sensing Resistors or FSRs, are robust polymer thick film (PTF) gadgets that resistance is inversely proportional to pressure carried out to the face of the sensor. This sensor is used as human contact manipulate in diverse programs. which include scientific systems, automobile electronics and in robotics and industrial programs. The force vs. resistance function proven in Fig. 1 (b) presents a widespread idea of force sensing resistor standard reaction conduct. For comfort, the pressure vs. resistance information is plotted on a semi-log layout. pressure sensing resistor is -cord sensor with a resistance that modifications on implemented force.

$$V_{out} = \frac{RmV +}{(Rm + Rfsr)} \quad (1)$$

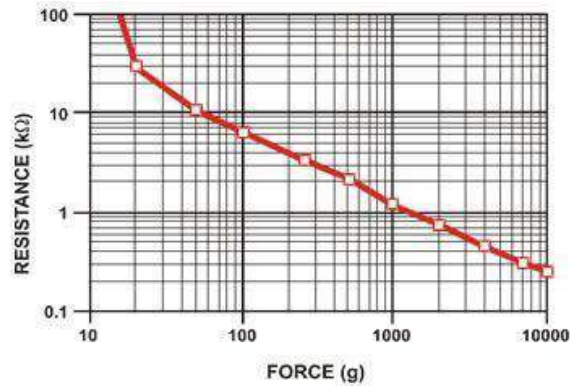


Fig -1: Resistance vs. Force.

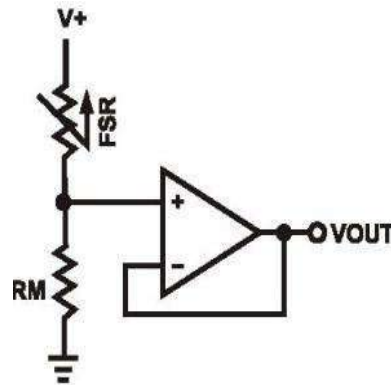


Fig -2: Circuit diagrams of FSR

2.2 MQ-THREE ALCOHOL SENSOR

MQ-3 Alcohol sensor is right for identifying the alcohol content material from breath. it could be positioned just front of the face. The sensor is responds to various gases. It determines by helmet unit that climate the rider is drunk or no longer. MQ-3 sensor has potentiometer to adjusting special awareness of gasses. We calibrate the detector for 0.4mg/L of Alcohol concentration in air and use value of resistance is 200 okΩ. MQ-3 has supports for each analog and virtual. MQ-three has a four pin particularly GND, VCC, Aout, Dout. Here we use digital output of this sensor that is offers output in phrases of excessive or low. It determined by way of our helmet unit weather rider is drunk.

2.3 ACCELEROMETER ADXL345

The ADXL345 is tinny, tri axial accelerometer with decision of thirteen bit. The output of accelerometer is digital and use 16 bit 2's supplement data. it's miles access to attach via Serial Peripheral Interface (SPI three-4 twine) or I2C interface. ADLX 345 is used for each dimension of static and dynamic acceleration. in this undertaking we use accelerometer measures the static acceleration of gravity. Unfastened-fall sensing notices if the motorbike is falling. And motorbike unit take choice that twist of fate is takes place or now not. on this assignment we interfaced ADXL345 with the aid of the usage of I2C digital interface approach. The CS linked to excessive to VDD I/O, the ADXL345 is requiring 2-cord connection. The minimal operational voltage of this device cannot greater than VDD I/O this is zero.3 V. For the right working condition, we use outside pull up resistor. The fee of pull up resistor is 3.three kilo ohm.

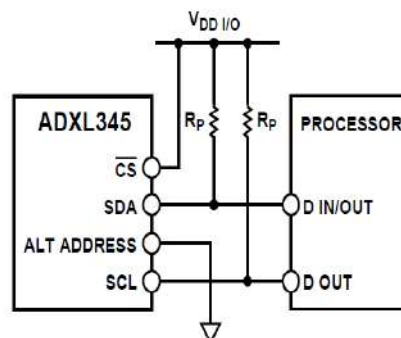


Fig -3: Interfacing diagram of Accelerometer

2.4 RF COMMUNICATION CIRCUIT

Helmet unit and motorcycle unit are connected by using wireless link of RF. RF conversation circuit carries encoder and decoder circuit. Encoder is on helmet facet that is using to transform parallel records into serial facts. The encoder is capable of encoding rubdown which incorporates of 12N records bits and N deal with bits. every cope with/statistics can stay set to with logical states. The oscillator frequency is selected by way of Rosc. We choose oscillator frequency is three kHz, with Rosc of 1M ohms. Minimal transmission of records is 4 words. Decoder is on motorbike facet, it used to decode serial data. It converts this serial facts in to parallel. The decoders are succesful to receive statistics that are spread by means of an encoder and apprehend it. the primary bits duration use as addresses and final 12N bits as our desired statistics, where N is stands for address range. in this decoder circuit oscillator frequency is 50 times greater than fOSCE (encoder oscillator frequency) that's chosen by means of price of Rosc. (Rosc is 1k ohms)

III. EXPLANATION

We already stated that we divide a undertaking in two devices namely helmet and motorbike. In helmet unit, the pressure sensing resister is positioned on interior upper part of the helmet wherein actually head changed into touched with sensor surface. And alcohol sensor is placed on in front of rider's mouth. it may experience without difficulty. solar panels are hooked up on higher facet of helmet that's in direct daylight. And the battery and everyday circuits became fixed within the helmet. Secondary controller and RF transmitter circuit was additionally located on in the helmet, antenna are placed out of doors the helmet.

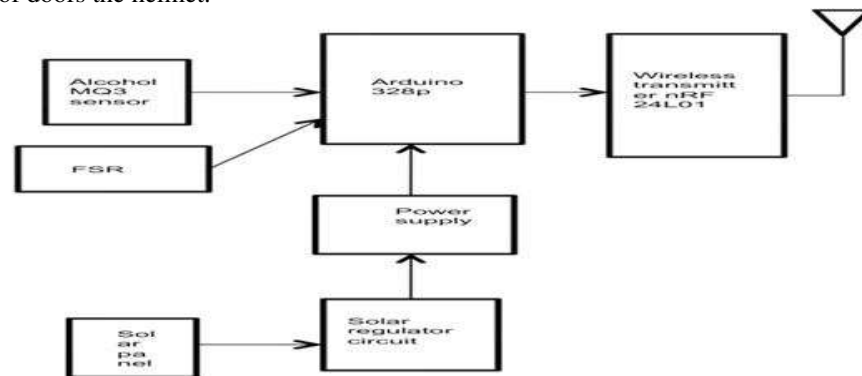


Fig -4: Block diagram of Helmet Unit

The motorcycle unit is hooked up on real motorbike. Accelerometer became fixed on motorcycle, for the fall detection. Our main controller is positioning in to storage case of motorbike. And decoder circuit is positioned on in handle of motorbike. We also stick a keyboard at the petrol tank. So we can without difficulty type the password.

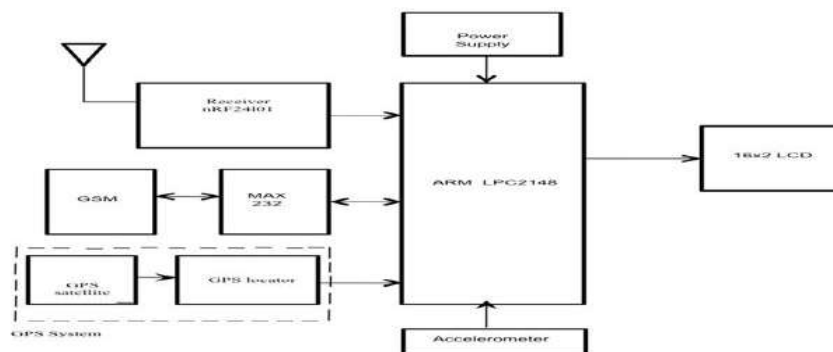


Fig -5: Block diagram of Bike Unit

IV. FLOWCHART AND ILLUSTRATION

Step one of challenge is it initializes all of the port and subsequent step is coincidence Detection the use of accelerometer if No coincidence then it's going to is going to 1/3 step. Third step is taking note of RF Module continuously for records and translates statistics using if conditions. Fourth step is test wether helmet is wore or not. If Helmet no longer wore then show Message "Please put on the helmet". Subsequent step is test the situation of under the influence of alcohol if rider is inebriated show message "you are under the influence of alcohol" and then ship the message to stored no. with area.. The sixth step, if accident detected, prevent the whole lot and send message with region.

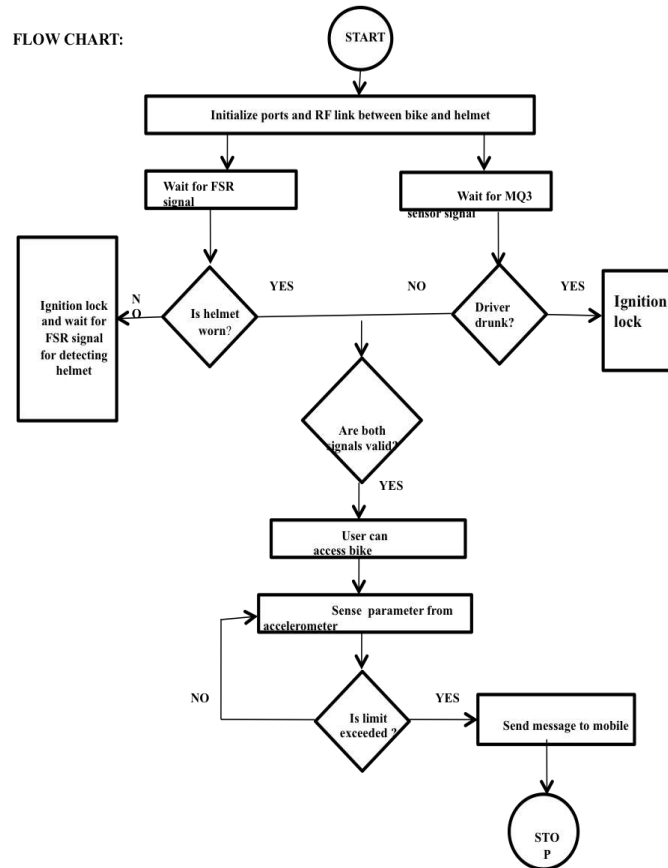


Fig -6: Flowchart for integrated proposed frame work

V. APPLICATION:

- It could be used in real time safety device.
- We will put in force the complete circuit into small module later.
- Less energy ingesting protection machine. This safety gadget technology can similarly be greater in car and additionally by using replacing the helmet with seat belt.

VI. SCOPE FOR FUTURE

- We can enforce numerous bioelectric sensors on the helmet to measure various hobby. we can use small camera for the recording the drivers activity.
- It could be used for passing message from the one car to every other vehicle via the usage of wi-fi transmitter.
- We have used solar panel for helmet power deliver by means of using equal power deliver we can charge our cellular phone.

VII. CONCLUSION

The outcomes of the undertaking have showed that the bike ignition will start if the helmet is worn. So, it'll robotically decrease the effect from accident and it could avoid bike from being stolen. Arduino lilypad is right in controlling all the gadget and the sensors. Executing the wi-fi machinewhichRadio Frequency Module to ship the message from helmet unit to the bike unit. Because of this wireless connection is better than stressed hyperlink.

REFERENCES

- [1] Manjesh N , Prof. Sudarshan raj "Safety measures for Two wheelers by Smart Helmet and Four wheelers by Vehicular Communication", International Journal of Engineering Research and Applications (IJERA) ISSN: 2248-9622 NATIONAL CONFERENCE on Developments,Advances & Trends in Engineering Sciences (NCDATES-
- [2] V.Krishna Chaitanya, K.Praveen Kumar, "Smart helmet using arduino", Hyderabad, 2013.
- [3] R. Prudhvi Raj, Ch. Sri Krishna Kanth, A. BhargavAdityaand K. Bharath, "Smart-tec Helmet," AEEE, India.
- [4] Manjesh N, Prof. Sudarshan Raj, "Smart Helmet Using GSM &GPS Technology for Accident Detection and Reporting System", International Journal of Electrical and Electronics Research, Vol. 2, Issue 4, October - December 2014.



- [5] SudharsanaVijayan, Vineed T Govind, Merin Mathews, SimnaSurendran, Muhammed Sabah, "Alcohol detection using smart helmet system", IJETCSE, Volume 8 Issue 1 – APRIL 2014.
- [6] Ruize Xu, Shengli Zhou, Li, W.J. "MEMS Accelerometer Based Nonspecific-User Hand Gesture Recognition", IEEE, Volume: 12 Issue: 5, 05 September 2011.
- [7] Muhammad Ali Mazidi and Janice Gillispie Mazidi, "The 8051 Microcontroller and Embedded Systems", Pearson Education.
- [8]. Y. Zhao, "Mobile phone location determination and its impact on intelligent transportation systems.



MATRUSRI ENGINEERING COLLEGE

(Approved by AICTE, Affiliated to Osmania University)

#16-1-486, Saidabad, Hyderabad - 500059



Sponsored by

MATRUSRI EDUCATION SOCIETY



ISBN: 97881-936274-0-2



Thermo Acoustic Refrigeration

¹T. Somasekhar, ²P.Naveen Kishore

¹Dept.of Mechanical Engineering Matrusri Engineering College Affiliated to Osmania University
 Saidabad, Hyderabad, telangana, India.

²Dept.of Mechanical Engineering Matrusri Engineering College Affiliated to Osmania University
 Saidabad, Hyderabad, telangana, India

Abstract ; Thermoacoustic refrigeration is an emerging refrigeration technology which does not require any moving parts or harmful refrigerants in its operation. This technology uses acoustic waves to pump heat across a temperature gradient. The vast majority of thermoacoustic refrigerators to date have used electromagnetic loudspeakers to generate the acoustic input. In this thesis, the design, construction, operation, and modeling of a thermoacoustic refrigerator are detailed. The developed theoretical and experimental tools can serve as invaluable means for the design and testing of other piezoelectrically-driven thermoacoustic refrigerator configurations.

Key Words — Thermo-Acoustics, Piezo-Electric effect, Drivers, Working Fluid, Thermal Acoustic Effect.

I. Introduction

Thermo acoustic refrigerator is a special kind of device that uses energy of sound waves or acoustic energy to pump heat from low temperature reservoir to a high temperature reservoir. The source of acoustic energy is called the „driver which can be a loudspeaker. The driver emits sound waves in a long hollow tube filled with gas at high pressure. This long hollow tube is called as „resonance tube“ or simply resonator. The frequency of the driver and the length of the resonator are chosen so as to get a standing sound wave in the resonator. A solid porous material like a stack of parallel plates is kept in the path of sound waves in the resonator. Due to thermo acoustic effect (which will be explained in detail in the animation), heat starts to flow from one end of stack to the other. One end starts to heat up while other starts to cool down. By controlling temperature of hot side of stack (by removing heat by means of a heat exchanger), the cold end of stack can be made to cool down to lower and lower temperatures. A refrigeration load can then be applied at the cold end by means of a heat exchanger.

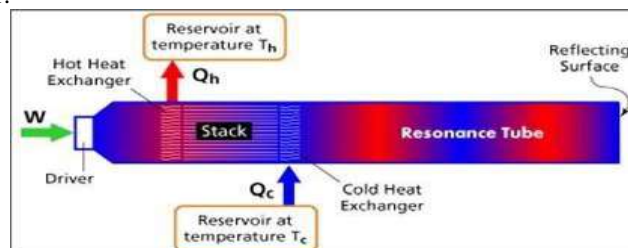


Figure 1.1: Temperature variation in device

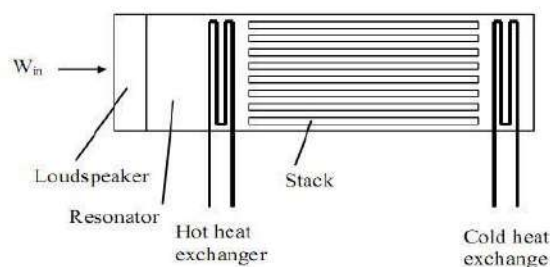


Figure 1.2 the basic principle of thermo -Acoustic refrigeration system

Thermo acoustics combines the branches of acoustics and thermodynamics together to move heat by using sound. While acoustics is primarily concerned with the macroscopic effects of sound transfer like coupled pressure and motion oscillations, thermo acoustics focuses on the microscopic temperature oscillations that accompany these pressure changes. Thermo acoustics takes advantage of these pressure oscillations to move heat on a macroscopic level. This results in a large temperature difference between the hot and cold sides of the device and causes refrigeration.

II. Methods And Procedures

2.1 Thermoacoustic Refrigerator Design

The design of thermoacoustic refrigerators is a field where a lot of research is currently being carried out. This literature contains many ongoing debates as to what the best design techniques may be. This chapter starts off with a basic design strategy for thermoacoustic refrigerators, and then goes on to discuss the individual components in detail, reviewing the relevant literature on the topic.

2.2 Design Overview

Thermoacoustic refrigerators can generally be broken up into four parts. These parts are known as the driver, the resonator, the stack, and the heat exchangers and are labeled for an example refrigerator in Figure 2.1:

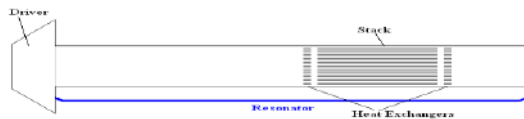


Figure 2.1: A Typical thermoacoustic refrigerator

2.3 Working Fluid

Another important design consideration is the choice of the working fluid which fills the resonator. Both the viscous and thermal penetration depths as well as the natural frequency of the resonator are dependent on the choice of working fluid. Belcer *et al.* points out that a high ratio of specific heat and small Prandtl number are desirable characteristics of the working fluid. The Prandtl number is of particular interest because it is equal to the square of the ratio of the viscous penetration depth to the thermal penetration depth. A small Prandtl number means that the viscous effects are small compared to the thermal effects.

Belcer *et al.* explore this concept further. He suggested that when mixing two binary gases, the minimum Prandtl number occurs when the lighter gas is approximately 66% by volume. He tests his theory and gets reasonable results. However, he concludes that the design applications must be taken into account before selecting a fluid for thermoacoustic devices, citing the example that when small temperature differences are the design goal, mixtures including polyatomic gases with small specific heat ratios may be desired.

Tijani *et al.* Conducted numerous experiments with different gas mixtures used as the working fluid in thermoacoustic refrigerators. Their experiments centered around mixing helium with other noble gases (*Xe, Kr, Ar, Ne*) and studying the effect of the resulting Prandtl numbers on refrigerator performance. They found that though the Prandtl number decreases as the mole fraction of helium to the other noble gas is decreased, the density of the overall working fluid increased. This increase in working fluid density reduces the cooling power of the system. Because of this tradeoff between efficiency and cooling power comes into play, the authors conclude that the optimal working fluid for helium-noble gas mixtures depends on the design goals of a specific refrigerator.

Giacobbe introduced methods for calculating the Prandtl number, viscosity, and thermal conductance of mixtures of gases. His paper describes experiments using mixtures of helium and other noble gases to validate his theoretical work. His results are in good agreement with his theory which allows this method to be used to obtain good estimations of the Prandtl number for gas mixtures to be made. 100g of weighed plastic granules are fed into the modified pressure cooker. The pressure cooker is modified by attaching a pressure gauge to maintain pressure and a thermocouple is attached to measure temperature. Heat is provided by using Nichrome coil heater which may be between 150-200°C. It is the temperature at which plastic begins to melt and vaporize. These vapors are passed through copper tubes which are connected to shell and tube heat exchanger. At the end of the heat exchanger, the distillate is collected. The amount of distillate obtained is measured.

2.4 Refrigerator Design

The starting point for the design of this thermoacoustic refrigerator was the driver as it was required. Once a suitable driver was selected, the choice of the resonator and stack followed as detailed in the following sections. This refrigerator was designed to be low cost and easy to assemble and study so that it can be modeled. Once models are created and validated, more expensive and difficult to construct piezoelectrically-driven thermoacoustic refrigerators will then be able to be modeled before massive amounts of effort are put in to construct them.

2.5 Driver Selection

Most piezoelectric drivers consist of a metallic diaphragm with piezoelectric material deposited on it. Electrodes are then attached to the two sides of the piezoelectric material. When voltage is applied across the electrodes, the piezoelectric material expands or contracts while the metal diaphragm is not affected by the voltage. The mismatch in expansion and contraction between these two materials which are bonded together causes a bending moment in the diaphragm. If an AC signal is applied, the diaphragm oscillates back and forth at the frequency of the signal, causing the air around it to oscillate as well.



Figure 2.2 speakers that act as drivers

2.6 Stack Design

Most thermoacoustic refrigerator stack designs are driven by cooling power requirements. For this design however, easily measurable cooling was the only requirement. Therefore, the stack and resonator designs were based off of the design given by Russel and Weibull.

The stack needed spacing on the order of 2 to 4 thermal penetration depths. The calculation of the thermal penetration depth is given in equation (2.16) above and is repeated below after substituting in frequency instead of angular frequency.

The variables that make up the thermal penetration depth are functions of the gas properties and the frequency. Air at room temperature was selected as the working fluid for this refrigerator. The properties for air at room temperature to be used are :

Thermal conductivity $k=0.0257$ W/m.K Density $\rho=1.205$ Kg/m³ Specific Heat Capacity $C_p=1005$ J/kg K
 These variables are then used with equation where f is the driving frequency of the refrigerator. This yields the following: $\delta = 1.3 \times 10^{-4}$

Recalling that the stack spacing should be around 2.5 thermal penetration depths, the targeted stack spacing is 0.325mm. A coil design for the stack was then selected for ease of manufacturing. The cross section of the stack was then required to be round. The stack cross sectional area selected to be much smaller than the speaker diaphragm was chosen in order to increase both pressure and volumetric flow rates in the resonator. The final selection was 0.875 (2.14 cm) diameter was used because the plastic tubes used for the resonator come in that standard size. The stack length was selected to be 35 mm following Russel and Weibull

2.7 Resonator Design

The resonator design was driven by the need to have a natural frequency near to 400 Hz so as to line up with the speaker natural frequency. It also needed to interface with the speaker and stack cross sections. Finally, it had to be easy to manufacture. A simple tube was selected to be used as the resonator geometry.

This tube made manufacturing very simple. It also made for easy calculation of the resonator natural frequency. At the driver end, the resonator was expanded to meet the speaker as shown in Figure 4.2. The other end was plugged with an aluminum cap as this is the hot end of the refrigerator and the aluminum would help heat to leave the system.

The end of the resonator with the aluminum plug is a pressure anti-node and velocity node. The end near the speaker has close to (but not exactly) the opposite boundary conditions (pressure node and velocity anti-node). The approximate resonator length is calculated as follows:

$$l = v/4f = 343/4 \cdot 40 = 21.4 \text{ cm}$$

The resonator length was varied somewhat after experiments were performed and the final resonator length was 9.45" (24 cm) which brought the natural frequency to 395 Hz. This variance in length is a result of the resonator boundary conditions at the speaker end being approximate. The resonator cross section had to be

round due to the stack. For ease of manufacturing, a 1" (2.54 cm) outer diameter, 0.875" (2.14 cm) inner diameter tube was to be used. The placement of the top of the stack was selected to be 1.85" (4.70 cm) from the speaker end of the resonator so that it would be well placed between the velocity and pressure nodes. The aluminum plug was simply selected to seal the end of the tube tightly.

2.8 Construction

The stack and resonator were made in house out of cheap, every day materials as detailed in the following sections. The driver was purchased as it is available commercially. A mount was built to hold the driver in place and is shown in the section on assembly.

Stack Construction

The stack spiral was made using 35 mm camera film. To enforce the spacing between the layers, nylon fishing line with a diameter of 0.35 mm was glued across the film as shown in Figure 4.3. After the glue dried, the film was rolled up as seen in Figure 4.3, and glued at the very end. The diameter of the rolled up stack is 0.875" (2.22 cm) and its height is 1.38 in (3.5 cm). The strip of film before being rolled up is approximately 20 in (50.8 cm).

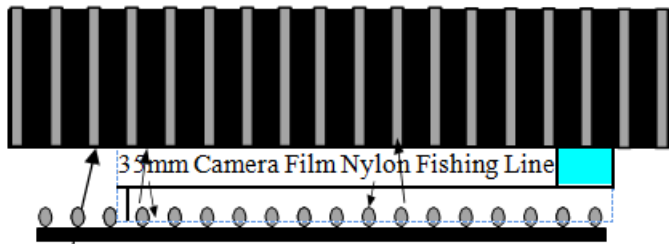
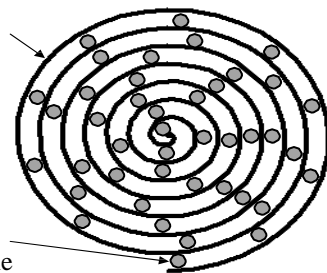


Figure 2.3: Top and side views of the stack before it is rolled up

35mm Camera Film



Nylon Fishing Line

Figure 2.4: Cross sectional view of the stack after it

2.9 Resonator Construction

The resonator was constructed from acrylic tubing with a 1" (2.54 cm) outer diameter and 0.875" (2.22 cm) inner diameter. An aluminum cap was machined to fit into the end of the tube. An acrylic base plate was used to create an interface between the speaker and the resonator, which was fastened to the resonator tube using an adhesive. Holes were drilled in the base plate which matched the speaker mounting holes for easy attachment to the speaker. The resonator is pictured in Figure 2.2.

2.9.1 Assembly

The stack was positioned inside the resonator tube by sliding it in from the top. The stack was pushed down until its top was 1.85" (4.70 cm) from the top of the resonator. Two small holes were then drilled in the side of the resonator so that thermocouples could be used to measure the internal temperature, one hole above the stack and one hole below it. Thermocouples were placed just through the holes and glue was used to both hold them in place and to reseal the holes. The aluminum cap was then placed at the top of the resonator. The speaker was placed in the mount which had been made for it. The resonator was then placed above the speaker and screws were used to fasten the whole thing together. Figures 2.7 show the assembled refrigerator. The dimensions of the refrigerator are displayed in Figure 2.5.

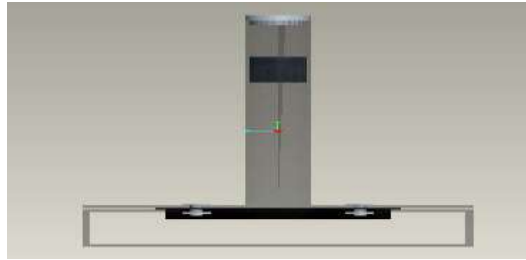


Fig: 2.5 Layout diagrams of thermoacoustic refrigeration



Figure 2.6: Assembled refrigerator

2.9.2 List of Materials

The list of materials used for the fabrication of the thermo acoustic refrigeration system is shown in the table.

Sl.No.	Parts	Qty.	Material
1	The Resonator	1	Glass tube
2	The Stack	1	Aluminum foil
3	Speaker	1	
4	Amplifier	1	
5	Thermocouples	2	-

Table 2.1: List of materials

III. Results And Discussions

In this case, the refrigerator was at its resonant frequency of 80 Hz and a current of 12 V and 200 mA respectively, *i.e.* input power is 7.6 watts. The thermocouple a data obtained at various times throughout the operation of the refrigerator are shown in Figures . It should be kept in mind that the thermocouples are measuring the internal temperatures just above and just below the stack.

The graphs are obtained at the beginning and throughout the experiment. The temperature variation at the stack is plotted.

S. no	Time t in Min	Thermocouple Readings in ⁰ c	
		At Hot End	At Cold End
1	0	30.75	30.75
2	10	33.75	30
3	15	36	29.75
4	25	39	29
5	30	41.75	28
6	35	44.75	26.75

Table 3.1 – Readings of Thermocouple at different time Periods

IV. Conclusion

From the values, we conclude that:

- There was four degrees drop in temperature at the cold chamber.
- For every three degrees rise in temperature at hot end there was one degree drop at cold end.
- The drop in temperature increases with increase in time.

References

- [1] J. C. Wheatley, T. Hofler, G. W. Swift and A. Migliori, Experiments with an Intrinsically Irreversible Acoustic Heat Engine, Physical Review Letters 50 (7), 499 (1983)
- [2] T. J. Hoffer, Thermoacoustic refrigerator design and performance, Ph.D. dissertation, Physics Department, University of California at San Diego, (1986)
- [3] The Pennsylvania State University, Graduate Program in Acoustics, thermo acoustics
- [4] M. E. H. Tijani, J. C. H. Zeegers and A. T. A. M. de Waele, Construction and performance of a thermoacoustic refrigerator, Cryogenics 42, 59 (2002)
- [5] International journal of emerging trends in engineering and development ISSN 2249-6149 Issue 1, Vol 2.
- [6] IOSR Journal of Mechanical and Civil Engineering (IOSR-JMCE) e-ISSN: 2278-1684,p-ISSN: 2320-334X, Vol 8, Issue 6 (Sep. - Oct. 2013), PP 15-24
- [7] G.W. Swift, "What is thermoacoustics? A brief description". Condensed Matter and Thermal Physics Group. Los Alamos National Laboratory, Los Alamos, New Mexico. 2004.
- [8] M.E.H. Tijani, J.C.H. Zeegers, A.T.A.M. de Waele, "Design of thermoacoustic refrigerators". Elsevier, Cryogenics 42 (2002) 49-57.
- [9] F. Zink, J. S. Viperman, L. A. Schaefer, "Environmental motivation to switch to thermoacoustic refrigeration". Applied Thermal Engineering 30 (2010) 119-126.
- [10] E. C. Nsofor, A. Ali, "Experimental study on the performance of the thermoacoustic refrigerating system". Applied Thermal Engineering 29 (2009) 2672-2679.
- [11] <http://hyperphysics.phy-astr.gsu.edu/hbase/sound/tralon.html>



All



ADVANCED SEARCH

Conferences > 2017 International Conference...

Investigation of linearly polarized RMPA embedded with 2D-EBG ground plane

Publisher: IEEE

Cite This

Cite This



Kunapareddy Koteswara Rao ; Pasumarthy Nageswara Rao ; Vangala Sumalatha **All Authors**

81 Full Text Views



Export to Collabratec

Alerts

- Manage
- Content Alerts
- Add to Citation
- Alerts

More Like This

- Performance improvement of small arrays of microstrip antennas on photonic band gap substrates
APMC 2001. 2001 Asia-Pacific Microwave Conference (Cat. No.01TH8577)
Published: 2001
- Microstrip antennas and arrays on photonic band gap substrates
Proceedings of the 2001 SBMO/IEEE MTT-S International Microwave and Optoelectronics Conference. (Cat. No.01TH8568)
Published: 2001

Show More

Abstract

Downl PDF

Document Sections

- I. Introduction
- II. Design Procedure
- III. 2D-EBG Design
- IV. Characterization of 2DEBG
- V. Conventional RMPA Design

Show Full Outline

- Authors
- Figures
- References
- Keywords
- Metrics
- More Like This

Abstract:The Performance of Rectangular Microstrip Patch Antenna (RMPA) over a 2D-EBG (Two Dimensional Electromagnetic Band Gap) ground plane is investigated and results obtained ... **View more**

Metadata

Abstract: The Performance of Rectangular Microstrip Patch Antenna (RMPA) over a 2D-EBG (Two Dimensional Electromagnetic Band Gap) ground plane is investigated and results obtained in numerical 3D electromagnetic simulation software are presented by comparing with a conventional RMPA over optically planar conducting ground. The band gap of a 2DEBG is centered at ISM band, and RMPA is made to operate within the band gap. So the first part of this paper is concentrated on characterization of 2DEBG bands. 2DEBG here is designed to resonate at 2.5 GHz with a forbidden band gap of 1.5 GHz, in phase reflection band gap of 41 MHz and a high impedance of 3540 Ω. The high surface impedance property of 2DEBG leads to RMPA miniaturization. The property of in-phase reflection band of 2DEBG enhances the gain upto 3.5 dB, when compared with the conventional arrangement. Due to surface wave band gap property, smoother radiation pattern and improvement in the radiation efficiency, and an operating band width of 3% has been achieved.

Published in: 2017 International Conference on Wireless Communications, Signal Processing and Networking (WiSPNET)

Date of Conference: 22-24 March 2017 **INSPEC Accession Number:** 17598729
Date Added to IEEE Xplore: 22 February 2018 **DOI:** 10.1109/WiSPNET.2017.8300200
Publisher: IEEE
ISBN Information: **Conference Location:** Chennai, India

 **Contents**

I. Introduction

The rapid development of wireless communication market is challenging the RF engineers to fulfill the increasing needs of end user. The challenges include in designing of compact size, wide-band, high gain, power efficient, cost effective, multipurpose system design.

Sign in to Continue Reading

Authors	▼
Figures	▼
References	▼
Keywords	▼
Metrics	▼

IEEE Personal Account

CHANGE USERNAME/PASSWORD

Purchase Details

PAYMENT OPTIONS
VIEW PURCHASED DOCUMENTS

Profile Information

COMMUNICATIONS PREFERENCES
PROFESSION AND EDUCATION
TECHNICAL INTERESTS

Need Help?

US & CANADA: +1 800 678 4333
WORLDWIDE: +1 732 981 0060
CONTACT & SUPPORT

Follow



[About IEEE Xplore](#) | [Contact Us](#) | [Help](#) | [Accessibility](#) | [Terms of Use](#) | [Nondiscrimination Policy](#) | [Sitemap](#) | [Privacy & Opting Out of Cookies](#)

A not-for-profit organization, IEEE is the world's largest technical professional organization dedicated to advancing technology for the benefit of humanity.

© Copyright 2021 IEEE - All rights reserved. Use of this web site signifies your agreement to the terms and conditions.

IEEE Account

» Change Username/Password
» Update Address

Purchase Details

» Payment Options
» Order History
» View Purchased Documents

Profile Information

» Communications Preferences
» Profession and Education
» Technical Interests

Need Help?

» **US & Canada:** +1 800 678 4333
» **Worldwide:** +1 732 981 0060
» Contact & Support

[About IEEE Xplore](#) | [Contact Us](#) | [Help](#) | [Accessibility](#) | [Terms of Use](#) | [Nondiscrimination Policy](#) | [Sitemap](#) | [Privacy & Opting Out of Cookies](#)

A not-for-profit organization, IEEE is the world's largest technical professional organization dedicated to advancing technology for the benefit of humanity.

© Copyright 2021 IEEE - All rights reserved. Use of this web site signifies your agreement to the terms and conditions.

Investigation of Linearly Polarized RMPA Embedded with 2D-EBG Ground Plane

Kunapareddy Koteswara Rao,¹ Pasumarthy Nageswara Rao² and Vangala Sumalatha³

¹Department of ECE, Vignana's Institute of Technology & Aeronautical Engineering College, Hyderabad.

²Department of ECE, Vardhman College of Engineering, Hyderabad.

³Department of ECE, Jawaharlal Nehru Technological University Anantapur (JNTUA).

Email: ¹kotesh2584@gmail.com ²nrraop@yahoo.com ³sumaatp@yahoo.com

Abstract—The Performance of Rectangular Microstrip Patch Antenna (RMPA) over a 2D-EBG (Two Dimensional Electromagnetic Band Gap) ground plane is investigated and results obtained in numerical 3D electromagnetic simulation software are presented by comparing with a conventional RMPA over optically planar conducting ground. The band gap of a 2DEBG is centered at ISM band, and RMPA is made to operate within the band gap. So the first part of this paper is concentrated on characterization of 2DEBG bands. 2DEBG here is designed to resonate at 2.5 GHz with a forbidden band gap of 1.5 GHz, in phase reflection band gap of 41 MHz and a high impedance of 3540 Ω . The high surface impedance property of 2DEBG leads to RMPA miniaturization. The property of in-phase reflection band of 2DEBG enhances the gain upto 3.5 dB, when compared with the conventional arrangement. Due to surface wave band gap property, smoother radiation pattern and improvement in the radiation efficiency, and an operating band width of 3% has been achieved.

Index Terms—EBG (Electromagnetic band gap), EM (Electromagnetic) Waves, AMC (Artificial Magnetic Conductor).

I. INTRODUCTION

The rapid development of wireless communication market is challenging the RF engineers to fulfill the increasing needs of end user. The challenges include in designing of compact size, wide-band, high gain, power efficient, cost effective, multipurpose system design.

In literature, numerous techniques are presented to sustain the antenna bandwidth at adequate level with a miniaturized antenna operating in multisystem environment. The techniques include, providing slots on the surface of radiating patch, inserting pins between patch and ground for shorting [1]. Metamaterials, EBG [2], [3], Double negative materials [4], [5], Left handed materials [6–8].

EBG is an energy band gap theory of semiconductor engineering to EM wave regions and these structures can be easily fabricated using conventional PCB technology. The EM characteristics of EBG structures have found useful application in Antenna Engineering. The surface wave band gap property of EBG helps the antenna system to achieve better gain, efficiency, lower side and back lobe levels, and better isolation between array elements [9–11]. Its structure consists of capacitive patches that are connected to a conducting ground plane by means of metal posts. The posts pass through a space layer that consists of dielectric material. This forces

the tangential magnetic fields impinging on its surface to become zero & hence named as Artificial Magnetic Conductor (AMC) [12–14]. This property helps to design low profile antennas [15–17]. Various forms of EBG structures were designed and applied for antenna engineering, to minimize the size of antenna and enhance its bandwidth and gain [18–24].

II. DESIGN PROCEDURE

A conventional microstrip patch antenna structure consists of either a rectangular or any other metallic pattern formed on a top surface of dielectric substrate, treated as a radiator or receiver of EM energy. Whereas back surface of dielectric substrate contains a conducting metal surface treated as ground. The patch antenna can direct radio waves to front surface direction due to ground conductor. Antenna directivity depends on the size of ground conductor, if ground size is small then the directivity of antenna is insufficient for radiation in front direction, so some radio waves leak to sides and the rear. This may cause interference.

An EBG structure exists in two or three dimensional periodic structures of dielectric or conductor and greatly attenuates two or three dimensional propagation of electromagnetic waves in certain frequency band. The architecture of 2D-EBG consists of protrusions or patches of square shape which are arranged over the top side of FR4 dielectric, while other side consists of conducting ground plane. The conductor posts or stubs are periodically arranged on conductor plane, which electrically connect the ground plane with protrusions. 2D-EBGs are exhibit special properties, such as (i) high surface impedance, (ii) in-phase reflection and (iii) surface wave suppression band. The high impedance property of 2DEBG allows in constructing low-profile antennas. The reflection phase of EBG helps for constructive addition of the incident and reflected Waves, thereby reducing backward radiation and enhancing forward radiation. The perfect magnetic conducting property in the structure helps to suppress the surface waves.

In this paper, 2DEBG as a ground is combined with patch antenna as a radiator. The shape of the antenna is a rectangular, with an edge feeding. The completed structure is etched on FR4 substrate backed by a 2D-EBG ground. The patch antenna is made to operate within band gap region of 2D-EBG; an RF signal radiated from the sides of the patch antenna can be attenuated by the resonance effect of 2D-EBG.

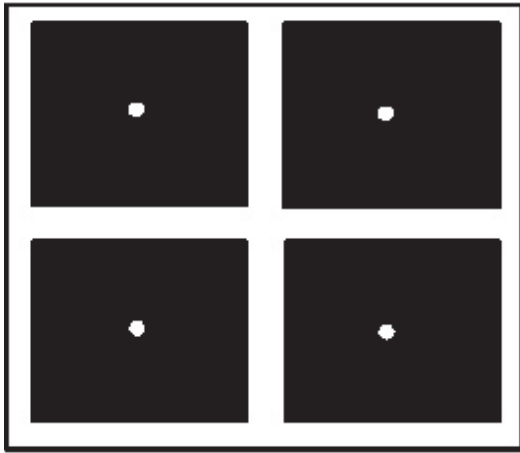


Fig. 1. Periodic array of 2DEBG unit.

As a result the invasion of radio waves into sides and rear of the patch antenna is suppressed, this avoids unnecessary radiation. More over the antenna can become low profile and achieve excellent directivity.

A 2DEBG structure is designed in ISM band, and its EM characteristics such as (i) high surface impedance, (ii) in-phase reflection and (iii) surface wave forbidden band are determined in the beginning of paper. Later, the radiation characteristics of RMPA, such as return loss, gain, and radiation pattern over the 2DEBG ground plane are investigated and obtained results are compared with the results of conventional RMPA. The complete structure is designed & analyzed using simulation software named as HFSS.

III. 2D-EBG DESIGN

Modern communication technology is facilitating, the development of novel EBG structures. The 2D-EBG structure is treated as resonating structure because of its lumped parameters L and C . The parallel inductances L are mostly formed by the conductor posts and their value depends on the length of the conductor posts. The series capacitances C are formed between adjoining conductor pieces and their value depends on the distance between adjoining conductor pieces and the size of conductor pieces. So center frequency of band gap is given by $w_0 = \frac{1}{\sqrt{LC}}$ where capacitance C is given as $C \approx \frac{w(\epsilon_1 + \epsilon_2)}{\pi} \cosh^{-1} \left(\frac{a}{g} \right)$ [2].

Inductance L is given as $L = \mu t$, where t is thickness, μ is permeability of a medium.

W : the patch width,

g : the gap width between patches,

h : the substrate thickness,

ϵ_r : the substrate permittivity,

r : the via radius.

Fig. 1 shows the top view of periodic array of two dimensional EBG. This consists of double sided FR4 substrate with dielectric constant of 4.4 and loss tangent of 0.009. Its top face is etched out so as to form a lattice of square patches.

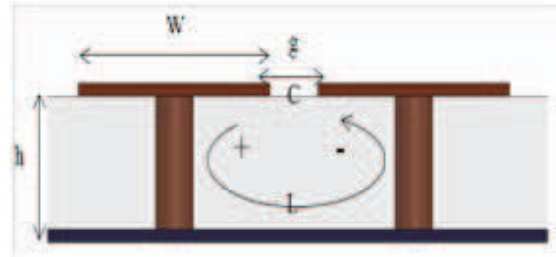


Fig. 2. Cross sectional view.

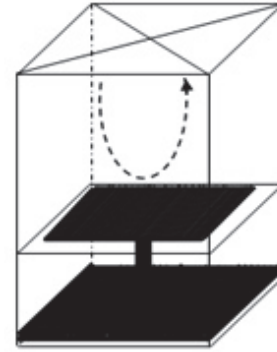


Fig. 3. Schematic diagram used to measure propagation characteristics.

Its bottom face consists of planar conducting surface. Top square patches are shorted to bottom conducting surface with the help of conducting stub or via that passes through the dielectric medium from top to bottom. The stub or via is placed exactly at the center of each unit cell. Fig. 2 shows the cross sectional view of 2DEBG unit

IV. CHARACTERIZATION OF 2DEBG

Fig. 3 shows the Schematic diagram or the arrangement used in numerical simulation tool for measurement of propagation characteristics of unit cell of 2DEBG as shown in Fig. 1.

The 2DEBG cell is placed inside of wave guide at its bottom and its top is applied with Floquet port. Its sides are applied with alternate boundary conditions. That means two of its opposite sides are applied with Perfect Electric Conducting surfaces while other two opposite sides are applied with Perfect Magnetic Conducting surfaces.

A. Reflection Characteristics

Fig. 4 displays Graph of reflection phase, drawn between scattering (S11 in dB) parameter verses frequency for incident TEM wave for Fig. 3. Here the reflection characteristics vary from $+180^\circ$ to -180° . The range between $+90^\circ$ to -90° is considered as in-phase reflection band. During this band magnitude of reflection co-efficient is +1 and in-phase band width is 41 MHz.

B. High Impedance Characteristics

Fig. 5 reveals the High impedance curve of Fig. 3. Practical high impedance surfaces are usually low loss and achieve a high impedance of 3540Ω .

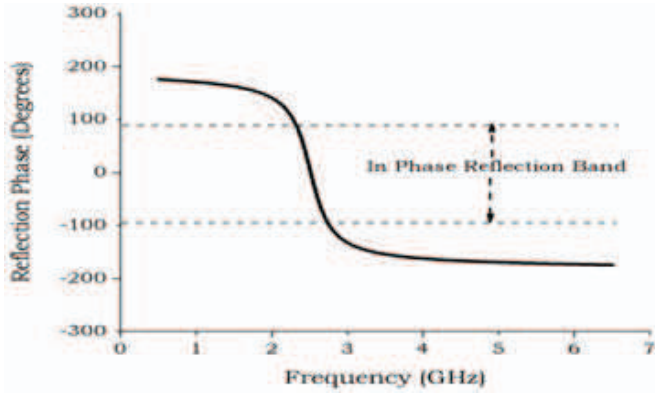


Fig. 4. Graph of reflection phase.

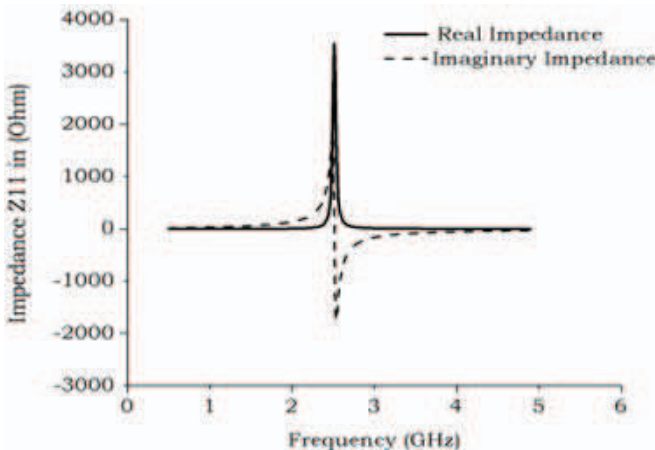


Fig. 5. High impedance curve.

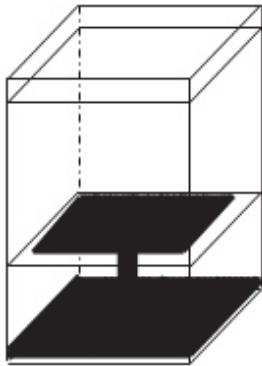


Fig. 6. Periodic boundaries with PML schematic diagram for measurement of stop band.

C. Dispersion Characteristics

Fig. 7 represents Schematic diagram for stop band gap measurement or the arrangement used in numerical simulation tool. The setup will give stop band characteristics of Fig. 6 by applying periodic boundaries with perfect matched layer over the top.

Below the resonance, the surface is inductive and supports TM surface waves. Above the resonance, the surface is

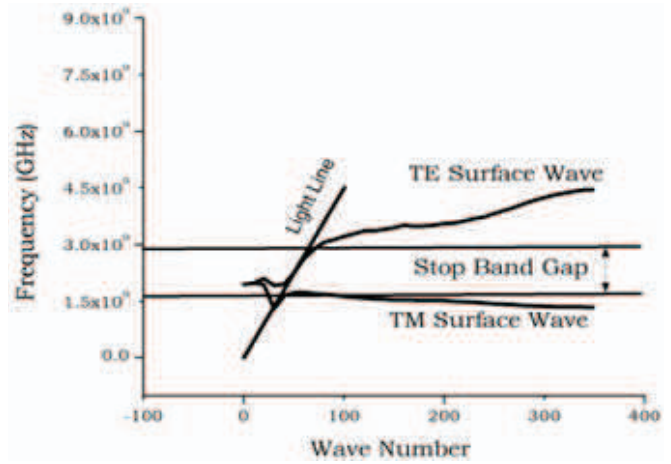


Fig. 7. Graph of dispersion curves.

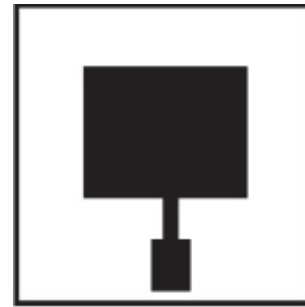


Fig. 8. Conventional design of patch antenna over FR4 substrate.

capacitive and supports TE surface waves. The gap between TE and TM waves is known as surface wave band or forbidden band gap. In present design, surface wave band gap of 1.5 GHz i.e from 1.5 GHz to 3 GHz is obtained.

V. CONVENTIONAL RMPA DESIGN

Fig. 8 shows Conventional design of patch antenna over FR4 substrate. Comprising a rectangular patch radiator on one side of FR4 substrate backed by an optically planar ground. In this design, a radiating patch is designed with conducting material of rectangular shape is on one side of FR4 dielectric substrate, with its relative permittivity of 4.2 and loss tangent of 0.009 and conductive planar ground plane on other side. The dimensions of patch are $33.3 \times 27.6 \text{ mm}^2$, which make the antenna to operate at 2.5 GHz.

VI. MINIATURED RMPA DESIGN

Fig. 9 shows the Miniatured Patch antenna with 2DEBG ground. The conventional design shown in Fig. 8, where its planar ground is replaced with 2DEBG ground. Since EBG is a resonating structure, lying near to another resonating structure like patch and have a property of high surface impedance. Then the resonating frequency of patch is lowered, Patch dimensions are miniaturized to $29.4 \times 24 \text{ mm}^2$ to bring back patches to resonate within the band gap of 2DEBG.

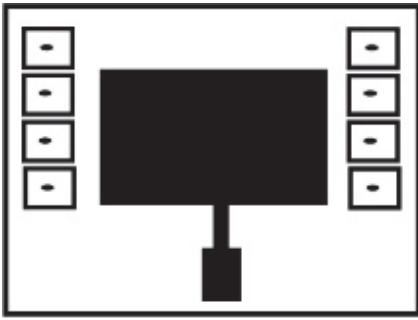


Fig. 9. Miniature size patch antenna surrounded by 2DEBG.

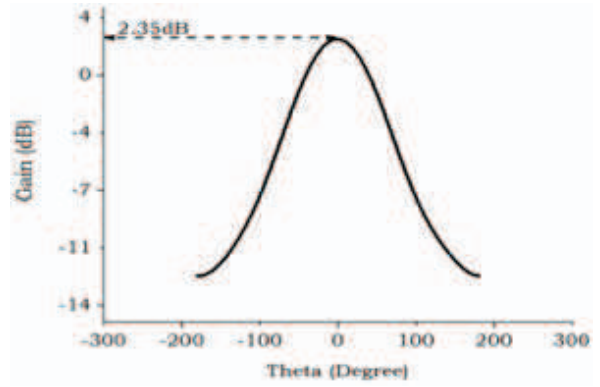


Fig. 12. Gain of conventional patch antenna over FR4 substrate.

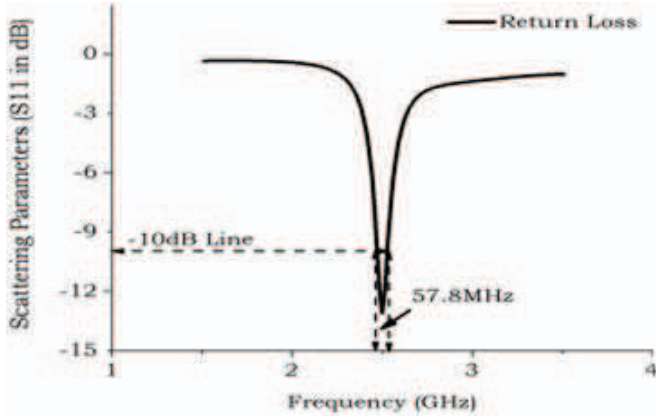


Fig. 10. Return loss of conventional patch antenna over FR4 substrate.

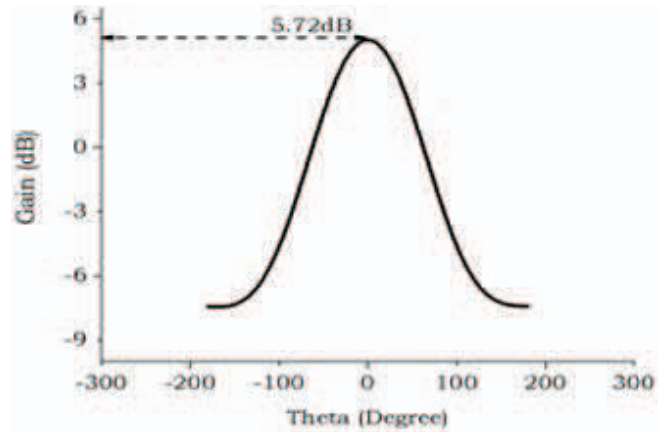


Fig. 13. Gain of antenna surrounded by 2DEBG.

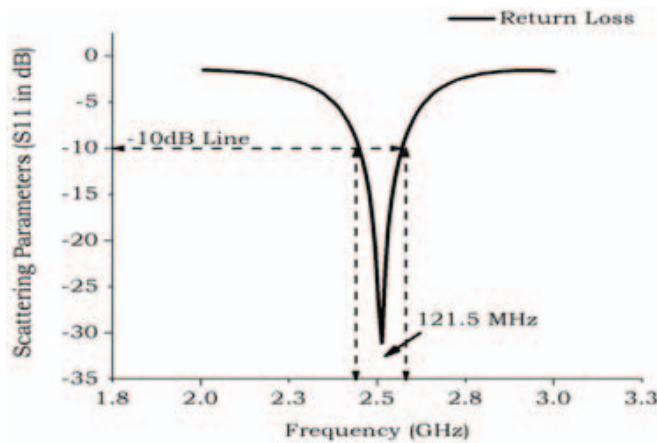


Fig. 11. Return loss of patch antenna surrounded by 2DEBG.

Fig. 10 shows the Return loss characteristics of conventional patch antenna for Figs. 8, 11 shows the Return Loss for characteristics for proposed antenna for Fig. 9 whereas the horizontal axis represents the frequency of EM signal transmitted from the antenna. The vertical axis represents the return loss in decibels of antenna. The bandwidth due to conventional structure is 57.8 MHz, whereas 2DEBG ground is 121.5 MHz. So we can conclude that the band width of patch is doubled due to 2D-EBG ground.

Fig. 12 shows the gain of the conventional patch antenna for Figs. 8, 13 shows the gain of antenna surrounded by 2DEBG structure for Fig. 9. Due to miniature structure of patch, its power handling capacity will be reduced, but due to the property of in phase reflection of 2DEBG, Ground reflected waves are added in phase with the radiated wave in forward direction resulting an improvement in gain achieved. The gain due to conventional design is 2.35 dB, whereas 2DEBG ground is 5.72 dB, hence gain improvement is achieved.

VII. CONCLUSION

The performance of RMPA with EBG structure is investigated and found the unique properties of 2DEBG are best suitable in the field of antenna engineering. By using 2DEBG structure as a ground plane for RMPA an enhancement in bandwidth of 3%, and gain upto 3.5 dB is achieved as compared with the conventional microstrip patch antenna. The proposed antenna is operating at 2.5 GHz within a forbidden band gap of 1.5 GHz, in phase reflection band gap of 41 MHz and a high impedance of 3540 Ω at the resonating frequency.

REFERENCES

- [1] K.-L. Wong, *Compact and Broadband Microstrip Antennas*. New York: Wiley, 2002.
- [2] D. Sievenpiper, L. Zhang, R. F. J. Broas, N. G. Alexopolous, and E. Yablonovitch, "High-impedance electromagnetic surfaces with a forbidden frequency", *IEEE Trans. Microw. Theory Tech.*, vol. 47, no. 11, pp. 2059–2074, Nov. 1999.
- [3] F.-R. Yang, K.-P. Ma, Y. Qian, and T. Itoh, "A uniplanar compact photonic-bandgap (UC-PBG) structure and its applications for microwave circuit", *IEEE Trans. Microw. Theory Tech.*, vol. 47, no. 8, pp. 1509–1514, Aug. 1999.
- [4] V. Veselago, "The electrodynamics of substances with simultaneously negative values of Permittivity ϵ and permeability μ ," *Soviet Phys. Uspekhi*, vol. 10, no. 4, pp. 509–514, 1968.
- [5] R. A. Shelby, D. R. Smith, and S. Schultz, "Experimental verification of a negative index of refraction", *Science*, vol. 292, no. 5514, pp. 77–79, Apr. 2001.
- [6] C. Caloz and T. Itoh, "Transmission line approach of left-handed (LH) materials and microstrip implementation of an artificial LH transmission line", *IEEE Trans. Antennas Propag.*, vol. 52, no. 5, pp. 1159–1166, May 2004.
- [7] A. Lai, C. Caloz, and T. Itoh, "Composite right/left-handed transmission line metamaterials", *IEEE Microw. Mag.*, vol. 5, no. 3, pp. 34–50, Sep. 2004.
- [8] G. V. Eleftheriades, A. K. Iyer, and P. C. Kremer, "Planar negative refractive index media using periodically L-C loaded transmission lines", *IEEE Trans. Microw. Theory Tech.*, vol. 50, no. 12, pp. 2702–2712, Dec. 2002.
- [9] R. Gonzalo, P. De Maagt, and M. Sorolla, "Enhanced patch-antenna performance by suppressing surface waves using photonic-bandgap substrates", *IEEE Trans. Microw. Theory Tech.*, vol. 47, no. 11, pp. 2131–2138, Nov. 1999.
- [10] J. S. Colburn and Y. Rahmat-Samii, "Patch antennas on externally perforated high dielectric constant substrates", *IEEE Trans. Antennas Propag.*, vol. 47, no. 12, pp. 1785–1794, Dec. 1999.
- [11] F. Yang and Y. Rahmat-Samii, "Microstrip antennas integrated with electromagnetic band-gap (EBG) structures: A low mutual coupling design for array applications", *IEEE Trans. Antennas Propag.*, vol. 51, no. 10, pp. 2936–2946, Oct. 2003.
- [12] Z. Li and Y. Rahmat-Samii, "PBG, PMC and PEC ground planes: A case study of dipole antennas", in *Proc. IEEE Antennas Propag. Soc. Int. Symp. Dig.*, Jul. 2000, vol. 2, pp. 674–677.
- [13] D. J. Kern, D. H. Werner, A. Monorchio, L. Lanuzza, and M. J. Wilhelm, "The design synthesis of multiband artificial magnetic conductors using high impedance frequency selective surfaces", *IEEE Trans. Antennas Propag.*, vol. 53, no. 1, pp. 8–17, Jan. 2005.
- [14] N. Christopoulos, G. Goussetis, A. P. Feresidis, and J. C. Vardaxoglou, "Metamaterials with multiband AMC and EBG properties", in *Proc. Eur. Microw. Conf.*, Oct. 2005, vol. 1, pp. 77–79.
- [15] F. Yang and Y. Rahmat-Samii, "Reflection phase characterizations of the EBG ground plane for low profile wire antenna applications", *IEEE Trans. Antennas Propag.*, vol. 51, no. 10, pp. 2691–2703, Oct. 2003.
- [16] J. Bell and M. Iskander, "A low-profile archimedean spiral antenna using an EBG ground plane", *IEEE Antennas Wireless Propag. Lett.*, vol. 3, pp. 223–226, 2004.
- [17] A. P. Feresidis, G. Goussetis, S. Wang, and J. C. Vardaxoglou, "Artificial magnetic conductor surfaces and their application to low-profile high-gain planar antennas", *IEEE Trans. Antennas Propag.*, vol. 53, no. 1, pp. 209–215, Jan. 2005.
- [18] S. Pioch and J.-M. Laheurte, "Size reduction of microstrip antennas by means of periodic metallic patterns", *Electron. Lett.*, vol. 39, no. 13, pp. 959–961, Jun. 2003.
- [19] S. Pioch and J.-M. Laheurte, "Parametric study of compact flat antennas based on periodic patterns", *Microw. Opt. Tech. Lett.*, vol. 40, no. 4, pp. 311–314, Jan. 2004.
- [20] M. Ermutlu, C. Simovski, M. Karkkainen, P. Ikonen, S. Tretyakov, and A. Sochava, "Miniaturization of patch antennas with new artificial magnetic layers", in *Proc. IEEE Int. Workshop Antenna Technol.: Small Antennas Novel Metamaterials (IWAT)*, March 2005, pp. 87–90.
- [21] K. Z. Rajab, R. Mittra, and M. T. Lanagan, "Size reduction of microstrip antennas using metamaterials", in *Proc. IEEE Antennas Propag. Soc. Int. Symp. Dig.*, Jul. 2005, vol. 2B, pp. 296–299.
- [22] H. Yang and J. Liang, "Analysis of a proximity coupled patch antenna on metalized EBG substrates", in *IEEE Antennas Propag. Soc. Int. Symp.*, Albuquerque, NM, Jul. 2006, pp. 2287–2290.
- [23] H. Mosallaei and K. Sarabandi, "Antenna miniaturization and bandwidth enhancement using a reactive impedance substrate", *IEEE Trans. Antennas Propag.*, vol. 52, no. 9, pp. 2403–2414, Sep. 2004.
- [24] H. Mosallaei and K. Sarabandi, "Design and modeling of patch antenna printed on magneto-dielectric embedded-circuit metasubstrate", *IEEE Trans. Antennas Propag.*, vol. 55, no. 1, pp. 45–52, Jan. 2007.
- [25] Indian Patent Application number 201641030225 dated 05.09.2016 in the name of 1. Kunapareddy Koteswa Rao 2. Pasumarthy Nageswar Rao and 3. Vangala Sumalatha.



NTSET-2018



12.

1ST NATIONAL CONFERENCE ON TRENDS IN SCIENCE, ENGINEERING AND TECHNOLOGY

(NTSET - 2018)

February 2nd & 3rd - 2018

TECHNICAL PAPER ABSTRACTS



ORGANIZED BY

MATRUSRI ENGINEERING COLLEGE

(Approved by AICTE, Affiliated to Osmania University)

#16-1-486, Saidabad, Hyderabad - 500059



Sponsored by

MATRUSRI EDUCATION SOCIETY

ISBN: 97881-936274-0-2

385



SURVIVAL PREDICTION FOR TITANIC DATA USING MACHINE LEARNING ALGORITHMS

¹P. Ravindra, ²Dr. P. Vijayapal Reddy,

¹Assistant Professor, ²Professor

^{1,2}Computer Science Engineering, Matrusri Engineering College, Hyderabad, India
¹ravindragec539@gmail.com

Abstract : RMS Titanic sinking is one of the most infamous shipwrecks in history. During its maiden voyage, the Titanic sank after colliding with an iceberg, killed many passengers including crew. This sensational tragedy shocked the international community and led to better safety regulations for ships. One of the reasons that the shipwreck led to such loss of life was that there were not enough lifeboats for the passengers and crew. Although there was some element of luck involved in surviving the sinking, some groups of people were more likely to survive than others, such as women, children, and the upper-class. In this paper we are going to make the predictive analysis of what sorts of people were likely to survive and using some tools in machine learning to predict which passengers survived the tragedy.

Index Terms - Machine learning, Logistic Regression, Decision Trees, Feature Engineering, Titanic Dataset

I. INTRODUCTION

Machine learning[8] means the application of any computer-enabled algorithm that can be applied against a data set to find a pattern in the data. This encompasses basically all types of data science algorithms, supervised, unsupervised, segmentation, classification, or regression". few important areas where machine learning can be applied are Handwriting Recognition, Language Translation, Speech Recognition, Image Classification, Autonomous Driving.

Some features of machine learning algorithms can be observations that are used to form predictions for image classification, the pixels are the features, For voice recognition, the pitch and volume of the sound samples are the features and for autonomous cars, data from the cameras, range sensors, and GPS.

II. LITERATURE SURVEY

Every machine learning algorithm works best under a given set of conditions. Making sure your algorithm fits the assumptions / requirements ensures superior performance. You can't use any algorithm in any condition. Instead, in such situations, you should try using algorithms such as Logistic Regression, Decision Trees, SVM, Random Forest etc. logistic regression and decision trees are the models used in this paper for prediction.

Logistic Regression[2][4][9][11] is used to model the probability of an event occurring depending on the values of the independent variables which can be categorical and numerical and to estimate the probability that an event occurs for a randomly selected observations versus the probability that the event does not occur and it is used to predict the effects of series of variables on a binary response variable and it is used to classify observations by estimating the probability that an observation is in a particular category. It is most commonly used in social and biological sciences.

The performance of Logistic regression[1] model can be measured using AIC (Akaike Information Criteria), Null Deviance and Residual Deviance, Confusion Matrix and McFadden R² is called as pseudo R². AIC is an analogous metric of adjusted R² in logistic regression is AIC. AIC is the measure of fit which penalizes model for the number of model coefficients. Therefore, we always prefer model with minimum AIC value. Null Deviance and Residual Deviance measure indicates the response predicted by a model with nothing but an intercept. Lower the value, better the model. Residual deviance indicates the response predicted by a model on adding independent variables. Lower the value, better the model. Confusion Matrix is nothing but a tabular representation of Actual vs Predicted values. This helps us to find the accuracy of the model and avoid overfitting. McFadden R² is used to analyze data with a logistic regression, an equivalent statistic to R-squared does not exist. However, to evaluate the goodness-of-fit of logistic models, several pseudo R-squared's have been developed. To find the accuracy of model in confusion matrix the formula is

$$accuracy = \frac{true\ positives + true\ negatives}{true\ positives + true\ negatives + false\ positives + false\ negatives}$$



Decision tree[3] is a hierarchical tree structure that can be used to divide up a large collection of records into smaller sets of classes by applying a sequence of simple decision rules. A decision tree model consists of a set of rules for dividing a large heterogeneous population into smaller, more homogeneous (mutually exclusive) classes. The attributes of the classes can be any type of variables from binary, nominal, ordinal, and quantitative values, while the classes must be qualitative type (categorical or binary, or ordinal). In short, given a data of attributes together with its classes, a decision tree produces a sequence of rules (or series of questions) that can be used to recognize the class. One rule is applied after another, resulting in a hierarchy of segments within segments. The hierarchy is called a tree, and each segment is called a node. With each successive division, the members of the resulting sets become more and more similar to each other. Hence, the algorithm used to construct decision tree is referred to as recursive partitioning. Decision tree applications are prediction tumor cells as benign or malignant, classify credit card transaction as legitimate or fraudulent, classify buyers from non-buyers, decision on whether or not to approve a loan, diagnosis of various diseases based on symptoms and profiles.

III. METHODOLOGY

The data we collected is still raw-data which is very likely to contain mistakes, missing values and corrupt values. Before drawing any conclusions from the data we need to do some data preprocessing which involves data wrangling and feature engineering. Data wrangling is the process of cleaning and unify the messy and complex data sets for easy access and analysis. Feature engineering[7] process attempts to create additional relevant features from existing raw features in the data and to increase the predictive power of learning algorithms.

Our approach to solve the problem starts with collecting the raw data need to solve the problem and import the dataset into the working environment and do data preprocessing which includes data wrangling and feature engineering then explore the data and prepare a model for performing analysis using machine learning algorithms and evaluate the model and re-iterate till we get satisfactory model performance then compare the results within the algorithm and select a model which gives a more accurate results.

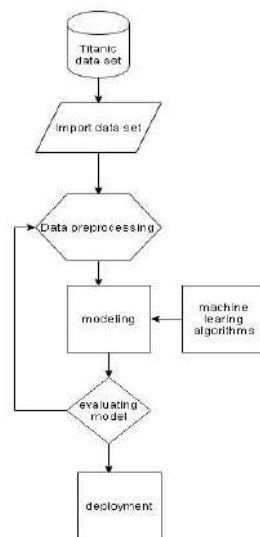


Fig:1 Operational flow chart

IV. EXPERIMENTAL ANALYSIS AND DISCUSSION

4.1 Data set description:

The original data has been split into two groups : training dataset(70%) and test dataset(30%). The training set is used to build our machine learning models. The training set includes our target variable, passenger survival status along with other independent features like gender, class, fare, and Pclass. The test set should be used to see how well our model performs on unseen data. The test set does not provide passengers survival status. We are going to use our model to predict passenger survival status. The test set should be used to see how well your model performs on unseen data. For the test set, we do not provide the ground truth for each passenger. It is your job to predict these outcomes. For each passenger in the test set, use the model we trained to predict whether or not they survived the sinking of the Titanic.

4.2 Results:

After training with the algorithms, we have validated our trained algorithms with test data set and measured the algorithms performance with goodness of fit with confusion matrix for validation. 70% of data as training data set and 30% as training data set.



The accuracy of predicting the survival rate using decision tree algorithm(83.7%) is high when compared with logistic regression(81.3%) for a given data set

Confusion matrix for decision tree

Trained data set

predictions	References	
	0	1
0	395	71
1	45	203

Test data set

predictions	References	
	0	1
0	97	20
1	12	48

Confusion matrix for logistic regression

Trained data set

predictions	References	
	0	1
0	395	12
1	21	204

Test data set

predictions	References	
	0	1
0	97	12
1	21	47

4.3 Enhancements and Reasoning:

Predicting the survival rate with others machine learning algorithms[8] like Random Forests , various types Support Vector Machines[8] may improve the accuracy of prediction for the given data set.

V. CONCLUSION

The analysis revealed interesting patterns across individual-level features. Factors such as socioeconomic status, social norms and family composition appeared to have an impact on likelihood of survival. These conclusions, however, were derived from findings in the given data set.

REFERENCES

- [1] Atakurt, Y., 1999, Logistic Regression Analysis and an Implementation in Its Use in Medicine, Ankara University Faculty of Medicine Journal, C.52, Issue 4, P.195, Ankara
- [2] Bircan H., Logistic Regression Analysis: Practice in Medical Data, Kocaeli University Social Sciences Institute Journal, 2004 / 2: 185-208
- [3] M Jamel Selim S Z The construction of decision tree vol. 61 pp. 177-188 1994.
- [4] J C. Bezdek Introduction of statistical model 1973.
- [5] K S A 1- Sultan S Z Selim Application of decision tree vol. 26 no. 9 pp. 1357-1361 1993.
- [6] Abdelghani Bellaachia and Erhan Guven. Predicting breast cancer survivability using data mining techniques.
- [7] <https://machinelearningmastery.com/discover-feature-engineering-how-to-engineer-features-and-how-to-get-good-at-it/>
- [8] Michalski R S, et al. Machine Learning: Challenges of the eighties. Machine Learning, 1986, 99-102.
- [9] Vapnik V.N. The Nature of Statistical Learning Theory[M]. New York □Springer-Verlag. 1995
- [10] V. Kumar, M. Steinbach, and P. N. Tan, "Introduction to data mining," Pearson, Addison Wesley, . London, 2006.
- [11] V. Vapnik, "Statistical learning theory," Wiley, New York, 1998.
- [12] V. Kumar, M. Steinbach, and P. N. Tan, "Introduction to data mining," Pearson, Addison Wesley, . London, 2006



MATRUSRI ENGINEERING COLLEGE

(Approved by AICTE, Affiliated to Osmania University)

#16-1-486, Saidabad, Hyderabad - 500059



Sponsored by

MATRUSRI EDUCATION SOCIETY



ISBN: 97881-936274-0-2





NTSET 2018



12.

1ST NATIONAL CONFERENCE ON TRENDS IN SCIENCE, ENGINEERING AND TECHNOLOGY

(NTSET - 2018)

February 2nd & 3rd - 2018

TECHNICAL PAPER ABSTRACTS



ORGANIZED BY

MATRUSRI ENGINEERING COLLEGE

(Approved by AICTE, Affiliated to Osmania University)

#16-1-486, Saidabad, Hyderabad - 500059



Sponsored by

MATRUSRI EDUCATION SOCIETY

ISBN: 97881-936274-0-2

CLOUD COMPUTING AND IOT IN HEALTHCARE SYSTEM

B. J. Praveena¹, C. Hari Priyanka²

^{1,2}Assistant Professor,

Computer Science Department, Matrusri Engineering College, Hyderabad, India

¹bjpraveena@gmail.com, ²haripriya.ksk@gmail.com

Abstract: The promising potential of cloud computing and its convergence with technologies such as cloud storage, cloud push, mobile computing leads to new developments for divers application domains, which provides a strong technical support for remote healthcare service as well. In this paper we propose a remote healthcare system which include both cloud computing and Internet of Things technologies. We have three parts: Portable medical device (built with IOT), Intelligent Terminals, Cloud Service Platform. Users can maintain and view their health data records anywhere at anytime only with proper Internet connection. Physicians can also view and diagnose the patient's health the same way. Cloud service platform also helps to avoid limitation of installing many applications on the phone.

Index Terms- Cloud computing, Cloud service platform, cloud push technology.

I. INTRODUCTION

Nowadays, the major concern is to have a portable medical help for the elderly and disabled persons in the society. Especially cardiovascular, other chronic diseases with longer ailing time and higher attendance rate not only bring much inconvenience to the patient and families but also the high health care cost is a considerable pressure. The goal is to have a smart, safe, convenient and inexpensive remote health care system. The revolutionary development of Mobile Internet, Cloud computing technology and sensor technology has made a remarkable difference in the health care system. The aim is to build a healthcare system by interfacing Mobile Internet, Cloud computing technology and sensor technology based on smart device (PDA, Smartphone, Tablets etc..) which can provide a health care system to the customers anywhere at any time with low cost.

II. ARCHITECTURE OVERVIEW

The healthcare system has three parts: Portable medical device (built with IOT), Intelligent Terminals, Cloud Service Platform. The portable medical device records the readings and sends those signals to intelligent terminal through wireless way (Bluetooth/Wi-Fi). The terminal will store, display and upload to the cloud service platform. Cloud service platform is built with cloud server, cloud storage and cloud push technology which is the core of the whole system.

Using Internet devices, user can view and maintain their health anywhere, anytime and physicians can check their patient's health condition and send the diagnosis report or advice to their patient and patient's family members anytime. The system also has online consultation feature to provide communication between patients and doctors.



Fig 1: Architecture of cloud-based Remote Health care system

III. OVERVIEW OF THE TECHNOLOGIES USED



Cloud Computing: Cloud computing has completely changed the point of view of the world these days. The most promising and adaptable technology in today's market is cloud computing. NIST (National Institute of Standards and Technology, USA) defined cloud computing in September, 2011 in "Special Publication" as:

"cloud computing is a model for enabling convenient, on-demand network access to a shared pool of configurable resources e.g., networks, servers, storage, applications and services) that can rapidly be provisioned and released with minimal management effort or service provider interaction."

A more formal definition that encapsulates the key benefits of cloud computing from a business perspective as well as its unique features from a technological perspective given by Sean Martson *et al.* [4] in their research paper is as follows:

"It is an information technology service model where computing services (both hardware and software) are delivered on-demand to customers over a network in a self-service fashion, independent of device and location. The resources required to provide the requisite quality-of-service levels are shared, dynamically scalable, rapidly provisioned, virtualized and released with minimal service provider interaction. Users pay for the service as an operating expense without incurring any significant initial capital expenditure, with the cloud services employing a metering system that divides the computing resource in appropriate blocks."

Cloud Computing is the use of hardware and software to deliver a service over a network (typically the Internet). With cloud computing, users can access files and use applications from any device that can access the Internet. An example of a Cloud Computing provider is Google's Gmail. Gmail users can access files and applications hosted by Google via the internet from any device. It keeps its critical data on Internet servers rather than distributing copies of data files to individual client devices. Video-sharing cloud services like Netflix, for example, stream data across the Internet to a player application on the viewing device rather than sending customers DVD or BluRay physical discs. Clients must be connected to the Internet in order to use cloud services. Some video games on the Xbox Live service, for example, can only be obtained online (not on physical disc) while some others also cannot be played without being connected. Some industry observers expect cloud computing to keep increasing in popularity in coming years.

Service Models:

a.) Software as a Service (SaaS): The capability provided to the consumer is to use the provider's applications running on a cloud infrastructure. The applications are accessible from various client devices through a thin client interface such as a web browser (e.g., web-based email). The consumer does not manage or control the underlying cloud infrastructure with the possible exception of limited user-specific application configuration settings.

b.) Platform as a Service (PaaS): The capability provided to the consumer is to deploy onto the cloud infrastructure consumer-created or acquired applications created using programming languages and tools supported by the provider. The consumer does not manage or control the underlying cloud infrastructure including network, servers, operating systems, or storage, but has control over the deployed applications and possibly application hosting environment configurations.

c.) Infrastructure as a Service (IaaS): The capability provided to the consumer is to provision processing, storage, networks, and other fundamental computing resources where the consumer is able to deploy and run arbitrary software, which can include operating systems and applications. The consumer does not manage or control the underlying cloud infrastructure but has control over operating systems, storage, deployed applications, and possibly limited control of select networking components (e.g. host firewalls).

Deployment Models:

Private Cloud: The cloud infrastructure is operated solely for an organization. It may be managed by the organization or a third party and may exist on premise or off premise.

Community Cloud: The cloud infrastructure is shared by several organizations and supports a specific community that has shared concerns (e.g., mission, security requirements, policy, and compliance considerations). It may be managed by the organizations or a third party and may exist on premise or off premise.

Public Cloud: The cloud infrastructure is made available to the general public or a large industry group and is owned by an organization selling cloud services.

Hybrid Cloud: The cloud infrastructure is a composition of two or more clouds (private, community, or public) that remain unique entities but are bound together by standardized or proprietary technology that enables data and application portability (e.g., cloud bursting for load-balancing between clouds).

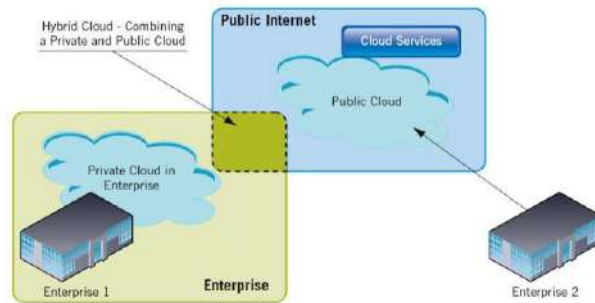


Fig 3 Picture illustrates Public, Private and Hybrid cloud deployment example.

Internet of Things: Internet of things is defined as Things having identities and virtual personalities operating in smart spaces using intelligent interfaces to connect and communicated within social, environment and user contexts. It can be considered the Future of Internet, where every object is connected to other objects. Every object is given a unique identity in the network. This allows the remote access through the network, anytime and at any location. IoT enabled objects communicate with each other, access information over the Internet, and interact with users creating smart, pervasive and always connected environments. IoT also enables machine to machine (M2M) communication which allows machines being controlled by the Internet and by other machines. This can revolutionize the way technology is used, as machine takes control of machine overcoming the constraints that people face while communicating with digital systems. Machines can monitor sensors all over the world to generate vast quantity of valuable information that would take human years to achieve.

IoT makes the concept of pervasive computing and ubiquitous computing a reality by allowing objects of our everyday life like cars, roadways, pacemakers, pill shaped cameras in our digestive tracks, billboards that adjust to passersby, refrigerators and even cattle's equipped with sensors to communicate with humans and assisting them in every step.

IV. CLOUD COMPUTING AND IOT IN HEALTH-CARE SYSTEM

1. SYSTEM KEY TECHNOLOGIES

A) Cloud platform

Currently the dominating leasing services for cloud computing platform are Microsoft Azure, Google GAE, Amazon EC2, Ali cloud and Baidu cloud, etc. The Ali cloud computing platform can be used as the dependence of the medical cloud platform, to form a remote healthcare system. In this the user can purchase cloud service according to their business volume. Optional configuration parameters are the number of CPU, operating system type, storage space amount, bandwidth, duration, etc

B) Portable medical device

The portable medical devices like BP , ECG ,Pulse monitor etc are built using audino and NFC technology. These devices record the Physiological signal and push them to the cloud for storage and for diagnosis purpose. The dives can also be built using raspberry pi for latest updates.

C) Intelligent Terminal

The Intelligent Terminals which can be used are PDA, Laptops, Smartphone, etc .The current mobile devices have Android and IOS as operating Systems. The applications which are developed in Ali cloud are using Flex builder which is not adaptable to the smart phones OS. So to build the communication between them we can use Web service technology.

V. SYSTEM IMPLEMENTATION

The portable medical device will record the physiological signals and push them to the intelligent medical device of the patient. The recorded data are then pushed to the cloud for storage and review purpose. Now the doctor will login in to the cloud and gets the readings. After diagnosing the report the doctor will send the treatment to the patient or the family members. This system is very useful for elderly and handicapped citizens. This system will definitely improve the medical reachability to everyone with less cost anywhere at anytime.

VI. CONCLUSION

After analyzing the developing trend of current mobile healthcare technology, this paper presents a new mobile healthcare model based on cloud computing. The application of this paper should be supported with strong internet connection. This model will make the healthcare reachable to all the citizens of different cadre.



REFERENCES

- [1] Lo'ai A. Tawalbeh, Rashid Mehmood, Elhadj Benkhelifa, Houbing Song, "Mobile Cloud Computing Model and Big Data Analysis for Healthcare Applications", *Access IEEE*, vol. 4, pp. 6171-6180, 2016, ISSN 2169-3536.
- [2] Gao Zhiqiang, He Lingsong, Tian Hang, "A Cloud Computing based Mobile healthcare service system" 2015 IEEE 3rd ICSIMA .
- [3] Hu Xiping, Zhang Zhimei, Dong Jiancheng, "Medical Information Based on Cloud Computing Concepts and Techniques", *Journal of Medical Information*, vol.31,2010,pp.6-9.
- [4] Danan Thilakanathan, Shiping Chen, et al, "A platform for secure monitoring and sharing of generic health data in the cloud", *Future Generation Computer System*, vol. 35,2014,pp102-113.
- [5] H.Alemdar, C.Erosy,"Wireless sensor networks for healthcare: A Survey. " *Computer Networks* 54.15(2010):26882710.
- [6] V.M. Rohokale,R. P. Neeli, R. Prasad, "A cooperative Ternet of Things(IOT) for rural healthcare monitoring and control", *IEEE 2nd International Conference on Wirless Communication, Vehicular Technology,Information Theory and Aerospace & Electronics Systems Technology(Wireless VITAE)*,2011.
- [7] F.Macias and G.Thomas,"cloud computing advantages in the Public Sector:How Today's Government,Education, and Healthcare Organizationa are Benefiting from Cloud Computing Enviornments.[White Paper],"2011.



MATRUSRI ENGINEERING COLLEGE

(Approved by AICTE, Affiliated to Osmania University)

#16-1-486, Saidabad, Hyderabad - 500059



Sponsored by

MATRUSRI EDUCATION SOCIETY



ISBN: 97881-936274-0-2





NTSET-2018



12.

1ST NATIONAL CONFERENCE ON TRENDS IN SCIENCE, ENGINEERING AND TECHNOLOGY

(NTSET - 2018)

February 2nd & 3rd - 2018

TECHNICAL PAPER ABSTRACTS



ORGANIZED BY

MATRUSRI ENGINEERING COLLEGE

(Approved by AICTE, Affiliated to Osmania University)

#16-1-486, Saidabad, Hyderabad - 500059



Sponsored by

MATRUSRI EDUCATION SOCIETY

ISBN: 97881-936274-0-2



PARSING SENTIMENT IN TELUGU LANGUAGE SENTENCES

¹G. Pratibha, ²Dr. Nagaratna Hegde, ³Ch. Abhilash Reddy, ⁴D. Maneesh

¹Assistant Professor, ²Professor, ^{3,4}B.E Student

^{1,3,4}CSE Matrusri Engineering College ,Hyderabad ,Telangana, India.

²Vasavi College of Engineering ,Hyderabad ,Telangana, India.

Abstract: In recent times, sentiment analysis in low resourced languages and regional languages has become emerging areas in natural language processing. Researchers are showing interest towards analysing sentiment in Indian languages such as Hindi, Telugu, Tamil, Bengali, Malayalam, etc. With the growing amount of information and availability of opinion-rich resources, it is sometimes difficult for a common man to analyse what others think about. In order to analyse the information and to see what others are thinking about the product or a service is the problem of Sentiment Analysis. Sentiment analysis or polarity labelling is an emerging field, so this needs to be accurate. In this paper, we explore various Machine Learning techniques for the classification of Telugu sentences into positive or negative polarities and also the implementation of the emoji's in the sentences are done and are classified.

Index Terms--

I. INTRODUCTION

In natural language processing(NLP),sentiment analysis is a technique that deals with analysing the sentiments, opinions ,emotions of an individual towards a product, events, news ,movies or organizations, etc. The primary task of sentiment analysis is to identify the polarity of a text in a given document. The polarity may be either positive, negative or neutral. Majority of the work in the field of sentiment classification has been done in the English Language. There has been very less research has been done for regional languages, especially Indian Languages.

Telugu is a most popular Dravidian language and are about 75 million native Telugu speakers. Telugu ranks fifteenth in the list of most-spoken languages worldwide. Currently there are a lot of web sites ,blogs etc., rich in Telugu content. Sentiment analysis can be applied to the input text in three categories namely, sentence level, document level, and aspect level. Sentence level analysis focuses on identifying sentence-wise polarity value in a given document. Document level analysis determines the polarity value based on consideration of the whole document. In aspect level analysis, it identifies the polarity of every aspect (word-wise) in a given text. In this work, we tried to classify the sentiment polarity of Telugu sentences using different Machine Learning Techniques viz., Naive Bayes, Logistic Regression, SVM (Support Vector Machines), MLP (Multilayer Perceptron) Neural Network, Decision Trees and Random Forest. We built models for two classification tasks: a binary task of classification of sentiment into positive and negative polarities and a ternary task of classification of sentiment into positive, negative and neutral polarities.

The rest of the paper is described as follows: In section 2, we discuss the previous works and related work. In section 3, we describe the datasets and classifiers used for our work. In section 4, we discuss about the methodology used in our paper which includes pre-processing, training and output. In section 5, we present the framework of our work which includes the tools and different Machine Learning techniques used in our work. In section 6, we present our experiments and discuss the results.

II. RELATED WORK

Sentiment analysis is a difficult task and a lot of research has been done in the past for English text and not been done for Telugu text with emojis. In this section we analysed some of the methodologies and approaches used for sentiment analysis and polarity classification.

To motivate more researchers towards the sentiment analysis in Indian languages, Patra et al. [15] conducted a shared task called SAIL (Sentiment Analysis in Indian Languages). In that event, many researchers have presented their method to analyse sentiment in Indian language such as Hindi, Bengali, Tamil, etc. Mukku et.al. [20] is the first reported work for sentiment analysis. They have used corpus provided by Indian Languages Corpora Initiative (ILCI) data and trained with the help of Doc2Vec model and for pre-processing, Doc2Vec tool that is used to give the representation of a sentence semantically provided by Gensim, a Python module. Machine learning techniques that are used to train the system such as SVM, regression, NB, MLP, decision tree and random forest classifiers. They have conducted experiments on binary and ternary sentiment classification.

Learning word vectors for sentiment analysis is a research work ,where Logistic Regression classifier is used as a predictor. [Maas et al., 2011] proposed a methodology which can grasp both continuous and multi-class sentiment information as well as non-sentiment annotations.



Distributed Representations of Sentences and Documents is the work by [Le and Mikolov, 2014] where they make fixed length paragraph vectors or sentence vectors which are quite useful for our work. We used the tool Doc2Vec for preprocessing the data.

III. DATASET

In this we describe the raw corpus and annotated data which are domain independent. That have been used in our experiments.

3.1 Raw Corpus

Indian Languages Corpora Initiative (ILCI) provided 7,21,785 raw Telugu sentences to corpus. These sentences were used for generating sentence vectors by training the Doc2vec model.

3.2 Annotated Data

The corpus consists of Telugu sentences each attached with a corresponding polarity tag. These sentences are used to train and evaluate the classifier models.

The corpus was prepared from raw data taken from the Telugu Newspapers. This newspaper raw data was first annotated by two native Telugu speakers separately. The data was then merged by a third native speaker who also validated it simultaneously. The annotation consists of three polarity tags i.e., Positive, Negative and Neutral.

We performed inter-annotator agreement using Cohen's kappa coefficient. We got the annotation consistency (k value) to be 0.92.

IV. METHODOLOGY

In this we explain the steps involved in our approach. Doc2Vec tool gives the representation of a sentence semantically with respect to dataset. This means that the sentence vector represents the meaning of the sentence. Therefore, classifying the semantic vector space according to training data can classify all the future instances of the same kind thus giving the solution to the problem of sentiment analysis.

4.1 Pre-Processing

In this we use the raw corpus data to identify the emoji's and replace the emoji with corresponding adjective from the database. We use the Doc2vec tool provided by Gensim, a python module. The sentences alone are taken from annotated data and passed through the trained Doc2Vec model. The model then returns sentence vectors for each of the sentences. Here we maintained the correspondence while converting between sentences and their tags.

4.2 Training

In this the sentence vector is obtained from the pre-processing phase and is attached to a corresponding tag. Therefore, the problem is reduced to a binary or ternary classification problem. We use machine learning Classifiers to train the sentence vectors and creates Classifier model. The models are evaluated using 5-fold cross validation where we divided the data into training and testing sets in the ratio 3:1.

4.3 Output

In this we discuss the resultant tag for a given input Telugu sentence. We will find the emoji from the given input sentence and is replaced with corresponding word from database and is converted into a sentence vector using a Doc2Vec model. This sentence vector is given to the trained classifier model which returns the output tag.

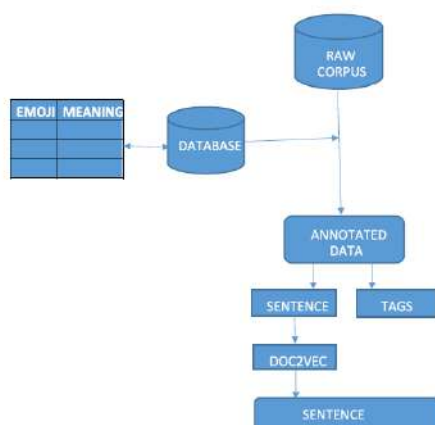


Fig 1.

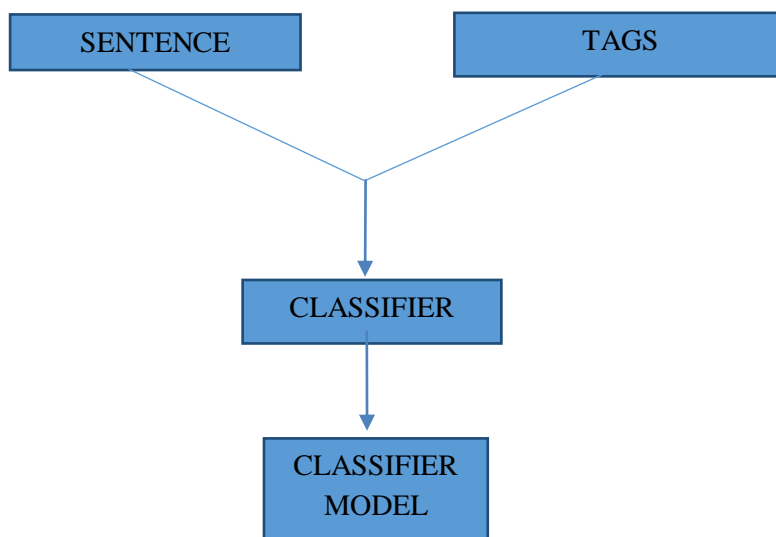


Fig 2.

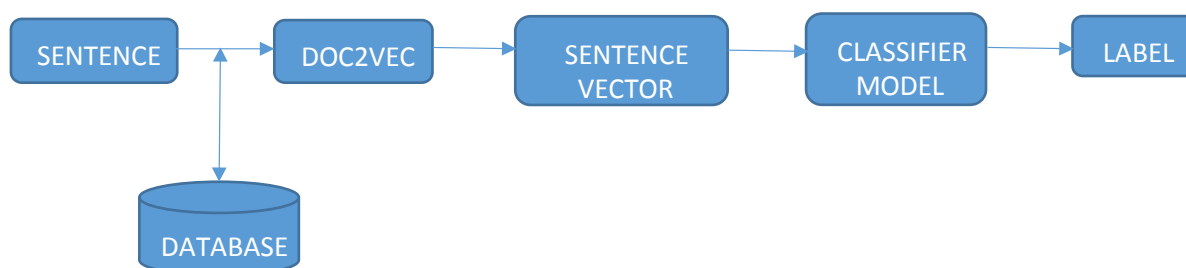


Fig 3.

V. FRAMEWORK

In this we explain the various Machine Learning Techniques employed and the tool used.

5.1 ML Techniques

We used the following Machine learning classifiers to classify.

Naive Bayes (NB): Naive Bayes classifier uses Bayes Theorem, which evaluates the probability of an event with respect to probability of another event which has previously occurred. This classifier works very efficiently for linearly separable and non-linearly separable problems.

Linear Regression (LR): Linear regression is one powerful classifier, which is a poly class logistic model. It is used to classify an object in the predefined classes by using probability with the help of independent variables.

Support Vector Machine (SVM): SVM classifier constructs a set of hyperplanes in a high-dimensional space which separates the data into classes. SVM takes the input and for each data row it predicts the class to which this input row belongs. It is a non-probabilistic linear classifier.

Multi-Layer Perceptron (MLP): A multilayer perceptron (MLP) is a feed-forward neural network which maps input data sets to the appropriate set of outputs. Feed-forward means the data flows only in one direction, in our case from input to output, i.e., in forward direction. Generally neural network has three layers: Input Layer, Hidden Layer and Output Layer. MLP consists of multiple layers of nodes in a directed graph, each layer is fully connected to the next layer.

Decision Trees (DT): Decision tree (DT) is a tool that uses a tree-like model for the decisions and likely outcomes. A decision tree is a tree in which each non-leaf node acts as an input feature which leads to a leaf node which is a label for a sentence. Each leaf of the tree is labeled with a class.

Random Forest (RF): Random Forest (RF) is a group of Decision Trees. Random Forests construct multiple decision trees and consider each of their scores for giving the final output. Random Forests reduce overfitting as multiple decision trees are involved. Decision Trees tend to overfit on a given data and hence they will give good results for training data but bad on testing data.

5.2 DOC2VEC TOOL: Doc2Vec is a tool in which sentences are converted into sentence vectors. This tool helps in pre-processing and training of data. Doc2vec is an extension of word2vec that learns to correlate labels and words, rather than words with other words.

VI. RESULTS

Results are taken from five iterations from Itr0 to Itr4 by changing the ratio of division of training and testing data and the average is taken from all. We can increase the accuracy by increasing the training data set size shown in Table 1.



Accuracy = CS/N*100, where CS is total number of statements correctly classified and N is total number of statements.

	Itr 0	Itr 1	Itr 2	Itr 3	Itr 4	Avg
NBC	63.55	65.42	64.96	63.91	65.20	64.60
LRC	66.94	68.16	65.25	68.33	67.58	67.25
SVM	68.94	68.35	65.60	67.76	66.90	67.51
MLP	65.71	63.53	62.95	63.48	68.36	63.81
DTC	54.47	56.30	55.26	54.81	53.56	54.88
RFC	65.94	67.76	69.06	66.01	70.21	67.79

Table 1

VII. CONCLUSION

Considering the fact that we got good results and our work being first attempt on the hybrid sentences. This approach produces a more focused and accurate sentiment summary of a given Telugu hybrid sentences which are useful for the users. This approach is not restricted by any domain. However, small changes in the pre-processing would be sufficient to use this algorithmic formulation in different languages.

VIII. FUTURE WORK

- To build a dictionary for emoji based sentiment which are frequently used for positive and negative opinion and to construct a lexicon-based system.
- To test the tool for irony detection.

REFERENCE

- [1] G.Pratibha, Asst.Professor, Matrusri engineering college, "An Hybrid Approach in Classification of Telugu Sentences".
- [2] Radhika Mamidi, LTRC, IIIT Hyderabad,"Enhanced Sentiment Classification of Telugu Text using ML Techniques".
- [3] "Scikit-learn: A machine learning in python",<http://www.Scikit-learn.org>.
- [4] Santosh Kumar Bharti, NIT Rourkela, "Sentiment Analysis using Telugu SentiWordNet"
- [5] Chekuri Rama Rao, "Telugu Vakyam", Andhra Pradesh Sahithya Academy, 1975.
- [6] Bh.Krishna Murthy and J.P.L.Gwynn, A Grammar of Modern Telugu., Oxford University press, 1985.
- [7] Quoc V. Le and Tomas Mikolov, "Distributed Representation of Sentences and Documents.", arXiv preprints, arXiv,1405.4053, 2014.
- [8] Martin Anthony and Peter L. Bhartlett, "Neural Network Learning: Theoretical Foundations", Cambridge University Press, 1999.
- [9] Ng, Andrew Y. and Jordan, Michael I, "On Discriminative Vs. Generative Classifiers: A Comparison of logistic regression and naïve Bayes", Advances in Neural Information Processing Systems 14,NIPS 2001.
- [10] Zellig S Harris, Distributional Structure, Word. 10-23: 146162, 1954.
- [11] Keerthi, S.S, Shavade, S. K, Bhattacharya. C & Murthy, K.R.K. "Improvements to Platt's SMO algorithm for SVM Classifier.", Neural Computation, vol. 13, Issue 3, March 2001, pp. 631-649.
- [12] Jiang, J.J. Cornath, D.W, "Semantic Similarity Based on Corpus Statistics and Lexical Taxonomy", arXiv preprint, arXiv: cmp-lg /9709008, pp. 1-15,1997.



MATRUSRI ENGINEERING COLLEGE

(Approved by AICTE, Affiliated to Osmania University)

#16-1-486, Saidabad, Hyderabad - 500059



Sponsored by

MATRUSRI EDUCATION SOCIETY



ISBN: 97881-936274-0-2



NTSET 2018



12.
1ST NATIONAL CONFERENCE ON TRENDS IN
SCIENCE, ENGINEERING AND TECHNOLOGY

(NTSET - 2018)

February 2nd & 3rd - 2018

TECHNICAL PAPER ABSTRACTS



ORGANIZED BY

MATRUSRI ENGINEERING COLLEGE

(Approved by AICTE, Affiliated to Osmania University)

#16-1-486, Saidabad, Hyderabad - 500059



Sponsored by

MATRUSRI EDUCATION SOCIETY

ISBN: 97881-936274-0-2



ANALYZING VARIOUS FACE RECOGNITION TECHNIQUES USING NEURAL NETWORKS

Dr. K. Sunil Manohar Reddy

Assistant Professor, Computer Science and Engineering, Matrusri Engineering College, Hyderabad, India

Abstract: Face recognition is a form of biometric identification and off late it has become the most important method to recognize various people in a real time system. Recognition is a method to identify a person in a still image or in video. It became important due to its applications in many safety and security related areas such as at airports, banks for authentication. New research studies of recognition in this area in recent years is focused towards using neural network methods. Going forward in research in this area is application of Fuzzy system. In this comparative study the focus will be on neural networks, fuzzy system and neuro-Fuzzy system.

Index Terms - Neural networks, face recognition, fuzzy system, Neuro-fuzzy.

I. INTRODUCTION

Face is a physical characteristic that a person posses to identify him/her self automatically. Face recognition is a process of identifying an image by matching with the images in the database. Face Detection is the process of claiming a person as an authorized user. It's a type of one – to –one matching. Facial images may be represented as a 2D or 3D. The 3D facial images are able to identify pose variations, has no effect due lightening. The main challenges one has to encounter in face recognizing are due to facial expressions, rotation effects, noise and distortion. Sometimes recognition is complex due to *interclass* and *intra class* similarities. In the first type two persons may appear to be similar such as twins where as in the second case same person but change in poses. Face recognition can be done in four different ways. Using

Knowledge Based Approach [1], [2], [3], [4] encodes faces based on rules. In **Feature Invariant** method identifies the facial feature that doesn't change due to expressions, pose, illumination etc. Hand coded templates are stored and then used for face detection in **Template Matching** which is the simplest of all methods. The images are trained using different learning methods of neural networks, PCA, SVM in

Appearance Based Method. Most of the research in face recognition in the recent years is based on the last method. From [2] the steps in face recognition are acquiring the face image, pre-processing is done to remove any noise in the image. Later two sets of data are selected, one for training and one for testing the new Image. The performance of any face recognition system is determined by the parameters False Acceptance Rate(FAR) – number of times a unauthorized users are accepted, False Rejection Rate (FRR) – number of times an authorized user has been rejected, Equal Error rate(EER)- FAR and FRR equals, Time to verify, Time taken to capture.

In this study Section II consists of Face recognition methods using Neural Networks, Section III focuses on Fuzzy System. Section IV describes a combination of both approaches Neuro-Fuzzy for face detection. In section V a comparative analysis is made on the two approaches that are neural networks and fuzzy system based on parameters. Section VI concludes on the Neuro-Fuzzy system.

II. FACE RECOGNITION USING NEURAL NETWORKS

2.1Back Propagation (BP)

From [4] a general back propagation network is used for face recognition. The author has proposed two algorithms for feature extraction i) View Based ii) Biometric based. Using a component based detector (CBD) the features of the face are extracted by selecting the sub images and calculating the biometric distance. The components that are selected in the face image are eyes, nose and mouth. From the sub image seven distance biometrics are calculated and normalized in terms of gray levels raging between the values 0 to 1. The resulting value is used as input to the classifier. BP uses both forward and reverse evaluation [5] to train the network and adjusting weights. The resulting training set is named as primary and secondary classifiers. During recognition if the face image doesn't matches with the primary then it matches with the secondary classifier.

2.2Self Organizing Maps (SOM)

SOM is a unsupervised learning method in neural networks which is mostly used a clustering algorithm. Maps the input space from higher dimension to low dimension. This algorithms follows the competitive learning method where the neurons compete with one another and the winning neuron is termed as the "Best Matching Unit(BMU) " which is very close to the input vector. At the end of the training phase the neurons are clustered based on the input space forming a Lattice. From [6] SOM is used to classify the face images even when there is change in facial expression. Here the author has proposed four SOM classifiers. The first SOM classifier (C1) applies to all neurons prior to testing phase. In this method there is no weight updating hence the neurons can be a winner or may be rejected or labeled a s unknown. In the second SOM classifier (C2) the class centroids are chosen for labeling as they are



known before training. In this method neuron belongs to only one class. In the third SOM Classifier (C3) which is a form of supervised SOM the input vectors are classified as pattern vector and class vector. The class vectors are of unit length whose value is to "1" the others are set to "0". In the last method SOM Classifier (C4) for each class assigned one SOM.

In the testing phase winning neuron is one among all of the SOM. In [7] the author presents a form of SOM that is used for facial skin segmentation recognition after plastic surgery. The different color spaces in Image processing are RGB, CMY, HIS, YIQ, IHLS. In this method [7] the given input face image which is normally based on RGB values are converted to IHLS. This color space method is used to improve color saturation and brightness of an image. The resulting images are processed by SOM in two stages. After conversion to IHLS the SOM starts with some random initial values for weight adjustments. The 256 neurons (16*16 colors) in the input space are reduced to 5 neurons after the second stage of the SOM. Then the resulting images is post processed to obtained facial segmentation.

III. FACE RECOGNITION USING FUZZY METHOD

Any image is converted into a set of integer values called "pixels". Face detection using fuzzy method can be done using two steps [8]. They are skin detection and edge detection. In the first step the given image values which are in the form of RGB values are converted to YCbCr values. Since RGB has different brightness values for Red, Green and Blue to overcome this YCbCr method is adopted. The Y component is the sum of R,G and B values, CB is obtained using B-Y, Cr is obtained using R-Y. The Cb, Cr values are used to identify if a pixel belongs to skin part or not. In the second step Fuzzy rules are applied to detect the edges of the face. A set of four pixels are chosen from a 2x2 widow size and sixteen inference rules are proposed to detect edges of the face[8]. An edge is present when there is a large difference between intensities of adjacent pixels.

In [9] fuzzy Retinex method was proposed for face image normalization. Initially the face and eye regions are detected using Adaboost algorithm. In the next step the image is normalized using Fuzzy Logic. Input to the fuzzy based normalization is the mean and standard deviation grey values of the facial image. Using the fuzzy Retinex method the global and local variations are overcome. Fuzzy membership function is derived for the input image. After normalization the face is recognized.

IV. FACE RECOGNITION USING NEURO - FUZZY (NF) SYSTEM

4.1BP and Fuzzy System

In [10] this method the input Facial image considered as image matrix. The rows that are identical are fed as input to the neural network. The number of input neurons are equal to the number of columns in data set matrix. The entire system is designed in two phases. First is the training phase and second is the recognition phase. In the first phase Back Propagation Neural Network is used for training the data sets. During training if there is any error it is feed back to adjust the weights. Once the network is converged the number of epoch and gradient is calculated. These two values are treated as input for Fuzzy Inference System (FIS). Based on the accuracy of the fuzzy membership values face recognition is done.

4.2 EigenFace and Neuro-Fuzzy System

In [11] this method Face features are extracted using Principal component Analysis (PCA) using Eigen faces. The PCA components are taken as input for the Neuro- Fuzzy System. Prior to this Fuzzification of PCA values are done. For each input and output values two membership values High and Low are derived. These values are fed as input to the BP Neural Network for Training Purpose. The hidden layer of BP takes the High and Low values as input. In the next step Genetic algorithms are used for recognition purpose.

4.3 Wavelet Gabor and Neuro-Fuzzy System

In [12] the author proposed a method of face detection using Wavelet Gabor for feature Extraction and NF system for face recognition. The features of the face are extracted by applying the Wavelet Gabor filter. NF is used to classify the input image. In this system BP is used for training purpose. The input layer is same as to that of the General BP but the hidden layer is fuzzification and rule antecedent layer. The output is rule inference layer. In the backward phase error is determined and minimized.

V. COMPARISON OF NEURAL NETWORKS AND FUZZY SYSTEM

Table 1: Comparison of Neural Networks and Fuzzy System

Parameters	Neural Networks	Fuzzy System
Knowledge Representation	Implicit	Explicit
Trainability	Trains itself by learning from data sets.	No Self Training. Training must be defined Explicitly.
Computational Algorithms	Low level	Structured Frame work
Initial Parameters	Fixed well	Randomly Chosen

VI. CONCLUSION



This study compares three different approaches for face recognition. Using only neural networks approach sometimes the network get trapped in local minima as to that of a back propagation Network. When we adopt only Fuzzy system for face recognition biometrics learning becomes an explicit function. In order to achieve a face recognition system that is fast and self adaptive based on the inputs extracted from the face image we can combine the two systems as Neuro-Fuzzy system. From the above analysis we can say the output performance of face recognition is much better in Neuro-Fuzzy system when compared to the individual system.

REFERENCES

- [1] Ming-Hsuan Yang, David J.Kriegman, Narendra Ahuja, "Detecting Faces in Images: A survey", IEEE Transaction on Pattern Analysis & Machine Intelligence Vol 24, No1, January 2002.
- [2] Mayank Agarwal, Nikunj Jain, Mr Manish Kumar and Himanshu Agarwal, "Face Recognition Using Eigen Faces and Artificial Neural Networks " International Journal of Computer Theory and Engineering, Vol 2, No 4, August 2010.
- [3] Cha Zhang and Zhengyou Zhang. "A Survey of Recent Advances in Face Detection", Technical Report, June 2010, MSR-TR-2010-66.
- [4] W.Zhao, R.Chellappa, P.J.Phillips and A.Rosenfeld," Face recognition : A Literature Survey ", ACM computing surveys, Vol 35, No 4, December 2003, pp 399-458.
- [5] M.Samer Charifa, Ahmad Suliman and Marwan Bikdash, "Face recognition using Hybrid General Back propagation Neural Networks ", 2007 IEEE International Conference on Granular Computing.
- [6] Isaque Q, Monterio, Samy D, Queiroz, Alex T Carneiro, Luis G. Souza and Guilherme A Barreto " Face Recognition Independent of Facial Expression Through SOM- Based Classifiers", vi International Telecommunications Symposium (ITS2006), September 3-6, 2006, Fortaleza -Ce Brazil.
- [7] Mohamad Amin Bakshali, Mousa Shamsi, Amir Golzarfar, " Application of SOM network to study Facial Skin segmentation after Facial Surgery " 2012 IEEE Symposium on Industrial Electronics And Application (ISIEA2012), September 23-26 2012, Bandung, Indonesia.
- [8] Rajandeep Kaur, Vijay Dhir, "Fuzzy Logic Based Novel Method of Face Detection ", International Journal Of Latest Research In Science & Technology, Vol 2, Issue 1,Page No 5558-566, January-February (2013).
- [9] Gi Pyo Nam and Kang Ryoung Park " New Fuzzy-based Retinex Method for illumination Normalization of Face Detection", International Journal Of Advanced Robotics System 2012, Vol 9,103:2012.
- [10] Shwetha Mehta, Shailender Gupta, Bharat Bhushan and C.K.Nagpal, "Face Recognition Using Neuro-Fuzzy Inference System", International Journal Of Signal Processing, Image Processing and Pattern Recognition, Vol 7, No 1 (2014), pp 331-344.
- [11] Prashanth.R.S and Saritha.R, "Face Recognition in Eigen Domain With Neuro- Optimization ", International Journal Of Image Processing and Vision Science Vol 1, Issue -2, 2012.
- [12] Raidah Salim," Neuro Fuzzy Network and Wavelet Gabor For Face Detection ", Journal Of Kufa for Mathematics and Computer Vol.1, No.8, Dec,2013, pp 48-57.



MATRUSRI ENGINEERING COLLEGE

(Approved by AICTE, Affiliated to Osmania University)

#16-1-486, Saidabad, Hyderabad - 500059



Sponsored by

MATRUSRI EDUCATION SOCIETY



ISBN: 97881-936274-0-2





NTSET 2018



12.

1ST NATIONAL CONFERENCE ON TRENDS IN SCIENCE, ENGINEERING AND TECHNOLOGY

(NTSET - 2018)

February 2nd & 3rd - 2018

TECHNICAL PAPER ABSTRACTS



ORGANIZED BY

MATRUSRI ENGINEERING COLLEGE

(Approved by AICTE, Affiliated to Osmania University)

#16-1-486, Saidabad, Hyderabad - 500059



Sponsored by

MATRUSRI EDUCATION SOCIETY

ISBN: 97881-936274-0-2



PARTICLE SWARM OPTIMIZATION METHODOLOGY FOR CLASSIFICATION OF IMAGES

G. Shyama Chandra Prasad¹, A. Pramod Kumar², A.V. Murali Krishna³

1 Associate Professor, Matrusri Engineering College, Hyderabad, T.S, India, gscprasad@gmail.com

2,3 Asst Professor, Matrusri Engineering College, Hyderabad, T.S, India, amaravarapu@gmail.com

Abstract: In this paper how Particle Swarm Optimization Radial Basis Function Neural Network is used for solving pattern recognition issues is discussed. To improve the pattern recognition efficiency PSO technique is used to find the weights and bias values and k-means algorithm is used to find the centroid values of the radial basis function neural network. Finally proved that this method shows better accuracy than the traditional RBF model.

Index Terms- Particle Swarm Optimization, Neural Network, Pattern Recognition, Radial Basis Function Network

I. INTRODUCTION

Particle Swarm Optimization (PSO) is a recently developed numerical method for optimization, which is simple, easy to apply and has a strong smart background, and it has been used in many fields such as function optimization, and pattern recognition. Particle Swarm Optimization algorithm is used to proceed global dynamic searching. PSO uses only one Swarm. Swarm is a collection of particles PSO is a simple method used to optimize the solution of problems with regards to the given requirement through iterative method. PSO has many particles and these are moving in the region of search-space based on the formula that consists of position and velocity. Every particle is affected by local positions and tries to reach the best positions in the search-space, which are updated as best position calculated by other particles. This leads the swarm to move in the direction of best solution. This method is used to find weights and bias values of RBFNN. In PSO initially all bias and weights are defined with random values and then move to optimal solutions. The solution of PSO is called particles; these are going through the problem space by following the current optimum particles. This paper is using a new method for image classification called Particle Swarm Optimization.

II. THE PROPOSED METHODOLOGY ARCHITECTURE

This paper has been analyzed in different designs of the Radial Basis Function Neural Network using traditional and PSO. The Figure 1 explains the Conceptual Outline of this paper. There are mainly four blocks shown in the diagram. The main part is in the third block. The third block shows Neural Network models which include two methods and they are as follows:

1. Traditional Radial Basis Function Neural Network (TRBF)
2. Particle Swarm Optimization RBF Neural Network (PSO RBF)

The above two methods are extensions of basic RBF Neural Network design. They are improved under some new aspects of these methods. The Radial Basis Function Neural Network (RBF NN) is a three layer design with weights and bias optimization values. Mainly our research focuses on computing optimization values using optimization methods. The Figure 1 shows that proposed methods improvement in RBF NN.

To compare the performance of several image features for retrieval systems or applications, bench mark image data sets used. This work uses Corel image data set. Generally in Radial Basis Function, input layer consists of input data which is extracted from image features. This work used different dimensions of the image features like Color, Texture, and Wavelet. In the hidden layer, it contains one more additional node than input node. This layer consists of centroids which are calculated using the following two methods.

1. Random
2. K-means clustering algorithm.

The above methods use Gaussian distribution function internally. In this work weights among hidden and output layers are computed with the following three optimization methods.

1. Inversion Matrix
2. PSO

Outputs are computed from processing layer and hidden layer plus Bias values. Generally Bias values are computed using PSO.

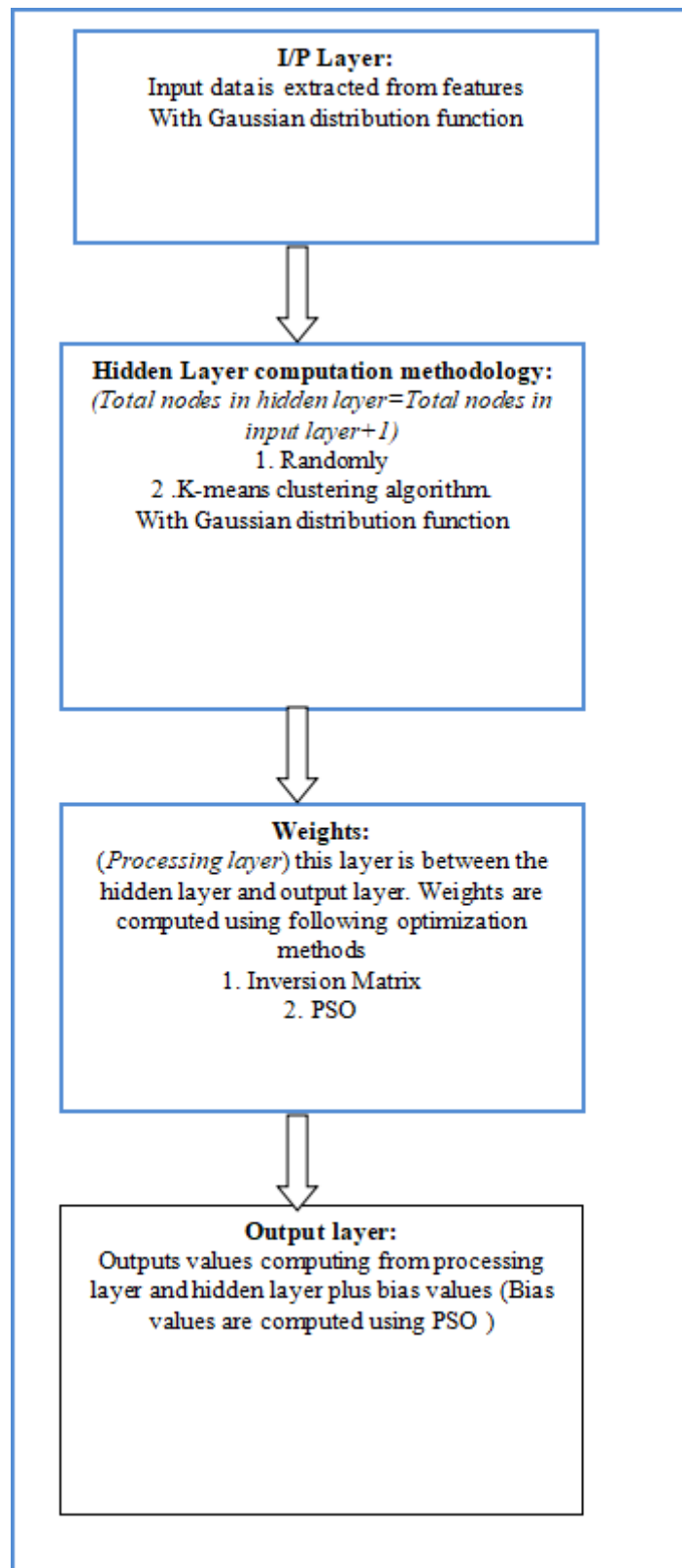


Figure 1 Architecture of the PSO

III. THE FLOWCHART

Particle swarm optimization (PSO) is a computational method that optimizes a problem by iteratively trying to improve a candidate solution with regard to a given measure of quality. This optimizes a problem by having a population of candidate solutions, here each particles, and moving these particles around in the search-space according to simple mathematical formulae over the particle's position and velocity. Each particle's movement is influenced by its local best known position but, is also guided toward the best known positions in the search-space, which are updated as better positions are found by other particles. This is expected to move the swarm toward the best solutions. Using Particle Swarm Optimization RBF Neural Networks weights and bias values are defined.



PSO-RBF Neural Networks uses image retrieval process using local minimum and global minimum. Swarm is a collection of particles. Each particle has five properties, they are position, error, velocity, bestPosition (Pbest) and bestError (Perror). PSO uses only one Swarm. Each Swarm has GlobalBestPosition (Gbest) and GlobalBestError(Gerror). Particles are moving in best direction based on MSE of the RBF. Each moved position compare with self bestError and GlobalBestError. Based on best values, Particle is updated with new position and updated GlobalBestPosition with BestPosition values.

Following are steps to compute Radial Basis Function weights and bias values.

Using Particle Swarm Optimization identify the weights and bias values for RBF Neural Networks.

- Totally 290 (28*10+10) numerical values are required to compute for the first training set.
- Following are the steps to find values:
 - Particle initialize:
 - **Position:** Random values (290) are between min and max values. Min and Max values are defined - 10 and 10.
 - **Position Error:** using initial position values compute K-Means Radial Basis Function network.
 - Find the MSE values
 - **Velocity:** Random values (290) are between min and max values.
 - **Particle Best Position (Pbest):** Initial position values set is Particle Best Position
 - **Particle Best Error (Pbest Error):** Initial position error is Particle Best Error.
 - Initial Find Best Global Position and Error based on all Particles
 - The next movement of the Particle based on Current Position and New Position.
 - (Particle movement only with Epochs, initial defined 100)
 - W inertia weight, C1 Local cognitive , C2 Global cognitive and r1 and r2 are random variables.
 - $\text{newVelocity}(j) = (w * \text{currP.velocity}(j)) + (c1 * r1 * (\text{currP.bestPosition}(j) - \text{currP.position}(j))) + (c2 * r2 * (\text{bestGlobalPosition}(j) - \text{currP.position}(j)))$;
 - New Position= Current Position + New Velocity
 - Find the MSE for New Position (Values)
 - If want move Particle from current to New Position, Error should be less compare with Pbest Error, Else Particle in current position.
 - If New Position Error is less than Global Best Error (Swarm Best), then update the Global Best Error and Position.
 - Particle selected randomly and movement up to number Epochs.
 - Final find the Best Global Position (Gbest) and Error.
 - Using this Gbest values, design the best PSO-Radial Basis Function Neural Network

In Particle Swarm Optimization main formal is,

$$\text{newVelocity}(j) = (w * \text{currP.velocity}(j)) + (c1 * r1 * (\text{currP.bestPosition}(j) - \text{currP.position}(j))) + (c2 * r2 * (\text{bestGlobalPosition}(j) - \text{currP.position}(j))) \dots (6)$$

Based on new Velocity, it will change the Particle position. One of the disadvantages of Particle Swarm Optimization is that only one Swarm limit of mathematical space. This is resolved by using Multi Swarm Optimization.

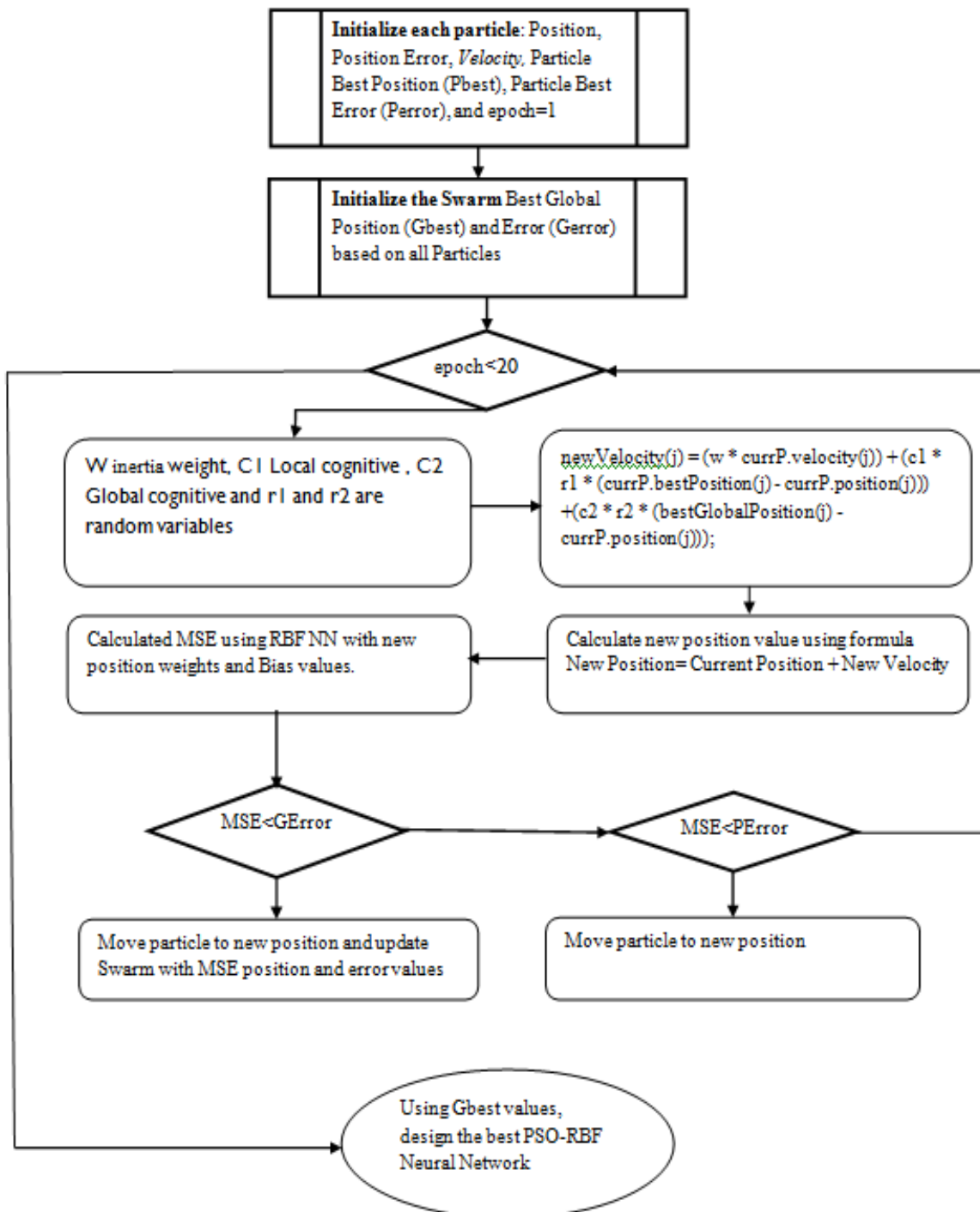


Figure 2 Flow Chart

IV. RESULTS

Data is collected from the Corel image database. Corel is available with 1000,5000,10000 images. For all these images extracted 27 features. These 27 Data features divided as three parts.

1. Color (Count -3): Mean value of each of the color spaces are chosen as color features [7].
2. Texture (Count -12): Variance, Coefficient of Variation, Energy and Entropy is calculated for each Color [7].
3. Wavelet features (Count -12): Decompose an image into sub-bands at one level with Approximation, Horizontal, Vertical and Diagonal for each color [7][8].

Using 1000 images, the following cases are defined for analyzing accuracy results, here all test data selected randomly. The test data are taken different values like 50,200,300,500,600,800 also the train data are considered as 950,800,700,500,400,200.



Parameters used for the proposed system

Table 1: Parameters used in the experiment

Paramater	Values
No of input nodes	27(No. of Features)
No of Hidden Nodes	28 (No. of input nodes +1)
No of Output Nodes	10 (No. of Classes)
Driving Function	Gaussian radial function
Learning Algorithm	MSE
Network	PSO RBF
Epochs	40
Goal	0.1 (error)
Standard Deviation	4
No of Swarms	100
No of particles for Swarm	100
Space Min and Space max	-10 and 10
W	0.72
r1 and r2	Rand value (between 0 and 1)

Performance Comparison

Table 2: All the cases with accuracy values for different systems

# Test Data	RBF	PSO-RBF
50	58	84
200	51.5	73.5
300	51	76.33
500	53.2	71.8
600	48	76.17
800	38	72.12

Finally, the present research demonstrates that the new method PSO RBF has better accuracy in comparison with other methods even in the case of when test data is very high and with less train data.

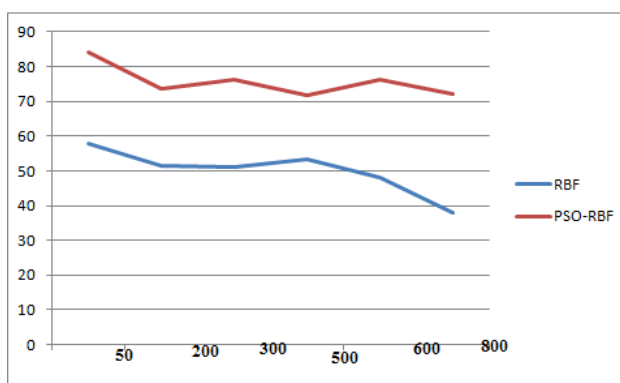


Figure 3 Comparison of accuracy values for various systems

V. CONCLUSION

In this paper accuracy assessment of images using traditional RBFNN and PSO RBFNN is emphasized. Traditional method has given 58, 51.5, 51, 53.2, 48 and 38% of test accuracy. This method uses Centroids values randomly and Weights and Bias values are calculated using Inversion Matrix method. Accuracy can be improved by defining proper weights and bias values, to improve the accuracy in this paper focused to use the right method for solving this problem that is Particle Swarm Optimization. Using PSO constructed best PSO-Radial Basis Function Neural Networks. This method achieved best accuracy results for different dynamic cases. PSO-RBF produced the following accuracy for test data: 84, 73.5 76.33, 71.8, 76.17 and 72.12% Test accuracy values .Compare with all existing methods, our research proposed method is more accuracy. Finally, PSO-RBF NN has given better results in the image classification over traditional RBFNN method.



REFERENCES

- [1] Jagriti Sharma¹ and Sunali Mehta², "Training of Radial Basis Function Using Particle Swarm Optimization", International Journal of Engineering Research and Development e-ISSN : 2278-067X, p-ISSN: 2278-800X, Volume 7, Issue 10, July 2013, PP. 01-10.
- [2] Qinghai Bai, "Analysis of Particle Swarm Optimization Algorithm", CIS, Vo3, No1, Feb 2010
- [3] Kennedy, J. and Mendes, R., "Population Structure and Particle Swarm Performance", Congress on Evolutionary Computation, 2002, pp. 1671-1676
- [4] Majid Moradi Zirkohi, Mohammad Mehdi Fateh and Ali Akbarzade, "Design Of Radial Basis Function Network Using Adaptive Particle Swarm Optimization And Orthogonal Least Squares. Software Engineering & Applications", 2010, 3, 704-708
- [5] Min Han, Member, IEEE, Wei Guo, Yunfeng Mu, "A Modified RBF Neural Network in Pattern Recognition", Proceedings of International Joint Conference on Neural Networks, Orlando, Florida, USA, August 12-17, 2007
- [6] Nabney IT, "Efficient training of RBF networks for classification", Proceedings of 9th ICANN, Volume 1, pp 210– 215.



MATRUSRI ENGINEERING COLLEGE

(Approved by AICTE, Affiliated to Osmania University)

#16-1-486, Saidabad, Hyderabad - 500059



Sponsored by

MATRUSRI EDUCATION SOCIETY



ISBN: 97881-936274-0-2



To Support Customers in Easily and Affordably Obtaining the Latest Peer-Reviewed Research,

Receive a 20% Discount on ALL Publications and Free Worldwide Shipping on Orders Over US\$ 295

Additionally, Enjoy an Additional 5% Pre-Publication Discount on all Forthcoming Reference Books

[Browse Titles \(https://www.igi-global.com/search/?p=&ctid=1%2c2\)](https://www.igi-global.com/search/?p=&ctid=1%2c2)



Internet of Things for Smart Cities

Pallavi Khare (Matrusri Engineering College, India) and Akhil Khare (MVSR Engineering College, India)

Source Title: Exploring the Convergence of Big Data and the Internet of Things (/book/exploring-convergence-big-data-internet/179213)

Copyright: © 2018

Pages: 17

DOI: 10.4018/978-1-5225-2947-7.ch008

**OnDemand PDF
Download:**

\$37.50

() Available

[Current Special Offers](#)

Abstract

The Internet of Things (IoT) is a system of interrelated computing devices, mechanical and digital machines, objects, animals or people that are provided with unique identifiers and the ability to transfer data over a network without requiring human-to-human or human-to-computer interaction. The Internet of Things (IoT) shall be able to incorporate transparently and seamlessly a large number of different and heterogeneous end systems, while providing open access to selected subsets of data for the development of a plethora of digital services. Building a general architecture for the IoT is hence a very complex task, mainly because of the extremely large variety of devices, link layer technologies, and services that may be involved in such a system.

Chapter Preview

Top

Introduction

The Internet of Things (IoT) is a recent communication paradigm that envisions a near future, in which the objects of everyday life will be equipped with microcontrollers, transceivers for digital communication, and suitable protocol stacks that will make them able to communicate with one another and with the users, becoming an integral part of the Internet. The IoT concept, hence, aims at making the Internet even more immersive and pervasive. Furthermore, by enabling easy access and interaction with a

wide variety of devices such as, for instance, home appliances, surveillance cameras, monitoring sensors, actuators, displays, vehicles, and so on, the IoT will foster the development of a number of applications that make use of the potentially enormous amount and variety of data generated by such objects to provide new services to citizens, companies, and public administrations.

Outline

This paradigm indeed finds application in many different domains, such as home automation, industrial automation, medical aids, mobile healthcare, elderly assistance, intelligent energy management and smart grids, automotive, traffic management, and many others (Atzori, Iera & Morabito, 2010). However, such a heterogeneous field of application makes the identification of solutions capable of satisfying the requirements of all possible application scenarios a formidable challenge. This difficulty has led to the proliferation of different and, sometimes, incompatible proposals for the practical realization of IoT systems. Therefore, from a system perspective, the realization of an IoT network, together with the required backend network services and devices, still lacks an established best practice because of its novelty and complexity. In addition to the technical difficulties, the adoption of the IoT paradigm is also hindered by the lack of a clear and widely accepted business model that can attract investments to promote the deployment of these technologies.

Scope of the Work

Today the application of the IoT paradigm to an urban context is of particular interest, as it responds to the strong push of many national governments to adopt ICT solutions in the management of public affairs, thus realizing the so-called Smart City concept. Although there is not yet a formal and widely accepted definition of "Smart City," the final aim is to make a better use of the public resources, increasing the quality of the services offered to the citizens, while reducing the operational costs of the public administrations. This objective can be pursued by the deployment of an urban IoT, i.e., a communication infrastructure that provides unified, simple, and economical access to a plethora of public services, thus unleashing potential synergies and increasing transparency to the citizens. An urban IoT, indeed, may bring a number of benefits in the management and optimization of traditional public services, such as transport and parking, lighting, surveillance and maintenance of public areas, preservation of cultural heritage, garbage collection, salubrity of hospitals, and school. Furthermore, the availability of different types of data, collected by a pervasive urban IoT, may also be exploited to increase the transparency and promote the actions of the local government toward the citizens, enhance the awareness of people about the status of their city, stimulate the active participation of the citizens in the management of public administration, and also stimulate the creation of new services upon those provided by the IoT. Therefore, the application of the IoT paradigm to the Smart City is particularly attractive to local and regional administrations that may become the early adopters of such technologies, thus acting as catalyzes for the adoption of the IoT paradigm on a wider scale.

Complete Chapter List

Search this Book:

[Reset](#)

Editorial Advisory Board and List of Reviewers	View Full PDF (/pdf.aspx?tid=187883&ptid=179213&ctid=15&t=Editorial Advisory Board and List of Reviewers&isxn=9781522529477)
Table of Contents	View Full PDF (/pdf.aspx?tid=187884&ptid=179213&ctid=15&t=Table of Contents&isxn=9781522529477)
Detailed Table of Contents	View Full PDF (/pdf.aspx?tid=187885&ptid=179213&ctid=15&t=Detailed Table of Contents&isxn=9781522529477)
Preface	View Full PDF (/pdf.aspx?tid=187886&ptid=179213&ctid=15&t=Preface&isxn=9781522529477)
Acknowledgment	View Full PDF (/pdf.aspx?tid=187887&ptid=179213&ctid=15&t=Acknowledgment&isxn=9781522529477)

Chapter 1**\$37.50**

Big Data and Cloud Computing: A Review of Supply Chain Capabilities and Challenges (/chapter/big-data-and-cloud-computing/187888) (pages 1-28)

Marcus Tanque, Harry J Foxwell

Sample PDF (/viewtitlesample.aspx?id=187888&ptid=179213&t=Big Data and Cloud Computing: A Review of Supply Chain Capabilities and Challenges&isxn=9781522529477)

Chapter 2**\$37.50**

Big Data Analytics in Aquaculture Using Hive and Hadoop Platform (/chapter/big-data-analytics-in-aquaculture-using-hive-and-hadoop-platform/187889) (pages 29-35)

P. Venkateswara Rao, A. Ramamohan Reddy, V. Sucharita

Sample PDF (/viewtitlesample.aspx?id=187889&ptid=179213&t=Big Data Analytics in Aquaculture Using Hive and Hadoop Platform&isxn=9781522529477)

Chapter 3**\$37.50**

Big Data Mining: A Forecast to the Future (/chapter/big-data-mining/187890) (pages 36-42)

V. Sucharita, P. Venkateswara Rao, A. Satya Kalyan, P. Rajarajeswari

Sample PDF (/viewtitlesample.aspx?id=187890&ptid=179213&t=Big Data Mining: A Forecast to the Future&isxn=9781522529477)

Chapter 4**\$37.50**

Cloud Computing Education Strategies: A Review (/chapter/cloud-computing-education-strategies/187891) (pages 43-54)

Syed Hassan Askari, Faizan Ahmad, Sajid Umair, Safdar Abbas Khan

Sample PDF (/viewtitlesample.aspx?id=187891&ptid=179213&t=Cloud Computing Education Strategies: A Review&isxn=9781522529477)

Chapter 5**\$37.50**

Computational Linguistic Distances and Big Data: Optimising the Speech Recognition Systems (/chapter/computational-linguistic-distances-and-big-data/187892) (pages 55-62)

Krishnaveer Abhishek Challa, Jawahar Annabattula

Sample PDF (/viewtitlesample.aspx?id=187892&ptid=179213&t=Computational Linguistic Distances and Big Data: Optimising the Speech Recognition Systems&isxn=9781522529477)

Chapter 6**\$37.50**

Big Data in Mobile Commerce: Customer Relationship Management (/chapter/big-data-in-mobile-commerce/187893) (pages 63-72)

Muhammad Anshari, Syamimi Ariff Lim

Sample PDF (/viewtitlesample.aspx?id=187893&ptid=179213&t=Big Data in Mobile Commerce: Customer Relationship Management&isxn=9781522529477)

Chapter 7**\$37.50**

Internet of Things: Concepts, Applications, and Challenges (/chapter/internet-of-things/187894) (pages 73-95)

Varsha Sharma, Vivek Sharma, Nishchol Mishra

Sample PDF (/viewtitlesample.aspx?id=187894&ptid=179213&t=Internet of Things: Concepts, Applications, and Challenges&isxn=9781522529477)

Chapter 8**\$37.50**

Internet of Things for Smart Cities (/chapter/internet-of-things-for-smart-cities/187895) (pages 96-112)

Pallavi Khare, Akhil Khare

Sample PDF (/viewtitlesample.aspx?id=187895&ptid=179213&t=Internet of Things for Smart Cities&isxn=9781522529477)

Chapter 9**\$37.50**

PIR-Enabled Security System for Internet of Things Using Raspberry Pi (/chapter/pir-enabled-security-system-for-internet-of-things-using-raspberry-pi/187896) (pages 113-128)

Mamillapally Nagaraju, Mulukutla Trivikram

Sample PDF (/viewtitlesample.aspx?id=187896&ptid=179213&t=PIR-Enabled Security System for Internet of Things Using Raspberry Pi&isxn=9781522529477)

Chapter 10**\$37.50**

Adaptive Control Strategies for Task Scheduler Using Internet of Things (/chapter/adaptive-control-strategies-for-task-scheduler-using-internet-of-things/187897) (pages 129-140)

Adiraju Prashantha Rao

Sample PDF (/viewtitlesample.aspx?id=187897&ptid=179213&t=Adaptive Control Strategies for Task Scheduler Using Internet of Things&isxn=9781522529477)

Chapter 11**\$37.50**

Centralized Fog Computing Security Platform for IoT and Cloud in Healthcare System (/chapter/centralized-fog-computing-security-platform-for-iot-and-cloud-in-healthcare-system/187898) (pages 141-154)

Chandu Thota, Revathi Sundarasekar, Gunasekaran Manogaran, Varatharajan R, Priyan M. K.

Sample PDF (/viewtitlesample.aspx?id=187898&ptid=179213&t=Centralized Fog Computing Security Platform for IoT and Cloud in Healthcare System&isxn=9781522529477)

Chapter 12**\$37.50**

An Intelligent Parking System in Smart Cities Using IoT (/chapter/an-intelligent-parking-system-in-smart-cities-using-iot/187899) (pages 155-180)

Amardeep Das, Prasant Kumar Dash, Brojo Kishore Mishra

Sample PDF (/viewtitlesample.aspx?id=187899&ptid=179213&t=An Intelligent Parking System in Smart Cities Using IoT&isxn=9781522529477)

Chapter 13 **\$37.50**

Data Mining for the Internet of Things (/chapter/data-mining-for-the-internet-of-things/187900) (pages 181-191)

Akhil Rajendra Khare, Pallavi Shrivasta

Sample PDF (/viewtitlesample.aspx?id=187900&ptid=179213&t=Data Mining for the Internet of Things&isxn=9781522529477)

Chapter 14 **\$37.50**

A Study on Performance of E-Commerce Web Applications (/chapter/a-study-on-performance-of-e-commerce-web-applications/187901) (pages 192-199)

Sreedhar G

Sample PDF (/viewtitlesample.aspx?id=187901&ptid=179213&t=A Study on Performance of E-Commerce Web Applications&isxn=9781522529477)

Chapter 15 **\$37.50**

Performance Improvement IoT Applications Through Multimedia Analytics Using Big Data Stream Computing Platforms (/chapter/performance-improvement-iot-applications-through-multimedia-analytics-using-big-data-stream-computing-platforms/187902) (pages 200-221)

Rizwan Patan, Rajasekhara Babu M, Suresh Kallam

Sample PDF (/viewtitlesample.aspx?id=187902&ptid=179213&t=Performance Improvement IoT Applications Through Multimedia Analytics Using Big Data Stream Computing Platforms&isxn=9781522529477)

Chapter 16 **\$37.50**

Predictive Analytics to Support Clinical Trials Get Healthier (/chapter/predictive-analytics-to-support-clinical-trials-get-healthier/187903) (pages 222-239)

Ankit Lodha, Anvita Karara

Sample PDF (/viewtitlesample.aspx?id=187903&ptid=179213&t=Predictive Analytics to Support Clinical Trials Get Healthier&isxn=9781522529477)

Chapter 17 **\$37.50**

Big Data and Internet of Things for Analysing and Designing Systems Based on Hyperspectral Images (/chapter/big-data-and-internet-of-things-for-analysing-and-designing-systems-based-on-hyperspectral-images/187904) (pages 240-260)

Peyakunta Bhargavi, Singaraju Jyothi

Sample PDF (/viewtitlesample.aspx?id=187904&ptid=179213&t=Big Data and Internet of Things for Analysing and Designing Systems Based on Hyperspectral Images&isxn=9781522529477)

Chapter 18 **\$37.50**

Can LTE-A Support Real-Time Smart Meter Traffic in the Smart Grid? (/chapter/can-lte-a-support-real-time-smart-meter-traffic-in-the-smart-grid/187905) (pages 261-281)

Elias Yaacoub

Sample PDF (/viewtitlesample.aspx?id=187905&ptid=179213&t=Can LTE-A Support Real-Time Smart Meter Traffic in the Smart Grid?&isxn=9781522529477)

Chapter 19

\$37.50

Mobile Cloud Gaming and Today's World (/chapter/mobile-cloud-gaming-and-todays-world/187906) (pages 282-295)

Hallah Shahid Butt, Sadaf Jalil, Sajid Umair, Safdar Abbas Khan

Sample PDF (/viewtitlesample.aspx?id=187906&ptid=179213&t=Mobile Cloud Gaming and Today's World&isxn=9781522529477)

About the Contributors

[View Full PDF \(/pdf.aspx?tid=187908&ptid=179213&ctid=17&t=About the Contributors&isxn=9781522529477\)](/pdf.aspx?tid=187908&ptid=179213&ctid=17&t=About the Contributors&isxn=9781522529477)

Index

[View Full PDF \(/pdf.aspx?tid=187909&ptid=179213&ctid=17&t=Index&isxn=9781522529477\)](/pdf.aspx?tid=187909&ptid=179213&ctid=17&t=Index&isxn=9781522529477)

Learn More

[About IGI Global \(/about/\)](/about/) | [Partnerships \(/about/partnerships/\)](/about/partnerships/) | [COPE Membership \(/about/memberships/cope/\)](/about/memberships/cope/) | [Contact \(/contact/\)](/contact/) | [Job Opportunities \(/about/staff/job-opportunities/\)](/about/staff/job-opportunities/) | [FAQ \(/faq/\)](/faq/) | [Management Team \(/about/staff/\)](/about/staff/)

Resources For

[Librarians \(/librarians/\)](/librarians/) | [Authors/Editors \(/publish/\)](/publish/) | [Distributors \(/distributors/\)](/distributors/) | [Instructors \(/course-adoption/\)](/course-adoption/) | [Translators \(/about/rights-permissions/translation-rights/\)](/about/rights-permissions/translation-rights/) | [Editorial Services \(/editorial-service-partners/\)](/editorial-service-partners/)

Media Center

[Webinars \(/symposium/\)](/symposium/) | [Blogs \(/newsroom/\)](/newsroom/) | [Catalogs \(/catalogs/\)](/catalogs/) | [Newsletters \(/newsletters/\)](/newsletters/)

Policies

[Privacy Policy \(/about/rights-permissions/privacy-policy/\)](/about/rights-permissions/privacy-policy/) | [Cookie & Tracking Notice \(/cookies-agreement/\)](/cookies-agreement/) | [Fair Use Policy \(/about/rights-permissions/content-reuse/\)](/about/rights-permissions/content-reuse/) | [Ethics and Malpractice \(/about/rights-permissions/ethics-malpractice/\)](/about/rights-permissions/ethics-malpractice/)

<http://www.facebook.com/pages/IGI-Global/138206739534176?ref=sgm>

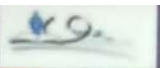
<http://twitter.com/igiglobal>

<https://www.linkedin.com/company/igi-global>



<https://publicationethics.org/category/publisher/igi-global>

Copyright © 1988-2021, IGI Global - All Rights Reserved



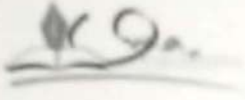
UMA PUBLICATIONS

GET READY FOR PLACEMENTS

Step By Step Guide to Prepare for
Technical Placements



Dr. G. Shyama Chandra Prasad



Uma Publications

ISBN : 978-81-920425-3-4

Get Ready for Placements - Step By Step Guide to Prepare for Technical Placements

Publisher : Himanshu Kulkarni,
Uma Publications
C/O R.B.Karkare, KarkareNiwas,
Mill Road, Kalamandir, Nanded.

Cell : +91 9421850831

Mail : umapublicationsned@gmail.com

Website : umapublishinghouse.com

Cover Design : Sriram Kulkarni

Cell : +91 9975477661

Layout : Ms.Swati Karkare

Printed by : Pooja Printers, Pune

Edition : 2017 Vol-1

All rights reserved by Uma Publications.

No part of the publication may be reproduced or distributed.

Rs.270/-

Table of Contents

I. General Interview Skills

1. On Campus Interview Process By Software Companies

1

2. General Interview questions

3

II. Programming Skills

3. C

4

4. Data Structures

90

5. C++ and OOPS

100

6. UNIX Concepts

122

III. Core Subjects

7. SQL

140

8. RDBMS Concepts

148

9. Operating Systems

149

10. Computer Networks

159

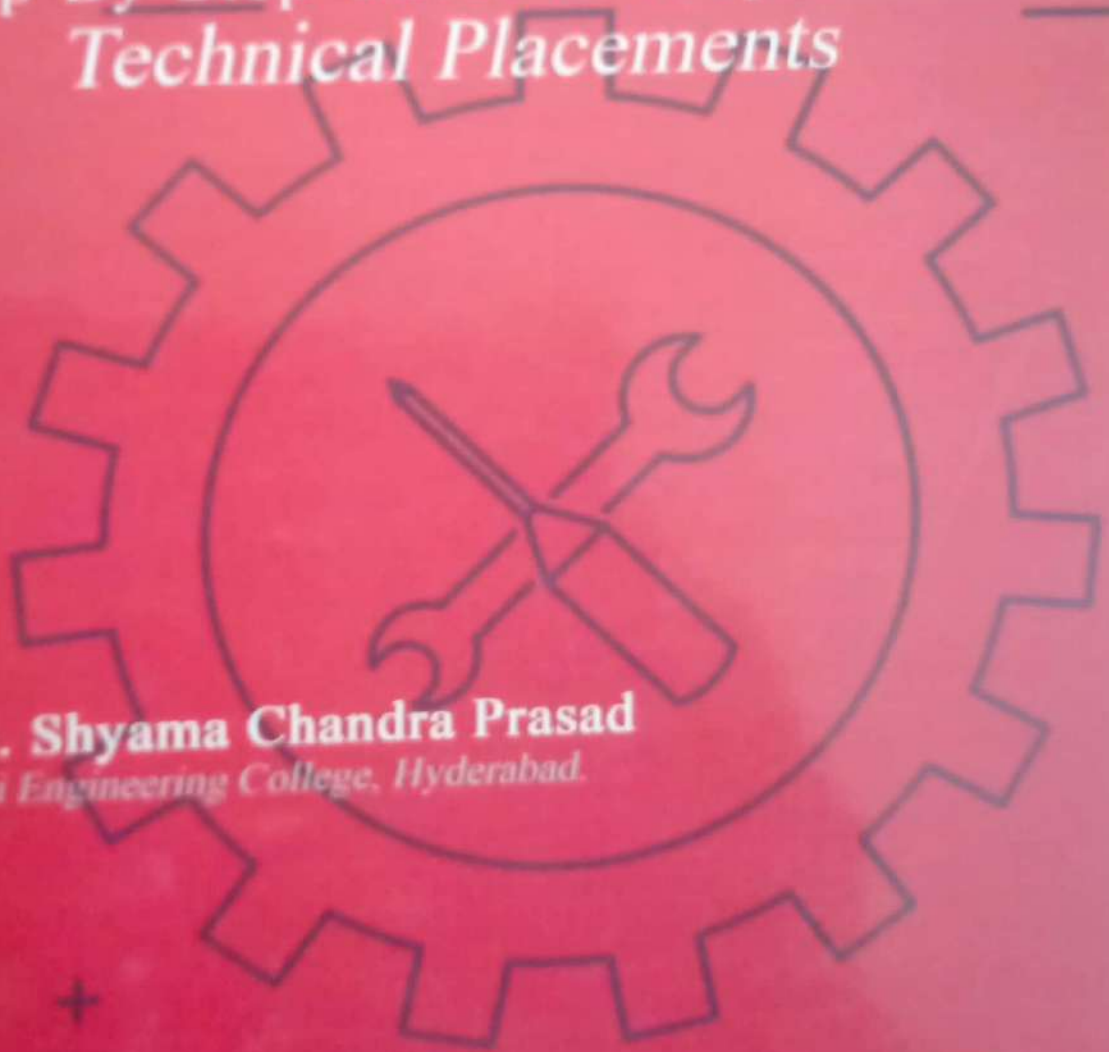
11. Design and Analysis of Algorithms

169

Bibliography

GET READY FOR PLACEMENTS

Step By Step Guide to Prepare for
Technical Placements



AUTHOR

Dr. G. Shyama Chandra Prasad
Matrusri Engineering College, Hyderabad.



UMA PUBLICATIONS



978-81-929425-3-4

To Support Customers in Easily and Affordably Obtaining the Latest Peer-Reviewed Research,

Receive a 20% Discount on ALL Publications and Free Worldwide Shipping on Orders Over US\$ 295

Additionally, Enjoy an Additional 5% Pre-Publication Discount on all Forthcoming Reference Books

[Browse Titles \(https://www.igi-global.com/search/?p=&ctid=1%2c2\)](https://www.igi-global.com/search/?p=&ctid=1%2c2)



Data Mining for the Internet of Things

Akhil Rajendra Khare (MVSR Engineering College, India) and Pallavi Shrivasta (Matrusri Engineering College, India)

Source Title: Exploring the Convergence of Big Data and the Internet of Things (/book/exploring-convergence-big-data-internet/179213)

Copyright: © 2018

Pages: 11

DOI: 10.4018/978-1-5225-2947-7.ch013

**OnDemand PDF
Download:**

\$37.50

Available

[Current Special Offers](#)

Abstract

The Internet of Things concept arises from the need to manage, automate, and explore all devices, instruments and sensors in the world. In order to make wise decisions both for people and for the things in IoT, data mining technologies are integrated with IoT technologies for decision making support and system optimization. Data mining involves discovering novel, interesting, and potentially useful patterns from data and applying algorithms to the extraction of hidden information. Data mining is classified into three different views: knowledge view, technique view, and application view. The challenges in the data mining algorithms for IoT are discussed and a suggested big data mining system is proposed.

Chapter Preview

Top

Introduction


Outline

The Internet of Things (IoT) and its relevant technologies can seamlessly integrate classical networks with networked instruments and devices. IoT has been playing an essential role ever since it appeared, which covers from traditional equipment to general household objects and has been attracting the attention of researchers from academia, industry, and government in recent years.

There is a great vision that all things can be easily controlled and monitored, can be identified automatically by other things, can communicate with each other through internet, and can even make decisions by themselves. In order to make IoT smarter, lots of analysis technologies are introduced into IoT; one of the most valuable technologies is data mining.

Data mining involves discovering novel, interesting, and potentially useful patterns from large data sets and applying algorithms to the extraction of hidden information. Many other terms are used for data mining, for example, knowledge discovery (mining) in databases (KDD), knowledge extraction, data/pattern analysis, data archaeology, data dredging, and information harvesting. The objective of any data mining process is to build an efficient predictive or descriptive model of a large amount of data that not only best fits or explains it, but is also able to generalize to new data (Figure 1). Based on a broad view of data mining functionality, data mining is the process of discovering interesting knowledge from large amounts of data stored in either databases, data warehouses, or other information repositories (Tsai, Lai & Vasilakos, 2014).

Figure 1. The data mining overview

 [978-1-5225-2947-7.ch013.f01](https://igiprodst.blob.core.windows.net:443/source-content/9781522529477_179213/978-1-5225-2947-7.ch013.f01.png?sv=2015-12-11&sr=c&sig=3KnEJ83kNDloUTz7TFjBYi8dXi7ulgOpQdOAg23QMcl%3D&se=2019-11-15T07%3A56%3A50Z&sp=r) (https://igiprodst.blob.core.windows.net:443/source-content/9781522529477_179213/978-1-5225-2947-7.ch013.f01.png?sv=2015-12-11&sr=c&sig=3KnEJ83kNDloUTz7TFjBYi8dXi7ulgOpQdOAg23QMcl%3D&se=2019-11-15T07%3A56%3A50Z&sp=r)

On the basis of the definition of data mining and the definition of data mining functions, a typical data mining process includes the following steps (Jiawei & Kamber, 2011)

Scope

We can view data mining in a multidimensional view.

1. In knowledge view or data mining functions view, it includes characterization, discrimination, classification, clustering, association analysis, time series analysis, and outlier analysis.
2. In utilized techniques view, it includes machine learning, statistics, pattern recognition, big data, support vector machine, rough set, neural networks and evolutionary algorithms.
3. In application view, it includes industry, telecommunication, banking, fraud analysis, bio data mining, stock market analysis, text mining, web mining, social network and e-commerce.

A variety of researches focusing on knowledge view, technique view and application view can be found in the literature. However, no previous effort has been made to review the different views of data mining in a systematic way, especially in nowadays big data; mobile internet and Internet of Things grow rapidly and some data mining researchers shift their attention from data mining to big data. There are lots of data that can be mined, for example, database data (relational database, No SQL database), data warehouse, data stream, spatiotemporal, time series, sequence, text and web, multimedia, graphs, the World Wide Web, Internet of Things data, and legacy system log. Motivated by this, we attempt to make a comprehensive survey of the important recent developments of data mining research. This survey focuses on knowledge view, utilized techniques view, and application view of data mining.

Top

Data Mining Functionalities

Data mining functionalities include classification, clustering, association analysis, time series analysis, and outlier analysis (Jing, Vasilakos, Wan et al., 2014).

Complete Chapter List

Search this Book:

Reset

Editorial Advisory Board and List of Reviewers	View Full PDF (/pdf.aspx?tid=187883&ptid=179213&ctid=15&t=Editorial Advisory Board and List of Reviewers&isxn=9781522529477)
Table of Contents	View Full PDF (/pdf.aspx?tid=187884&ptid=179213&ctid=15&t=Table of Contents&isxn=9781522529477)
Detailed Table of Contents	View Full PDF (/pdf.aspx?tid=187885&ptid=179213&ctid=15&t=Detailed Table of Contents&isxn=9781522529477)
Preface	View Full PDF (/pdf.aspx?tid=187886&ptid=179213&ctid=15&t=Preface&isxn=9781522529477)

Acknowledgment

[View Full PDF \(/pdf.aspx?tid=187887&ptid=179213&ctid=15&t=Acknowledgment&isxn=9781522529477\)](#)

Chapter 1

\$37.50

Big Data and Cloud Computing: A Review of Supply Chain Capabilities and Challenges (/chapter/big-data-and-cloud-computing/187888) (pages 1-28)

Marcus Tanque, Harry J Foxwell

Sample PDF (/viewtitlesample.aspx?id=187888&ptid=179213&t=Big Data and Cloud Computing: A Review of Supply Chain Capabilities and Challenges&isxn=9781522529477)

Chapter 2

\$37.50

Big Data Analytics in Aquaculture Using Hive and Hadoop Platform (/chapter/big-data-analytics-in-aquaculture-using-hive-and-hadoop-platform/187889) (pages 29-35)

P. Venkateswara Rao, A. Ramamohan Reddy, V. Sucharita

Sample PDF (/viewtitlesample.aspx?id=187889&ptid=179213&t=Big Data Analytics in Aquaculture Using Hive and Hadoop Platform&isxn=9781522529477)

Chapter 3

\$37.50

Big Data Mining: A Forecast to the Future (/chapter/big-data-mining/187890) (pages 36-42)

V. Sucharita, P. Venkateswara Rao, A. Satya Kalyan, P. Rajarajeswari

Sample PDF (/viewtitlesample.aspx?id=187890&ptid=179213&t=Big Data Mining: A Forecast to the Future&isxn=9781522529477)

Chapter 4

\$37.50

Cloud Computing Education Strategies: A Review (/chapter/cloud-computing-education-strategies/187891) (pages 43-54)

Syed Hassan Askari, Faizan Ahmad, Sajid Umair, Safdar Abbas Khan

Sample PDF (/viewtitlesample.aspx?id=187891&ptid=179213&t=Cloud Computing Education Strategies: A Review&isxn=9781522529477)

Chapter 5

\$37.50

Computational Linguistic Distances and Big Data: Optimising the Speech Recognition Systems (/chapter/computational-linguistic-distances-and-big-data/187892) (pages 55-62)

Krishnaveer Abhishek Challa, Jawahar Annabattula

Sample PDF (/viewtitlesample.aspx?id=187892&ptid=179213&t=Computational Linguistic Distances and Big Data: Optimising the Speech Recognition Systems&isxn=9781522529477)

Chapter 6

\$37.50

Big Data in Mobile Commerce: Customer Relationship Management (/chapter/big-data-in-mobile-commerce/187893) (pages 63-72)

Muhammad Anshari, Syamimi Ariff Lim

Sample PDF (/viewtitlesample.aspx?id=187893&ptid=179213&t=Big Data in Mobile Commerce: Customer Relationship Management&isxn=9781522529477)

Chapter 7**\$37.50**

Internet of Things: Concepts, Applications, and Challenges (/chapter/internet-of-things/187894) (pages 73-95)

Varsha Sharma, Vivek Sharma, Nishchol Mishra

Sample PDF (/viewtitlesample.aspx?id=187894&ptid=179213&t=Internet of Things: Concepts, Applications, and Challenges&isxn=9781522529477)

Chapter 8**\$37.50**

Internet of Things for Smart Cities (/chapter/internet-of-things-for-smart-cities/187895) (pages 96-112)

Pallavi Khare, Akhil Khare

Sample PDF (/viewtitlesample.aspx?id=187895&ptid=179213&t=Internet of Things for Smart Cities&isxn=9781522529477)

Chapter 9**\$37.50**

PIR-Enabled Security System for Internet of Things Using Raspberry Pi (/chapter/pir-enabled-security-system-for-internet-of-things-using-raspberry-pi/187896) (pages 113-128)

Mamillapally Nagaraju, Mulukutla Trivikram

Sample PDF (/viewtitlesample.aspx?id=187896&ptid=179213&t=PIR-Enabled Security System for Internet of Things Using Raspberry Pi&isxn=9781522529477)

Chapter 10**\$37.50**

Adaptive Control Strategies for Task Scheduler Using Internet of Things (/chapter/adaptive-control-strategies-for-task-scheduler-using-internet-of-things/187897) (pages 129-140)

Adiraju Prashantha Rao

Sample PDF (/viewtitlesample.aspx?id=187897&ptid=179213&t=Adaptive Control Strategies for Task Scheduler Using Internet of Things&isxn=9781522529477)

Chapter 11**\$37.50**

Centralized Fog Computing Security Platform for IoT and Cloud in Healthcare System (/chapter/centralized-fog-computing-security-platform-for-iot-and-cloud-in-healthcare-system/187898) (pages 141-154)

Chandu Thota, Revathi Sundarasekar, Gunasekaran Manogaran, Varatharajan R, Priyan M. K.

Sample PDF (/viewtitlesample.aspx?id=187898&ptid=179213&t=Centralized Fog Computing Security Platform for IoT and Cloud in Healthcare System&isxn=9781522529477)

Chapter 12**\$37.50**

An Intelligent Parking System in Smart Cities Using IoT (/chapter/an-intelligent-parking-system-in-smart-cities-using-iot/187899) (pages 155-180)

Amardeep Das, Prasant Kumar Dash, Brojo Kishore Mishra

Sample PDF (/viewtitlesample.aspx?id=187899&ptid=179213&t=An Intelligent Parking System in Smart Cities Using IoT&isxn=9781522529477)

Chapter 13**\$37.50**

Data Mining for the Internet of Things (/chapter/data-mining-for-the-internet-of-things/187900) (pages 181-191)

Akhil Rajendra Khare, Pallavi Shrivasta

Sample PDF (/viewtitlesample.aspx?id=187900&ptid=179213&t=Data Mining for the Internet of Things&isxn=9781522529477)

Chapter 14**\$37.50**

A Study on Performance of E-Commerce Web Applications (/chapter/a-study-on-performance-of-e-commerce-web-applications/187901) (pages 192-199)

Sreedhar G

Sample PDF (/viewtitlesample.aspx?id=187901&ptid=179213&t=A Study on Performance of E-Commerce Web Applications&isxn=9781522529477)

Chapter 15**\$37.50**

Performance Improvement IoT Applications Through Multimedia Analytics Using Big Data Stream Computing Platforms (/chapter/performance-improvement-iot-applications-through-multimedia-analytics-using-big-data-stream-computing-platforms/187902) (pages 200-221)

Rizwan Patan, Rajasekhara Babu M, Suresh Kallam

Sample PDF (/viewtitlesample.aspx?id=187902&ptid=179213&t=Performance Improvement IoT Applications Through Multimedia Analytics Using Big Data Stream Computing Platforms&isxn=9781522529477)

Chapter 16**\$37.50**

Predictive Analytics to Support Clinical Trials Get Healthier (/chapter/predictive-analytics-to-support-clinical-trials-get-healthier/187903) (pages 222-239)

Ankit Lodha, Anvita Karara

Sample PDF (/viewtitlesample.aspx?id=187903&ptid=179213&t=Predictive Analytics to Support Clinical Trials Get Healthier&isxn=9781522529477)

Chapter 17**\$37.50**

Big Data and Internet of Things for Analysing and Designing Systems Based on Hyperspectral Images (/chapter/big-data-and-internet-of-things-for-analysing-and-designing-systems-based-on-hyperspectral-images/187904) (pages 240-260)

Peyakunta Bhargavi, Singaraju Jyothi

Sample PDF (/viewtitlesample.aspx?id=187904&ptid=179213&t=Big Data and Internet of Things for Analysing and Designing Systems Based on Hyperspectral Images&isxn=9781522529477)

Chapter 18**\$37.50**

Can LTE-A Support Real-Time Smart Meter Traffic in the Smart Grid? (/chapter/can-lte-a-support-real-time-smart-meter-traffic-in-the-smart-grid/187905) (pages 261-281)

Elias Yaacoub

Sample PDF (/viewtitlesample.aspx?id=187905&ptid=179213&t=Can LTE-A Support Real-Time Smart Meter Traffic in the Smart Grid?&isxn=9781522529477)

Chapter 19

\$37.50

Mobile Cloud Gaming and Today's World (/chapter/mobile-cloud-gaming-and-todays-world/187906) (pages 282-295)

Hallah Shahid Butt, Sadaf Jalil, Sajid Umair, Safdar Abbas Khan

Sample PDF (/viewtitlesample.aspx?id=187906&ptid=179213&t=Mobile Cloud Gaming and Today's World&isxn=9781522529477)

About the Contributors

[View Full PDF \(/pdf.aspx?tid=187908&ptid=179213&ctid=17&t=About the Contributors&isxn=9781522529477\)](/pdf.aspx?tid=187908&ptid=179213&ctid=17&t=About the Contributors&isxn=9781522529477)

Index

[View Full PDF \(/pdf.aspx?tid=187909&ptid=179213&ctid=17&t=Index&isxn=9781522529477\)](/pdf.aspx?tid=187909&ptid=179213&ctid=17&t=Index&isxn=9781522529477)

Learn More

[About IGI Global \(/about/\)](/about/) | [Partnerships \(/about/partnerships/\)](/about/partnerships/) | [COPE Membership \(/about/memberships/cope/\)](/about/memberships/cope/) | [Contact \(/contact/\)](/contact/) | [Job Opportunities \(/about/staff/job-opportunities/\)](/about/staff/job-opportunities/) | [FAQ \(/faq/\)](/faq/) | [Management Team \(/about/staff/\)](/about/staff/)

Resources For

[Librarians \(/librarians/\)](/librarians/) | [Authors/Editors \(/publish/\)](/publish/) | [Distributors \(/distributors/\)](/distributors/) | [Instructors \(/course-adoption/\)](/course-adoption/) | [Translators \(/about/rights-permissions/translation-rights/\)](/about/rights-permissions/translation-rights/) | [Editorial Services \(/editorial-service-partners/\)](/editorial-service-partners/)

Media Center

[Webinars \(/symposium/\)](/symposium/) | [Blogs \(/newsroom/\)](/newsroom/) | [Catalogs \(/catalogs/\)](/catalogs/) | [Newsletters \(/newsletters/\)](/newsletters/)

Policies

[Privacy Policy \(/about/rights-permissions/privacy-policy/\)](/about/rights-permissions/privacy-policy/) | [Cookie & Tracking Notice \(/cookies-agreement/\)](/cookies-agreement/) | [Fair Use Policy \(/about/rights-permissions/content-reuse/\)](/about/rights-permissions/content-reuse/) | [Ethics and Malpractice \(/about/rights-permissions/ethics-malpractice/\)](/about/rights-permissions/ethics-malpractice/)

<http://www.facebook.com/pages/IGI-Global/138206739534176?ref=sgm>

<http://twitter.com/igiglobal>

<https://www.linkedin.com/company/igi-global>



<https://publicationethics.org/category/publisher/igi-global>

Copyright © 1988-2021, IGI Global - All Rights Reserved